A Study into the Influence of Amyloid-beta Peptide Oxidation on the Rate of Fibril Formation, with a Synthesis of 2-oxo-histidine

Hannah Mary Garrett

A thesis submitted to

THE UNIVERSITY OF LONDON

For the degree of

DOCTOR OF PHILOSOPHY

School of Biological and Chemical Sciences

Queen Mary, University of London

May 2012

I herewith certify that any material in this thesis that is not my own work has been properly acknowledged.

Hannah Garrett

I dedicate this thesis to my family and friends but in particular to my late father, Christopher John Wright, who first showed me the wonder of science.

ACKNOWLEDGEMENTS

Although a PhD thesis only has one name on the title page it is never a solo effort. There are so many people who have advised and supported me over the last four years and without them it is unlikely this thesis would be here. It is impossible to thank everyone who has made this possible but I would like to mention a few of these people.

Firstly, I would like thank my two supervisors, Dr Peter Wyatt and Dr John Viles, for giving me the opportunity to undertake this project, for advising me throughout and for being a constant source of suggestions of how to go forward with the project when things didn't quite go to plan. They have inspired me with their enthusiasm for their work and their breadth and depth of knowledge of their fields.

Secondly, I would like to thank the other academics at Queen Mary who have advised and supported me throughout my PhD. Professor Mike Watkinson chaired my panel meetings in a way that ensured I gained the most from them and throughout my PhD has kept me on course. Dr Robin Maytum always brought interesting discussions to my panel meetings and, when I felt like giving up, was incredibly supportive and reminded me of the benefits of a PhD. Professor Vaughan Griffiths kindly replaced Dr Maytum on my panel and brought a new perspective to the meetings, which highlighted important approaches to a PhD that I had not previously considered. Dr Adrian Dobbs, despite not being on my panel, has always encouraged me to increase my knowledge of organic chemistry by teaching me, allowing me to attend several of his group meetings and by being a good friend throughout my PhD.

SBCS at Queen Mary is truly blessed in having such a lovely, supportive and friendly community of researchers. Without the friendly faces and comforting chats that I experienced every day in the college, the PhD would have been a much harder process. In addition, the many conversations over cups of tea early in the morning and late in the evenings regarding mechanisms, appropriate reagents and which music was the best to work to, were invaluable.

Dr Ana María Blanco Rodríguez has been a good friend and supportive work colleague throughout my PhD. The many evening meals we had together were a good way to unwind after a tough day in the lab. Freda Chio is the most hard working person I have ever met and really inspired me, first as a project student in the Wyatt group and secondly as a fellow PhD student in the Chemistry department, to keep going. I really enjoyed studying the theory of organic chemistry with her and can only slightly apologise for exasperating her when always asking what the correct nomenclature was

for every chemical structure I came across. She has been a kind and conscientious friend throughout. Niranjeni Pathumakanthar has the most perseverance I have ever seen in a PhD student. Despite all her hardships she is a lovely, cheerful soul with whom I have enjoyed many lunches and conversations across a fume hood. I wish her all the best with completing her PhD. Dr Farid Uddin has been another true friend throughout my whole PhD. He is both a source of indispensible knowledge of chemistry and has a wicked sense of humour. My PhD would not have been half as enjoyable without his presence in the lab.

Dr Rendy Tan, Dr Becky Nadal and Dr Claire Sarrell were all current members of the Wyatt and Viles groups when I joined in 2004. Without them I would never have got up to speed on the many new techniques and knowledge required to do my PhD. Watching them go on to complete their post docs and PhDs was a real inspiration for completing my own project. The other members, past and present, of the Wyatt and Viles groups have made these groups feel like real families; Ahmed Dellali, Jahangir Malik, Zhe Li, Yu Peng, Zhang Yi, Nadine Younan and Helen Stanyon.

Finally, but by no means least, my friends and family have been such an encouraging and supportive network throughout my PhD, despite not always understanding the slightly frazzled, PhD-crazed person I had become. My new husband John Garrett has always been a rock throughout my PhD to whom I could turn at any moment for support and love. He even still agreed to marry me after four years of experiencing the PhD stress first-hand and for that I will always admire and love him. My parents have constantly supported me throughout my life and helped me to strive to whatever goal I set myself. They have always taken a keen interest in how my PhD is progressing and my mother even knows the title of my thesis. Rosie and Lucy have been such great sisters throughout my PhD, always with support and able to make me laugh. Finally, my closest friends, Jess, Mary, Zoe, Claire, Lorraine and Amy, have listened to my trials and tribulations and in return provided kind words and fun anecdotes.

It is with all this kindness, good will and support that I have completed this PhD and for that I will be eternally grateful.

Thank you also to the EPSRC and Queen Mary, University of London for my funding.

ABSTRACT

The Amyloid Cascade Hypothesis states that fibrillation of the amyloid beta (Aβ) peptide is the primary cause of Alzheimer's pathology. The trigger for the fibrillation is a subject of much debate, although it is clear, oxidative stress is a key feature of Alzheimer's aetiology. This thesis explores a possible role of oxidation of Aβ, in particular the effect of histidine and methionine side-chain oxidation, on Aβ fibril growth rates. Within chapters 2 and 3 of this thesis is a discussion of various approaches to chemical synthesis of 2-oxo-histidine with a view to the incorporation of the oxidised amino acids into Aβ peptide using Fmoc approaches. Chapter 2 describes attempted chemical transformation of (protected) L-histidine into L-oxohistidine. Dimethyldioxirane oxidised Boc-His-OMe yielded products containing isopropylidene groups, while oxidation using a Cu(II)/ascorbate generated 2-oxo-histidine but gave very low yields. Within chapter 3, a successful synthesis of protected 2-oxo-histidine is described, via the known imidazolin-2-one-4-carboxylic. Chapter 4 analyses Aβ(1-40) fibrillation kinetics by treating the intact peptide with various oxidants. Contrary to previous reports, hydrogen peroxide alone did not slow fibrillation rates. Cu(II)/Cu(I)-catalysed oxidation increased the likelihood of amorphous aggregation over fibrillation. This thesis shows oxidation of Aβ has a profound influence on fibril growth and that incorporation of a stable oxidised histidine into Aβ is a realisable goal.

TABLE OF CONTENTS-

LIST OF ABBREVIATIONS

Å	Angstrom (≡ 0.1 nm)
ø	diameter
δ_x	chemical shift (x = nucleus)
ε	C-2 of the imidazole ring
Δ ε	molar ellipticity
θ	ellipticity
μM	micromolar
λ	wavenumber
ρ	resistivity
Aβ	amyloid beta (peptide) (also known as A4)
Ac	acetyl
AD	Alzheimer's disease
ADDLs	Aβ-derived diffusible ligands
AFM	atomic force microscopy
AFU	arbitrary fluorescence units
AGE	advanced-end product of glycation
Agp	*Agrobacterium phytochrome*
ApoE	apolipoprotein E
APP	amyloid precursor protein
Ar	aromatic
ASPD	amylospheroid
ATR-IR	attenuated total reflectance infra red spectroscopy
AU	arbitrary units
$[B]_t$	maximal fluorescence (well-plate)
BCA	bicinchonic acid
Boc	*tert*-butyloxycarbonyl
BOM	benzyloxymethyl
BSA	bovine serum albumin
c_0	column pore volume
CAN	cerium(IV) diammonium nitrate
Cbz	carbobenzloxy
CD	circular dichroism
c_i	interstitial column volume
CNS	central nervous system
COD	cyclooctadiene
COSY	correlation spectroscopy
CSF	cerebrospinal fluid
DBU	1,8-diazabicyclo[5.4.0]undec-7-ene
dec.	decomposed
DEPT	distortionless enhancement by polarization transfer
DFT	density functional theory
DIBAl-H	diisobutylaluminium hydride
DLS	dynamic light scattering
DMB	dimethoxybenzoyl
DMDO	dimethyldioxirane
DMPO	5,5-Dimethyl-1-Pyrroline N-Oxide
DNA	deoxyribonucleic acid
DTT	dithiothreitol

DuPHOS	1,2-bis(phospholano)benzene
EDTA	ethylenediaminetetraacetic acid
EI-MS	electron impact mass spectrometry
EM	electron microscopy
EPR	electron paramagnetic resonance
ER	endoplasmic reticulum
FAB-MS	fast atom bombardment mass spectrometry
fAD	familial Alzheimer's disease
FMOC	(fluorenyl)methoxycarbonyl
FPLC	fast protein liquid chromatography
FT-IR	Fourier transform infra red spectroscopy
HEPES	(4-(2-hydroxyethyl)-1-piperazineethanesulfonic acid)
HPLC	high performance liquid chromatography
HSA	human serum albumin
HSQC	heteronuclear single quantum coherence
HWE	Horner-Wadsworth-Emmons (reaction)
Hz	hertz
IR	infra red
IUPAC	International Union of Pure and Applied Chemistry
k_{app}	apparent fibril growth rate
K_{AV}	retention factor (SEC)
kDa	kilodaltons
k_e	elongation constant
k_n	nucleation constant
K_{SEC}	distribution coefficient (SEC)
L-DOPA	L-3,4-dihydroxyphenylalanine
Lit.	literature
MCO	metal catalysed oxidation
MDa	megadaltons
mdeg	millidegrees
mM	Millimolar
mp	melting point
MPa	megapascals
M_r	relative molecular mass
m/z	mass charge ratio
NDP	nucleation dependent polymerisation
NFT	neurofibrillary tangle
NHE	normal hydrogen electrode
nm	nanometre
nM	nanomolar
NMR	nuclear magnetic resonance
NOE	Nuclear Overhauser effect
PHF	paired helical filament
PHOS	phosphine
pI	isoelectric point
p*K*a	acid dissociation constant
pM	picomolar
PMB	*p*-methoxybenzoyl (also known as MPM)
ppm	parts per million
R_f	retention factor

R_h	hydrodynamic radius
r.t.	room temperature
ROS	reactive oxygen species
RP-HPLC	reverse-phase high performance liquid chromtography
SDS-PAGE	sodium dodecyl sulfate polyacrylamide gel electrophoresis
SEC	size exclusion chromatography
t_{50}	time to half maximal growth
Th-T	thioflavin-T
t_{lag}	lag phase (nucleation)
TLC	thin layer chromatography
TRH	thyrotrophin releasing hormone
UHQ	ultra high quality
UV	ultra-violet
V_c	column volume
V_e	elution volume
V_i	pore volume

Amino acids are referred to by both their 1 and 3 letter codes throughout this thesis:

Ala	A	alanine
Arg	R	arginine
Asp	D	aspartate
Asn	N	asparagine
Cys	C	cysteine
Gln	Q	glutamine
Glu	E	glutamate
Gly	G	glycine
His	H	histidine
Iso	I	isoleucine
Leu	L	leucine
Lys	K	lysine
Met	M	methionine
Phe	F	phenylalanine
Pro	P	proline
Ser	S	serine
Thr	T	threonine
Trp	W	tryptophan
Tyr	Y	tyrosine
Val	V	valine

Chapter 1

INTRODUCTION 1

1.1. Alzheimer's Disease (AD)

Alzheimer's Disease (AD) was first characterised in 1906 by Alois Alzheimer upon examination of one of his patients, Auguste D, 55 years old. She had presented with the symptoms of disorientation, impaired memory, difficulties reading and writing, and hallucinations (Alzheimer, A., 1906). Upon post-mortem the cerebral cortex of the patient's brain was found to be thinning and, within the remaining tissue, two abnormalities were noted, co-localised with neuronal degeneration; intracellular neurofibrillary tangles (NFT) within cell bodies and proximal dendrites, and extracellular amyloid plaques within the blood plasma, cortical interstitium and cerebrospinal fluid (CSF) (Figure 1.1).

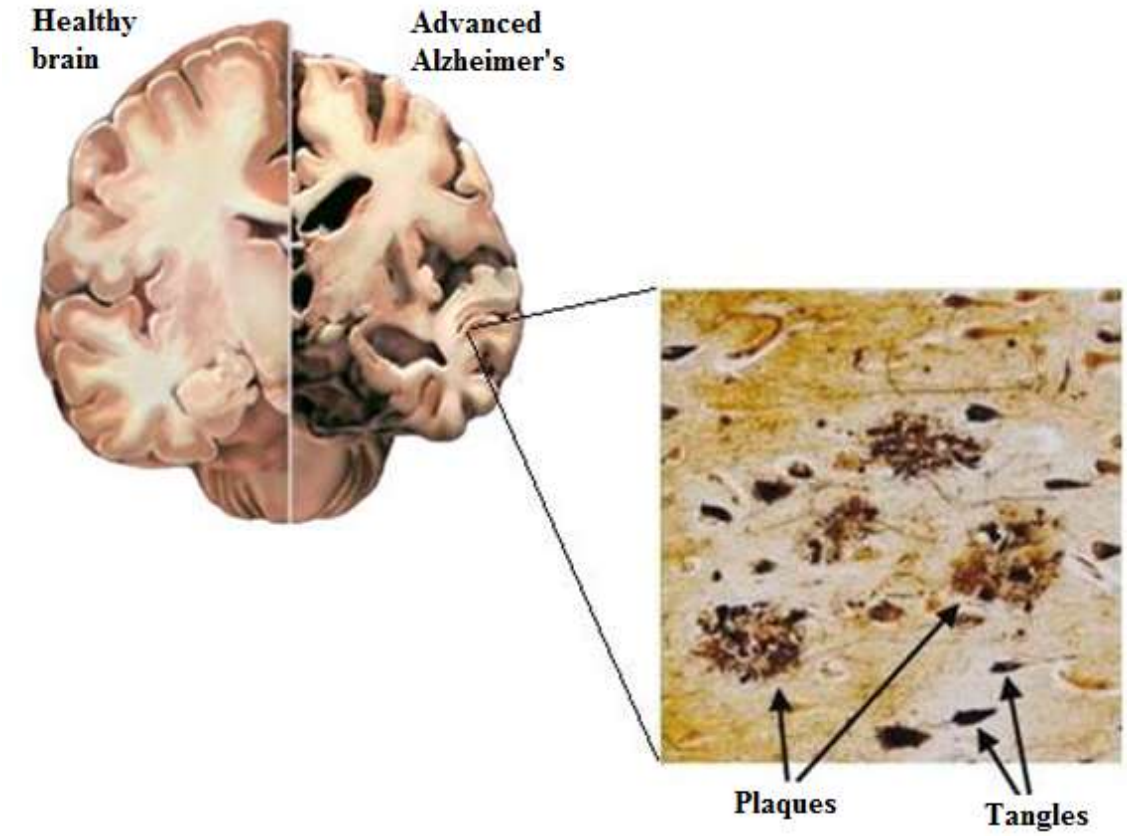

Figure 1.1: Neuropathology of AD. Histological section of cerebral cortex showing both extracellular amyloid plaques and intracellular neurofibrillary tangles (Blennow, K., *et al*., 2006).

In the 1960s, Terry *et al.* and Kidd found the main component of plaques to be amyloid fibrils (Kidd, M., 1964, Terry, R. D., *et al.*, 1964) and further work in 1984 and 1985 by two groups, Glenner and Wong and Masters *et al*., identified the aggregated proteinaceous component of these plaques to be the ~4 kDa amyloid beta (Aβ) peptide

(initially named A4) (Glenner, G. G. and Wong, C. W., 1984, Masters, C. L., *et al.*, 1985). Around the same time, NFTs were found to be composed of paired helical filaments (PHFs) containing a hyperphosphorylated form of the microtubule-associated protein, tau (Grundke-Iqbal, I., *et al.*, 1986). Further work in the 1980s and 1990s deduced more molecular mechanisms behind AD, culminating in the Amyloid Cascade Hypothesis in 1992 (see Section 1.3.). Since then research has strived to elucidate the exact aetiology of Alzheimer's disease.

1.2. The amyloid beta (Aβ) peptide

1.2.1. Evidence for Aβ as the toxic species in AD

Throughout the field of AD research there are currently two schools of thought as to what is the toxic species in the disease; the "tauists" who believe it is the intracellular protein tau and the "baptists" who propose it is the extracellular peptide, Aβ.

There are several lines of evidence that Aβ is the primary toxic species in AD aetiology. Firstly, Aβ is directly toxic to neuronal cell cultures and causes both neurodegeneration and impaired learning and memory in animal models (Nakamura, S., *et al.*, 2001, Zhang, Y., *et al.*, 2002). Secondly, several mutations of APP, the precursor protein from which Aβ is derived, and related APP-processing proteins lead to early-onset familial cases of AD (fAD) (Lazo, N. D., *et al.*, 2005). Such AD-causing mutations do not exist for the tau protein. Thirdly, Down's Syndrome sufferers present with AD by 50 years of age and this is thought to be due to the increased gene dosage of APP on chromosome 21, which is trisomic in the disease. Therefore, Aβ is likely the primary toxic agent in AD aetiology. It is likely that, although tau is not the primary toxic species in AD, it is still required for toxicity as a downstream mediator of toxicity, with several studies showing that without tau, Aβ toxicity it limited (Oddo, S., *et al.*, 2006, Rapoport, M., *et al.*, 2002, Roberson, E. D., *et al.*, 2007, Shipton, O. A., *et al.*, 2011).

In the literature there is an "Alternative Hypothesis" of Aβ's role in AD pathology that states that Aβ is either a bystander in AD or has a neuroprotective role in AD. Any proteinaceous deposits, be they amyloid plaques or neurofibrillary tangles, are

hypothesised to be simply downstream developments in the disease progression (Castellani, 2009). However, evidence for a neuroprotective role for Aβ is dependent on the peptide's concentration and aggregation state, with picomolar and possibly nanomolar concentrations being neuroprotective while higher, disease-related concentrations proving neurotoxic (Puzzo, D., *et al.*, 2008, Yankner, B. A., *et al.*, 1990). At the Aβ concentrations seen in AD pathology, Aβ is the primary toxic species in the disease.

1.2.2. Cleavage of the amyloid precursor protein (APP) generates the Aβ peptide.

The Aβ peptide is not a primary translation product but is instead derived from the endoproteolytic processing of a ubiquitous cell-surface protein; amyloid precursor protein (APP) (residues 672 to 714, Figure 1.2(C)) (Kang, J., *et al.*, 1987, Robakis, N. K., *et al.*, 1987). APP is a type I membrane spanning glycoprotein of approximately 770 amino acids with three main isoforms; 695, 751 and 770 and has an enriched expression in brain tissue. One fundamental event in AD aetiology is the cleavage of the APP protein to generate the Aβ peptide.

Neurons are unique in that the APP they produce can be cleaved by two possible pathways; the amyloidogenic pathway (Figure 1.2(A)) and the non-amyloidogenic pathway (Figure 1.2(B)) (Busciglio, J., *et al.*, 1993, Selkoe, D. J., 2001). Only the amyloidogenic pathway involving two cleavages by the β-and γ-secretases generates the Aβ peptide. The second cleavage by γ-secretase can occur anywhere between residues 711 and 715 of APP leading to several isoforms of Aβ (Figure 1.3). however, 90 % of cleavages generate Aβ(1-40) or Aβ(1-42) (Thinakaran, G. and Koo, E. H., 2008). In the healthy brain the cleavage to generate Aβ(1-40) is more common leading to an abundance of Aβ(1-40) over Aβ(1-42), but this balance can shift in AD pathology towards more Aβ(1-42). Aβ isolated from plaques is also found with post-translational modifications which make Aβ both more resistant to proteolysis leading to increasing Aβ levels (Atwood, C. S., *et al.*, 2002, Kuo, Y.-M., *et al.*, 1998), and, in many cases, more liable to aggregate (Fabian, H., *et al.*, 1994, He, W. and Barrow, C. J., 1999).

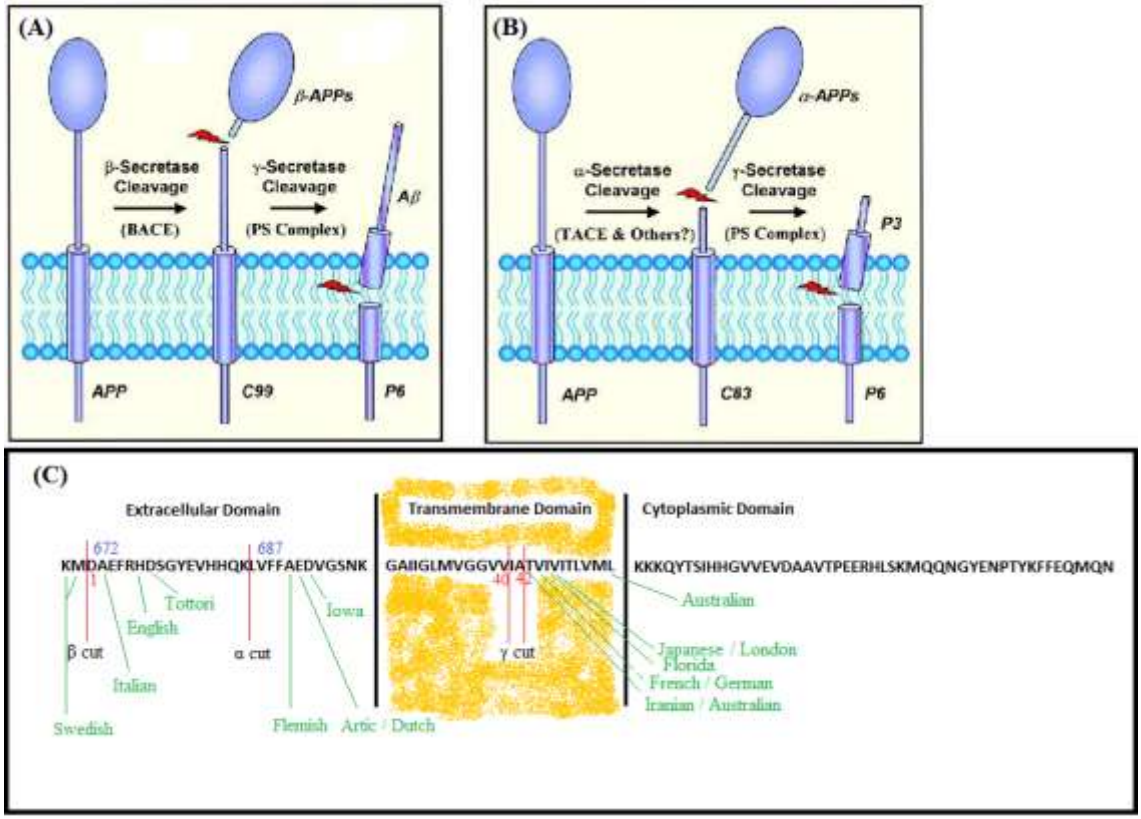

Figure 1.2: The two pathways of proteolytic degradation of the amyloid precursor protein (APP). **(A)** Amyloidogneic cleavage pathway. **(B)** Non-amyloidogenic cleavage pathway. **(C)** Cleavage relative to sequence. Residues 670 - 770 of APP are shown. Blue numbers refer to codons in the APP sequence, whereas red numbers refer to codons in the holoprotein, Aβ. The neuronal cell membrane is illustrated in yellow. Note some minor secretase cleavage sites are not shown. Shown in green are the 16 kindreds currently known for familial cases of AD. Adapted from Kosik *et al.*, 1999, Barrow 1999 and Lazo *et al.*, 2005 (Barrow, C. J., 1999, Kosik, K. S., 1999, Lazo, N. D., *et al.*, 2005).

Aβ(1-39)	**DAEFRHDSGYEVHHQ**	**KLVFFAEDVGSNKGAIIGLMVGGV**
Aβ(1-40)	**DAEFRHDSGYEVHHQ**	**KLVFFAEDVGSNKGAIIGLMVGGVV** *
Aβ(1-41)	**DAEFRHDSGYEVHHQ**	**KLVFFAEDVGSNKGAIIGLMVGGVVI**
Aβ(1-42)	**DAEFRHDSGYEVHHQ**	**KLVFFAEDVGSNKGAIIGLMVGGVVIA** *
Aβ(1-43)	**DAEFRHDSGYEVHHQ**	**KLVFFAEDVGSNKGAIIGLMVGGVVIAT**
	Hydrophilic	**Hydrophobic and amyloidogenic**

Figure 1.3: The Aβ sequence can vary between 39 to 43 residues. The amino acid sequence of Aβ showing the differentiation between the hydrophilic region of Aβ and hydrophobic region. The most common isoforms are Aβ(1-40) and Aβ(1-42) as illustrated with *.

1.2.3. Aβ(1-40) and Aβ(1-42) have different aggregation behaviours and toxicities.

Aβ(1-42) is more hydrophobic than Aβ(1-40) due to the addition of two non-polar residues, isoleucine and alanine, at the C-terminus (Kuo, Y.-M., *et al.*, 1998). This causes Aβ(1-42) to self-associate more than Aβ(1-40), leading to significantly faster fibrillisation rates than for Aβ(1-40) (Jarrett, J. T., *et al.*, 1993) and deposition as plaques earlier in AD pathology (Saido, T. C., *et al.*, 1996). Aβ(1-42) is more protease resistant and thus has extended longevity compared to Aβ(1-40). It forms larger intermediate species on the way to fibres, known as oligomers, than Aβ(1-40), with typical Aβ(1-42) species being pentameric and hexameric (paranuclei) and Aβ(1-40) oligomers exist as an equilibrium between monomers, dimers, trimers and tetramers (Bitan, G., *et al.*, 2003, Chen, Y. R. and Glabe, C. G., 2006). Aβ(1-42) also exclusively forms aggregated species most associated with Aβ neurotoxicity – ADDLs and amylospheroids (see Section 1.2.8.) – which are not formed by Aβ(1-40) (Hoshi, M., *et al.*, 2003, Lambert, M. P., *et al.*, 1998). In general Aβ(1-42) is more neurotoxic than Aβ(1-40) and thus Aβ(1-42) is known as the 'amyloidogenic species' of Aβ.

The estimated concentration of Aβ in healthy individuals is 0.2 ± 0.09 nM in the blood and between 0.6 nM and 8 nM in the CSF, predominately as the Aβ(1-40) isoform (Gravina, S. A., *et al.*, 1995, Mehta, P. D., *et al.*, 2000, Seubert, P., *et al.*, 1992, Vigo-Pelfrey, C., *et al.*, 1993). In the AD brain the concentration of total Aβ increases approximately 6-fold to 75 nM soluble Aβ and 5 μM insoluble Aβ (Kuo, Y. M., *et al.*, 1996, Mclean, C. A., *et al.*, 1999). The concentration of Aβ(1-42) increases 12-fold in overall brain tissue but decreases in blood plasma and CSF indicating increased sequestration in plaques (Kuo, Y. M., *et al.*, 1996, Pesaresi, M., *et al.*, 2006, Sjogren, M., *et al.*, 2002, Tapiola, T., *et al.*, 2009). These increases in Aβ concentrations in the AD brain relative to healthy brain are due to both greater production of Aβ coupled with impaired Aβ clearance (Lazo, N. D., *et al.*, 2005).

1.2.4. Aβ structure

The determination of the structure of full length Aβ has been complicated by the propensity of the peptide to form non-crystalline amyloid fibres preventing solution NMR studies and X-ray diffraction studies. However, solid-state NMR and site-directed spin labelling has enabled the structure to be determined (Roychaudhuri, R., *et al.*, 2009).

The structure of monomeric Aβ

The Aβ peptide is amphipathic with two distinct regions (Figure 1.3); the hydrophobic *C*-terminal (residues 16-42), which contains mainly non-polar residues, and the largely hydrophilic *N*-terminal (1-15). Within the *C*-terminus two regions control Aβ fibrillisation via the hydrophobic effect; residues 15 – 21 and residues 31 – 36 (Soto, C., 2004, Wetzel, R., 2006). In particular the Met35 residue has been shown to be important to Aβ neurotoxicity, Aβ paranuclei formation, and thus subsequent fibrillisation (Nakamura, M., *et al.*, 2007, Varadarajan, S., *et al.*, 2001, Varadarajan, S., *et al.*, 1999). This residue is also linked to oxidative stress induced by the peptide. The hydrophilic region of the peptide does not fibrillise in solution but instead forms the non-amyloidogenic random coil conformation. This region contains all the metal binding sites, modulates pH-dependence of the peptide's structure and controls the conformational state of the peptide (Barrow, C. and Zagorski, M., 1991).

In aqueous environments, Aβ has a random coil structure with some bend and turn character (Riek, R., *et al.*, 2001, Zhang, S., *et al.*, 2000). In a membrane/micelle environment Aβ forms a predominately alpha helical structure with two helices; Helix 1 from residues 15-24 and Helix 2 from residues 28-36 (Coles, M., *et al.*, 1998, Shao, H., *et al.*, 1999). In both environments Aβ can undergo a conformation change to a β-sheet form, which has a propensity to form amyloid fibres (Glenner, G. G., *et al.*, 1972, Halverson, K., *et al.*, 1990). The *N*-terminal residues 1-8 remains disordered throughout (Torok, M., *et al.*, 2002).

The structure of fibrillar Aβ

Site-specific spin-labelling and solid state NMR have shown that, within each β-sheet form of the Aβ monomer, residues 12-24 (β1) and 30-40 (β2) (Figure 1.4(A)) in Aβ(1-40) and residues 18-26 (β1) and 31-42 (β2) in Aβ(1-42) make up the β-sheets that are aligned perpendicular to the fibril axis in a β-strand-turn-β-strand motif, with the remaining residues being solvent exposed and random coil (Figure 1.4(A)) (Antzutkin, O. N., *et al.*, 2000, Nelson, R. and Eisenberg, D., 2006, Tycko, R., 2006, Whittemore, N. A., *et al.*, 2005). These two sheets are joined by a β-turn between residues 25-29, which is stabilised by a salt bridge between Asp23 and Lys28 in Aβ(1-42) (Figure 1.4(B)) (Luhrs, T., *et al.*, 2005, Nelson, R. and Eisenberg, D., 2006, Petkova, A. T., *et al.*, 2002). These β-strands self-assemble and are held together by intermolecular backbone-backbone hydrogen bonding in a cross-β structure (Figure 1.4(C)). Based on studies on other amyloid proteins this likely forms a steric zipper structure (Nelson, R. and Eisenberg, D., 2006, Sawaya, M. R., *et al.*, 2007). This self-assembly leads to oligomers and then rod-like protofibrils (aka fibrils), which have a beaded appearance due to their formation via elongation of spherical aggregates (Blackley, H. K. L., *et al.*, 1999, Hartley, D. M., *et al.*, 1999, Nybo, M., *et al.*, 1999, Walsh, D. M., *et al.*, 1999). Fibrils have been measured as 150 nm long with a 2.5 - 3.9 nm diameter for Aβ(1-40) and a 4 - 6 nm diameter for Aβ(1-42) (Kirschner, D. A., *et al.*, 1986, Nelson, R. and Eisenberg, D., 2006). Five or six parallel fibrils around a hollow core make up a mature fibre (Burkoth, T. S., *et al.*, 2000, Inouye, H., *et al.*, 1993, Miyakawa, T., *et al.*, 1986, Terry, R. D., *et al.*, 1964). Atomic force microscopy (AFM) and transmission electron microscopy (TEM) show fibres are > 1 μM in length, 10-15 nm in diameter, un-branched, twisted and have a regular periodicity in thickness of ~ 150 nm (Burkoth, T. S., *et al.*, 2000, Roher, A. E., *et al.*, 1996, Terry, R. D., *et al.*, 1964). They are non-crystalline and insoluble with the direction of the polypeptide backbone perpendicular to the fibril axis. They exhibit birefringence with Congo Red dye and bind the dyes thioflavins S and T (Atwood, C. S., *et al.*, 2002, Sipe, J. D., 2000, Soto, C., 2004).

Fibres aggregate together to form amyloid plaques. Amyloid fibres, across all amyloid diseases, share similar structural and spectroscopic characteristics. This hierarchical structure of Aβ fibres is built up linearly as shown in Figure 1.5 with an

initial conformational change in the Aβ peptide from its native form (see above) to a β-sheet form (Halverson, K., *et al.*, 1990).

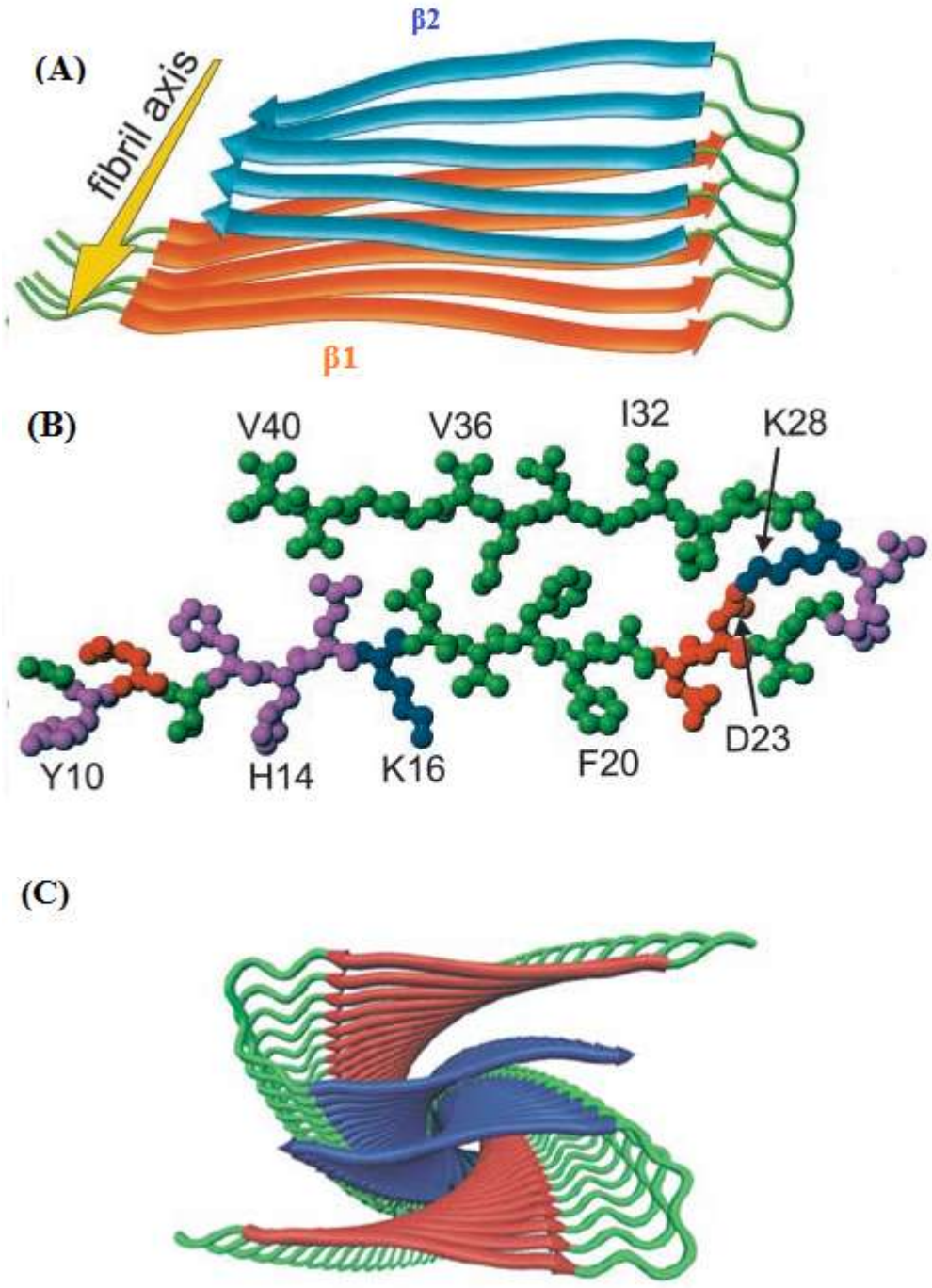

Figure 1.4: Models of the Aβ(1-40) protofilament. (A) Residues1-8 are disordered and not shown. Residues 9-40 form two β-sheets – 12-24 (orange) and 30-40 (blue) joined by a turn. The yellow arrow is the direction of the fibril long axis. **(B)** Residues 9-40 coloured based on residue side chain; hydrophobic (green), polar (magenta), negative (red), positive (blue). K28 (Lys28) and D23 (Asp23) form a stabilising salt bridge at the bend (Petkova, A. T., *et al.*, 2002). **(C)** The β-strand is made up of parallel β-sheets in a cross-β arrangement (Tycko, R., 2006).

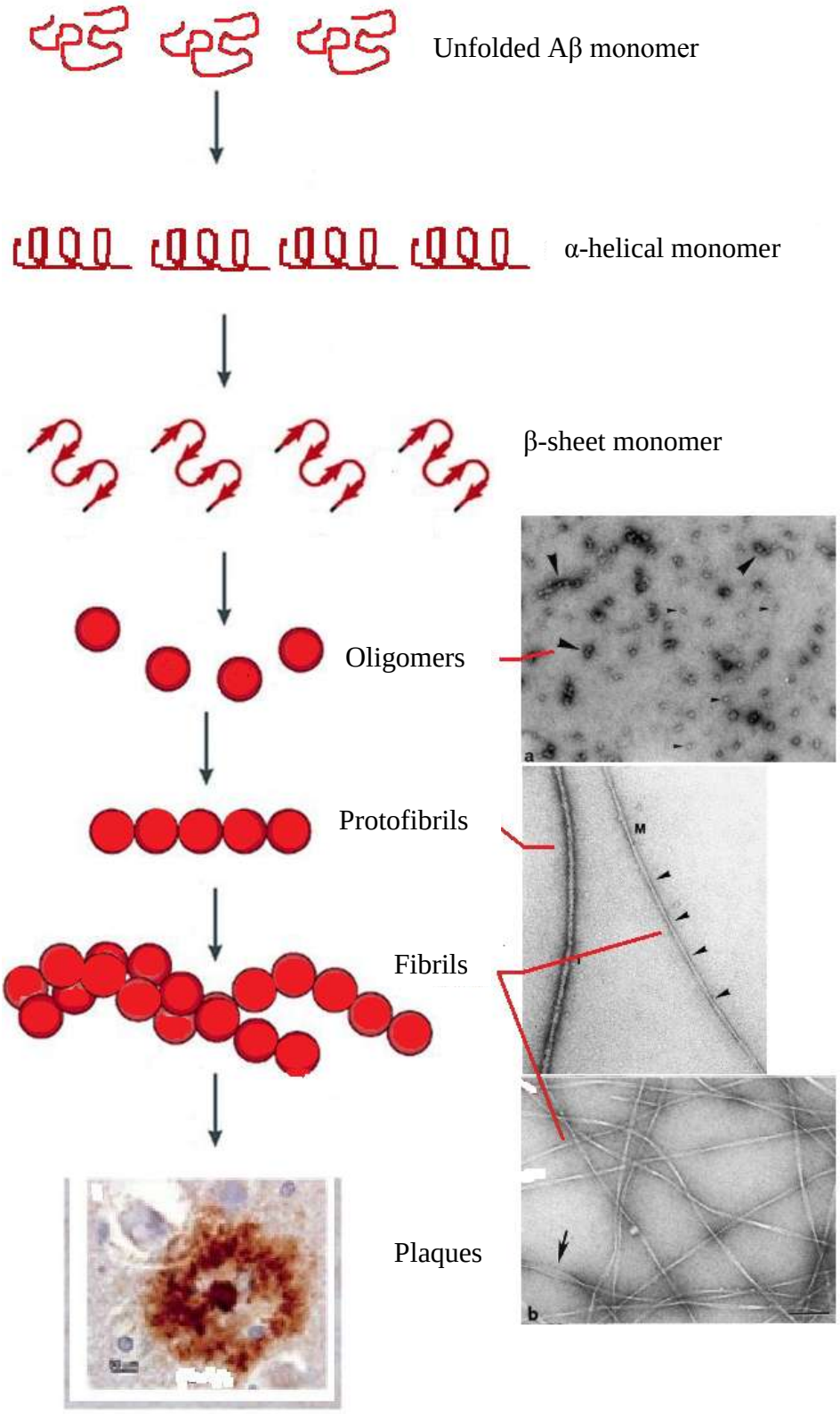

Figure 1.5: Amyloidogenic pathway of Aβ aggregation. The electromicrographs are taken from Seilheimer *et al.*, 1997 (Seilheimer, B., *et* al., 1997).

1.2.5. The kinetic models of Aβ fibrillisation

The fibrillisation of Aβ is a 'nucleation-dependent-polymerisation' (NDP) event (Figure 1.6(A)) (Jarrett, J. T., *et al.*, 1993, Wetzel, R., 2006). It involves three main stages; a nucleation or stationary lag phase, an elongation phase and a final plateau phase. These stages can be represented by a fibril growth curve (Figure 1.6(B)).

Dynamic light scattering (DLS) studies at acidic pH allow slowed-down kinetics to be studied. These studies have shown spherocylinder micelles of Aβ to forming, which are seeds for equilibrium, in a constant pre-equilibrium with both monomers and further aggregating species. At a critical concentration these seeds form fibre nuclei (nucleation) (Lomakin, A., *et al.*, 1997, Wetzel, R., 2006, Yong, W., *et al.*, 2002). Nucleation is slow because it is energetically unfavourable with entropy outweighing enthalpic gains due to the need to bury hydrophobic residues (Bieschke, J., *et al.*, 2006). This generates a lag phase in fibril concentration growth, although this lag phase can be removed if the concentration of Aβ is high and the Aβ culture is seeded with a nucleating species (Jarrett, J. T. and Lansbury, P. T., 1993).

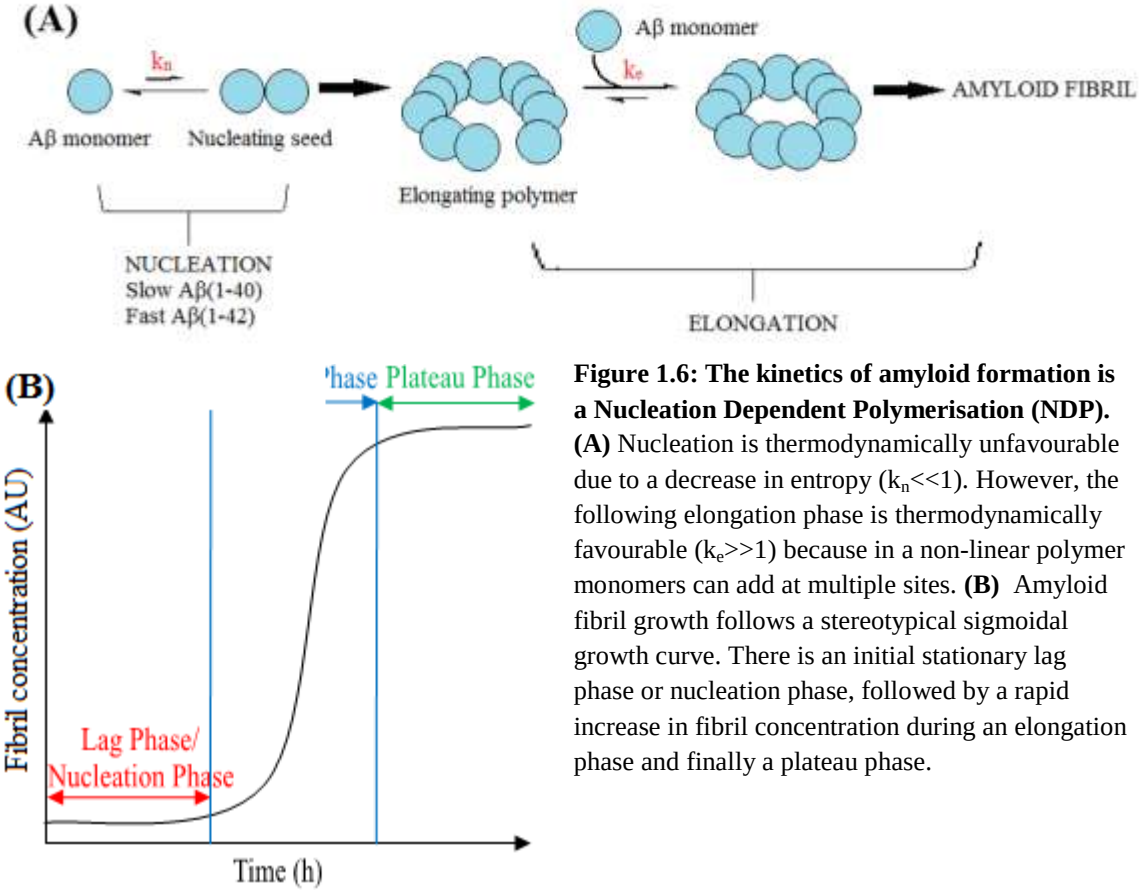

Figure 1.6: The kinetics of amyloid formation is a Nucleation Dependent Polymerisation (NDP). **(A)** Nucleation is thermodynamically unfavourable due to a decrease in entropy (k_n<<1). However, the following elongation phase is thermodynamically favourable (k_e>>1) because in a non-linear polymer monomers can add at multiple sites. **(B)** Amyloid fibril growth follows a stereotypical sigmoidal growth curve. There is an initial stationary lag phase or nucleation phase, followed by a rapid increase in fibril concentration during an elongation phase and finally a plateau phase.

Once a critical concentration of nucleating seed species has formed elongation begins (Jarrett, J. T. and Lansbury, P. T., 1993). This leads to a rapid increase in fibril concentration (Walsh, D. M., *et al.*, 1999). Elongation involves both monomers adding to the end of fibrils and fibrils themselves self-associating. In addition, fragmentation of fibres generates new fibril ends for monomer addition (Harper, J. D., *et al.*, 1999, Nichols, M. R., *et al.*, 2002).

Finally a plateau phase follows where maximal fibril growth has occurred, monomer concentrations have fallen below the critical concentration and the fibres are in a thermodynamic equilibrium with the critical concentration of nucleating seeds.

1.2.6. Factors that influence Aβ fibrillisation

Thioflavin-T (Th-T) studies on *in vitro* Aβ(1-40) have shown that fibrillisation rates are dependent on several factors; temperature, pH, Aβ length and sequence, ionic strength, solvent hydrophobicity, Met35 oxidation, metal ions, seed concentration and Aβ concentration, which it follows with first-order kinetics (Khandogin, J. and Brooks, C. L., 3rd, 2007, Mclaurin, J., *et al.*, 2000, Roychaudhuri, R., *et al.*, 2009, Sarell, C. J., *et al.*, 2010, Stine, W. B., Jr., *et al.*, 2003). It should be noted when consulting literature studies that the *in vivo* environment experienced by Aβ is different to these *in vitro* environments because the former is influenced by molecular crowding; interactions with numerous metals, lipids, such as cholesterol and gangliosides, and proteins, such as Apolipoprotein E and laminin (Bronfman, F. C., *et al.*, 1996, Hayashi, H., *et al.*, 2004, Mclaurin, J., *et al.*, 2000, Van Den Berg, B., *et al.*, 2000, Yanagisawa, K. and Matsuzaki, K., 2002). This may explain why the critical concentration of Aβ for fibrillisation *in vivo* is so much lower (pM) than *in vitro* (nM) (Selkoe, D. J., 1994). However, studies on *ex situ* plaques combined with radio-iodinated Aβ have shown that the same first-order kinetics occurs *in vivo* (Esler, W. P., *et al.*, 1996) and *in vitro* Aβ fibres have been found to have the same morphology, tinctorial, immunological and spectroscopic characteristics as fibres extracted from amyloid plaques, thus validating *in vitro* studies (Giaccone, G., *et al.*, 2005, Soto, C., 2004).

1.2.7. Off-pathway Aβ aggregation

As well as the classical polymerisation described above, several pathways, and hence several resulting structures, have been found for Aβ assembly. These pathways are distinguished as "on-pathway" if they result in fibres and "off-pathway" if they result in other structures (Figure 1.7). The folding pathways taken by Aβ depend on its concentration. Below 100 μM Aβ amyloid fibrils form, while above 100 μM Aβ micelles form (30-50 monomers) as Aβ begins to act as a surfactant (Westlind-Danielsson, A. and Arnerup, G., 2001). At very high Aβ concentrations (300 – 600 μM) Aβ(1-40) only has been shown to spontaneously form highly stable, 20 – 200 μm diameter spheres from fibres (Hoshi, M., *et al.*, 2003).

Several "on-pathway" structures are reasonably stable and have been isolated from fibrillising Aβ cultures. They tend to be composed of either dimer and trimer or hexameric units of Aβ and include hexameric, 18-mer and 24-mer oligomers and the dodecameric species the Aβ*56 and amyloid derived diffusible ligands (ADDLs) (Bernstein, S. L., *et al.*, 2009, Bitan, G., *et al.*, 2003, Huang, T. H. J., *et al.*, 2000, Roychaudhuri, R., *et al.*, 2009). These last two structures are discussed more in Section 1.2.8. as potentially toxic species of Aβ.

Off-pathway species include pore-like structures called annuli (Lashuel, H. A., *et al.*, 2003), and globular structures such as globulomers (dodecamer), the "Aβ oligomer" (octadecamer), amylospheroids (ASPDs) and amyloid balls, of diameters 10 – 15 nm and 20 – 200 nm respectively (Hoshi, M., *et al.*, 2003, Murray, M. M., *et al.*, 2009, Yu, L., *et al.*, 2009). Several of these, especially the larger globular species, have only been detected *in vitro*, although they have been shown to be neurotoxic if their diameter exceeds 10 nm (Gellermann, G. P., *et al.*, 2008, Kusumoto, Y., *et al.*, 1998, Roychaudhuri, R., *et al.*, 2009). One example of an off-pathway Aβ species, which has been detected *in situ* within brain tissue, is the unstructured amorphous aggregate. These aggregates are non-toxic to neuronal and glial cell cultures and this has led to the hypothesis that the neurotoxicity of Aβ requires an on-pathway fibril structure (Howlett, D. R., *et al.*, 1995, Lorenzo, A. and Yankner, B. A., 1994).

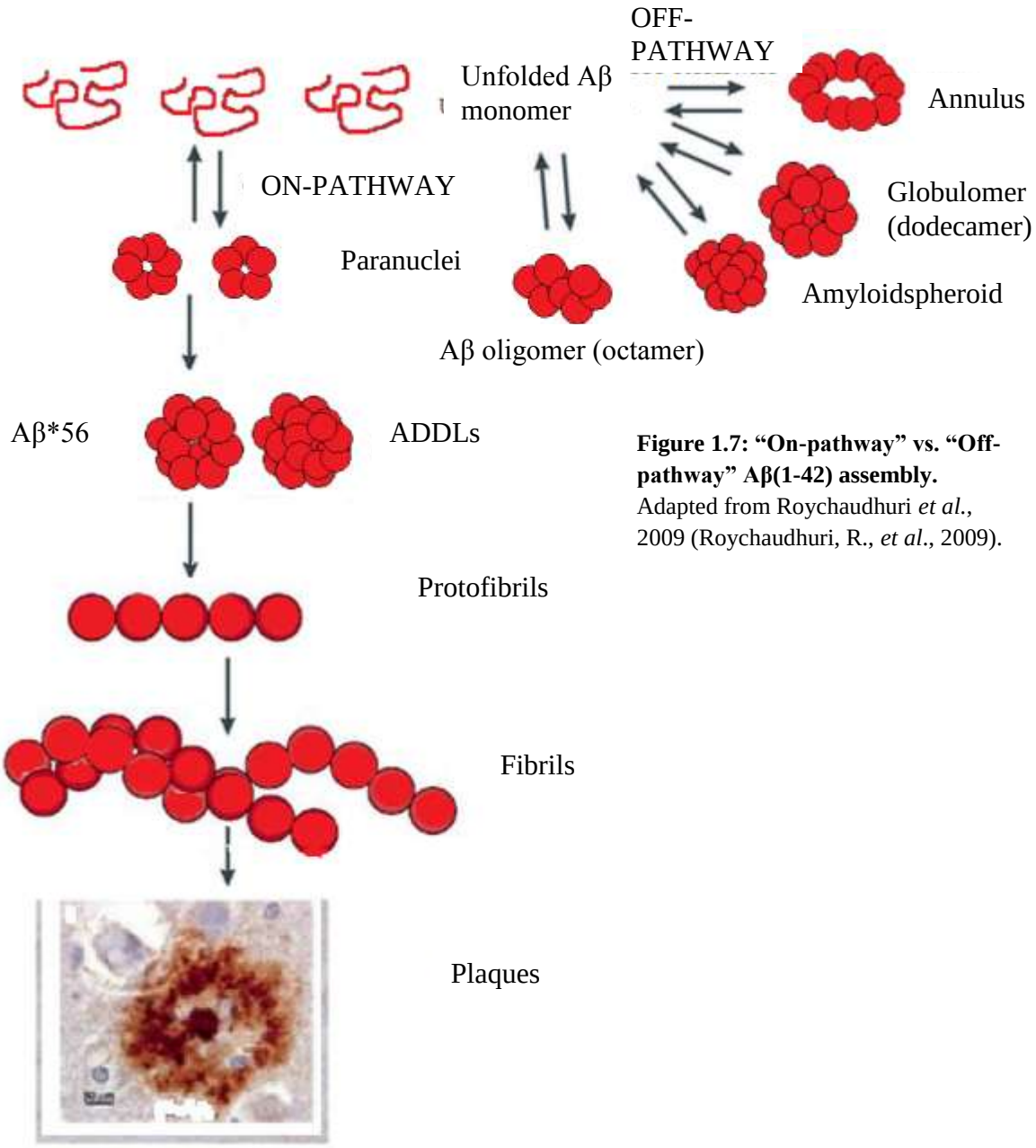

Figure 1.7: "On-pathway" vs. "Off-pathway" Aβ(1-42) assembly.
Adapted from Roychaudhuri *et al.*, 2009 (Roychaudhuri, R., *et al.*, 2009).

1.2.8. Toxic species of Aβ

Amyloid plaques are associated with dystrophic, dysmorphic and dead neurons in the AD brain (Benzing, W. C., *et al.*, 1993, Spires, T. L. and Hyman, B. T., 2004). Therefore, initially it was thought that amyloid plaques, and the amyloid fibres they contained, were the toxic species in the disease (Lorenzo, A., *et al.*, 1993, Pike, C. J., *et al.*, 1991, Weldon, D. T., *et al.*, 1998). However, subsequent studies, which inhibited plaque formation did not prevent the neurotoxic properties of the peptide (Bieschke, J.,

et al., 2008, Forloni, G., *et al.*, 1997, Lambert, M. P., *et al.*, 1998). In addition, some studies found a lack of correlation between the prevalence of AD pathology and the concentration of amyloid plaques in AD patients and the occurrence of memory deficits and synaptic dysfunction in mice before amyloid deposition (Aizenstein, H. J., *et al.*, 2008, Giannakopoulos, P., *et al.*, 2003, Katzman, R., *et al.*, 1988, Mucke, L., *et al.*, 2000). Instead, plaque formation is now thought of as a neuroprotective mechanism which traps smaller toxic aggregates of Aβ, but unfortunately inadvertently causes further neurodegeneration through obstruction of axonal transport, activating microglial clearance mechanisms and recruiting cellular components (Frautschy, S. A., *et al.*, 1991, Kowall, N. W., *et al.*, 1991, Meyer-Luehmann, M., *et al.*, 2008, Zhang, Y., *et al.*, 2002).

Current dogma now states that it is the smaller pre-fibrillar aggregates of Aβ which exhibit cellular toxicity. Freshly prepared Aβ kills fibroblasts (Klein, W. L., *et al.*, 2004) and leads to the production of highly toxic substrates, such as hydrogen peroxide (H_2O_2). This production reduces as Aβ peptide cultures age and presumably form larger aggregates (Figure 1.8) (Lue, L.-F., *et al.*, 1999, Mclean, C. A., *et al.*, 1999, Tabaton, M., *et al.*, 1994). In addition, the concentrations of soluble forms of Aβ correlate better with AD progression (Simmons, L. K., *et al.*, 1994).

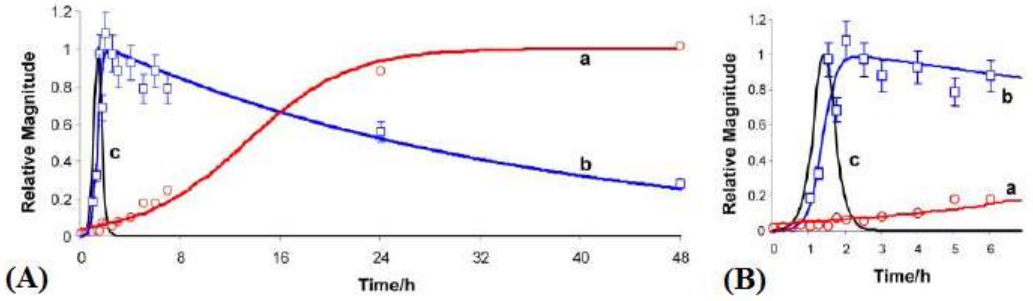

Figure 1.8: Hydrogen peroxide production by Aβ(1-40) early in aggregation profile. (A) Curve **a** shows the aggregation profile of Aβ(1-40) as measured with Th-T fluorescence. Curve **b** shows hydrogen peroxide production as predicted by an EPR spectrum for DMPH-OH. Curve **c** shows the simulated hydrogen peroxide production. **(B)** This is an enlargement of the early part of Figure 1.14A (Klein, W. L., *et al.*, 2004).

Monomeric forms of Aβ are not neurotoxic (Chromy, B. A., *et al.*, 2003, Ferreira, S. T., *et al.*, 2007, Kagan, B., 2005, Kayed, R., *et al.*, 2003), therefore toxic species of Aβ must be between monomeric and fibrillar size. The actual size of these neurotoxic Aβ species is yet to be elucidated, although there is literature evidence that the following Aβ aggregates are toxic species; oligomers (pentameric and hexameric) (Ferreira, S. T.,

et al., 2007, Gong, Y., *et al.*, 2003, Lambert, M. P., *et al.*, 1998, Oda, T., *et al.*, 1995), Aβ-derived diffusiable ligands (ADDLs) also known as Aβ*56 (dodecameric) (Klein, W. L., *et al.*, 2004, Lacor, P. N., *et al.*, 2007, Lacor, P. N., *et al.*, 2003, Lambert, M. P., *et al.*, 1998, Westerman, M. A., *et al.*, 2002); dimers and trimers (Crouch, P. J., *et al.*, 2005, Shankar, G. M., *et al.*, 2007), amylospheroids (ASPDs), the only non-β-sheet form of toxic Aβ recorded to date (Hoshi, M., *et al.*, 2003), and finally protofibrils (Haass, C. and Steiner, H., 2001, Hartley, D. M., *et al.*, 1999, Nilsberth, C., *et al.*, 2001). Detection and correlation of Aβ oligomeric forms with toxicity is complicated by the fact oligomers are often transient intermediate species and hence oligomeric preparations of Aβ are unlikely to be homogenous. Therefore, smaller subsets of oligomers may actually be the most toxic form of Aβ. However, it is most likely the case that both oligomers and protofibrils are the neurotoxic Aβ species (Bhatia, R., *et al.*, 2000, Hoshi, M., *et al.*, 2003, Kayed, R., *et al.*, 2003).

1.3. The Amyloid Cascade Hypothesis

In 1992 Hardy and Selkoe devised the Amyloid Cascade Hypothesis, which described how the intial misfolding of the Aβ peptide and its subsequent fibrillisation induced neurotoxicity via a cascasde of molecular events, including a loss of ion homeostasis, for important ions, such as the signalling ion Ca^{2+} and redox-active metal ions, and oxidative stress, eventually leading to neuronal apoptosis (Figure 1.9) (Hardy, J. and Selkoe, D. J., 2002, Hardy, J. A. and Higgins, G. A., 1992).

Aβ exerts this toxicity by binding plasma membrane receptors and disrupting intracellular signalling pathways, damaging cellular membranes and thus altering neuronal conductance and initiating inflammation and reactive oxygen species (ROS) production (Balleza-Tapia, H. and Pena, F., 2009, Snyder, E. M., *et al.*, 2005, Velazquez, P., *et al.*, 1997, Yankner, B. A., 1996). Its oxidation of lipids may also prevent tau dephosphorylation thus linking the two proteinergic agents of AD (Mattson, M. P., *et al.*, 1997). In conclusion, the Aβ peptide mediates neurodegeneration via numerous different mechanisms complicating attempts to develop therapeutics against AD.

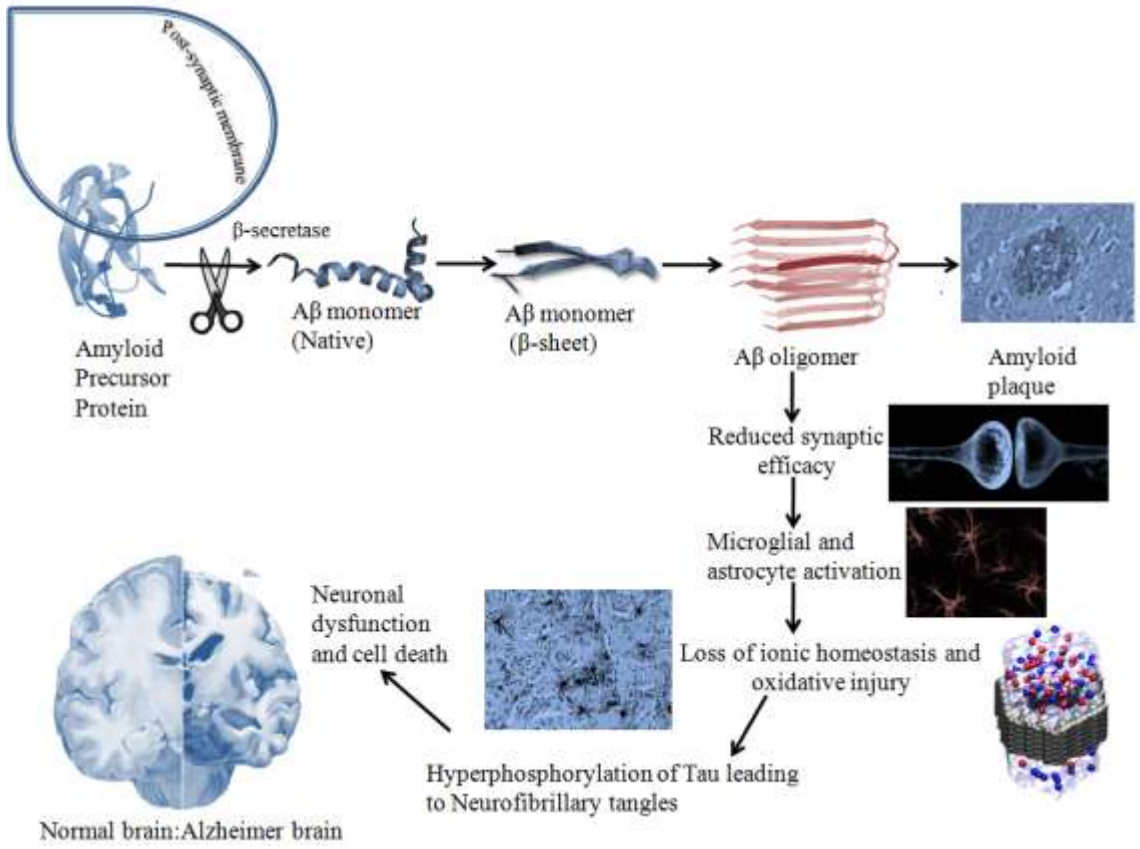

Figure 1.9: The Amyloid Cascade Hypothesis. The Amyloid Cascade Hypothesis states that it is the misfolding of Aβ and subsequent fibrillisation to oligomers which triggers neurodysfunction and neurodegeneration seen in AD pathology. Downstream targets include synaptic dysfunction, loss of ion homeostasis and tau hyperphosphorylation and subsequent aggregation to neurofibrillary tangles (NFTs) (Hardy, J., Selkoe, D. J., 2002).

1.4. Current therapies

The therapeutics for AD are currently lagging behind those for comparably common diseases such as cancer. It is still nearly impossible to detect pre-clinically with diagnosis relying purely on neurological tests that do not distinguish between different types of dementia and no confirmation of the disease until post-mortem. Current therapeutics, such as acetylcholinesterase inhibitors, are symptomatic only and often cause significant side effects (Nordberg, A., 2003). Therapeutics cannot simply reduce the concentrations of Aβ because the peptide is hypothesised to have cellular functions including as an initiator of neurite sprouting after neuronal lesions (Geddes, J. W., *et al.*, 1986), as an antioxidant (see Section 1.5.3.), as an apolipoprotein capable of controlling cholesterol homeostasis (Koudinov, A. R., *et al.*, 2001) and as a modulator of neurotransmitter receptors and neuronal excitation, and thus controlling memory

forming processes such as long-term potentiation (LTP) (Wu, J., *et al.*, 1995a, b). Indeed targeting Aβ itself with therapies, such as Aβ vaccination, can lead to detrimental side effects such as inflammatory responses (Orgogozo, J. M., *et al.*, 2003, Senior, K., 2002).

Therefore, ideally therapeutics should target the triggers of Aβ misfolding, of which there are several hypothesised in the literature. These include elevated levels of Aβ causing a concentration-dependent seeding effect (Hortschansky, P., *et al.*, 2005, Lomakin, A., *et al.*, 1996), changes in physiological condtions such as pH and ionic strength closer to the conditions e.g. pI (PH 5.3) of Aβ where fibrillisation is most rapid (Sarell, C. J., *et al.*, 2010, Snyder, S. W., *et al.*, 1994), metal ions binding Aβ and altering fibril growth rates (Sarell, C. J., *et al.*, 2010) and chemical modifications of Aβ, such as oxidation of the tyrosine, methionine and histidine residues in Aβ (see Section 1.5.3.), altering the net charge and hydrophobicity of the peptide and thus its fibrillisation rates.

Interestingly, some of the most recent successful clinical trials have involved antioxidants, such as Vitamin E and α-lipoic acid (Grundman, M., 2000, Hager, K., *et al.*, 2007, Sano, M., *et al.*, 1997), and metal chelators,such as Desferrioxamine and Clioquinol (Crapper-Mclachlan, D. R. C., *et al.*, 1991, Liu, G., *et al.*, 2010, Ritchie, C. W., *et al.*, 2003). This may indicate that metal-catalysed oxidation (MCO) may be very important in AD pathology.

1.5. Oxidative Stress

1.5.1. Oxidative stress increases with age.

Oxidative stress relates to tissue damage caused by reactive oxygen species (ROS) when cellular antioxidant systems become overwhelmed. ROS include both radicals, e.g.superoxide $O_2^{\cdot-}$, hydroxyl radicals $HO^{\cdot}$and peroxy radicals ROO^{-}, and non-radicals e.g. hydrogen peroxide H_2O_2, peroxynitritie ($ONOO^{-}$) and lipid-derived aldehydes and ketones (Berlett, B. S. and Stadtman, E. R., 1997, Butterfield, D. A. and Stadtman, E. R., 1997, Kowalik-Jankowska, T., *et al.*, 2004, Wong, S. F., *et al.*, 1981). These ROS are derived from several sources, including lipid peroxidation, ionising radiation and the

terminal respiratory electron chain of mitochondria (Halliwell, B., 1992, Olanow, C. W., 1993). However, the most frequent mechanism is metal-catalysed oxidation (MCO) and this generates the most reactive ROS, the hydroxyl radical (Stadtman, E. R. and Berlett, B. S., 1997).

A consequence of living in an aerobic environment is that oxidation products accumulate over time, causing cumulative cellular damage, and these are the cause of several age-related disorders (Butterfield, D. A. and Stadtman, E. R., 1997, Zhu, X. W., *et al.*, 2005). Indeed studies have shown that the greater the level of oxygen that an animal is exposed to, the shorter its lifespan (Halliwell, B. and Gutteridge, J. M. C., 1985) and Stadtman *et al.* reported that protein oxidation, as indicated by measuring the protein carbonyl content of tissue, increases with age (Figure 1.10) (Stadtman, E. R. and Berlett, B. S., 1997). Several studies have shown oxidative stress and aging to be intricately linked (Agarwal, S. and Sohal, R. S., 1993, Edamatsu, R., *et al.*, 1995, Forster, M. J., *et al.*, 1996, Mecocci, P., *et al.*, 1993, Smith, C. D., *et al.*, 1991, Sohal, R. S., *et al.*, 1995, Starke-Reed, P. E. and Oliver, C. N., 1989, Takahashi, R. and Goto, S., 1990, Youngman, L. D., *et al.*, 1992). Levels of antioxidants which scavenge ROS, such as vitamins A, C and E, bilirubin, superoxide dismutase and glutathione, tend to decrease with age (Halliwell, B., 1992, Perkins, A. J., *et al.*, 1999, Stadtman, E. R. and Berlett, B. S., 1997). Thus it is an alteration in the balance between oxidant production and antioxidants that causes increasing oxidative stress with increasing age.

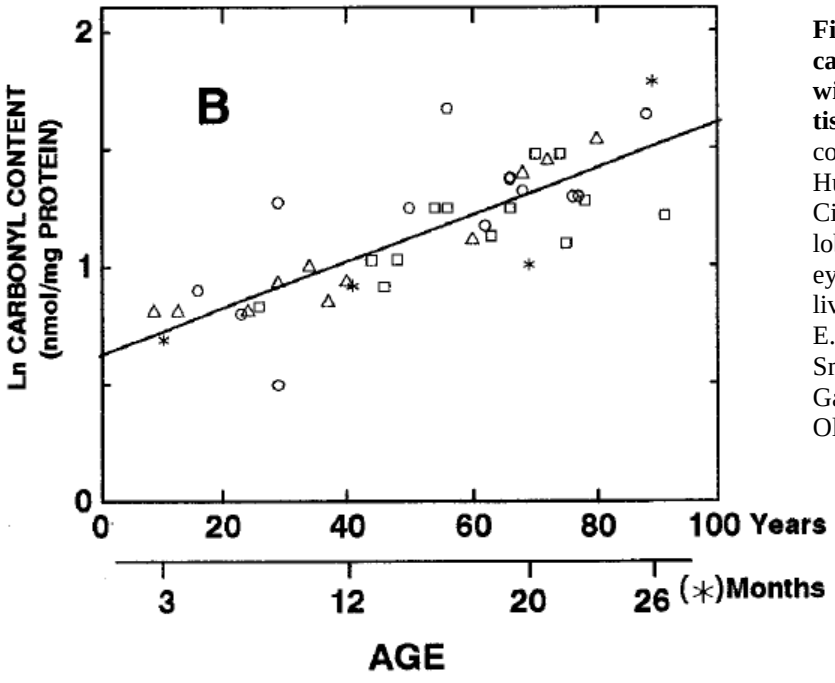

Figure 1.10: Increasing carbonyl content of proteins with age across numerous tissue types. Carbonyl content of: Triangles – Human dermal fibroblasts. Circles – Human occipital lobe tissue. Squares – Human eye lens cortex. Stars – Rat liver hepatocytes (Stadtman, E. R., and Berlett, B. S., 1997, Smith, M. A., *et al.*, 1994, Garland, D., *et al.*, 1988, Oliver, C. N., 1987).

1.5.2. Oxidative stress in the central nervous system (CNS) and AD

Oxidative stress has been shown to cause synaptic dysfunction and apoptosis in neural cultures (Greenlund, L. J. S., *et al.*, 1995, Kamsler, A. and Segal, M., 2004), although low levels of ROS are required for normal neuronal function such as LTP (Serrano, F. and Klann, E., 2004). The central nervous system (CNS) is particularly vulnerable to oxidative stress due to several properties. It has a high oxygen consumption rate i.e. 20 % of body's consumption by only 2 % of body weight, due to most energy being derived from oxidative metabolism (Coyle, J. T. and Puttfarcken, P., 1993, Jiang, D. L., *et al.*, 2010). It has a high concentration of peroxidizable polyunsaturated fatty acid side chains present in membranes (Halliwell, B., 1992). With the exception of the liver, the brain has the highest concentration of redox active metals in the body (Popescu, B. F. G. and Nichol, H., 2011, Youdim, M. B. H., 1988), which coupled with low concentrations of iron-binding proteins, such as transferrin, in the cerebrospoinal fluid (CSF) leads to high concentrations of free iron (Gruener, N., *et al.*, 1991). Compared to other tissues, the brain tissue has low concentrations of antioxidant enzymes, such as catalase, superoxide dismutase and glutathione peroxidase(Coyle, J. T. and Puttfarcken, P., 1993, Halliwell, B. and Gutteridge, J. M. C., 1985), and high concentrations of reductants such as ascorbic acid (500 μM), 10-fold the level found in the blood and further concentrated in neural tissue to approximately 10 mM in neurons and 1 mM in glia (Halliwell, B., 1992, Spector, R. and Eels, J., 1984). Finally the low mitotic cellular renewal in brain tissue means oxidative damage is not compensated for with regeneration of neurons (Lee, H.-G., *et al.*, 2007).

A recurrent finding from analysis of the post-mortem AD brain is evidence of severe oxidative stress. This was first reported by Martins *et al.* in 1986 with the finding of increased activity of the hexose monophosphate pathway enzymes indicative of increased oxidative stress (Martins, R. N., *et al.*, 1986). Oxidative stress starts early in AD pathology, preceding both Aβ fibrillisation and NFT formation, and continues throughout the disease progression, with neurons associated with NFTs and amyloid plaques found to contain oxidised nucleic acids (DNA and RNA), oxidised proteins and oxidised lipids (Castegna, A., *et al.*, 2002, Ding, Q., *et al.*, 2005, Nunomura, A., *et al.*, 1999, Sayre, L. M., *et al.*, 1997, Smith, C. D., *et al.*, 1991, Subbarao, K. V., *et al.*, 1990, Sun, A. Y., *et al.*, 2001). Markers of oxidative stress are found in regions of the brain

associated with neurodegeneration such as the inferior parietal cortex and hippocampus, frontal pole, inferior parietal lobe and superior middle temporal gyrus but not the cerebellum (Figure 1.11) (Aksenov, M. Y., *et al.*, 2001, Hensley, K., *et al.*, 1995, Hensley, K., *et al.*, 1998, Korolainen, M., A., *et al.*, 2006).

Further findings indicative of a role of oxidative stress in AD include elevated concentrations of redox active transition metals in the AD brain, especially within plaques (Markesbery, W. R., 1997, Smith, M. A., *et al.*, 1997a), a lowered pH (6.6) in the AD brain, which promotes metal redox reactions required for MCO (Yates, C. M., *et al.*, 1990), the concentration in plaques of numerous factors linked to oxidative stress e.g. Cu/Zn-SOD, Mn-SOD, catalase and AGE-modified tau (Grundke-Iqbal, I., *et al.*, 1990, Smith, M. A., *et al.*, 1994a, Smith, M. A., *et al.*, 1997b, Smith, M. A., *et al.*, 1994b, Smith, M. A., *et al.*, 1994c), elevated concentrations of ROS in the AD brain (Atwood, C. S., *et al.*, 2000, Giulian, D., *et al.*, 1998) and upregulation of some antioxidant enzymes and metal-binding proteins in the AD brain in regions associated with AD pathology (Kish, S., *et al.*, 1986, Lovell, M. A., *et al.*, 1995, Martins, R. N., *et al.*, 1986, Premkumar, D. R. D., *et al.*, 1995, Smith, M. A., *et al.*, 1994a).

Both the tau protein and the Aβ peptide are found oxidised in AD pathology. Tau is found oxidised at Cys322 and this leads to protein dimerisation and polymerisation to insoluble filaments (Schweers, O., *et al.*, 1995, Troncoso, J. C., *et al.*, 1993). Aβ is also found oxidised (Boros, S., *et al.*, 2004) and itself is predicted to have many roles in the oxidative stress of AD (see Section 1.5.3.).

-

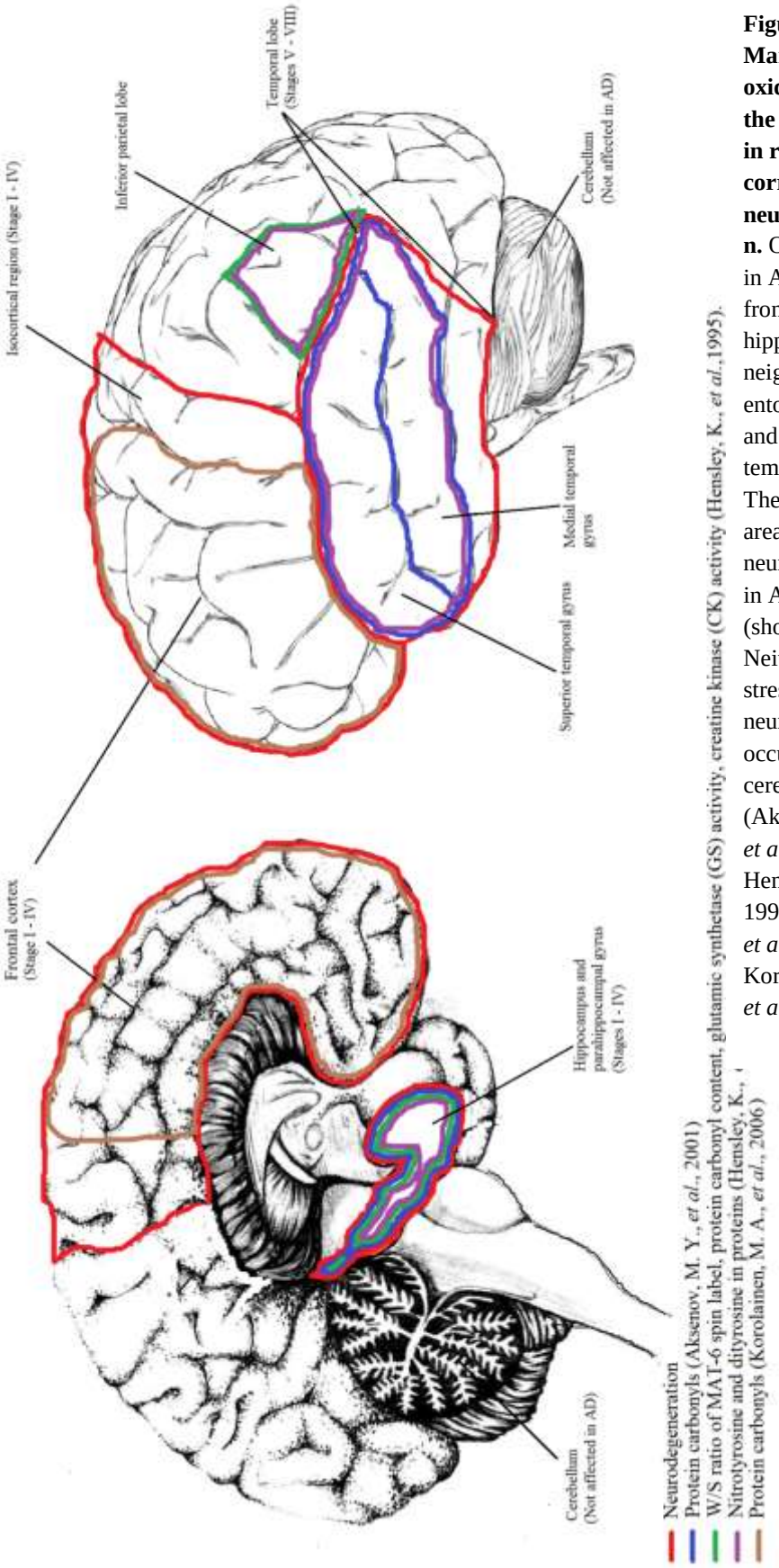

Figure 1.11: Markers of oxidative stress in the AD brain are in regions correlated with neurodegeneration. Oxidative stress in AD occurs in the frontal cortex, hippocampus, and neighbouring entorhinal cortex, and areas of the temporal lobe. These are also areas of neurodegeneration in AD pathology (shown in red). Neither oxidative stress or neurodegeneration occurs in the cerebellum (Aksenov, M. Y., *et al.*, 2001, Hensley, K., *et al.*, 1995, Hensley, K., *et al.*, 1998, Korolainen, M., A., *et al.*, 2006).

1.5.3. The role of Aβ in AD oxidative stress

Aβ as a pro-oxidant in AD pathology

The Aβ peptide may not just be toxic due to its aggregation state (see Section 1.2.8). It may also mediate toxicity by being a pro-oxidant in AD pathology. Several studies have correlated Aβ neurotoxicity with levels of cellular oxidants e.g. neurons depleted of antioxidants are more susceptible to Aβ-mediated toxicity (White, A. R., *et al.*, 1999). In addition, Aβ neurotoxicity can be inhibited by radical scavengers and antioxidants such as catalase, vitamin E and gossypin (Behl, C., 1997, Yatin, S. M., *et al.*, 2000, Yoon, I., *et al.*, 2004). Targeting Aβ with antisense oligonucleotides reduces oxidative stress in transgenic mice models (Poon, H. F., *et al.*, 2004) and *in situ* studies have shown that markers of oxidative stress are elevated in the tissues of animal models expressing Aβ and neuronal cultures exposed to Aβ (Akama, K. T., *et al.*, 1998, Bondy, S. C., *et al.*, 1998, Butterfield, D. A., *et al.*, 1994, Della Bianca, V., *et al.*, 1999, Klegeris, A. and Mcgeer, P. L., 1997, Matsuoka, Y., *et al.*, 2001, Murray, I. V. J., *et al.*, 2005, Rival, T., *et al.*, 2009, Smith, M. A., *et al.*, 1998, Sultana, R. and Butterfield, D. A., 2008, Yatin, S. M., *et al.*, 1999).

Aβ has been proposed to promote oxidative activities in cells including stimulating RAGE receptors within neurons, which causes oxidative stress, stimulating nitric oxide and superoxide production by microglia, converting cholesterol to neurotoxic 7-hydroxycholesterol and entering mitochondria to induce ROS generation within these organelles (Li, M., *et al.*, 1996, Mcdonald, D. R., *et al.*, 1997, Meda, L., *et al.*, 1995, Nelson, T. J. and Alkon, D. L., 2005, Pratico, D., 2008, Thomas, T., *et al.*, 1996, Yan, S. D., *et al.*, 1996). It has also been reported to decrease the activity of endogenous antioxidants such as glutathionine peroxidase, superoxide dismutase, ascorbic acid, vitamin E and glutathione (Kato, M., *et al.*, 1997, Melo, J. B., *et al.*, 2009, Wan, L., *et al.*, 2011).

In addition, to promoting oxidative processes, the Aβ peptide has been proposed to produce ROS itself. Hensley *et al.*, first reported electron paramagnetic resonance (EPR) and mass spectrometric data, which seemed to show that Aβ produced radicals upon fragmentation (Hensley, K., *et al.*, 1994). However, this spontaneous generation of ROS by Aβ was disputed by several studies which showed Aβ-induced radical

production required metals (Dikalov, S. I., *et al.*, 1999, Huang, X., *et al.*, 1999a, Huang, X., *et al.*, 2004, Turnbull, S., *et al.*, 2001) and thus Hensley's initial study was explained as having involved trace metals in solution.

Huang *et al.* reported Aβ to produce equimolar concentrations of hydrogen peroxide, by the reduction of molecular oxygen and either Cu^{2+} or Fe^{3+} (Huang, X., *et al.*, 1999a, Huang, X., *et al.*, 1999b). This hydrogen peroxide production was then correlated to the toxicity of the peptide and has been shown to be enough to oxidise other proteins (Antunes, F. and Cadenas, E., 2001, Harris, M. E., *et al.*, 1995). The toxicity of Aβ can be inhibited by the hydrogen-peroxide scavenger catalase and neuronal cell clones, which are resistant to Aβ toxicity, are also often resistant to H_2O_2 toxicity (Behl, C., *et al.*, 1994), implying that the peptide's toxicity is mediated by H_2O_2 (Behl, C., *et al.*, 1994, Huang, X., *et al.*, 1999a, Rival, T., *et al.*, 2009). Further studies reported that Aβ was capable of further reducing this H_2O_2 to generate hydroxyl radicals via Fenton's chemistry (Dikalov, S. I., *et al.*, 2004, Guilloreau, L., *et al.*, 2007).

This pro-oxidant activity of Aβ has been proposed to be mediated specifically by smaller aggregates of the peptide while plaques, which negatively correlate with oxidative damage, may be redox-silencing traps for the Aβ peptide (Cuajungco, M. P., *et al.*, 2000, Smith, D. G., *et al.*, 2007). There is some dispute whether monomeric Aβ or oligomeric/fibrillar Aβ is the more redox active (Drake, J., *et al.*, 2003, Fang, C.-L., *et al.*, 2010, Jiang, D. L., *et al.*, 2010, Monji, A., *et al.*, 2001). The two major Aβ isoforms have been reported to have different pro-oxidant activity with the Aβ(1-42) peptide generating 5 times the concentration of hydroxyl radicals than the Aβ(1-40) peptide (Huang, X., *et al.*, 1999a).

Aβ as an antioxidant in AD pathology

Despite evidence from the studies described above it is not current dogma in the field of Alzheimer's research that Aβ is a pro-oxidant and in fact several studies have reported Aβ to be an antioxidant in the disease. Some of these studies have reported that antioxidants do not protect against the neurotoxicity of Aβ (Lockhart, B. P., *et al.*, 1994, Lorenzo, A. and Yankner, B. A., 1994), and inconsistent results found by Zhang *et al.* for the action of H_2O_2 scavengers led this group to propose that inhibition of Aβ neurotoxicity by catalase was due to induction of a conformational change in the

peptide rather than ROS scavenging (Zhang, Z., *et al.*, 1996). Further evidence against Aβ being a pro-oxidant is the fact oxidative stress occurs early in AD aetiology, prior to increases in Aβ concentrations and deposition (Drake, J., *et al.*, 2003, Nunomura, A., *et al.*, 2001, Pratico, D., *et al.*, 2001). In addition, application of low concentrations of Aβ (0.1 – 1.0 nM) to cellular cultures has been shown to protect against certain types of oxidative stress e.g. ascorbate-stimulated lipid peroxidation (Kontush, A., 2001, Kontush, A., *et al.*, 2001a).

There are two mechanisms by which Aβ is hypothesised to act as an antioxidant against MCO; scavenging already formed ROS such as hydroxyl radicals or chelating redox-active metals and preventing ROS formation by MCO. Both are proposed to act via the Met35 residue, with Aβ rapidly chelating redox active metals and in doing so being oxidised to Met35 sulfoxide and then slowly scavenging ROS after this oxidation which leads to further oxidation of Met35-sulfoxide to Met35-sulfone (Baruch-Suchodolsky, R. and Fischer, B., 2008). In terms of the second mechanism, the H_2O_2 and hydroxyl radical production rates of Aβ-metal complex are less than for the free metal, for both Cu^{2+} (Guilloreau, L., *et al.*, 2007) and Fe^{3+} (Khan, A., *et al.*, 2006). However, most redox active metals are not in a free form in physiological settings and Aβ-Cu produces more ROS than these other protein-Cu complexes (Guilloreau, L., *et al.*, 2007, Hureau, C. and Faller, P., 2009). Therefore Aβ may not be as useful an antioxidant as previously hypothesised.

It may be the case that Aβ has a dual-role of both pro-oxidant and antioxidant dependant on certain conditions; Cu^{2+} ions concentration (Hayashi, T., *et al.*, 2007), the presence of ascorbate (Murray, I. V. J., *et al.*, 2005, Zou, K., *et al.*, 2002) or whether it binds Cu^{+} or Cu^{2} (Baruch-Suchodolsky, R. and Fischer, B., 2008, 2009). Finally Aβ concentration is thought to control the antioxidant behaviour of Aβ with high disease-related concentrations i.e. μM concentrations rather than normal nM concentrations, needed for antioxidant behaviour (Baruch-Suchodolsky, R. and Fischer, B., 2008, Kontush, A., *et al.*, 2001b). This is likely due to increased aggregation of Aβ at higher concentrations of the peptide and the increased redox metal ion binding affinity of aggregated Aβ compared to the monomeric peptide (Baruch-Suchodolsky, R. and Fischer, B., 2008). Several groups have proposed oligomeric Aβ to be antioxidant, whereas fibrillar and monomeric Aβ is pro-oxidant (Karr, J. W. and Szalai, V. A., 2008, Nadal, R. C., *et al.*, 2008, Sponne, I., *et al.*, 2003, Zou, K., *et al.*, 2002).

This condition dependent behaviour of Aβ has led to the hypothesis that Aβ has a dual role in AD pathology; as an antioxidant in its monomeric form and as a pro-oxidant in its oligomeric form (Atwood, C. S., *et al.*, 2003, Kontush, A., 2001, Nadal, R. C., *et al.*, 2008). A final consideration is that oxidative stress can control the production of Aβ, via H_2O_2 production damaging the APP promoter and peroxidation of phospholipids in the plasma membrane altering the activity of γ-secretase, degrading the enzymes which usually catabolise the peptide, all leading to further Aβ production (Frederikse, P. H., *et al.*, 1996, Misonou, H., *et al.*, 2000, Paola, D., *et al.*, 2000, Shinall, H., *et al.*, 2005).Therefore, with oxidative stress controlling Aβ concentrations and high concentrations of Aβ becoming pro-oxidant, a positive feedback loop is set up in AD pathology of increasing oxidative stress.

Aβ and metal catalysed oxidation (MCO)

In AD there is a loss of metal homeostasis with altered concentrations of free metal ions in AD brains (Atwood, C. S., *et al.*, 1999) and increased concentrations particularly in areas of neurodegeneration (Deibel, M. A., *et al.*, 1996, Thompson, C. M., *et al.*, 1988). These metal ions include the redox active Cu^{2+} and Fe^{3+} ions (Cornett, C. R., *et al.*, 1998, Dong, J., *et al.*, 2003, Lovell, M. A., *et al.*, 1998). Metal ions have been found to alter APP expression and trafficking (Rival, T., *et al.*, 2009, Venti, A., *et al.*, 2004) and alter the fibrillisation properties of Aβ by binding the peptide, altering its net charge and encouraging amorphous aggregation instead of fibrillisation (Atwood, C. S., *et al.*, 1999, Chevion, M., 1988, Sarell, C. J., *et al.*, 2010, Stadtman, E. R., 1990, Stadtman, E. R. and Berlett, B. S., 1991, 1997). However, one of the most likely effects of increased redox active metal concentrations in AD is an increased occurrence of metal-catalysed oxidation (MCO).

Metal-catalysed oxidation is the production of reactive oxygen species (ROS) by the redox activity of metals such as copper ions and iron ions. These metals transfer single electrons and cycle between their reduced (Cu^{+} and Fe^{2+}) and oxidised state (Cu^{2+} and Fe^{3+}). By transferring these electrons to species such as oxygen and hydrogen peroxide in reactions such as the Haber Weiss Reaction and Fenton's Reaction these metals can generate ROS including the superoxide anion and hydroxyl radicals (Fifure 1.9). MCO is a site-specific process thus these highly reactive hydroxyl radicals oxidise

neighbouring targets (Opazo, C., *et al.*, 2002). Opazo *et al.* proposed Aβ to act as a metalloprotein, forming a complex with these redox active metal ions (Figure 1.12) (Baruch-Suchodolsky, R. and Fischer, B., 2008, Halliwell, B. and Gutteridge, J. M. C., 1985, Huang, X., *et al.*, 1999a). Indeed, the residues of Aβ involved in metal co-ordination tend also to be the residues required for ROS production by the peptide (Figure 1.13).

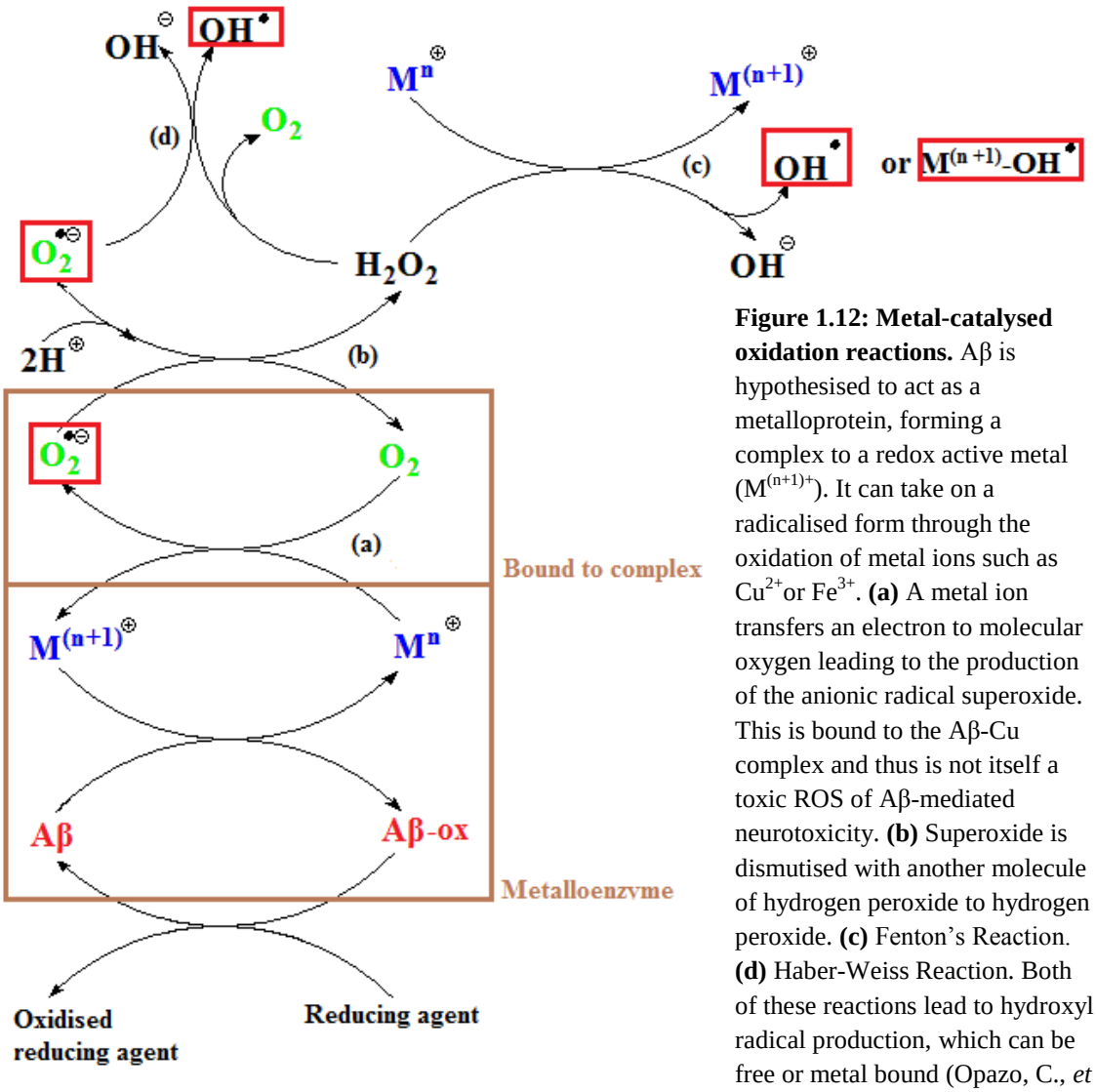

Figure 1.12: Metal-catalysed oxidation reactions. Aβ is hypothesised to act as a metalloprotein, forming a complex to a redox active metal ($M^{(n+1)+}$). It can take on a radicalised form through the oxidation of metal ions such as Cu^{2+} or Fe^{3+}. **(a)** A metal ion transfers an electron to molecular oxygen leading to the production of the anionic radical superoxide. This is bound to the Aβ-Cu complex and thus is not itself a toxic ROS of Aβ-mediated neurotoxicity. **(b)** Superoxide is dismutised with another molecule of hydrogen peroxide to hydrogen peroxide. **(c)** Fenton's Reaction. **(d)** Haber-Weiss Reaction. Both of these reactions lead to hydroxyl radical production, which can be free or metal bound (Opazo, C., *et al.*, 2002, Hewitt, N., and Rauk, A., 2009).

(A)
DAEFRHDSGYEVHHQKLVFFAEDVGSNKGAIIGLMVGGV

(B)
DAEFRHDSGYEVHHQKLVFFAEDVGSNKGAIIGLMVGGV

Figure 1.13: A comparison of Aβ residues which bind copper and Aβ residues linked to ROS production.
A summary of the literature reports of:
(A) Residues potentially involved in Cu^{2+} co-ordination (blue) and Cu^{+} co-ordination (green).
(B) Residues involved in Cu^{2+} reduction (red) and ROS scavenging (yellow).

Different types of MCO systems include Fenton's Reagents (Cu^{2+}/H_2O_2), Udenfriend's Reagents (Fe^{3+}/ascorbic acid) and the Cu^{2+}/ascorbic acid system. Of the two redox active metals, the reduction of Cu^{2+} by Aβ is more efficient than the reduction of Fe^{3+}, and Cu^{2+} ions generate hydroxyl radicals from H_2O_2 at several times the rate of Fe^{3+} (Dikalov, S. I., *et al.*, 2004, Guilloreau, L., *et al.*, 2007, Jiang, D., *et al.*, 2007). In addition, for redox cycling of the metal to occur, and hence greater than equimolar concentrations of H_2O_2 to be generated by the Aβ-metal complex, an external reducing agent is required of a lower redox potential that the Aβ-metal complex (0.28 – 0.34 V *vs*. NHE), e.g. ascorbic acid (0.051 – 0.058 V *vs*. NHE) (Khossravi, M. and Borchardt, D. R., 1998). It should be noted that ascorbate has a dual role as a pro-oxidant and an antioxidant. As a pro-oxidant it can reduce Cu^{2+} to Cu^{+} whereas as an antioxidant it can scavenge ROS (Stadtman, E. R. and Berlett, B. S., 1997).

Because MCO is site specific, the binding of redox active metals to Aβ and subsequent production of ROS such as the hydroxyl radical likely leads to oxidation of the Aβ peptide itself. This oxidation could lead to peptide bond cleavage or peptide cross-linking leading to large-insoluble aggregates. However, another outcome of Aβ oxidation may be amino acid side chain modifications (Table 1.1), particularly of aromatic and/or metal binding amino acids, which alter the net charge and hydrophobicity of the peptide, thus altering its fibrillisation rate. Hence MCO may be one of the elusive triggers of the Amyloid Cascade.

Amino acid	Products of oxidation
Arginine	Carbonyl derivatives
Threonine	
Proline	
Lysine	
Leucine	Hydroxyleucine
Methionine	Methionine sulfoxide/methionine sulfone
Phenylalanine	Hydroxyphenylalanine
Tyrosine	Dityrosine and nitrotyrosine derivatives
Tryptophan	Hydroxytryptophan, kynurenine derivatives, nitrotryptophan
Cysteine	Disulfide derivatives
Histidine	2-oxo-histidine, 4-OH-glutamate, aspartic acid, asparagine
Glutamic acid	α-ketoacyl derivatives

Table 1.1: Expected products of amino acid oxidation.

Histidine, methionine and tyrosine residues of Aβ are likely oxidised by MCO

Several factors determine an amino acid's susceptibility to oxidation. Amino acids in a hydrophilic peptide environment are more readily oxidised than amino acids in a hydrophobic region, due to their greater exposure to the aqueous medium. In Aβ this would favour oxidation within the hydrophilic *N*-terminal (1-28) region rather than the hydrophobic *C*-terminus (29-42). In addition, the type of oxidising system can determine amino acid susceptibility to oxidation. As described above Aβ seems to be primarily involved in MCO, which produces highly reactive short-lived ROS which target their nearest neighbours. The redox active metal ion Cu^{2+} has been shown to bind the Aβ peptide via the three histidines (His6, His13 and His14) and the *N*-terminus as part of a square-planar complex (Figure 1.14) (Huang, X., *et al.*, 1999a, Nakamura, M., *et al.*, 2007, Smith, D. P., *et al.*, 2006). These three histidine residues of Aβ are required for the reduction of Cu^{2+}, as shown by comparison with rat Aβ, which contains one less histidine than human Aβ and is subsequently less redox active (Ali, F. E., *et al.*, 2003, Inoue, K., *et al.*, 2006, Kowalik-Jankowska, T., *et al.*, 2004, Nadal, R. C., *et al.*, 2008, Schiewe, A. J., *et al.*, 2004, Schoneich, C. and Williams, T. D., 2002, Schoneich, C. and Williams, T. D., 2003). Therefore, these residues are the nearest targets of any ROS generated by MCO with the Cu^{2+} ion.

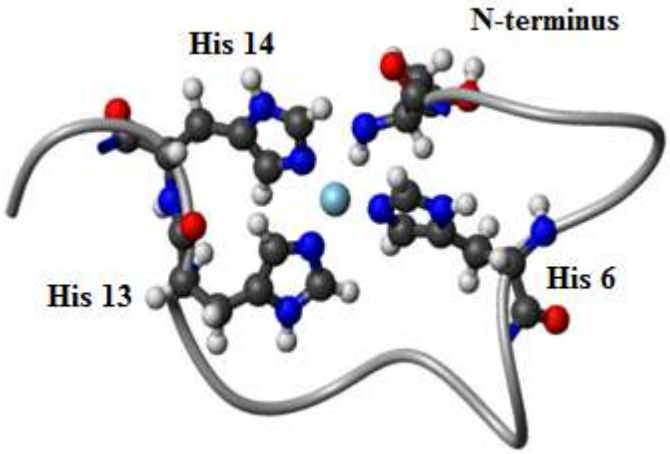

Figure 1.14: Cu^{2+} ions bind Aβ as part of a square planar complex. The first mole of Cu^{2+} ions is co-ordinated to Aβ via the three histidines of the peptide and its *N*-terminus amino groups in a square-planar geometry. Modified from Syme and Nadal *et al*. (Syme, C. D., *et al.*, 2004).

Indeed the three histidine residues of Aβ, in particular His13 and His14, have been identified as oxidised in several *in vitro* studies where the Aβ peptide has been exposed to MCO conditions such as Cu^{2+} ions and either H_2O_2 or ascorbic acid (Nadal, R. C., *et al.*, 2008, Schoneich, C. and Williams, T. D., 2002). The product of this histidine oxidation is often identified as 2-oxo-histidine (Kowalik-Jankowska, T., *et al.*, 2004) or asparate and asparagine (Uchida, K. and Kawakishi, S., 1989b), which are oxidation products derived from 2-oxo-histidine (Scheme 1.1(B)) (Giunta, S., *et al.*, 2000, Nadal, R. C., *et al.*, 2008, Nishino, S. and Nishida, Y., 2001, Schiewe, A. J., *et al.*, 2004, Schoneich, C. and Williams, T. D., 2003).

Several studies have found other residues in Aβ such as methionine (Met35) and Tyrosine (Tyr10) oxidised after MCO to the products given in Scheme 1.1(C), either in addition or instead of histidine residues (Head, E., *et al.*, 2001, Shearer, J. and Szalai, V. A., 2008). In addition, although 90 % of Aβ isolated from amyloid plaques upon post mortem is found oxidised (Dong, J., *et al.*, 2003), only the Met35 residue is found to be the likely target in the Aβ sequence (Atwood, C. S., *et al.*, 2000, Baruch-Suchodolsky, R. and Fischer, B., 2008).

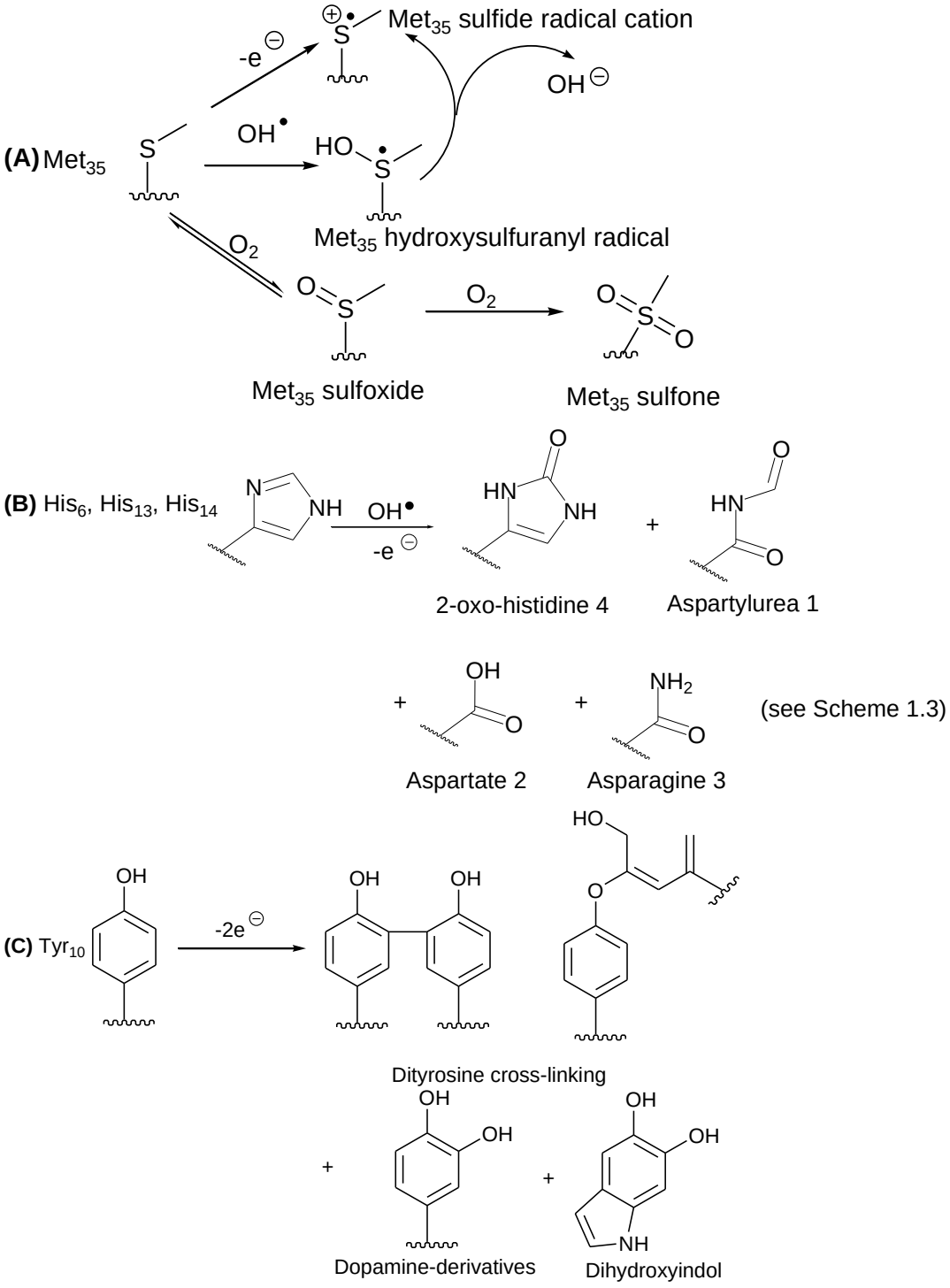

Scheme 1.1: Amino acid oxidation products associated with Aβ. Common oxidation products of the three most likely oxidised amino acids in the Aβ sequence; **(A)** methionine, **(B)** histidine and **(C)** tyrosine. For simplicity the amino acid backbone and β-carbon are not shown.

This finding might be due to the analysis techniques used, e.g.raman spectroscopy, being unable to detect certain oxidised residues. In addition, Aβ peptides isolated from AD plaques is found with both a 32 % histidine loss and a percentage gain in arginine,

glutamate and glutamine, the end products of histidine oxidation (Nadal, R. C., *et al.*, 2008, Schiewe, A. J., *et al.*, 2004). MCO may continue after production of 2-oxo-histidine to provide these ring-ruptured products. Therefore, histidine oxidation in Aβ is a likely event in AD pathology. Aβ tends to be found di-oxidised at Met35 and one histidine residue (Sundberg, R. J. and Martin, R. B., 1974). Therefore, the two main residues found oxidised are histidine (His6, His 13 and His14) and methionine (Met35).

The three histidines of the Aβ peptide

Histidine (His or H) **5** is a 156 Da basic amino acid (pI 7.61) with a positively charged imidazole side chain (pK_a 6.04) at neutral pH, meaning that at physiological pH histidine can act as a buffer. A pyridine-type nitrogen in the imidazole ring side chain allows histidine to bind metals, such as Cu^{2+} and Zn^{2+} ions (Fraser, P. E., *et al.*, 1994). This property and the basic nature of the imidazole side chain give this residue its biological activity.

The imidazole ring can be represented by two tautomers (Scheme 1.2). The labelling of histidine is discussed further in Chapter 6.

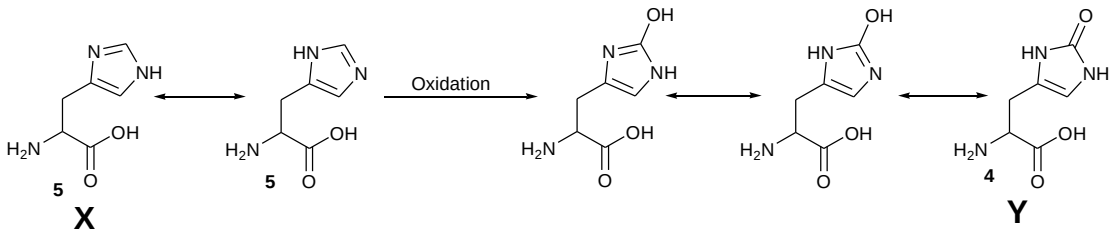

Scheme 1.2: The tautomeric forms of L-histidine 5 and 2-oxo-histidine 4. L-histidine has two tautomers of the imidazole ring, which exists predominately in the **X** tautomer but undergoes fast hydrogen atom exchange to the minor tautomer. 2-Oxo-histidine exists in a tautomeric state of three tautomers although it is primarily believed to exist in the cyclic urea tautomer **Y**.

As described above in Section 1.2.8., the Aβ peptide has a toxicity that is linked to its fibrillisation state, with oligomeric and protofibrillar forms being considered the most neurotoxic. Although, the histidine residues of Aβ are not important for determining the peptide's pre-fibrillar β-sheet packing (Hou, L., *et al.*, 2004), they are important for the process of fibrillisation and subsequent fibril stabilisation (Fraser, P. E., *et al.*, 1994, Hilbich, C., *et al.*, 1991, Mclaurin, J. and Fraser, P. E., 2000), with histidine substitutions leading to altered length and surface tension of Aβ protofibrils and the

formation of stable, amorphous, ribbon like-aggregates beyond the protofibrillar stage (Hou, L., *et al.*, 2004). This is likely due to these histidines forming intramolecular interactions via glycoaminoglycans, binding metals, forming salt-bridges via their imidazole moieties to carboxylates in aspartate and glutamate residues, e.g. Asp23-His13, (Figure 1.15) (Lazo, N. D., *et al.*, 2005), and undergoing hydrogen bonding (Giulian, D., *et al.*, 1998). These all contribute to an amorphous aggregate structure instead of the usual amyloid fibrillar structure. In general, as histidine is the only amino acid able to buffer at physiological pH, these three amino acids are very important for determining the electrostatic charge of the Aβ peptide in physiological environments.

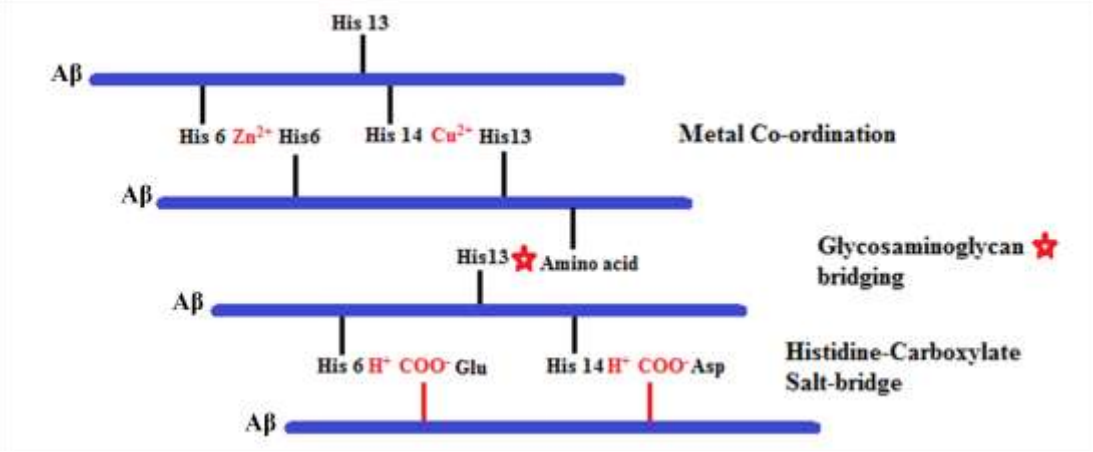

Figure 1.15: Modification of the histidines in Aβ promotes amorphous aggregation over fibrillisation.

There are numerous mechanisms by which Aβ is proposed to exert its toxicity. One is the activation of microglia leading to brain inflammation seen in Alzheimer's pathology and His13 and His14 in the Aβ sequence have been shown to be part of a HHQK (His-His-Gln-Lys) tetrad which binds and activates these microglia (Smith, D. G., *et al.*, 2010). Another mechanism of Aβ toxicity, is the binding of Aβ oligomers to cellular membranes, and mutation studies have shown His14 to be vital for this binding and subsequent neurotoxicity, via electrostatic interactions between the charged head groups of phosphatidylserines and the imidazoles of histidines (Díaz, J. C., *et al.*, 2006). The channels that are proposed to form when Aβ binds to these membranes are also reliant on His13 and His14 being present in the Aβ sequence, as shown by mutation studies (Nakamura, M., *et al.*, 2007). The three histidines of Aβ have also been shown to be important in determining the antioxidant behaviour of Aβ, as these residues have been

implicated as scavengers of potentially harmful free radicals (Traore, D. A. K., *et al.*, 2009).

Histidine oxidation in other proteins has been shown to alter metal affinities (Meister Winter, G. E. and Butler, A., 1996), alter protein function (Lewisch, S. A. and Levine, R. L., 1995) and alter protein turnover (Liaw, S.-H., *et al.*, 1993, Schoneich, C., 2004). Histidine oxidation in the Aβ sequence may be protective as oxidised Aβ has a lower affinity for Cu^{2+} ions and thus may be less likely to generate ROS by Cu^{2+} reduction (Schoneich, C., 2000, Uchida, K. and Kawakishi, S., 1994). However, if histidine oxidation leads to greater Aβ fibrillisation rates, then such oxidation may not be protective at all and this is discussed more in Chapter 4.

These effects of histidine oxidation in other proteins and the numerous roles of the histidine residues in the Aβ sequence on AD aetiology, indicate that oxidation of histidine residues could greatly alter this aetiology.

The most likely product of histidine oxidation is 2-oxo-histidine.

Histidine can be oxidised by MCO on either the imidazole ring or on the amino acid backbone (Scheme 1.3). Oxidation of the imidazole side-chain of *N*(α)-Bz-His-OH **5b** has been shown by Uchida and Kawakishi to lead to 2-oxo-histidine **4**, a 172.5 Da mono-oxygen C-2 adduct of histidine **4,** also known as *β*(2oxoimidazolonyl)alanine (Uchida, K. and Kawakishi, S., 1989b, 1990b) or to ring-ruptured products such as asparagine **3**, aspartate **2**, aspartylurea **1**, formylasparagine **8**, 4-hydroxyglutamate **9** and glutamic acid **10** (Ali, F. E., *et al.*, 2003, Levine, R. L., *et al.*, 1996). Oxidation of the amino acid backbone involves hydrogen abstraction at the α or β carbon leading to compounds such as α-ketoacids, aldehydes, amides, imidazole acetic acids, imidazole lactic acids, imidazole acsetonitriles or carboxylic acids (Ali, F. E., *et al.*, 2003).

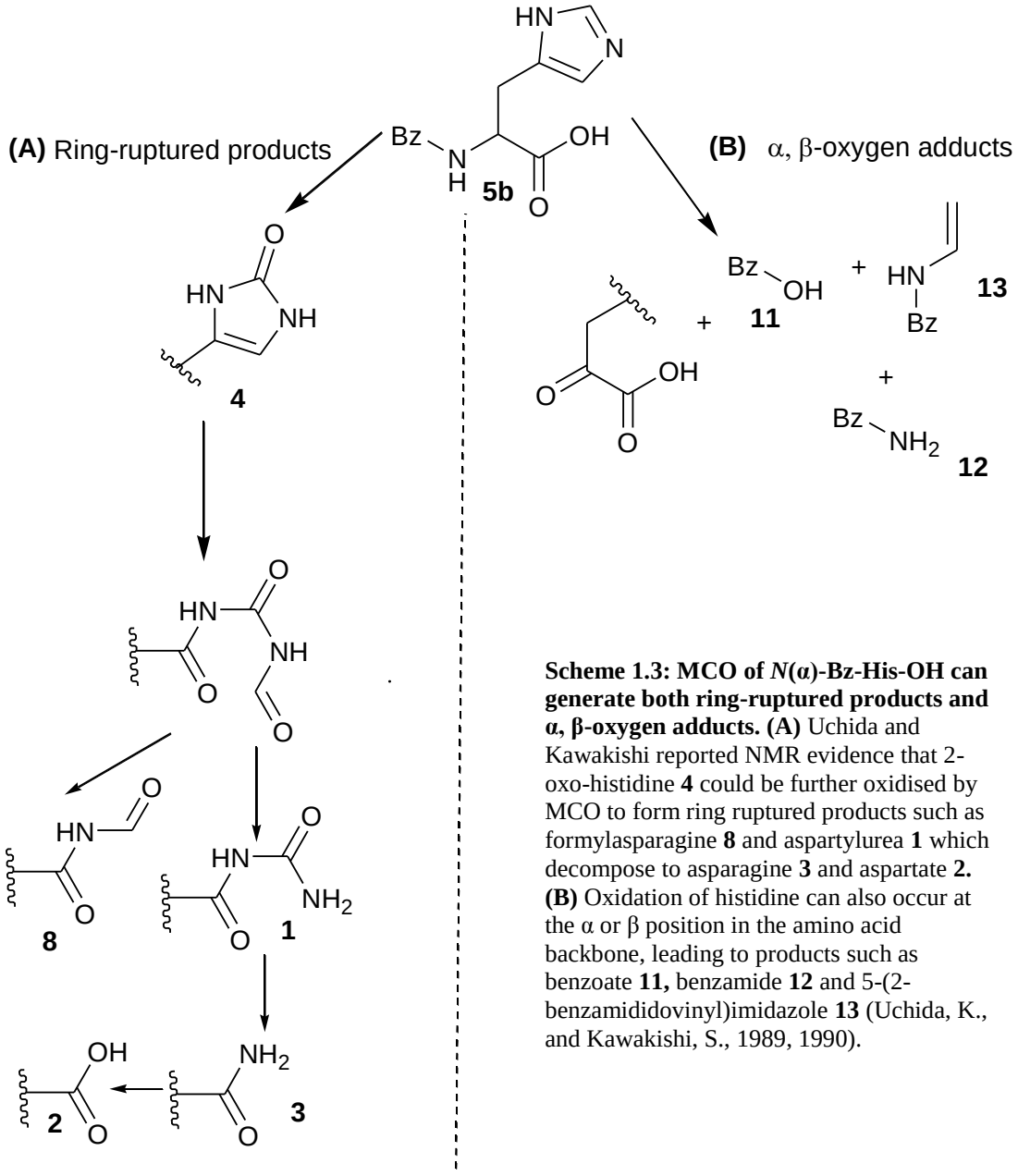

Scheme 1.3: MCO of *N*(α)-Bz-His-OH can generate both ring-ruptured products and α, β-oxygen adducts. (A) Uchida and Kawakishi reported NMR evidence that 2-oxo-histidine **4** could be further oxidised by MCO to form ring ruptured products such as formylasparagine **8** and aspartylurea **1** which decompose to asparagine **3** and aspartate **2. (B)** Oxidation of histidine can also occur at the α or β position in the amino acid backbone, leading to products such as benzoate **11,** benzamide **12** and 5-(2-benzamididovinyl)imidazole **13** (Uchida, K., and Kawakishi, S., 1989, 1990).

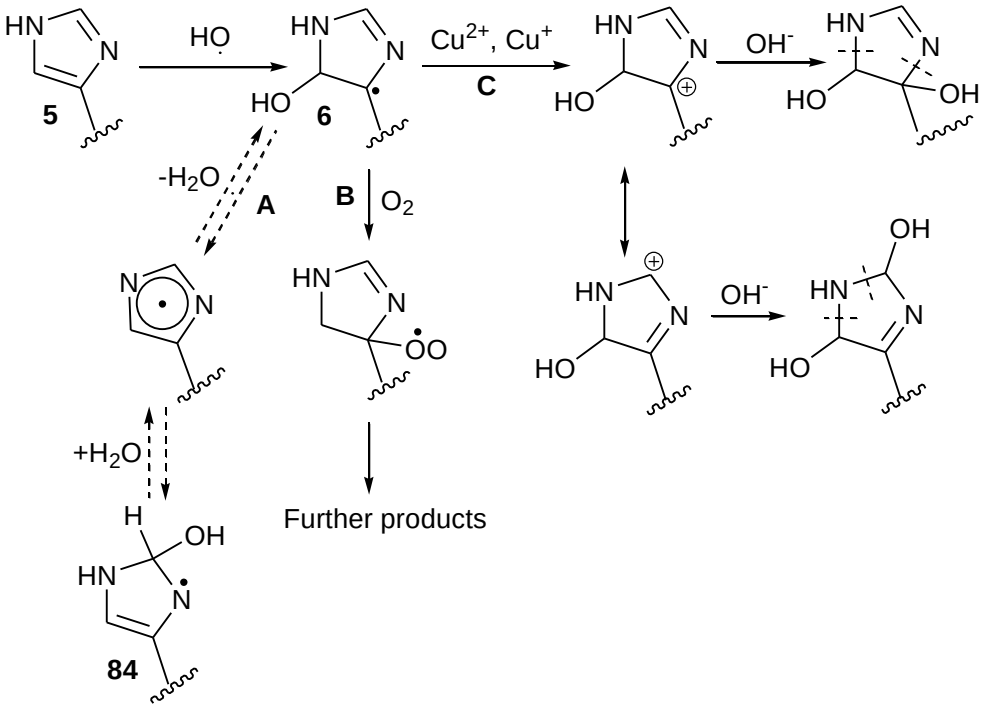

Scheme 1.4: Oxygen addition to C5 during histidine oxidation. Hydroxyl radicals can add at the C-5 position. They can then either react with molecular oxygen **(B)** to form a peroxy radical which will further react, or they can reduce Cu^{2+} (**C**), which will ultimately lead to the imidazole ring fragmenting (as shown by the dotted lines). One, theorised reaction of the C-5 adduct **6** is shown **(A),** where in the presence of transition metals or a basic environment, water elimination of the C-5 adduct **6** converts it to a radical precursor of the C-2 adduct **84.** These reactions all apply to the C-4 adduct **7** (Schoneich, C., 2000).

Mono-oxygen addition to the imidazole ring is the main product of MCO, with oxygen addition at C-2 **4**, C-4 **7** or C-5 **6**. Addition of oxygen at C-4 **7** and C-5 **6** has been detected by Schoneich using EPR studies (Lassmann, G., *et al.*, 2000) and in some cases these adducts have been predicted to be the predominant form (Schoneich, C., 2000). However, these oxygen adducts are predicted not to be stable and are likely to either leads to ring fragmentation or conversion to 2-oxo-histidine **4** (Scheme 1.4) (Schoneich, C., 2000). The production of 2-oxo-histidine is also reported to be MCO system specific e.g. Uchida *et al.* found Fe^{3+}-based redox systems, Fenton's or Udenfriend's, incapable of producing 2-oxo-histidine **4** (Uchida, K. and Kawakishi, S., 1989b).

Oxo-histidine has also been detected following application *in vitro* of Cu^{2+} ions and ascorbate to numerous proteins. Evidence includes addition of +16 mass units to proteins (Zhao, F., *et al.*, 1997), amino acid analysis showing a decrease in histidine content of proteins (Lewisch, S. A. and Levine, R. L., 1995, Requena, J. S. R., *et al.*, 2001), detection of an earlier eluting amino acid in amino acid analysis (Zhao, F., *et al.*,

1997), decreased C-2 ^{1}H-NMR peak intensities for histidine within proteins under MCO conditions (Khossravi, M., *et al.*, 2000, Uchida, K. and Kawakishi, S., 1990c), ^{1}H-NMR peaks that match those of the model *N*(α)-Bz-His-OH **5b** (Meister Winter, G. E. and Butler, A., 1996, Retsky, K. L., *et al.*, 1998, Uchida, K. and Kawakishi, S., 1993, 1994) and co-elution of the oxidised amino acid isolated from HPLC columns with a known sample of 2-oxo-histidine **4** (Santa Maria, C., *et al.*, 1995).

Initially, there were concerns in the literature that, although 2-oxo-histidine **4** could be detected *in vitro* after application of MCO, this form of oxidised histidine may not form *in vivo*. Studies on CuZnSOD isolated from liver that reported an age-dependent loss of histidine (Ghezzo-Schoneich, E., *et al.*, 2001) could not be replicated by later mass spectrometry studies (Atwood, C. S., *et al.*, 2000). In addition, although Aβ released from brain tissue showed loss of histidine residues (Lee, J. and Helmann, J. D., 2006) it was not identified as containing 2-oxo-histidine **4**. However, studies on the transcription factor PerR have shown that after exposure to H_2O_2, histidine will incorporate oxygen *in vivo* (Traore, D. A. K., *et al.*, 2009). Traore *et al.* advanced on this study by isolating 2-oxo-histidine **4** from PerR protein oxidised *in vivo* and providing a crystal structure of the oxidised amino acid (Figure 1.16) (Hovorka, S. W., *et al.*, 2002, Schoneich, C., 2000, Schoneich, C. and Williams, T. D., 2002). Therefore, it is likely that 2-oxo-histidine **4** is a relevant form of oxidised histidine *in vivo*.

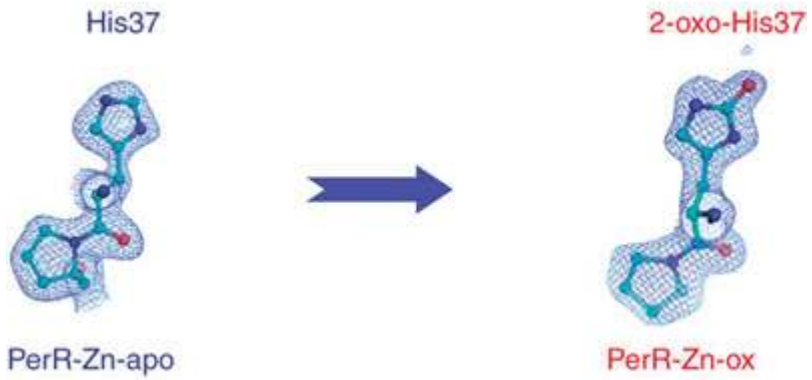

Figure 1.16: Density map and corresponding crystal structure of the His37 residue in PerR-Zn after application of hydrogen peroxide. A crystal structure of His37 after application of hydrogen peroxide reveals the oxidation product is 2-oxo-histidine **4**.

Therefore the most likely product of histidine oxidation in Aβ exposed to MCO is 2-oxo-histidine (Atwood, C. S., *et al.*, 2002, Sayre, L. M., *et al.*, 1997, Uchida, K. and Kawakishi, S., 1986, 1989b, 1993). It contains a neutral cyclic urea rather than the

basic imidazole of histidine, at neutral pH, and hence is less nucleophilic than histidine, giving it a reduced proton affinity relative to histidine (Lewisch, S. A. and Levine, R. L., 1995) and causing it to exit later than histidine **5** from reverse-phase HPLC (RP-HPLC) columns (Lam, A. K. Y., *et al.*, 2010). DFT calculations predict that 2-oxo-histidine exists as a mixture of three tautomers (Scheme 1.2) especially in an aqueous environment (Ren, Y., *et al.*, 2005). The most stable tautomer is the cyclic urea form thus 2-oxo-histidine **4** has no aromatic character unlike histidine.

2-Oxo-histidine **4** is stable in an acid environment e.g. at the 0.05 M $HClO_4$ (Traore, D. A. K., *et al.*, 2009) and the 6 M HCl needed for amino acid analysis as long as dithiothreitol (DTT) is used (Lewisch, S. A. and Levine, R. L., 1995). However, it is not stable in a basic environment and thus its stability can be increased by keeping pH below 8.0 (Lewisch, S. A. and Levine, R. L., 1995, 1999). In addition, freeze drying at 20 °C or storage as a protein hydrolysate has been shown to reduce the oxidised residue's degredation rates (Ren, Y., *et al.*, 2005). This must be considered when using this amino acid in solid phase peptide synthesis.

2-Oxo-histidine can also form 2-oxo-His-2-oxo-His or Lys-2-oxo-His protein cross-links (Meister Winter, G. E. and Butler, A., 1996) thus promoting peptide aggregation. Therefore, the oxidation of histidines in the Aβ peptide to 2-oxo-histidine is highly likely to alter the behaviour of the Aβ peptide.

Mechanisms of hidtidine oxidation to 2-oxo-histidine by MCO

There is some debate in the literature regarding the mechanism by which histidine is oxidised by MCO. Scheme 1.6 shows the initially accepted mechanism; oxidation by a hydroxyl radical generated by single-electron reduction of a redox active transition metal followed by single-electron reduction of H_2O_2. This radical then attacks histidine at the C-2 position forming a radical species, which is oxidised to a carbocation. Subsequent proton loss leads to 2-oxo-histidine **4** (Uchida, K. and Kawakishi, S., 1986, 1989b). There are some variations on this mechanism, such as the formation of the radical at a ring nitrogen instead of C-4 (Zhao, F., *et al.*, 1997) and delocalisation of the radical and carbocation throughout the imidazole ring system (Garrison, 1987, Simic, M. G., 1978). This mechanism has been backed up by EPR studies showing hydroxyl radicals readily adding to the aromatic ring system (Lassmann, G., *et al.*, 2000). Other

studies have also confirmed the action of H_2O_2, Cu^+ ions and Cu^{2+} ions in this MCO reaction with the use of H_2O_2 inhibitos catalase and thiourea and the metal chelators BCA and EDTA (Khossravi, M. and Borchardt, D. R., 1998). H_2O_2 alone did not oxidise histidine, indicating that H_2O_2 must be reduced by MCO to form hydroxyl radicals before histidine oxidation can occur (Khossravi, M. and Borchardt, D. R., 1998, Stadtman, E. R. and Berlett, B. S., 1991, Uchida, K. and Kawakishi, S., 1990a, Zhao, F., *et al.*, 1997).

However, several studies dispute the hydroxyl radical mechanism with the findings that hydroxyl radical scavengers, e.g. mannitol, sodium formate, isopropanol and 5,5-Dimethyl-1-Pyrroline N-Oxide (DMPO), do not prevent oxidation of histidine by MCO (Stadtman, E. R. and Berlett, B. S., 1997, Vogt, W., 1995). In addition DFT calculations predict free hydroxyl radicals tend to add at the C-4 and C-5 position of histidine, not the C-2 position (Zhao, F., *et al.*, 1997). Instead for C-2 oxygen addition, an alternative caged mechanism for MCO of histidine is predicted (Scheme 1.5) (Khossravi, M. and Borchardt, R. T., 2000), where an azametallacyclic complex forms between the imidazole of histidine, ascorbate, Cu^{2+}/Cu^+ ions and other compounds such as buffer salts and water (Uchida, K. and Kawakishi, S., 1994). This mechanism involves a single electron transfer from the imidazole to a bound Cu^{2+} ion, leading to a ring radical**.** The His-Cu(I) complex then reacts with molecular oxygen to give a peroxy radical. An electron transfer then occurs from the bound Cu^+, converting the ring radical into an anionic state. This then degrades to a hydroperoxy species which is reduced to 2-oxo-histidine by Cu^{2+}, as part of a oxocopper(III) species (Uchida, K., 2003) (Scheme 1.5) (Kurahashi, T., *et al.*, 2001, Uchida, K. and Kawakishi, S., 1989a). The expected 2-hydroperoxy intermediate has been identified by ^{13}C-NMR (Farber, J. M. and Levine, R. L., 1986). Other evidence for this mechanism include the detection of charge transfers with colour changes of *N*-benzoylhistidine-Cu^{2+} complexes after addition of ascorbate (Imanaga, Y., 1955) and calculations which show that histidine has a higher reactivity for electron transfer (6×10^7 M^{-1} s^{-1}) than hydroxyl radical addition (5×10^9 M^{-1} s^{-1}) (Bernaducci, E., *et al.*, 1981) and that metal charge transfers are energetically favourable (Uchida, K. and Kawakishi, S., 1989b). However, Imanaga *et al.* found no evidence for complexes of histidine and ascorbate (Hureau, C. and Faller, P., 2009).

In the Aβ peptide, oxidation by hydroxyl radicals is less likely than a charge transfer as Cu-Aβ has a much lower redox potential than either of the Tyr10 or Met35 residues and is relatively stable to electron transfers from endogenous versions of these residues (Schoneich, C., 2000, Zhao, F., *et al.*, 1997). However, heavy-oxygen isotope studies have shown that the source of oxygen in 2-oxo-histidine formation during MCO is not water but ambient oxygen (Zhao, F., *et al.*, 1997) and this means that the MCO mechanism involves a hydroxyl or peroxy radical and not an electron transfer mechanism (Cooper, 1985).

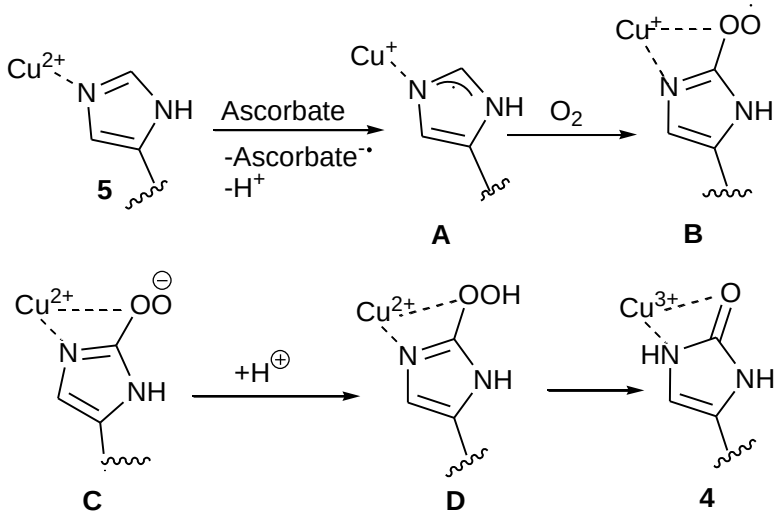

Scheme 1.5: Mechanism of MCO of histidine to 2-oxo-histidine via a hydroperoxy intermedate – a "caged" mechanism. Uchida and Kawakishi propose a mechanism of MCO of histidine **5** to form 2-oxo-histidine **4**, which proceeds via a 2-hydroperoxy intermediate **C** as has been identified by Kurahashi *et al.*, 2002 (Kurahashi, T., *et al*., 2002). This process starts with a one electron transfer from the imidazole to a bound Cu^{2+} ion, leading to a ring radical bound to Cu^{+}. Loss of H^{+} from C-2 leads to the radical intermediate **A.** The His-Cu(I) complex then reacts with molecular oxygen to give the peroxy radical **B.** An electron transfer then occurs from the bound Cu^{+} converting the oxygen radical into an anionic state **C.** This then undergoes a proton transfer to a hydroperoxy species **D**. An oxidation of Cu^{2+} to a Cu^{3+} species and loss of water gives 2-oxo-histidine **4**. In general, copper ions are considered complexed in an azametallacyclic complex (Uchida, K. And Kawakishi, S., 1994, Uchida, K., 2003). For simplicity's sake only the five-membered ring of histidine is shown. In addition, the complex is only shown between Cu^{2+} and imidazole, not ascorbate, water or any buffer salts.

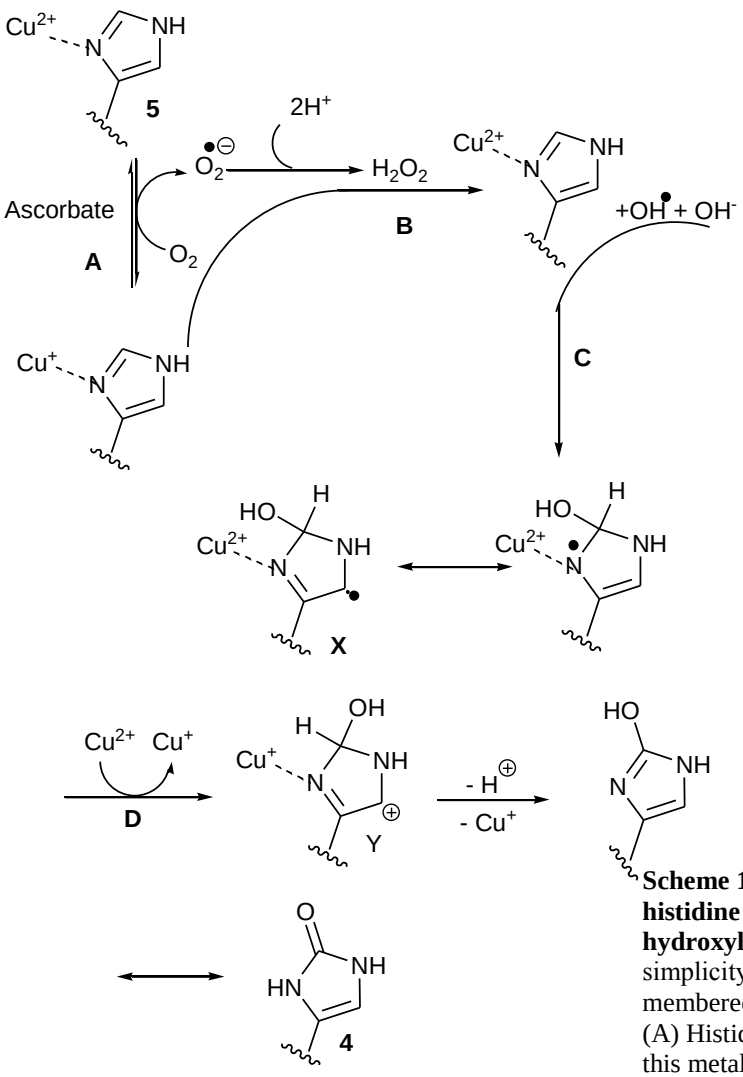

Alternative forms of X and Y:

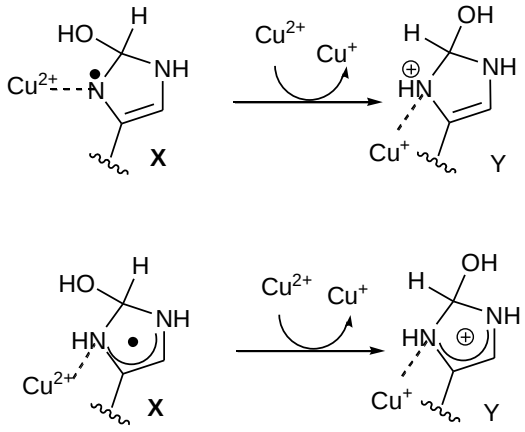

Scheme 1.6: Mechanism of MCO of histidine to 2-oxo-histidine via hydroxyl radical production. For simplicity's sake only the five-membered ring is shown.
(A) Histidine **5** binds a Cu^{2+} ion and this metal is reduced by ascorbate to Cu^{+}.
(B) This then generates a hydroxyl radical by reducing hydrogen peroxide.
(C) The hydroxyl radical attacks the C-2 of histidine giving a hydroxylated histidine radical.
(D) Electron transfer then occurs from this histidine radical to Cu^{2+}, to form 2-oxo-histidine. Cu^{+} then dissociates from 2-oxo-histidine **4** (Schoneich, C., 2000, Schoneich, C., 2000, Hovorka, S. W., 2002).
There is some variation on the intermediates X and Y (Zhao, F., *et al*., 1997, Uchida, K., and Kawakishi, S., 1986, 1989).

The likely physiological effect of Aβ oxidation

Due to the reversible oxidation of methionine this amino acid may act as a scavanger of ROS, preventing them reacting with other targets (Hou, L., *et al.*, 2002, Johansson, A.-S., *et al.*, 2007, Maiti, P., *et al.*, 2010). However, oxidation of histidine is irreversible and therefore can be considered as peptide damage.

The effects of methionine oxidation in Aβ on the peptides solubility, neurotoxicity and fibrillisation has been previously studied using non-radical based H_2O_2 mediated oxidations (Barnham, K. J., *et al.*, 2003, Bitan, G. and Teplow, D. B., 2004, Yan, Y., *et al.*, 2008). Aβ-Met35-Ox has been extensively analysed in the literature and has been found to have increased solubility in aqueous medium and thus dissociation from lipid membranes, to remain in a random coil form and not undergo the transition to alpha helix seen in wild-type Aβ and to not form the toxic paranuclei seen with Aβ(1-42) (see Section 1.2.8.) (Hureau, C. and Faller, P., 2009, Johansson, A.-S., *et al.*, 2007, Naylor, R., *et al.*, 2008, Pike, C. J., *et al.*, 1995, Seilheimer, B., *et al.*, 1997). There is some literature dispute over whether Aβ-Met-Ox is more neurotoxic than wild-type Aβ (Hou, L., *et al.*, 2002, Johansson, A.-S., *et al.*, 2007, Maiti, P., *et al.*, 2010). There is also some literature dispute over whether Aβ-Met-Ox is more likely to fibrillise than normal Aβ (see Chaoter 4). However, in general the effects of Met35 oxidation on Aβ structure and fibrillisation can be easily studied by simply using a non-radical based oxidation system such as H_2O_2, without other residues within the Aβ sequence being oxidised, and this has been done by groups such as Hou *et al.*, Johansson *et al.* and Maiti *et al.* (Sarell, C. J., *et al.*, 2010, Syme, C. D., *et al.*, 2004).

In comparison, histidine cannot be oxidised selectively in the Aβ sequence, without oxidising other residues. Thus this PhD project proposed to synthesise oxidised histidine in a high yielding synthesis with a product which is both enantiomerically pure in the biologically-relevant L-enantiomer form and has appropriate protecting groups for solid peptide synthesis. This oxidised histidine could then be incorporated into the sequence for Aβ(1-42) to generate a form of the peptide where the oxidised residues are solely the three histidine; His6, His13 and His14 (Figure 1.17).

DAEFRH-oxDSGYEVH-oxH-oxQKLVFFAEDVGSNKGAIIGLMVGGVVIA

Figure 1.17: The location of oxidised histidines in solid-phase peptide synthesised Aβ(1-42)-His-ox.

Using literature methods (Gangopadhyay, S., *et al.*, 1992, Garrison, 1987, Hureiki, L., *et al.*, 1994, Karim, E. and Mahanti, M. K., 1992, Laloo, D. and Mahanti, M. K., 1990, Pereira, W. E., *et al.*, 1973, Pinto, I., *et al.*, 1990, Rangappa, K. S., *et al.*, 1998, Satyanarayana, M. V., *et al.*, 1993, Uchida, K. and Kawakishi, S., 1989b, 1990b, Yong, S. H. and Karel, M., 1978), a comparison could then be made between the native Aβ peptide and this synthesised Aβ-His-ox peptide in terms of both secondary structure changes, for example their propensity to refold to the amyloidogenic β-sheet form rather than the native α-helical or random coil form (Sections 1.2.4.), and altered fibrillisation behaviours, both in terms of overall changes in fibrillisation rate, effects on fibrillisation lag times and alterations in either the nucleation or elongation phases of the peptides aggregation behaviour (Sections 1.2.5.). Together this information should give a clearer insight into how histidine oxidation of the Aβ peptide alters the peptides amyloidogenic fibrillising behaviour, thus providing further evidence that oxidation is the elusive trigger of the Amyloid Cascade Hypothesis (see Section 1.3.).This may ultimatedly reveal how oxidation contributes to the aetiology of Alzheimer's Disease.

Chapter 2

ATTEMPTED SYNTHESIS OF 2-OXO-HISTIDINE FROM L-HISTIDINE

2.1. Introduction

Chapter 1 suggested 2-oxo-histidine **4** as the most physiologically relevant form of oxidised histidine in Aβ exposed to metal-catalysed oxidation (MCO). This Chapter, and Chapter 3, will discuss attempts to generate protected, enantiomerically pure 2-oxo-histidine, starting in Chapter 2 with syntheses from L-histidine.

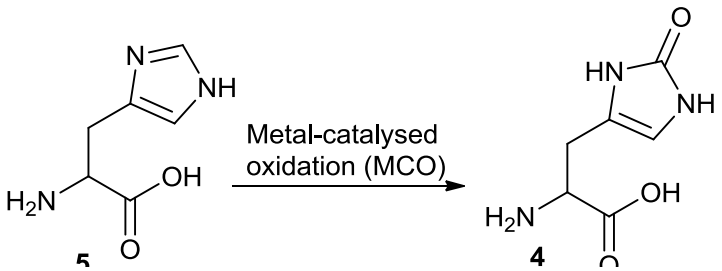

Scheme 2.1: 2-oxo-histidine is the most likely product of metal-catalysed oxidation of histidine.

2.1.1. Literature syntheses of 2-oxo-histidine from L-histidine

Histidine **5** oxidation generally requires harsher conditions, i.e. metal-catalysed or radical-based oxidations, than methionine oxidation, which can be effected by H_2O_2 alone (Tsuji, K., *et al.*, 1992). Histidine **5** exposed to H_2O_2 simply forms 1:1 histidine-hydrogen peroxide hydrogen-bonded adducts, which are crystallise in aqueous solution (Ali, F. E., *et al.*, 2003) and *in vivo* (Uchida, K., 2003).

It was first shown in 1937 by Edlbacher and Segesser that the imidazole of histidine readily decomposes upon aeration with L-ascorbic acid in the presence of trace metals and in doing so generates ammonia (Lewisch, S. A. and Levine, R. L., 1995, Von Edlbacher, S. and Von Segesser, A., 1937). Since then the most commonly quoted synthesis of 2-oxo-histidine in the literature has been the synthesis of *N*(α)-benzoyl protected 2-oxo-histidine **5b** with an aerated Cu^{2+}/Cu^{+}/ ascorbate system (Scheme 2.2(A)) (Meister Winter, G. E. and Butler, A., 1996, Uchida, K. and Kawakishi, S., 1986, 1989, 1993). This is a metal-catalysed oxidation (MCO) which is mirrored by oxidising conditions in the Alzheimer's brain (Ali, F. E., *et al.*, 2003, Schoneich, C. and Williams, T. D., 2003).

A relatively recent literature synthesis of 2-oxo-histidine is that described by Saladino *et al* (Scheme 2.2(B)). They reported that the relatively mild oxidant dimethyldioxirane (DMDO) could be applied to *N*(α)-Boc protected histidine methyl ester **5a** to generate *N*(α)-Boc-His-OMe **4a** (Saladino, R., *et al.*, 1999). This synthesis

was reported to have higher yields than MCO - 59 % compared to 0.1 % (Lewisch, S. A. and Levine, R. L., 1995) - and has other advantages such as allowing use of the relatively manipulative and protein synthesis friendly Boc protecting groups (see Section 2.1.2.) due to the use of non-acidic oxidising conditions and without the requirement for ion exchange chromatography for product purification. Therefore, this PhD project began by attempting to replicate this reported synthesis of *N*(α)-Boc-His-OMe **4a** using DMDO.

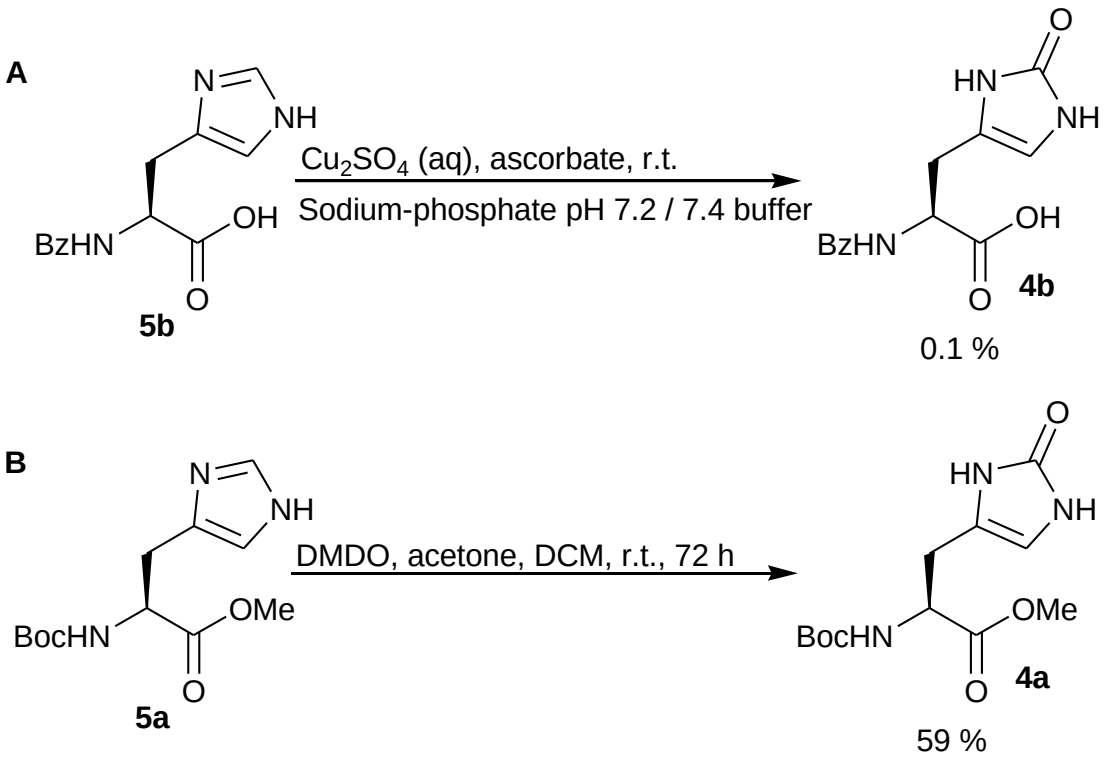

Scheme 2.2: Literature syntheses of 2-oxo-histidine. (A) The most common synthesis in the literature is an oxidation of *N*(α)-Bz-His-OH **5b** with a Cu^{2+}/Cu^{+}/ascorbate system. However, the yields of *N*(α)-Bz-2-oxo-His-OH **4b** are low i.e. ~0.1 % (Uchida, K. and Kawakishi, S., 1989). **(B)** Saladino *et al*. report a synthesis of *N*(α)-Boc-2-oxo-His-OMe **4a** using DMDO, with significantly higher yields reported i.e. 59 % (Saladino, R., *et al.*, 1999).

2.1.2. Incorporation of 2-oxo-histidine into the Aβ sequence

For this PhD, once 2-oxo-histidine was synthesised, the initial plan was to incorporate this into the Aβ (1-42) sequence at positions 6, 13 and 14. The resulting peptide could then be used to study the effects of histidine-only oxidation on the structure and fibrillisation behaviour of Aβ.

There are certain considerations that should be made when synthesising 2-oxo-histidine **4** for use in solid phase synthesis of Aβ(1-42) because Aβ is a "difficult sequence" (Tickler, A. K., *et al.*, 2004). Its highly hydrophobic *C*-terminus increases its tendency to aggregate, leading to the fully synthesised peptide being insoluble. This aggregation inhibits coupling, deprotection steps and purification during peptide synthesis (Lewisch, S. A. and Levine, R. L., 1995). There are certain solutions for these problems and these are presented in Figure 2.1, although some modifications involving basic conditions may not be suitable for 2-oxo-histidine **4** (see Chapter 1 Section 1.5.3.) (Bladon, C. M., 1990). In general they aim to prevent hydrophobic interactions and acidic conditions near the peptide's pI. For the same reason, one of the most important solutions to consider is the use of Boc groups rather than traditional Fmoc groups to protect the *N*(α) of coupling amino acids, as the basic conditions used to deprotect Fmoc groups are likely to degrade 2-oxo-histidine **4**. However, as orthogonal protection is required of the *N*(α) and *N*(τ)/*N*(π) groups, the use of Boc groups as the *N*(α)-protecting group would require groups on the ring nitrogens that are not labile in the presence of TFA e.g. benzyloxymethyl (BOM), and these are not compatible with solid-phase synthesis. Therefore, more investigation into potential ring nitrogen protecting groups is required. The side-chain of 2-oxo-histidine **4** would require protecting and this could be done with *O*-alkyl groups as these would remove the electrophilic carbonyl group and hence increase amino acid stability under the basic conditions of solid phase peptide synthesis.

It was proposed to do a model synthesis with a short histidine-containing peptide e.g. thyrotropin releasing hormone (TRH; *p*Glu-His-Pro-NH_2) (Figure 2.2) before synthesis of the full Aβ(1-42) peptide is attempted . This would allow conditions to be established for oxo-histidine manipulations in solid phase peptide synthesis, with a central histidine residue exposed to both amino and carboxyl coupling conditions.

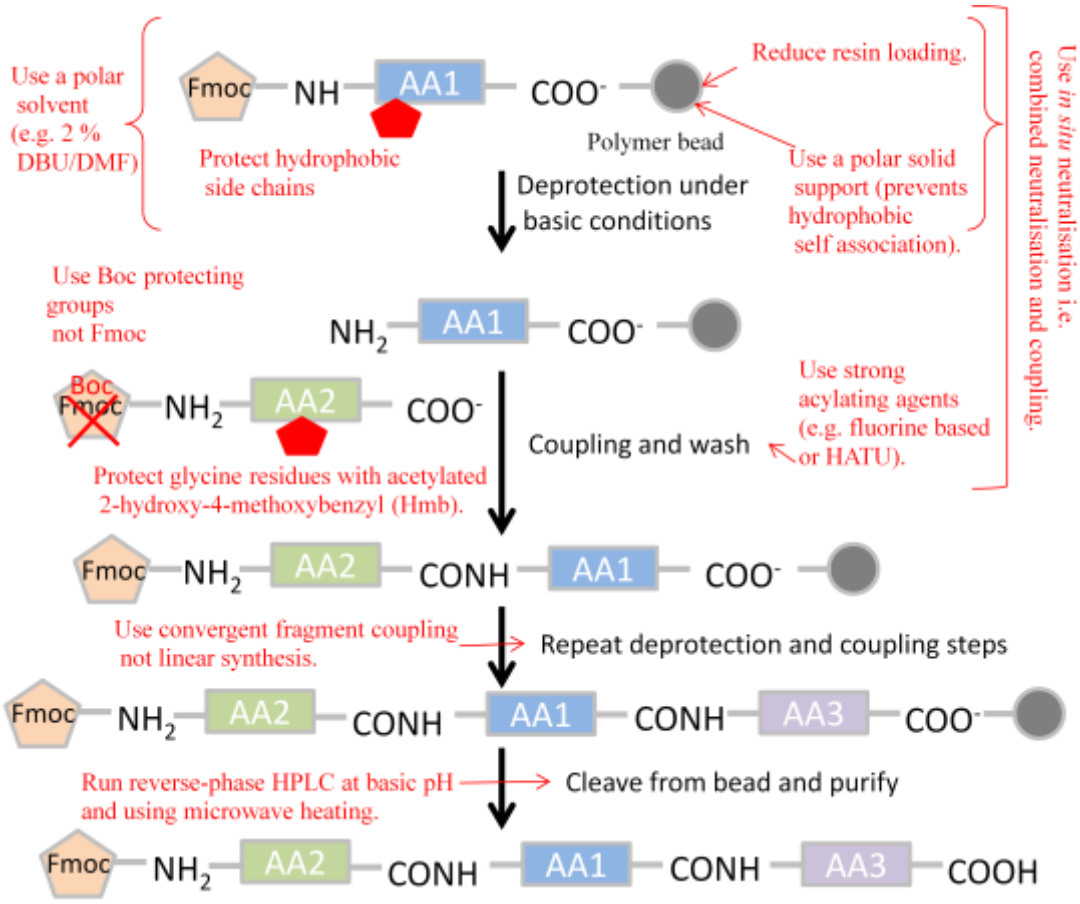

Figure 2.1: Optimising solid phase peptide synthesis for amyloidogenic peptides.

The scheme above illustrates the general steps behind solid phase peptide synthesis. Illustrated in red are the possible modifications put forward in the literature for improving syntheses of "difficult peptides" such as amyloidogenic peptides. In addition, instead of traditional solid phase synthesis, O-acyl isopeptides which undergo an *O-N* intramolecular acyl migration to form the correct peptide sequence, can be used. (Bailey, P. D., 1992, Barrow, C. and Zagorski, M., 1991, Barrow, C. J., 1999, Barrow, C. J., *et al.*, 1992, Blennow, K., *et al.*, 2006, Chan, W. C. and White, P. D., 2004, Clippingdale, A. B., *et al.*, 1999, Cohen-Anisfeld, S. T. and Lansbury, P. T., 1993, Colombo, R., *et al.*, 1984, Fukuda, H., *et al.*, 1999, He, W. and Barrow, C. J., 1999, Hendrix, J. C., *et al.*, 1992, Jobling, M., *et al.*, 1999, Kim, Y. S., *et al.*, 2004, Liu, S. T., *et al.*, 1999, Milton, N. G., 1999, Murakami, K., *et al.*, 2003, Quibell, M., *et al.*, 1994, 1995, Sampson, W. R., *et al.*, 1999, Sohma, Y., *et al.*, 2005, Tickler, A. K. and Wade, J. D., 2001, Wade, J. D., *et al.*, 2003).

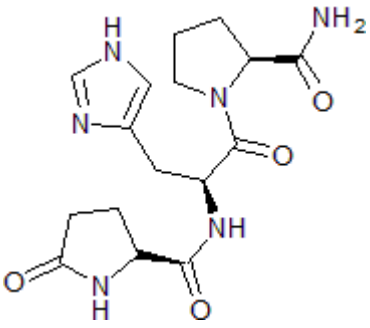

Figure 2.2: Thyrotropin Releasing Hormone (TRH). Thyrotropin Releasing Hormone (TRH) has the amino acid sequence *p*Glu-His-Pro-NH_2). This tripeptide, with histidine in the central position would be ideal for testing the suitability of 2-oxo-histidine **4** and its protecting groups to solid phase peptide synthesis.

2.1.3. Aims

The histidine residues of Aβ are likely oxidised in AD pathology to 2-oxo-histidine **4**. We propose to synthesise a protected, enantiomerically pure form of 2-oxo-histidine **4** for incorporation into the Aβ(1-42) peptide via solid phase peptide synthesis.

This chapter will discuss the initial three synthetic strategies used to approach 2-oxo-histidine 4; all starting from L-histidine. The first two were oxidations using either dimethyldioxirane (DMDO) or a metal-catalysed oxidation (MCO) system, in particular a Cu^{2+}/Cu^{+}-ascorbate system. The third strategy was a Bamberger cleavage of the imidazole ring with subsequent ring closure to include a carbonyl group at C-2.

2.2. Results

L-histidine **5** is a good starting material for the synthesis of 2-oxo-histidine **4** for several reasons. It is readily available and can be purchased as the pure L-enantiomer, thus preventing the need to induce chirality at a later stage. In addition, synthesis from L-histidine **4** has the advantage over *de novo* syntheses, such as those described in Chapter 3, of having fewer synthetic steps, as the amino acid functionality is already present and the side-chain is almost identical to that of the product.

2.2.1. Synthesis of protected histidine derivatives

The two oxidations of L-histidine, which were originally attempted for this thesis - dimethyldioxirane (DMDO)-mediated oxidation and metal-catalysed oxidation (MCO) – started from protected forms of L-histidine as starting materials. The protecting groups chosen for this required a compromise between being able to survive the conditions of oxidation and still being able to be removed to prepare the oxidised amino acid for peptide synthesis. The following two sections explain the choices of the protecting groups and describe protecting procedures.

*Synthesis of N(α)-Boc-His-OMe **5a***

The attempted DMDO-mediated oxidations of L-histidine (Section 2.2.2.) used a histidine derivative protected at the carboxy-terminus with a methyl ester and at the amino terminus with a *tert*-butyloxycarbonyl (Boc) group. This is denoted *N*(α)-Boc-His-OMe **5a** in this thesis.

Boc groups have the advantage over many other protecting groups in that they are easy to remove upon dissolution in trifluoroacetic acid (TFA), mineral acids or LiBr in MeCN (Hernandez, J. N., *et al.*, 2003), although a cation scavenger is often required (Wuts, P. G. M. and Greene, T. W., 2006). The majority of these cleavage methods do not induce racemisation, unlike for other protecting groups, which use alkaline hydrolysis (Hernandez, J. N., *et al.*, 2003). Boc groups are also less susceptible to nucleophilic attack than protecting groups such as methyl esters (Wuts, P. G. M. and Greene, T. W., 2006), thus allowing ester hydrolysis to be

performed whilst retaining the Boc group. As mentioned in Figure 2.1, they have been shown to increase yields of Aβ synthesis and reduce the likelihood of this peptide undergoing a conformational change to the highly aggregating β-sheet form.

Their disadvantage is their high sensitivity to mineral acids and some organic acids, which makes purification methods such as ion-exchange chromatography difficult for amino acids thus protected. This sensitivity also makes it more likely Boc groups will degrade under acidic oxidising conditions, meaning that they can only be used with basic or neutral oxidants such as DMDO.

A methyl ester was added to the carboxy terminus of L-Histidine hydrochloride **5e** using thionyl chloride and methanol under reflux, to form HisOMe.2HCl **5c** before Boc-protection. Methyl esters have the advantage of being easily removed by acid/base catalysed hydrolysis. However, this property does make them sensitive to hydrolysis in non-neutral aqueous conditions and can lead to histidine racemisation, hence protection of the amino nitrogen is required.

This project compared two methods (Scheme 2.3) for synthesis of *N*(α)-Boc-His-OMe **5a**:

1) A one-step synthesis starting from HisOMe·2HCl **5c**.
2) A two-step synthesis; first protecting HisOMe·2HCl **5c** to form *N*(α), *N*(τ)-DiBoc-His-OMe **5d** and then deprotecting this to form *N*(α)-Boc-His-OMe **5a**.

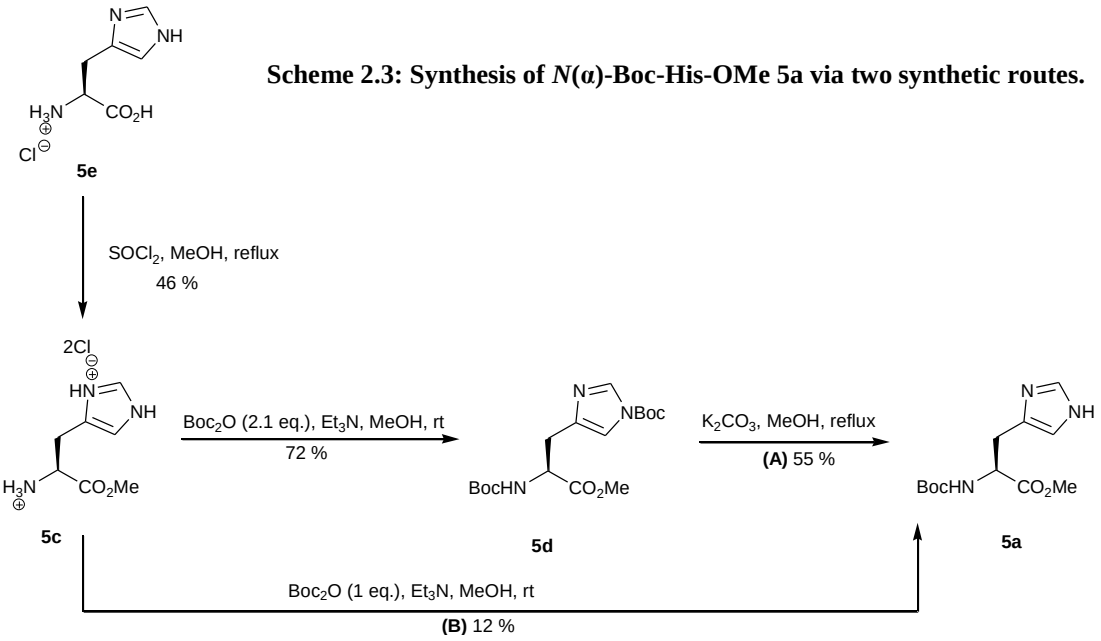

Scheme 2.3: Synthesis of *N*(α)-Boc-His-OMe 5a via two synthetic routes.

The latter was found to be higher yielding, despite the extra synthesis step, at 40 % relative to 12 %.

For the synthesis from HisOMe·2HCl **5c** we chose a protection using Boc anhydride and the base triethylamine in methanol, similar to that used by Brown *et al.* (Brown, T., *et al.*, 1982). There are alternative methods, as described by Hanford *et al.*, which use a base such as pyridine to generate the free base before adding Boc anhydride (Hanford, B. O., *et al.*, 1968). However, these methods tend to generate a mixture of mono-Boc and di-Boc protected histidine and thus require extra purification.

For the synthesis from *N*(α), *N*(τ)-DiBoc-His-OMe **5d** the method chosen was that of Dancer *et al.*, which uses potassium carbonate in hot methanol to selectively remove the *N*(τ)-Boc group with methanolysis (Dancer, J., *et al.*, 1996). Alternative methods for Boc removal tend not to be selective and remove both Boc groups, such as the use of dry HCl acidolysis (Gibson, F. S., *et al.*, 1994).

A successful synthesis of *N*(α)-Boc-His-OMe **5a** from both synthetic methods was indicated from ^{1}H-NMR data showing the methyl ester as a downfield methyl singlet at *ca* δ_H 3.70 and showing the presence of the Boc group as a nine proton singlet at δ_H 1.41 and a urethane carbonyl peak at *ca* 1700 cm^{-1} in the IR spectrum. However, due to the difference in yields the method starting from *N*(α), *N*(τ)-DiBoc-His-OMe **5d** was employed for further syntheses.

*Synthesis of N(α)-Bz-His-OH **5b***

Benzoyl protected histidine (*N*(α)- Bz-His-OH) **5b** was used for the attempted metal-catalysed oxidations of L-histidine **5**. Apart from their relative stability to hydrolysis, benzoyl groups have the advantage over Boc groups of being crystalline, easing product purification and characterisation. They also provide a chromophore which aids analysis of oxidation products by UV absorption.

One major disadvantage of benzoyl groups is the difficulty in removing them, which often requires quite strongly acidic hydrolysis. However, as 2-oxo-histidine **4** had been reported as stable to acid environments, this should not present a problem for this synthesis (Meister Winter, G. E. and Butler, A., 1996).

N(α)-Bz-His-OH **5b** was synthesised using the method shown in Scheme 2.4 using the protecting reagent benzoyl chloride and the base sodium bicarbonate. The successful protection was shown by the presence of a five proton multiplet at δ_H 7.68 - 7.79 and a melting point (243 °C) consistent with that reported in the literature (Otani, T. T. and Briley, M. R., 1979).

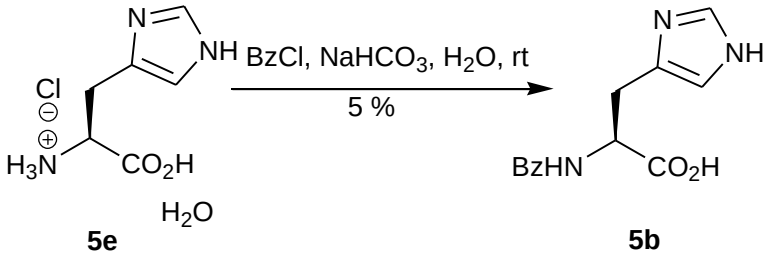

5e **5b**

Scheme 2.4: Synthesis of *N*(α)-Bz-His-OH 5b.

2.2.2. Attempted Dimethyldioxirane (DMDO)-mediated oxidation of *N*(α)-Boc-His-OMe **5a**

*Synthesising dimethyldioxirane (DMDO) **21***

Dimethyldioxirane (DMDO) **21** is a mild, selective oxidant derived from acetone (Curi, D., *et al.*, 1999). Due to its electrophilic nature it can be used to insert oxygen into unactivated C-H bonds at ambient temperatures, without the need for metal ions, within short reaction times and with good yields (Simakov, P. A., *et al.*, 1998). It has selectivity for side chains of protected amino acids as opposed to α-C-H bonds,

despite the latter having a lower dissociation energy, because the reaction is favoured by electron donating substituents on the C-H (Saladino, R., *et al.*, 1999). In general, a solvent with high polarity is required to promote the reaction (Shustov, G. V. and Rauk, A., 1998).

One advantage of using DMDO to oxidise protected histidine derivatives is that the only reagent is DMDO and the only major side-product is acetone, although dangerous peroxy species are possible by-products. However, it is not considered particularly harmful to the environment and can be prepared from commercially readily-available reagents (Curi, D., *et al.*, 1999). In addition, it can react in neutral solvents (Curi, D., *et al.*, 1999). DMDO is relatively mild and thus unlikely to affect the protecting groups.

One downside is that DMDO is unstable, due to fast radical-chain decomposition (Bravo, A., *et al.*, 1998), and thus requires synthesis almost immediately before the oxidation reaction. Although one-pot syntheses combining DMDO synthesis and DMDO-mediated oxidation are reported (Murray, R. W. and Singh, M., 1998), we chose a separate synthesis of DMDO using a simple vacuum distillation method described by Adam *et al.* because of the low solubility of oxone in acetone, the possibility of remaining oxone degrading DMDO to acetone, dioxygen and sulphates (Curi, D., *et al.*, 1999) and the reported higher yield obtained using this synthetic method (Adam, W., *et al.*, 1991). Despite other groups using quite elaborate distillation apparatus (Murray, R. W. and Singh, M., 1998), Adam *et al.* have argued against the need for high efficiency condensers and helium atmospheres (Adam, W., *et al.*, 1991). Our method differed from Adam *et al.*'s only in the use of a room temperature vacuum distillation as opposed to one at 15 °C.

The synthesis of DMDO is quite low yielding, i.e. 5 % (Bravo, A., *et al.*, 1998) as it suffers from the competing Baeyer-Villiger oxidation, especially at high pH (Scheme 2.5) (Curi, D., *et al.*, 1999). Using an iodine/thiosulfate back titration the concentration of the final solution of DMDO in acetone obtained in this project was determined to be 40 mM, which indicated a 1.7 % yield.

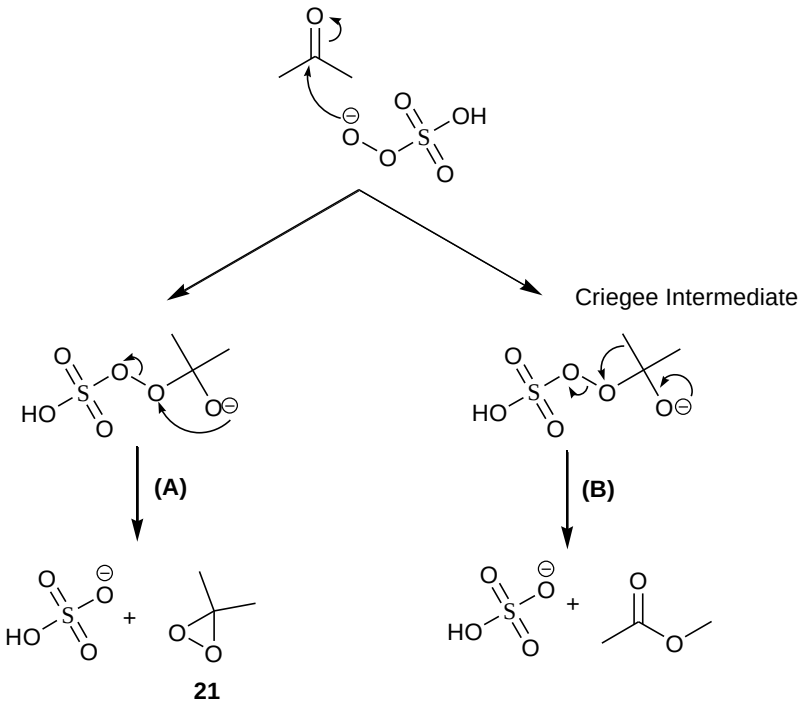

Scheme 2.5: Mechanisms of DMDO 21 synthesis from acetone and potassium peroxymonosulfate and the competing Baeyer-Villiger reaction. Acetone and potassium peroxymonosulfate will combine to form a Criegee intermediate. This can either undergo cyclisation to DMDO **21** (**A**) or can undergo the Baeyer-Villiger reaction (**B**)**.** This competing reaction explains the low yields obtained during DMDO synthesis.

*Attempted oxidation of L-histidine with DMDO **21***

Despite the low yield of DMDO synthesised we expected a moderately high yield of the subsequent protected 2-oxo-histidine as described by Saladino *et al.*, who reported a 59 % yield of *N*(α)-Boc-2-oxo-His-OMe **4a** from *N*(α)-Boc-His-OMe **5a** using DMDO (Saladino, R., *et al.*, 1999). We repeated Saladino *et al.*'s synthesis on a scale of 1.2 mmol of *N*(α)-Boc-His-OMe **5a** as starting material, also at room temperature, but for only 12 h as opposed to 3 days, since after this time TLC analysis indicated the starting material was no longer present. We also used 10 mol. eq. DMDO in acetone as opposed to 2.5 mol. eq. and used acetone exclusively whereas Saladino *et al.* used a small volume of DCM in addition. However, instead of forming *N*(α)-Boc-2-oxo-His-OMe **4a**, we formed a complex mixture of oxidation products.

In general, 2-oxo-histidine **4** formation from L-histidine **5** is indicated from NMR data by the loss of the imidazole H-2, or a broadening of the signal here if the enol tautomer is stabilised, and with the shift of the imidazole H-4 protons from

approximately δ_H 7.2 to approximately δ_H 6.3 (Lam, A. K. Y., *et al.*, 2010, Meister Winter, G. E. and Butler, A., 1996, Uchida, K. and Kawakishi, S., 1989). ^{13}C-NMR data are available from similar compounds containing the imidazoline-2-one structure, e.g. the citronamides (Figure 2.3, **14**), with C-2 resonance at δ_H 154.7 and C-4 resonance at δ_C 107.3 (Carroll, A. R., *et al.*, 2009).

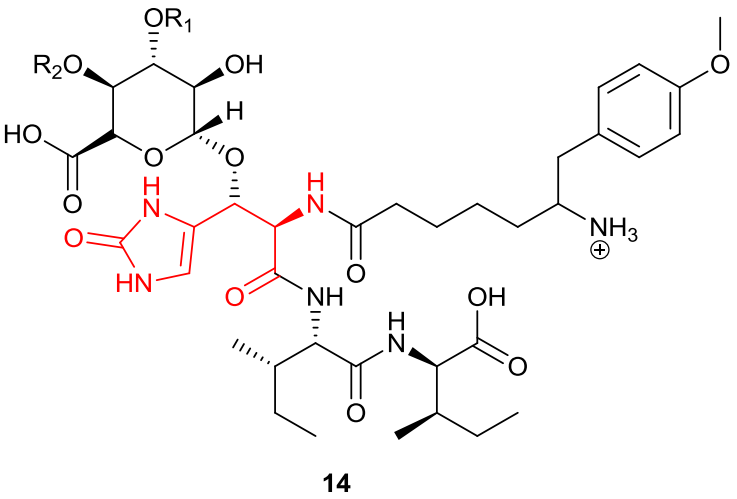

14

Figure 2.3: Citronamide 14 with a 2-oxo-histidine-type functionality. Carroll *et al.* isolated two citronamides **14** which contained a 2-oxo-histidine-type functionality, shown in red. The ^{13}C-NMR resonances detected for C-2 was δ_C 154.7 and for C-4 resonance δ_C 107.3 (Carroll, A. R., *et al.*, 2009).

In particular two compounds were isolated following flash chromatography both of which incorporated the isopropylidene groups seen in acetone and DMDO at C-2; a C-5 oxygen adduct **22** and its formylated intermediate **23c** (Scheme 2.6). We attempted the oxidation using two different reaction conditions; 12 h at room temperature or 27 h at 2 °C. In case the products were not stable at room temperature. The former produced only the non-formylated compound **22** whereas the combination of colder conditions and longer reaction times produced both products.

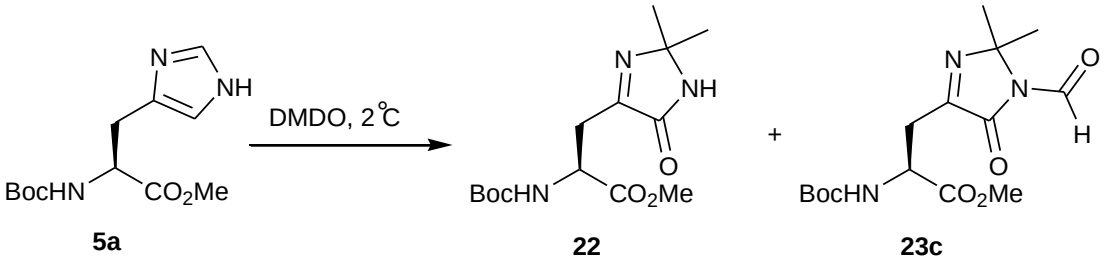

5a **22** **23c**

Scheme 2.6: DMDO-mediated oxidation of *N*(α)-Boc-His-OMe 5a yielded two compounds. Compound **22** was isolated from both DMDO oxidation attempts on *N*(α)-Boc-His-OMe (**5a**) and was determined as the structure above. Compound **23c** was only isolated from the reaction at 2 °C over 27 h. The structure is an *N*-formylated derivative of compound **22**.

The structure of the 5-oxo derivative **22** was proposed based on ^{1}H-NMR (Figure 2.4), ^{13}C-NMR (Figure 2.5), DEPT-135, HSQC (Figure 2.6) and COSY data and EI-MS data. The amino acid backbone was still present as shown by the presence of diastereotopic β-CH_2 protons at δ_H 3.00 and δ_H 3.07 (Figure 2.4), with the β-C at δ_C 30.8 (Figure 2.5), and a multiplet α-CH resonance at δ_H 4.71-4.79 (Figure 2.4) and an α-C resonance at δ_C 51.1 (Figure 2.5). The protecting groups remained intact with *t*-Bu CH_3 peaks at δ_H 1.44, δ_C 28.3, and methyl ester CH_3 peaks at δ_H 3.72 and δ_C 52.4. The H-2 peak of the starting material, *ca* δ_H 7.55, is also no longer present and instead, the isopropylidene group is indicated by the ^{1}H-NMR spectrum (Figure 2.4), with two peaks at δ_H 1.45 and δ_H 1.46 and from the ^{13}C-NMR with resonances at δ_C 26.7 and δ_C 27.0 (Figure 2.5). The ^{1}H-NMR spectrum (Figure 2.4) also reveals the loss of the imidazole ring protons on the 5-carbon (δ_H 6.79). There are three carbonyl peaks (δ_C 155.4, 165.0, 171.7), indicating the additional of a carbonyl relative to the starting material (Figure 2.5). Finally, a NH peak at δ_H 7.65 indicates the stabilization of the original imidazole tautomerism.

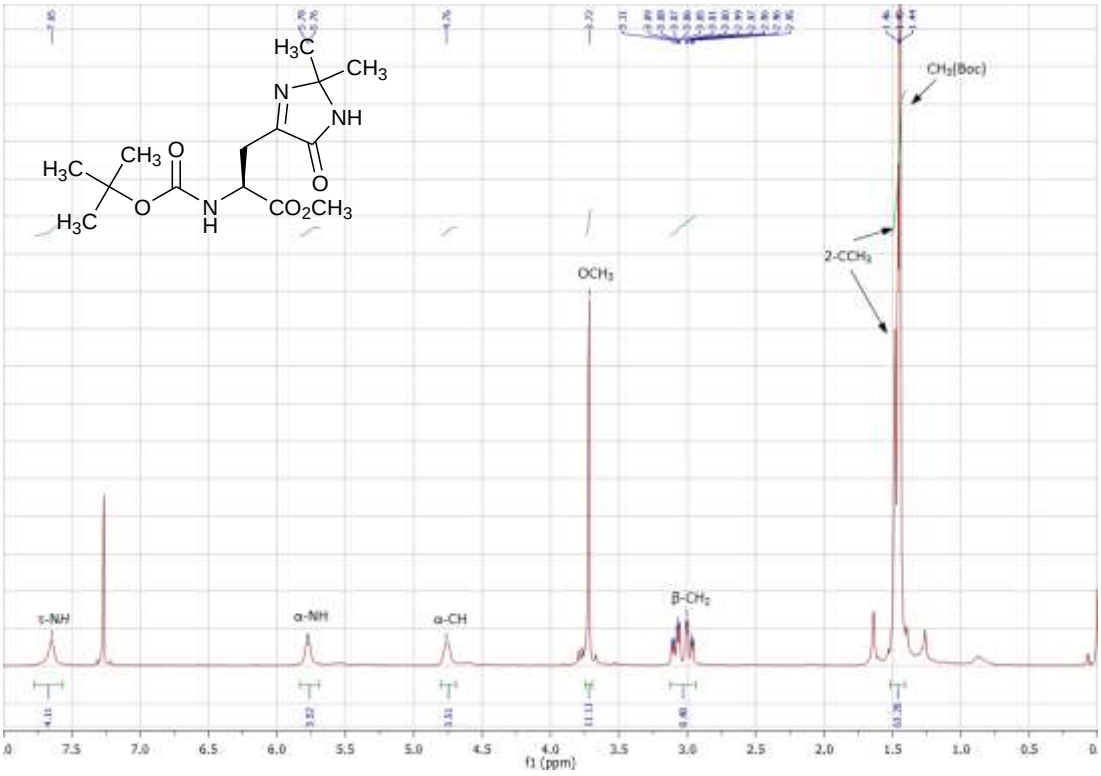

Figure 2.4: ^{1}H-NMR (400 MHz, $CDCl_3$) spectrum of 2-Boc-amino-3-(2,2,-dimethyl-5-oxo-2,5-dihydro-1*H*-imidazol-4-yl)-propionic acid methyl ester 22.

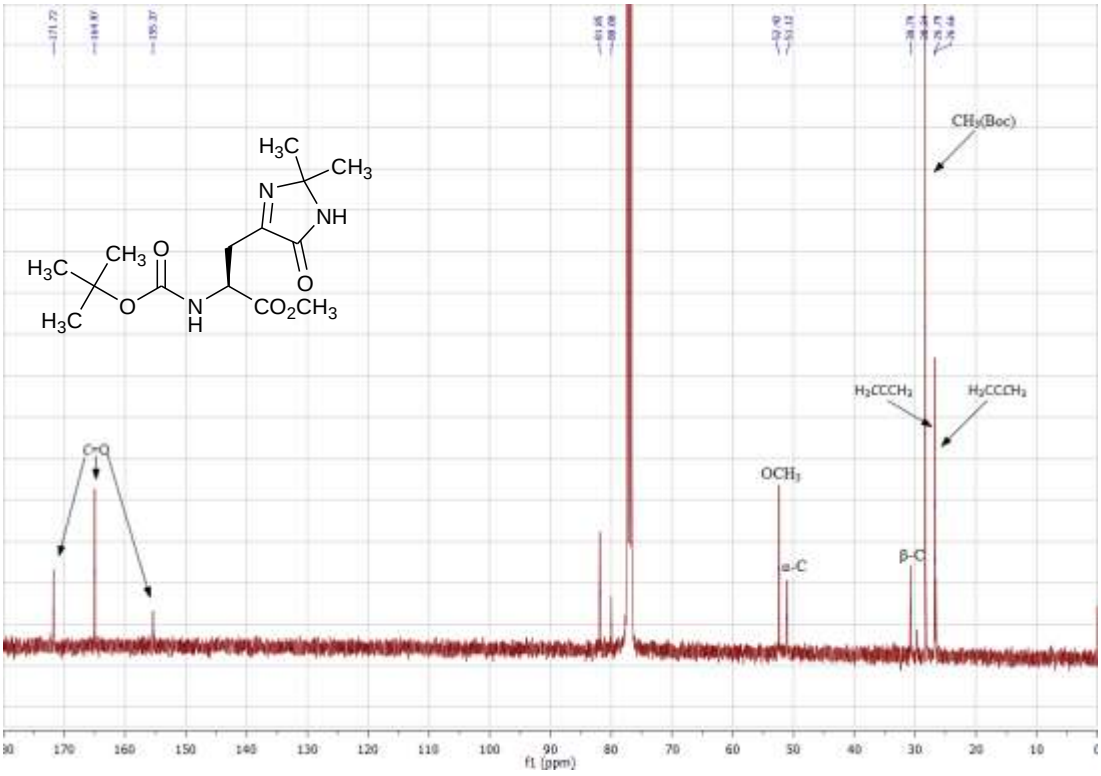

Figure 2.5: ^{13}C-NMR (100.65 MHz, $CDCl_3$) spectrum of 2-Boc-amino-3-(2,2,-dimethyl-5-oxo-2,5-dihydro-1*H*-imidazol-4-yl)-propionic acid methyl ester 22.

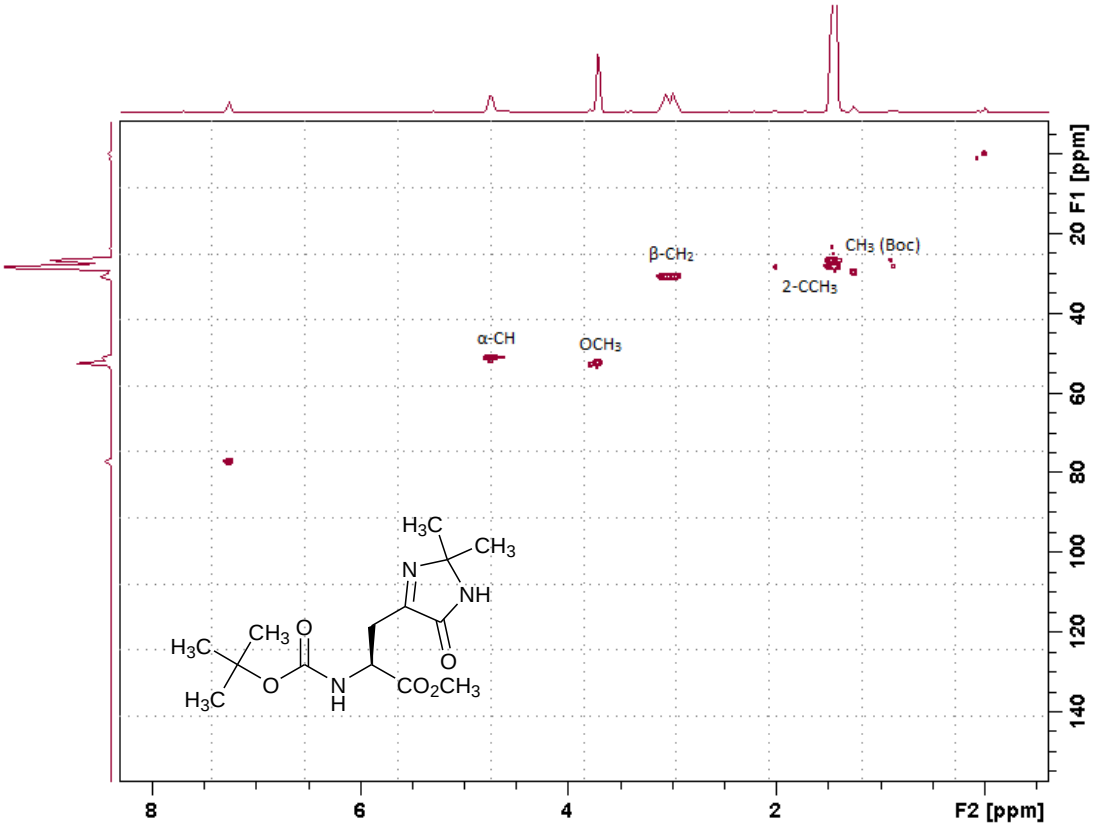

Figure 2.6: ^{1}H – ^{13}C HSQC (δ_H(400 MHz, $CDCl_3$), δ_C(100.65 MHz, $CDCl_3$)) NMR spectrum of 2-Boc-amino-3-(2,2,-dimethyl-5-oxo-2,5-dihydro-1*H*-imidazol-4-yl)-propionic acid methyl ester 22.

The EI-MS data reveals a molecule of mass 314.1713, which is consistent with the addition of the isopropylidene group of DMDO and an oxygen atom with the subsequent loss of two hydrogen atoms, likely the two ring protons. There is one problem with this structure and that is the ^{13}C-NMR spectrum (Figure 2.5) is missing a carbon environment, in particular the imine C-4 of the ring system in structure **22**. However, this carbon is present based on the mass spectrometry data for this compound and thus is suspected to unseen in the ^{13}C-NMR data due to peak overlap.

Compound **23** was analysed using ^{1}H-NMR (Figure 2.7), ^{13}C-NMR (Figure 2.8), DEPT-135, HSQC and COSY (Figure 2.9) data, ESI-MS data and FT-IR and from this data several structures were proposed (Scheme 2.7).

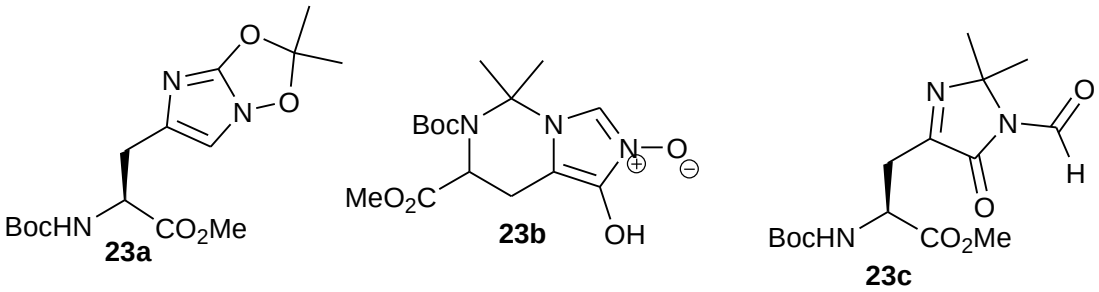

Scheme 2.7: Possible structures proposed for compound 23.

As for **22**, peaks can be seen for the amino acid backbone and protecting groups. Two methyl groups neighbouring a quaternary carbon are indicated with ^{1}H-NMR peaks at δ_H 1.61 and δ_H 1.62 (Figure 2.7) along with ^{13}C-NMR peaks at δ_C 24.6 and δ_C 24.8 (Figure 2.8) indicative of an isopropylidene group. The EI-MS data indicate a molecular weight of 342.1663, which corresponds to a molecular formula of $C_{15}H_{23}N_3O_6$. This suggested addition of a whole DMDO molecule to *N*(α)-Boc-His-OMe and the loss of two hydrogen atoms with an extra carbon and oxygen incorporated into the structure compared to compound **22.**

The first structure proposed was **23a**. This had the correct molecular formula, incorporated the isopropylidene groups and showed the clear addition of the DMDO molecule as part of a bicyclic system. However, the quaternary carbon of this group did not have a corresponding downfield ^{13}C-NMR peak (Figure 2.8) for its positioning between two oxygens and therefore this carbon was deemed to be between two nitrogens as shown in structure **23b** and **23c**.

The second structure proposed was **23b.** The chemical shift of the proton at δ_H 9.02 (Figure 2.7) reveals this is in a very electronegative environment. Hence, it was initially predicted that this was H-2 in a cyanate environment. However, the

COSY data (Figure 2.9) shows coupling between the α-CH and an NH, hence the α-NH cannot be bound in a bicyclic ring system.

Therefore structure **23c** was proposed which is a formyl derivative of structure **22**. This is a proposed product of a side-reaction in the predicted mechanism of the synthesis of compound **22** given in Scheme 2.9. The downfield proton was now predicted to be a formyl proton. The only data disputing this is the lack of an extra carbonyl in the FT-IR data, with the only carbonyls in this structure being the Boc urethane (1706 cm^{-1}) and the carboxylate ester (1750 cm^{-1}). However, this could be due to peak overlap and so structure **23c** is the most likely match for the characterization data.

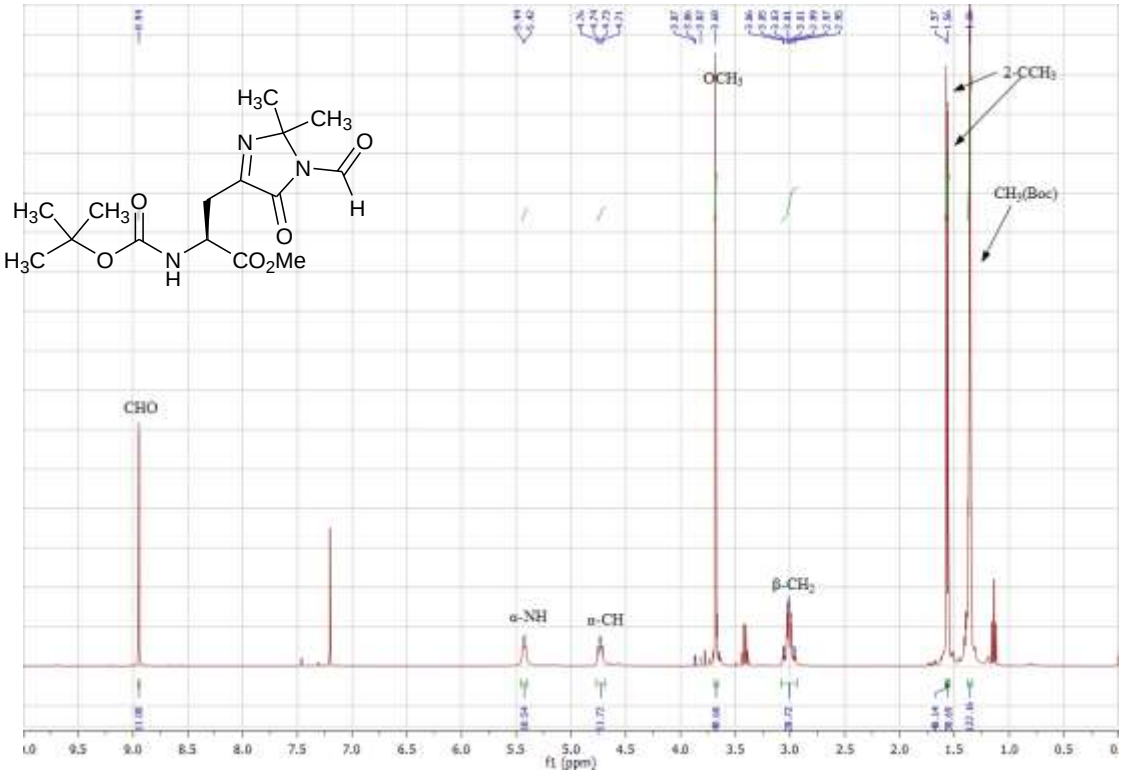

Figure 2.7: ^{1}H-NMR (400 MHz, $CDCl_3$) spectrum of 2-Boc-amino-3-(2,2-dimethyl-5-oxo-2,5-dihydro-1*H*-imidazol-4-yl)-*N*(τ)-formyl-propionic acid methyl ester 23.

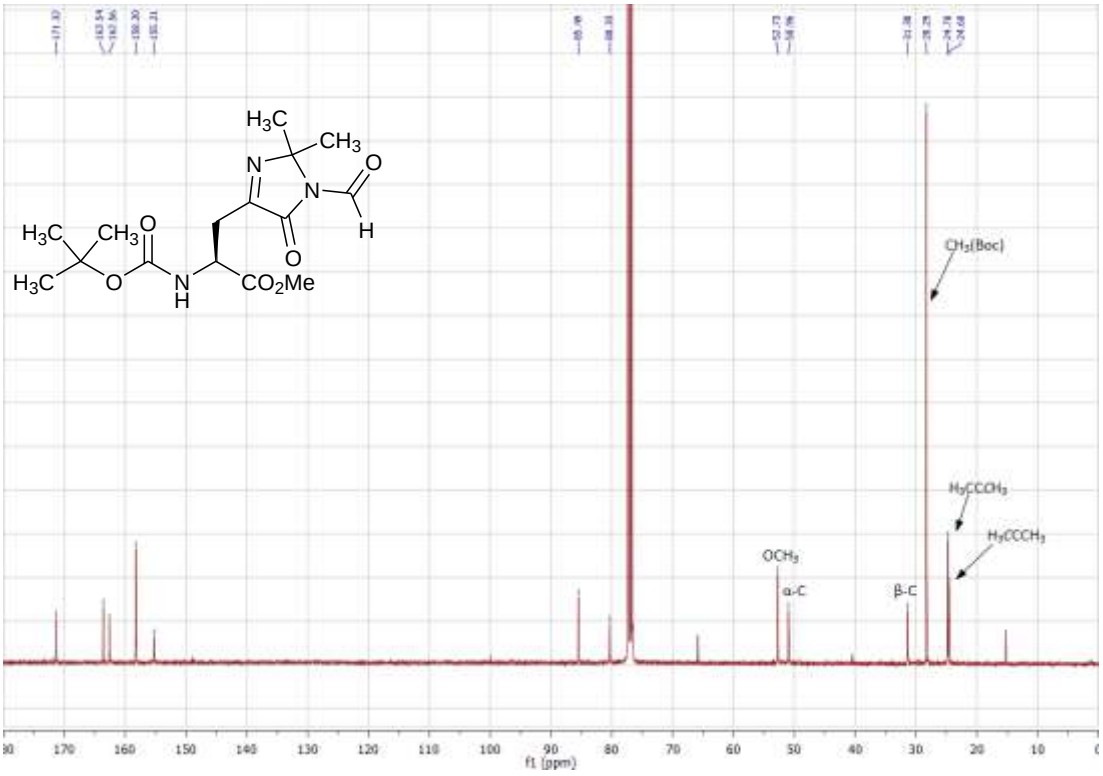

Figure 2.8: ^{13}C-NMR (100.65 MHz, $CDCl_3$) spectrum of 2-Boc-amino-3-(2,2-dimethyl-5-oxo-2,5-dihydro-1*H*-imidazol-4-yl)-*N*(τ)-formyl-propionic acid methyl ester 23.

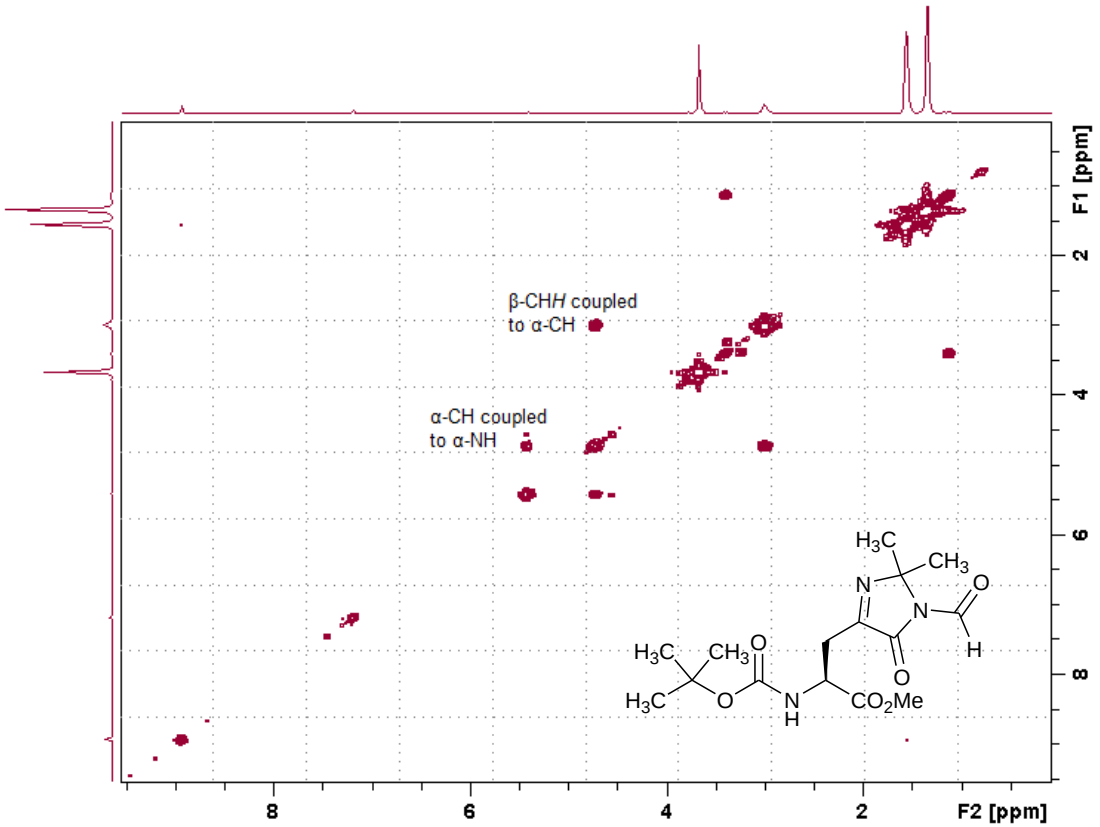

Figure 2.9: ^{1}H – ^{13}C HSQC (δ_H(400 MHz, $CDCl_3$), δ_C(100.65 MHz, $CDCl_3$)) NMR spectrum of 2-Boc-amino-3-(2,2-dimethyl-5-oxo-2,5-dihydro-1*H*-imidazol-4-yl)-*N*(τ)-formyl-propionic acid methyl ester 23.

Studying Saladino *et al.*'s paper more thoroughly reveals that the ^{13}C-NMR data presented by the authors does not match the expected *N*(α)-Boc-2-oxo-His-OMe **4a** structure. For example, despite the two non-carbonyl carbons (C-4 and C-5) of the imidazole ring existing in very similar chemical environments they are denoted as having very different chemical shifts in the paper by Saladino *et al.* i.e. δ_C 158.15 and δ_C 80.39 respectively (Table 2.1). In addition, Saladino *et al.* propose a mechanism that goes via an oxiranyl derivative with subsequent hydrogen shift rearrangement (Saladino, R., *et al.*, 1999). However, this mechanism is proposed in the rest of the literature to be relevant only to DMDO oxidation of fully saturated compounds and thus is unlikely to be applicable to an imidazole ring system which contains alkene and imine-type functionalities. In predicting the likely products of DMDO on imidazole it is probably more helpful to study its action on similar compounds such as benzimidazoles and indoles.

Interestingly, the ^{13}C-NMR data for compound **23c** has very similar peak chemical shifts to the "protected 2-oxo-histidine" product reported by Saladino *et al.* (Table 2.1), with the exception of the lack of isopropylidene peaks at δ_c 24.6 and δ_C 24.8 and the quaternary carbon peak at δ_C 155.2. It may be speculated that this relatively weak peak was present but indistinguishable from noise in the data of Saladino *et al.* and that the upfield peaks were mistaken for solvent peaks, and that in fact the compound synthesised and proposed to be Boc-protected 2-oxo-histidine **5a** by Sala-dino *et al.* is in fact the same as compound **23c**.

Peaks reported by Saladino *et al.*, 1999		**Peaks of compound 23c**	
δ (ppm)	Structure assignment	δ (ppm)	Structure assignment
		24.6	H_3CCCH_3
		24.8	H_3CCCH_3
28.00	$(CH_3)_3$ (Boc)	28.3	$(CH_3)_3$ (Boc)
31.05	β-*C*	31.4	β-*C*
50.70	α-*C*	51.0	α-*C*
52.47	OCH_3	52.7	OCH_3
80.39	$C(CH_3)_3$ (Boc)	80.3	*C*
85.46	*C-4*	85.5	*C*
		155.2	*C*
158.15	*C-5*	158.2	*CH*
162.51	$COOCH_3$	162.6	*C*O
163.50	*C-2*	163.5	*C*O
171.27	$(CH_3)_3COCO$ (Boc)	171.3	*C*O
Structure proposed by Saladino *et al.*		Structure proposed for compound 23	

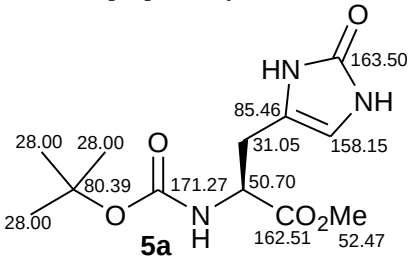

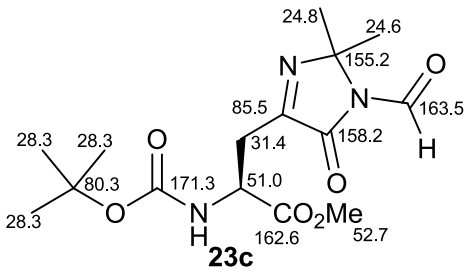

Table 2.1: Comparison of the ^{13}C-NMR peak chemical shifts of Saladino *et al.*'s oxidised histidine product 5a (Saladino, R., *et al.*, 1999) and compound 23c. Proposed assignments are given for each structure.

Literature studies on DMDO oxidation would predict preferable addition across the alkene bond (between C-4 and C-5 in imidazole) and not the semi-imine bond (N=C-2 in imidazole). For example tetrahydrobenzimidazoles undergo a pinacol-like rearrangement to form a 5-imidazolone derivative (Scheme 2.8(A)) (Lovely, C. J., *et al.*, 2004, Sivappa, R., *et al.*, 2007), *N*-acyl indoles undergo epoxide addition across the akylated carbon and the carbon adjacent to the nitrogen leading to indolin-2-ones and indolin-3-ones along with methyleneindolines (Adam, W., *et al.*, 1994, Zhang, X. and Foote, C. S., 1993) (Scheme 2.8(B)) and in carbethoxypyridines and pyrrolidine ene carbamates, DMDO-mediated oxidation leads to epoxide formation across the alkene (Scheme 2.8(E)) (Burgess, L. E., *et al.*, 1996). These all replicate the oxidation of simple enamines, where DMDO oxidises the olefinic carbons equivalent to C-4 and C-5 in imidazole (Adam, W., *et al.*, 1992) (Scheme 2.8(C)).

Addition across alkenes rather than imines, to give imidazol-5-one products, is seen exclusively in these literature procedures due to the relative stability of the carbocation intermediate and this is likely true for the L-histidine derivative used in this PhD project. In indole systems, Zhang *et al.* also found a significant effect of R-substituent on the alkylated carbon on the yields of these three products. For example methyl/ethyl groups on C-3 led to a carbocation forming at the benzylic carbon, which led to aromatic ring conjugation and thus the indolin-2-one. *i*-propyl/*t*-butyl groups on C-2 led to the carbocation at C-2, which led to *N*-stabilisation and thus the indolin-3-one and elimination products (Zhang, X. and Foote, C. S., 1993). Translating to L-histidine this has alkylation on C-4 in the form of a methylene group so oxygen addition would be expected at C-5.

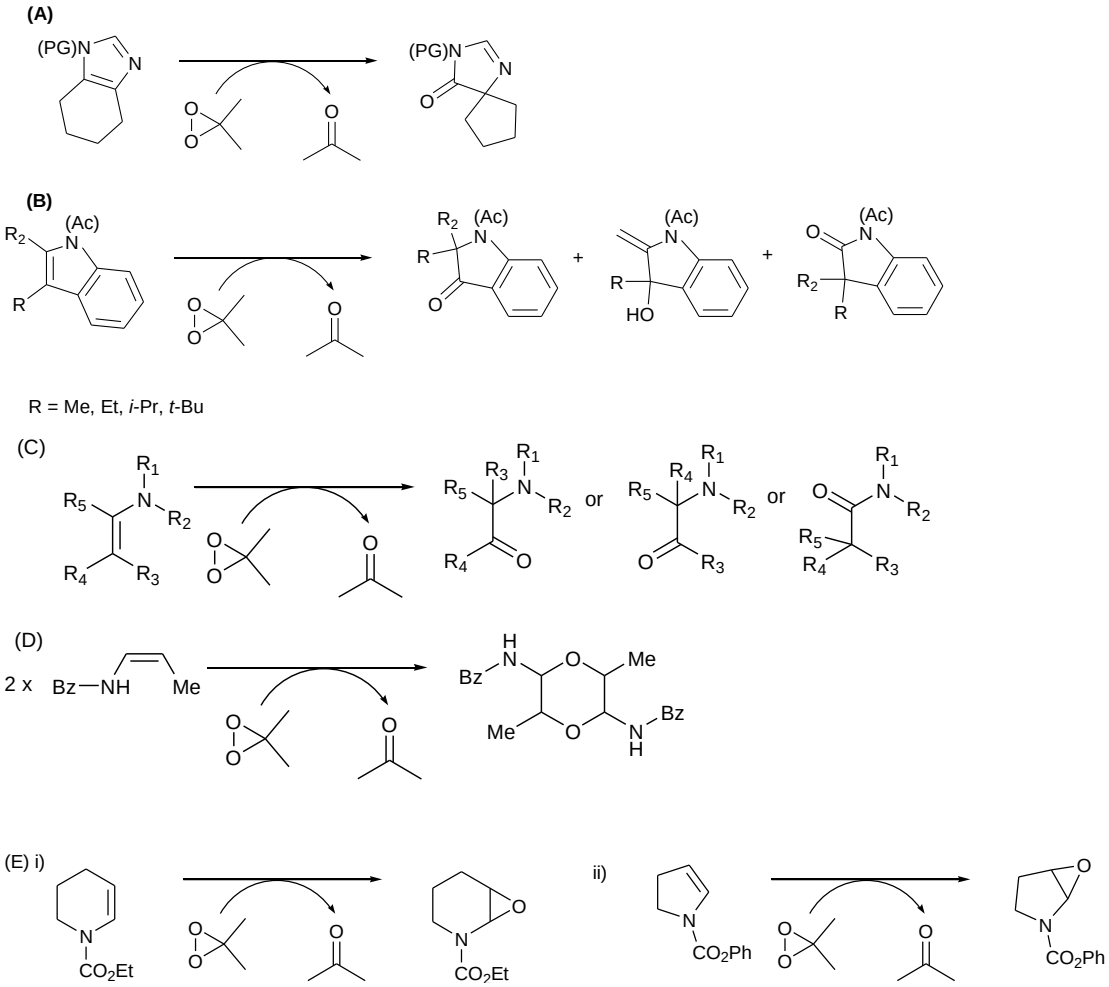

Scheme 2.8: Selectivity of oxygen addition to imidazole-type systems using DMDO. (A) Sivappa *et al.* and Lovely *et al.* studied tetrahydrobenzimidazoles. These react via a pinacol-like rearrangement to form a 5-imidazolone derivative (Lovely, C. J., *et al.*, 2004, Sivappa, R., *et al.*, 2007). (B) Zhang *et al.* and Adam *et al.* studied *N*-acyl indoles (Adam, W., *et al*., 1994, Zhang, X., and Foote, C. S., 1993). (C) Adam *et al.* looked at simple enamines. Products are dependent on R substituents (Adam, W., *et al*., 1992). (D) In a separate study Adam *et al.* found epoxides formed from enamines could dimerise via a zwitteronic intermediate (Adam, W., and Reinhardt, D., 1995). (E) Burgess *et al.* found carbethoxypyridine and pyrrolidine ene carbamates to form epoxides upon addition of DMDO in acetone (Burgess, L. E., *et al.*, 1996).

Therefore, if we accept that DMDO adds oxygen at C-5, as in compound **22** from our synthesis, then the mechanism of this oxidation is likely as shown in Scheme 2.9. The weak O-O bond of DMDO is broken as the 4-C=C-5 double bond undergoes nucleophilic attack of the electron deficient oxygen of DMDO. The resulting zwitterionic species undergoes a hydride transfer from C-5 to C-4 and the formation of a ketone at C-4 to stabilise the resulting positive charge. Ring hydrolysis then follows at C-2 and finally acetone closes the ring with the addition of isopropylidene groups, the last step being similar to that reported by Samsonov *et al.* on cyclohexadiene diamines (Samsonov, V. and Volodarskii, L., 1980). This mechanism does go via an oxidation of C-2 but this product is not stable and is oxidised further. The mechanism in Scheme 2.9 also predicts formation of the formylated structure **23c**, where without the hydrolysis of the formylated intermediate, acetone reacts to form **23c**.

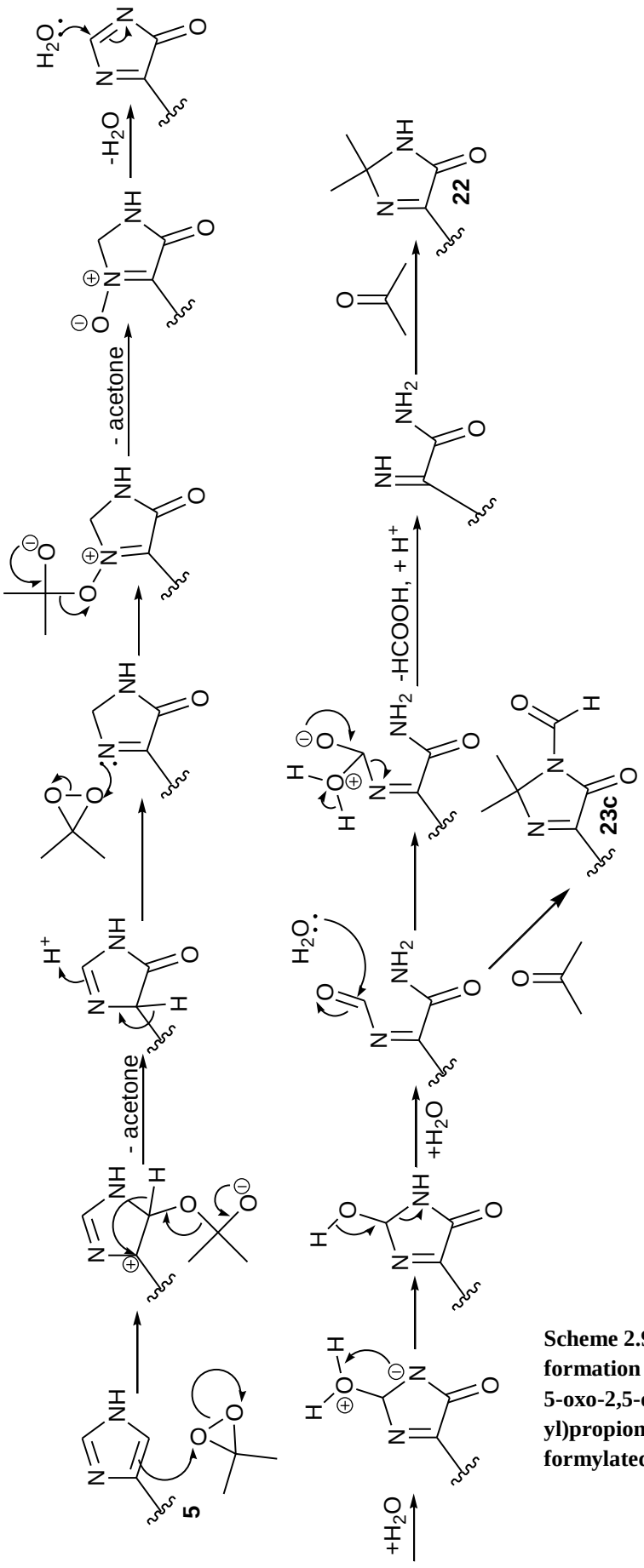

Scheme 2.9: Proposed mechanism for formation of 2-Boc-amino-3-(2,2-dimethyl-5-oxo-2,5-dihydro-1*H*-imidazol-4-yl)propionic acid methyl ester 22 and its formylated derivative 23.

It is possible that other oxygen adducts are formed from the DMDO oxidation of *N*(α)-Boc-His-OMe **5a**, especially in view of the poor yields of **22** and **23** and based on the ^{1}H-NMR of the crude product which showed numerous minor components exhibiting Boc groups, imidazole CH chemical shifts indicating oxygen addition and many vinylic peaks. However, these products may not be stable at room temperature or even at 0 °C. This was found by Zhang *et al.* with their work on DMDO-mediated oxidation of *N*-acylindoles, where many products formed at -78 °C, yet only four were persistent enough to be characterised at 0 °C (Zhang, X. and Foote, C. S., 1993). Therefore, it is predicted that more oxygen adducts may have formed from the DMDO-mediated oxidation of *N*(α)-Boc-His-OMe **5a** but that they were not possible to characterise due to their poor stability at room temperature.

In conclusion, DMDO-mediated oxidation of *N*(α)-Boc-His-OMe **5a**, despite the claims of Saladino *et al.*, is not a feasible synthetic route for generating *N*(α)-Boc-2-oxo-His-OMe **4a** from L-histidine **5**. Instead, the oxidation generates oxygen adducts that add at C-5 in the imidazole ring and which incorporate the isopropylidene groups of either acetone or DMDO.

2.2.3. Attempted Cu(II)/ascorbate metal-catalysed oxidation of *N*(α)-Bz-His-OH **5b**.

The majority of 2-oxo-histidine syntheses reported in the literature start with *N*(α)-Bz-histidine **5b** and use a metal-catalysed oxidation (MCO) using Cu^{2+}/Cu^{+} and either H_2O_2 or ascorbate to oxidise histidine via Fenton's chemistry (Meister Winter, G. E. and Butler, A., 1996, Uchida, K. and Kawakishi, S., 1986, 1989). This is also believed to be the most physiologically relevant mechanism of histidine oxidation (see Chapter 1, Section 1.5.3.).

A consideration to make when using MCO to oxidise L-histidine is that Fenton's reagents react in a highly pH dependent manner, giving the highest yields at neutral to strongly basic pH depending on the environment of histidine, e.g. pH 10.0 for *N*(α)-Bz-His-OH (Uchida, K. and Kawakishi, S., 1990) and pH 7.5 for histidine in glutamine synthetase (Levine, 1983). In general, it is important that the pH of the reaction is greater than pH 6.5, to ensure efficient binding of Cu^{2+} to histidine (Casella, L. and Gulloti, M., 1983, Sarell, C. J., *et al.*, 2009). In addition, at pH 7.4, ascorbate is a better reductant than at lower pHs, (although it may also be a better

antioxidant, see Chapter 1, Section 1.5.3.). The product of MCO on histidine, 2-oxo-histidine **4**, is not stable at greater than pH 8.0 (see Section 2.1.1.) and hence a pH of 7.2 was chosen for this synthesis attempt.

The reaction was carried out at room temperature. Cu^{2+} ions were supplied in the form of $CuSO_4$ and the reducing agent used was ascorbic acid (Scheme 2.10).

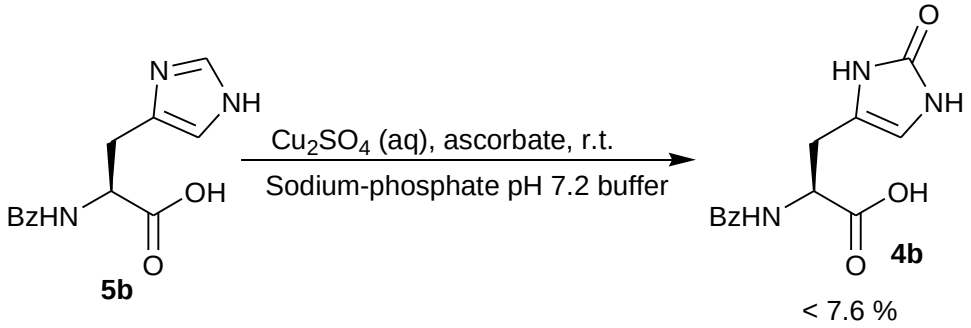

Scheme 2.10: Metal-catalysed oxidation of *N*(α)-Bz-His-OH 5b with a Cu^{2+}/ascorbate system yields *N*(α)-Bz-2-oxo-His-OH 4b in low yield.

We used *N*(α)-Bz-histidine **5b** as the histidine-containing starting material. We found some evidence for the formation of *N*(α)-Bz-2-oxo-histidine **4b** with the expected upfield shift in the 5-C resonance from δ_H 6.29 to δ_H 6.86, as described by Winter and Butler (as δ_H 5.6) and Uchida and Kawakishi as (δ_H 5.98). In addition, reverse-phase-HPLC-MS, run on the sample in negative ion mode, revealed a peak at *m/z* 273.1 (16.5 %) indicative of *N*(α)-Bz-2-oxo-histidine **4b** (M - H^+). This reverse-phase-HPLC mass spectrometry was performed on an Agilent 1100 Series LC-MS with SL Ion Trap MSD and used a similar solvent system to that reported by Lewisch and Levine (acetonitrile and water) as successful for isolation for 2-oxo-histidine (Lewisch, S. A. and Levine, R. L., 1995).

The ^{1}H-NMR of the crude product showed substantial evidence for ascorbate and oxidised ascorbate – monohydroascorbate **24** and dehydroascorbate **25** (Scheme 2.11) - with a large multiplet at δ_H 3.48 - 5.05. Therefore, as done by Lewisch and Levine (Lewisch, S. A. and Levine, R. L., 1995), a purification by ion exchange chromatography was attempted. A cation exchange resin (Dowex, AG 50W-X8 resin) was acidified with 2 M HCl and the crude oxidation product added in a 50:50 mixture of distilled water and methanol. The column was eluted with distilled water and *N*(α)-Bz-2-oxo-histidine **4b** was expected to elute in the void volume as reported by Lewsich and Levine (Lewisch, S. A. and Levine, R. L., 1995). However, the isolation of this product from the remaining ascorbic acid and oxidised ascorbic acid

proved difficult and the yield obtained was still low (< 7.6 %). Literature yields obtained are reported as being very low, e.g. 0.1 % (Lewisch, S. A. and Levine, R. L., 1995), and it was decided that this synthetic method would be abandoned as an ineffective route to protected 2-oxo-histidine.

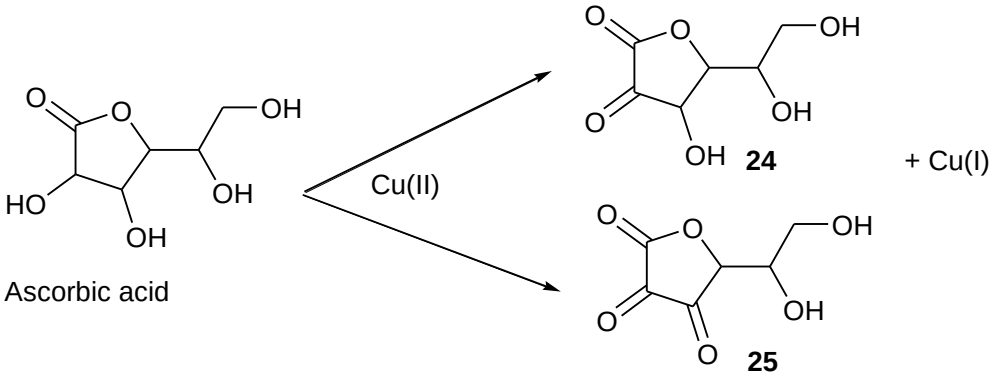

Scheme 2.11: The two products of ascorbic acid oxidation under radical conditions. Any oxidative reaction mixtures involving ascorbic acid and Cu^{2+} ions will be expected not to contain ascorbic acid but instead oxidised ascorbic acid i.e., dehydroascorbic acid **25** and monohydroascorbic acid **24.**

2.2.4. Attempted Bamberger cleavage and subsequent ring closure

The third synthetic method attempted was not an oxidation but an acylation and cleavage of the imidazole ring between the two nitrogens of the ring, a Bamberger reaction, and then a ring closure to include a carbonyl at C2.

A similar synthetic route has been used to generate Im-*H*-2 substituted derivatives of *N*(α)-Bz-His-OMe **5b** where the substituents have included trifluoromethyl (Kimoto, H., *et al.*, 1978), methyl, ethyl, phenyl and benzyl groups (Van Der Merwe, P., 1928, Windaus, A. and Langenbeck, W., 1922). These syntheses do not produce racemisation of the original L-enantiomer of histidine via oxazolone formation if the carboxyl group is protected as its ester (Ashley, J. N. and Harington, C. R., 1930, Kimoto, H., *et al.*, 1978).

First step: Acylation and Bamberger cleavage of imidazole ring

The Bamberger reaction was first described by Bamberger in 1893 as a reaction capable of opening up the imidazole ring between the two nitrogens to form a 1,2-diacylamidoethene derivative, by the use of an acylating agent in the presence of an aqueous base e.g. Na_2CO_3 (Heath, H., *et al.*, 1951), K_2CO_3, $NaHCO_3$ (Altman, J. and

Wilchek, M., 1989) and at ambient temperature (Bamberger, E., 1893, Grace, M. E., *et al.*, 1980). The mechanism of the reaction is given in Scheme 2.12 with the rate-determining step reported by Grace *et al.* as the formation of **26**, the hydroxyimidazoline, which can be readily hydrolysed by base catalysis into the Bamberger product (Grace, M. E., *et al.*, 1980).

Warshawsky *et al.* and Grace *et al.* optimised this cleavage by reducing the concentration of base while increasing the concentration of protected imidazole derivative, histamine, and acylating agent (Grace, M. E., *et al.*, 1980, Warshawsky, A., *et al.*, 1989). Excess acyl chloride and extended reaction times are required for the Bamberger cleavage to overcome the competing hydrolysis of the acylating agents (Grace, M. E., *et al.*, 1980), otherwise in most cases only the mono-acylated intermediate is isolated (Altman, J., *et al.*, 1984, Patchornik, A., *et al.*, 1957, Vliegenthart, J. F. and Dorland, L., 1970). In this PhD project an excess of acylating reagents was used to reduce the effects of potential hydrolysis on reaction yield.

It is not unusual for an *N*-formyl derivative of the Bamberger product (see Table 2.2(B)) to form as well as the full Bamberger product (Table 2.2(A)) (Grace, M. E., *et al.*, 1980), and this is detected in our syntheses described below. Some literature claims that water alone is enough to effect the final cleavage of this formyl group to give the full Bamberger product, as shown in Scheme 2.12 (Loosemore, M. J. and Pratt, R. F., 1976), however most groups claim either a base, e.g. 10 % $NaHCO_3$ (Altman, J. and Wilchek, M., 1989), or refluxing methanol (Altman, J., *et al.*, 1990, Altman, J., *et al.*, 1985) is needed for this deformylation (Grace, M. E., *et al.*, 1980). Basic conditions are preferable as refluxing in alcohol may induce *cis*/*trans* isomerisation in the Bamberger product (Altman, J., *et al.*, 1990). Grace *et al.* also report that to increase the ratio of full product:formyl product the reaction can be done at higher temperature or with longer reaction times (Grace, M. E., *et al.*, 1980).

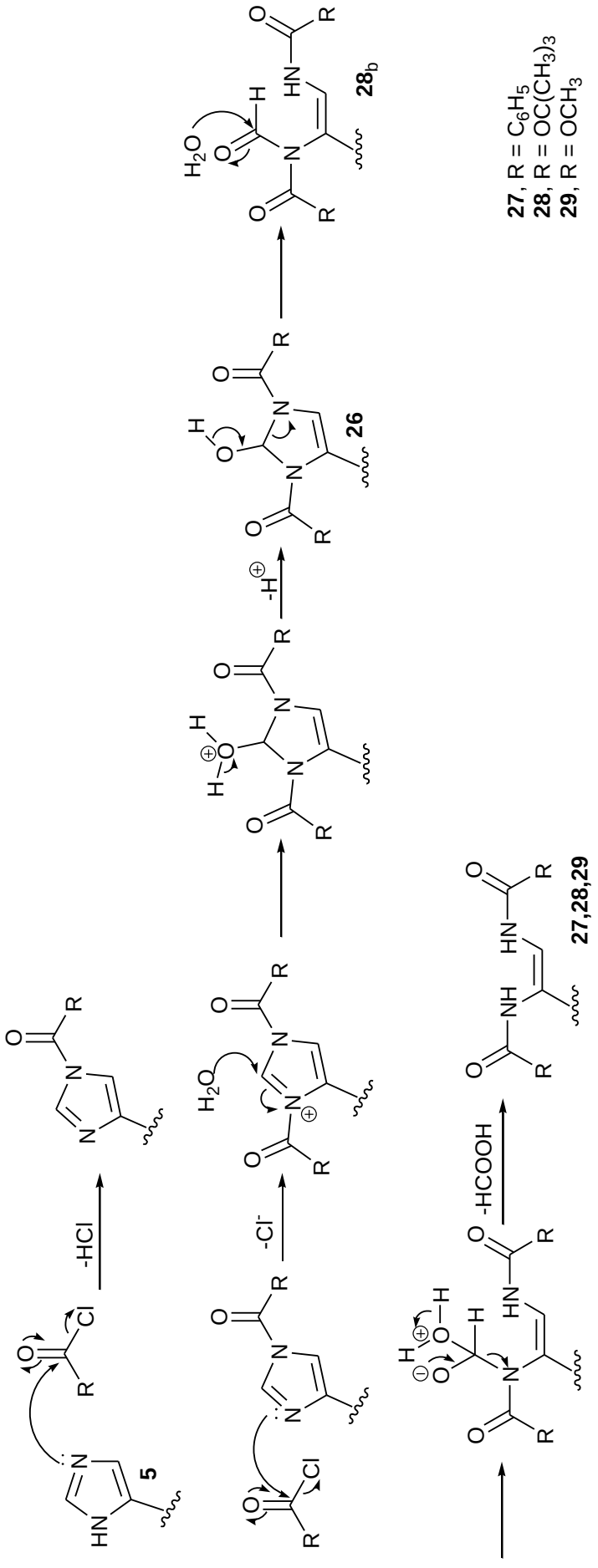

Scheme 2.12: Mechanism for Bamberger cleavage of an imidazole ring. The Bamberger reaction opens up the imidazole ring between the two nitrogens by the use of an acylating agent (RCOCl) in the presence of an aqueous base at low temperature. The first step is the acylation of each nitrogen to form a diacylimidazolium ion. The addition of water to form a tetrahedral intermediate **26**, the rate determining step as indicated by Grace *et al.*, is followed by cleavage across C2-*N*(τ) to form a formylated derivative, which has been isolated in the case of product **28a**. Further base catalysed (B) hydrolysis cleaves this as formic acid leaving the Bamberger product **27**, **28**, **29** (Grace, M. E., *et al*., 1980).

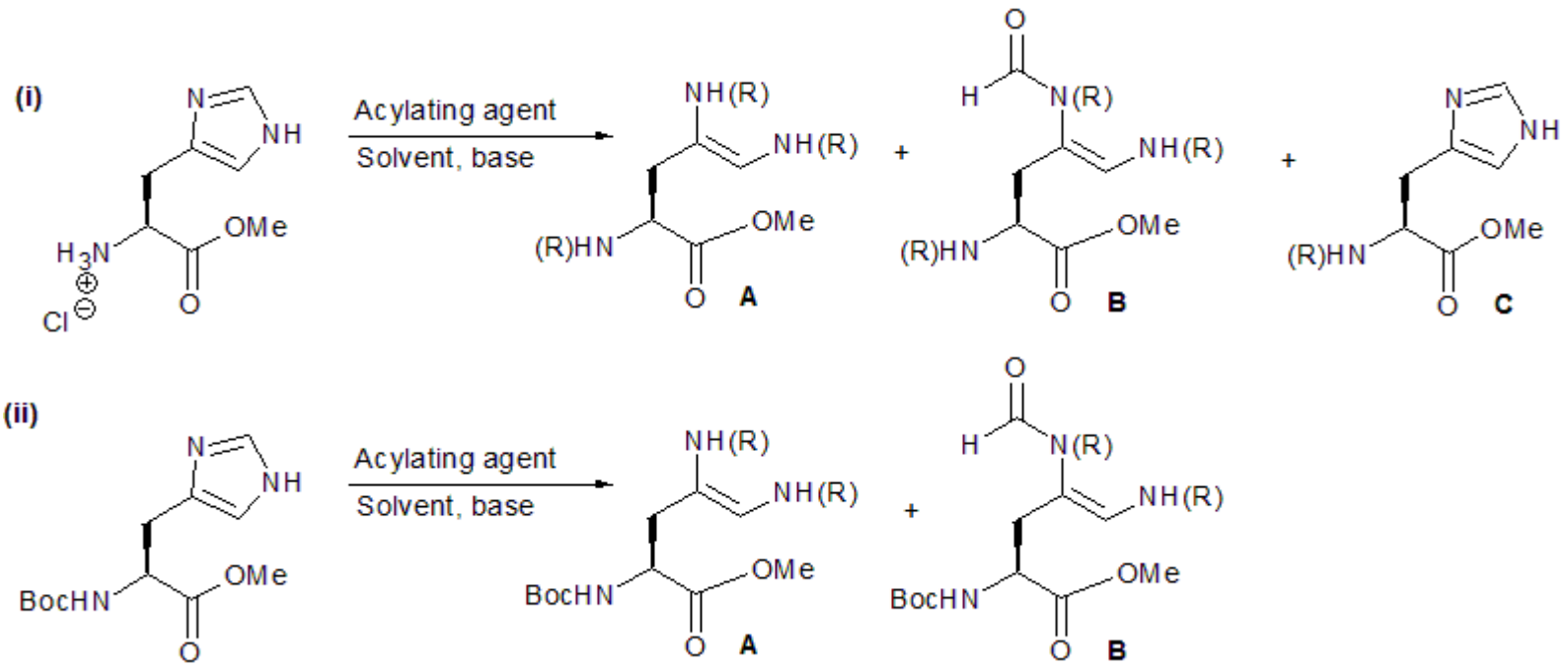

	Starting material	Acylating agent	Base	Solvent	Product	Yield (%)
A	HisOMe·2HCl (**5c**)	BzCl	$NaHCO_3$	MeCN	No reaction	N/A
B	HisOMe·2HCl (**5c**)	BzCl	$NaHCO_3$	Toluene:water	No reaction	N/A
C	HisOMe·2HCl (**5c**)	BzCl	$NaHCO_3$	EtOAc:water	Full Bamberger product (**A**) (**27**)	31

	Starting material	**Acylating-agent**	**Base**	**Solvent**	**Product**	**Yield (%)**
D	*N*(α)-Boc-His-OMe (**5a**)	BzCl	$NaHCO_3$	EtOAc:water	Full Bamberger product (**A**) (**28**)	20
					Formylated Bamberger product (**B**) (**28a**)	3.2
E	HisOMe·2HCl (**5c**)	ZCl	$NaHCO_3$	EtOAc:water	Mono-acylated product (**C**)	Minor in crude
F	HisOMe·2HCl (**5c**)	ZCl	$NaHCO_3$	$CHCl_3$	Mono-acylated product (**C**)	Minor in crude
G	HisOMe·2HCl (**5c**)	MeOCOCl	$NaHCO_3$	EtOAc:water	Full Bamberger product (**A**) (**29**)	31
H	*N*(α)-Boc-His-OMe (**5a**)	MeOCOCl	$NaHCO_3$	EtOAc:water	No reaction	N/A
I	HisOMe·2HCl (**5c**)	Boc_2O	NaOAc	MeCN:water	Formylated Bamberger product (**B**)	Minor in crude
					Mono-acylated product (**C**) (**5a**)	Major in crude

Table 2.2: Summary of the Bamberger reactions attempted on HisOMe.2HCl 5c (i) and *N*(α)-Boc-His-OMe 5a (ii). The figure illustrates the full Bamberger product (**A**), its formylated intermediate (**B**), and a non-Bamberger mono-acylated product (**C**) with mono-acylation on the *N*(τ) assumed based on similar literature examples (see Section 2.2.1. and Brown *et al*, 1982). R is the acyl group. All reactions were carried out at room temperature.

Acyl group	Substrate	References
Benzoyl (Bz)	Benzimidazole	(Hofmann, K., 1953)
	His-OMe·2HCl (**5**$_c$)	(Heath, H., *et al.*, 1951)
	Diethyl[2-(4-imidazoyl)ethyl]malonate	(Altman, J. and Wilchek, M., 1989)
	Ethyl imidazolylpropanoate	(Altman, J., *et al.*, 1984)
tert-butyloxycarbonyl (Boc)	*N*-tosylhistamine	(Altman, J., *et al.*, 1985)
	Imidazole	(Grace, M. E., *et al.*, 1980)
Benzyl carbamate (Cbz)	Ethyl imidazolylpropanoate	(Altman, J., *et al.*, 1984)
Methyl carbamate	Ethyl imidazolylpropanoate	(Altman, J., *et al.*, 1990)
	His-OMe·2HCl (**5**$_c$)	(Glinka, T., *et al.*, 2008)

Table 2.3: Bamberger reactions in the literature. Bamberger reactions in the literature use a variety of acylating reagents and substrates.

Previously work on the Bamberger reaction had been done by the Wyatt group and it was found that HisOMe·2HCl **5c** could be successfully cleaved across the two ring nitrogens using benzoyl chloride to produce the free vinyl diamide 2,4,5-tris-Bz-amino-pent-4-enoic acid-OMe **27** (Jumnah, R., 1991). This PhD project expanded on this synthesis using different acylating reagents as have been reported in the literature (Table 2.3). Previous acyl groups used in Bamberger reactions on L-histidine include benzoyl groups (Altman, J., *et al.*, 1990, Heath, H., *et al.*, 1951, Mizusaki, K. and Makisumi, S., 1981), ethoxycarbonyl groups (Loosemore, M. J. and Pratt, R. F., 1976, Vliegenthart, J. F. and Dorland, L., 1970), methyl carbamate (Glinka, T., *et al.*, 2008) and benzyl carbamate (Patchornik, A., *et al.*, 1957). In general, histidine is less reactive than imidazole for the Bamberger cleavage and in some cases has been found only to proceed as far as the formyl stage (Grace, M. E., *et al.*, 1980).

Each of these acyl groups has certain advantages and disadvantages to the overall synthesis, besides those discussed on pages 147 - 149. Benzoyl chloride is a stronger electrophile than other potential acylating agents such as Boc anhydride and hence can be added in lower amounts. However, unlike urethane groups, benzyl groups cannot provide a carbonyl for internal cyclisation in the second step of this

synthesis. Benzyl chloroformate has the advantage over methyl chloroformate of providing crystalline products and being less sensitive to hydrolysis, although if it does hydrolyse to form benzyl alcohol this is more difficult to remove than the relatively volatile MeOH. We studied a range of acyl groups to try and optimise both the yield of the Bamberger product and that of the subsequent cyclisation.

In an attempted replication of Jumnah's method (Jumnah, R., 1991) the benzoyl Bamberger product **27** of His-OMe·2HCl **5c** was successfully synthesised. Initially, a one-phase solvent system of acetonitrile was used, as had been used for Bamberger reactions reported by Altman *et al.* (Altman, J., *et al.*, 1985) (Table 2.2(A)), in an effort to reduce hydrolysis of the acylating reagent. However, despite leaving the reaction for 10 days, thin layer chromatography (TLC) monitoring revealed only starting material. Therefore it was decided that two-phase solvent systems would be used with an aqueous base. Traditionally benzene-water systems have been used (Heath, H., *et al.*, 1951) but we replaced benzene with toluene as a similar non-polar solvent but with lower toxicity (Table 2.2(B)). However, with this solvent system no Bamberger product was formed with the only new product appearing to contain a formyl group. These formylated Bamberger products were isolated from reactions with other acylating reagents and are discussed further below.

Next an ethyl acetate-water solvent system was used (Table 2.2(C)) and in this case there was successful synthesis of the benzoyl Bamberger product **27**. The ^{1}H-NMR analysis revealed the expected aromatic peaks of the benzoyl groups in the correct integral ratios at δ_H 7.42 - 7.62 (10 H) and δ_H 7.79 - 7.95 (5 H) and the expected lack of a H-2 signal. Mass spectrometry analysis also revealed a molecular ion at the expected mass of 470.1 (100%). The yield was only 31 %, which may be due to hydrolysis of benzoyl chloride to benzoic acid, but it exceeds yields obtained by Jumnah (13 %) (Jumnah, R., 1991)

There are advantages to the use of orthogonal acylating and α-protecting groups; simplification of the analysis of Bamberger products and selective deprotection of these two functionalities. Therefore, we attempted the Bamberger reaction with benzoyl chloride on *N*(α)-Boc-His-OMe **5a** as a starting material. An identical base and solvent system was used to the synthesis from His-OMe·2HCl **5c** (Table 2.2(D)), although the reaction time was almost tripled as indicated by the persistence of starting material on TLC analysis. Despite this extended reaction time

and although the Bamberger reaction was successful, the yield of **28** was low at 20 %. An additional new product was also isolated from the crude product; a formylated derivative of the Bamberger product **28a** in a 3 % yield. This eluted later than the Bamberger product **28** from the flash chromatography column, indicating a greater polarity, and the presence of a formyl group was revealed conclusively by a ^{1}H-NMR peak at δ_H 9.17. Coupling (~8 Hz) of the remaining C*H* (δ_H 6.65) from the original imidazole ring to a benzoylated N*H* (δ_H 10.0) revealed that the formyl group was on the benzoylated nitrogen next to the quaternary carbon from the original ring. In this formylated product **28a** the benzoyl groups were still added in the correct ratio (i.e. 10 H instead of the 15 H seen for the non-Boc protected starting material). This formylated product **28a** also formed in a toluene-water solvent system. In general, though, the full Bamberger product **28** was formed in greater yield than the formylated product **28a** without the need for basic conditions or refluxing in methanol, as reported by previous studies (see page 87) (Altman, J., *et al.*, 1985).

In conclusion, benzoyl chloride could be used to successfully generate Bamberger products of both His-OMe·2HCl **5c** and *N*(α)-Boc-His-OMe **5a** albeit in low yields. However, it was predicted that cyclisation on this product would be more difficult than one which contained urethane functionality. Therefore, we chose to explore different acylating agents.

Jumnah had previously reported that the use of benzyl chloroformate gave higher yields of Bamberger products than benzoyl chloride. In addition, Altman *et al.* had previously commented that for *N*-tosylhistamine **30**, a similar product to *N*-protected histidine, the use of benzyl chloroformate gave the imidazolin-2-one derivative **31** without the need for the second cyclisation step (Altman, J., *et al.*, 1985) (Scheme 2.13).

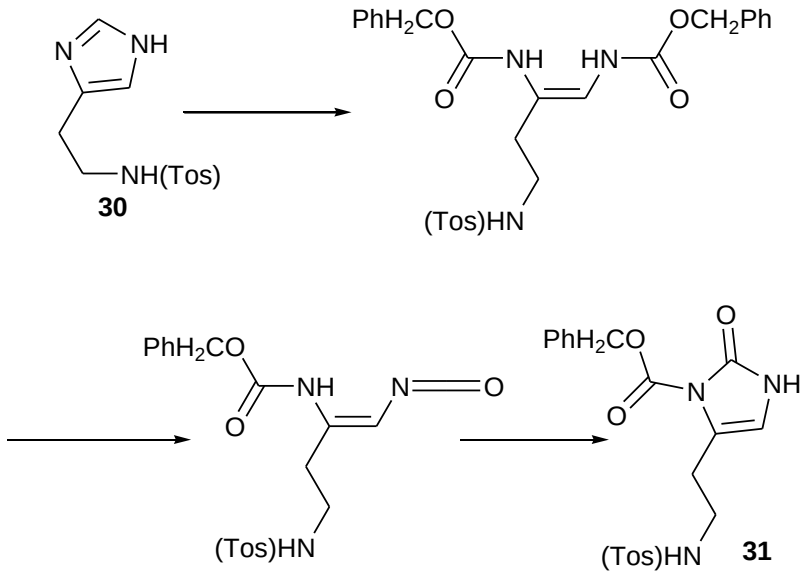

Scheme 2.13: Formation of a 2-oxo derivative of histamine 30 via a Bamberger reaction. Adapted from Altman *et al.*, 1985 (Altman, J., *et al*., 1985).

Hence, this acylating reagent was trialled in both a chloroform-water solvent system (Table 2.2(F)) and an ethyl acetate-water solvent system (Table 2.2(E)) on His-OMe.2HCl **5c**. However, with both solvent systems the crude product did not show any evidence of a fully cleaved Bamberger product and in both cases mostly starting material was recovered. NMR data did indicate some reaction; mono-acylated histidine for the chloroform two-phase system and formylated product for the ethyl acetate two-phase system.

The next acylating agent tested was methyl chloroformate in an ethyl acetate-water solvent system with a sodium bicarbonate base (Table 2.2(G)). This successfully generated the Bamberger product **29** over a similar time period and with a similar yield (31 %) as the reaction with benzoyl chloride. The expected methyl protons of the MeOCO were seen in the correct integral ratios (3.67 (3 H), 3.71 (3 H), 3.72 (3 H)) and there was a lack of a H-2 proton. A formylated product was indicated in the ^{1}H-NMR spectrum of the crude product but this was not isolated. This acylation was also trialled on *N*(α)-Boc-His-OMe **5a** but only starting material was isolated (Table 2.2(H)).

In a final attempt to find a higher yielding acylating agent, Boc_2O was used. This can form urethane functionality required for intramolecular cyclisation when bound to the imidazole nitrogens. The reaction was carried out in acetonitrile and water rather than with ethyl acetate, and the starting material was His-OMe.2HCl **5c**.

The base used was sodium acetate rather than sodium bicarbonate (Table 2.2(I)). When the Bamberger reaction was attempted, the main product, indicated by ^{1}H-NMR of the crude product, was the mono-acylated histidine, *N*(α)-Boc-His-OMe **5a**, despite the mixture being left to react for 14 days. In addition, a lot of starting material was recovered and some evidence of a formylated product.

In conclusion, three products (Scheme 2.14) were formed under these reaction conditions, the full Bamberger cleavage product **27**, **28**, **29**, the formylated Bamberger product **28a** and the mono-acylated product **5a** (see Table 2.2). The only two successful acylating reagents for generating Bamberger products were found to be benzoyl chloride and methyl chloroformate, which are the two reagents reported in the literature to be successful for generating the Bamberger product of His-OMe·2HCl **5c** (Glinka, T., *et al.*, 2008, Heath, H., *et al.*, 1951). Although, there were advantages to starting with *N*(α)-protected histidine **5a**, histidine methyl ester hydrochloride **5c** was found to produce the cleanest reactions. Therefore, for the ring closure step the starting material chosen was the tribenzoyl Bamberger product **27**.

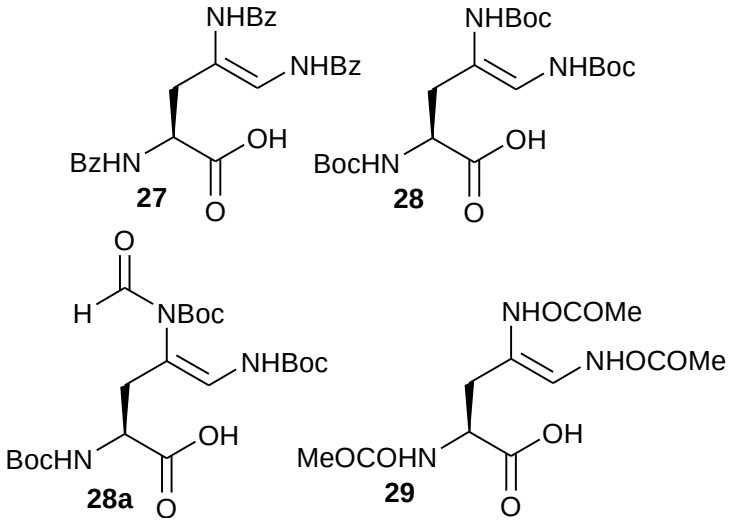

Scheme 2.14 Summary of major products formed by the Bamberger reaction. Three derivative of the full Bamberger product were successfully synthesised **27** (benzoyl), **28** (Boc) and **29** (methyl carbamate) in addition to a formylated derivative with Boc groups **28a**.

Second step: Ring closure with carbonyl at C2

The second step of this attempted synthesis is a ring closure with addition of carbonyl at C-2 in the imidazole ring. There are two main approaches for this ring closure:

1) Internal source of carbonyl group (Scheme 2.15(A)) – if the *N*-bound acyl group forms a urethane then the carbonyl within this group can be incorporated at C2 to close the ring and form an imidazolin-2-one derivative. Therefore, this cyclisation could occur if the acyl groups used were Cbz, methoxycarbonyl or Boc, but not if they were Bz. Use of a non-nucleophilic base, e.g. *t*-butoxide, might be sufficient to effect the cyclisation. Literature examples include Altman *et al.* (Altman, J., *et al.*, 1985).
2) External source of carbonyl group (Scheme 2.15(B)) – in the cases where urethane functionality is not already part of the Bamberger product, a carbonyl-containing reagent, such as diethyl carbonate, is likely to be required with either a strong acid/base catalyst or high temperatures. There are several examples in the literature (Ashley, J. N. and Harington, C. R., 1930, Van Der Merwe, P., 1928, Windaus, A. and Langenbeck, W., 1922).

However, the only successful Bamberger product containing urethane functionality was the methyl carbamate derivative **29** and was only produced in quite low yield. Thus all cyclisation attempts were using an external source of carbonyl group on the benzoyl derivative 2,4,5-tris-Bz-amino-pent-4-enoic acid-methyl ester **27**.

Ring closure of imidazoyl Bamberger products has been done successfully in the literature with incorporation of methyl, ethyl, phenyl and benzyl at C-2 with the use of carboxylic anhydrides at high temperatures (Ashley, J. N. and Harington, C. R., 1930, Van Der Merwe, P., 1928, Windaus, A. and Langenbeck, W., 1922). In addition, trifluoroacetic anhydride at reflux will generate 2-trifluoromethyl-histidine from the imidazoyl Bamberger product (Kimoto, H., *et al.*, 1978). In general, the reagents used to ring close the Bamberger products are carbonyl-containing electrophilic reagents (Scheme 2.16).

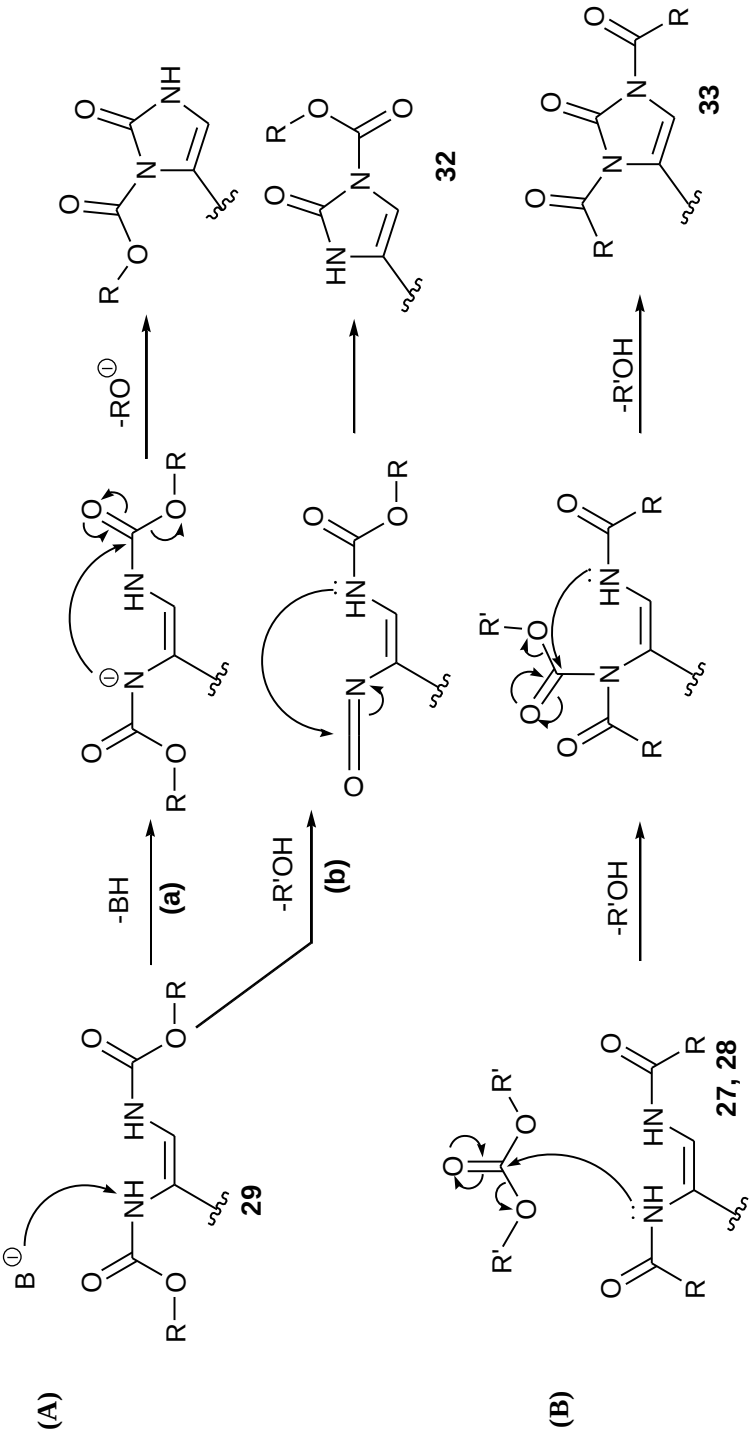

Scheme 2.15: Mechanisms of ring closure of the Bamberger product. (A) External source of carbonyl group – A base is used to deprotonate one of the acylated nitrogens in the Bamberger product **27**, **28**, **29**. This then attacks at the carbonyl of the other ring nitrogen's acyl group bridging across the nitrogens to form an imidazolin-2-one derivative **(a).** Alternatively the mechanism can go via an isocyanate intermediate **(b).**
(B) Internal source of carbonyl group – an acylated nitrogen of the Bamberger product attacks the carbonyl of the reagent with the loss of an alcohol. A further attack from the other acylated nitrogen bridges the carbonyl across the two nitrogens.

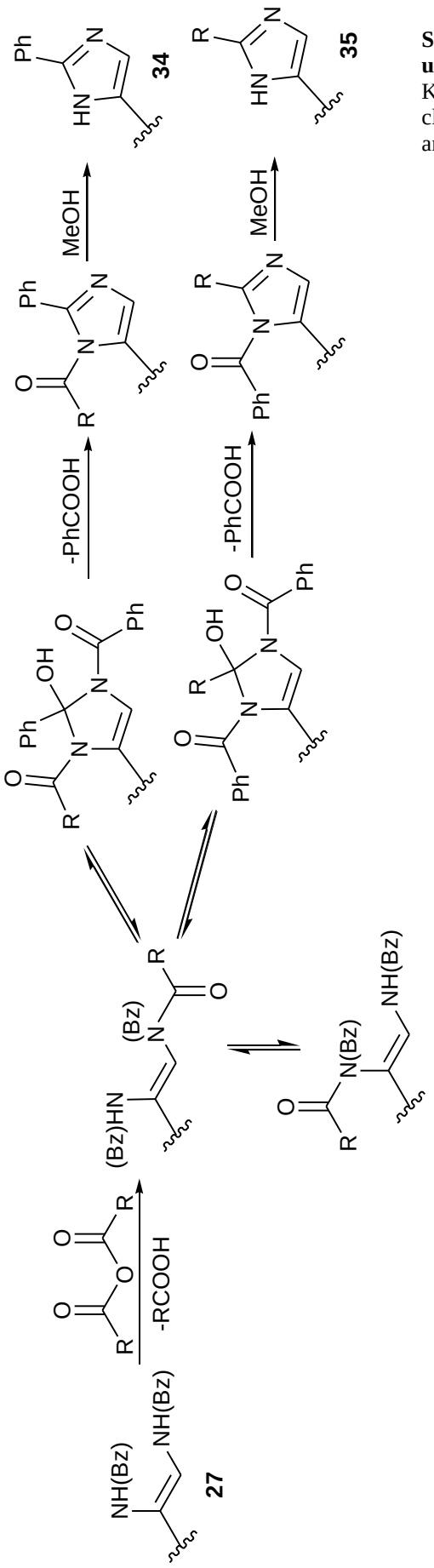

Scheme 2.16: Ring closure of Bamberger products using a carboxylic anhydride.
Kimoto *et al.* proposed this mechanism for the ring closure of a Bamberger product **27** using a carboxylic anhydride (Kimoto, H., *et al*., 1978).

It was envisaged that triphosgene could be used as an electrophilic reagent for the formation of 2-oxo-histidine derivatives from Bamberger products. This is a solid trimer of the toxic gaseous phosgene. It has three carbons in the same oxidation state which can be incorporated as the carbonyl and thus is only required in 0.33 mole equivalence. This reagent has been used successfully to ring close *o*-aminobenzamides to form quinazolinediones (Cortez, R., *et al.*, 1991) and α-amino alcohols to produce oxazolidinones (Pridgen, L. N., *et al.*, 1989).

The initial attempted cyclisation with triphosgene was conducted at 0 °C under an inert atmosphere (Scheme 2.17(a)). Triphosgene (0.3 mole equivalents) was added to 2,4,5-tris-Bz-amino-pent-4-enoic acid-methyl ester **27** suspended in anhydrous THF. 2 Molar equivalents of sodium hydride were added to increase the nucleophilicity of the nitrogens in the Bamberger product **27**. The occurrence of a reaction was indicated by the mixture changing from colourless to yellow and formation of a white precipitate. Despite evidence of the Bamberger product salt intermediate forming, overall the reaction yielded only starting material.

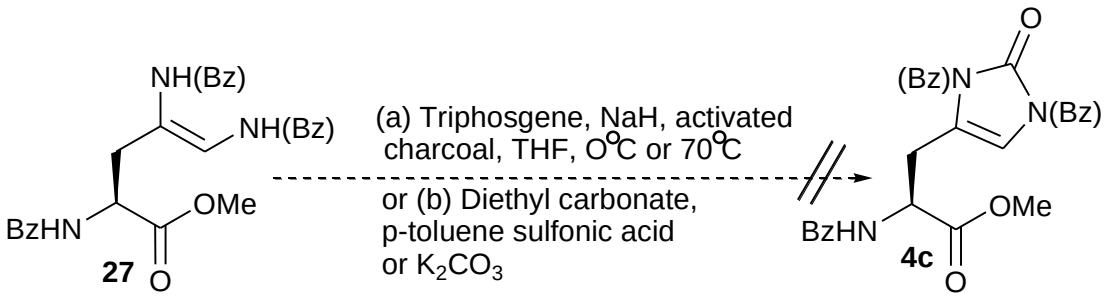

Scheme 2.17: Attempted cyclisation of 2,4,5-tris-Bz-amino-pent-4-enoic acid-methyl ester 27.

It was suspected that the nucleophilicity of the acylated nitrogens was still compromised by extensive delocalisation of the 4-C=C-5 double bond electrons. However, there was reluctance to add more base in case of racemisation of the amino acid backbone chiral centre. In addition, the formation of a white precipitate suggested that the intermediate sodium salt had formed successfully. Therefore, to try and increase the reactivity of the triphosgene reagent the reaction was repeated at 70 °C. The reaction was left for 6 hours until a tan-brown emulsion formed. However, as before, ^{1}H-NMR of the crude product indicated only starting material.

A second cyclisation agent was then examined; diethyl carbonate (Scheme 2.17(b)). Initially an acid catalyst was then used because this could protonate the diethyl carbonate reagent providing a better electrophile for attacking the acylated

nitrogens of the Bamberger product **27**. The acid catalyst used was *p*-toluene sulfonic acid and it was added at 1 mole equivalent relative to the Bamberger product **27**. The reaction product was expected to be in equilibrium with the starting material and hence, to try and promote the forward reaction diethyl carbonate was added in excess and the mixture was heated to 140 °C for 22 h. However, ^{1}H-NMR of the crude product showed a lack of α-C*H* or β-CH_2 peaks indicating that the amino acid functionality had not survived the reaction.

Hence, a base catalyst was trialled for the same reasons as discussed above; to increase the nucleophilicity of the acylated nitrogens within the Bamberger product starting material **27**. Potassium carbonate was used as the base at 1 mole equivalent to the starting material. Again the reaction was heated to 140 °C for 22 h and once again the ^{1}H-NMR showed no evidence of amino acid functionality.

Therefore, the reaction was repeated but with only a 1 h 20 min reaction time. This time the amino acid components survived the reaction conditions but, as for the attempted cyclisation with triphosgene, only starting material was recovered. Therefore, it was concluded that the conditions required for cyclisation of the Bamberger product **27** were too severe for the stability of the amino acid functionality present in the Bamberger product **27**.

2.3. Discussion

In conclusion, the three synthetic methods attempted to synthesise protected 2-oxo-histidine from L-histidine have been unsuccessful. However, there are both ^{1}H-NMR and mass spectrometric data which indicate the presence of a low yield of *N*(α)-benzoyl protected 2-oxo-histidine **4b** from a Cu^{2+}/Cu^{+}/ascorbate metal-catalysed oxidation.

The initial attempted oxidation of L-histidine was conducted on *N*(α)-Boc-His-OMe **5a** and yielded two novel compounds **22** and **23**, both containing isopropylidene groups. This was based on a literature procedure for synthesising *N*(α)-Boc-2-oxo-His-OMe **4a** described by Saladino *et al.*, however, upon further analysis of their ^{13}C-NMR data for *N*(α)-Boc-2-oxo-His-OMe **4a** it was deemed an unfeasible strategy for generating 2-oxo-histidine (Saladino, R., *et al.*, 1999). In addition, literature on DMDO-mediated oxidation of compounds similar to imidazole indicate that oxygen addition at C-4/C-5 in the imidazole ring, as seen with product **22**, was more likely than at the C-2 position (Adam, W., *et al.*, 1992, Sivappa, R., *et al.*, 2007, Zhang, X. and Foote, C. S., 1993).

The second potential synthetic strategy for generating 2-oxo-histidine in the literature is the use of a metal-catalysed oxidation system, in particular Cu^{2+}/Cu^{+}/ascorbate (Hovorka, S. W., *et al.*, 2002, Schoneich, C., 2000, Uchida, K., 2003, Uchida, K. and Kawakishi, S., 1986). With this system we generated *N*(α)-Bz-2-oxo-His-OMe **4b** but in very small yields and also within an environment of high concentrations of ascorbate and oxidised ascorbate. Despite several attempted purifications with ion exchange chromatography and reverse-phase HPLC, this 2-oxo-histidine could not be successfully extracted and, due to the poor yield, this MCO system was abandoned as a potential synthetic strategy for generating 2-oxo-histidine.

The third synthetic strategy attempted was an acylation and cleavage of the imidazole ring followed by ring closure to include a carbonyl at C-2. The initial step showed some success with use of the acyl groups, benzoyl and methyoxycarbonyl, in an EtOAc-water solvent system and using the base $NaHCO_3$. However, cyclisation attempts with triphosgene yielded only starting material, while cyclisation attempts with diethyl carbonate, either degraded the amino acid functionality of the histidine

or yielded starting material.

Hence, it was decided that a different synthetic strategy from that starting from L-histidine should be undertaken. Therefore, syntheses starting with the known compound imidazolin-2-one **36** were studied. This is discussed further in Chapter 3.

Chapter 3

SYNTHESIS OF 2-OXO-HISTIDINE FROM UREA

3.1. Introduction

Chapter 2 discussed attempted synthesis of 2-oxo-histidine **4** from L-histidine **5**, however, these attempts were unsuccessful in providing 2-oxo-histidine in synthetically useful quantities. Therefore, it was proposed to start a synthesis from the imidazolin-2-one **36** ring system, a carboxylic derivative **49** of which can be formed by the known synthesis from urea **17** and (+)-tartaric acid **36** (Duschinsky, R. and Dolan, L. A., 1946, Hilbert, G. E., 1932) (Scheme 3.1).

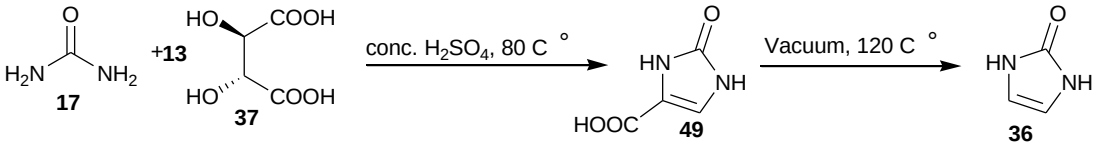

Scheme 3.1: Synthesis of the carboxylic derivative 49 of imidazolin-2-one 36 from urea 17 and (+)-tartaric acid 36. (Duschinsky, R. and Dolan, L. A., 1946, Hilbert, G. E., 1932)

3.1.1. A retrosynthetic analysis of 2-oxo-histidine identifies derivatives of the imidazolin-2-one ring system **36** as a starting point.

From a retrosynthetic analysis, 2-oxo-histidine **4** there are several potential synthetic routes (Scheme 3.2). Simple cleavage of either the C-α, C-β bond (Scheme 3.2(A)) or C-γ, C-β bond (Scheme 3.2(B)) indicates syntheses from either a glycine enolate equivalent or serine derivative respectively, and these are discussed further in Section 3.2.2.

However, the most successful synthesis discussed in this thesis used an alternative approach by first considering an α, β-dehydro derivative of 2-oxo-histidine. Further retrosynthetic analysis on this intermediate predicted the required coupling of an imidazolin-2-one-derived cation synthon and a glycine anion synthon. The synthetic equivalents used for this project were a protected form of the aldehyde, 4-formylimidazolin-2-one **38**, and a protected form of the phosphonate, phosphonoglycine trimethyl ester **39** (Scheme 3.2(C)).

In terms of forming the aldehyde **38** there are several related synthetic strategies reported in the literature. Nakajima *et al.* report on a coupling of imidazolin-2-one **36** to ethyl formate using a Grignard reagent (Nakajima, M., 1958).

The Vilsmeier-Haack reaction has also been used recently to formylate imidazolin-2-one **36** (Ma, Z., *et al.*, 2011). This synthesis is explored further in Section 3.2.2. A second synthetic approach is that described by Dransfield *et al.* in their syntheses of several dienes (Dransfield, P. J., *et al.*, 2006). This synthesis protected the ring nitrogens of 4-carboxyimidazolin-2-one, esterified the carboxylic acid group to an ester, reduced this to an alcohol and then oxidised this up to the aldehyde. This literature procedure is the basis of the synthesis described in Section 3.2.1.

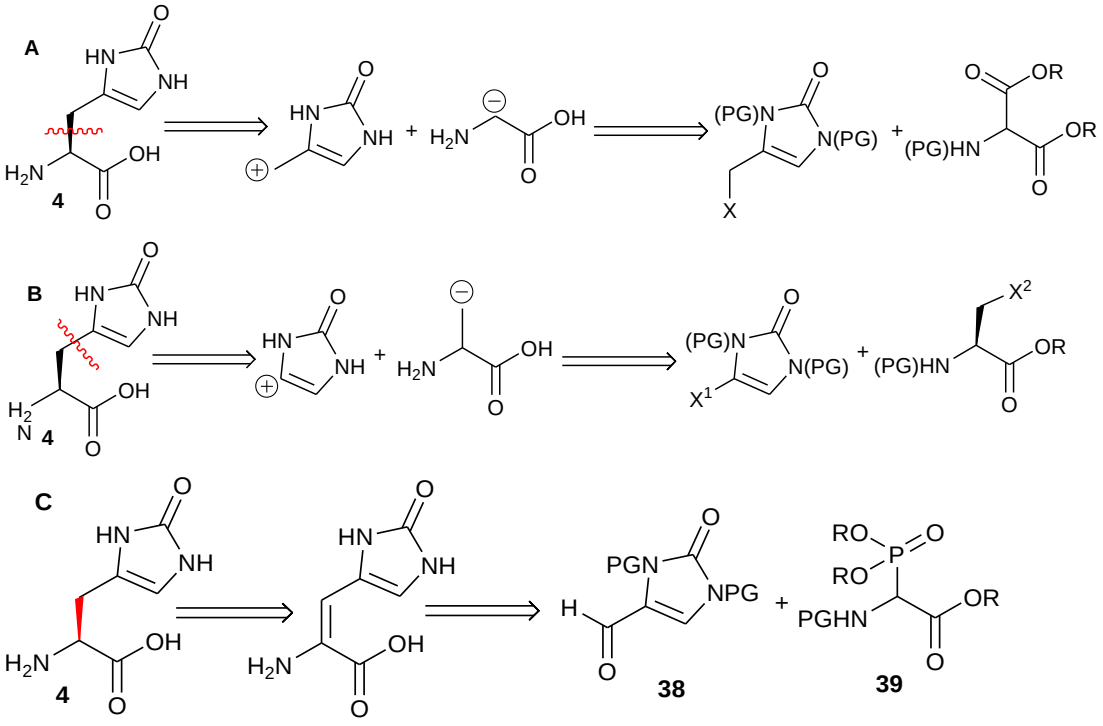

Scheme 3.2: A retrosynthetic analysis of 2-oxo-histidine 4.
(A) Cleavage of the C-α, C-β bond predicts synthons who synthetic equivalents could be a glycine enolate equivalent and an activated imidazoline species.
(B) Another set of synthons could be generated by cleaving the C-4, C-β bond, which would be equivalent to a serine derivative and a halogenated imidazoline derivative.
(C) By forming the chiral centre of 2-oxo-histidine **4** by asymmetric reduction, retrosynthetic analysis of the dehydro starting material predicts the use of a Wittig style coupling between an imidazolene aldehyde **37** and a phosphonate **38.**
R is an alkyl group.
PG is a protecting group.

3.1.2. Synthesising the imidazolin-2-one ring system **36** from urea **17** and tartaric acid **37**

Imidazolin-2-one **36** (Scheme 3.3) is a well-characterised ring system that has been studied extensively in the literature.

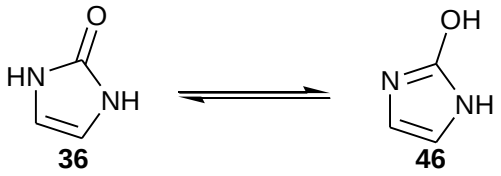

36 **46**

Scheme 3.3: Tautomeric forms of imidazolin-2-one 36.

In 1892 Marckwald claimed to have devised a synthesis of imidazolin-2-one **36** from an amino acetal **47** (Scheme 3.4(A)) (Marckwald, W., 1892). However, this synthesis was prone to polymerisation of the ureidoacetal intermediate **48** instead of cyclisation to the imidazolin-2-one species **36** (Aiman, C. E. and Daugs, E. D., 1994, Duschinsky, R. and Dolan, L. A., 1946). Despite some improvements to the method, e.g. use of an alcoholic solvent (Aiman, C. E. and Daugs, E. D., 1994), it was still far from an ideal synthesis of imidazolin-2-one.

Thus is 1932, Hilbert *et al*. proposed an alternative two-step synthesis (Hilbert, G. E., 1932). The first step is a condensation of urea **17** and tartaric acid **37** in concentrated sulfuric acid to form 4-carboxyimidazolin-2-one **49** (Scheme 3.4(B)). The pure carboxylic acid **49** can be precipitated by pouring the reaction mixture onto ice and has been used subsequently by several groups to generate this carboxylic acid **49** as an end product (Dransfield, P. J., *et al.*, 2006, Otter, B. A., *et al.*, 1968). The second step of this imidazolin-2-one synthesis is a decarboxylation of the carboxylic acid **49**. This can be carried out in several ways, although the most common method is refluxing in aqueous base (Baxter, R. L., *et al.*, 1992, Zav'yalov, S. I., *et al.*, 1972) (Scheme 3.4(B)), which avoids the high temperatures (230 – 240 °C) of other decarboxylation methods such as sublimation (Scheme 3.4(C)) (Hilbert, G. E., 1932, Nakajima, M., 1958). Another potential synthesis is that described by Fenton and Wilks which uses a condensation of maleic acid **50** with urea **17** (Scheme 3.4(D)) (Fenton, H. J. H. and Reginald, W. A. W., 1909), however there is little characteristic data to back up this synthesis. Therefore, this PhD uses the two-step synthesis starting from urea **17** and tartaric acid **37** described by Hilbert *et al.* (Hilbert, G. E., 1932) (Scheme 3.4(A)).

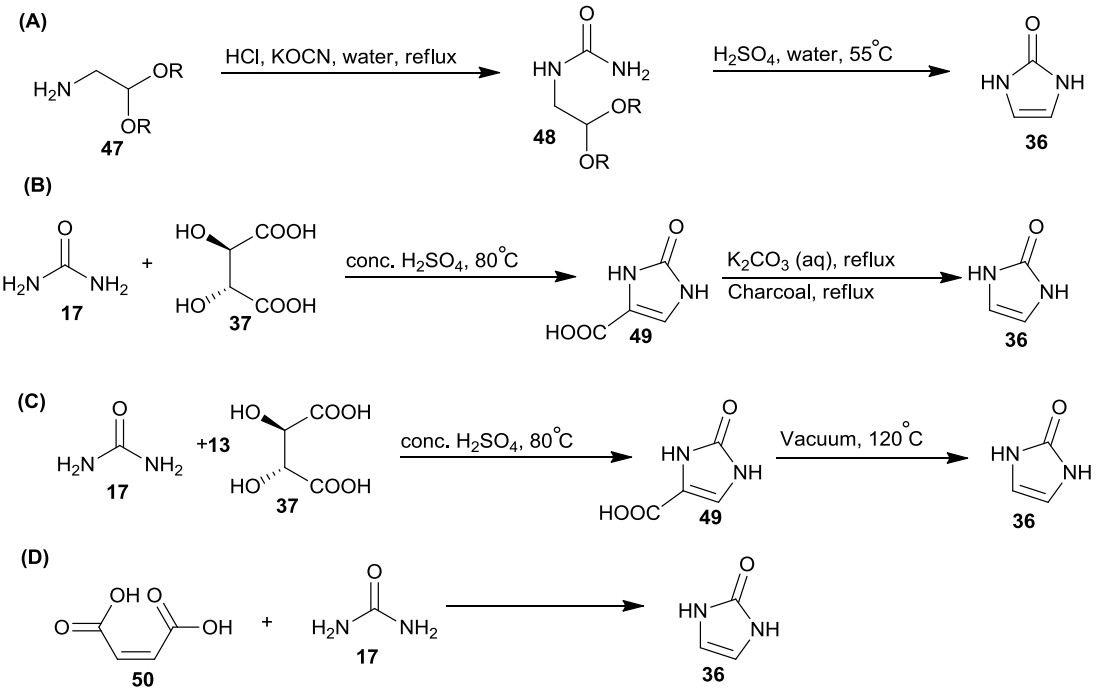

Scheme 3.4: Two-step synthesis of imidazolin-2-one from urea 45 and (+)−tartaric acid 46.
(A) Markwald's Method: The reaction of an aminoacetal **47** with a cyanate to form ureidoacetal **48.** This is followed by an acid-catalysed condensation to form imidazolin-2-one **36** (Duschinsky, R., and Dolan, L. A., 1946)**.**
(B) This synthesis is composed of two steps (Hilbert's Method); condensation of urea **17** and (+)-tartaric acid **37** to form 4-carboxyimidazolin-2-one **49** (Hilbert, G. E., 1932, Hagenmaier, H., *et al*., 1979) and decarboxylation of 4carboxyimidazolin-2-one **49** to form imidazolin-2-one **36 (**Zav'yalov, S. I., *et al*., 1972, Baxter, R. L., 1992)
(C) Sublimation of 4-carboxyimidazolin-2-one **49** at 120 °C (Hilbert, G. E., 1932).
(D) The condensation of maleic acid **50** and urea **17 (**Fenton, H. J. H., and Wilks, W. A. W., 1909).

3.1.3. Imidazolinones as important biological molecules

Chapter 1 discussed the importance of histidine residues in sequences for biological processes, specifically for the Aβ peptide, and postulated how these roles could be affected by histidine oxidation. However, imidazolinone derivatives have other biological activities as well (Diness, F. and Meldal, M., 2009). Imidazolinones are implicated in receptor antagonists (Burgey, C. S., *et al.*, 2006, Carling, R. W., *et al.*, 1999, Reitz, D. B., *et al.*, 1993), phosphodiesterase (PDE) inhibitors (Andrés, J. I., *et al.*, 2002), β-adrenergic receptor agonists (Naylor, E. M., *et al.*, 1999), GABA receptor ligands (Desimone, R. W. and Blum, C. A., 2000), natural antibiotics (Fiedler, H.-P., *et al.*, 1982) and bacterial antifungal compounds. Thus novel synthetic methods increasing the functionality and synthetic potential of this group

may have uses beyond simply constructing oxidised histidine. In addition, imidazolinones can act as either nucleophiles or electrophiles and are substrates for copper-catalysed cross-coupling to aryl groups (Diness, F. and Meldal, M., 2009), which may indicate how 2-oxo-histidine will react in oxidised proteins such as Aβ.

3.1.4. Aims

The aim of this chapter is to use the imidazolin-2-one **36** ring system to generate enantiomerically pure 2-oxo-histidine **4** with suitable protecting groups for solid phase peptide synthesis of the Aβ peptide.

3.2. Results

3.2.1. Synthesis from 4-carboxyimidazolin-2-one **49**

As discussed in Section 3.1.1. the object of this synthesis was to couple the aldehyde 4-formylimidazolin-2-one **38** and the phosphonate, phosphonoglycine trimethyl ester **39** (Scheme 3.1) in a Horner-Wadsworth-Emmons (HWE) reaction to form a protected dehydro-derivative of 2-oxo-histidine **40**, which could then be reduced to form protected 2-oxo-histidine **4**. Suitable protection of the nitrogens was required, so initially *para*-methoxybenzyl (PMB) groups were used to protect the ring nitrogens, while benzyloxycarbonyl (Cbz) groups were used to protect the amino nitrogen.

para-methoxybenzyl (PMB) as a nitrogen protecting group

PMB groups (also known as MPM groups) are reported as being suitable protecting groups for imidazole rings (Kamijo, T., *et al.*, 1983). In terms of imidazolin-2-one ring systems, previous ring-nitrogen protections have used PMB as the second nitrogen-protecting group after mono-benzylations of the ring. PMB groups have been shown to be stable to reactions similar to those described below (Dransfield, P. J., *et al.*, 2006). However, the use of di-PMB protection on imidazolin-2-one ring systems has not been used to date.

PMB groups were considered to be advantageous because they are reported to be removable by a simple cerium(IV) diammonium nitrate (CAN)-mediated oxidation (Bartoli, G., *et al.*, 2003, Smith, A. B., *et al.*, 1992, Yamaura, M., *et al.*, 1985), which was not expected to have an effect on the imidazolin-2-one **36** ring system given its oxidised structure.

PMB groups are typically added using a 4-methoxybenzyl halide and the base NaH in DMF. They are stable to a range of reaction conditions including hot aqueous alkali, aqueous acid, mild oxidants such as potassium permanganate, cold Lewis acids, several nucleophilic reagents e.g. CN^- and ArO^- and mild catalytic hydrogenolysis (Buckle, D. R. and Rockell, C. J. M., 1982).

*Obtaining protected 1,3-bis(PMB)-4-formylimidazolin-2-one **38a***

This multi-step synthesis started with urea **17** and (+)-tartaric acid **37** and resulted in the synthesis of 1,3-bis(PMB)-4-formylimidazolin-2-one **38a** (Scheme 3.5). The initial product, 4-carboxyimidazolin-2-one **49**, has the correct heterocyclic ring for 2-oxo-histidine **4**. The synthesis of protected 4-formylimidazolin-2-one **38** from 4-carboxyimidazolin-2-one **49** is well documented by Dransfield *et al.* (Dransfield, P. J., *et al.*, 2006), although with use of a different set of protecting groups.

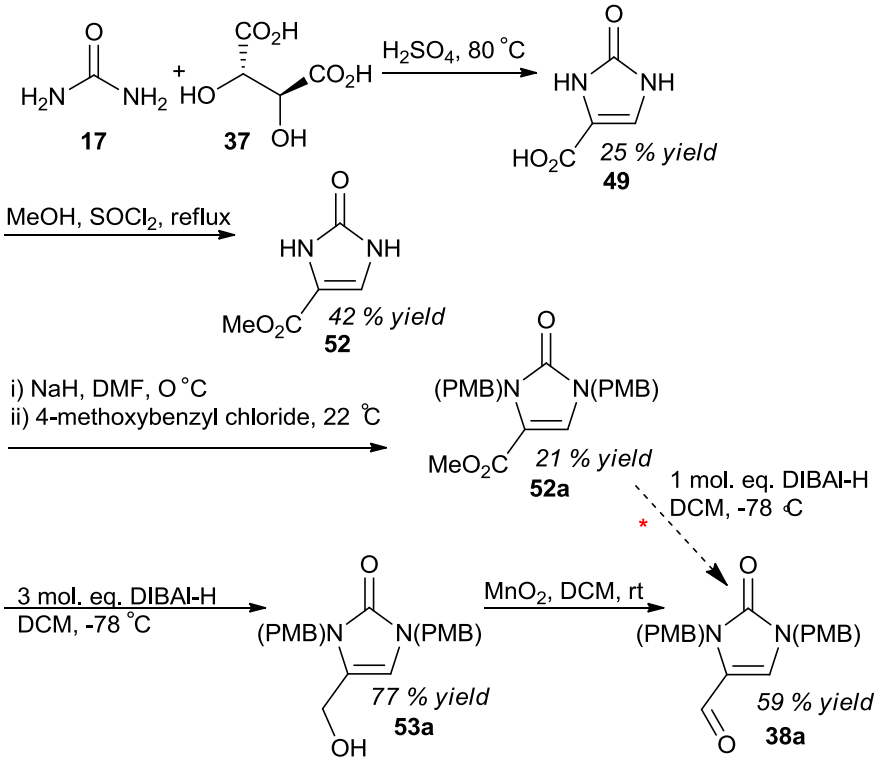

Scheme 3.5: Synthesis of 1,3-bis(PMB)-4-formylimidazolin-2-one 38a. The red star indicates an attempted one step reduction of methyl ester **52a** to aldehyde **38a**.

The carboxylic acid, 4-carboxyimidazoline-2-one **49** was synthesised from urea **17** and (+)-tartaric acid **37** heated in concentrated sulfuric acid. The presence of a single C*H* environment (δ_H) in both the ^{1}H-NMR (δ_H 7.13) and the ^{13}C-NMR spectra (δ_C 115.0) indicated the ring system had formed and both IR and ^{13}C-NMR evidence was obtained for the presence of two carbonyls. This indicated that this product was likely 4-carboxyimidazolin-2-one **49**.

This carboxylic acid **49** was then converted into the protected imidazoline aldehyde **38a** via four steps, which were based on those described by Dransfield *et al.* and Dilley *et al.* (Dilley, A. S. and Romo, D., 2001, Dransfield, P. J., *et al.*, 2006).

Firstly, **49** was esterified using thionyl chloride and methanol to yield 4-methoxycarbonylimidazolin-2-one **52**. Alternative syntheses, which use heating in concentrated sulfuric acid with the corresponding alcohol, are reported in the literature but with poor yields (50 – 55 %) (Hilbert, G. E., 1932, Otter, B. A., *et al.*, 1968). Esterified product **52** gave IR data with a new carbonyl band at 1728 cm^{-1} typical of an α,β-unsaturated ester and ^{1}H-NMR data revealed the addition of a new OMe group with the correct 3H integral at δ_H 3.70, which compared favorably to the OMe peak reported for **49** by Otter *et al.* (δ_H 3.74) (Otter, B. A., *et al.*, 1968). The syntheses also achieved a higher yield (80 %) than the alternative syntheses mentioned above.

The PMB protective groups were added next, to the nitrogens of the imidazole using 4-methoxybenzyl chloride and sodium hydride base, in strictly anhydrous conditions to prevent ester hydrolysis to the original carboxylic acid **49**. The work-up also used acidic aqueous phases to try to neutralize any remaining sodium hydroxide, and thus prevent base-catalysed hydrolysis. The crude product required some column chromatography in ethyl acetate and petrol and recrystallisation from ether and *n*-hexane but this yielded crystalline 1,3-bis(PMB)-4-methoxycarbonylimidazolin-2-one **52a** with NMR data showing new aryl ring environments (δ_H 6.91 - 6.78, 7.19 and 7.32, δ_C 113.4 (2 *C*H), 114.0 (*C*H), 114.4 (*C*H), 120.1 (*C*H), 127.2 (*C*H), 129.5 (*C*H), 129.6 (*C*H), 130.2 (2 *C*), 153.4 (*C*), 158.9 (*C*)), OMe protons (δ_H 3.76 and 3.79) and benzyl CH_2 environments (δ_H 4.76 and 5.16, δ_C 45.1 and 47.2). Two additional CH_3 groups were also detected in the DEPT-135 data (δ_C 55.2 and 55.3) indicative of the OMe of the PMB groups. The expected mass of 383.1602 ($M + H^+$) was also confirmed by high resolution mass spectrometry.

Reduction of the methyl ester group in this compound **52a** using diisobutylaluminium hydride (DIBAl-H) with recrystallisation gave the alcohol **53a** in comparable yields to the Bn/BOM protected analogue synthesised by Dransfield *et al.* (92 % relative to Dransfield *et al.*'s 87 %) (Dransfield, P. J., *et al.*, 2006). Initially Rochelle salt (potassium sodium tartrate) was used in the work-up, as this chelates aluminium released from DIBAl-H to prevent it forming hydroxide gels. These gels can disrupt partitioning of the crude product between DCM and water. However, subsequent work-ups simply used more MeOH to break-up these gels and produced

comparable yields, so the use of Rochelle salt was removed from the work-up. The IR showed one fewer carbonyl band than the starting material and an alcohol O-H band at 3270 cm^{-1}. NMR showed evidence of a new CH_2 (δ_C 108.9) as a doublet (δ_H 4.20), with splitting attributed to the neighbouring alcohol group, and loss of peaks associated with the third OMe group in the ester starting material **52a**. In addition, the mass spec. data gave the correct corresponding mass for the alcohol structure ($M + H^+$; 355.1654).

The alcohol **53a** was then oxidised to 1,3-bis(PMB)-4-formylimidazolin-2-one **38** using manganese dioxide. Mass spectrometry of the aldehyde showed a mass of 353 as expected. Both ^{1}H-NMR and ^{13}C-NMR showed peaks indicative of an aldehyde (δ_H 9.12 and δ_C 178.6) and loss of peaks from the starting material, which corresponded to the C-5 alcohol adduct. The IR data showed a new aldehyde carbonyl at 1703 cm^{-1}. This aldehyde **38a** was immediately frozen until needed, as it is reported to autooxidise back to the carboxylic acid **49** if left at room temperature in aerobic conditions (Hagenmaier, H., *et al.*, 1979).

An attempt was made to reduce the protected methyl ester **52a** to aldehyde **38a** in one step (as shown in Scheme 3.5 by the red star *****) rather than two steps via the alcohol **53a**. This has not been reported in the literature in relation to imidazolin-2-one derivatives but it has been reported on alkyl esters converted to alkyl aldehydes (Mears, R. J., *et al.*, 2006, Qin, H.-L. and Panek, J. S., 2008), and Thenappan and Burton state that distinguishing between an alcohol product and an aldehyde product is as simple as using 3 mole equivalents of DIBAl-H instead of stoichiometric quantities, with the latter only generating 3 % alcohol (Thenappan, A. and Burton, D. J., 1990). Therefore, the mole equivalence of DIBAl-H used in the reduction of ester **52a** was reduced from three to one. However, ^{1}H-NMR of the crude product showed no formyl peak and only the protected alcohol **53a** was recovered, so the synthesis was left unmodified.

*Obtaining a dehydro derivative of N(α)-Cbz, N(π),N(τ)-bis(PMB)-oxo-His-OMe **40a** via a Horner Wadsworth-Emmons (HWE) reaction*

The Horner-Wadsworth-Emmons (HWE) reaction is a modified Wittig reaction (Horner, L., *et al.*, 1958, Horner, L., *et al.*, 1959, Wadsworth, W. S. and Emmons, W. D., 1961, Wadsworth, W. S. J. and Emmons, W. D., 1973). This reaction couples an aldehyde or ketone to a phosphonate, as opposed to the usual triphenyl phosphonium ylide used in the Wittig Reaction. A strong base, such as NaH, is used to deprotonate the phosphonate, giving an anionic species that is a better nucleophile that traditional phosphonium ylids.

Many groups have reported the HWE reaction to generate dehydroamino acids from phosphorylglycine esters and aldehydes (Armstrong, R. W., *et al.*, 1992, Baldwin, J. E., *et al.*, 1993, Ciattini, P. G., *et al.*, 1988, Daumas, M., *et al.*, 1989, Debenham, S. D., *et al.*, 1997, Hammadi, A., *et al.*, 1992, Marino, S. T., *et al.*, 2004, Ratcliffe, R. W. and Christensen, B. G., 1973, Schmidt, U., *et al.*, 1992, Shin, C.-G., *et al.*, 1987), which can be enantioselectively hydrogenated using a chiral rhodium-phosphine catalyst (Marino, S. T., *et al.*, 2004, Schmidt, U., *et al.*, 1982, Schmidt, U., *et al.*, 1984). It also avoids the potentially acidic conditions and high temperatures, which can induce racemisation, of the alternative dehydroamino acid forming Erlenmeyer-Plöchl amino acid synthesis (Marino, S. T., *et al.*, 2004).

Schmidt *et al.* note the importance of protecting the ring nitrogens when synthesising histidine via a HWE reaction (Schmidt, U., *et al.*, 1984), and thus our precursor aldehyde **38** is ring nitrogen protected. This protected aldehyde **38a** has been coupled using the HWE reaction in a couple of literature reports(Dilley, A. S. and Romo, D., 2001, Dransfield, P. J., *et al.*, 2006), however, this was to a vinyl chloride and vinyl acetate and not to prepare amino acid derivatives. Nevertheless, these literature reports show that this imidazolin-2-one derivative is stable under the conditions of HWE reactions, e.g. strong base, unlike 2-oxo-histidine (see Chapter 1, Section 1.5.3.), and can give high yields, e.g. 89 % (Dransfield, P. J., *et al.*, 2006).

There are several syntheses of the phosphoryl glycine derivatives required for the HWE in the literature and these are summarised by Ferris *et al.* (Ferris, L., *et al.*, 1996). It is now most commonly generated by a Michaelis-Arbusov reaction of an α-alkoxyl glycine ester and a trialkyl phosphite (Schmidt, U., *et al.*, 1982, Schmidt, U.,

et al., 1984), as a high yielding, inexpensive synthetic route (Shankar, R. and Scott, A. I., 1993), and thus this is the synthetic route that this project took. Initially the triethyl ester **39a** was to be used and this was synthesised by modification of the procedures described by Williams *et al.* who use benzyl carbamate **55** and glyoxylic acid monohydrate **56** to form the analogous trimethyl ester (Scheme 3.6) (Williams, R. M., et al., 1990).

The addition of the diethoxyphosphinyl group was based on the procedure described by Coleman and Carpenter (Coleman, R. S. and Carpenter, A. J., 1993), which used a one-pot synthesis without isolation, in which the intermediate halide was used in a Michaelis-Arbuzov reaction with triethyl phosphite. This formed ethyl *N*-(benzyloxycarbonyl)-*α*-diethoxyphosphinylglycinate **(**Scheme 3.6**)** as phosphonate **39a**.

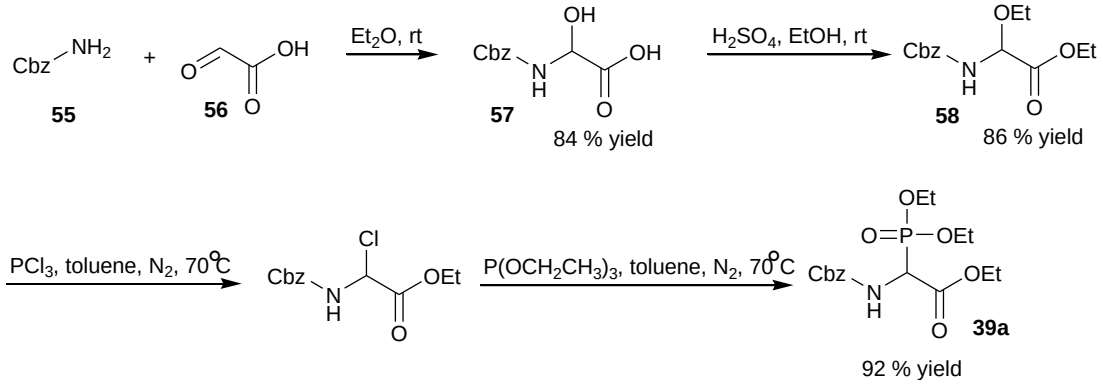

Scheme 3.6: Preparation of ethyl *N*-(Cbz)-*α*-ethoxyglycinate 39a.

However, the trimethyl ester can be purchased commercially and has the advantage over the triethyl ester of being more crystalline and being more easily hydrolysed upon deprotection (Schmidt, U., *et al.*, 1984). It is also more commonly used in the literature than the triethyl ester with a 95-fold greater number of publications citing the trimethyl ester on the Beilstein database than the trimethyl ester. Hence, this phosphonate **39b** was chosen for the HWE reaction.

The *N*-terminus protection used for the phosphonate **39b**, and hence the overall dehydroamino acid after coupling, was the carboxybenzyl (Cbz) group. This, along with the acetyl (Ac) group have been used successfully in the literature during synthesis of the phosphonate and under the conditions of HWE (Coleman, R. S. and Carpenter, A. J., 1993, Williams, R. M., *et al.*, 1990). In general, the Cbz group has the advantage over the Ac group of being removed under milder conditions - hydrogenation with a palladium catalyst - rather than the strongly acidic hydrolysis

conditions required to remove the Ac group. Hydrogenation as a deprotecting route would also have the advantage that, within the same reaction, Boc anhydride can be added to reprotect the amino function with a Boc group (Sakaitani, M., *et al.*, 1988), to give the desired N*(α)* protection required for Aβ synthesis (see Chapter 2, Section 2.1.2.). However, for the reasonably acid stable 2-oxo-histidine (see Chapter 1, Section 1.5.3.), with a ring system that may undergo hydrogenation, the acetyl protecting group may be more suitable that Cbz.

Several literature reports used 1,8-diazabicyclo[5.4.0]undec-7-ene (DBU) as the base for the HWE reaction instead of sodium hydride because it gave higher yields and stereoselectivity (Schmidt, U., *et al.*, 1992, Vaswani, R. G. and Chamberlin, A. R., 2008, Wang, W., *et al.*, 2002). This project also used this base for the additional reasons that it is a liquid, and hence easy to dispense, and it is soluble in organic solvents. Literature reports have also found DCM to be a higher yielding solvent than THF and thus this project used this solvent than THF and thus this project used this solvent (Vaswani, R. G. and Chamberlin, A. R., 2008).

Aldehyde **38a** was successfully coupled to phosphonate **39b** in a HWE reaction and generated an α,β-unsaturated precursor **40** to protected 2-oxo-histidine (Scheme 3.7). Characterisation of the product from the HWE reaction showed the expected olefinic proton at δ_H 6.49, with a downfield quaternary carbon (α-C) peak in the ^{13}C-NMR characteristic of an alkene (δ_C 119.5). In addition, peaks associated with both the Cbz and PMB groups were seen in the correct ratio indicating successful coupling of the aldehyde and the phosphonate to form a de-hydro derivative of 2-oxo-histidine.

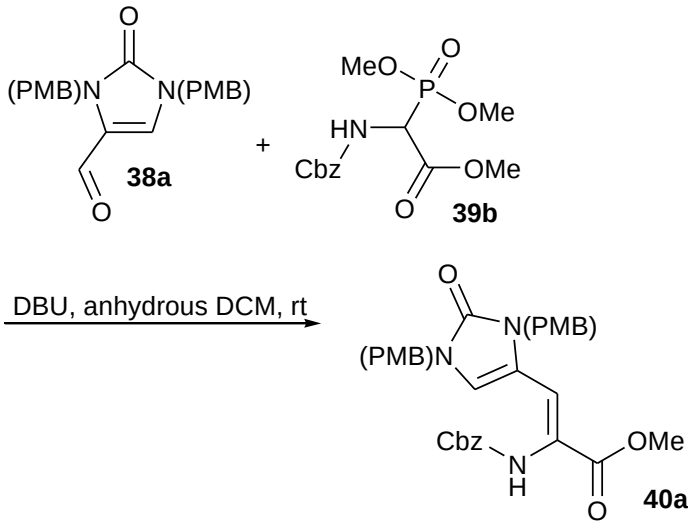

Scheme 3.7: Horner-Wadsworth-Emmons reaction to generate the *N*(α)-Cbz, *N*(τ),*N*(π)-PMB-dehydro-amino acid derivative 40a.

The characterisation data does not distinguish the configuration (*E* or *Z*) of the dehydro derivative **40a**. Use of 1D-NOE would be limited due to the lack of protons on the double bond with which to couple. However, based on literature reports on similar compounds, the likely predominant form is the *Z* isomer and this is how the dehydro derivative is represented in this PhD thesis. Schmidt *et al.* found the dehydro derivative of histidine, formed by a HWE reaction between the acetyl form of phosphonate **39c** and a non-oxidised analogue of the imidazoline aldehyde **38a**, to have a > 20 ratio of *Z*/*E*. It should be noted that Coleman and Carpenter have reported this diastereomeric selectivity to be highly base specific (Coleman, R. S. and Carpenter, A. J., 1993), and that Schmidt *et al.* use a different base to the one used in this PhD, i.e. potassium *t*-butoxide as opposed to DBU. However, subsequent papers by Schmidt *et al.* and Wang *et al.* used DBU as the base for their HWE reactions to form didehydroamino acid esters and also found a *Z*-selectivity (Schmidt, U., *et al.*, 1992, Wang, W., *et al.*, 2002), indicating that this is the likely isomer of **40a** formed.

Attempted asymmetric hydrogenation

The aim of this multi-step synthesis was to generate 2-oxo-histidine in the enantiomerically pure L-histidine form **4**. Starting from the dehydro-derivative **40a** required the introduction of a correctly configured chiral centre at the α-carbon. Therefore, initially a chiral catalyst was chosen to attempt α,β hydrogenation of the dehydro derivative **40a**.

In general, rhodium catalysts lead to hydrogenations with higher enantioselectivity than are seen if other metals, such as iridium, are used (Burk, M. J., *et al.*, 1993). Enantioselective rhodium catalysts were developed from the achiral rhodium-phosphine, Wilkinson's catalyst (chlorotris(triphenylphosphine)rhodium(I)) (Knowles, W. S., 2002). The use of phosphine ligands allows use of higher hydrogenation pressures to ensure faster reactivity, without losses in selectivity (Nagel, U. and Albrecht, J., 1998). Burk *et al.* then developed DuPHOS-based rhodium(I) catalysts (1,2-bis ((2S, 5S) with the DuPHOS ligands being electron rich bisphospholane ligands; 1,2-bis(phospholano)benzene (Nagel, U. and Albrecht, J., 1998). These catalysts have the advantage of having high efficiency (1/2500 ratio

catalyst/substrate), being commercially available, reacting quickly, producing high enantiomeric excess (> 99 %) and not being affected by changes in temperature or pressures below 50 atm, over which point there are slight reductions in selectivity (Knowles, W. S., 2002, Nagel, U. and Albrecht, J., 1998). They also hydrogenate both the *Z*- and *E*-isomer of the dehydroamino derivative to give the same absolute configuration (Knowles, W. S., 2002, Marino, S. T., *et al.*, 2004), which is not always the case for all chiral catalysts. Several groups have successfully used Burk's DuPHOS catalyst to enantioselectively hydrogenate α-enamides with aromatic substituents with a high enantioselectivity (Marino, S. T., *et al.*, 2004, Wang, W., *et al.*, 2002). A search of the literature on rhodium catalysts suitable to hydrogenate dehydroamino acids shows DuPHOS catalysts to have the highest enantiomeric excesses.

These catalysts work by generating two diastereomic catalyst-substrate complexes, with the minor diastereomer having much greater reactivity than the major diastereomer and thus generating the predominant product enantiomer (Scheme 3.8) (Halpern, J., 1982, Nagel, U. and Albrecht, J., 1998). These two catalyst-substrate diastereomers reacts via two catalytic cycles; the minor manifold pathway and the major manifold pathway (Scheme 3.8). The cyclooctadiene (COD) ligand of the catalyst is first hydrogenated and this loses affinity for the rhodium metal so it is displaced by two solvent molecules to form a bis-solvent-catalyst complex. The substrate then displaces these solvent molecules and chelates the rhodium metal side on via both its olefinic group and its amido oxygen. This complex can exist in two diastereomeric forms, the minor form reacting with hydrogen substantially faster than the major form to form a dihydro complex. This is the first irreversible step in the hydrogenation and hence the geometry of the dihydro complex, rather than the geometry of the substrate, determines the enantioselectivity of the hydrogenation (Nagel, U. and Albrecht, J., 1998), explaining why the E- and Z-isomers of the dehydro derivative are equally well hydrogenated.

Burk *et al.* compared a range of catalysts to generate α,γ-unsaturated dehydroamino acid derivatives and found the Et-DuPHOS-Rh(I) **59** to have the highest enantioselectivity (> 99 %) and, possibly more importantly, to have the highest regioselectivity; reducing the C-α=C-β double bond over the C-γ=C-δ double bond, which is as desired in our dehydro derivative of 2-oxo-histidine **40a** (Burk, M.

J., *et al.*, 1998a). The absolute configuration generated by Et-DuPHOS-Rh(I) catalysts is the same configuration as the catalyst (Burk, M. J., *et al.*, 1993), therefore to generate protected L-2-oxo-histidine, equivalent to *(S)*-2-oxo-histidine, a (*S*,*S*)-Et-DuPHOS-Rh(I) would be required.

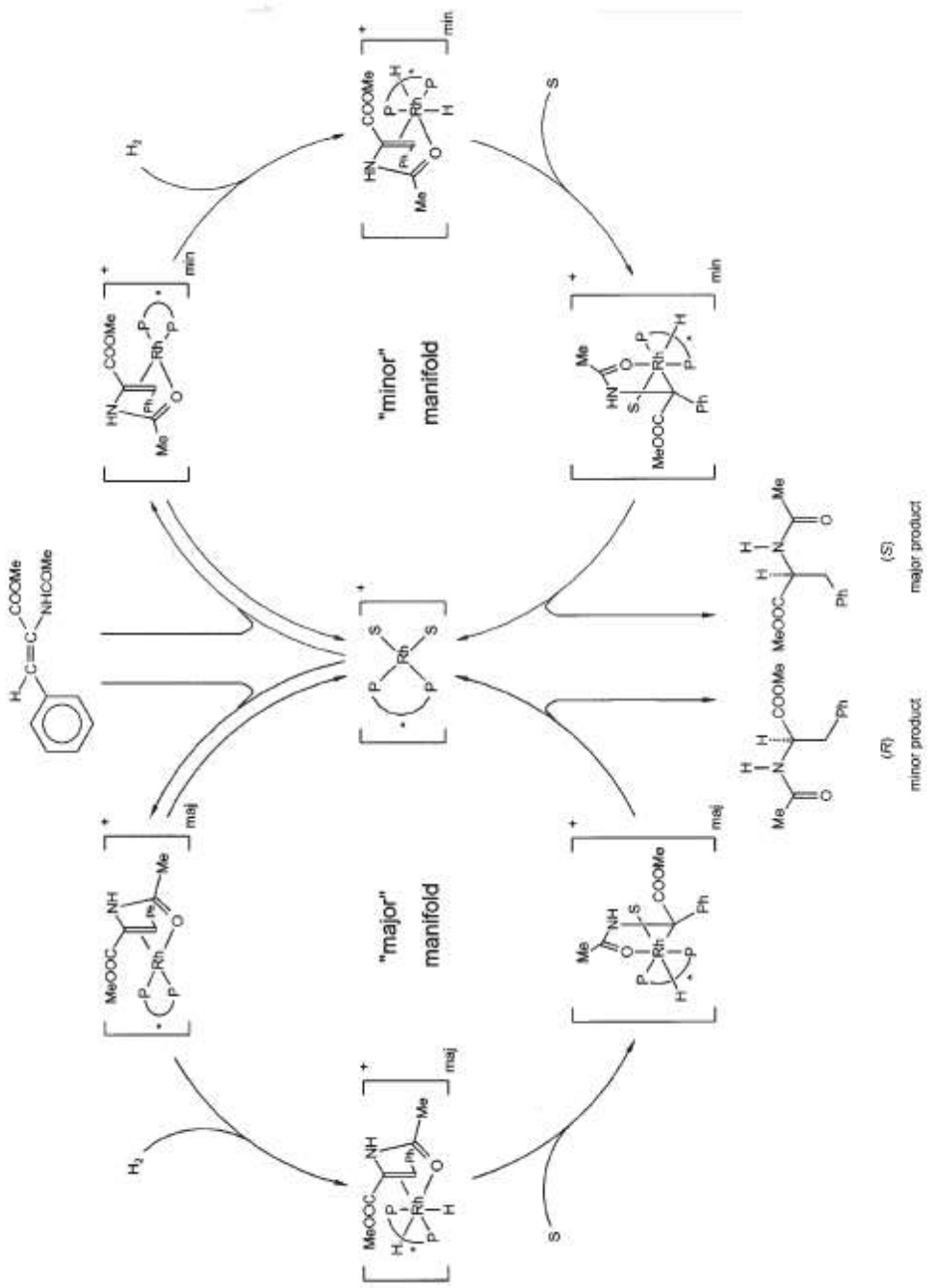

Scheme 3.8: The two catalytic cycles for hydrogenation by soluble rhodium complexes. The COD ligand of the catalyst is first hydrogenated and thus loses affinity for the rhodium metal so is displaced by two solvent molecules to form a bis-solvent-catalyst complex. The substrate then displaces these solvent molecules and chelates the rhodium metal side-on via both its olefinic group and its amido oxygen. The catalyst-substrate complex forms two diastereomers which react via two catalytic cycles; the minor manifold pathway and the major manifold pathway. The minor form reacts with hydrogen substantially faster than the major form to form a dihydro complex. This is the first irreversible step in the hydrogenation and hence the geometry of the dihydro complex, rather then the geometry of the substrate, determines the enantioselectivity of the hydrogenation (Nagel, U., and Albrecht, J., 1998).

In this project, hydrogenation of the dehydro derivative **40a** was attempted using the chiral rhodium catalyst;
1,2-bis[(2*S*, 5*S*)-2,5-dimethyl phosphono]benzene(cyclooctadiene)rhodium(I)tetraflu oroborate abbreviated to (*S*, *S*)-Et-DuPHOS-Rh(I) **59**. The catalyst was added at a 1:40 ratio with the substrate, the dehydro derivative **40a**.The hydrogenation was carried out in methanol, which had previously been reported to allow the greatest enantiomeric selectivity and regioselectivity when using Et-DuPHOS-Rh(I) catalysts over a range of solvents (Burk, M. J., *et al.*, 1998a, Fabrello, A., *et al.*, 2010). The flask was evacuated before the catalyst was added to reduce oxidation of the catalyst (Scheme 3.9). The hydrogenation was initially carried out under atmospheric conditions (i.e. approx. 1 – 2 bar) but only starting material was recovered. The hydrogenation was then attempted again in an autoclave under approximately 10 bar of hydrogen but, again, only starting material was recovered.

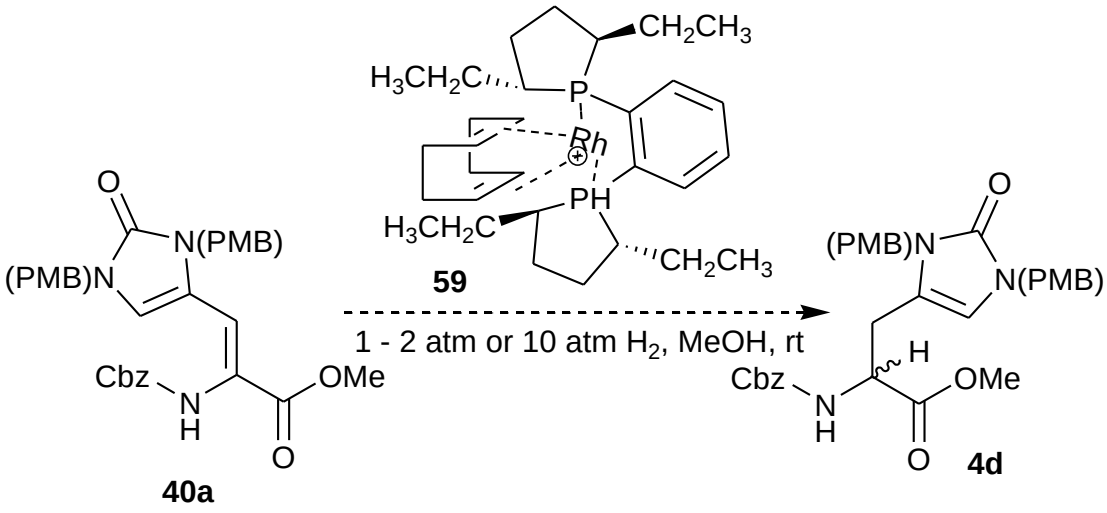

-

Scheme 3.9: Attempted enantioselective hydrogenation of the *N*(α)-Cbz dehydro derivative 40a. This used the catalyst (*S*, *S*)-Et-DuPHOS-Rh(I) **59**.

Non-enantioselective hydrogenation

To check if general hydrogenation of the dehydro derivative **40a** was possible an achiral catalyst, platinum oxide (PtO_2, Adam's catalyst), was used. The same hydrogenation conditions were used as for the chiral catalyst **59** but at a 1:3 molar ratio of catalyst to substrate. This did successfully yield a protected derivative of 2-oxo-histidine **4d** (Scheme 3.10) with the expected β-CH_2 pair of

doublets-of-doublets at δ_H 2.67 and δ_H 2.72 (δ_C 28.1 and 44.2) and a doublet for the α-CH at δ_H 4.41 (δ_C 114.1) (Figure 3.1 and Figure 3.2). However, this is will be a racemic product and hence not suitable for peptide synthesis of Aβ.

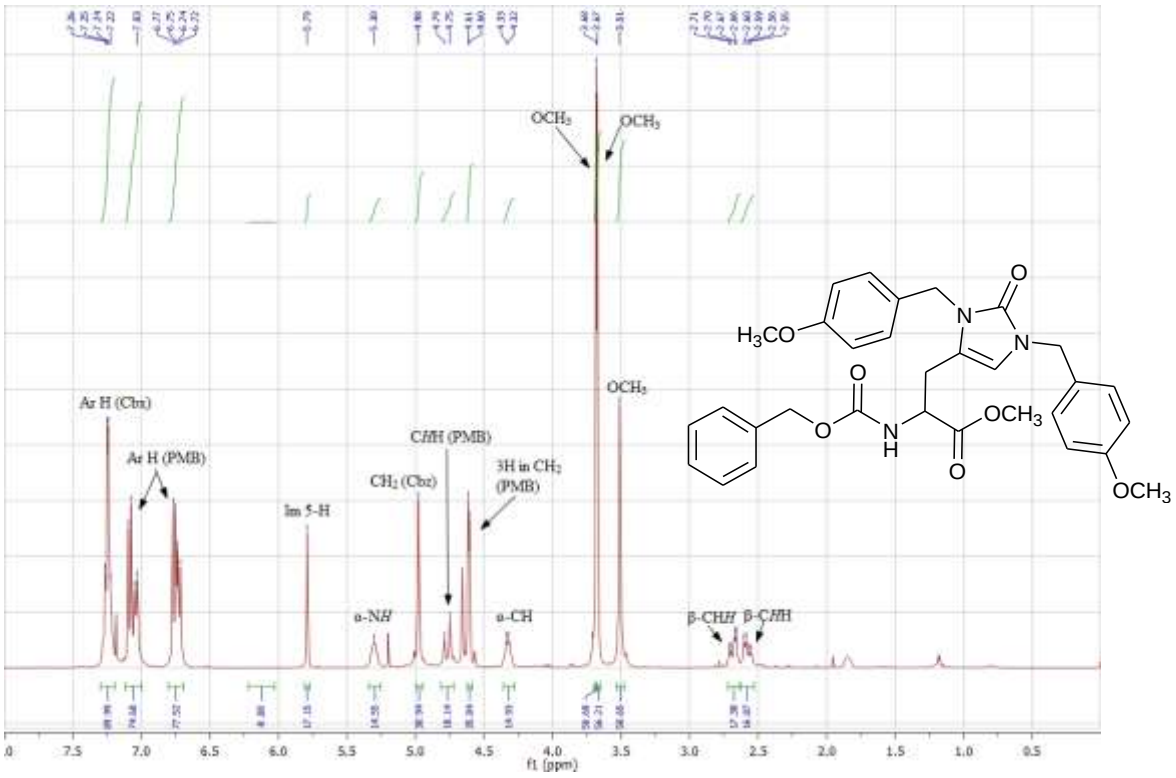

Figure 3.1: ^{1}H-NMR (400 MHz; $CDCl_3$) spectrum of *N*(α)-Cbz, *N*(π), *N*(τ)-Bis(PMB)-2-oxo-His-OMe 4d.

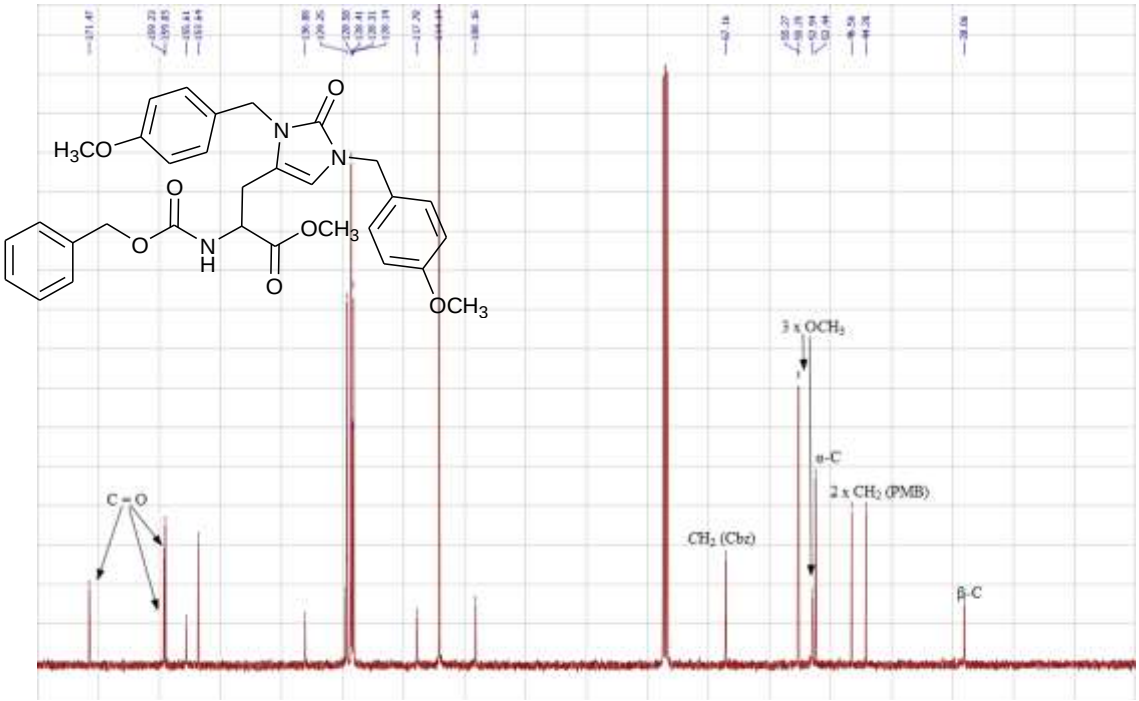

Figure 3.2: ^{13}C-NMR (100.65 MHz; $CDCl_3$) spectrum of *N*(α)-Cbz, *N*(π), *N*(τ)-Bis(PMB)-2-oxo-His-OMe 4d.

Two additional compounds were isolated from the crude product of the hydrogenation; a C-4,C-5 dihydro, α,β-dehydro derivative of 2-oxo-histidine **60** and a C-4,C-5 dihydro 2-oxo-histidine derivative **61,** as a 45:55 mixture of two diastereomers (Scheme 3.10). This shows that the 4-C=C-5 double bond of imidazole is reduced more readily than the corresponding double bond in non-oxidised histidine derivatives, which have a greater aromatic character.

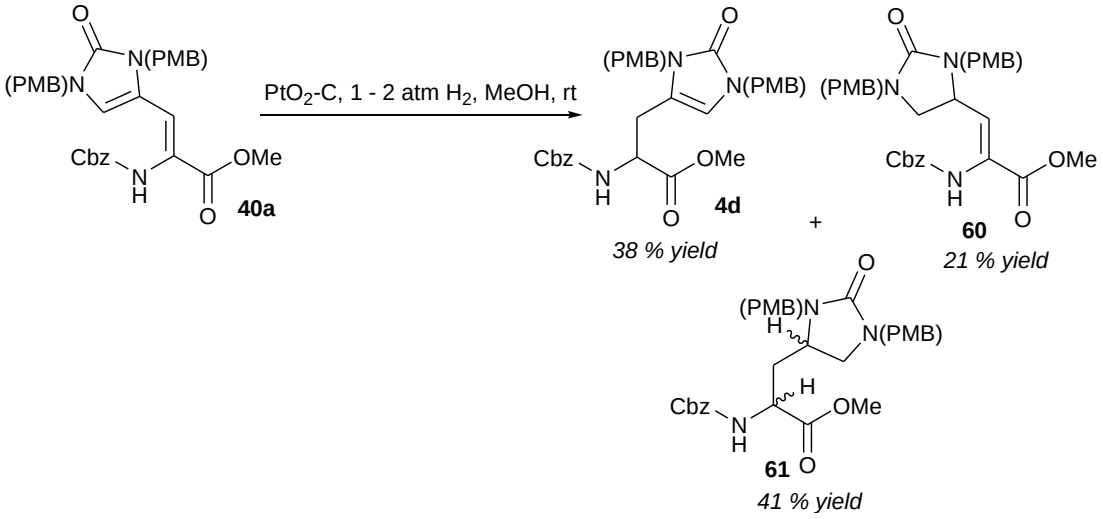

Scheme 3.10: Hydrogenation of the *N*(α)-Cbz, *N*(τ),*N*(π)-bis(PMB)-dehydro-derivative of 2-oxo-histidine 40a with a platinum catalyst.

The C-4,C-5 dihydro, α,β-dehydro derivative of 2-oxo-histidine **60** showed the remaining olefinic proton at the β-carbon (δ_H 6.13, δ_C 130.2, Figure 3.3 and Figure 3.4) indicating this bond had not been hydrogenated. In addition, the C-5 proton signal was now presenting as an AB system of two doublets at δ_H 2.90 and δ_H 3.38 (δ_C 46.3) indicating **60** now had diastereotopic C*H*$_2$ environments (Figure 3.3). The new chiral centre was identified as C-4, which presented as a doublet of doublets of doublets at δ_H 4.06 (δ_C 51.1) coupled to both the β-CH and the H$_2$C-5 (Figure 3.5).

The C-4,C-5 dihydro 2-oxo-histidine derivative **61** presented the expected α,β reduction with a pair of diastereotopic doublets of doublets at δ_H 1.59 and δ_H 2.20 (δ_C 53.5, Figure 3.6 and Figure 3.7) coupled to both the new chiral centre at the α-CH (δ_H 4.12 – 4.20, δ_C 128.1) and the new chiral centre at C-4 (δ_H 3.23 - 3.34, δ_C 114.0, Figure 3.8). As with product **60**, this product presented with the diastereotopic H-5 (δ_H 2.74 and 3.14, δ_C 47.9) protons and the new chiral centre at C-4.

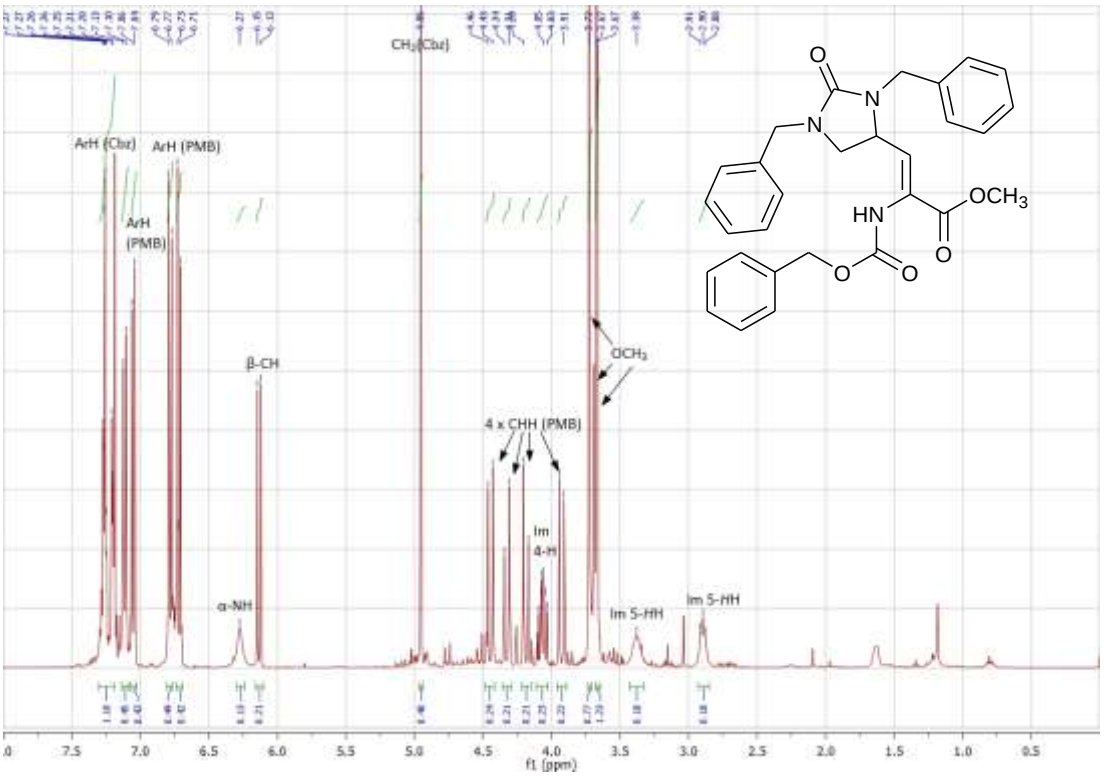

Figure 3.3: ^{1}H-NMR (400 MHz; $CDCl_3$) spectrum of *N*(α)-Cbz, *N*(π), *N*(τ)-Bis(PMB)-α,β-dehydro-4,5-dihydro-2-oxo-His-OMe 60.

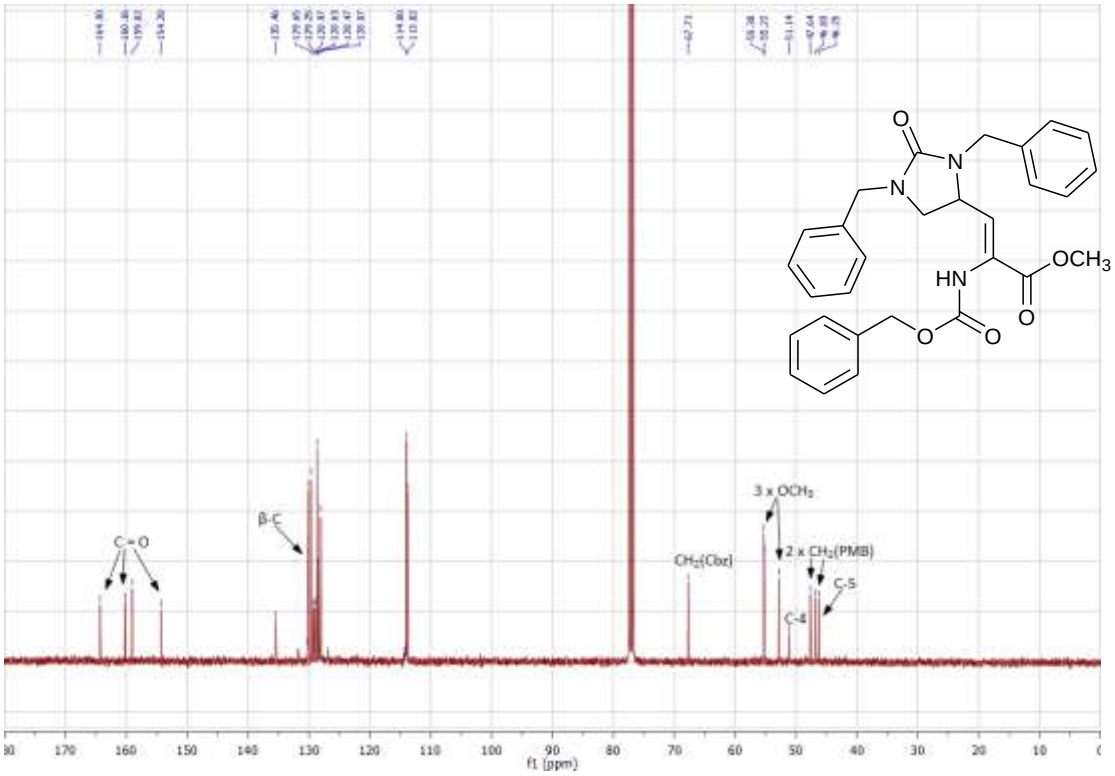

Figure 3.4: ^{13}C-NMR (100.65 MHz; $CDCl_3$) spectrum of *N*(α)-Cbz, *N*(π), *N*(τ)-Bis(PMB-α,β-dehydro-4,5-dihydro-2-oxo-His-OMe 60.

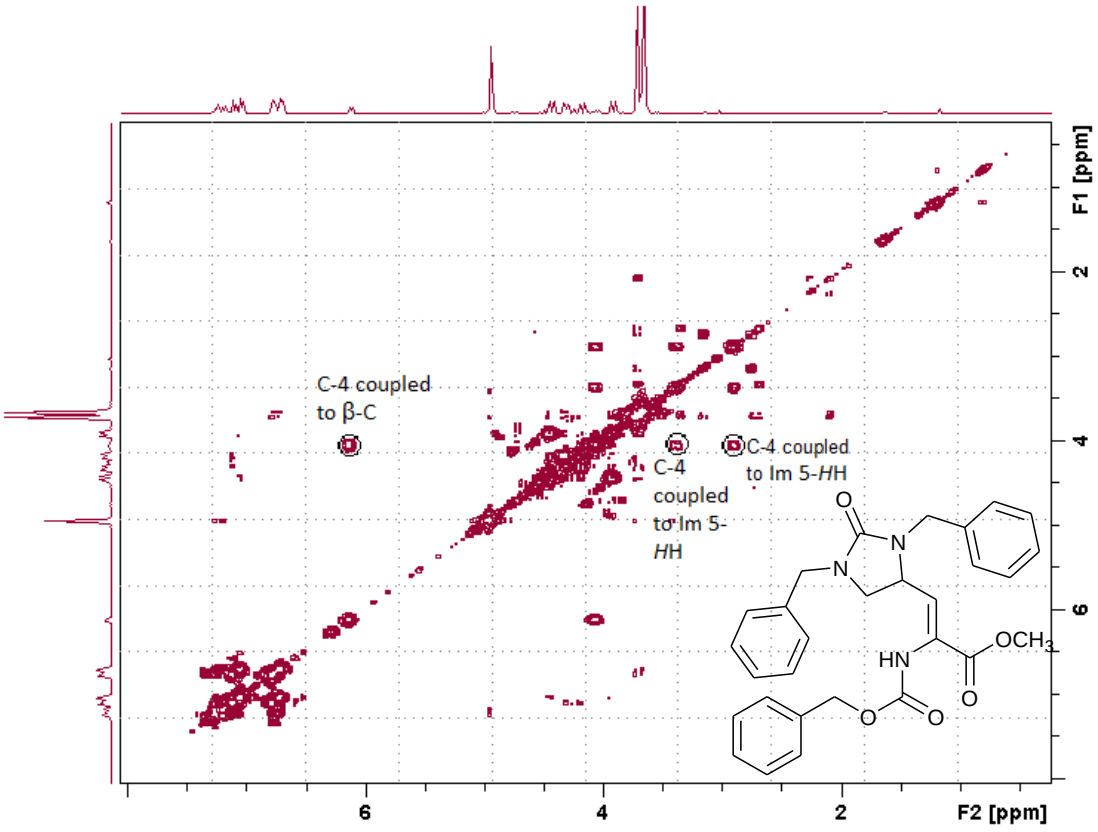

Figure 3.5: ^{1}H – ^{1}H COSY (400 MHz; $CDCl_3$) NMR spectrum of *N*(α)-Cbz-*N*(π),-*N*(τ)-Bis(PMB)-α,β-dehydro-4,5-dihydro-2-oxo-His-OMe 60.

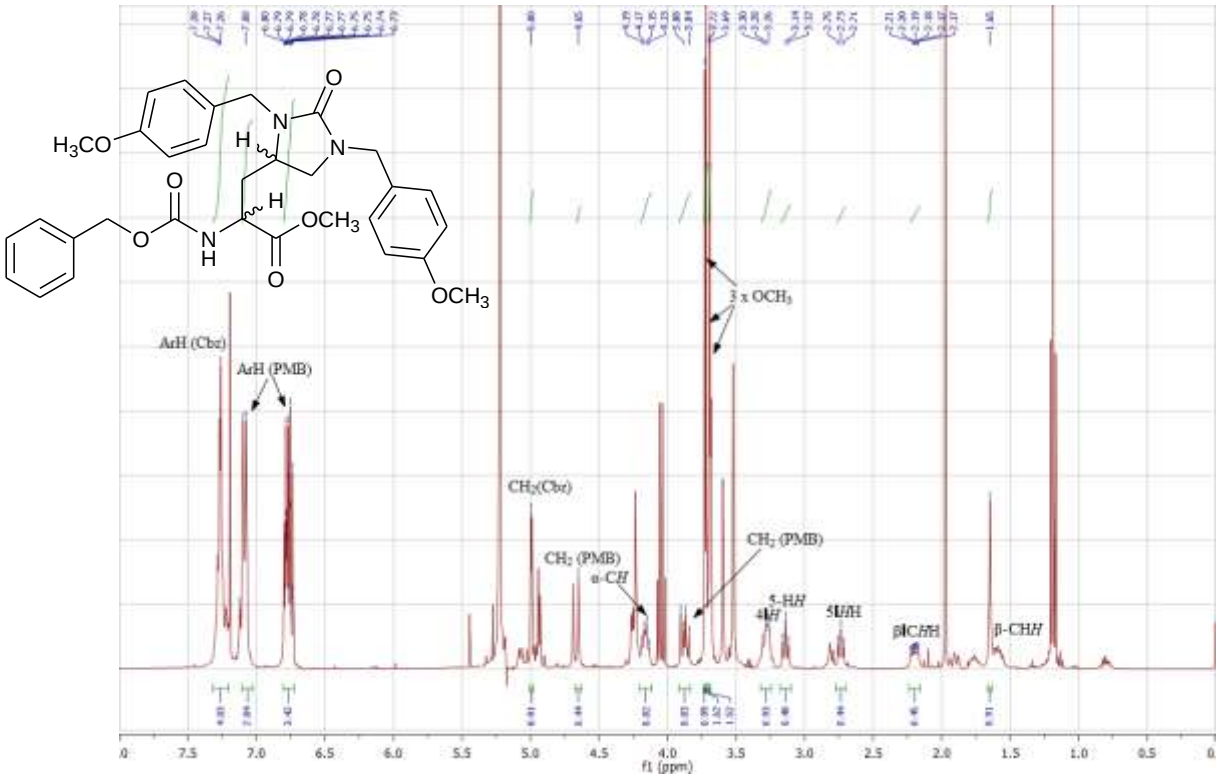

Figure 3.6: ^{1}H-NMR (400 MHz; $CDCl_3$) spectrum of *N*(α)-Cbz, *N*(π), *N*(τ)-Bis(PMB)-4,5-dihydro-2-oxo-His-OMe 61.

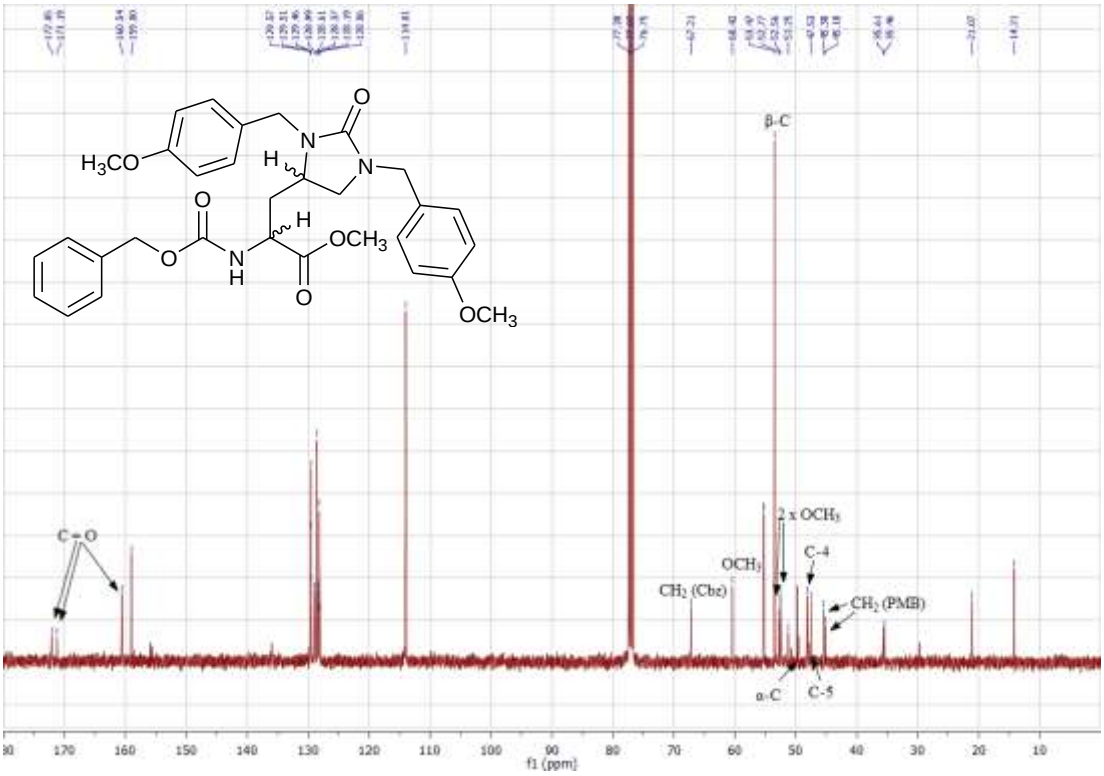

Figure 3.7: ^{13}C-NMR (100.65 MHz; $CDCl_3$) spectrum of *N*(α)-Cbz, *N*(π), *N*(τ)-Bis(PMB)-4,5-dihydro-2-oxo-His-OMe 61.

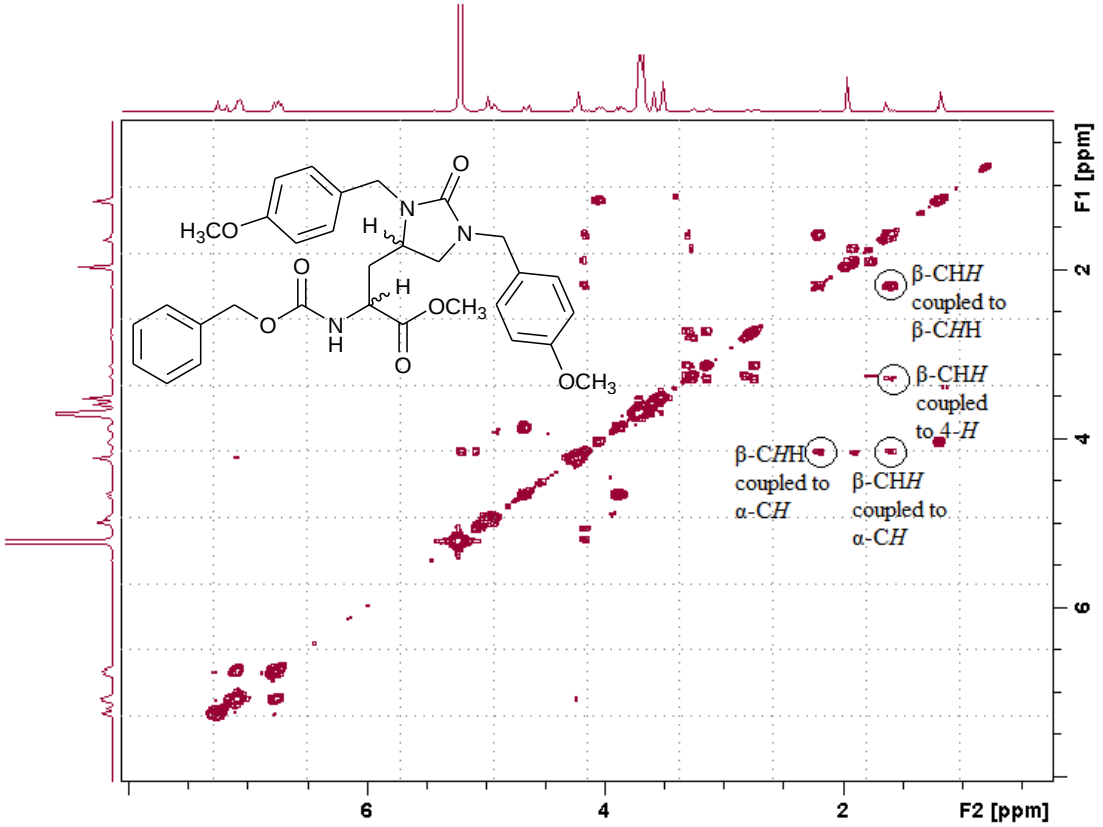

Figure 3.8: ^{1}H – ^{1}H COSY (400 MHz; $CDCl_3$) NMR spectrum of *N*(α)-Cbz, *N*(π), *N*(τ)-Bis(PMB)-4,5-dihydro-2-oxo-His-OMe 61.

Of the three hydrogenation products generated in this reaction the most high yielding (41 %) is the derivative **61** with both the 4-C=C-5 and α-C=β-C double bonds reduced. Of the two mono-reduced products the most common product is α-C=β-C dihydro derivative (2-oxo-his) **4d** with a 38 % yield compared to the 21 % yield of the 4-C=C-5 dihydro derivative **60** indicating that the imidazole ring is less reactive to hydrogenation than the α-C=β-C double bond.

Use of the N(α)-Acetyl group

It was at this time that a paper was found describing the necessity of an amide group as the amino-protective groups in these hydrogenations, in order to allow co-ordination of the rhodium cation of the catalyst complex via the amide oxygen (Burk, M. J., *et al.*, 1998b). Burk *et al.* found this true for α,γ-dienamide esters, which have a similar pattern of unsaturation as 2-oxo-histidine (Burk, M. J., *et al.*, 1998a). Carbamates such as *N*-Cbz were found not to chelate the rhodium metal. In addition, the universal enantiomeric selectivity across both *Z*-isomers and *E*-isomers is slightly less for N*(α)*-Cbz protected enamides than N*(α)*-Ac protected enamides (i.e. 92 % ee compared to > 99 % ee) (Burk, M. J., *et al.*, 1993) and other studies have found *N*-Ac protected dehydro derivatives to give a better enantiomeric excess than *N*-Cbz dehydro derivatives (Kreuzfeld, H.-J., *et al.*, 1993). In addition, an Ac protecting group may, as discussed above, allow a different selection of rhodium chiral catalysts, which were not suitable for *N*-Cbz protected dehydro derivative, to be trialled on the *N*-Ac-dehydro derivative.

Therefore, the enantioselective hydrogenation using the (*S*, *S*)-Et-DuPHOS-Rh(I) catalyst **59** was trialled on the Ac-dehydro derivative **40b** (Scheme 3.13). This required the synthesis of the dehydro-derivative of 2-oxo-histidine to be redesigned to incorporate an acetyl protecting group at the amino terminus rather than a Cbz group. It was decided that this protecting group would be introduced onto the phosphonate before the HWE coupling.

Schmidt *et al.* note that the *N*-Cbz group can easily be cleaved and replaced with an *N*-acetyl group without adding any more complications to the subsequent HWE reaction (Schmidt, U., *et al.*, 1984). Indeed, several *N*-protecting groups can be used such as *N*-Boc, *N*-chloroacetyl and *N*-formyl, but not *N*-trifluoroacetyl

(Schmidt, U., *et al.*, 1984). However, Schmidt *et al.* used a two-step method (Schmidt, U., *et al.*, 1984) for generating the Ac-phosphonate **39c** from the Cbz-phosphonate **39b** which seemed unnecessary based on the similarity in reagents used in both steps and the fact that the isolated intermediate was likely to be unstable. Therefore, the method used in this project was based on that described by Hoshina *et al.* which used a one-pot synthesis of the Ac-phosphonate **39c** from the Cbz-phosphonate **39b** via a hydrogenation with a Pd/C catalyst in conjunction with an acetylation by acetic anhydride (Scheme 3.11) (Hoshina, Y., *et al.*, 2007). This synthesis also uses acetic acid as the solvent instead of either a two component methanol-DCM solvent system or methanol, used in other syntheses (Schmidt, U., *et al.*, 1984, Vaswani, R. G. and Chamberlin, A. R., 2008), to try and prevent methyl acetate forming as a by-product. The Ac-phosphonate **39c** was successfully synthesised, as shown by a similar melting point to those reported in the literature (Mazurkiewicz, R. and Kuznik, A., 2006, Schmidt, U., *et al.*, 1984), the loss of the Cbz-group-associated benzyl protons from the ^{1}H-NMR and the addition of an acetyl CH_3 at δ_H 2.06, as reported by Hoshina *et al.* (δ_H 2.09). The ^{31}P-NMR also showed a pure compound with only one peak (δ_P 20.0).

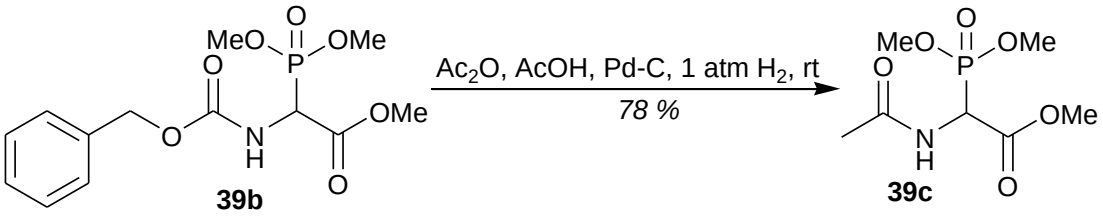

Scheme 3.11: Synthesis of ethyl *N*-(Ac)-*α*-dimethoxyphosphinylglycinate (39b).

The Ac-phosphonate **39c** was successfully coupled to the PMB-protected aldehyde **38a** using the HWE condensation used on the original Cbz-phosphonate (Scheme 3.12). The Ac and PMB associated protons signals presented in the correct ratios and the olefinic environments associated with the α,β double bond were seen at δ_H 6.28 and δ_C 116.4. However, on attempted hydrogenation of the Ac-dehydro derivative **40b** with the (*S*, *S*)-Et-DuPHOS-Rh(I) catalyst **59**, only starting material was obtained (Scheme 3.13).

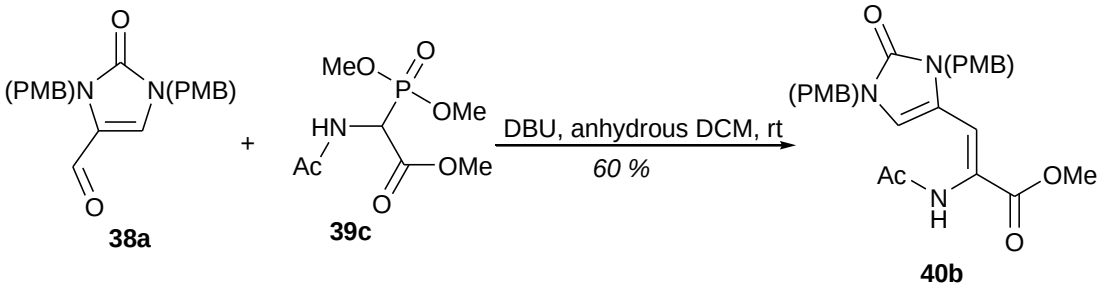

Scheme 3.12: Horner-Wadsworth-Emmons reaction to generate the *N*(α)-Ac, *N*(τ),*N*(π)-PMB -dehydro-amino acid derivative 40b.

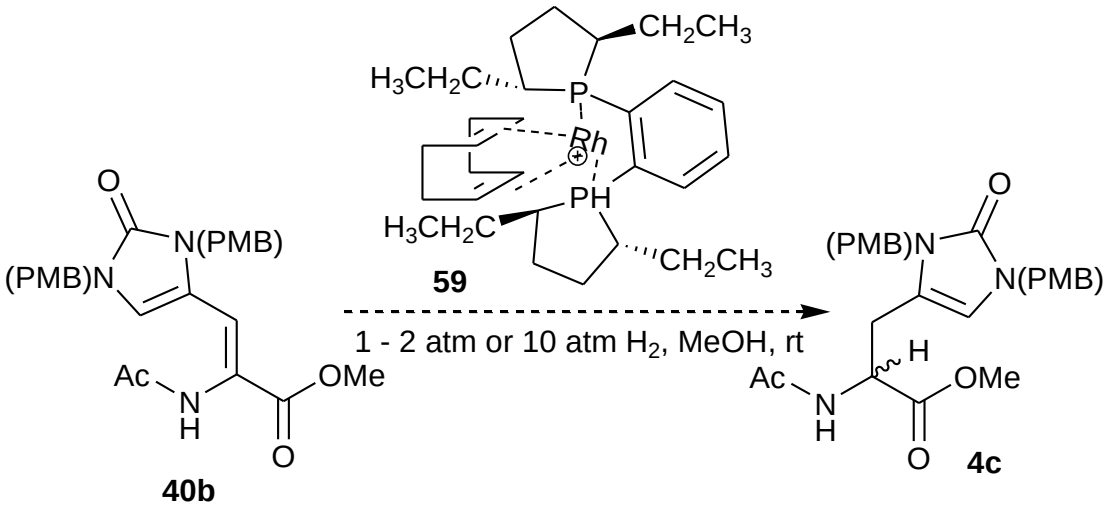

Scheme 3.13: Attempted enantioselective hydrogenation of the *N*(α)-Ac dehydro derivative 40b. This used the catalyst (*S, S*)-Et-DuPHOS-Rh(I) **59**.

The catalyst (*S, S*)-Et-DuPHOS-Rh(I) **59** is reported in the literature as being highly air sensitive (Burk, M. J., *et al.*, 1999, Guernik, S., *et al.*, 2001), especially when in solution. Hence, an analysis of the structure and function of this catalyst **59** was then done. A ^{1}H-NMR spectrum of the catalyst run in $CDCl_3$ showed mostly upfield methyl and olefinic protons, not expected of the catalyst's ligands. A test of functionality was then done by analysing the effect of the catalyst on a typical model hydrogenation of methyl-2-acetamido-acrylate **62** to 2-acetamidopropionic acid methyl ester **63** (Scheme 3.11) (Burgemeister, K., *et al.*, 2007, Cobley, C. J., *et al.*, 2003). Only starting material **62** was obtained. Therefore, use of this chiral catalyst was abandoned. There may be more potential for an enantioselective hydrogenation of protected N*(α)*-Cbz-2-oxo-his with use of (*S,S*)-Pr-DuPHOS-Rh(I) catalyst **59**, which has been successfully been shown to hydrogenate N*(α)*-Cbz-alanine (Burk, M. J., *et al.*, 1993) or the non-air sensitive ferrocenyldiphosphine rhodium catalyst

(Kang, J., *et al.*, 1998). However, this required further time and resources than were available for this PhD project.

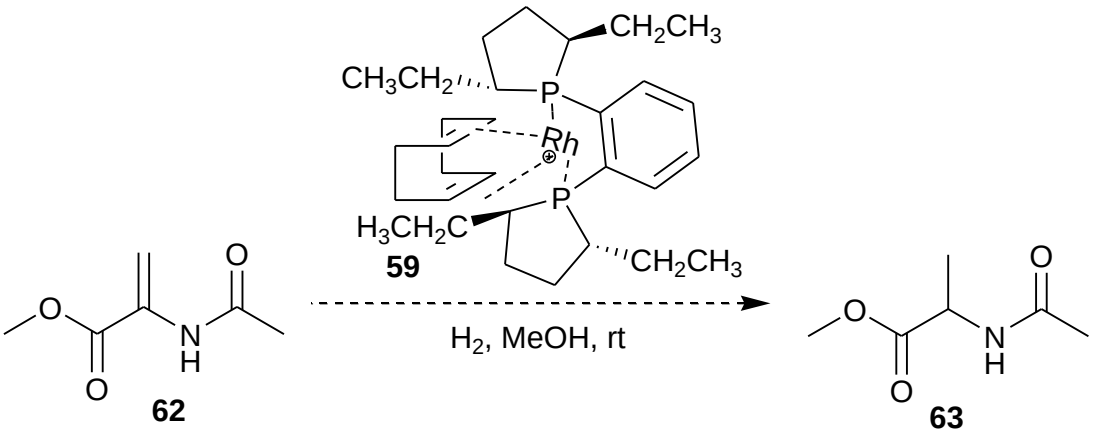

Scheme 3.14: Model reduction of methyl-2-acetamido-acrylate 62.

As a non-asymmetric hydrogenation was now the only route to protected 2-oxo-histidine from the dehydro-derivative **40** it was now an imperative to find a method of separating the enantiomers of 2-oxo-histidine generated by such a hydrogenation. One proposed method was the use of enzymes which would selectively deprotect a single enantiomer of the oxidised amino acid at the amino terminus, thus allowing easy separation of the deprotected enantiomer from the protected enantiomer using column chromatography. One such enzyme is Hog renal acylase (aka Acylase 1 from porcine kidney) (Bretschneider, T., *et al.*, 1988). This will only cleave acetyl groups from the amino terminus of L-configured amino acids and thus allows separation of racemic mixtures of protected 2-oxo-histidine by solvent extraction.

Therefore, with this method in mind, a non-asymmetric hydrogenation of the Ac-dehydro derivative **40b** was attempted using Adam's catalyst (Scheme 3.15), with similar hydrogenation conditions as had been previously done on the Cbz-dehydro derivative **40a**. However hydrogenation of the Ac-dehydro-derivative (**7,** R = Ac) with PtO_2 led to reduction of the PMB benzyl groups, with a multitude of upfield hydrocarbon peaks in the ^{1}H-NMR of the crude product. It appeared that the N*(α)*-Cbz protection was affording some protection of the N*(τ)*,N*(π)*-PMB groups from hydrogenation, which was not afforded by the N*(α)*-Ac protection. Therefore, it was decided to abandon syntheses using N*(α)*-Ac protection.

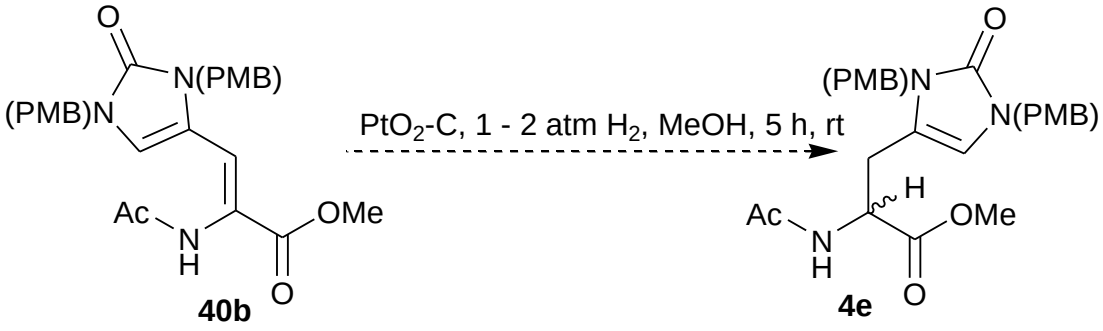

Scheme 3.15: Attempted hydrogenation of the *N*(α)-Ac, *N*(τ),*N*(π)-bis(PMB)-dehydro-derivative of 2-oxo-histidine 40b with a platinum catalyst.

Attempted deprotection of N(α)-Cbz, N(π),N(τ)-bis(PMB)-oxo-his OMe ***4d***

As discussed above, PMB protecting groups for the ring nitrogens were considered advantageous over groups such as BOM because the literature reported that they could be removed by oxidation with cerium(IV) diammonium nitrate (CAN) (Bull, S. D., *et al.*, 2001, Johansson, R. and Samuelsson, B., 1984, Smith, A. B., *et al.*, 1992, Yamaura, M., *et al.*, 1985), instead of the usual hydrogenation required to deprotect other protecting groups such as BOM groups. This reduces the chance of the C-4,C-5 double bond of the imidazolin-2-one ring system being reduced as was seen in the formation of products **60** and **61**.

Therefore, a deprotection using CAN was attempted on the protected 2-oxo-histidine derivative **4d** (Scheme 3.16(A)). This was performed in acetonitrile, as this is a solvent unlikely to be oxidised. Both 4-methoxybenzaldehyde **64** in 96 % yield and traces of PMB alcohol **65** (identified by TLC) were recovered, implying CAN deprotects by both oxidative and hydrolytic mechanisms. This second mechanism has been implied in the literature by the recent finding that CAN can have Lewis acid like behaviour (Scheme 3.17) (Caruso, T., *et al.*, 2006).

But the only amino acid derivative recovered was over oxidised so that the ring now contained two nitrone groups **66**. This structure is supported by imine bands in the IR at 1613 cm^{-1} and ^{1}H-NMR at δ_H 8.64 (Figure 3.9). The mass spectrometry data - 564.2335 ($M + H^+$), 581.2599 ($M + NH_4^+$), 586.2149 ($M + Na^+$) - predicted the mass of the product to be approximately 563.23. The product was also found to dimerise under electrospray ionisation (ESI) conditions giving an $M + NH_4^+$ ion at 1144.4890. All three protecting groups were indicated as intact by ^{1}H-NMR.

This is a novel compound, but it was little use as a deprotection product of 2-oxo-histidine. The yield obtained was less than 4 % for this over-oxidised amino acid, but no other product with an intact imidazolin-2-one ring was detected by ^{1}H-NMR. This indicates that, although deprotection was successful, the remaining amino acid derivative was destroyed by the oxidative conditions. However, using less CAN is unlikely to cause deprotection, as Yamaura *et al.* have reported poor deprotection yields at low CAN concentrations (Yamaura, M., *et al.*, 1985). In addition, CAN has been shown to promote intramolecular cyclisation between ketones in imidazolinone ring systems and neighbouring alkyl chains (Zancanella, M. A. and Romo, D., 2008) and so may not be appropriate for deprotection of imidazolin-2-one ring systems.

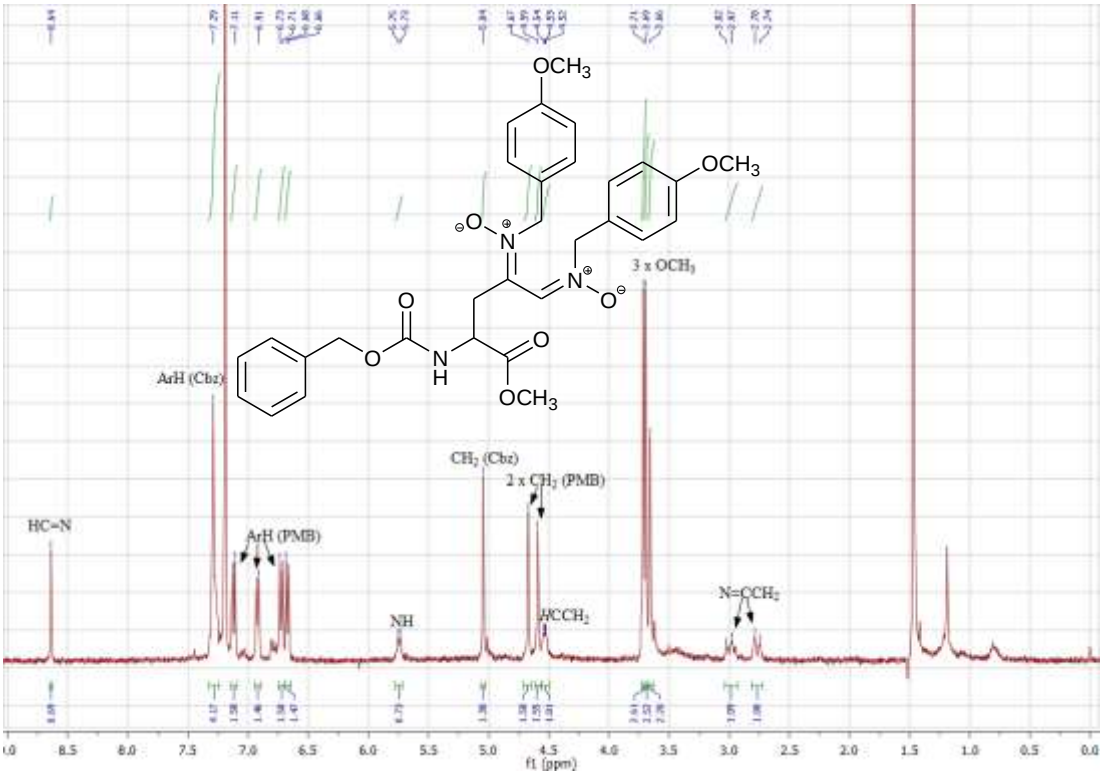

Figure 3.9: ^{1}H-NMR (400 MHz; $CDCl_3$) spectrum of 2-carboxybenzylamino-4,5-bis-(PMB-imino)pentanoic-acid methyl ester *N*(4), *N*(5)-dioxide 65.

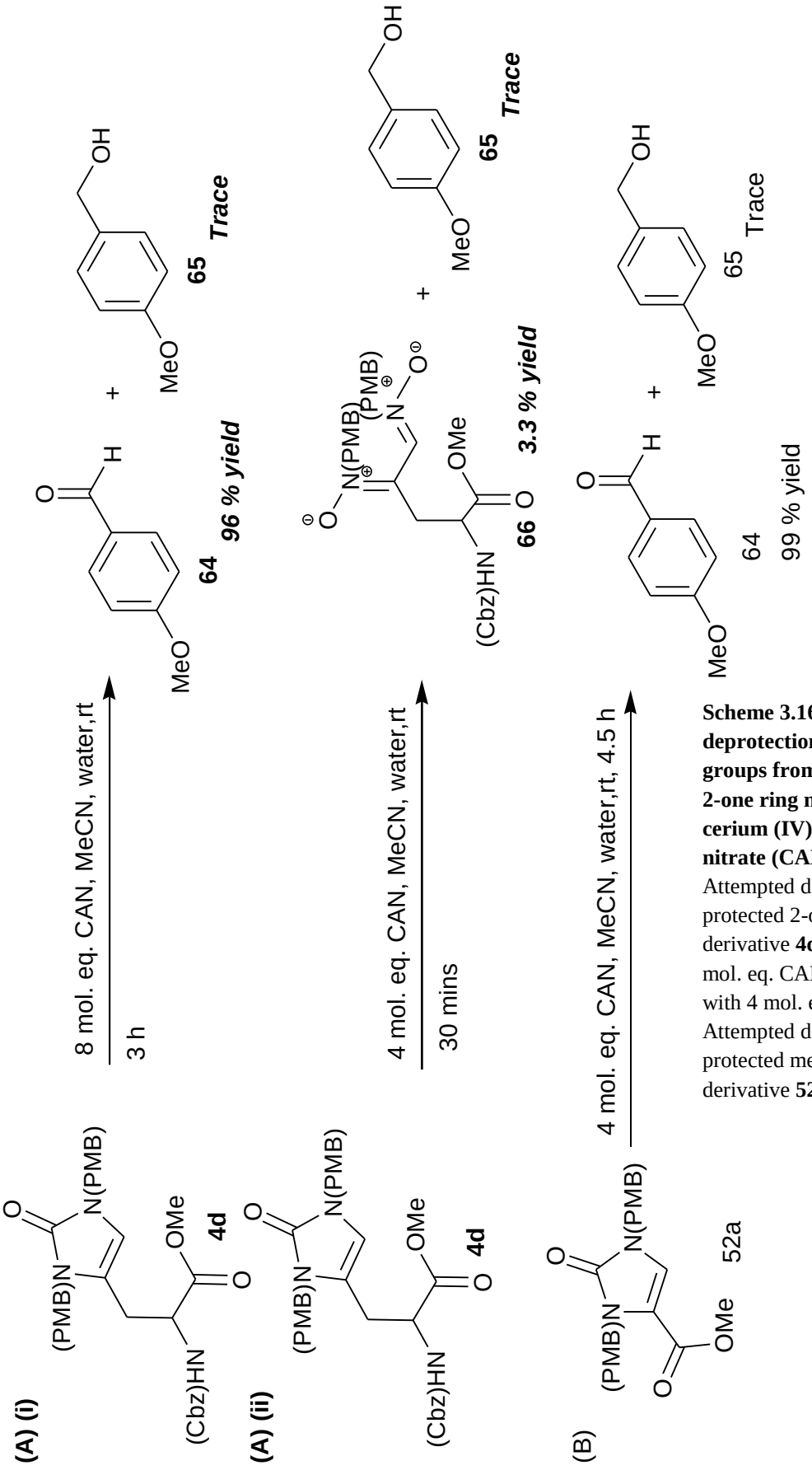

Scheme 3.16: Attempted deprotection of PMB groups from imidazolin-2-one ring nitrogens using cerium (IV) ammonium nitrate (CAN). (A) Attempted deprotection of protected 2-oxo-histidine derivative **4d**. **(i)** 3 h with 8 mol. eq. CAN. **(ii)** 30 min with 4 mol. eq. CAN. **(B)** Attempted deprotection of protected methyl ester derivative **52a**

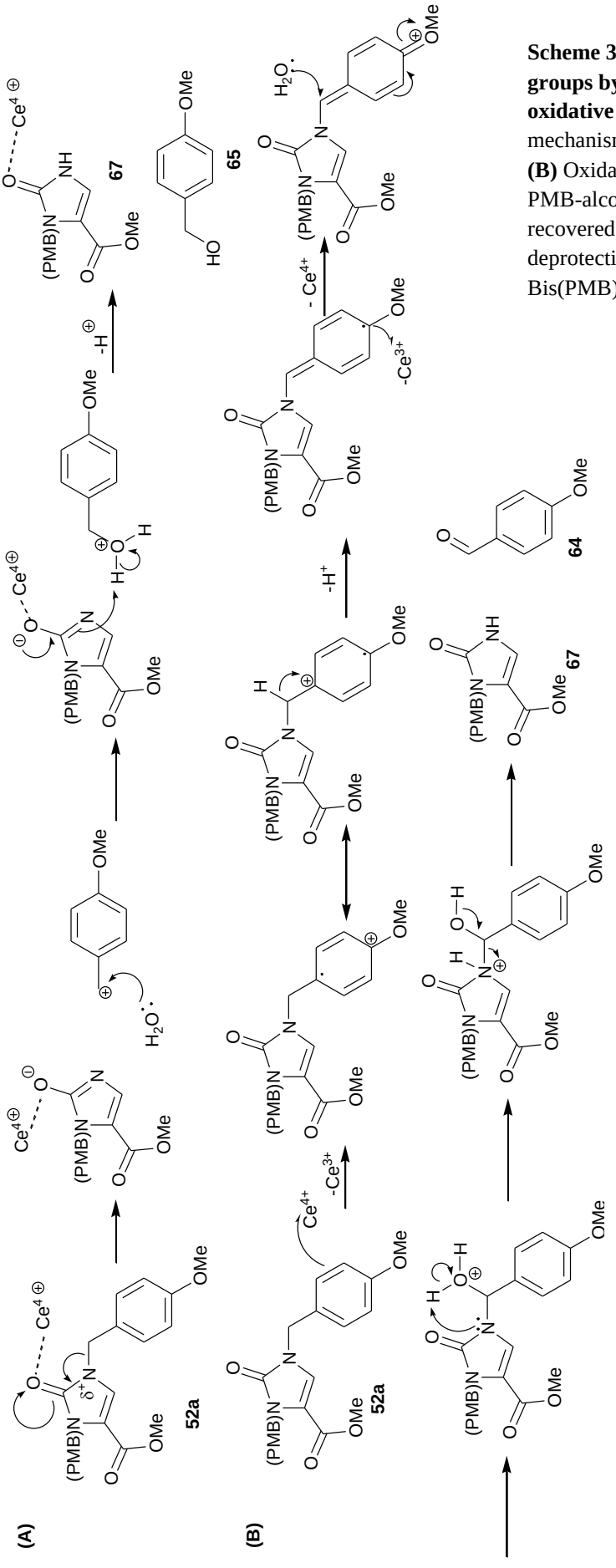

Scheme 3.17: CAN removes PMB groups by both hydrolytic and oxidative mechanisms. (A) Hydrolytic mechanisms generate PMB-aldehyde **64**. **(B)** Oxidative mechanisms generate PMB-alcohol **65.** Both have been recovered from CAN-mediated deprotections of *N*(α)-Cbz, *N*(π), *N*(τ)-Bis(PMB)-2-oxo-His-OMe **4d**.

CAN-mediated deprotection was then attempted on a simpler model system, the PMB-methyl ester **52a** (Scheme 3.16(B)), but, despite 4-methoxybenzaldehyde **64** being isolated, the deprotected methyl ester could not be extracted into an organic solvent so as to separate it from cerium ions. This made NMR based characterisation impossible due both to domination of the spectra with ammonium ion peaks and to peak broadening due to paramagnetic Ce^{3+}. Therefore, CAN-mediated oxidation was abandoned as a deprotection method.

PMB groups are also reported in the literature to be removable by strongly acidic conditions (Yamaura, M., *et al.*, 1985). Therefore, the second method of deprotection tested was an acid-based deprotection. Initially TFA was trialled. Room temperature reactions (4 h incubation) on the PMB-methyl ester **52a** (Scheme 3.18(A)), based on procedures used by Chida *et al.* (Chida, N., *et al.*, 1993), led to simply starting material being recovered. Reactions under reflux, based on procedures used by Brooke *et al.* (Brooke, G. M., *et al.*, 1997) (96 h incubation) (Scheme 3.18(B)) led to deprotection but only of one PMB group leaving the mono-PMB-methyl ester **67**. ^{1}H-NMR showed the new free NH with a broad peak at δ_H 10.90 and the integrals of the PMB associated protons were reduced by half compared to the original di-PMB protected product **52a**. The specific regiochemistry of this compound was determined using a 1D-NOE experiment (Figure 3.10). The ring proton was irradiated at δ_H 7.47 and an enhanced peak was observed at δ_H 4.68 i.e. CH_2 of the PMB group. This indicated that the remaining PMB group was positioned next to the ring proton as opposed to next to the methyl ester group (Figure 3.10).

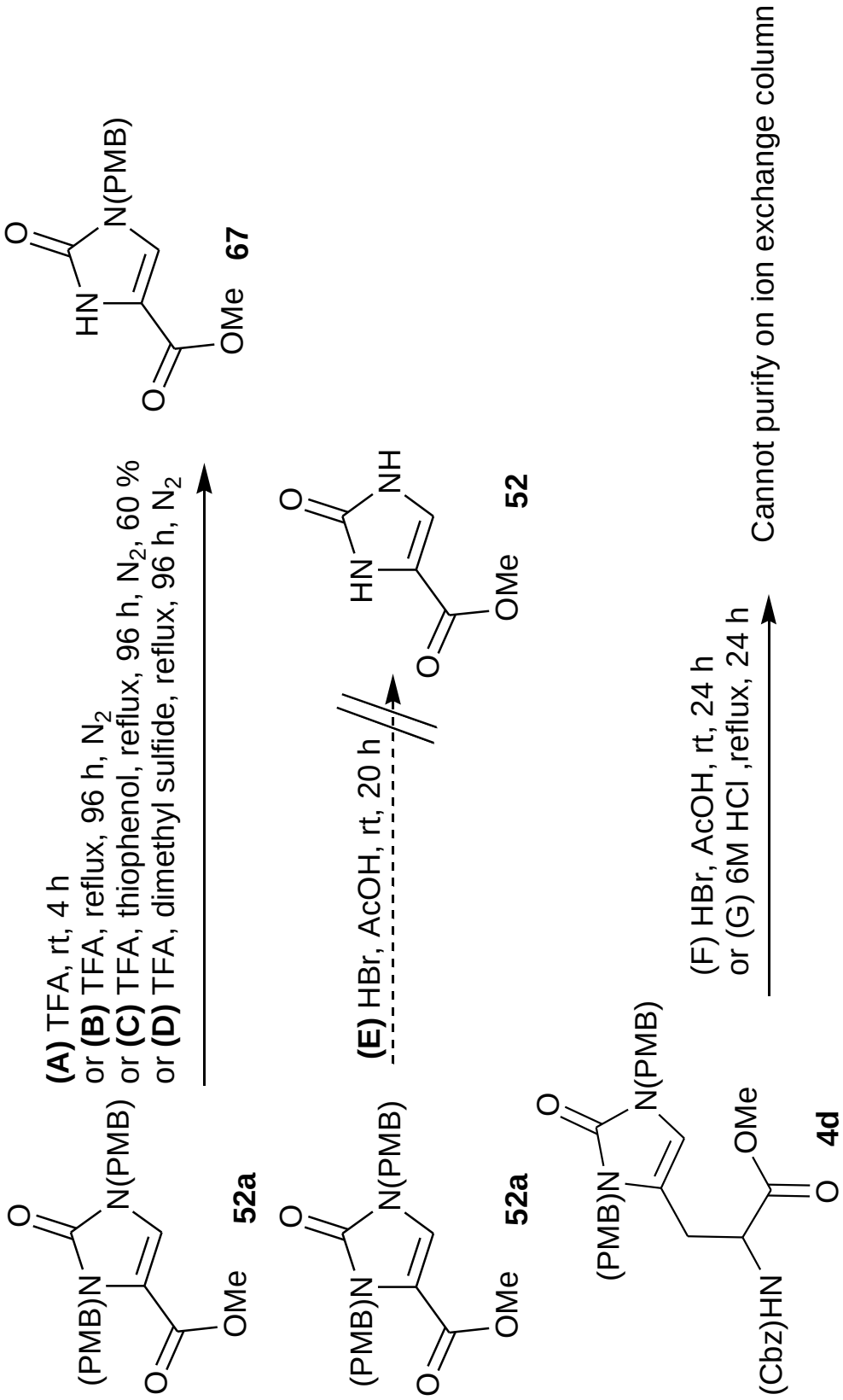

Scheme 3.18: Attempted deprotection of PMB groups from imidaozlin-2-one ring nitrogens using acid hydrolysis.

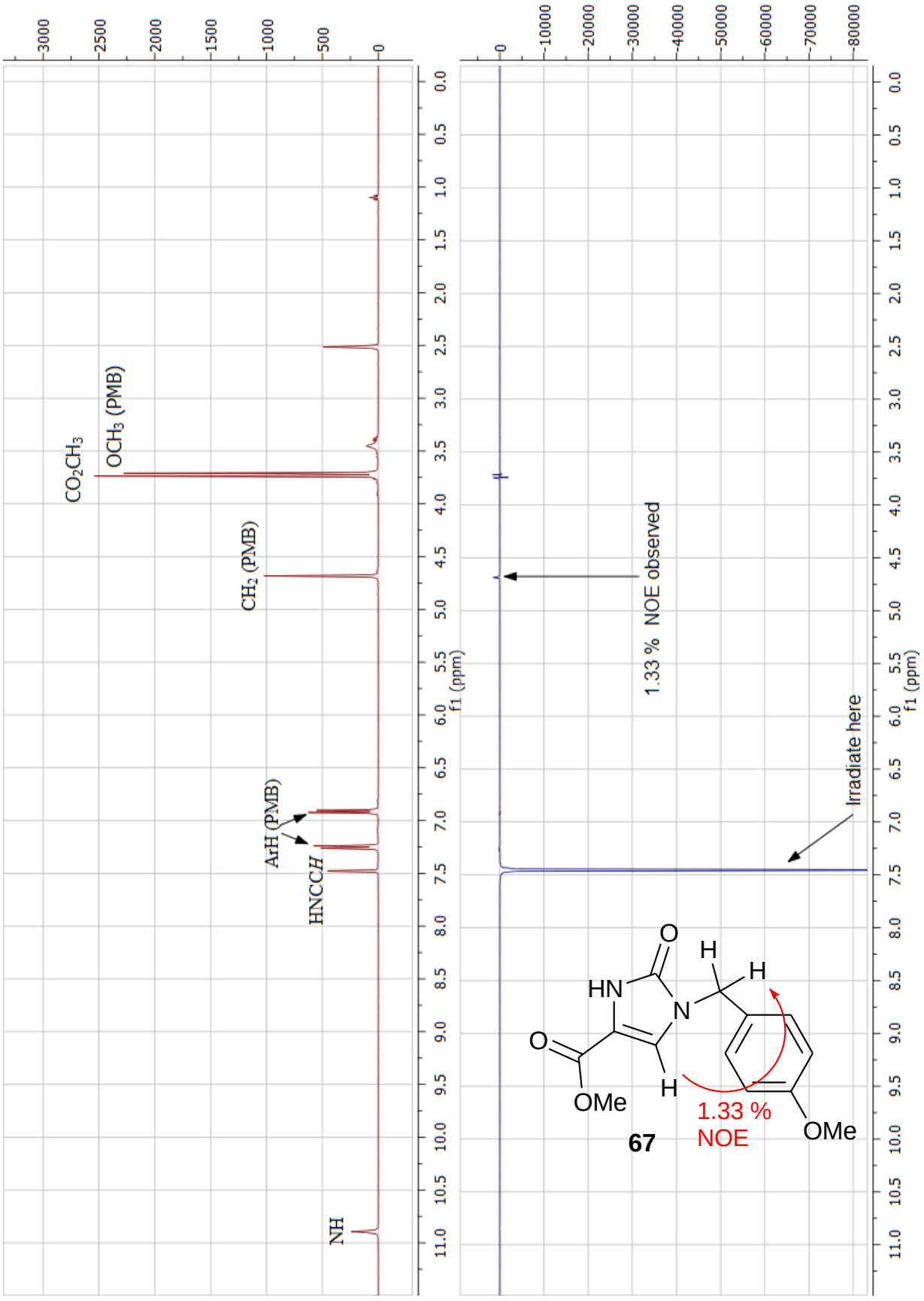

Figure 3.10: 1D NOE (400 MHz, DMSO) spectrum of 1-PMB-4-methoxycarbonylimidazolin-2-one 67. This indicates, after deprotection with TFA, the remaining PMB group of methyl ester 67 is positioned next to the ring. The ring proton was irradiated at δ_H 7.47 ppm and an enhanced peak was observed at δ_H 4.68 ppm i.e. CH_2 of the PMB group.

Some literature examples of TFA-mediated deprotections indicate the importance of using a nucleophilic scavenger such as anisole (Boger, D. L., *et al.*, 2000, Forbes, I. T., *et al.*, 1992, Wood, J. L., *et al.*, 1995) in the reactions to remove the electrophilic PMB-deprotection product. Although there are few nucleophilic sites in the unprotected 2-oxo-histidine derivative, the deprotections on the PMB-methyl ester **52a** were repeated for completeness, using TFA and one of two easily available nucleophile scavengers; thiophenol (Scheme 3.18(C)) (Tam, J. P., *et al.*, 1985) or dimethyl sulphide (Scheme 3.18(D)) (Lundt, B. F., *et al.*, 1978). With use of the former scavenger mono-PMB-methyl ester **67** was obtained along with unreacted thiophenol, whereas for the latter the PMB groups remained.

Another acid used for attempted deprotections on PMB-methyl ester **52a** was hydrobromic acid at room temperature for 20 h but only starting material was recovered (Scheme 3.18(E)). To see whether hydrobromic acid would have any effects on the Cbz and OMe protecting groups an attempted deprotection of the fully protected 2-oxo-his **4d** with hydrobromic acid at room temperature for 24 h was attempted but it was not possible to purify the product with ion exchange chromatography as the product would neither bind to anion (IRA400 OH resin) or cation (DOWEX 50W-X8) exchange columns (Scheme 3.18(F)). This may be due to 2-oxo-histidine being less basic than histidine and therefore less likely to bind to these columns. The crude product indicated both formyl peaks (δ_H 8.2), PMB peaks (δ_H 6.7-7.0) and amino acid peaks (e.g. δ_H 2.9-3.1 for βCH_2).

Finally, a quite extreme deprotection of the fully protected 2-oxo-his **4d** using a 24 h reflux with 6M HCl (Scheme 3.18(G)) produced an initially promising ^{1}H-NMR of the crude reaction mixture with a halving in the integrals of PMB-related peaks indicating mono-deprotection, and loss of the Cbz-aromatic peaks at δ_H ~7.3 . However, as for the hydrobromic acid based deprotection, purification of this using ion exchange chromatography proved impossible.

Due to the difficulty in removing the second PMB-group from our protected molecules we decided to attempt synthesis using different protecting groups; benzyloxymethyl (BOM) and dimethoxybenzyl (DMB). The literature also gives examples of other groups, such as 2-(trimethylsilyl)ethoxycarbonyl (Teoc) (Lanman, B. A., *et al.*, 2007) or benzyl (Bn) (Wang, S., *et al.*, 2006), being used to protect

imidazolin-2-one, but these protecting groups are more difficult to manipulate or can cause intramolecular cyclisation upon deprotection.

Benzyloxymethyl (BOM) as a nitrogen protecting group

BOM groups are stable to TFA, basic conditions and aqueous carboxylic acids (Brown, T., *et al.*, 1982). Brown *et al.* concluded this was the best protecting group with which to protect imidazole nitrogens and could be carried through to solid phase peptide synthesis and still be stable (Brown, T., *et al.*, 1982). They were one of the orthogonal protecting groups initially discussed in the Dransfield *et al.* paper from which the synthesis discussed above is based (Dransfield, P. J., *et al.*, 2006). However, this project initially did not use the BOM group as a potential ring nitrogen protecting group because of the requirement for hydrogenation in order to remove these groups at deprotection, which may target the 4-C=C-5 bond of the ring system in 2-oxo-histidine.

*Attempted alterations to synthesis of 2-oxo-histidine **4** with use of the BOM-protecting group*

The synthetic route to the dehydro derivative **40c** is summarised in Scheme 3.19 and follows a similar synthetic route to that with the PMB intermediates. One difference was the production of two products upon protection of the methyl ester **52**, the expected methyl ester **52b** and an ester substitution to a BOM ester **68** at the C-4 position. This is likely due to impurities in the benzyl chloromethyl ether, such as benzyl chloride, acting as a friedel craft-type alkylating agent. The extent of this transesterification was considerable, with higher yields obtained for the BOM ester **68** than the methyl ester **52b**. There may have been some evidence for this with the PMB protection of **52** with extra peaks seen in the crude product NMR in a 2:1 ratio with the expected product **52a**. However, such an ester substituted product was not isolated and was not the major product, unlike with the BOM protection. In general, the protection of the methyl ester with BOM-Cl was lower yielding (6 %) than the protection with PMB-Cl (21 %). This is probably due to the poor purity of

commercial benzyl chloromethyl ether (60 % quoted by Sigma Aldrich) in comparison to 4-methoxybenzyl chloride (98 % quoted by Sigma Aldrich).

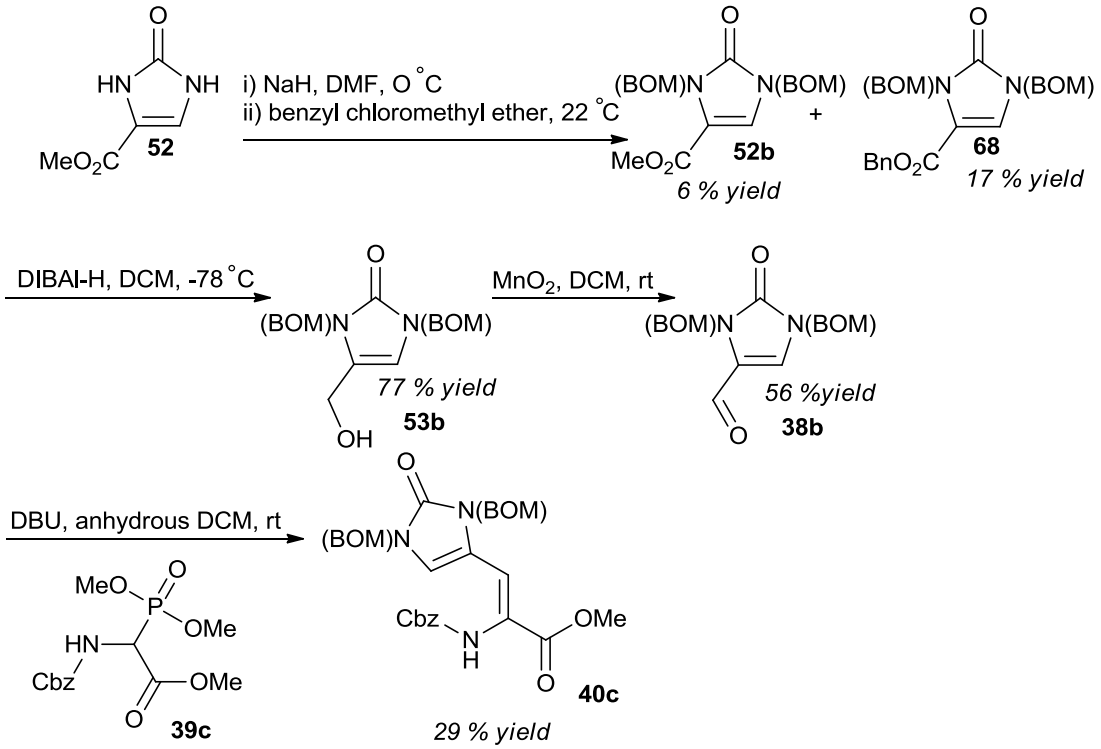

Scheme 3.19: Synthesis of the *N*(α)-Cbz, *N*(τ), *N*(π)-bis(BOM)–dehydro derivative of 2-oxo-histidine 39c.

This substituted ester could still be used for the DIBAl-H reduction as the side product alcohol could be isolated by column chromatography or, in the case of PMB alcohol, by recrystallisation. The alcohol **53b** was successfully oxidised to the aldehyde **38b** using MnO_2. The characterisation data for the BOM-aldehyde **38b** compared favourably with those reported by Ma *et al.* with all peaks within 0.03 ppm of those reported, with the aldehyde peak at δ_H 9.34 in particular measured as being between the peak recorded by Ma *et al.* (δ_H 9.33) (Ma, Z., *et al.*, 2011) and that recorded by Dransfield *et al.* (δ_H 9.36) (Dransfield, P. J., *et al.*, 2006), noting that the latter was recorded in a different solvent.

Synthesis of the dehydro derivative with BOM protecting groups was lower yielding than that with PMB protecting groups with an overall yield of 0.13 % (BOM) compared to 0.95 % (PMB). However, it could be done successfully indicating BOM could be a viable alternative to the PMB group for protecting the ring nitrogens.

Dimethoxybenzyl (DMB) as a nitrogen protecting group

The use of DMB as a nitrogen protecting group, along with trimethylsilylethyl (Tse) groups, in an imidazoline-2-one system exposed to strong acids and mild oxidising agents, has been demonstrated previously by several groups (Dransfield, P. J., *et al.*, 2006, Dransfield, P. J., *et al.*, 2005, Wang, S., *et al.*, 2006, Zancanella, M. A. and Romo, D., 2008). The group can be easily removed using potassium persulfate (Huffman, W. F., *et al.*, 1977, Qian, X., *et al.*, 2002), *p*-toluenesulfonic acid (Chern, C. Y., *et al.*, 2003), DDQ (Grunder-Klotz, E. and Ehrhardt, J.-D., 1991, Mori, S., *et al.*, 1988), or TFA-mediated hydrolysis with or without cation scavengers (Deshong, P., *et al.*, 1985, Schlessinger, R. H., *et al.*, 1985, Shimshock, S. J., *et al.*, 1991, Wood, J. L., *et al.*, 1995, Wood, J. L., *et al.*, 1997, Wood, J. L., *et al.*, 1996), which will also remove the Cbz groups (Lundt, B. F., *et al.*, 1978). They are also easily deprotected from electron-rich systems (Watson, D. J., *et al.*, 2001), of which the imidazolin-2-one ring system is an example, making them ideal nitrogen protecting groups for this project.

This PhD looked at the isomeric 2,4- and 3,4-dimethoxybenzyl groups, with the 2,4 form predicted to be easier to remove due to the stability of the carbocation formed. This has the advantage over PMB as a protecting group that the extra electron-donating methoxy group stabilises the carbocation produced as an intermediate in the deprotection process.

The chlorides **69** and **70** required to add these groups were synthesised according to literature methods from the corresponding alcohols (Howell, S. J., *et al.*, 2001, Nicoletti, T. M., *et al.*, 1990, Smyth, M. S., *et al.*, 1993). However, upon attempted protection of the methyl ester **52** with these chlorides (Scheme 3.20(A); for 2,4-DMB-Cl **69**, and Scheme 3.20 (B); for 3,4-DMB-Cl (**70**)), using a NaH/DMF method similar to literature procedures (Leigh, C. D. and Bertozzi, C. R., 2008, Paterson, I., *et al.*, 2009), a complex mixture of products, as shown by TLC, was produced. ^{1}H-NMR showed numerous methoxy environments indicating that this was not an efficient protecting strategy for the methyl ester. The 2,4-DMB-Cl **69** also polymerised rapidly to form a purple crystalline solid upon exposure to air.

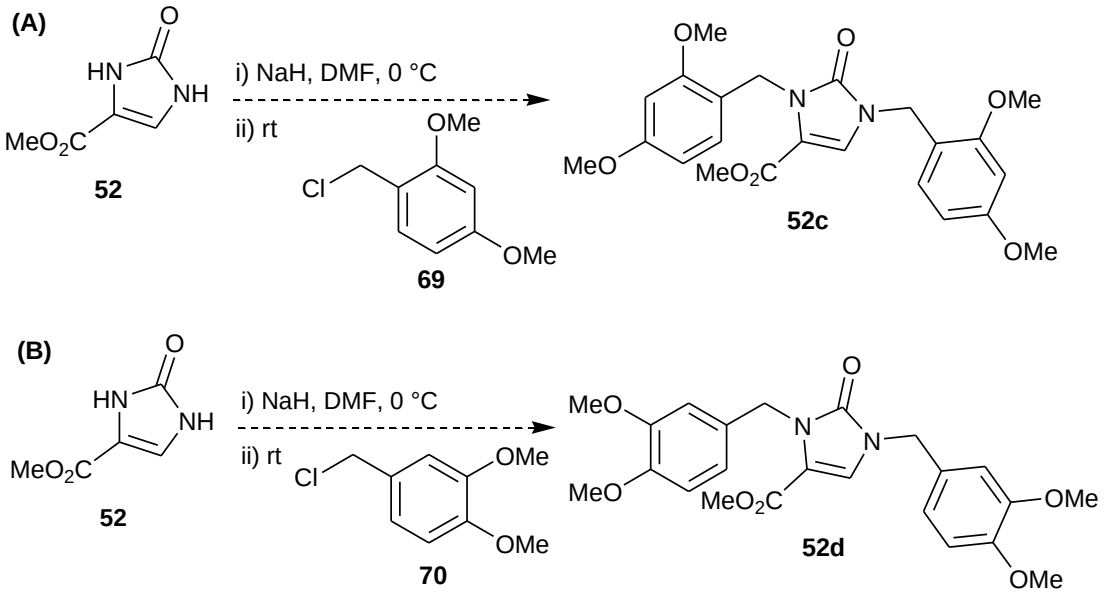

Scheme 3.20: Attempted protection of methyl ester 52 with dimethoxybenzyl groups.
(A) Attempted protection with 2,4-dimethoxybenzyl chloride **69**. **(B)** Attempted protection with 3,4-dimethoxybenzyl chloride **70**.

3.2.2. Alternative syntheses from urea **17** attempted

There are alternative synthetic routes to 2-oxo-histidine which may seem more elegant than those described above. Indeed with the seven steps required to go from urea and tartaric acid to protected 2-oxo-histidine, overall yields are below 1 %. Therefore, other simpler syntheses based on the imidazolin-2-one ring system were attempted.

*Alcohol activation of hydroxymethylimidazolin-2-one **53** with subsequent substitution with a glycine enolate*

An alternative proposed synthesis from 4-hydroxymethylimidazolin-2-one **53** to 2-oxo-histidine requires the alcohol to be activated by the introduction of a good leaving group. This leaving group can then be substituted with a glycine enolate equivalent e.g. diethyl acetamidomalonate **71** (see Section 3.1.1.) (Burgoyne, D. L., *et al.*, 1991, Jones, R. G. and Mclaughlin, K. C., 1949, Kuwano, R. and Kondo, Y., 2004, Steinhuebel, D., *et al.*, 2006). Ester hydrolysis and decarboxylation then leaves the protected amino acid **4**. This has an advantage over the previously described

synthesis in that the glycine enolate **71** is at the same oxidation level as the desired 2-oxo-histidine product and thus avoids the use of a α-C=β-C reduction step with the associated risk of reduction of the C-4=C-5 double bond in the imidazole ring. In addition, diethyl acetamidomalonate **71** is inexpensive and readily available (Steinhuebel, D., *et al.*, 2006).

There are several good leaving groups that can be incorporated at the C-4,C-5 carbon of the imidazolin-2-one ring system instead of the alcohol (Scheme 3.21). These include tosyl and mesyl groups (Burgoyne, D. L., *et al.*, 1991), alkyl carbonates (Kuwano, R. and Kondo, Y., 2004, Steinhuebel, D., *et al.*, 2006, Yeung, K.-S., *et al.*, 2001), alkyl halides (Anilkumar, G., *et al.*, 2002, Bayle-Lacoste, M., *et al.*, 1990, Choi, Y., *et al.*, 2003, Jones, R. G. and Mclaughlin, K. C., 1949, Krogsgaard-Larsen, P., *et al.*, 1984, Lisowski, V., *et al.*, 2001) and alkyl acetates (Yokogi, M. and Kuwano, R., 2007). Alkyl halides were avoided because they can be quite low yielding (Jones, R. G. and Mclaughlin, K. C., 1949), can undergo reversible reactions and can be difficult to synthesise. Out of the alcohol activation procedures presented in Scheme 3.21, the following were studied in this project; tosylation/mesylation and carbonate formation.

Tosylation has been successfully employed by Burgoyne *et al.* to generate a dibenzyloxybenzyl substituted glycine (Scheme 3.21(B)) (Burgoyne, D. L., *et al.*, 1991). For this project, both a tosylation and mesylation were attempted on alcohol **53**. The procedure used was very similar to that used by Burgoyne *et al.* (Burgoyne, D. L., *et al.*, 1991), although the solvent used was either anhydrous DCM or anhydrous diethyl ether rather than benzene. For the tosylation (Scheme 3.22) both sodium hydride and pyridine were trialed as bases. Pyridine was initially avoided due to the likelihood it would be react with the tosylated ring system **72** to form a pyridinium salt. However, ^{1}H-NMR of the crude product after NaH was used as the base showed no peak shift indicative of the sodium salt forming. Therefore, pyridine was used as the base for the tosylation. For the mesylation, triethylamine was used as the base. In both cases the reaction was performed under a nitrogen atmosphere.

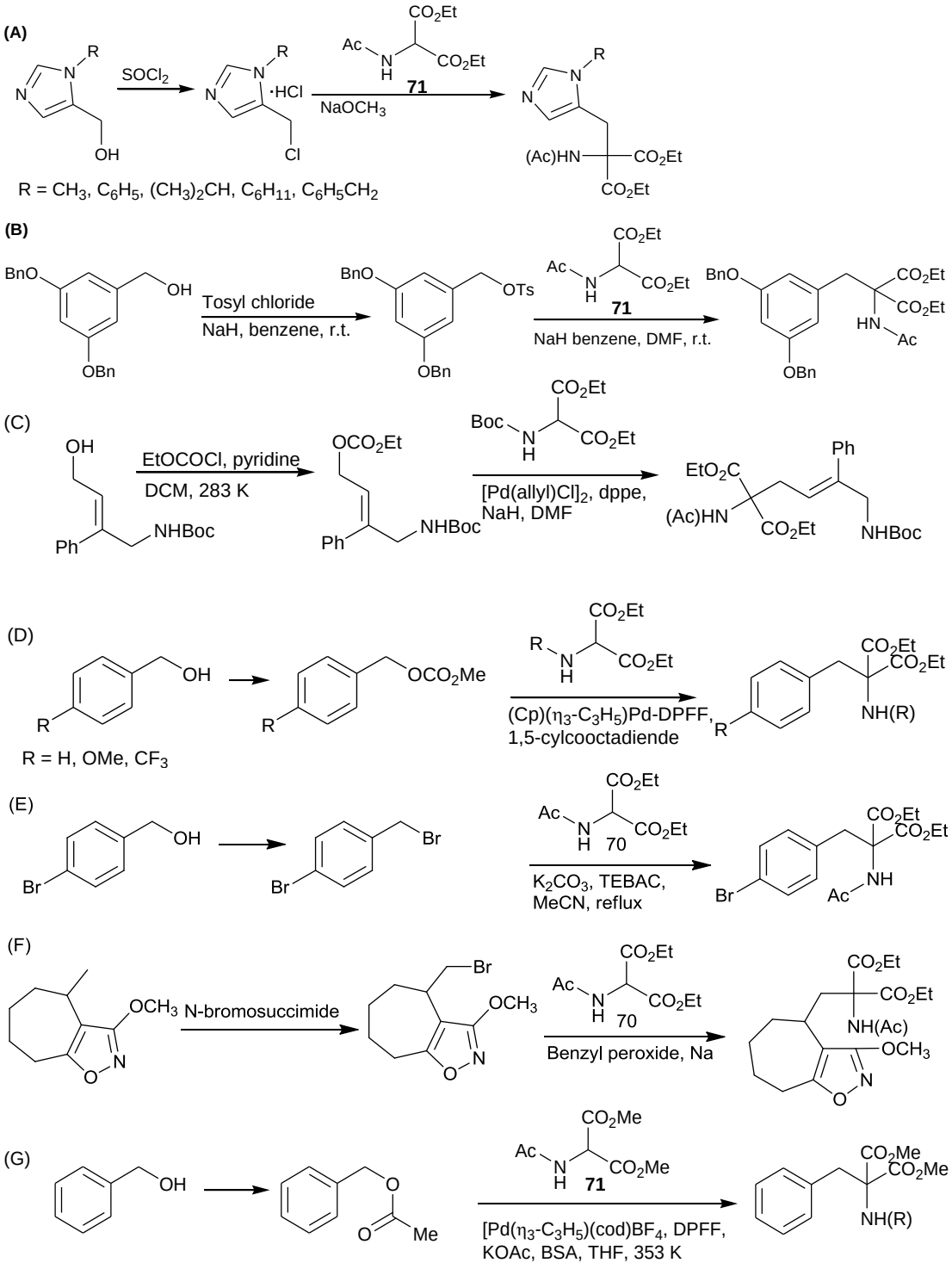

Scheme 3.21: Literature examples of activated alcohols coupled to glycine enolates.
(A) 1-substituted imidazole chlorides (Jones, R. G., and McLaughlin, K. C., 1949).
(B) Dibenzyloxybenzyl tosylates (Burgoyne, D. L., *et al.*, 1991).
(C) Vinyl amine ethyl carbonates (Steinhuebel, D. L., *et* al., 2006).
(D) Benzyl methyl carbonates (Kuwano, R., and Kondo, Y., 2004).
(E) Bromo-benzyl bromides (Bayle-Lacoste, M., *et* al., 1990).
(F) Tetrahydrocycloheptaisoxazolone bromides (Krogsgaard-Larsen, P., *et al.*, 1984).
(G) Benzyl acetates (Yokogi, M., and Kuwano, R., 2007).
(H) Alkyl acetates (Yokogi, M. and Kuwano, R., 2007).

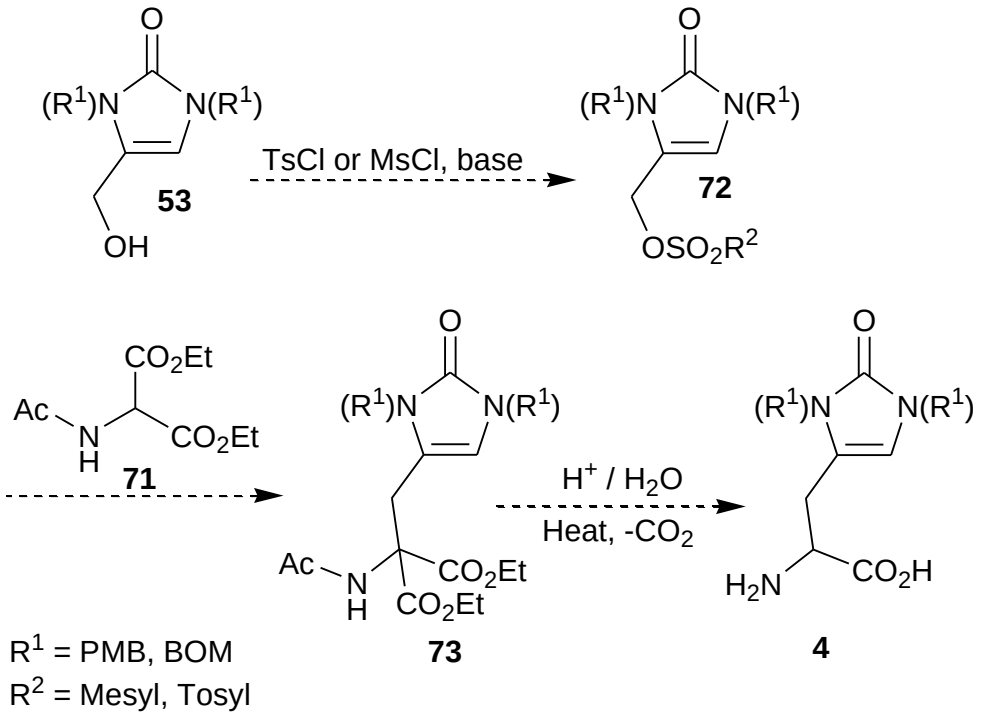

Scheme 3.22: Proposed alternative synthesis of 2-oxo-histidine via an alkylation of a glycine enolate equivalent. This synthesis takes the alcohol **53** and activates it to either a tosyl or mesyl group **72.** This can then undergo a coupling to a glycine enolate equivalent e.g. diethyl acetamidomalonate **71** to form diester **73**. Deprotection and decarboxylation can then give 2-oxo-histidine **4**.

However, the use of either TsCl or MsCl did not result in the conversion of the alcohol into a tosyl or mesyl ester respectively but instead yielded 5-methyl-imidazolin-2,4-dione **74** (Scheme 3.23), an isomer of the alcohol **53** in 25 % yield. The remaining crude was starting material. In the IR spectrum of the fraction containing purified product **74a** no alcohol bands, present in **53** at ~ 3200 cm^{-1}, were seen. Instead two carbonyls were present as bands at 1768 cm^{-1} and 1704 cm^{-1}. The ^{13}C-NMR spectrum (Figure 3.12) showed two carbonyl peaks at δ_C 173.4 and δ_C 156.1. In addition the ^{1}H-NMR spectrum (Figure 3.11) shows a new methyl group (doublet at δ_H 1.30) coupled to a ring proton (quartet at δ_H 3.70) indicating a methyl group (δ_C 15.1) attached to an imidazoline ring carbon next to a ring CH (δ_C 54.7). The C-5 C*H* singlet peak seen in the starting material at approximately δ_H 6.04 was absent from the spectrum of the imidazolin-2,4-dione **24**. The ^{1}H-NMR data (Figure 3.11) also showed an AB system (δ_H 4.47 and δ_H 4.59) indicative of the aryl CH_2 protons being in diastereotopic environments induced by the formation of a new chiral centre at C-4 in the imidazole ring.

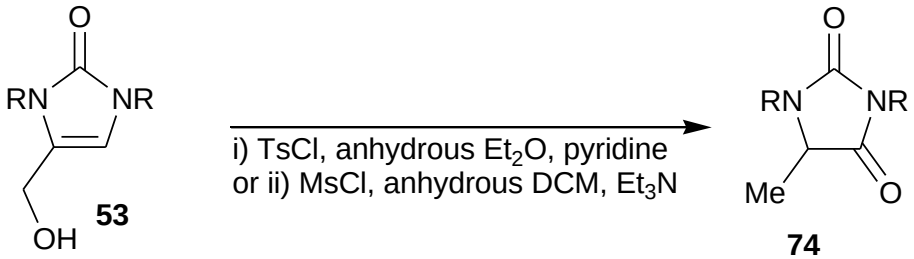

R = PMB, BOM

Scheme 3.23: Isomerisation of protected 4-methylhydroxylimidazolin-2-one 53 induced by TsCl and MsCl. This occurs with both TsCl and MsCl as a reagent and for 4-methylhydroxylimidazolin-2-one protected with either PMB **74a** or BOM **74b** groups.

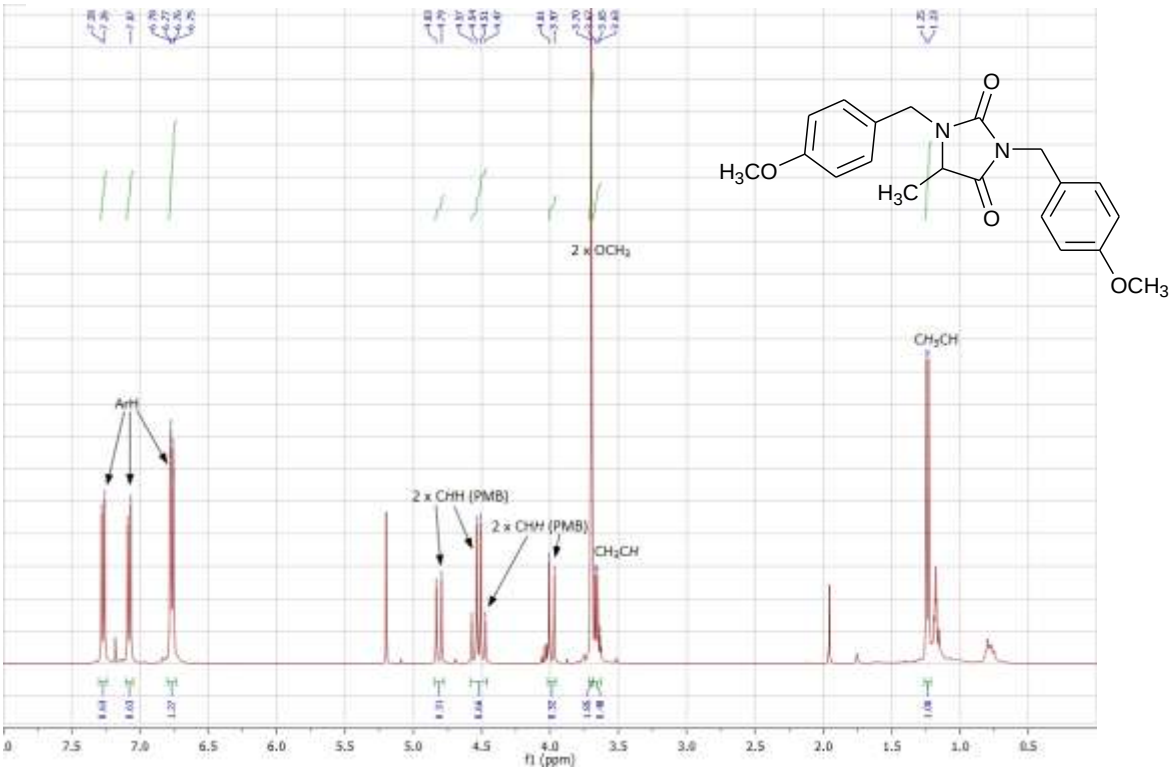

Figure 3.11: ^{1}H-NMR (400 MHz, $CDCl_3$) spectrum of 1,3-bis(PMB)-5-methylimidazolidine-2,4-dione 74a.

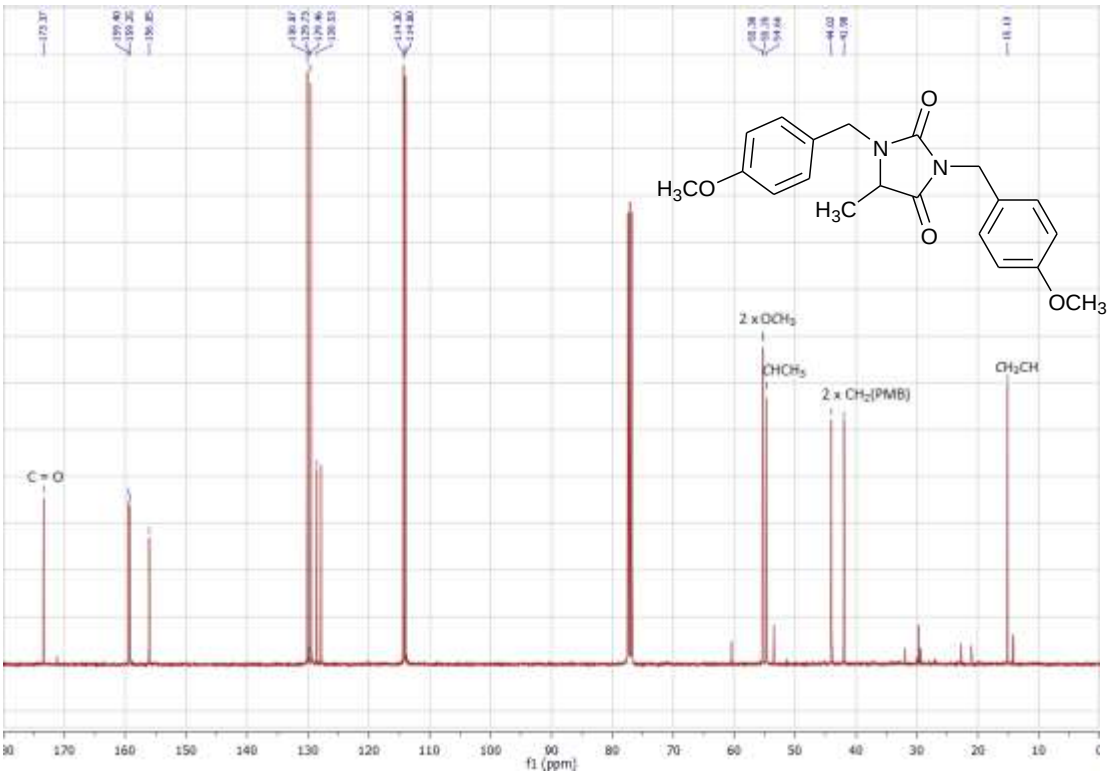

Figure 3.12: ^{13}C-NMR (100.65 MHz, $CDCl_3$) spectrum of 1,3-bis(PMB)-5-methylimidazolin-2,4-dione 74a.

One potential mechanism for this isomerisation is given in Scheme 3.24. Interestingly, this isomerisation occurs for both the PMB-protected alcohol **53a** and the BOM-protected alcohol **53b**.

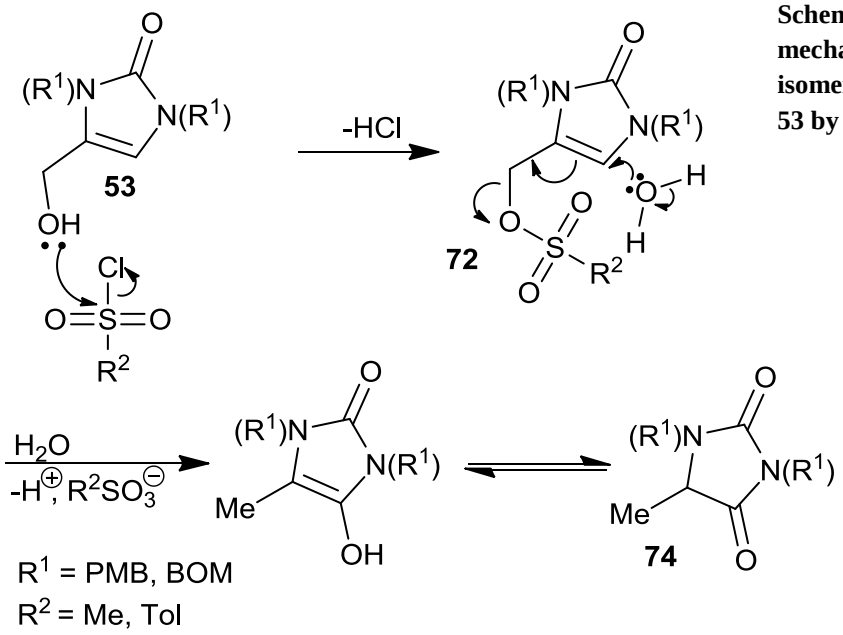

Scheme 3.24: Proposed mechanism for the isomerisation of alcohols 53 by sulfonyl chlorides.

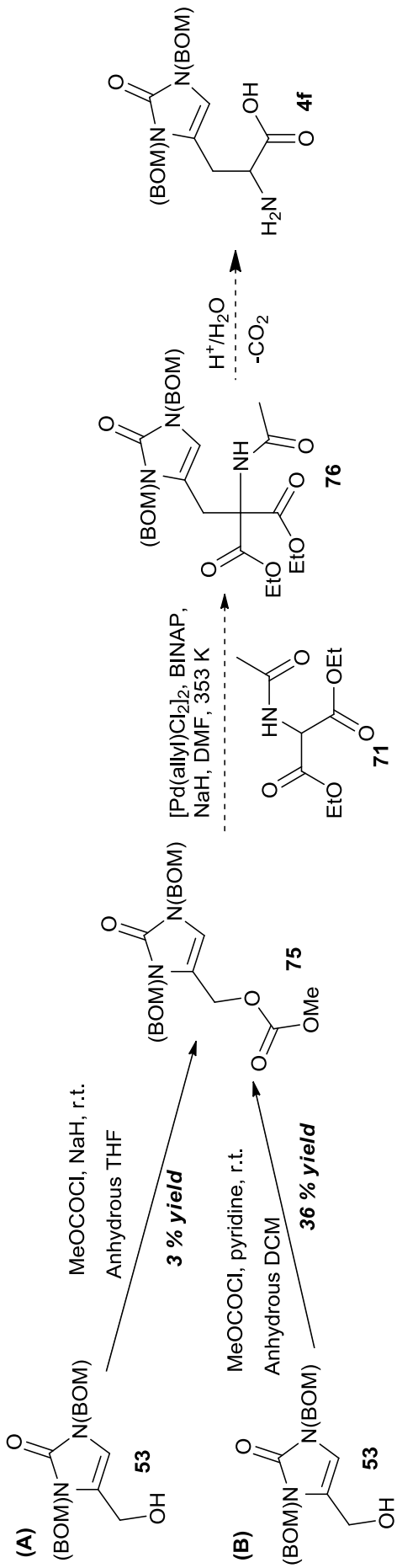

Another activation of the protected alcohol, this time exclusively with ring nitrogen BOM protection **53b**, was the conversion to the methyl carbonate **75**. It was envisaged that this could then be coupled to the glycine enolate equivalent discussed above, diethyl acetamidomalonate **71** (Scheme 3.24). Similar methods have been used for coupling allylic carbonates to diethyl acetamidomalonate (Steinhuebel, D., *et al.*, 2006) (Scheme 3.20(C)) and coupling of benzyl ethyl carbonates to a selection of glycine enolate equivalents (Kuwano, R. and Kondo, Y., 2004) (Scheme 3.20(D)).

Scheme 3.25: Activation of 1,3-bis(BOM)-4-hydroxymethyl-imidazolin-2-one 53 as a methyl carbonate 75. Two synthetic methods to make the carbonate **40** were compared: **(A)** Using NaH as the base. **(B)** Using pyridine as the base.

Two methods were compared for the synthesis of the methyl carbonate **75** from the alcohol **53b** (Scheme 3.25). One used NaH as a base in anhydrous THF and generated the methyl carbonate **75** in very poor yields (3 %, Scheme 3.25(A)). A better method used pyridine as the base in anhydrous DCM and generated the methyl carbonate **75** in 36 % yield (Scheme 3.25(B)). In both cases the characterisation confirmed the formation of the methyl carbonate with an expected high resolution MS peak at 413.1704 ($M + H^+$) and NMR peaks for the new methyl ether group (δ_H 3.69, δ_C 55.0). The product was found not to be stable to chromatography on standard flash silica gel and so columns were pre-treated with triethylamine before chromatography was performed on the carbonate. In addition, organic layers were washed with pH 7.4 phosphate buffer rather than HCl.

The coupling of the carbonate **75** to diethyl acetamidomalonate **71** was then attempted (Scheme 3.25) using firstly NaH in DMF to form the sodium salt of the malonate and then adding BINAP with the $Pd(allyl)Cl_2$ catalyst and diethyl acetamidomalonate for the coupling. These conditions were similar to the conditions used by Steinhuebel *et al.* but using the more readily available BINAP ligand rather than dppe (Steinhuebel, D., *et al.*, 2006). However, the coupling step did not generate the expected histidine derivative **4f**. Instead, carbon-carbon bond formation occurred on the unsubstituted ring carbon to form an isomer **77** of the expected product (Scheme 3.26). The mass spectrometric data showed the expected mass of 554.2494 ($M + H^+$) for the carboxylated protected histidine derivative **4f**. However, the ^{1}H-NMR data showed the loss of the ring proton at δ_H 6.29 and addition of an extra methyl CH_3 peak at δ_H 1.78. The remaining peaks were derived from diethyl acetamidomalonate; δ_H 2.05 for the acetyl CH_3, δ_H 4.01 – 4.03 and δ_H 1.21 for the ethyl ester peaks, δ_H 7.89 (br) for the amide NH peak, indicating that the malonate had bound to the imidazolin-2-one ring system, just not at the expected carbon. Therefore the isomer **77** was assigned as the structure of the product.

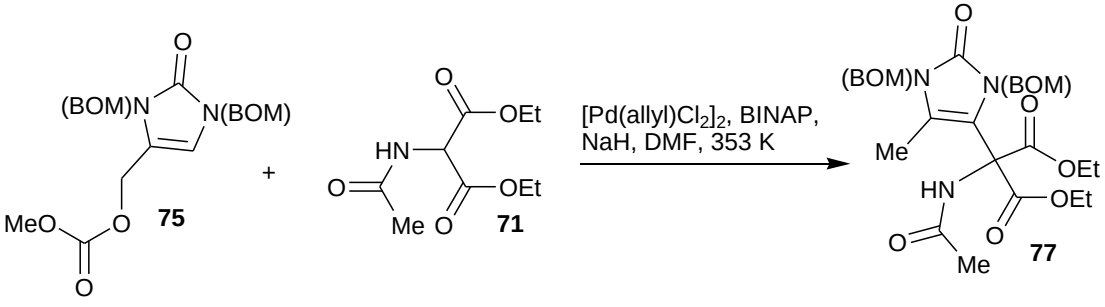

Scheme 3.26: Formation of unwanted isomer 77 from Pd-catalysed coupling of carbonate 75 with diethyl carbonate 71.

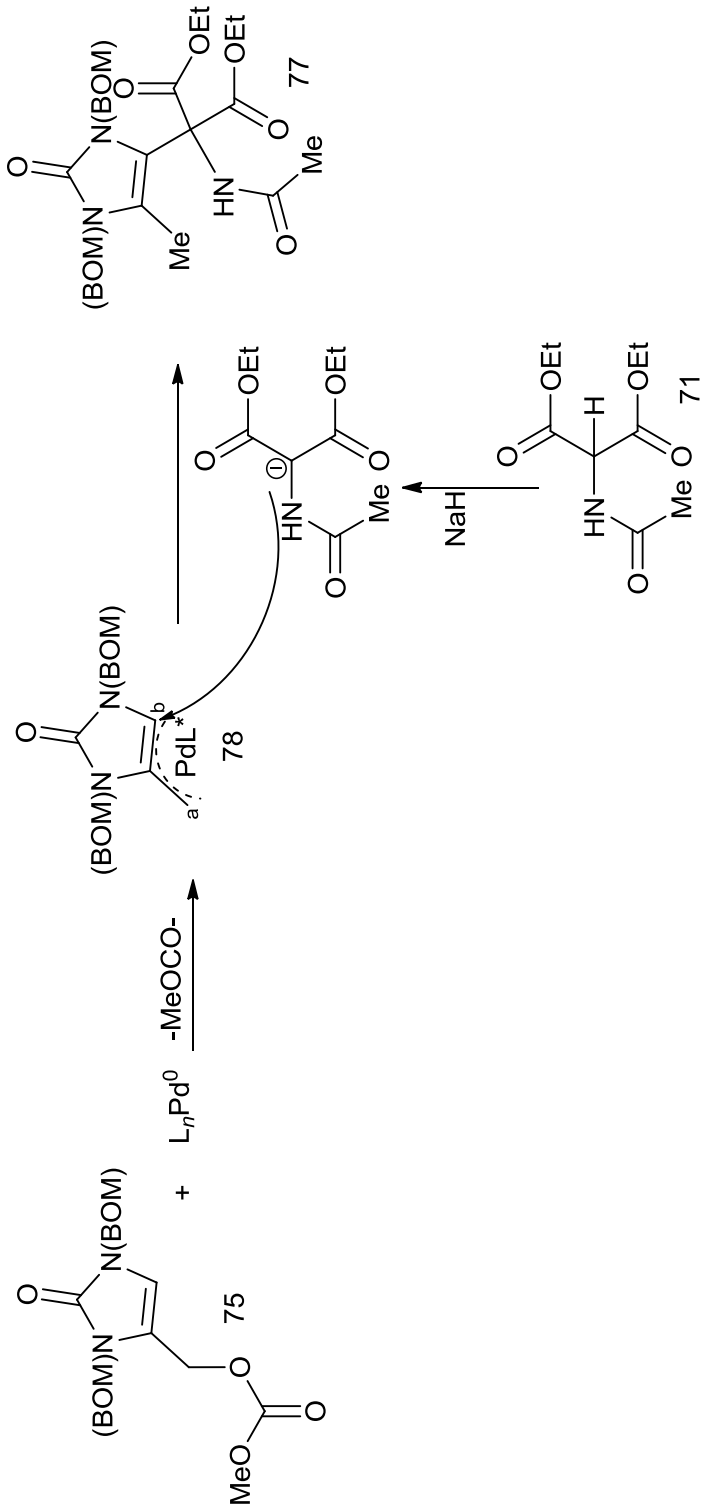

The mechanism proposed for this coupling is given in Scheme 3.27 and is based on the general mechanism for palladium(0)-catalyzed allylic alkylations, specifying diethyl acetamidomalonate **71** with strong base as a stabilized carbanion, and the carbonate **75** as the allylic substrate. It is proposed that the malonate **70** adds to the allylic cation system at the C-5 position (Scheme 3.27(b)), as opposed to the C-4 position (Scheme 3.27(a)) which would lead to the carboxylated histidine derivative **4f** due to the stabilisation of the positive charge in the π-allylpalladium intermediate **78** at C-5 (Scheme 3.27(b)) by the neighbouring τ-nitrogen. This isomer **77**, although a novel compound, does not aid in the synthesis of protected 2-oxo-histidine.

Scheme 3.27: Proposed mechanism for formation of the carbonate-derived isomer 77. The malonate **71** can add at either a or b in the π-allylpalladium intermediate **78** but addition at b is stabilised by the neighbouring τ-nitrogen.

A two-step synthesis of 4-formylimidazolin-2-one **38**, for use in the HWE reaction, was considered. This started with a decarboxylation of 4-carboxyimidazoline-2-one **49** to yield imidazolin-2-one **36**, as described in Section 3.1.2. and then proceeded via a modified Vilsmeier-Haack reaction (Scheme 3.28).

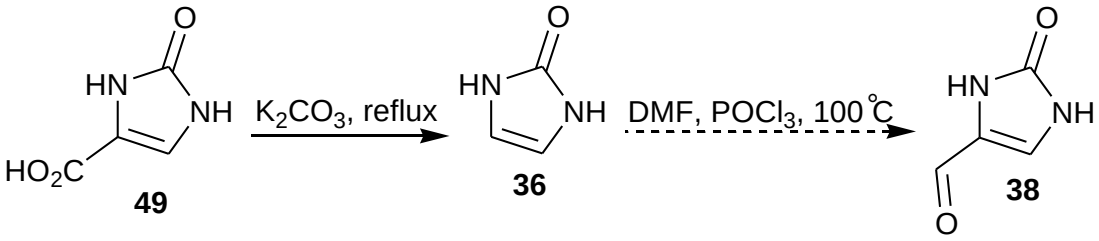

Scheme 3.28: Attempted use of the Vilsmeier-Haack reaction to synthesise 4-formylimidazolin-2-one 38.

This modified Vilsmeier-Haack reaction used dimethylformamide (DMF) and phosphoryl chloride, which combine to generate the electrophilic species, a dimethyl chloromethyleniminium ion, that can formylate electron-rich aromatics and olefinic carbons at high temperatures and so should introduce a formyl group at C-4 of imidazolin-2-one. The reaction mixture was heated to 100 °C for 1.5 h. Ice was added and the mixture left to warm to room temperature. A very fine precipitate formed which required centrifugation to separate it from the filtrate. A ^{1}H-NMR spectrum of the crude product in DMSO-d_6 showed evidence of an aldehyde product (δ_H 9.77) in a 4:1 ratio with a product displaying a more downfield proton (δ_H 10.1). The only comparable unprotected 4-formylimidazolin-2-one **38** structure in the literature is that of an extraction from bacterial anti-fungal sugar (Hagenmaier, H., *et al.*, 1979). This product was analysed using a ^{1}H-NMR in D_2O and showed a formyl peak at δ_H 9.20, therefore the peak at δ_H 9.77 in the crude product may indicate the formation of 4-formylimidazolin-2-one **38** by this modified Vilsmeier-Haack reaction.

Although the ^{1}H-NMR of the crude product showed no evidence of DMF contamination, without peaks around δ_H 2.8 – 2.9, evidence for phosphoryl chloride contamination was seen, with substantial large splitting (12.7 Hz) of the C-5 proton peaks characteristic of phosphorus splitting. This crude product had limited solubility in both organic solvents and water and this hindered purification attempts, which included recrystallisation from water and column chromatography in both

methanol and ethyl acetate-based solvent systems. Eventually this synthetic approach was abandoned, however it was decided that further syntheses should use imidazoline derivatives with protection on the nitrogens of the ring to improve solubility.

Since experiments finished for this PhD project a paper has been published by Ma *et al.* which describes a one-pot Vilsmeier-Haack reaction to generate BOM-protected 4-formylimidazolin-2-one (Ma, Z., *et al.*, 2011).

*Halogenation of imidazolin-2-one **36** and Negishi cross-coupling to an activated serine derivative **79***

Finally another approach to synthesise 2-oxo-histidine from imidazolin-2-one **36** was proposed. This involved halogenation of imidazolin-2-one **36** and subsequent Negishi cross-coupling to a serine derivatized organozinc reagent **79** (Scheme 3.29). The serine derivative is activated by first substituting the alcohol with iodide and then co-coordinating this iodide to zinc to form the activated derivative **79**, synthetically equivalent to a β-alanine anion (see Section 3.1.1.). An advantage of this approach is that the innate chirality in the serine derivative would avoid the need to induce stereoselectivity at a later stage by performing an asymmetric step. This approach has been used to successfully synthesise novel amino acids with aromatic side chains using both aryl iodides and aromatic bromides (Scheme 3.30) (Jackson, R. F. W., *et al.*, 1992, Oswald, C. L., *et al.*, 2008). The approach tolerates numerous functionalities in the aryl groups, including heteroarenes such as pyridyl and pyrimidyl side chains (Jackson, R. F. W., *et al.*, 1992, Oswald, C. L., *et al.*, 2008, Tabanella, S., *et al.*, 2003, Walker, M. A., *et al.*, 1997). In addition, reactivity may be enhanced by co-ordination to trace metals (Oswald, C. L., *et al.*, 2008), which is a likely behavior of the imidazolin-2-one ring.

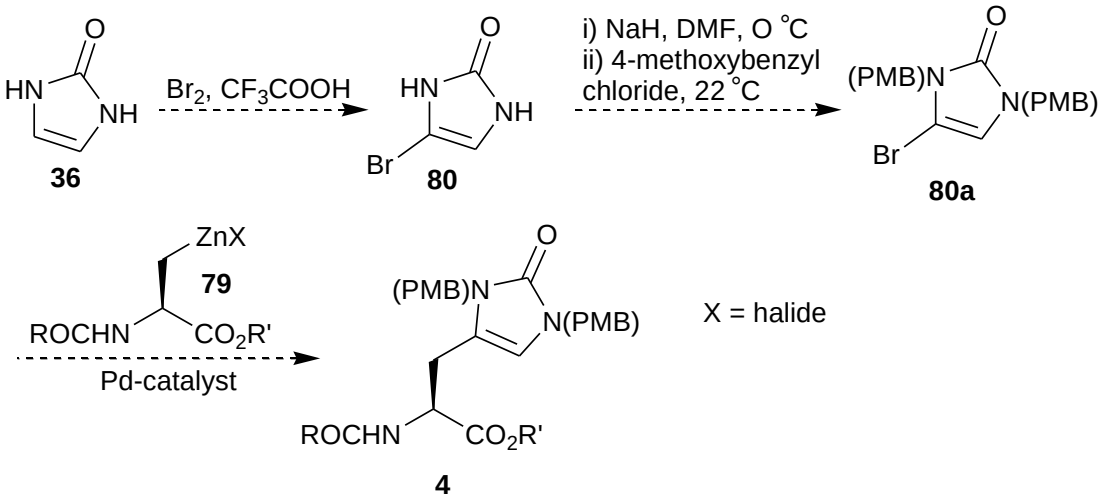

Scheme 3.29: Attempted synthesis of 2-oxo-histidine by a Negishi cross-coupling of imidazolin-2-one bromide 80 and an activated serine derivative 79. The C-4/5 of imidazoline-2-one **36** is activated as a bromide, which is then coupled via a Negishi cross-coupling to an activated serine derivative **79** to generate an enantiomerically pure form of 2-oxo-histidine **4**. Use of an imidazolin-2-one bromide **80** requires bromination followed by ring-nitrogen protection.

It was decided that bromination would be conducted before ring nitrogen protection because the electron-rich PMB groups are sensitive to bromination. Bromination was attempted on imidazolin-2-one **38** with just over 1 mol. eq. of bromine in either acetic acid or TFA to reduce the likelihood of the dibromo product forming. The reaction was undertaken under strongly acidic conditions with concentrated sulfuric acid added to the acetic acid solvent system to encourage bromination of the semi-aromatic 4-C=C-5 double bond. Bromine was seen to be consumed from the solution with the loss of red colouration to the reaction mixture with time. However, the product could not be isolated from the starting material by recrystallisation, had limited solubility in organic solvents and the ^{1}H-NMR of the crude product showed a complex mixture of products most of which did not appear to be the mono-brominated imidazolin-2-one **81**.

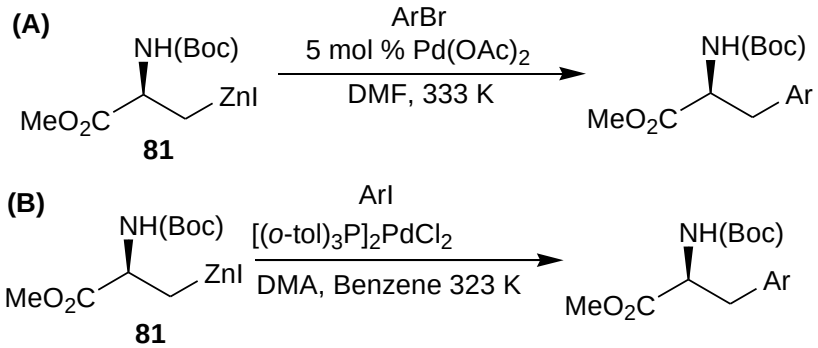

Scheme 3.30: Previous Negishi cross-coupling of activated serine derivatives and aromatic or oxo-compounds to give novel amino acids.
(A) Negishi cross-coupling of zinc iodide-serine derivative **81** with aryl bromides using palladium catalysts (Oswald, C. L., *et al*., 2008).
(B) Negishi cross-coupling of zinc iodide-serine derivative **81** with aryl iodides using palladium catalysts (Jackson, R. F. W., *et al*., 1992).

3.3. Discussion

A racemic form of protected 2-oxo-histidine has successfully been synthesised; *N*(α)-Cbz, *N*(π),*N*(τ)-Bis(PMB)-2-oxo-His-OMe **4d**. Future work will need to develop an enantioselective synthesis of this compound and determine the most suitable protective groups for Fmoc synthesis. This novel amino acid can then be used to synthesise peptides containing oxidized histidine residues in order to study the effects of histidine oxidation on the physiological behaviour of these peptides. Initially a short peptide synthesis such as that for Thyrotropin Releasing Hormone (TRH) (see Chapter 2, Section 2.1.2.) could be used to determine the oxidised residue's versatility to peptide synthesis conditions before incorporation into the Aβ(1-42) sequence at positions 6, 13 and 14 (Figure 3.13). The rate of fibril formation of this peptide can then be measured using a Th-T assay.

DAEFRH-oxDSGYEVH-oxH-oxQKLVFFAEDVGSNKGAIIGLMVGGVVIA

Figure 3.13: The location of oxidised histidines in solid-phase peptide synthesised Aβ(1-42)-His-ox.

Since these studies have been done a total synthesis of racemic 2-oxo-histidine has been claimed by Lam *et al.* (Lam, A. K. Y., *et al.*, 2010). This synthesis is shown in Scheme 3.31 and is based on a synthesis of racemic 2-thiooxo-histidine **82** reported by Furuta *et al.* (Furuta, T., *et al.*, 1992). A similar synthesis of the (L)-2-thioxo-histidine **82** using a Bamberger cleavage has recently been described in a patent by Trampota (Scheme 3.32) (Trampota, M., 2009). This involved forming a Bamberger product of L-histidine with benzoyl chloride in the presence of base which was then hydrolysed to form an (L)-ketobenzamide **83a**. This was then subjected to deprotection via acid-catalysed hydrolysis and subsequently reacted with potassium thiocyanate to obtain the (L)-thioxohistidine **82**. A similar synthesis is under investigation in the Wyatt group (Scheme 3.33) (Oyedele, T. A. O., 2011) and optimum conditions are being sought for formation of (L)-2-oxo-histidine by reaction of an (L)-ketoaminoacid with potassium cyanate.

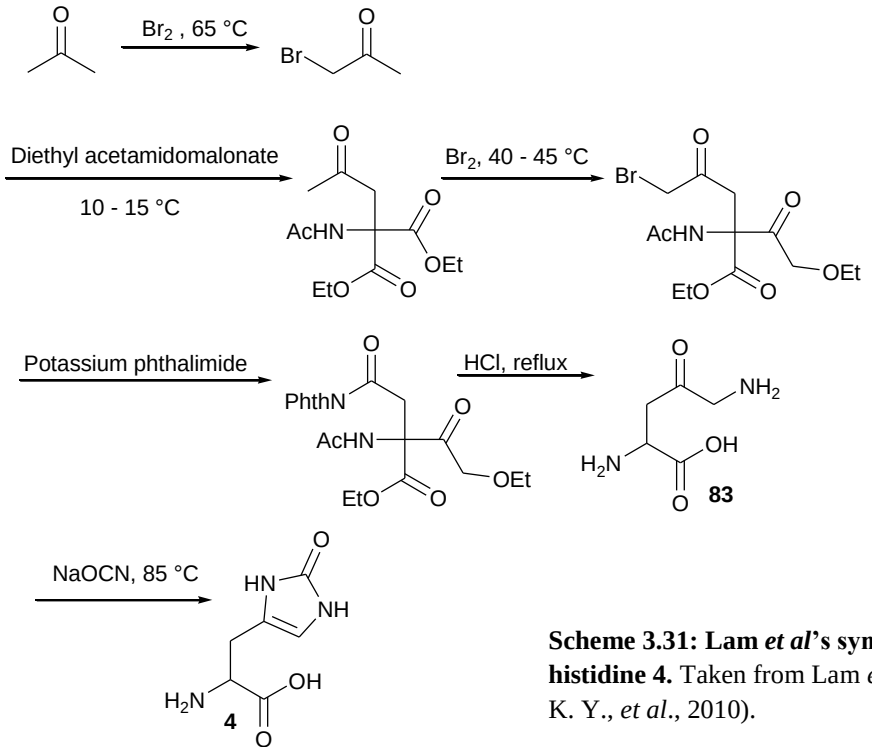

Scheme 3.31: Lam *et al*'s synthesis of 2-oxo-histidine 4. Taken from Lam *et al.*, 2010 (Lam, A. K. Y., *et al*., 2010).

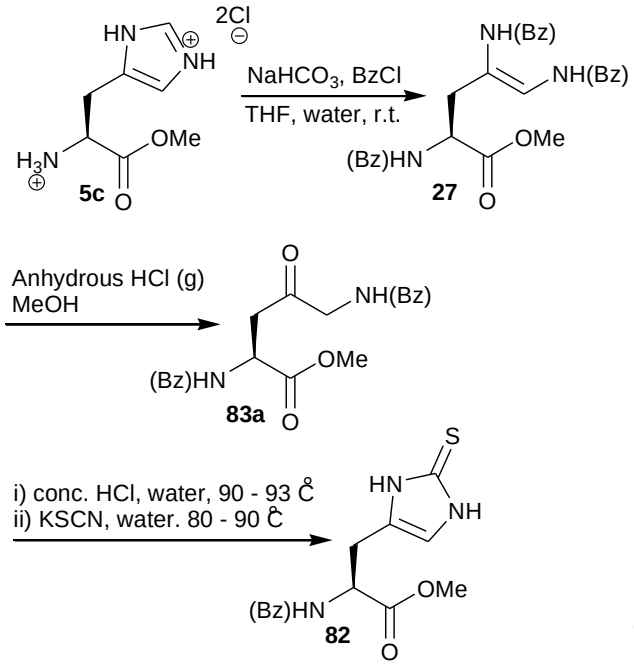

Scheme 3.32: Synthesis of protected (L)-2-thioxo-histidine 81 using a Bamberger cleavage (Trampota, M., 2009).

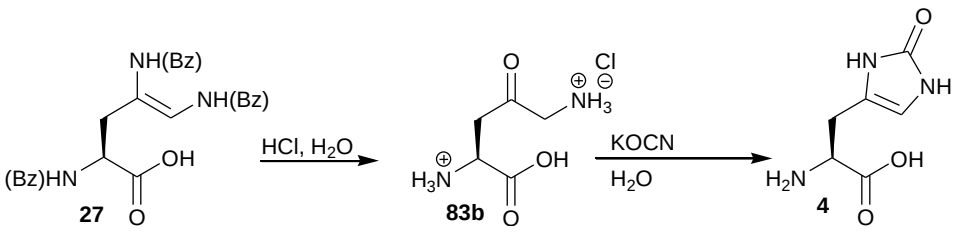

Scheme 3.33: Attempted adaptation of Lam *et al*'s synthesis of 2-oxo-histidine conducted by Oyedele and Wyatt (Oyedele, T, A. O., 2011).

An analysis of ring nitrogen protecting groups showed that both PMB and BOM groups can be used successfully to the dehydro-derivative stage of synthesis although the latter groups give lower synthetic yields. The PMB group proved difficult to deprotect leaving polar compounds, which were difficult to isolate. In addition, these groups may not be suitable for solid phase peptide synthesis and thus alternative groups such as *t*-butoxymethyl groups could be used on the imidazolin-2-one ring system. As discussed in Chapter 2, Section 2.1.2. the amino terminus of 2-oxo-histidine requires either Boc or Fmoc protection rather than the Cbz protection used in this thesis. In general, further analysis of appropriate protecting groups is needed.

In conclusion this thesis presents a multi-step synthesis to a protected form of 2-oxo-histidine **4d** for further progress towards synthesising peptides containing oxidised histidine, which can be used to analyse the effects of histidine oxidation on peptide structure and functionality.

Chapter 4

THE INFLUENCE OF OXIDATION ON Aβ FIBRIL GROWTH

4.1. Introduction

Chapter 1 concluded that Aβ is likely exposed to metal-catalysed oxidation of histidine and methionine residues *in vivo* due to Cu^{2+} ions being highly concentrated in plaques and known to bind Aβ via the three histidines and *N*-terminus with high affinity (Dong, J., *et al.*, 2003, Sarell, C. J., *et al.*, 2009, Syme, C. D., *et al.*, 2004). This copper ion, Cu^{2+}, is redox active and will generate hydrogen peroxide and hydroxyl radicals via metal catalysed oxidation (MCO) (Nadal, R. C., *et al.*, 2008, Stadtman, E. R. and Berlett, B. S., 1991). Chapters 2 and 3 discussed synthetic attempts towards 2-oxo-histidine for incorporation into the Aβ sequence. Although this peptide synthesis of Aβ-His-Ox was never realised during the timescale of this PhD, whole peptide studies were done under oxidising conditions, in order to analyse the effect of oxidation on the rate of Aβ fibrillisation; the hallmark of AD pathology according to the Amyloid Cascade Hypothesis. This is the topic of this chapter.

The two types of oxidation investigated were:

1) Hydrogen Peroxide (H_2O_2) alone, which causes methionine oxidation to methionine sulfoxide ($2e^-$ oxidation). In Aβ this would be at residue Met35.
2) Metal catalysed oxidation via either H_2O_2 and Cu^{2+} ions or ascorbate and Cu^{2+} ions, which causes both methionine ($1e^-$ oxidation) and histidine oxidation most likely to the 2-oxo-histidine form (see Chapter 1, page 51). In Aβ this would be at residues His6, His13, His14 and Met 35. Note ascorbate may reduce oxidised methionine (Schoneich, C., 2002). In this project this oxidation is conducted under aerobic conditions.

These processes have been described in detail in Chapter 1, Section 1.10.5. The two MCO systems are reported to generate different forms of histidine due to different complexes forming with Aβ (Ueda, J. I., *et al.*, 1995); Cu^{2+}/ascorbate giving 2-oxo-histidine and the Fenton's reagents, Cu^{2+}/H_2O_2, giving ring-ruptured and α, β-oxygen adducts (Cooper, 1985, Khossravi, M. and Borchardt, D. R., 1998, Uchida, K. and Kawakishi, S., 1990, 1993). In general, however, it can be considered

that Cu^{2+}/Cu^{+}-catalysed oxidation efficiently converts histidine into an oxidised form in the Aβ sequence.

4.1.1. Previous studies into the effects of oxidation on fibril growth

The only previous study that has been conducted on the effects of MCO on Aβ aggregation is that by Dyrks *et al.* (Dyrks, T., *et al.*, 1992). This study used both the Aβ(1-42) peptide and the Aβ(1-42)+Met, which is equivalent to the Aβ sequence with an additional *N*-terminal methionine residue. Dyrks *et al.* used two methods to oxidise Aβ; a H_2O_2 based method devised by Solar *et al.*, which used an oxygen-binding protein to ensure a high oxygen concentration for efficient oxidation (Solar, I., *et al.*, 1990), and a second metal-catalysed oxidation (MCO) method as described by Halliwell and Gutteridge, which used iron as the redox active metal (Halliwell, B. and Gutteridge, J. M. C., 1984). Analysis on SDS-PAGE gels of peptides derived from these oxidations found both to produce higher-size bands relative to controls, indicative of faster aggregation under oxidation. Dyrks *et al.* also found that the use of radical scavengers, such as ascorbate and trolox, prevented Aβ aggregation and concluded that not only did radical-based oxidation of Aβ accelerate fibril growth; it was a prerequisite for it. However, this early study did not measure amyloid fibrils specifically but only aggregate size because SDS-PAGE does not distinguish between the formation of amorphous aggregates and the formation of fibrils.

Apart from the Dyrks *et al.* study, all literature on the effects of oxidation on Aβ fibril kinetics involves oxidation of methionine alone. These studies contain contradictory results although more recent studies seem to have reached a consensus that methionine oxidation leads to decreased Aβ fibrillisation rates.

The first three studies after Dyrks *et al.* were those by Snyder *et al.*, Seilheimer *et al.* and Lorenzo *et al.*, which either found an increased rate of fibrillisation (Snyder, S. W., *et al.*, 1994) or no change in fibrillisation (Lorenzo, A., *et al.*, 1993, Seilheimer, B., *et al.*, 1997) after oxidation of Met35 to methionine sulfoxide. However, like Dyrks *et al.*, these studies used analyses that simply measured overall aggregation, rather than fibrillisation specifically; absorbance change indicative of turbidity change, analytical ultracentrifugation and HPLC-MS.

In addition, these studies used high concentrations of Aβ peptide, i.e. 45 μM - 100 μM, which can increase the chances of amorphous aggregates forming instead of fibrillar aggregates (Sarell, C. J., *et al.*, 2010). So, for both these reasons, Seilheimer *et al.*, Snyder *et al.* and Lorenzo *et al.* appear to have been measuring the effects of methionine oxidation on the rate of amorphous aggregate formation, not fibril formation. It is also likely that methionine oxidation in the Aβ sequence increases the formation of amorphous aggregates at the expense of fibrils and the reasons for this are hypothesised in Section 4.4.1.

A later study by Varadarajan *et al.* also found no effect of Met35 oxidation on Aβ fibrillisation kinetics (Varadarajan, S., *et al.*, 2001). However, it is likely that the samples were left too long, i.e. at least 24 h, before the analysis of fibre morphology by electron microscopy (EM) was conducted, thus allowing both oxidised and unoxidised samples to reach the plateau phase of fibrillisation. In addition, upon closer inspection of the electron micrographs, the morphologies do appear dissimilar between oxidised and unoxidised samples with unoxidised peptides appearing sparser and shorter, as would be expected if shorter, oligomeric neurotoxic species were forming.

All other studies on the effects of methionine oxidation on Aβ fibrillisation kinetics have found a decrease in fibrillisation rate and this is the general consensus currently in the literature (Hou, L., *et al.*, 2002, Hou, L., *et al.*, 2004, Johansson, A.-S., *et al.*, 2007, Maiti, P., *et al.*, 2010, Palmblad, M., *et al.*, 2002, Watson, A. A., *et al.*, 1998). However, there are still some criticisms of these studies. For example, Watson *et al.* claim to have used an Aβ(1-40) concentration of 1.2 mM at pH 6.5 (Watson, A. A., *et al.*, 1998). This is outside of the solubilisation range of Aβ(1-40). The solubilisation techniques used by Palmblad *et al.* and Watson *et al.* may also be likely to cause amorphous aggregation. Their solubilisation techniques involve direct dissolving of Aβ into the experimental media; pH 3 acetic acid and dilute hydrogen peroxide, respectively. Snyder *et al.* commented that this solubilisation technique leads to 'non-homogeneous solvation'; an initially high local aggregation-promoting Aβ concentration. For this PhD study, all peptides were solubilised at 5 °C at strongly alkaline pH to prevent aggregation via this process.

The pHs used in these studies are also of concern. Palmblad uses the extreme pH 3 for their studies by conducting them in acetic acid and not surprisingly found a complete prevention of fibrillisation (Palmblad, M., *et al.*, 2002). In addition, the use

of co-solvents such as acetic acid may promote α-helical formation, an intermediate secondary structure en route to the β-sheet form required for fibrillisation (Hou, L., *et al.*, 2002). At a lesser extreme is Watson *et al.*'s study, which is conducted at both pH 4 and 6.5 (Watson, A. A., *et al.*, 1998), however, this is bringing Aβ(1-40) closer to its isoelectric point (pI) of ~5.3 than is physiologically relevant. This is likely affecting kinetics, as discussed further in 4.4.2. For this PhD project, no co-solvents were used and experiments were conducted at pH 7.4, as this is the most physiologically relevant pH and prevents amorphous aggregation associated with being close to the Aβ(1-40) peptide's pI.

The molar ratio of H_2O_2 to Aβ varies widely between studies, typically 200 mol. eq. to 40,000 mol. eq. (800 μM to 2 M) (Table 4.1) (Hou, L., *et al.*, 2002, Johansson, A.-S., *et al.*, 2007, Palmblad, M., *et al.*, 2002, Watson, A. A., *et al.*, 1998). The concentration of H_2O_2 in bodily fluids ranges from 0.05 μM to 117 μM (Banerjee, D., *et al.*, 2002, Lászó, G., 2006). These levels are probably higher in the oxidative stress environment of AD, and the increase in overall peroxide levels between normal and AD age-matched controls has been estimated at 1.3–fold (Squitti, R., *et al.*, 2006). Therefore, with CSF Aβ concentration at ~75 nM (Mclean, C. A., *et al.*, 1999) there is a 2000-fold greater concentration of H_2O_2 in CSF than Aβ, therefore this molar ratio would be more suitable for modelling the effects of H_2O_2 on Aβ fibrillisation *in vivo*. As discussed in Section 4.3.1. a range of H_2O_2 concentrations were analysed as part of this PhD, which attempted to cover amounts of H_2O_2 present in healthy and AD brain.

First Author	Concentration of H_2O_2 used	Concentration of Aβ used	Ratio H_2O_2:Aβ	References
Hou	2 M	50 μM	40,000-fold	Hou *et al.*, 2002 Hou *et al.*, 2004
	10 mM		200-fold	
Watson	0.9 M	1.2 mM	750-fold	Watson *et al.*, 1998
Palmblad	800 μM	2 μM	400-fold	Palmblad *et al.*, 2002
		4 μM	200-fold	
Johansson	800 mM	10 μM	80,000-fold	Johansson *et al.*, 2007
		100 μM	8,000-fold	

Table 4.1: Varying ratios of H_2O_2 to Aβ in literature studies on Aβ fibrillisation. A summary of H_2O_2 and Aβ concentrations used by studies in the literature on Aβ fibrillisation oxidation by H_2O_2 only.

The analysis methods used in these literature studies also deserve some criticism. Again, methods that do not discriminate amorphous aggregates and amyloid fibrils were used, such as size-exclusion chromatography (SEC) (Johansson, A.-S., *et al.*, 2007) and fourier transform ion cyclotron resonance mass spectrometry (FTICR-MS) (Palmblad, M., *et al.*, 2002). However, these methods can give an indication of the size of oligomeric species forming, as discussed in Section 4.1.2. Other methods are indirect measures of fibrillisation, in that they detect β-sheet formation, a precursor to fibril formation, rather than fibrillisation itself. Examples of these methods are UV-CD (Hou, L., *et al.*, 2002, Maiti, P., *et al.*, 2010, Watson, A. A., *et al.*, 1998) and NMR (Hou, L., *et al.*, 2004). The ideal methods for detecting fibrillisation are Th-T-binding assays (Hou, L., *et al.*, 2002) and electron microscopy (Maiti, P., *et al.*, 2010), and the former was used in this project's investigation into the effects of varying oxidation techniques on Aβ fibrillisation kinetics.

In general the most authoritative papers on the effects of methionine oxidation on Aβ fibrillisation may be regarded as Hou *et al.*, Johansson *et al*. and Maiti *et al.* (Hou, L., *et al.*, 2002, Johansson, A.-S., *et al.*, 2007, Maiti, P., *et al.*, 2010). In all three of these studies, H_2O_2-mediated oxidation of Aβ increased the time for fibres to form *in vitro*. This behaviour seems to run counter to the observation that amyloid plaques contain a high proportion of Met35-Ox Aβ (Dong, J., *et al.*, 2003).

4.1.2. Previous studies into the effects of oxidation on oligomeric state

If oxidation inhibits fibrillisation, it may be interesting to determine at which point fibrillisation is arrested i.e. is it at the monomer-dimer stage or does oxidation promote formation of oligomeric species in competition with fibres. These oligomeric species could be more neurotoxic than the fibrillar form e.g. the pentameric Aβ* (Aβ56 kDa) species (see Chapter 1, Section 1.6.1.). This has indeed been indicated for an indirect effect of oxidative stress on Aβ i.e. the action of oxidised metabolites on Aβ in the studies by Bieschke *et al.* (Bieschke, J., *et al.*, 2005).

The only study for the effects of MCO on Aβ oligomeric state is Dyrks *et al.*, who found only a high molecular weight smear on their SDS-PAGE gels after

oxidation of Aβ(1-42). They concluded that MCO of Aβ led to larger oligomeric species forming than for Apo. This study also found that oxidation led to aggregates which were more resistant to degradation, possibly explaining the role of oxidative stress in accelerating AD pathology.

Previous studies on the effects of oxidation by H_2O_2 alone are summarised in Table 4.2. All studies apart from Dyrks *et al.* found smaller Aβ species formed under H_2O_2 oxidation. The actual size of these smaller species is yet to be determined. The four remaining studies use varying techniques to measure oligomeric size from morphology analysis, AFM and EM, to the more quantitative, molecular size-determining SEC and MS. In the case of Palmblad *et al.*'s study the fourier transform ion cyclotron resonance-MS (FTICR-MS) technique has a particular advantage in that it is highly sensitive and thus can be used with relatively low, physiologically relevant, Aβ concentrations (Palmblad, M., *et al.*, 2002). Johansson *et al.* and Palmblad *et al.* agree that monomers or dimers are the most likely forms of Met35 oxidised Aβ(1-40) and Aβ(1-42), although they disagree on the specific size of the unoxidised species. This may be due to the different conditions and incubation times used for each study.

Hou *et al.* and Bitan *et al.* disagree slightly on what form the oxidised species takes, with the former stating it is globular amyloid-based oligomeric form while the latter states it is a non-amyloid amorphous aggregated form. This discrepancy may simply be because amorphous aggregates and globular oligomeric species are difficult to distinguish using AFM. Bitan *et al.*'s theory that Met35 oxidation causes the usual paranuclei forming Aβ(1-42) peptide to revert to the non-paranuclei forming Aβ(1-40) aggregation pathway is an attractive hypothesis (Bitan, G., *et al.*, 2003). However, without a method of species size determination which also incorporates an amyloid-specific binding dye such as Congo red or Th-T, this discrepancy cannot be resolved. Nevertheless this PhD study will aim to resolve the size of oligomeric species formed under both Cu^{2+}/Cu^{+}-catalysed oxidation and oxidation by H_2O_2 alone, both under aerobic conditions, using SEC.

Reference	First author	Aβ fragment	Oligomeric species found before oxidation	Oligomeric species found after oxidation	Technique used
Dyrks *et al.*, 1992	Dyrks	Aβ(1-42)	Monomers	Tetramers and octamers (50%) & larger aggregates (50%)	SDS-PAGE
Hou *et al.*, 2002	Hou	Aβ(1-42)	Protofibrils (3.6 ± 0.6 nm ⌀, 21 ± 4 nm periodicity) and filaments (0.65 ± 0.07 nm ⌀, no periodicity)	Globular, oligomeric species (0.7-3.3 nm ⌀)	AFM
Palmblad *et al.*, 2002	Palmblad	Aβ(1-40)	Monomers and dimers & trimers & tetramers	Monomeric and dimeric only until 100 h	SEC & FTICR-MS
Johansson *et al.*, 2007	Johansson	Aβ(1-42)	Trimers and tetramers	Mostly monomers & dimers	SEC
Bitan *et al.*, 2003	Bitan	Aβ(1-42)	Quasi-Globular Paranuclei	Revert back to non-paranuclei, amorphous aggregates as found for Aβ(1-40)	Photoinduced Cross-linking Unmodified Proteins (PICUP) & EM

Table 4.2: Summary of previous studies on the effects of hydrogen peroxide only oxidation of Aβ on its oligomeric state.

4.1.3. Aims

Although there are numerous lines of evidence to link oxidative stress with AD, there have been relatively few studies on the effect of Cu^{2+}/Cu^{+}-catalysed oxidation on Aβ fibrillogenicity. In contrast, the effect of H_2O_2-promoted oxidation of Aβ on fibril growth kinetics has been studied by a number of groups, however these studies have not always been in agreement. With this in mind, in this chapter we investigate how oxidation by H_2O_2 alone and Cu^{2+}/Cu^{+}-catalysed oxidation of Aβ influences fibre and oligomer formation.

4.2. Experimental methods and background theory

The majority of chemicals were purchased from Sigma Aldrich at the highest purity available. Deuterium oxide was purchased from GOSS Scientific Instruments Ltd. Water used was of ultra high quality (UHQ) with $\rho > 10^{-18}\,\Omega^{-1}\,cm^{-1}$.

4.2.1. Origin of Aβ peptide stocks

Aβ peptides and peptide fragments were synthesised using solid-phase Fmoc chemistry (ABC; Imperial College London and Zinisser Analytic). The peptides synthesised were Aβ(1-40) and Aβ(1-28). The *C*-termini and *N*-termini of the full peptides were left native as carboxyl and amino groups respectively. The peptide fragments were synthesised with a native amino terminus and an ethyl ester at the carboxyl terminus. After removal from the resin and deprotection, peptides were purified via RP-HPLC. Mass spectrometry was used to characterise these peptides and ^{1}H-NMR confirmed the peptides were not oxidised at the Met35 residue. Peptides were freeze dried for transportation and found to contain 20 % moisture by weight.

These lyophilized peptides were solubilised at 0.7 mg ml^{-1} Aβ in pH 10.5 UHQ water. This has been shown to be the best method for solubilising Aβ in order to avoid aggregation and precipitation and produce fibres typical of amyloids (Fezoui, Y., *et al.*, 2000). Aβ stocks contains salts of TFA the removal of acid labile groups and the cleavage of completed peptide sequences from solid supports during synthesis (Teplow, D. B., 2006). This means that upon solubilising to neutral pH, the initial Aβ microenvironment is an acidic milieu with pHs of 3-4, which then bypasses pH 5.3 on the way to neutral pH. This pH corresponds to the isoelectric point (pI) of Aβ and hence exposes the peptide to an environment where aggregation and precipitation is strongly promoted (Barrow, C. J., *et al.*, 1992, Fezoui, Y., *et al.*, 2000, Teplow, D. B., 2006, Wood, S. J., *et al.*, 1996). Fezoui *et al.* have shown that by using the strongly alkaline (pH~10.5) pre-treatment of Aβ, stocks of the peptide are seed (pre-existing aggregate) free and this allows repeatable data to be recorded using the peptide stocks without batch-to-batch variability (Fezoui, Y., *et al.*, 2000).

The solution of Aβ in UHQ water was incubated at 5 °C for 72 h with gentle agitation on a rocker before being separated into aliquots and stored at −80 °C until required. The concentration of Aβ was determined using its Tyr10 absorption at 280 nm (ε_{280} = 1280 M^{-1} cm^{-1}). Seed-free preparations could be determined by checking for a substantial lag-phase using a growth assay, although samples are expected to contain low MW species such as dimers and trimers.

4.2.2. Oxidation method

Oxidation was achieved using either H_2O_2 alone or via MCO, the latter using a $H_2O_2/Cu^{2+}/Cu^{+}$ system or an ascorbate/Cu^{2+}/Cu^{+} system. Both of these were conducted under aerobic conditions. Cu^{2+} was added to the samples in the form of copper(II) chloride at a substoichiometric ratio of 0.1 mol. eq. to Aβ (typically 1 μM $CuCl_2$ to 10 μM Aβ). H_2O_2 and ascorbate levels were at 10 mol. eq. (typically 100 μM H_2O_2 or 100 μM ascorbate to 10 μM Aβ).

Temperature was controlled throughout analysis of samples due to its significant effects on Aβ fibrillisation (Barrow, C. J., *et al.*, 1992). The pH was also controlled using a HEPES/NaCl buffer. HEPES was chosen because of its low binding affinity for Cu^{2+} ions (Sokolowska, M. and Bal, W., 2005) and its lack of interference with Aβ fibrillisation (Qin, Z., 2010). For the well plate assays the buffer was 50 mM HEPES/160 mM NaCl, with the concentration of NaCl being the physiological concentration of saline (1.6 p.c.) as defined by Lazarus-Barlow (Lazarus-Barlow, W. S., 1896). For SEC analysis the buffer was 50 mM HEPES/150 mM NaCl. For UV-CD analysis the buffer was 0.25 mM HEPES/0.8 mM NaCl so that the salt concentration did not cause absorbance outside of the dynamic range of the CD machine. UHQ water ($\rho = 10^{-18}$ $\Omega^{-1}cm^{-1}$) was used to make up these buffers.

Samples were made up in a specific order with addition of H_2O_2 or ascorbate after addition of Th-T to reduce potential oxidative decomposition of the dye. The pH was adjusted after addition of H_2O_2 to a pH of 7.4 with small additions of 10 mM HCl or 10 mM NaOH. Aβ(1-40) was added last to each sample, which was then immediately analysed. The concentration of Aβ(1-40) varied for each analysis,

although molar ratios of reagents were kept consistent. This is discussed further in Section 4.3.1.

Aβ fibrillisation was monitored using a Th-T binding well-plate assay (Section 4.2.3.) and UV-circular dichroism (UV-CD) (Section 4.2.4.). Size-exclusion chromatography (SEC) (Section 4.2.5.) was used to analyse the size of Aβ(1-40) species formed.

4.2.3. Thioflavin-T binding well-plate assay

Thioflavin-T (Th-T) as an amyloid fibril detecting dye

Thioflavin-T (Th-T) binds predominantly to crossed β-sheet structures in amyloid fibres (Figure 4.1) and is commonly used for detecting amyloid fibrils (Levine, H., 1995, Uversky, V. N., *et al.*, 2001). When bound to fibrils, Th-T fluoresces strongly with an emission at 482 nm and an excitation maximum at 450 nm (Naiki, H., *et al.*, 1989). Unbound Th-T is virtually non-fluorescent at these wavelengths. Thus the intensity of the fluorescence gives a quantitative measure of fibril growth.

Several models have been proposed to explain the exclusivity of fluorescence when bound to amyloid fibres but not monomeric species. These include the Monomeric Model (Krebs, M. R. H., *et al.*, 2005), the Excimer Model (Groenning, M., *et al.*, 2007), the Micelle Model (Khurana, R., *et al.*, 2005) and the Lateral Stacking Model (Wu, C., *et al.*, 2008). The Lateral Stacking Model may explain Th-T binding best and incorporates mechanisms proposed from all three of the other models. This model states that Th-T binds to monomers via aromatic ring-ring interactions and hydrophobic interactions in the grooves of β-sheets. As monomers come together to form an oligomeric species, bound Th-T molecules are then laterally stacked (Wu, C., *et al.*, 2008), which leads to a fluorescence enhancement via the mechanisms described in other papers; Th-T dimerisation leading to excimer formation (Groenning, M., *et al.*, 2007) and steric interactions between Th-T molecules and fibril side chains (Krebs, M. R. H., *et al.*, 2005) (Figure 4.1).

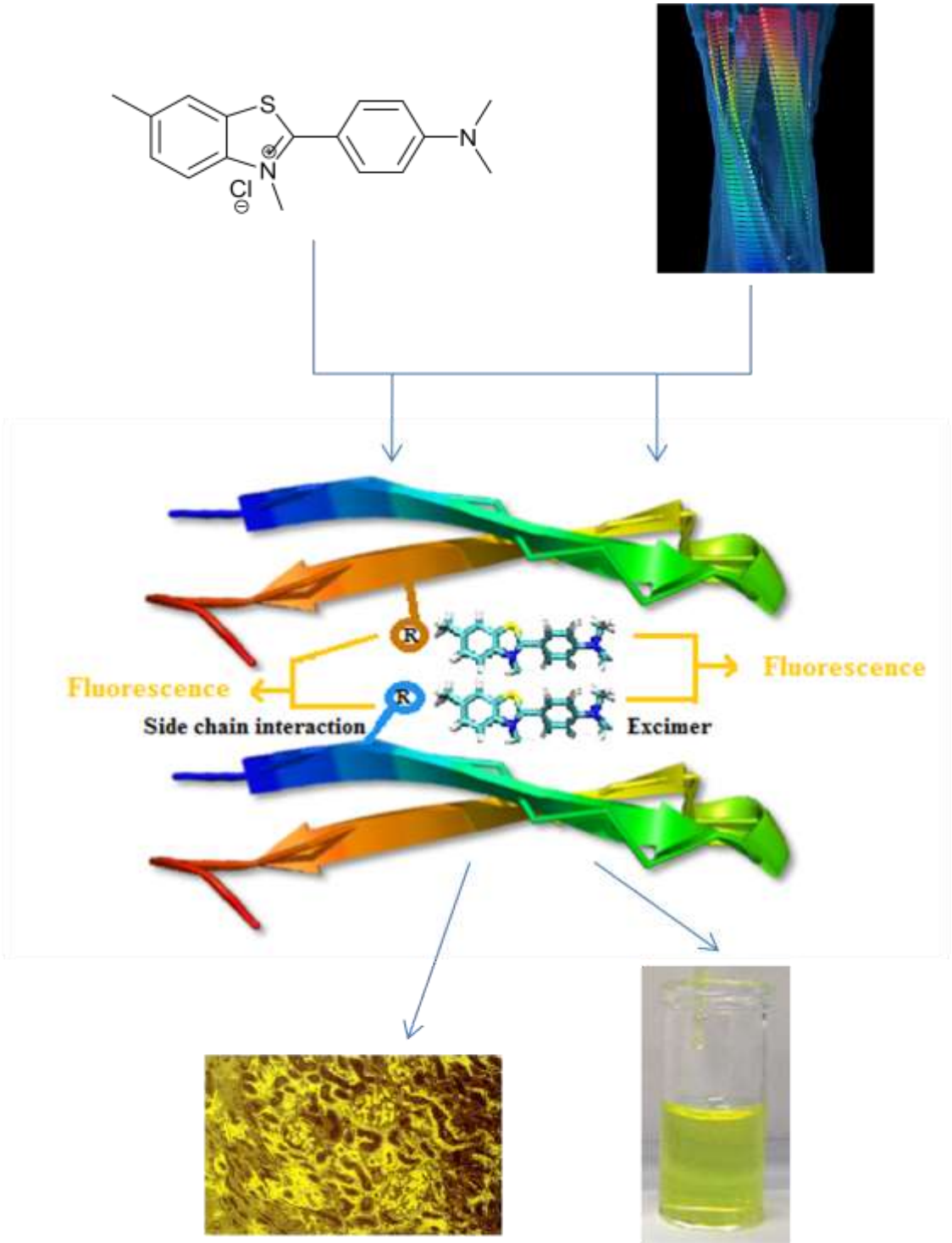

Figure 4.1: Thioflavin-T (Th-T) structure and fluorescence when bound to amyloid fibrils. The structure shown is of Thioflavin-T (Th-T). It is a dye which fluoresces only when bound to fibres containing a crossed β-sheet structure, i.e. amyloid fibres. The lateral stacking of the Th-T molecules (Wu, C., *et al.*, 2008) is believed to cause steric interactions with the side chains of the Aβ residues (Krebs *et al.*, M. R. H., 2005) and excimer formation (Groenning, M., *et al.*, 2007) leading to enhanced Th-T fluorescence at 482 nm. The appearance of this in both an *in situ* histological slide of amyloid fibrils (Williams, A. D., *et al.*, 2004) and an *in vitro* fibril solution is shown. The image of an amyloid fibre was taken from Dobson *et al.*, 1999 (Dobson, C. M., 1999).

Th-T was added at a molar ratio of 2.0 to Aβ(1-40) concentration, as fibril Aβ is saturated at these levels. The Th-T stock was dissolved in UHQ water at a concentration of 2 mM and kept foil wrapped at 5 °C to prevent light-induced decomposition.

This dye was used for the fibrillisation studies in this PhD project because it binds to Aβ(1-40) at the relevant pH 7.4 due to its positively charged state at this pH, with a suitable binding affinity (K_d = 2 μM) and is not NaCl sensitive (Levine, H., 1993).

Well-plate methodology

A BMG-Galaxy fluoro-star fluorescence (96) well plate reader was used to measure Th-T fluorescence because it allows temperature and agitation to be controlled and can perform automated measurements at specific time points. A typical well plate reader apparatus is shown schematically in Figure 4.2.

Samples were placed in a sterile, flat bottomed 96 well plate (Becton Dickinson) using a 300 μl sample volume. Only the central 60 wells were used because the outer wells are prone to undergo evaporation during the study. The plates were sealed with Starseal polyolefin film sealing tape (Starlabs) to minimise evaporation.

Temperature was controlled using an in-machine incubator set at 30 °C. Fibril growth kinetics are very sensitive to peptide concentration, which was tightly controlled by making up a single stock of each condition and then separating this into each set of wells as repeats. Reagents, such as $CuCl_2$ solution and H_2O_2, were added at an approximate volume of 5 μl per 1800 μl of stock sample to reduce diluting effects.

Wavelengths used were 440 nm for excitation and 490 nm for emission detection. Typically measurements of fluorescence intensity (AFU) were taken every 1 h directly after a 3 mm width orbital agitation for 1 min. Within each measurement, 100 flashes (readings) were taken and averaged.

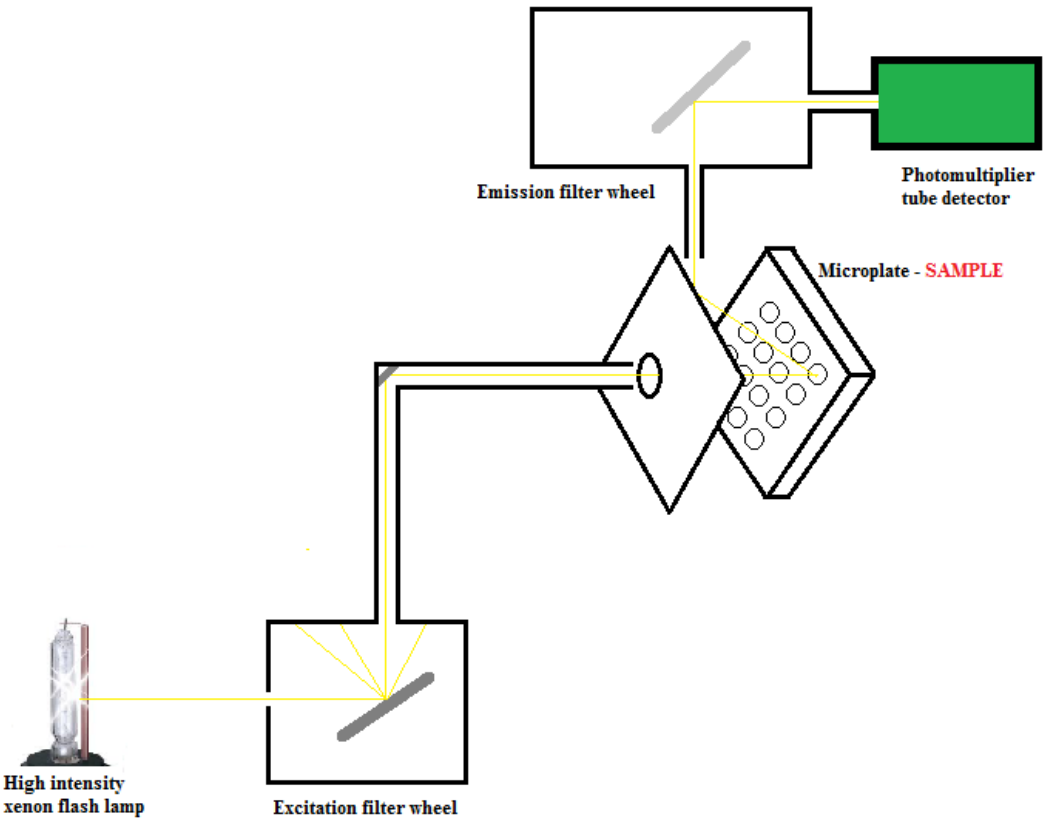

Figure 4.2: Well-plate reader apparatus. A basic schematic of the well-plate reader apparatus. A xenon flash lamp produces a high intensity light beam. An excitation filter wheel can be set to split the light so that a single excitation wavelength exits the filter. This is fed via fibre optic tubes to a specific well plate sample well. The fluorescence produced by the sample is then emitted back to an emission filter wheel, which resolves the beam so only the fluorescence at the desired wavelength is transmitted via further fibre optic fibres to the photomultiplier detector. This gives an output for fluorescence intensity for that well.

Measurement gain was optimised after an initial preliminary study at each Aβ(1-40) concentration. To do this, once the fibril growth curves obtained from this preliminary study showed maximum fibril growth i.e. has reached the plateau (equilibrium) phase, several measurements were taken over a range of gains and the results of three wells plotted against intensity of fluorescence. An example is given in Figure 4.3. The optimal gain in this case would be 49 %, as this gives the greatest differential in fluorescence intensity between the wells without being close to the machine's saturation level, 65,000 AFU. The optimal gain for each Aβ concentration was found and applied in future analyses. These gains ranged from 49 - 55%.

Data were averaged across traces, as indicated in the captions to data figures. The data were also zeroed to the initial fluorescence reading typically over the first 30 h to allow for both noise at the beginning of a well plate run due to condensation

and plate warming and also for a substantial part of the lag phase of each growth curve before the elongation phase began.

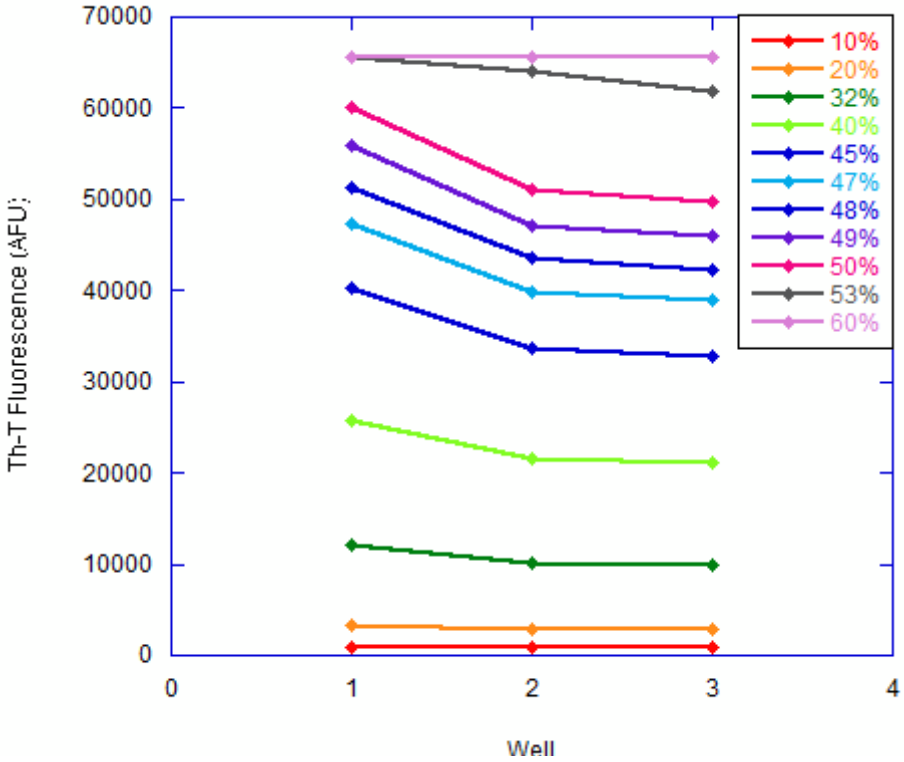

Figure 4.3: Optimising the gain for well plate analysis. Once the plateau phase had been reached for a preliminary Th-T binding well plate assay of 5 μM Aβ(1-40),this plate was used to find the optimal gain for this concentration of Aβ to use for future fibrillation analyses. Several measurements were made over a range of gains (10 – 60 %) and the Th-T fluorescence of three wells was plotted. For the example above the optimal gain is 49 %. This gives the greatest differential between wells but is not too close to the saturation of the instrument at 65,000 AFU.

Fibril growth curve analysis

The output from the well-plate reader is a fibril growth curve, as described in Chapter 1 and shown in Figure 1.6, where Th-T fluorescence intensity can be seen as a direct indicator of fibril formation. The curve describes three phases; an initial lag phase, an elongation phase and a plateau phase. The lag phase is also known as a nucleation phase in reference to the time taken for monomeric Aβ to become a nucleating species. The elongation phase refers to the time taken for the addition of monomeric Aβ to nucleating species and thus the formation of fibres. The plateau phase refers to equilibrium where there is no net increase in the number of amyloid fibres.

The fibril growth curves obtained in this study were fitted to two equations in order to obtain parameters by which to compare and characterise growth curves. The curve fitting software used was Origin Lab's Origin 8.5.0 SR0. If the fitting would not converge under suitable initial parameters or if the expected sigmoidal growth curve shape was not achieved with a data set, these data were discarded as unsuitable for analysis. In addition, upon obtaining parameters from this curve fitting, any parameters which lay outside 1.5*interquartile range of the data set were excluded from the analysis as outliers.

The first equation used to fit growth curves (Figure 4.4) is described by Uversky *et al.*, 2001 (Equation 1) (Uversky, V. N., *et al.*, 2001). It gives values for:

t_{50} - (annotated x_0 by Uversky *et al.*) half-maximal fibril growth in h.
$t_{lag} = t_{50} - 2\tau$; lag phase in h.
$k_{app} = 1/\tau$; apparent fibril growth rate in h^{-1}.

$$Y = (y_i + m_i t) + \frac{(v_f + m_f t)}{1 + e^{\frac{t - t_{50}}{\tau}}} \qquad \textbf{(Eq. 1)}$$

The other parameters in Eq. 2 are:
Y – concentration of fibres.
t – (annotated x by Uversky *et al.*) time.

The term $y_i + m_i t$ refers to the lag phase of the curve, while the term $v_f + m_f t$ refers to the plateau phase. Both these expressions allow for a slope in these two phases. Uversky *et al.* note that Equation 1 does not relate to underlying molecular mechanisms of fibrillisation but instead simply provides a model for comparing how different growth conditions affect fibril growth kinetics. They used this equation successfully to analyse the effect of pH change on α-synuclein fibrillisation (Uversky, V. N., *et al.*, 2001).

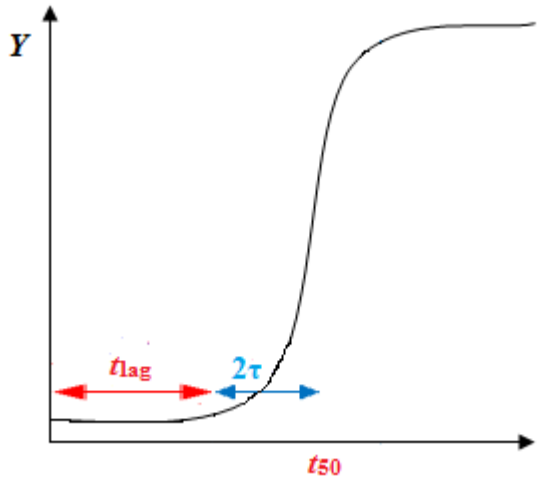

Figure 4.4: Application of parameters from the curve fitting equation described by Uversky *et al.* to the fibre growth curve shown in Figure 1.7. Parameters from the growth curve fitting equation described by Uversky *et al.* are fitted to the sigmoidal growth curve associated with Aβ fibrillation. t_{50} is the time to half maximal growth of fibrils and hence refers to halfway through the elongation phase. t_{lag} is the time of the lag phase. 2τ is the difference between these two values and ½ of this value gives the apparent fibre growth rate, k_{app} (Uverksy, V.N., *et al.*, 2001).

The second equation used to fit growth curves (Figure 4.5) is that described by Morris *et al.* (Equation 2) (Morris, A. M., *et al.*, 2008) and gives values for:

k_n – (annotated k_1 by Morris *et al.*) nucleation rate; the rate at which monomeric Aβ species become nucleating in h^{-1}.

k_e - (annotated k_2 by Morris *et al.*) elongation rate; the rate at which monomeric Aβ adds onto the nucleating species in h^{-1}.

$[B]_t$ - the maximal fluorescence in AFU corresponding to the maximal concentration of Aβ fibres.

$$[B]_t = [A]_t - \frac{\frac{k_n}{k_e} + [A]_0}{1 + \frac{k_n}{k_e[A]_0}\exp(k_n + k_e[A]_0)\,t} \qquad \textbf{(Eq. 2)}$$

The other parameters in Eq. 2 are:

$[A]_t$ - the concentration of Aβ monomer at time *t*.

$[A]_0 = [B]_t - [A]_t$; the total Aβ concentration.

t = time.

These parameters can be applied to Figure 1.6 as shown in Figure 4.5. The equation was based on the Finke-Watzky (F-W) 2-step mechanism of aggregation (Figure

4.6), for transition metal nanocluster formation (Watzky, M. A. and Finke, R. G., 1997), which can just as easily be applied to fibril growth. Morris *et al.* showed that this mechanism could accurately describe 14 sets of literature data on neurological protein aggregation with an $R^2 \geq 0.98$ (Morris, A. M., *et al.*, 2008), including several data sets involving Aβ aggregation (Bieschke, J., *et al.*, 2005, Dong, J., *et al.*, 2006, Vestergaard, M., *et al.*, 2005, Zirah, S., *et al.*, 2006). The mechanism described an initial slow continuous nucleation step (A→B) with rate constant k_n followed by a rapid, autocatalytic growth step (A+B→2B) with rate constant k_e similar to the two step Nucleation-Dependent-Polymerisation (NDP) mechanism described in Chapter 1 (Jarrett, J. T. and Lansbury, P. T., 1993). A was defined as 'unfolded, or misfolded, ready-to-aggregate protein' where B is the 'growing surface area of the aggregating protein' and included both oligomeric and fibrillar species (Morris, A. M., *et al.*, 2008).

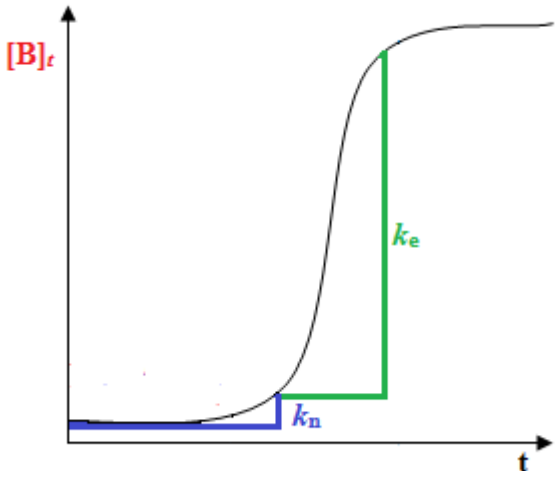

Figure 4.5: Application of parameters from the curve fitting equation described by Morris *et al.* to the fibre growth curve shown in Figure 1.7. Parameters from the growth curve fitting equation described by Morris *et al.* are fitted to the sigmoidal growth curve associated with Aβ fibrillation. k_n is the rate of nucleation and hence is related to the lag phase of the curve. k_e the elongation rate and hence is related to the elongation phase of the curve. $[B]_t$ is the concentration of oligomeric Aβ at time *t* and when extracted from curve fitting data indicates the maximal fibril concentration (Morris, A. M., *et al.*, 2008).

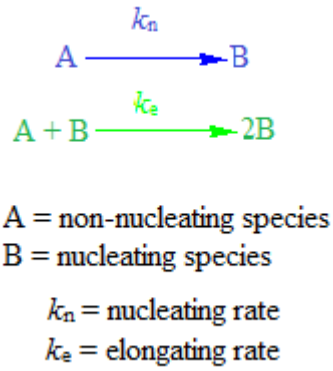

Figure 4.6 Finke-Watzky (F-W) 2-step mechanism for nucleation and growth phenomenon. This was used as a model for the fibre growth curve equation devised by Morris *et al.*, 2008, Equation 2.

This description of fibril growth had the advantage over the previously most cited mechanism, the 'Subsequent Monomer Addition Mechanism for Aggregation of Proteins'(Eisenverg, H., 1971) (abbreviated here to SMAMAP), in that it provides easy curves for fitting and it clearly illustrates the two initial phases of nucleation and elongation (Morris, A. M., *et al.*, 2008). Other mechanisms of protein aggregation have involved modifications of the SMAMAP model so that it incorporates elongation via species of various sizes ('Random association mechanism') (Thusius, D., *et al.*, 1975), assumes that the rate constant of dimer formation is unique but all subsequent additions have the same rate constant (Wegner, A. and Engel, J., 1975) and finally involves a monomer activation state to a nucleating species (Frieden, C. and Goddette, D. W., 1983). These were all precursors to Morris *et al.*'s model based on the F-W 2-step mechanism. Even more complicated, unwieldy mechanisms have been devised that describe polymerisation as either beginning with heterogeneous nucleation – polymers growing onto existing polymers - or homogeneous nucleation – polymers growing from seeds (Ferrone, F. A., *et al.*, 1980). In addition, Lansbury devised the 'passive autocatalysis mechanism' which indicated three rates as important, essentially the nucleation rate, the elongation rate and the dissociation rate (Come, J. H., *et al.*, 1993). Finally, Saito *et al.* devised a 3-step mechanism which included, before the nucleation step, a monomer-micelle step (Kamihira, M., *et al.*, 2000, Lomakin, A., *et al.*, 1997). However, Morris *et al.* showed that this could be reduced to the F-W 2-step mechanism without losing any accuracy (Morris, A. M., *et al.*, 2008).

There are some limits to Equation 2. The model does not take account of the effect of species size on k_n and k_e and it assumes the concentration of monomer is constant during the nucleation phase. The latter assumption means the equation

needs an ample lag phase to get an accurate nucleation rate and this must be considered when analysing the data described in this chapter.

Statistical tests of significance

Tests of significant difference between two data sets were performed using unpaired, two-tailed, t-tests. Initially an F-test was performed to determine whether the data sets had equal variance using the formula Equation 3.

$$F = \frac{S_1^2}{S_2^2} \quad \textbf{(Eq. 3)}$$

where n_i is the sample size of the *i*th data set and S_i^2 is an unbiased estimator of the variance of the *i*th data set given in Equation 4.

$$S^2 = \frac{1}{n-1}\sum_{i=1}^{n}(X_i - \overline{X})^2 \quad \textbf{(Eq. 4)}$$

F-test 95% probability critical value tables were obtained from the StatSoft Electronic Statistics Textbook (Statsoft). There were n−1 degrees of freedom.

In the cases of equal variance a homoscedastic Student's t-test was used to test for significant differences between the means of the two data sets using the formula in Equation 5.

$$t = \frac{\overline{X}_1 - \overline{X}_2}{S_{X_1X_2} \cdot \sqrt{\frac{1}{n_1} + \frac{1}{n_2}}} \quad \textbf{(Eq. 5)}$$

where $\overline{X}_i$ is the mean of the *i*th data set, n_i is the sample size of *i*th data set and $S_{X_1X_2}$ is the pooled standard deviation as given in Equation 6.

$$S_{X_1X_2} = \sqrt{\frac{(n_1-1)S_{X_1}^2 + (n_2-1)S_{X_2}^2}{n_1 + n_2 - 2}} \quad \textbf{(Eq. 6)}$$

The degrees of freedom were given by $n_1 + n_2 - 2$.

In the cases of unequal variance a heteroscedastic Welch's t-test was used to test for significant differences between the means of the two data sets using the formula in Equation 7.

$$t = \frac{\overline{X}_1 - \overline{X}_2}{\sqrt{\frac{s_1^2}{n_1} + \frac{s_2^2}{n_2}}} \qquad \textbf{(Eq. 7)}$$

where $\overline{X}_i$ is the mean of the *i*th data set, n_i is the sample size of *i*th data set and s_i^2 is an unbiased estimate of the variance of the *i*th data set as described above. The degrees of freedom were given by the Welch-Satterthwaite equation (Equation 8).

$$\text{d.f.} = \frac{(s_1^2/n_1 + s_2^2/n_2)^2}{(s_1^2/n_1)^2/(n_1 - 1) + (s_2^2/n_2)^2/(n_2 - 1)} \qquad \textbf{(Eq. 8)}$$

t-test 95% probability critical value tables were obtained from the StatSoft Electronic Statistics Textbook (Statsoft).

4.2.4. UV-Circular Dichroism (UV-CD) analysis

A theoretical background to UV-Circular Dichroism (UV-CD)

UV-Circular Dichroism (UV-CD) is a spectroscopic measurement of the differential absorbance of left and right circularly polarised light by a sample. Samples such as proteins, which are optically active, have non-zero values for this differential absorbance.

The instrument used to measure this, a CD spectrometer, has a set-up as shown in Figure 4.7. This instrument generates a monochromatic, linearly polarised light source which is then given a periodic variation in polarisation from left- to right-circularly polarised light which is passed through the sample before being detected. Any differences in the absorbance between each polarisation of light are then recorded and from this a measure of ellipticity calculated.

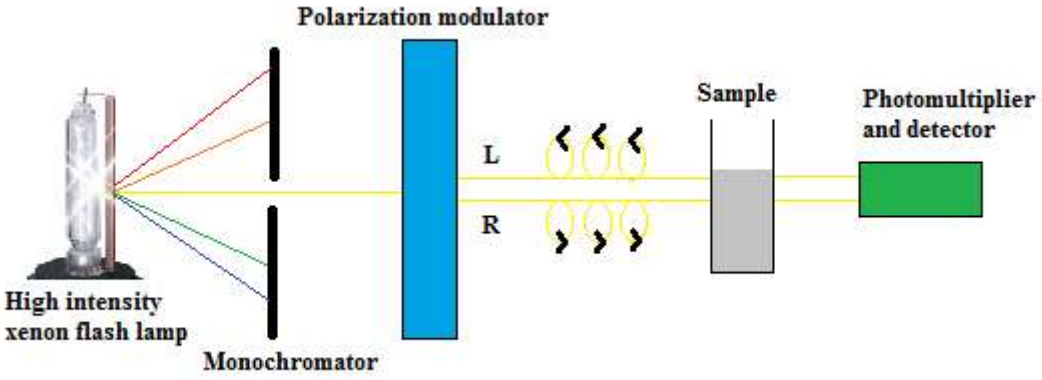

Figure 4.7: UV-CD spectrometer apparatus. A high intensity xenon lamp generates a light source which is both made monochromatic and polarised linearly by a monochromator. This light then passes through a polarization modulator where it is given a periodic variation in polarization ranging from left to right circular directions. This is then passed through the sample and a photomultiplier and detector records the differential absorbance of each light polarisation by the sample. (Adapted from Drake, A. F., 1994)

Proteins have an optical activity, and thus a differential absorbance of left and right circularly polarised light. The amide bond within the polypeptide backbones of proteins acts as a chromophore with two electronic absorptions; one at approximately 190 nm due to a π - π^* transition and one at approximately 210 nm due to a $n - \pi^*$ transition. These transitions, and hence the extent of the absorptions, become optically active due to the chirality of the α-carbon adjacent to the amide group and hence the orientations of its substituents. This orientation is heavily influenced by the secondary structure of the protein and hence UV-CD spectra can be used to as an indicator of this conformational level of a protein. The distinct spectra produced by certain conformations are shown in Figure 4.8.

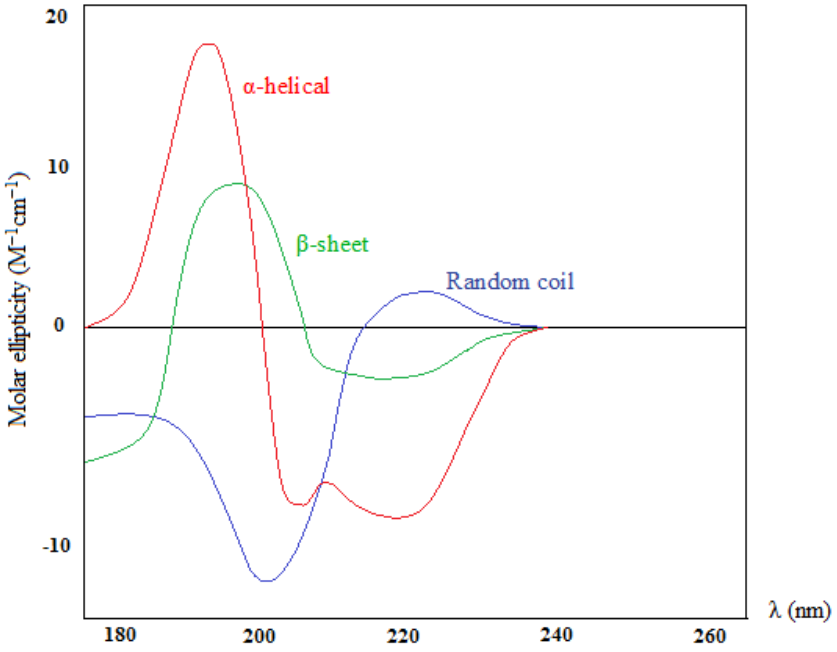

Figure 4.8: Characteristic UV-CD spectra of protein secondary structures. α-helical proteins display UV-CD spectra (red) typically with two negative bands at 222 nm and 208 nm and a positive band at 192 nm. β-sheet proteins give UV-CD spectra (green) with a weak negative band at 217 nm and a positive band at 195 nm. Random coil structures give a negative band at 198 nm and a weak positive band at 218 nm.

UV-Circular Dichroism (UV-CD) methodology

CD measurements were made on a Chirascan CD Spectrometer (Applied Photophysics). During measurements temperature was controlled using a Peltier Temperature Controller at 37 °C. Between measurements the sample was kept at 37 °C in an incubator with a 100 rpm rotation. The latter was to provide gentle agitation to the samples, another factor which can promote fibril formation.

Measurements were made at 95 minutes, 200 h, 305 h, 390.5 h, 561 h, 632.5 h, 680.5 h and 730.5 h. For each measurement, three repeats were recorded, which were later averaged. Sampling points were taken every 0.5 nm, with 3 seconds for each point. Spectra were obtained from 190 – 270 nm. Three background readings of the buffer were taken before measurements of the samples commenced and the average of these was subtracted from the averaged data sets for each measurement. Data were also zeroed at 260 nm and smoothed using the Applied Photophysics' Chirascan Viewer program.

Although the CD spectrometer measures light absorption, for historical reasons the units for data obtained from the CD machine is the ellipticity of linear polarised light passing through the sample and thus is given as an angle in millidegrees (θ). This can be converted into a measure of sample absorbance using an adaptation of Beer's Law. The output is a measure of molar ellipticity (Δε) with units $M^{-1}cm^{-1}$ using Equation 9.

$$\Delta\varepsilon = \frac{\theta}{33{,}000.\,c.\,l} \qquad \textbf{(Eq. 9)}$$

where c is the concentration in M and l is the path length in cm. The sample cell used had a 1 mm path length.

4.2.5. Size-exclusion chromatography (SEC) analysis

Background theory to size-exclusion chromatography (SEC)

Size-exclusion chromatography (SEC) is a form of chromatography which separates components of a solution predominantly according to their size rather than by their enthalpic interactions with the stationary phase. It has the advantage of being quick, convenient and involves separation with very narrow bands. It is often used as a method for finding the approximate molecular weight (M_r) and hydrodynamic radius (R_h) of macromolecules, although the specific property that molecules are separated by using size-exclusion chromatography is molecular hydrodynamic volume (Mori, S. and Barth, H. G., 1999). The technique involves passing the macromolecules in solution (the mobile phase) through a column of an inert gel medium stationary phase with pores of a nominal size, e.g. polyacrylamide or dextran, under a low pressure (Mori, S. and Barth, H. G., 1999). A basic schematic diagram of the size-exclusion apparatus is shown in Figure 4.9.

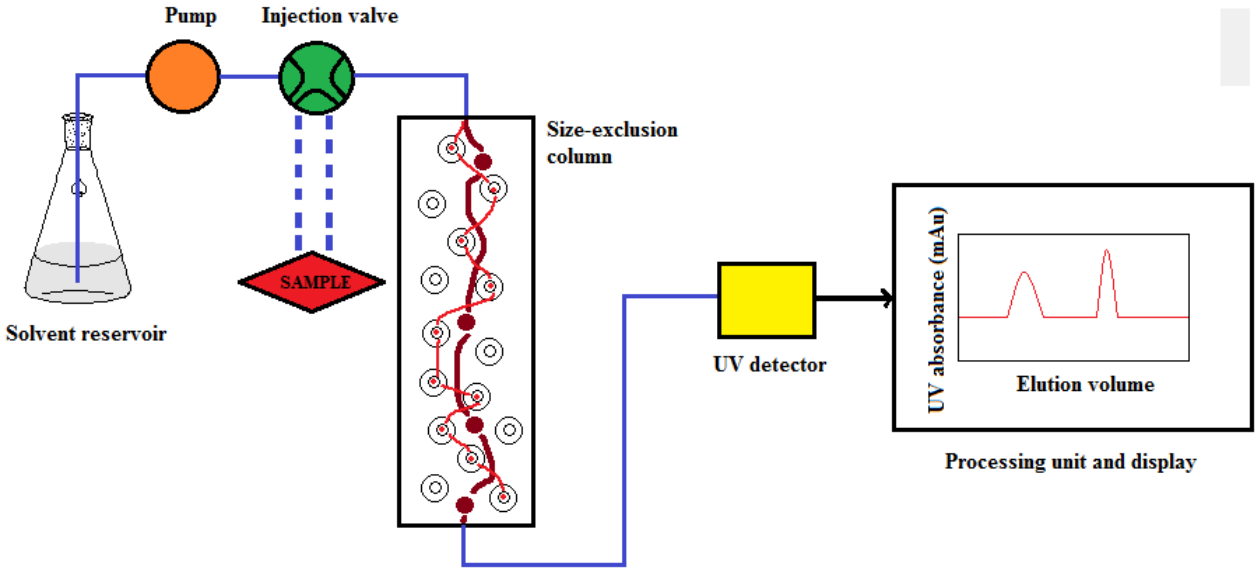

Figure 4.9: Size-exclusion chromatography apparatus. A basic schematic diagram of a size-exclusion chromatography apparatus. A pump causes flow of solvent (mobile phase) through the column via an injection valve which can allow diversion of the mobile phase via a sample. The column then separates molecules in the sample solution by their size. Smaller molecules (red) penetrate more of the pores in the column stationary phase and hence take longer to elute from the column than large molecules (brown). Only two molecule sizes are shown for simplicity's sake. The eluate from the column is then analysed using UV detection which produces a trace of UV absorbance against elution volume/time.

The elution time of each macromolecule depends on the volume of column the macromolecule travels through. This means the smaller the molecule, the more pore volume the molecule will penetrate and the more time it will take for the macromolecule to fully elute the column. In reality the theory behind particle separation is not this simple as there will be some variation in pore and particle size for each defined size. Therefore, elution curves are actually Gaussian distributions. The eluant from the column is analysed constantly using detection such as UV absorbance (Figure 4.10). The elution volume (V_e) decreases approximately linearly with the log of the molecular weight. Thus using macromolecules of known molecular weight, a relationship between elution volumes and molecular weight can be determined via a calibration curve and this can be used to convert the elution volumes of sample proteins to their molecular weight (Figure 4.10). This is discussed in detail below.

The Void Volume (V_0) of the column is the volume of mobile phase that passes through the column containing particles too large to interact at all with the

stationary phase. The Column Volume (V_c) is the maximum volume of mobile phase that passes through the column before molecules too small to be separated by the column start to elute as a final single band.

The behaviour of molecules on size-exclusion columns can be described by Equation 10.

$$V_e = V_i \cdot K_{SEC} + V_0 \quad \textbf{(Eq.10)}$$

where V_i is the pore volume accessible to the molecules and K_{SEC} is a thermodynamic parameter defined as the ratio of column pore volume (c_i) to interstitial column volume (c_0) (Equation 11). It is often referred to as the SEC distribution coefficient.

$$K_{SEC} = \frac{c_i}{c_0} \quad \textbf{(Eq. 11)}$$

For size-exclusion to reliably separate molecules based on their molecular size then the criteria $0 < K_{SEC} > 1$ must be satisfied. If $K_{SEC} = 0$, the molecules will elute in the void volume. If $K_{SEC} = 1$, the molecules will elute after the column volume and if $K_{SEC} > 1$ then the molecules are likely interacting with the stationary phase in an enthalpic manner and are not eluting based on molecular size alone. Electrostatic charges, for example, may also be influencing elution volume in this case (Mori, S. and Barth, H. G., 1999). These factors must be taken into consideration when designing a SEC experiment. Depending on the size of molecules, different packing material is used with different pore size. For example for studying the oligomeric size of Aβ(1-40) around the expected Aβ*56 size, Superdex 75 was used, which measures molecular weights from 3,000 – 70,000 Da.

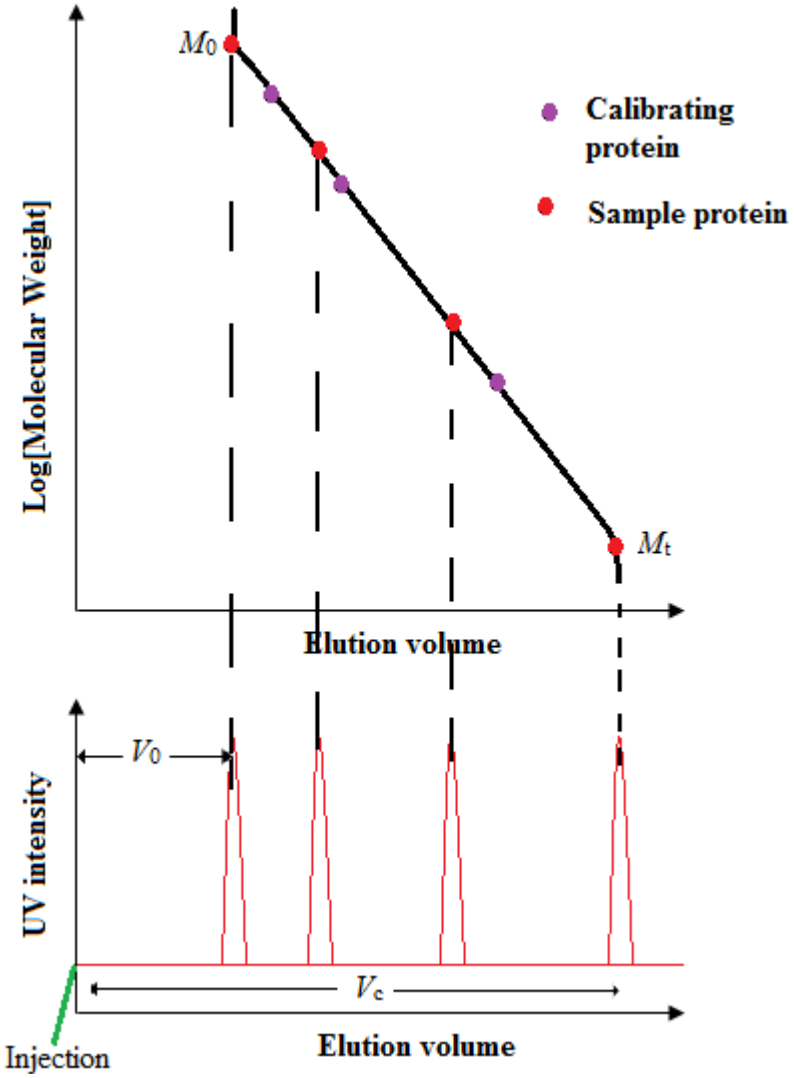

Figure 4.10: Typical SEC calibration curve for a protein sample. SEC is a relative rather than absolute method for measuring molecular weight and therefore requires a calibration curve. The lower trace shows a typical output from a SEC processing unit with elution volume plotted against UV intensity and peaks showing proteins exiting the column. The upper trace shows a typical calibration curve determined by running proteins of known molecular weight down the column. Molecular weights of sample proteins can be read off this based on their elution volumes. V_0 represents the void volume of the column. It is not until the end of this volume that reliable molecular weights can be determined and this point is marked as M_0, the exclusion limit of the column. V_c represents the column volume, which is the maximum volume of the column from which reliable molecular weights can be determined. It is marked as M_t, the total permeation limit of the column. Adapted from Mori and Barth 1999 (Mori, S., and Barth, H. G.. 1999).

General SEC methodology

Analytical size-exclusion chromatography was carried out using a Superdex-75 10/300 GL column (3,000 < M_r > 70,000) with a UV detector set at 280 nm in order to detect UV active compounds eluting from the column. This was housed within an

ÄKTA FPLC unit. The UV data were processed using Unicorn Software. The concentration of Aβ(1-40) used was 10 μM with an injection volume of 500 μl. The column conditions were isocratic. For all experiments at pH 7.4 a 50 mM HEPES/150mM NaCl buffer was used as described above. For experiments at pH 10.5 samples were run in alkaline saline solution ([NaCl] = 150 mM) only, with careful adjustment of pH using small amounts of 10 mM NaOH and 10 mM HCl. In all cases UHQ water (ρ > 18 MΩ cm) was used. All buffers were filtered and degassed before use.

For sets of readings taken at increasing time intervals a stock sample was kept incubated in a water bath set at 30 °C and 500 μl aliquots were taken at 2 hour intervals. As for the well-plate and UV-CD analyses, Aβ(1-40) was used instead of Aβ(1-42).This is even more important for SEC because of the latter's tendency to form insoluble aggregates over 24 h which can cause irreversible changes to the column packing material (Kuo, Y.-M., *et al.*, 1998).

The void volume of the column was determined by measuring the elution volume of blue dextran (M_r 2 MDa) and was found to be 8.57 ml at pH 7.4 and 7.99 ml at pH 10.5. This volume is indicated with grey shading in the figures discussed in Section 4.3. The column volume was determined by running acetone (M_r = 58.1 Da) down the column and was found to be 19.5 ml. This is where the trace terminates in these figures, because, as explained in above, outside of these regions, molecules eluting the column are not been separated by molecular weight alone.

Before and after each measurement the column was cleaned with 1.5 column volumes of 2 M NaOH, to dissociate any remaining Aβ(1-40) aggregates and allow thorough cleaning of the column, and then 2 column volumes of distilled water to restore pH. The column was stored in either 0.2 % azide or distilled water, depending on the period of storage. The injection loop was also syringed through with NaOH and water. Between different mobile phases the column pumps were washed and the column was re-equilibrated using 1.5 column volumes of the relevant cleaning agent or experimental buffer to ensure the column was a uniform environment before the sample was run down it.

For each measurement 1.2 – 1.5 column volumes of elution buffer was run down the column following sample injection. The flow rate used was 0.5 ml min^{-1} to prevent the column pressure limit (1.8 MPa) being exceeded.

Determining molecular weight from SEC elution volume

In order to determine the molecular weight of Aβ(1-40) species exiting the column it was necessary to calibrate the column. This involved running proteins of known molecular weight down the column. These proteins were all globular, compact proteins and included bovine serum albumin (BSA), M_r = 66.4 kDa and lysozyme, M_r= 14.6 kDa. At this salt concentration (150 mM NaCl) BSA forms both dimers and monomers. For pH 7.4 the dimeric form of BSA (M_r = 132 kDa) gave a band within the void volume and thus could not be used for calibration. Although at pH 10.5 this dimer did show a band within the reliable part of the column, the column specifications state that no proteins greater than 70,000 Da can be measured on the column so this could not be used for calibration purposes.

An attempt was made to use *Agrobacterium phytochrome* (Agp1) (M_r = 34683.37 Da) and the prion protein fragment, PrP(57-90) (M_r = 3370.45 Da) as calibrating proteins. The behaviour of each on the SEC column is shown in Figure 4.11(A) and Figure 4.11(B) respectively. Both proteins showed poor resolution on the SEC column, with PrP(57-90) showing significant degradation and Agp1 showing excessive aggregation and possibly some degradation. Therefore, only lysozyme and BSA were used to construct the calibration curve.

Calibrating proteins were run in the same buffers as were the samples, and thus two separate calibrations were performed for pH 7.4 and pH 10.5. Each protein (5 mg ml^{-1}) was run down the column in conjunction and the resulting chromatogram is shown in Figure 4.11. For pH 7.4 (Figure 4.11(A)) two repeats were run of the calibrating proteins and the average elution columns used in calibration calculations. The elution volumes were very similar indicating a high reproducibility of this method. For pH 10.5 (Figure 4.11(B)) only one run of calibrating proteins was done.

Elution volumes were then converted into a retention factor, K_{AV}, using Equation 12.

$$K_{AV} = \frac{V_e - V_0}{V_c - V_0} \qquad \textbf{(Eq. 12)}$$

where V_e is the elution volume of the calibrating protein. V_0 is the void volume of the column and V_c is the total column volume as measured with acetone.

K_{AV} was then plotted against log(M_r) of the calibrating proteins to produce a straight line graph with equation $y = ax + b$. This equation can be used to convert the K_{AV} of sample proteins using Equation 13 to the log of their molecular weight.

$$\log(M_r) = \frac{K_{AV} - b}{a} \qquad \textbf{(Eq. 13)}$$

A simple inverse log function then gives the molecular weight (M_r).

However, unstructured proteins have considerably larger hydrodynamic radii than folded proteins of equivalent molecular weight. Danielsson *et al.* gave the formula in Equation 14 to relate hydrodynamic radius (R_h) and molecular weight (M_r) for unstructured proteins (Danielsson, J., *et al.*, 2002).

$$R_h = 0.027 M_r^{0.5} \qquad \textbf{(Eq. 14)}$$

Talmard *et al.* found that R_h of Aβ species calculated from this formula matched R_h determined using pulse field gradient (PFG) NMR whereas SEC gave an even larger value for R_h (Talmard, C., *et al.*, 2007). The SEC is calibrated with globular proteins whereas Aβ species are unstructured. This would lead to calibrating proteins of a similar molecular weight to Aβ exiting the column later, making Aβ appear larger than it is, specifically so that a monomeric Aβ species would appear hexameric (Talmard, C., *et al.*, 2007). In addition, papers such as Teplow, 2006, have indicated that low molecular weight Aβ will elute from a size exclusion column at 5-15 kDa and that monomer may appear as heptamer (Teplow, D. B., 2006).

There were some cases when application of this formula was not appropriate. For example Aβ complex with Zn^{2+} ions leads to a more structured peptide which increases lag time on the column. However, in general, it can be stated that monomeric Aβ may appear anywhere from pentameric to heptameric on a column calibrated with globular proteins.

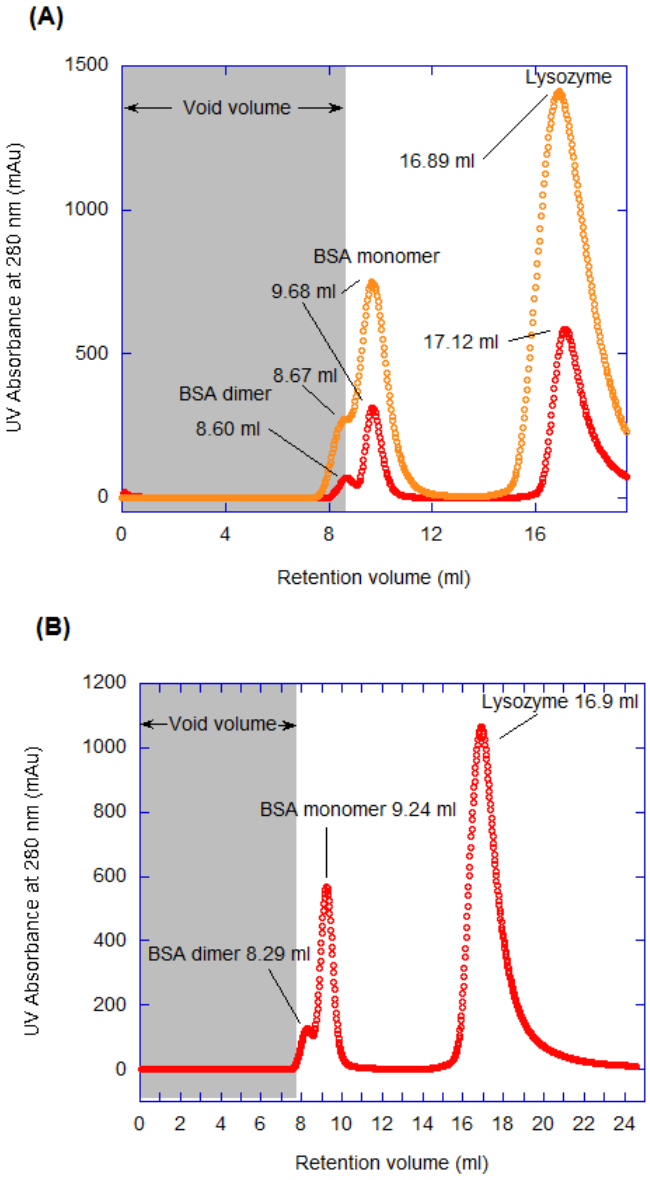

Figure 4.11: Chromatogram of BSA and lysozyme used for calibration of SEC. UV traces of eluting products from a size exclusion after injection of 5 mg^{-1} ml each of bovine serum albumin (BSA) and lysozyme. **(A)** Proteins run in pH 7.4 50 mM HEPES/150 mM NaCl buffer. Two repeats were done. **(B)** Proteins run in pH 10.5 150 mM NaCl UHQ H_2O.

4.3. Results

4.3.1. Fibril growth rates of oxidised and unoxidised Aβ(1-40)

Initially the effects of oxidation on the fibrillisation kinetics of Aβ were studied, including both the nucleation and elongation rates of fibril formation. The first section of the results will discuss these studies.

Determining the optimal concentration of Aβ(1-40) for fibril growth assays

Initially, well-plate assays were run on Aβ(1-40) alone, in order to establish the optimal concentration of peptide to obtain growth curves over a time period which would allow detection of both increased and decreased rates of fibril growth under various oxidising conditions. The assay used was a Th-T fluorescence binding assay at two different Aβ(1-40) concentrations, 10 μM and 20 μM. The data are shown in Figure 4.12(A). The fibril growth curves were then fitted to the two equations described in Section 4.2.3. and the values obtained were then averaged across five traces (10 μM Aβ(1-40)) or six traces (20 μM Aβ(1-40)) to give various kinetic parameters with standard errors given in parentheses (Table 4.3 and Table 4.4).

Doubling the concentration of Aβ(1-40) nearly doubled the apparent fibril growth rate (k_{app}) from 0.064 ± 0.008 h^{-1} with 10 μM Aβ(1-40) to a k_{app} of 0.11 ± 0.01 h^{-1} for 20 μM Aβ(1-40) (Table 4.3). The time taken to half maximal growth of the Aβ(1-40) fibres was tripled for 10 μM Aβ(1-40) with a t_{50} of 231 ± 11 h compared to just 75 ± 3 h for 20 μM Aβ(1-40) (Table 4.3, Figure 4.12(B)) and statistical testing (t-test) showed this change to be significant ($p < 0.05$) (Table 4.5). The apparent discrepancy between these two indicators of fibril growth rate, k_{app} and t_{50}, can be explained by the vastly different nucleation rates for these two concentrations with a nucleation rate of just $5\times10^{-7} \pm 3\times10^{-7}$ h^{-1} for 10 μM Aβ(1-40) versus the significantly faster $10\times10^{-5} \pm 3\times10^{-5}$ for 20 μM Aβ(1-40) ($p < 0.05$) (Table 4.4, Figure 4.12(C)). The t_{50} is highly dependent on nucleation rate and thus the apparent numerical differences in the extent of the effect of concentration of Aβ(1-40) on fibril growth can be explained. This is also illustrated by the greater difference in lag phase between the two concentrations – a four-fold

difference between 200 ± 2 h for 10 μM Aβ(1-40) and 56 ± 2 h for 20μM Aβ(1-40) (Table 4.3) – which is a significant component of the time to half maximal growth.

To varying degrees, these quantitative measurements all indicate the same conclusion, that a doubling in Aβ(1-40) concentration causes a significant ($p < 0.05$) increase in the rate of fibril growth and thus must be taken into consideration when designing assays to determine the effects of peptide oxidation on fibril growth.

It is interesting to note that although doubling the concentration of Aβ(1-40) significantly increased the nucleation rate it did not profoundly affect the elongation rate, which was in fact only marginally faster at the lower peptide concentration; $3.6\times10^{-6} \pm 0.3\times10^{-6}$ h^{-1} for 10 μM Aβ(1-40) and $2.9\times10^{-6} \pm 0.2\times10^{-6}$ h^{-1} for 20 μM Aβ(1-40) (Table 4.4, Figure 4.12(D)). These data suggest that under these conditions nucleation, as defined by Equation 2, is considerably more influenced by concentration than is elongation.

As expected maximal Th-T fluorescence intensity is approximately half when the concentration of Aβ(1-40) is halved; 15,900 ± 270 AFU for 10 μM Aβ(1-40) compared to 29,300 ± 290 AFU for 20 μM Aβ(1-40) (Table 4.4). This demonstrates that the Th-T fluorescence binding assay gives meaningful quantitative measurements of fibril formation.

From these data it was decided that the best Aβ(1-40) concentration to use for the oxidation assays was 10μM Aβ(1-40) as this would allow an adequate range of t_{lag} values around the control Apo t_{lag} of 200 ± 8 h, should oxidation either increase or decrease fibril growth rates. In addition, previous publications had indicated that at Aβ concentrations greater than 10μM Aβ, amorphous aggregates form and thus amyloid fibres could not be detected under certain conditions, e.g. in the presence of Cu^{2+} ions (Sarell, C. J., *et al.*, 2010). This indicated that higher concentrations of Aβ(1-40) may not be favourable for amyloid fibre formation and may instead favour amorphous aggregation.

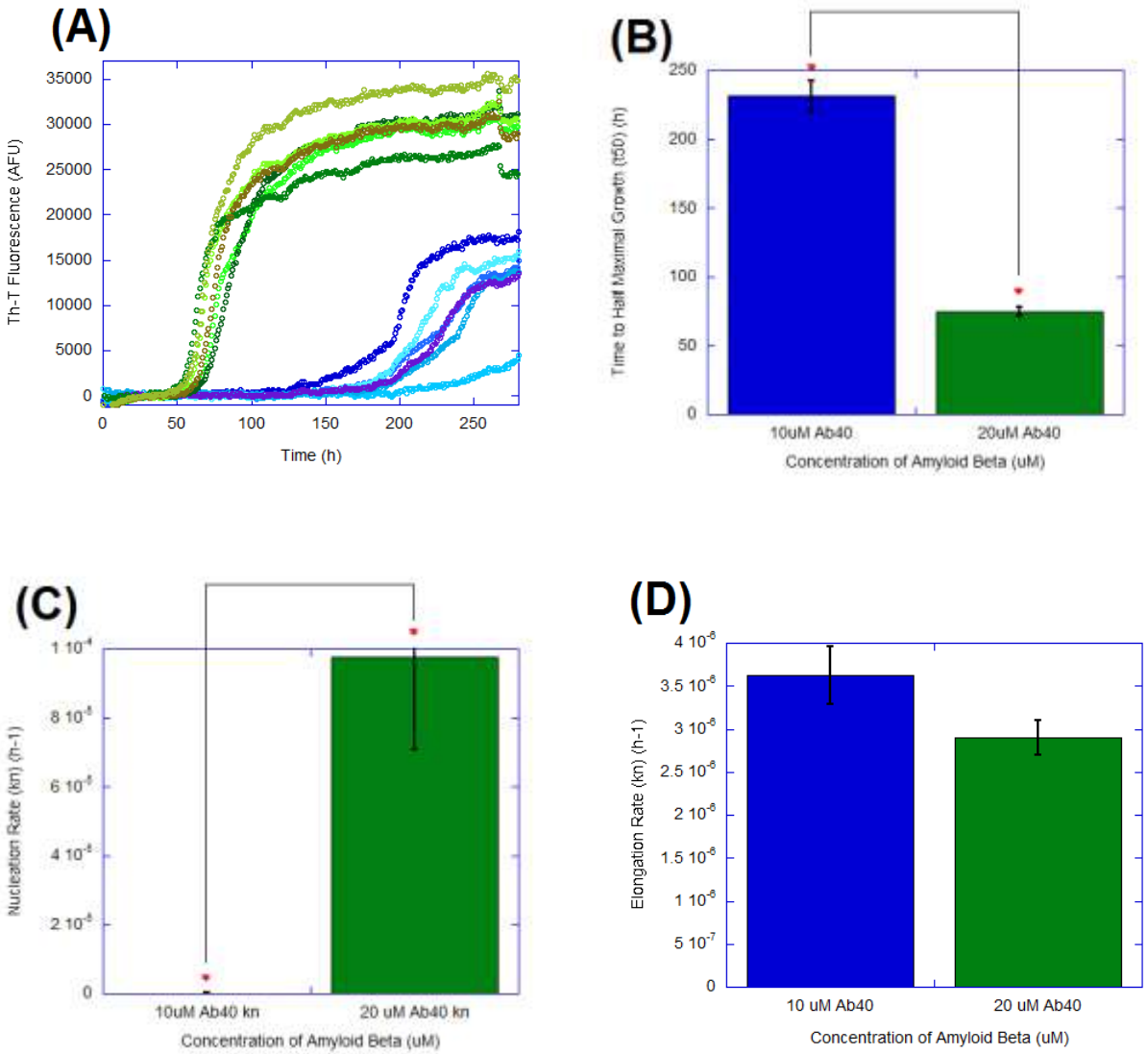

Figure 4.12: Effect of Aβ(1-40) concentration on fibril growth. (a) Fibril growth curves of Aβ(1-40) at 10 µM (blue) and 20 µM (green) with 2 mol. eq. Th-T at 30 °C, pH 7.4 (50 mM HEPES, 160 mM NaCl Buffer). Th-T fluorescence values are zeroed at 30 h . Six traces are shown for each concentration. (b) Summary plot showing the mean time to half maximal growth (t_{50}) for each concentration of Aβ(1-40) used; 10 µM (blue) and 20 µM (green) Aβ(1-40). Error bars are for standard error of 5 traces (10 µM) and 6 traces (20 µM). Halving the concentration of Aβ(1-40) significantly decreases the fibril growth rate. Significant changes are indicated with a red star. c) Summary plot showing the nucleation rate (k_n) for each concentration of Aβ(1-40) used; 10 µM (blue)and 20 µM (green) Aβ(140). Error bars are for standard error of 4 traces (10 µM) and 6 traces (20 µM). Halving the concentration of Aβ(1-40) significantly decreases nucleation rate, so much so that the two sets of data cannot be plotted on the same chart. Significant changes are indicated with a red star .d) Summary plot showing the elongation rate (k_e) for each concentration of Aβ(1-40) used; 10 µM (blue) and 20 µM (green) Aβ(1-40). Error bars are for standard error of the mean of 5 traces (10 µM) and 6 traces (20 µM). Halving the concentration of Aβ(1-40) has no significant effect on elongation rate.

Aβ(1-40) concentration (μM)	**Mean t_{50} (h)**	**Mean t_{lag} (h)**	**Mean k_{app} (h^{-1})**
10	231.4 (11.2) n = 5	200.0 (8.4) n = 5	0.064 (0.0081) n = 5
20	74.9 (3.2) n = 6	56.4 (2.1) n = 6	0.11 (0.013) n = 6

Table 4.3: t_{50}, t_{lag} and k_{app} values for varying concentrations of Aβ(1-40).
Calculated using the equation specified by Uversky *et al.*, 2001 (Uversky, V., *et al.*, 2002) by fitting the curves shown in Figure 4.12(A). In parentheses are the standard errors for each measurement.

Aβ(1-40) concentration (μM)	**Mean k_n ($x10^{-7}$))**	**Mean k_e ($x10^{-7}$)**	**Mean $[B]_t$ (AFU)**
10	1.71 (0.75) n = 4	36.2 (3.3) n= 5	15900 (269.0) n = 3
20	976.0 (270.0) n = 6	29.0 (2.0) n = 6	29300 (288.0) n = 4

Table 4.4: k_n, k_e and $[B]_t$ values for varying concentrations of Aβ(1-40).
Calculated using the equation specified by Morris *et al.*, 2008 (Morris, A. M., *et al.*, 2008) by fitting the curves shown in Figure 4.12(A). In parentheses are the standard errors for each measurement.

Statistic	**Value**	**Critical value**	**Conclusion**
F-statistic	10.291	5.1922 (4, 5)	Unequal variances - Welch's t-test
t-statistic	13.408	2.1318 (4.7966)	Means significantly differ

Table 4.5: Tests of significant difference on t_{50} from Figure 4.12(A).
Calculated using the equations specified in Section 4.2.3. Degrees of freedom for each test are given in brackets.

The effects of H_2O_2 oxidation on Aβ(1-40) fibril growth rates

In Figure 4.13 the kinetics of fibril growth under various oxidising conditions are compared using well plate-Th-T binding assay on 10 μM Aβ(1-40). Comparison of unoxidised Aβ(1-40) (Figure 4.13(A)) with H_2O_2-oxidised Aβ(1-40) (Figure 4.13(B)) indicates that the rate at which fibres are formed is significantly increased with H_2O_2 oxidation ($p < 0.05$) (Table 4.8). In particular, the time to half maximal fluorescence (t_{50}) is reduced from 221 ± 7 h for un-oxidised Aβ to 104 ± 4 h for the H_2O_2 oxidised Aβ(1-40) (Table 4.6). The difference in t_{50}s was shown to be significant according to an unpaired t-test ($p < 0.05$) (Figure 4.13(D)).

Comparison of the elongation and nucleation rates suggests that it is the lag phase (nucleation rate) that is most influenced by H_2O_2 oxidation. H_2O_2 oxidation reduces the lag phase from 192 ± 4.5 h to 73 ± 3.7 h. The nucleation rate ($1.5\times10^{-4} \pm 0.5\times10^{-4}$ h^{-1}) is increased 950-fold compared to un-oxidised ($1.6\times10^{-7} \pm 0.7\times10^{-7}$ h^{-1}) while the elongation rate ($4.3\times10^{-6} \pm 0.3\times10^{-6}$ h^{-1}) is only increased 1.2-fold compared to Apo ($3.6\times10^{-6} \pm 0.3\times10^{-6}$ h^{-1}) (Table 4.7). This indicates that although oxidising Aβ significantly increases the rate at which the peptide nucleates it has little effect on the rate at which the nucleating species then elongates. It is also notable that the total amount of fibres generated at equilibrium is comparable.

Oxidising condition	**Mean t_{50} (h)**	**Mean t_{lag} (h)**	**Mean k_{app} (h^{-1})**
Apo	221.2 (7.3) n = 5	192.0 (4.5) n = 5	0.075 (0.0094) n = 3
Cu^{2+}	52.1 (3.5) n = 5	49.7 (6.6) n = 5	0.276 (0.032) n = 5
H_2O_2	104.8 (4.3) n = 4	72.8 (3.7) n = 4	0.0606 (0.0023) n = 2
Cu^{2+} and H_2O_2	131.7 (45.8) n = 2	95.5 (17.6) n = 2	0.031 (N/A) n = 1

Table 4.6: t_{50}, t_{lag} and k_{app} values for 10 µM Aβ(1-40) under oxidising conditions.
Calculated using the equation specified by Uversky *et al.*, 2001(Uversky, V., *et al.*, 2002) by fitting the curves shown in Figure 4.13(A). In parentheses are the standard errors for each measurement.

Aβ(1-40) concentration (µM)	**Mean k_n ($x10^{-7}$))**	**Mean k_e ($x10^{-7}$)**	**Mean $[B]_t$ (AFU)**
Apo	1.60 (0.67) n = 4	36.4 (3.3) n = 5	15700 (110.1) n = 3
Cu^{2+}	730.0 (337.0) n = 6	133.0 (21.5) n = 6	10400 (680.6) n = 5
H_2O_2	1530 (513.0) n = 5	42.8 (3.0) n = 4	13500 (1560.0) n = 5
Cu^{2+} and H_2O_2	4680 (3020) n = 2	26.4 (6.86) n = 2	10300 (517.3) n = 2

Table 4.7: k_n, k_e and $[B]_t$ values for 10 µM Aβ(1-40) under oxidising conditions.
Calculated using the equation specified by Morris *et al.* (Morris, A. M., *et al.*, 2008) by fitting the curves shown in Figure 4.13(A). In parentheses are the standard errors for each measurement.

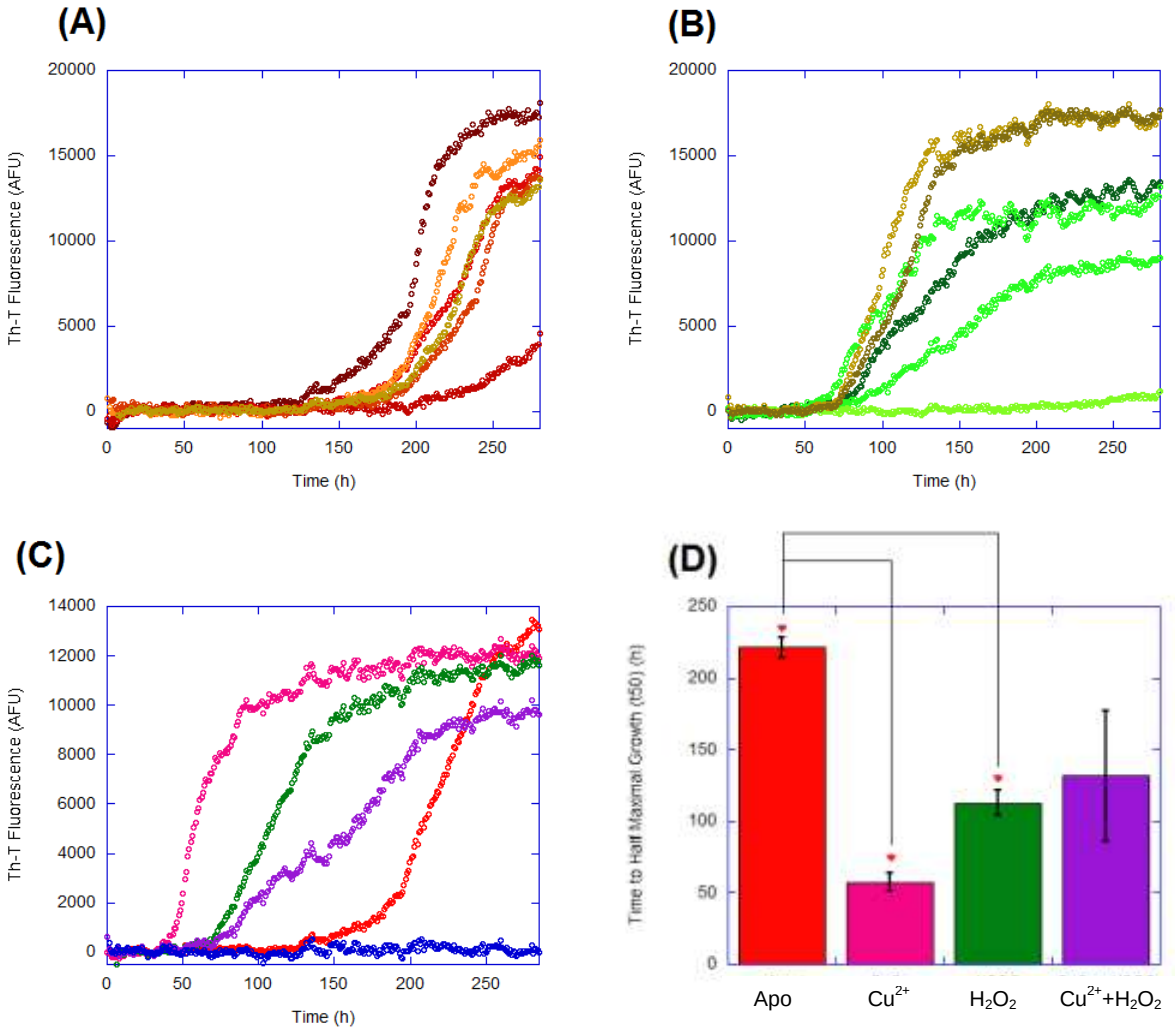

Figure 4.13: Cu^{2+} and hydrogen peroxide based oxidation of 10 µM Aβ(1-40) accelerates fibril growth. (a) All six growth curves for Apo (10µM Aβ(1-40)). Th-T fluorescence values are zeroed at 30 h. (b) All six growth curves for addition of H_2O_2 (100 µM). Th-T fluorescence values are zeroed at 30 h. (c) Fibril growth curves of 10 µM Aβ(1-40) with 20 µM Th-T at 303K, pH 7.4 (50 mM HEPES, 160 mM NaCl buffer). Th-T fluorescence values are zeroed at 30 h and are averaged across six traces (red, green, blue), five traces (pink) or two traces (purple). Conditions used were Apo (red), 1 µM $CuCl_2$ (pink), 100 µM H_2O_2 (green), 1 µM $CuCl_2$ and 100 µM H_2O_2 (purple), 1 µM $CuCl_2$ and 100 µM ascorbate (blue). pH was rechecked after addition of H_2O_2 and readjusted to be pH 7.4. (d) Summary plot showing the mean time to half maximal growth (t_{50}) for each oxidising condition as referenced for Figure 5.11(C). Error bars are for standard error of the mean of 5 traces (both Apo and H_2O_2) , 6 traces ($CuCl_2$) and 2 traces ($CuCl_2$ and H_2O_2). All three conditions increase fibril growth rate compared to Apo. Significant differences are indicated by a red star.

Oxidising condition	F-statistic	F-critical	Variance Conclusion	t-statistic	t-critical	Mean conclusion
Apo vs. Cu^{2+}	4.5627	6.3882(4, 4)	Equal variances (Student's t-test)	18.583	1.9432 (95 %, 6)	Means significantly differ
Apo vs. H_2O_2	3.7040	9.1172 (4, 3)	Equal variances (Student's t-test)	11.155	1.8946 (95 %, 7)	Means significantly differ
Apo vs. Cu^{2+} and H_2O_2	15.432	7.7086 (1, 4)	Unequal variances (Welch's t-test)	1.9308	6.3138 (95 %, 1)	Means do not significantly differ

Table 4.8: Tests of significant difference on t_{50} from Figure 4.13(A).
Calculated using the equations specified in Section 4.2.3. Degrees of freedom for each test are given in brackets.

The effects of Cu^{2+}/Cu^{+}-catalysed oxidation on Aβ(1-40) fibril growth rates

The effect of fibril growth rates when Aβ(1-40) is oxidised using Cu^{2+}/Cu^{+}-catalysed oxidation has also been studied with both a H_2O_2 and Cu^{2+} incubation and a Cu^{2+} and ascorbate incubation. The behaviour relative to H_2O_2 driven oxidation is quite different. It is notable that some of the well plate samples did not generate any fibril growth while for others the final maximal Th-T fluorescence was reduced relative to unoxidised Aβ(1-40). In particular, Cu^{2+} and ascorbate incubated Aβ(1-40) resulted in no detectable Th-T fluorescence even after more than 250 h (Figure 4.13(C)), while for Cu^{2+} and H_2O_2 only two wells generated fibres out of the 6 wells set up. It should be noted that with only two fibre growth curves available reliable kinetic data cannot be determined for the Cu^{2+} and H_2O_2 preparations.

The lack of fibre detection suggests that Cu^{2+}/Cu^{+}-catalysed oxidation under these conditions inhibits fibre growth perhaps by generating non Th-T-binding amorphous aggregates. Alternatively, the oxidising conditions may be degrading the Th-T dye. However, it will be shown later in this chapter that the latter is not the case.

As a control the effect of Cu^{2+} ions only, which will not oxidise Aβ appreciably, was also studied and it was found that just 0.1 mol equivalents of Cu^{2+} ions led to a four-fold decrease in t_{50} values from 221 ± 7 h for Apo Aβ(1-40) to just 52 ± 4 h for 1 μM $CuCl_2$ (Table 4.6). These results, regarding the ability of Cu^{2+} to bind to Aβ and thus accelerate fibre formation, parallel findings recently published

by Sarell *et al.* (Sarell, C. J., *et al.*, 2010), and thus provide validity to the assays run in this project.

Fibril growth at high concentration of oxidised Aβ(1-40)

The Th-T dye may be sensitive to free radical oxidation and so interfere with the detection of fibres. It was therefore proposed that the assay should be re-run at a higher concentration of Aβ(1-40) i.e. 20 μM to enable faster fibril growth and hence hopefully allow fibril growth curve formation before Th-T degradation. In addition, the data shown in Figure 4.12 indicate that 20 μM might be a better concentration of Aβ(1-40) to use than 10 μM because of improved signal-to-noise for fibre detection values.

The assay was re-run at 20 μM Aβ(1-40) and the resulting data are shown in Figure 4.14, including a complete fibril growth curve for the Cu^{2+} and ascorbate condition. Perhaps the most striking difference in the fibril growth curves obtained under the various oxidising conditions is the marked reduction in the maximal Th-T fluorescence generated for the Cu^{2+}/Cu^{+}-catalysed oxidation from ~25,000 AFU for unoxidised Aβ down to ~4,000 AFU for the Cu^{2+}/Cu^{+}-catalysed Aβ. This may be due to either the Th-T degradation discussed above or to the production of insoluble amorphous aggregates, which do not cause Th-T fluorescence.

Figure 4.14(A) displays the results of a well-plate Th-T assay on 20 μM Aβ(1-40) under the same oxidising conditions as Figure 4.13. The traces displayed are averages of up to six data sets. The data were fitted to the two curve equations described by Uversky *et al.* and Morris *et al.* to give the parameters seen in Tables 4.9 and 4.10 respectively. The t_{50}s deduced from fitting Uversky *et al.*,'s equation are plotted in Figure 4.14(B) and their significance is analysed using unpaired t-test methodology as shown in Table 4.11.

As for the 10 μM Aβ(1-40) data, t_{50} values for 20 μM Aβ(1-40) (Table 4.9) show that fibril growth was generally faster with the addition of either Cu^{2+} alone (50 ± 1 h) or hydrogen peroxide (68 ± 4 h) compared to unoxidised Aβ(1-40) (75 ± 3 h). Only the effect of Cu^{2+} was deemed a significant ($p < 0.05$) increase by statistical t-test values given in Table 4.11.

Cu^{2+} and H_2O_2 incubation lead to an increase in the time to generate fibres, with a t_{50} of 100 ± 14 h, compared to unoxidised Aβ(1-40), with a t_{50} of 75 ± 3 h.
The other Cu^{2+}/Cu^{+}-catalysed condition, with ascorbate, appears to significantly increase the time for half maximal growth of Aβ fibres, with a t_{50} of 128 h. However, although 6 repeats were run for this condition, only one sample generated a Th-T fluorescence signal and even this was with a greatly reduced intensity of ~4,000 AFU compared to unoxidised Aβ (~25,000 AFU). With only one fibril trace generated it is not possible to make reliable inferences as to the significance of this observation.

In conclusion, Figures 4.13 and 4.14 show some variation in the behaviour of fibril growth kinetics of Aβ(1-40) under the conditions applied. However, in general, oxidation of Aβ(1-40) by H_2O_2 tends to accelerate the rate of fibre formation. In contrast Cu^{2+}/Cu^{+}-catalysed oxidation tends to result in reduced fibre formation. For a limited number of traces there are some fibres generated but the maximal intensity of Th-T fluorescence is significantly reduced.

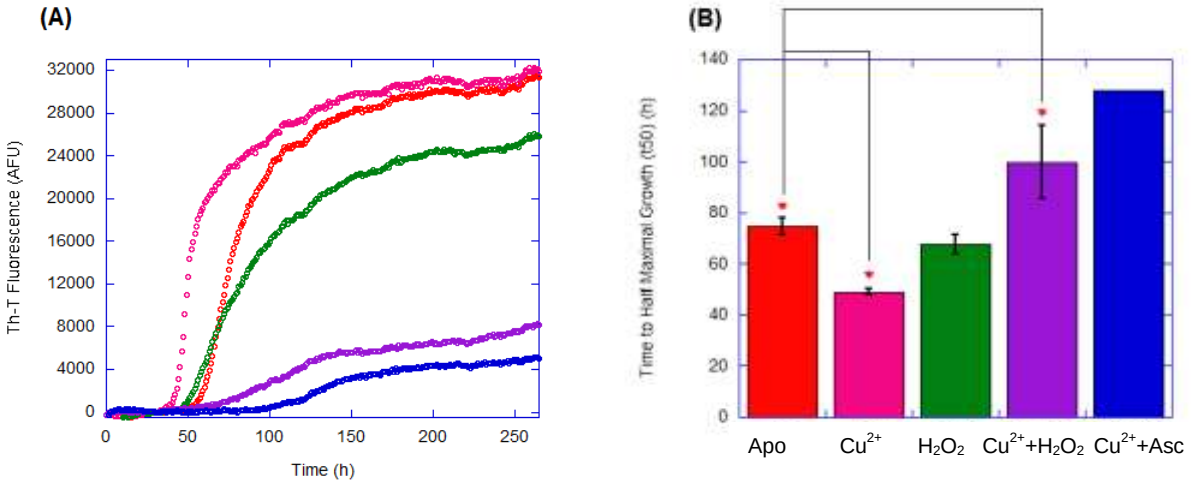

Figure 4.14: Cu^{2+} and hydrogen peroxide based oxidation of 20 µM Aβ(1-40) accelerates fibril growth. (a) Fibril growth curves of 20 µM Aβ(1-40) with 40 µM Th-T at 303K, pH 7.4 (50 mM HEPES, 160 mM NaCl buffer). Th-T fluorescence values are zeroed at 30 h and are averaged across six traces (red, pink, green), two traces (purple) or one trace (blue). Conditions used are Apo (red), 2 µM $CuCl_2$ (pink), 200 µM H_2O_2 (green), 2 µM $CuCl_2$ and 200 µM H_2O_2 (purple), 2 µM $CuCl_2$ and 200 µM ascorbate (blue). (b) Summary plot showing the mean time to half maximal growth (t_{50}) for each oxidising conditions as referenced for Figure 5.12(A). Error bars are for standard error of the mean of 6 traces (Apo, $CuCl_2$ only and H_2O_2 only) 2 traces ($CuCl_2$ and H_2O_2) and 1 trace ($CuCl_2$ and ascorbate). pH was re-checked after addition of H_2O_2 and readjusted to be pH 7.4. Contrary to the data shown in Figure 5.11(C) the Cu^{2+}-catalyzed oxidation condition appears to significantly decelerate fibril growth relative to Apo. H_2O_2 alone may increase fibril growth slightly although statistical tests show this difference is not significant.

Oxidising condition	**Mean t_{50} (h)**	**Mean t_{lag} (h)**	**Mean k_{app} (h^{-1})**
Apo	74.7 (3.2) n = 6	57.3 (2.0) n = 6	0.12 (0.016) n = 6
Cu^{2+}	49.1 (1.1) n = 6	34.8 (2.5) n = 6	0.15 (0.019) n = 6
H_2O_2	67.8 (3.8) n = 6	28.1 (6.6) n = 6	0.057 (0.0020) n = 4
Cu^{2+} and H_2O_2	99.8 (14.2) n = 2	82.0 (19.1) n = 2	0.12 (0.034) n = 2
Cu^{2+} and ascorbate	127.6 (N/A) n = 1	102.6 (N/A) n = 1	0.080 (N/A) n = 1

Table 4.9: t_{50}, t_{lag} and k_{app} values for 20 µM Aβ(1-40) under oxidising conditions.
Calculated using the equation specified by Uversky *et al.*, 2001(Uversky, V., *et al.*, 2002) by fitting the curves shown in Figure 4.14(A). In parentheses are the standard errors for each measurement.

Aβ(1-40) concentration (µM)	**Mean k_e ($x10^{-7}$)**	**Mean $[B]_t$ (AFU)**
Apo	35.9 (3.2) n = 6	28000 (26.5) n = 4
Cu^{2+}	34.9 (2.70) n = 6	28100 (30.9) n = 5
H_2O_2	25.9 (0.63) n = 4	23100 (79.7) n = 6
Cu^{2+} and H_2O_2	110.0 (23.1) n = 2	6080 (681.7) n = 2
Cu^{2+} and ascorbate	148.0 (N/A) n = 1	4210 (N/A) n = 1

Table 4.10: k_e and $[B]_t$ values for 20 µM Aβ(1-40) under oxidising conditions.
Calculated using the equation specified by Morris *et al.*, 2008 (Morris, A. M., *et al.*, 2008) by fitting the curves shown in Figure 4.14(A). In parentheses are the standard errors for each measurement. The k_n has been removed due to unusual curve fitting.

Oxidising condition	F-statistic	F-critical	Variance Conclusion	t-statistic	t-critical	Mean conclusion
Apo vs. Cu^{2+}	8.3852	5.0503 (5, 5)	Unequal variances (Welch's t-test)	7.5256	1.9432 (95 %, 6)	Means significantly differ
Apo vs. H_2O_2	1.4249	5.0503 (5, 5)	Equal variances (Student's t-test)	1.3786	1.8125 (95 %, 10)	Means do not significantly differ
Apo vs. Cu^{2+} and H_2O_2	6.4735	6.6079 (1, 5)	Equal variances (Student's t-test)	2.8208	1.9432 (95 %, 6)	Means significantly differ

Table 4.11: Tests of significant difference on t_{50} from Figure 4.14(A).
Calculated using the equations specified in Section 4.2.3. Degrees of freedom for each test are given in brackets.

Dependence of Aβ fibrillisation on H_2O_2 concentration

To investigate further whether different concentrations of H_2O_2 would exert different effects on Aβ fibrillisation rates, the Th-T binding assay on 10 μM Aβ(1-40) was conducted at six different H_2O_2 concentrations. Figure 4.15 shows the Th-T fluorescence fibril growth data using a range of H_2O_2 concentrations (0, 10, 50, 100, 200 and 1,000 μM). The traces displayed are averages as indicated in the Figure's caption. The fibril growth curves were fitted to the two equations described by Uversky *et al.* and Morris *et al.* to give the lag phase, rates of nucleation and elongation and maximal fluorescence as displayed in Tables 4.12 and 4.13 respectively. The t_{50} data deduced from fitting were analysed for significance and this produced the values given in Table 4.14.

Slight variations in the t_{50}s were observed over the range of H_2O_2 concentrations used (Figure 4.15(B); however, none of these differences were significant (Table 4.14). Values of t_{lag} for the various H_2O_2 concentrations were also quite similar to that of unoxidised Aβ(1-40) (Table 4.12).

The maximal intensity of the Th-T signal, at equilibrium, was reduced and the numbers of growths curves obtained decreased with increasing amounts of H_2O_2. This may indicate that Aβ oxidised by H_2O_2 is forming amorphous aggregates instead of fibrils that activate Th-T. This is a significant effect of H_2O_2 on Aβ(1-40) fibril growth.

However, there is one other possibility to explain these results; that oxidation of Th-T is also taking place and this could be affecting the Th-T fluorescence signal.

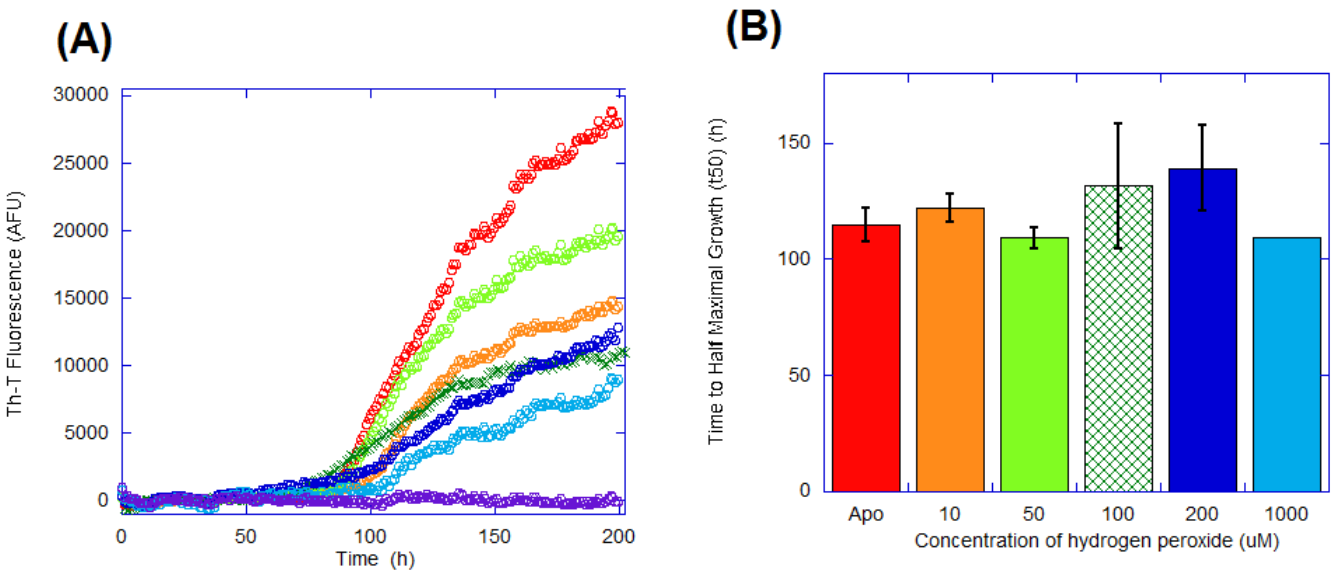

Figure 4.15: The effect of varying hydrogen peroxide concentration on Aβ(1-40) fibril growth. (a) Fibril growth curves of 10 µM Aβ(1-40) with 20 µM Th-T at 303K, and varying concentrations of H_2O_2 , pH 7.4 (50 mM HEPES, 160 mM NaCl Buffer). H_2O_2 concentrations used were Apo (red), 10 µM (orange), 50 µM (light green), 100 µM (dark green), 200 µM (dark blue), 1 mM (light blue), 2 mM (purple). The 100 µM data was recorded on a separate occasion to the rest of the data shown and hence is illustrated with crosses (x) as opposed to circles (o). pH was rechecked after addition of H_2O_2 and readjusted to be pH 7.4. Th-T fluorescence values are either one trace (light blue) or are averaged across three traces (dark blue), six traces (dark green), eight traces (red) or nine traces (orange, light green, purple).(b) Summary plot showing the mean time to half maximal growth (t_{50}) for each hydrogen peroxide concentration as referenced for Figure 5.14(A). Error bars are for standard error of the mean of 9 traces (10 µM, 50 µM), 8 traces (Apo), 5 traces (100 µM), 3 traces (200 µM) and 1 trace (1 mM). None of the hydrogen peroxide concentrations appears to cause a significant change in fibril growth rate compared to Apo.

Hydrogen peroxide concentration (µM)	**Mean t_{50} (h)**	**Mean t_{lag} (h)**	**Mean k_{app} (h^{-1})**
Apo	115.0 (7.2) n = 8	95.4 (6.1) n = 7	0.15 (0.016) n = 7
10	114.0 (2.9) n = 7	101.5 (0.76) n = 6	0.14 (0.011) n = 9
50	109.2 (4.4) n = 9	92.0 (3.2) n = 9	0.14 (0.011) n = 8
100	104.8 (3.8) n = 4	68.2 (6.1) n = 4	0.051 (0.012) n = 5
200	139.2 (18.3) n = 3	115.9 (25.4) n = 3	0.11 (0.036) n = 3
1000	109.6 (N/A) n = 1	103.0 (N/A) n = 1	0.30 (N/A) n = 1

Table 4.12: t_{50}, t_{lag} and k_{app} values for 10 µM Aβ1-40) with varying concentrations of hydrogen peroxide. Calculated using the equation specified by Uversky *et al.*, 2001(Uversky, V., *et al.*, 2002) by fitting the curves shown in Figure 4.15(A). In parentheses are the standard errors for each measurement. The 100 µM data was recorded on a separate occasion to the rest of the data shown. No fibril growth curves were obtained for the 2 mM H_2O_2 condition.

Hydrogen peroxide concentration (μM)	**Mean k_n (x10^{-7}))**	**Mean k_e (x10^{-7})**	**Mean $[B]_t$ (AFU)**
Apo	42.5 (20.9) n = 6	27.9 (5.0) n = 8	29500 (2440) n = 8
10	11.9 (4.7) n = 8	68.9 (4.0) n = 8	14700 (118.6) n = 8
50	141.3 (33.9) n = 8	38.7 (4.4) n = 9	18900 (305.0) n = 7
100	1230 (405.1) n = 5	44.7 (3.3) n = 5	12900 (1510) n = 5
200	574.0 (526.0) n = 3	40.1 (5.2) n = 3	14200 (1300) n = 3
1000	154.9 (N/A) n = 1	27.1 (N/A) n = 1	16500 (N/A) n = 1

Table 4.13: k_n, k_e and $[B]_t$ values for 10 μM Aβ1-40) with varying concentrations of hydrogen peroxide. Calculated using the equation specified by Morris *et al.*, 2008 (Morris, A. M., *et al.*, 2008) by fitting the curves shown in Figure 4.15(A). In parentheses are the standard errors for each measurement. The 100 μM data was recorded on a separate occasion to the rest of the data shown. No fibril growth curves were obtained for the 2 mM H_2O_2 condition.

Hydrogen peroxide concentration (μM)	**F-statistic**	**F-critical**	**Variance Conclusion**	**t-statistic**	**t-critical**	**Mean conclusion**
Apo vs. 10	1.2013	3.8660 (6, 7)	Equal variances (Student's t-test)	0.091295	1.7709 (95 %, 13)	Means do not significantly differ
Apo vs. 50	2.3489	3.5005 (7, 8)	Equal variances (Student's t-test)	1.4360	1.7531 (95 %, 15)	Means do not significantly differ
Apo vs. 100	7.2828	8.8867 (7, 3)	Equal variances (Student's t-test)	0.95309	1.8125 (95 %, 10)	Means do not significantly differ
Apo vs. 200	2.4409	4.7374 (2, 7)	Equal variances (Student's t-test)	1.5321	1.8331 (95 %, 9)	Means do not significantly differ

Table 4.14: Tests of significant difference on t_{50} from Figure 4.15(A). Calculated using the equations specified in Section 4.2.3. Degrees of freedom for each test are given in brackets.

Cu^{2+}/Cu^{+}-catalysed oxidation does not interfere with Th-T detection.

Some batches of Aβ(1-40) used in these assays, despite vigorous solubilisation and disaggregation procedures, still behaved as seeded in the assays, i.e. they produced no lag phase. This is a common occurrence as indicated in the literature (Dobeli, H., *et al.*, 1995). An example from this PhD study is shown in Figure 4.16. These data sets were not useful for extracting meaningful kinetic parameters. However, they do illustrate that growth curves can be successfully obtained for all five conditions for up to six repeats, even for the radical-based oxidative conditions.

An appreciable Th-T fluorescence intensity can be obtained for both the H_2O_2 and Cu^{2+}/Cu^{+}-catalysed oxidation and the oxidation by H_2O_2 alone, with only a slight decrease for the ascorbate and Cu^{2+}/Cu^{+}-catalysed oxidation condition. As these samples are seeded this promotes fibrillisation over amorphous aggregation (see Chapter 1, Section 1.5.3.). Therefore, in previous, non-seeded samples, the drop in Th-T intensity can be attributed to amorphous aggregates forming, not Th-T degradation under oxidising conditions.

To confirm the results found so far using the Th-T binding assay for the effects of oxidation on Aβ(1-40) fibrillisation results, a second technique was used. This procedure, which does not use an in-sample dye that is thus exposed to reaction conditions, was circular dichroism (CD) (Section 4.3.2.).

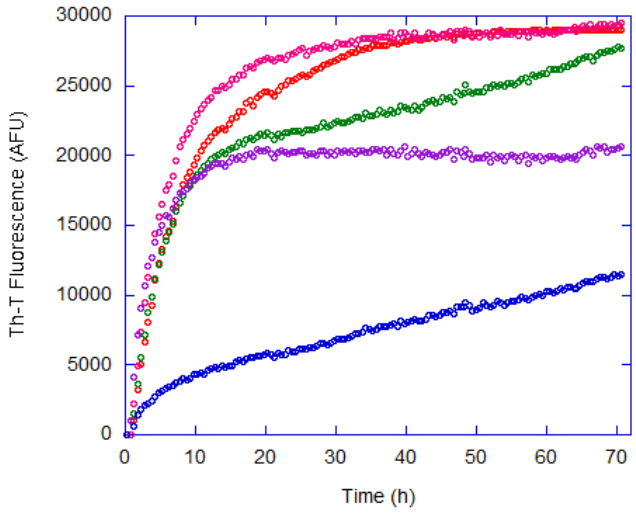

Figure 4.16: Aβ(1-40) with Cu^{2+} and ascorbate can show fibril growth curves for seeded samples. Fibril growth curves of seeded 20 µM Aβ(1-40) with 40 µM Th-T at 303K, pH 7.4 (50 mM HEPES, 160 mM NaCl buffer). Th-T fluorescence values are zeroed at 30 h and are averaged across six traces. Conditions used are Apo (red), 2 µM $CuCl_2$ (pink), 200 µM H_2O_2 (green), 2 µM $CuCl_2$ and 200 µM H_2O_2 (purple), 2 µM $CuCl_2$ and 200 µM ascorbate (blue). pH was re-checked after addition of H_2O_2 and readjusted to be pH 7.4

Delay in Th-T binding mature fibres

Figure 4.17 shows the change in Th-T fluorescence with time of two separate wells that were both filled with 5 µM Aβ(1-40) but with Th-T added at either the beginning of the study, or at 174.5 h, when the first well had shown maximal fibril growth. This shows that Th-T takes over 30 h to bind mature Aβ fibres rather than undergoing an instantaneous binding event. An alternative explanation is that Th-T is needed to facilitate growth; however, it is generally accepted that this is not the case (Nicotera, T. M., 2007). Therefore, it is likely that Th-T added to mature fibres will exhibit a delay in fluorescence of greater than 30 h before maximal fluorescence is detected. Interestingly Th-T added to concentrated (50 µM) Aβ as monomer can show the formation of maximal Th-T fluorescence in considerably less than 30 h (Sarell, C. J., *et al.*, 2010). Thus the fluorescence signal shown in Figure 4.17 reflects the time taken for Th-T to diffuse into all parts of the mature fibres' core.

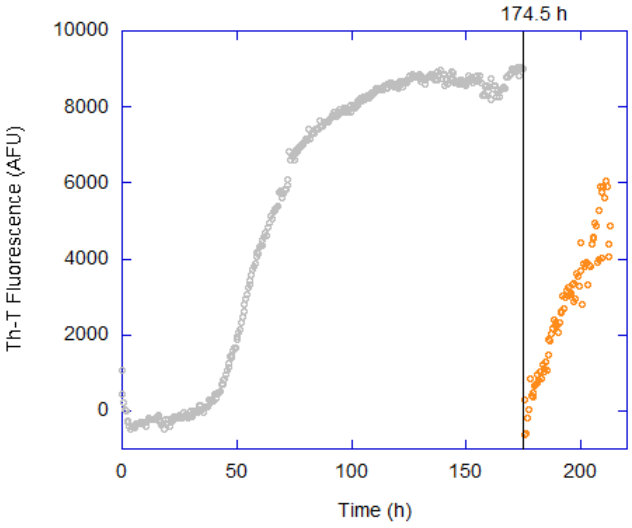

Figure 4.17: Th-T takes over 30 h to bind mature Aβ fibres. Fibril growth curves of 5 µM Aβ(1-40) at 303K, pH 7.4 (50 mM HEPES, 160 mM NaCl Buffer). 10 µM Th-T was either added at 0 h (grey trace) or at 174.5 h (orange trace). Th-T fluorescence values are zeroed at 30 h. Data are from two individual wells.

4.3.2. β-sheet formation with oxidation of Aβ

Circular dichroism (CD) is a spectroscopic technique which does not require any fluorophore or chemical additive, thus problems associated with competitive oxidation of the additive are avoided. Hence, the effects of Aβ(1-40) oxidation on

fibril growth rate were studied using CD to detect fibrillisation. This method measures changes in the amount of β-sheet over time. As conformational switching from a random coil to β-sheet is a requirement for fibrillisation, this change can be used as an indication of fibrillisation rates.

Across all oxidising conditions and Apo, the only spectrum to show any change was that for the Apo condition (Figure 4.18). Here, a slight shift from mostly random coil to partially β-sheet was seen. This can be visualised in Figure 4.18(B) where the decrease in the 198 nm band characteristic of random coil and the increase in the 217 nm band characteristic of β-sheet is plotted. However, a full shift from random coil to β-sheet could not be recorded before the peptide precipitated, hence the general decrease in signal seen in Figure 4.18(A). This is also indicated by the general drift of the maximum trough from 198 nm to 202 nm and the lack of an isosbestic point, suggesting not all of the peptide recorded for the initial random coil structures was soluble during the later measurements.

Very low NaCl concentration and low Aβ peptide concentrations were needed to obtain measurements using UV-CD (see Section 4.3.2.). These low concentrations meant the peptide took a lot longer to fibrillise. Because of this none of the oxidising conditions studied produced data that showed changes in secondary structure over 730 h. After 700 h there was a general loss of CD signal, which indicated peptide was precipitating out of solution (data not shown). Because no change was seen at all in secondary structure under oxidising conditions it can be assumed that oxidation causes a slowing in fibrillisation but this decrease cannot be quantified.

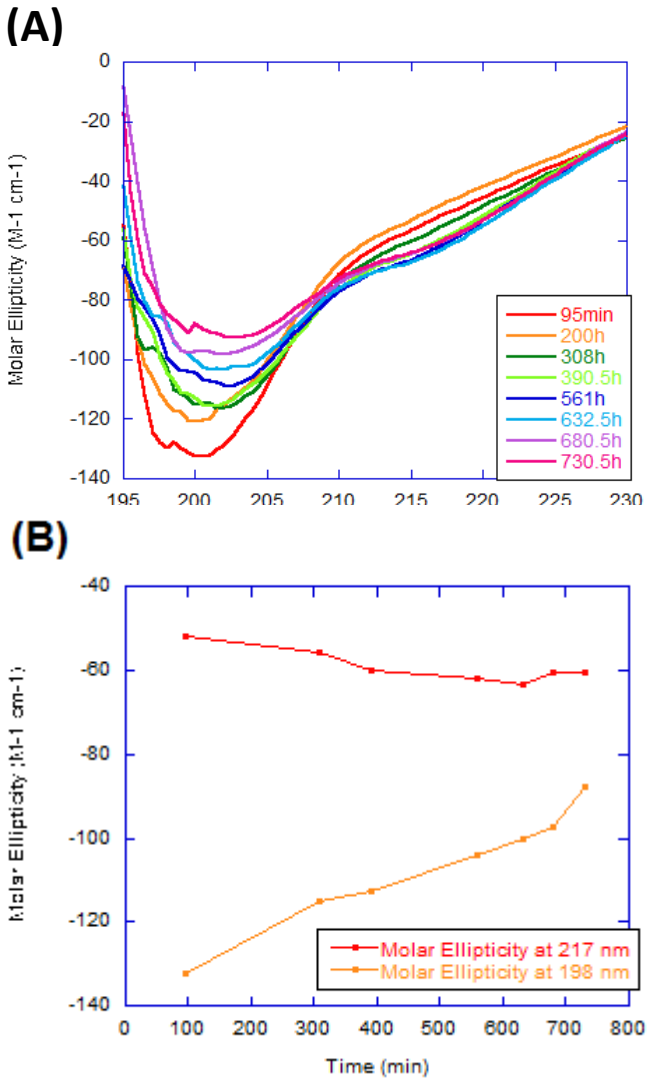

Figure 4.18: Aβ fibril growth involves a beta sheet transition but also aggregate precipitation. (a) UV-CD spectra of the secondary structure of 5 µM Aβ(1-40), 310K, pH 7.4 (0.25 mM HEPES, 8 mM NaCl buffer). 8 readings were taken at 95 min (red), 200 h (orange) 308 h (dark green), 390.5 h (light green), 561 h (dark blue), 632.5 h (light blue), 680.5 h (lilac), 730.5 h (pink). An in-spectrometer incubator at 310K was used for each reading. Between readings the sample was stored at 310 K and shaken at 100 rpm. (b) A plot of the change in molar ellipticity at 198 nm (orange - indicative of random coil) and 217 nm (red - indicative of β-sheet) with time.

4.3.3. The oligomeric state of oxidised Aβ(1-40) as detected by SEC

We were interested in studying if oxidation of Aβ influenced the formation of oligomeric species of Aβ(1-40).

pH 7.4 studies

Freshly prepared Aβ(1-40) was generated from a solubilised stock of Aβ and analysed using size-exclusion chromatography (SEC). Figure 4.19 (Table 4.15) shows a size-exclusion chromatograph where 10 μM Aβ(1-40) has been injected at volume 0 ml.

This chromatogram is dominated by a band with an elution volume of 14.1 ml. The calibration curve suggests these elution volumes correspond to a M_r of 26,500 Da. At first we were surprised that a fresh Aβ(1-40) preparation would elute with an apparent molecular weight close to a hexameric Aβ(1-40) oligomer, instead of the molecular weight of Aβ(1-40) monomer, which is 4,327 Da. However, with the correction devised by Talmard *et al.* (seepage 185) this band would correspond to monomeric Aβ(1-40). This correction is based on the fact that a column calibrated with folded, globular proteins will lead to an unfolded protein, such as Aβ(1-40), eluting from the SEC more rapidly than its mass would suggest. It has been shown previously that unfolded monomeric Aβ will elute a SEC column with an apparent molecular weight of 26 kDa (Talmard, C., *et al.*, 2007).

Aβ(1-40) was then incubated for 17 h under various oxidising conditions and size-exclusion chromatograms were obtained (Figure 4.20, Table 4.16). For Cu^{2+} ions, H_2O_2 and the combination of these two reagents the single elution band was produced indicative of a hexameric Aβ(1-40) species (on average an elution volume of 14.1 ml indicating a molecular weight of 26,500 Da before correction). However, the second radical-based oxidation with ascorbate and Cu^{2+} ions produced an additional band with an elution volume of 17.4 ml; a low molecular weight species (i.e. < 1,000 Da). Ascorbate was known to be observable on the UV trace and it was suspected that as this band was at a similar elution volume to the small molecule acetone (M_r 58 Da) this may correspond to the elution of other small molecules, due to ascorbate or products of ascorbate oxidation; dehydroascorbate (M_r 174 Da) or monodehydroascorbate (M_r 176 Da) (Figure 2.11). Hence, a control run of ascorbate, after a 17 h incubation at 30 °C and pH 7.4 with Cu^{2+} ions, was done on the size-exclusion column. Figure 4.21 (Table 4.17) shows the result of this control alongside the trace for the incubation of these two reagents with Aβ(1-40). As

expected the extra non-monomeric-Aβ(1-40) species band in this latter trace appears at a similar elution volume to the control band for ascorbate i.e. at 16.9 ml.

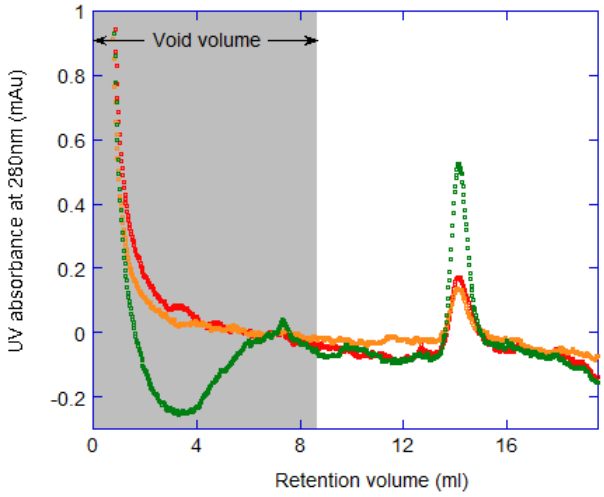

Figure 4.19: Size exclusion chromatogram of fresh Aβ(1-40) shows one predominant oligomeric species. A UV trace of eluting products from a size exclusion column is shown after injection of fresh 10 µM Aβ(1-40) at volume 0 ml with 50 mM HEPES, 150 mM NaCl pH 7.4 buffer. Three data sets are shown, two of which are from the same stock (red and orange traces) and the third from a stock made up on a separate occasion (green). The major peak shown represents monomer. The void volume was determined using blue dextran. For elution volumes at the peaks see Table 5.16.

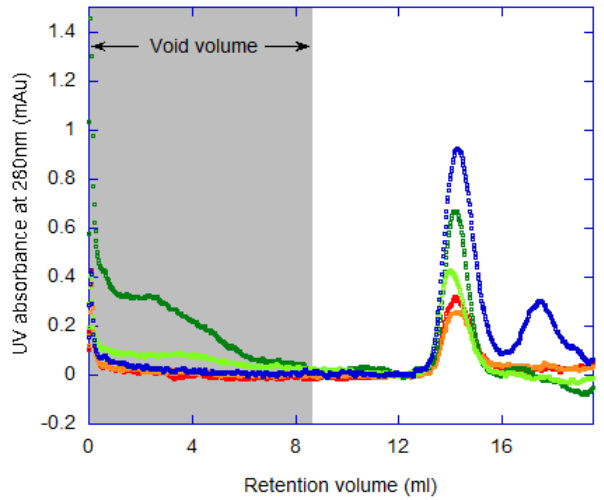

Figure 4.20: Size exclusion chromatogram of Aβ(1-40) under different oxidising conditions after a 17 h incubation at 30 °C. Five UV traces of eluting products from a size exclusion column are shown after separate injections of 10 µM Aβ(1-40) at volume 0 ml with 50 mM HEPES, 150 mM NaCl pH 7.4 buffer and varying oxidising conditions; Apo (red), 1 µM Cu^{2+} (orange), 100 µM H_2O_2 (dark green), 1 µM Cu^{2+} and 100 µM H_2O_2 (light green), 100 µM ascorbate and 1 µM Cu^{2+} (blue). Each sample was incubated for 17 h at 30 °C before injection. The void volume was determined using blue dextran. Data are zeroed at 12 ml. For elution volumes at the peaks see Table 5.17.

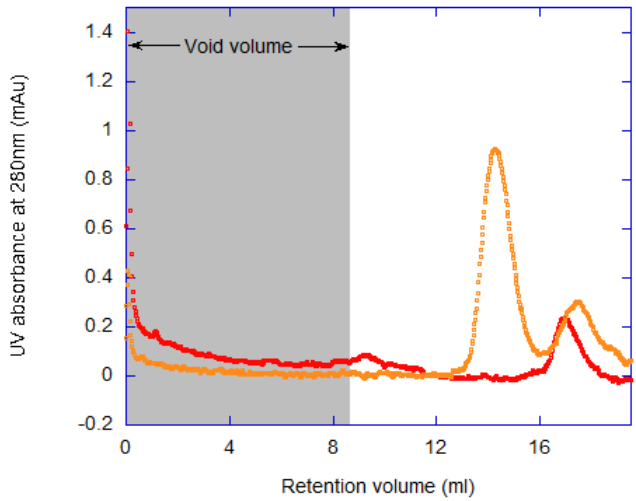

Figure 4.21: Size exclusion chromatogram of ascorbate and Cu^{2+} /Cu^{+} control. Two UV traces of eluting products from a size exclusion column are shown. Two samples of 100 µM ascorbate and 1 µM Cu^{2+} were incubated for 17 h at 303K, one with 10 µM Aβ and one without. These were injected separately at volume 0 ml with 50 mM HEPES, 150 mM NaCl pH 7.4 buffer. The void volume was determined using blue dextran. Data are zeroed at 12 ml. For elution volumes at the peaks see Table 5.18.

Trace	Elution volume at peak (ml)	Molecular weight (Da)
Aβ(1-40) Stock 1 (red)	14.14	26400
Aβ(1-40) Stock 1 (orange)	14.04	27000
Aβ(1-40) Stock 2 (green)	9.42, 14.15	70000, 26400

Table 4.15: The elution volumes for peaks in Figure 4.19. Molecular weights are calculated using an equation derived from a calibration curve based on data in Figure 4.11(A).

Trace	Elution volume at peak (ml)	Molecular weight (Da)
Apo (red)	14.12	26500
Cu^{2+} (orange)	14.22	26000
H_2O_2 (dark green)	14.16	26300
Cu^{2+} and H_2O_2 (light green)	14.02	27100
Cu^{2+} and Ascorbate (blue)	14.18, 17.40	26200, 13500

Table 4.16: The elution volumes for peaks in Figure 4.20. Molecular weights are calculated using an equation derived from a calibration curve based on data in Figure 4.11(A).

Trace	Elution volume at peak (ml)	Molecular weight (Da)
Cu^{2+} and Ascorbate only (red)	16.93	14800
Cu^{2+} and Ascorbate and Aβ(1-40) (orange)	14.18, 17.40	26200, 13500

Table 4.17: The elution volumes for peaks in Figure 4.21. Molecular weights are calculated using an equation derived from a calibration curve based on data in Figure 4.11(A).

Therefore, in general, after a 17 h incubation with each condition, Aβ(1-40) seems to show no more variation in oligomeric species than unoxidised Aβ. Further studies were carried out to see whether species size varied over the 17 h incubation. The results of three different conditions are shown in Figure 4.22 (Table 4.18).

A sample of 10μM Aβ(1-40) was incubated at 30 °C, pH 7.4 and aliquots were taken and injected onto the size-exclusion column at approximately 2 h intervals as indicated. Figure 4.22(A) shows the results of this procedure on Aβ(1-40) alone. Initially (17 min reading) some minor high and low molecular bands appear at 8.82 ml (M_r 79,000 Da), 12.6 ml (M_r 36,300 Da) and 17.2 ml (M_r 14,000 Da). If Aβ was still exhibiting characteristics of an unstructured peptide, these would correspond to approximately trimer, 1.4-mer and a fragment respectively. However, if it was becoming more globular as it formed aggregates, which is more likely, these bands may indicate the appearance of higher order oligomers.

These extra three bands disappear by 2.5 h although the low molecular weight band reappears for the 4.5 h alongside another with an elution volume of 19.12 ml (M_r 9400 Da), which corresponds to a low molecular weight species. Throughout all

the readings a band at approx. 14.0 ml (M_r 27,000 Da) was recorded which reveals that the hexameric species was present over the whole 13 h under these conditions.

The addition of H_2O_2 (Figure 4.22(B)) also produced a monomeric species with an average elution volume (V_e) of 14.1 ml (M_r 26,700 Da) throughout all of the readings. Even after 13 h incubation there is no evidence of the formation of oligomeric species. Larger Aβ(1-40) oligomers eluting in the void volume are not apparent. Also the intensity of the hexameric band is maintained during incubation indicating that the only Aβ(1-40) species produced is hexameric.

Finally a radical based oxidation of Aβ(1-40) was conducted using Cu^{2+} ions and ascorbate as shown in Figure 4.22(C). The two bands for monomeric Aβ(1-40) and oxidised ascorbate were seen at on average 14.20 ml (M_r 26100 Da) and 17.20 ml (M_r 14,000 Da) respectively. Some higher molecular weight bands were observed at approximately 4.5 h with bands at 9.87 ml (M_r 64,000 Da) and 11.36 ml (M_r 47,000 Da). These extra bands were not observed for longer incubation times. In general, the only significant band seen throughout these time-dependent readings is the monomeric Aβ(1-40) band under both unoxidised and oxidised conditions.

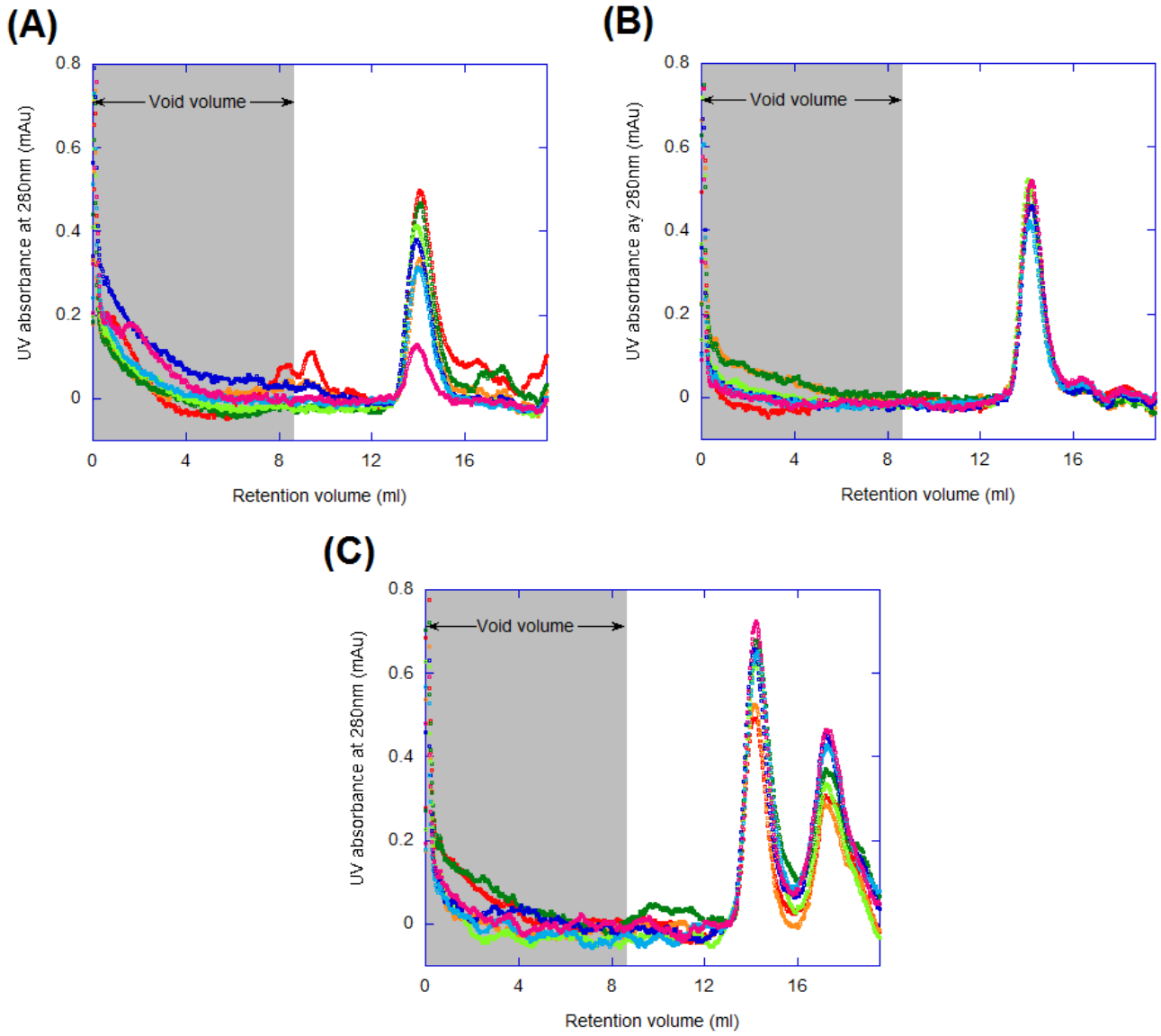

Figure 4.22: Periodic size exclusion runs of Aβ(1-40) with and without oxidising conditions over a ~13 h period. (a) A sample of 10 µM Aβ(1-40) was incubated at 30 °C. Aliquots were taken at different time points and injected onto a size exclusion column at volume 0 ml. Eluting products were detected using UV as shown. 50 mM HEPES, 150 mM NaCl pH 7.4 buffer was used and the void volume was determined using blue dextran. Readings were taken at 17 min (red), 2 h 29 min (orange), 4 h 36 min (dark green), 6 h 56 min (light green), 9 h 2 min (dark blue), 11 h 9 min (light blue), 13 h 14 min (pink). (b) As for (a) but with a sample of 10 µM Aβ(1-40) and 100 µM H_2O_2. Readings were taken at 5 min (red), 2 h 6 min (orange), 4 h 21 min (dark green), 6 h 30 min (light green), 8 h 35 min (dark blue), 10 h 41 min (light blue), 12 h 46 min (pink). (c) As for (a) but with a sample of 10 µM Aβ(1-40), 1 µM $CuCl_2$ and 100 µM ascorbate. Readings were taken at 3 min (red), 2 h 11 min (orange), 4 h 23 min (dark green), 6 h 30 min (light green), 8 h 37 min (dark blue), 10 h 52 min (light blue), 13 h 2 min (pink). For elution volumes at the peaks see Table 5.19.

Trace	Elution volume at peak (ml)	Molecular weight (Da)
Apo	8.82, 12.60, 17.20, 19.12, 13.90, 14.00, 14.10	79300, 36300, 14000, 9440, 27800, 27200, 26600
H_2O_2	14.00, 14.10, 14.20, 17.46, 19.23	27200, 26600, 26100, 13300, 9230
Cu^{2+} and Ascorbate	9.87, 11.36, 14.10, 14.20, 14.30, 17.10, 17.20	63800, 46900, 26600, 26100, 25600, 14300, 14000

Table 4.18: The elution volumes for peaks in Figure 4.22 Molecular weights are calculated using an equation derived from a calibration curve based on data in Figure 4.11(A).

pH10.5 studies

A final investigation was done to confirm the interpretation that unfolded Aβ monomer eluted from the SEC column with an apparent molecular weight of 26 kDa. pH 10.5 is highly solubilising for Aβ and will favour monomer. Therefore, a 20 µM sample of Aβ(1-40) was injected onto the column at volume 0 ml on Figure 4.23 and the column was eluted with 160 mM NaCl in pH 10.5 UHQ H_2O. A single major band was observed at an elution volume of 13.46 ml along with a very minor band at 19.40 ml (Figure 4.23, Table 4.19). Using a new calibration curve, based on proteins run at this pH, these bands corresponded to 28,800 Da and 8,900 Da respectively, which using Talmard *et al.*,'s corrections corresponds to monomeric and a low molecular weight fragment (~ 1,000 Da) respectively. Therefore, as at high pH the only Aβ(1-40) species is monomer, the major peak at pH 7.4 is also likely to be monomeric because the derived molecular weights are of a similar magnitude.

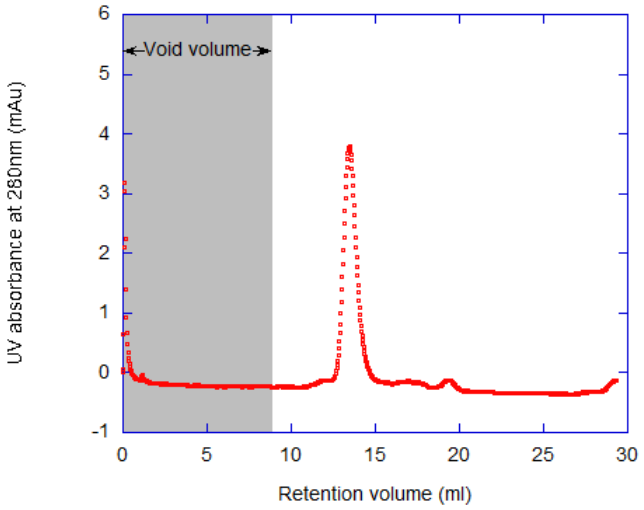

Figure 4.23: Size exclusion chromatogram of Aβ(1-40) at pH 10.5. A UV trace of eluting products from a size exclusion column are shown. 20 μM Aβ was injected at volume 0 ml with 160 mM NaCl in pH 10.5 UHQ H_2O. The void volume was determined using blue dextran. For elution volumes at the peaks see Table 5.20.

Trace	Elution volume at peak (ml)	Molecular weight (Da)
pH 10.5 Aβ(1-40)	13.46, 19.40	28800, 8900

Table 4.19: The elution volumes for peaks in Figure 4.23. Molecular weights are calculated using an equation derived from a calibration curve based on data in Figure 4.11(B).

4.4. Discussion

4.4.1. The effect of H_2O_2-only oxidation Aβ(1-40) fibrillisation

It is clear from the fibril growth experiments that oxidation by H_2O_2 alone either accelerates fibre formation, especially of the nucleation phase, or has no significant effect. Although various experimental trials of H_2O_2 oxidised Aβ have been studied in this project, in no cases is there a reduction in the rate of fibre formation. This is in stark contrast to previous literature reports (Hou, L., *et al.*, 2002, Hou, L., *et al.*, 2004, Johansson, A.-S., *et al.*, 2007, Maiti, P., *et al.*, 2010, Palmblad, M., *et al.*, 2002, Watson, A. A., *et al.*, 1998).

Several of these reports used different procedures to those used in this project. For example, Hou *et al.* and Watson *et al.* used higher concentrations of Aβ, 50 μM and 1.2 mM respectively (Hou, L., *et al.*, 2002, Watson, A. A., *et al.*, 1998). Such high concentrations of Aβ are likely to lead to amorphous aggregation. Palmblad *et al.* and Watson *et al.* also used a solubilisation technique which is likely to subject Aβ to initially high concentrations and thus is also likely to favour amorphous aggregation (Palmblad, M., *et al.*, 2002, Watson, A. A., *et al.*, 1998). This amorphous aggregation may occur at the expense of fibrillisation explaining the decreases seen in fibrillisation rates reported in these studies.

Palmblad *et al.* and Watson *et al.* also used different pHs to this study which may explain the differing results (Palmblad, M., *et al.*, 2002, Watson, A. A., *et al.*, 1998). A final difference between previous studies and this study is the concentration of H_2O_2 used. For example Hou *et al.* used 10 mM and Watson *et al.* used 0.9 M, which are both greater than the 1 mM maximum H_2O_2 concentration this project could achieve fibril growth at. Therefore, these observations of experimental technique may go some way to explaining the different findings of this project and previous studies.

In addition, in order to explain the findings of this project at the molecular level, it is necessary to consider how the biophysical properties of the peptide (see Chapter 1, Section 1.5.3.), are altered by oxidation. These include hydrophobicity, hydrogen-bonding capacity, and protonation state, and thus the total charge on Aβ. Oxidation of Aβ(1-40) by H_2O_2 alone occurs specifically at methionine. In most

cases, and in Aβ isolated from senile plaques (Dong, J., *et al.*, 2003), methionine is oxidised to methionine sulfoxide (Nadal, R. C., *et al.*, 2008, Schoneich, C., 2005), although the sulfone is also noted in the literature (Maiti, P., *et al.*, 2010).

Methionine sulfoxide is a stronger hydrogen bond acceptor than the original methionine due to the addition of oxygen (Watson, A. A., *et al.*, 1998), and thus the oxidation of Met35 to methionine sulfoxide will lead to this residue contributing more to Aβ(1-40) hydrogen bonding (Hung, A., *et al.*, 2008). Previous papers, which have found a decrease in Aβ fibrillisation after H_2O_2 oxidation, have implied that this conversion to methionine sulfoxide may disrupt the specific hydrogen bonding between β-sheets which leads to a β-hairpin structure. This would then promote amorphous aggregation leading to decreases in observed fibrillisation rates (Hung et al.., 2008). However, the degree of specificity of hydrogen bonding required for Aβ fibre formation is debatable. For example Wetzel *et al.* report that there is no specific relationship between the number of hydrogen bonds in an Aβ fibre and that fibre's stability (Jarrett, J. T., *et al.*, 1993, Williams, A. D., *et al.*, 2004). Therefore, methionine oxidation may strengthen overall hydrogen bonding of the Aβ(1-40) peptide and thus promote the formation of β-sheets, leading to increased nucleation and thus fibrillisation rates. In addition, methionine oxidation in other peptides has been shown to induce conformational changes from α-helix to β-strand (Nishino, S. and Nishida, Y., 2001, Schenck, H. L., *et al.*, 1996), which is the precursor to fibrillisation. This is one of the effects of H_2O_2 oxidation seen in this thesis.

The second effect seen with H_2O_2 oxidation is a lack of change in fibril growth rates. Previous studies that reported a decrease in Aβ(1-40) fibrillisation rates with oxidation by H_2O_2 alone used very high concentrations of H_2O_2, 200 mol. eq. to 40,000 mol. eq., and it may be the case, as discussed in Chapter 1, Section 1.10.5, that this oxidises other residues such as glutamine, threonine and tyrosine. Hence it may be the case that decreasing fibrillisation rates seen in previous literature reports were due to oxidation of amino acids other than methionine. In the experiments reported in this thesis, which use a much lower H_2O_2 concentration, it is more likely that only methionine is oxidised. Therefore, as fewer amino acids are affected, there is less change in hydrogen bonding capability of the Aβ(1-40) peptide and this may explain the lack of change seen in some oxidation by H_2O_2 alone experiments. Methionine sulfoxide has a reduced hydrophobicity relative to methionine. In addition, molecular dynamics studies have predicted that oxidation of methionine

alters the residue's orientation so it contributes more to the Aβ surface polarity (Triguero, L., *et al.*, 2008a) and hence is more exposed to an aqueous environment. There is some controversy over how the change in surface polarity with methionine oxidation would affect Aβ fibrillisation rates. Methionine sulfoxide is a larger and more polar residue than methionine (Kim, Y. H., *et al.*, 2001) and thus this increases the surface polarity (Triguero, L., *et al.*, 2008b). This would be expected to reduce β-sheet self-association into fibres and thus reduce Aβ fibrillisation rates (Bitan, G., *et al.*, 2003, Hou, L., *et al.*, 2002). However, some groups argue that surface polarity change does not explain altered Aβ fibrillisation rates after methionine oxidation. When Maiti *et al.* performed molecular dynamic calculations on Aβ-Met-Ox they found little change in fibrillisation rate relative to unoxidised peptide despite oxidised methionine having a dipole of approximately 5.24 Debye relative to just 1.6 Debye for unoxidised methionine (Maiti, P., *et al.*, 2010).

It should be noted that these oxidising conditions may also promote more cross-linking, which may further promote amorphous aggregate formation relative to amyloid formation (Butterfield, D. A. and Stadtman, E. R., 1997). The decreased maximal fluorescence intensity and decreased number of fibre growth curves obtained when H_2O_2 only was used in this PhD backs up the prediction that amorphous aggregates are formed under this condition.

In conclusion, oxidation by H_2O_2 alone is expected to reduce surface hydrophobicity of Aβ, promoting peptide folding and fibrillisation, increase hydrogen bonding capacity of the Met35 residue, which may either contribute more to Aβ β-sheet formation or have little effect, and increase the residue's polarity, although this is unlikely to alter overall peptide fibrillisation rates. It is not surprising therefore that we observe either an increase in fibrillisation rates or no significant effects when Aβ(1-40) is oxidised by H_2O_2 alone.

4.4.2. The effect of Cu^{2+}/Cu^{+}-catalysed oxidation on Aβ(1-40) fibrillisation

Metal catalysed oxidation (MCO), in this case Cu^{2+}/Cu^{+}-catalysed oxidation, produced an apparent decrease in fibrillisation rates of Aβ(1-40) and often a complete inhibition of fibril formation. This occurred for both a H_2O_2/Cu^{2+} system and an ascorbate/Cu^{2+} system; although only the former was shown to be a

significant effect ($p < 0.05$). In order to explain the effects of Cu^{2+}/Cu^{+}-catalysed oxidation on fibrillisation rate the effects of histidine oxidation, as well as methionine oxidation, on Aβ must be considered. The likely cause of these decreased fibrillisation rates is an increased propensity of Aβ(1-40) to form amorphous aggregates instead of amyloid fibres after $Cu^{2+}Cu^{+}$-catalysed oxidation.

The conversion of histidine to 2-oxo-histidine alters its pK_a. The pK_a associated with peptide-bound histidine are given in Figure 4.24 (A). The pK_a for 2-oxo-histidine (Figure 4.24 (B)) have not been experimentally determined, although it contains an electron withdrawing urea instead of a simple imidazole and thus the pK_a is expected to be a lot lower than that of histidine. At neutral pH therefore unoxidised Aβ(1-40) will be approximately 17 % protonated compared to His-Ox Aβ(1-40), which will effectively be neutrally charged. This difference in electrostatic nature of the oxidised peptide is likely to disrupt the specific cross-β structure of the amyloid fibre associated with unoxidised Aβ leading to amorphous aggregation.

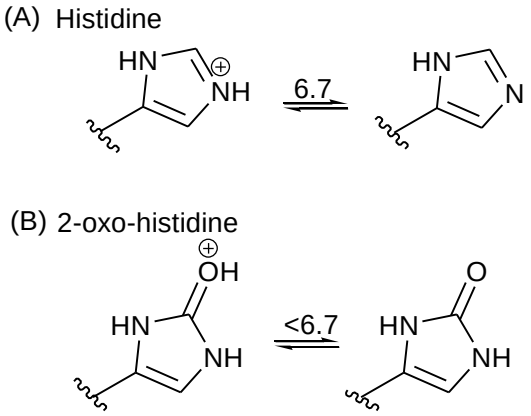

Figure 4.24: Protonation of histidine and 2-oxo-histidine. Peptide-bound histidine had one pK_a associated with it; the pK_a of the imidazole $N(\tau)$ which is 6.7 (A). Due to the electron-withdrawing of the urethane in 2-oxo-histidine, the pK_a is significantly lower than 6.7 (B).

It addition, 2-oxo-histidine does have a greater hydrogen-bond capacity than native histidine and therefore it is likely that oxidised histidine interferes with the specific hydrogen bonding of the Aβ peptide, and thus formation of β-sheets. Again, this will lead to amorphous aggregates forming instead of fibrils and this would give an apparent decrease in fibril formation, as indicated by the results of this PhD project. This explanation is backed up by the finding that maximal Th-T fluorescence decreases under Cu^{2+}/Cu^{+}-catalysed oxidising conditions, indicating that non Th-T binding amorphous aggregates are forming in this case instead of amyloid fibres. In

conclusion, the effect of Cu^{2+}/Cu^{+}-catalysed oxidation on Aβ(1-40) is to promote amorphous aggregation formation over amyloid fibrillisation.

There were some concerns that the presence of H_2O_2 and, in particular, radical based oxidants might interfere with Th-T bound fibril detection by degrading the Th-T. This may explain why Hou *et al.* chose to delay initiation of methionine oxidation at varying intervals to allow some progress in Aβ growth to the elongation phase before Th-T was exposed to the oxidising agents (Hou, L., *et al.*, 2002). In some previous studies procedures to remove oxidants before addition of Th-T have been employed. However the seeded experiment run in this project indicated that Th-T is resistant to degradation under oxidising conditions (Heegaard, P. M. H., *et al.*, 2004, Jayaraman, S., *et al.*, 2007, Kim, N. H. and Kang, J. H., 2003). The explanation above indicates that decreased Th-T fluorescence intensity is expected under Cu^{2+}/Cu^{+}-catalysed oxidation conditions because Aβ(1-40)-HisOx forms amorphous aggregates, which do not bind Th-T, rather than amyloid fibres, which do.

Attempted use of UV-CD to study Aβ(1-40) fibrillisation rates

UV-CD was also used to analyse the effects of oxidation on Aβ(1-40) fibrillisation because this technique did not involve any growth indicators internal to the sample. However, due to the low peptide and salt concentrations, needed to prevent absorbance exceeding the machine's dynamic range, the samples did not show fibril growth before precipitation of amorphous aggregates occurred (Snyder, S. W., *et al.*, 1994), apart from a slight shift to the β-sheet form of the Apo peptide. The oxidised samples took even longer to form β-sheets.

Therefore, the Th-T binding well-plate assay data was used exclusively to determine the effects of oxidation of Aβ(1-40) fibrillisation rates.

4.4.3. Oxidation and Aβ oligomers

SEC studies found that across two pHs, 7.4 and 10.5, unoxidised, fresh Aβ(1-40) exists in a monomeric form. Both oxidation by H_2O_2 alone and Cu^{2+}/Cu^{+}-catalysed oxidation were found not to generate detectable small oligomeric species of

Aβ(1-40). Only monomeric Aβ(1-40) was detected throughout a 17 h incubation with either of these conditions.

It should be noted that the range of the SEC column is only 3 – 70 kDa. Oligomers and fibres could be considerably larger, however, there is no evidence that larger species eluted in the void volume. Indeed, the intensity of the main Aβ (monomer) band remains constant throughout the incubation, suggesting appreciable amounts of oligomers/fibres were not formed under these conditions over 17 hour incubations.

4.4.4. Conclusion

In contrast to the literature this PhD study has found oxidation of Aβ(1-40) using H_2O_2 alone either increases or has little effect on fibrillisation rates. Any effect it appears to have is in increasing the nucleation phase rather than the elongation phase. These effects are likely mediated by the increased hydrogen-bond capacity and decreased hydrophobicity of methionine sulfoxide, which promote β-sheet formation and folding to bury the methionine sulfoxide residue respectively.

These effects are highly biologically relevant as H_2O_2 concentrations increase 1.3–fold in AD (Squitti, R., *et al.*, 2006) and not surprisingly Met35 of Aβ extracted from plaques has been found to have a high sulfoxide content (Dong, J., *et al.*, 2003). Therefore, if oxidation by H_2O_2 alone of Aβ is occurring *in vivo* it may be a significant factor in contributing to increased fibrillisation of the peptide in AD pathology. It is notable that H_2O_2 oxidation did not cause formation of the highly toxic oligomeric form of the peptide, Aβ*, which would have eluted on the SEC at 56 kDa. Instead it seems that any extra fibrillisation is continuing to higher molecular weight forms of the peptide.

In addition, Aβ plaques have been found to be the site of high concentrations of redox active metals (Huang, X., *et al.*, 1999). These bind Aβ with a high affinity (Sarell, C. J., *et al.*, 2009) and hence it is highly likely that Aβ is exposed to Cu^{2+}/Cu^{+}-catalysed oxidation as opposed to oxidation by H_2O_2 alone in the AD brain. The *in vitro* studies described above suggest that this oxidation leads to a propensity of Aβ(1-40) to form amorphous aggregates as opposed to the amyloid fibres which are associated with Aβ-induced toxicity. The mechanism by which

copper catalysed oxidation might promote amorphous aggregation of Aβ is not clear. However, the oxidised histidine ring system will become a stronger hydrogen-bond acceptor and consequently will be capable of forming hydrogen bonds with amides from the main chain, disrupting hydrogen-bond networks along the backbone required for the cross-beta structure in amyloid fibres. In addition, the charge of the peptide will be closer to neutral for Aβ containing 2-oxo-histidine as opposed to the unoxidised peptide, due to the much lower p*K*a of this oxidised residue compared to its native form. Consequently amorphous self-association will be favoured over amyloid formation. However, these experiments are performed at micromolar levels of Aβ and physiologically Aβ levels are considerably lower, around the nM mark. At this considerably lower concentration of Aβ fibrils may form over amorphous aggregates.

In conclusion, oxidation by H_2O_2 alone leads to an increase in Aβ fibrillisation. In the environment of the AD brain, where disrupted metal homeostasis has led to increased concentrations of redox active metals (Bush, A. I., 2003), Aβ is more exposed to Cu^{2+}/Cu^{+}-catalysed oxidation, which may delay the toxicity-related fibrillisation that the peptide undergoes as described by the Amyloid Cascade Hypothesis.

Chapter 5

CONCLUSION

Protein oxidation is a physiological process associated with age-related diseases (Adams, J. D. J., 1991, Coyle, J. T. and Puttfarcken, P., 1993). These diseases include Alzheimer's Disease (Markesbery, W. R., 1997), with oxidation of the Amyloid beta (Aβ) peptide reported to occur (Dong, J., *et al.*, 2003, Head, E., *et al.*, 2001, Shearer, J. and Szalai, V. A., 2008). This is a peptide whose fibrillisation is a seminal event in the aetiology of the disease as described by the Amyloid Cascade Hypothesis (Hardy, J. A. and Higgins, G. A., 1992) (Figure 5.1).

Chapter 4 of this thesis presents evidence that oxidation of the Aβ peptide can alter these disease-related fibrillisation rates. Previous literature has focused on the effects of H_2O_2-only mediated oxidation, on Aβ fibrillisation kinetics. This oxidation method exclusively oxidises Met35 in the Aβ sequence (Hou, L., *et al.*, 2004). These studies report that this oxidation causes a decrease in fibrillisation rates (Hou, L., *et al.*, 2002, Hou, L., *et al.*, 2004, Johansson, A.-S., *et al.*, 2007, Maiti, P., *et al.*, 2010, Palmblad, M., *et al.*, 2002, Watson, A. A., *et al.*, 1998). Firstly, in contrast to the literature, this thesis presents evidence that H_2O_2-only mediated oxidation of Aβ(1-40) actually either increases or has little effect on fibrillisation rates (Figure 5.1). In the environment of the AD brain, where H_2O_2 concentrations increases 1.3-fold (Squitti, R., *et al.*, 2006), this may therefore represent a trigger of increased Aβ fibrillisation in the disease.

Secondly, in the environment of the AD brain, where metal homeostasis is severely disrupted and redox-active metal ions such as Cu^{2+} and Fe^{3+} can reach concentrations of 340 μM – 400 μM and 1 mM respectively (Bush, A. I., 2003, Dong, J., *et al.*, 2003, Lovell, M. A., *et al.*, 1998), the more physiologically probable oxidation that the Aβ peptide is exposed to is metal catalysed oxidation (MCO), in particular Cu^{2+}/Cu^{+}-catalysed oxidation. Indeed, Aβ binds Cu^{2+} ions with a high affinity (Sarell, C. J., *et al.*, 2009) and hence Aβ is likely exposed to this highly site-specific oxidation mechanism. The only previous study on the effects of this oxidation mechanism on Aβ is that by Dyrks *et al.* who found an increase in fibrillisation rates with MCO of Aβ (Dyrks, T., *et al.*, 1992). However, this study used SDS-PAGE to measure Aβ aggregation rates, which does not distinguish between the disease-causing amyloid fibres of Aβ (Seilheimer, B., *et al.*, 1997) and the relatively non-toxic amorphous aggregates of the peptide (Howlett, D. R., *et al.*, 1995, Lorenzo, A. and Yankner, B. A., 1994).

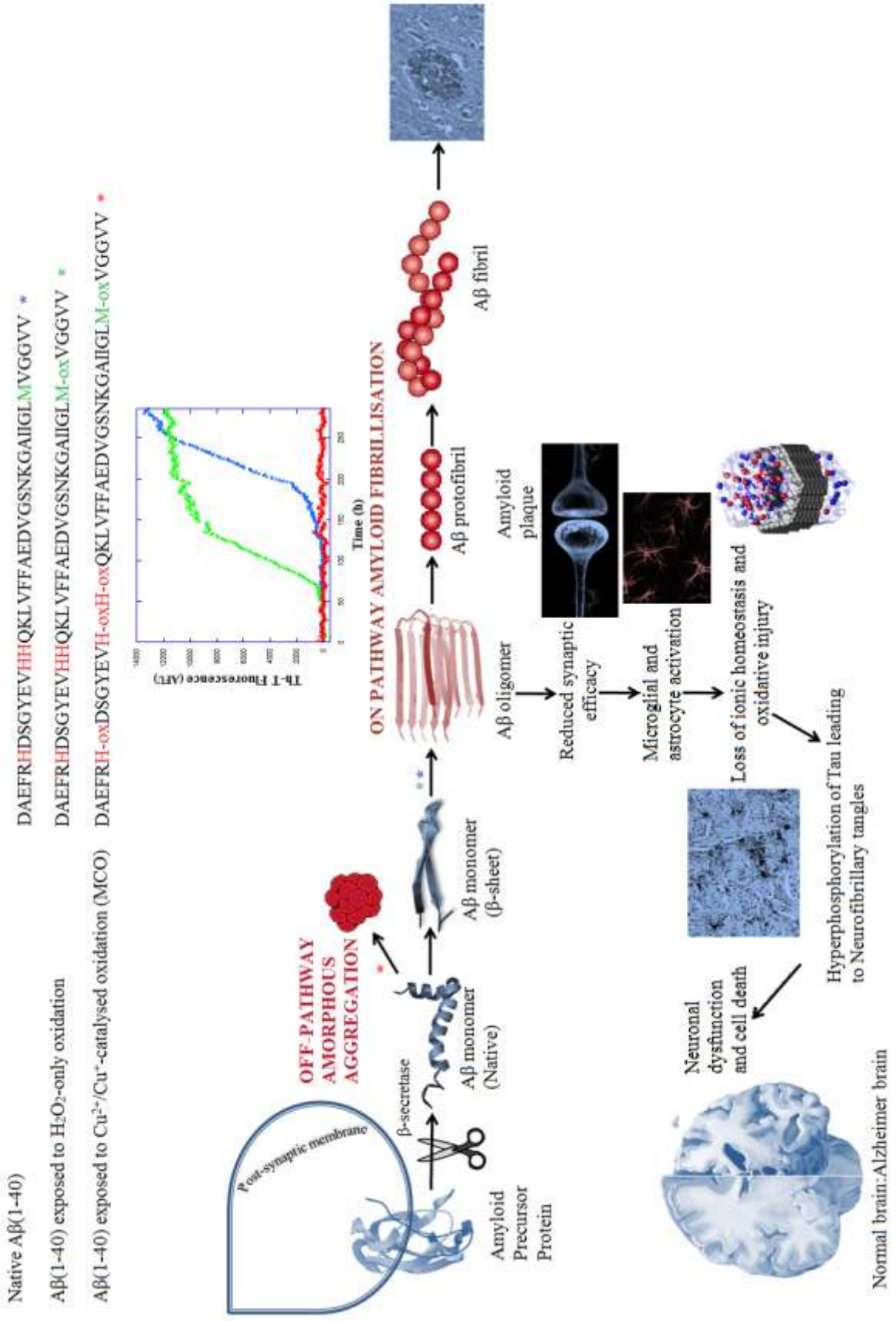

Figure 5.1: Summary of the role of oxidation in the Amyloid Cascade Hypothesis. Aβ(1-40) exposed to H_2O_2 mediated oxidation (green) exhibits faster on-pathway fibrillisation, which has been linked via the Aβ oligomer to neurodegeneration. Aβ(1-40) exposed to Cu^{2+}/Cu^{+}-catalysed oxidation (red) is diverted onto the non-toxic off-pathway amorphous aggregation pathway. The fibrillisation rate of native Aβ is shown in blue.

This thesis presents the first study into the effects of MCO on Aβ fibrillisation using a technique that can detect the specific cross-β structure of the Aβ peptide; Th-T binding fluorescence well-plate assays. This study found that Aβ fibrillisation rates are decreased after Cu^{2+}/Cu^{+}-oxidation indicating that MCO of the Aβ peptide is likely promoting folding to the non-toxic amorphous form of the peptide rather than the toxic amyloid fibrillar form (Figure 5.1). Therefore, increasing oxidative stress in AD pathology may actually reduce toxicity of the Aβ peptide, although it is still likely to promote the disease state via other mechanisms such as DNA and RNA oxidation and further loss of metal homeostasis (Atwood, C. S., *et al.*, 1999, Mecocci, P., *et al.*, 1994, Nunomura, A., *et al.*, 1999).

MCO of the Aβ peptide targets both methionine and histidine residues (Inoue, K., *et al.*, 2006, Nadal, R. C., *et al.*, 2008, Schiewe, A. J., *et al.*, 2004, Schoneich, C. and Williams, T. D., 2002). Oxidation of methionine, to methionine sulfoxide, differs from oxidation of histidine to its most common physiological form, 2-oxo-histidine **4** (Schoneich, C. and Williams, T. D., 2002, Traore, D. A. K., *et al.*, 2009), as the former is reversible. The methionine sulfoxide reductases can convert methionine sulfoxide back into the native methionine form (Schoneich, C., 2005) and this is a likely mechanism by which Aβ can act as a scavenger of toxic reactive oxygen species (ROS) (Nadal, R. C., *et al.*, 2008). However, histidine oxidation of the Aβ peptide represents irreversible damage to the peptide. Therefore, to study how Aβ fibrillisation kinetics alter with increasing oxidative stress it is necessary to study the effects of histidine-only oxidation on the peptide. The whole-peptide oxidation methods used in Chapter 4 cannot be applied to this study because histidine cannot be oxidised exclusively without oxidising other residues. Thus, this PhD project proposed to synthesise protected, enantiomerically pure, oxidised histidine and then incorporate this into the sequence for Aβ(1-42) (Figure 5.2) for further analysis of the effect of histidine specific oxidation on Aβ(1-42) structure and fibrillisation.

DAEFRH-oxDSGYEVH-oxH-oxQKLVFFAEDVGSNKGAIIGLMVGGVVIA

Figure 5.2: The location of oxidised histidines in solid-phase peptide synthesised Aβ(1-42)-His-ox.

Chapter 2 describes initial attempts to synthesise 2-oxo-histidine from L-histidine (Scheme 5.1). Synthesis from L-histidine has the advantages of the starting material being available as the pure L-enantiomer, thus preventing the need to induce chirality at

a later stage, and the synthesis including few steps. The first attempted synthesis used a DMDO-mediated oxidation of mono-Boc protected L-histidine methyl ester **5a**, which was reported in the literature to generate mono-Boc protected 2-oxo-L-histidine methyl ester **4a** via a single oxygen transfer (Saladino, R., *et al.*, 1999). However, this thesis reports that the products of this oxidation in fact incorporate whole DMDO molecules into their structure with isopropylidene groups as shown in structures **22** and **23**, the latter being the formyl intermediate of the former (Scheme 5.1(A)). A second synthesis attempted to replicate literature synthesis of mono-Bz protected 2-oxo-L-histidine **4b** (Meister Winter, G. E. and Butler, A., 1996, Uchida, K. and Kawakishi, S., 1986, 1989), however, as described in the literature (Lewisch, S. A. and Levine, R. L., 1995), yields were low and purification from the side products of oxidised ascorbate was challenging (Scheme 5.1(B)). A final attempted synthesis from L-histidine **5** used a two step synthesis, starting with a Bamberger cleavage of the imidazole ring (Scheme 5.1(C(i))) followed by a second step to close the ring with the addition of a carbonyl at C-2 (Scheme 5.1(C(ii))). The benzoyl derivative of mono-Boc protected L-histidine methyl ester **28** was successfully synthesised as were two derivatives of the Bamberger product of L-histidine methyl ester; a methyl carbamate derivative **29** and a benzoyl derivative **27**. Ring closure was attempted on the diamidoethane **27** using triphosgene and diethyl carbonate but the former reagent led to only starting material being recovered and the latter to destruction of the amino acid functionality.

Chapter 3 presented a synthesis of protected 2-oxo-histidine, starting from urea **17** and tartaric acid **37**. These were coupled together to form the known ring system 4-carboxyimidazolin-2-one **49**. This product was further derivatized to form 4-formylimidazolin-2-one **38a**, which was subsequently coupled to a phosphonate **39b** using a Horner-Wadsworth-Emmons reaction to generate a dehydro-derivative of protected L-histidine **40a**. Platinum-catalysed hydrogenation was then used to generate a protected form of 2-oxo-histidine (Scheme 5.2). However, at the end of this experimental work this product still required further work to ensure its suitability to solid-phase peptide synthesis; resolution of this racemate to an enantiomerically pure form, and re-protection using groups suitable to peptide synthesis.

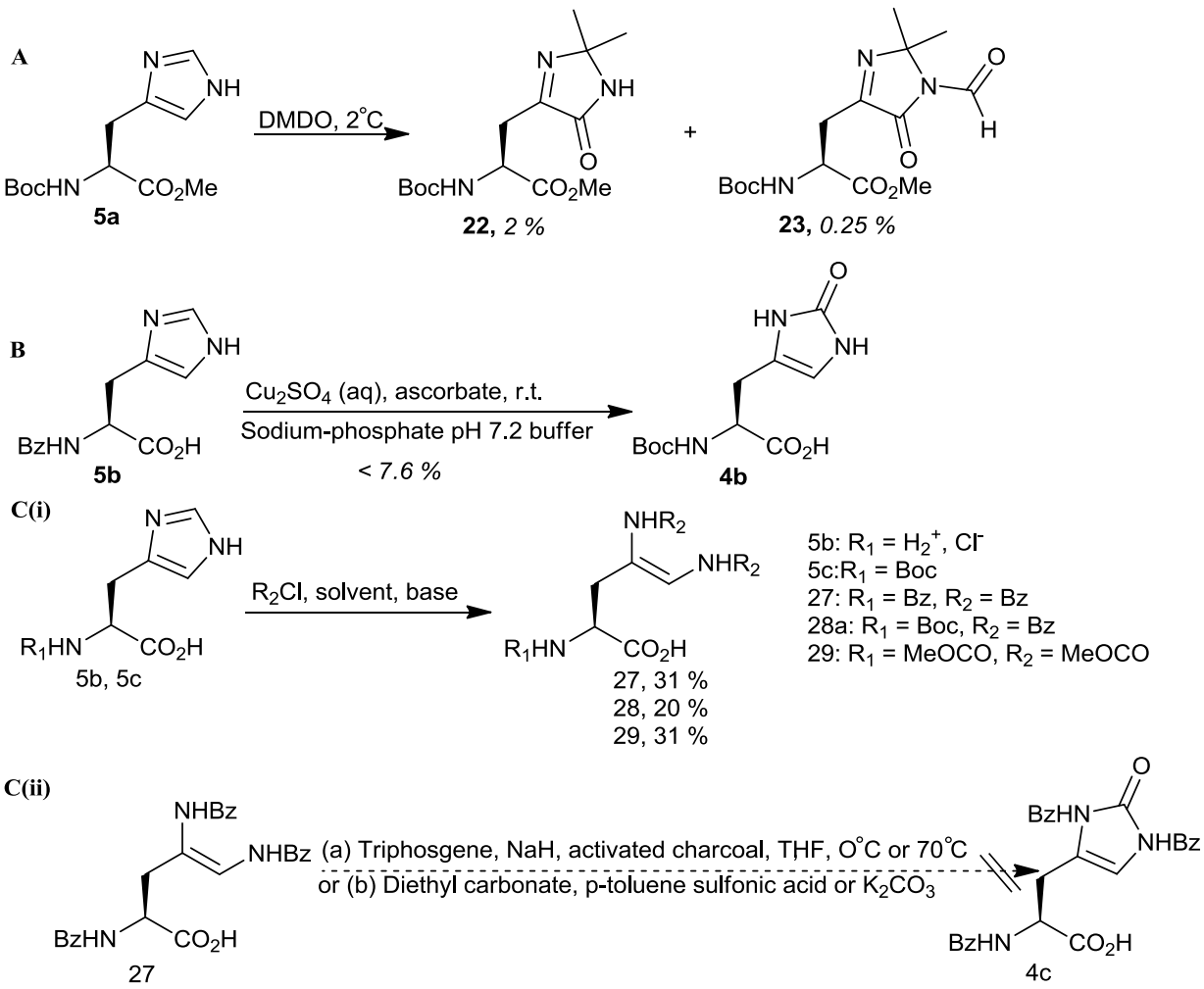

Scheme 5.1: Summary of attempted syntheses of 2-oxo-histidine 4 from L-histidine.
(A) DMDO-mediated oxidation of *N*(α)-Boc-His-OMe **5a**.**(B)** Cu^{2+}/Cu^{+}-catalysed oxidation of *N*(α)-Bz-His-OH **5b**. **(C) (i)** Bamberger cleavage of either *N*(α)-Boc-His-OMe **5a** or His-OMe.2HCl **5c**. **(ii)** Attempted ring closure of the benzoyl Bamberger product of L-histidine **27**.

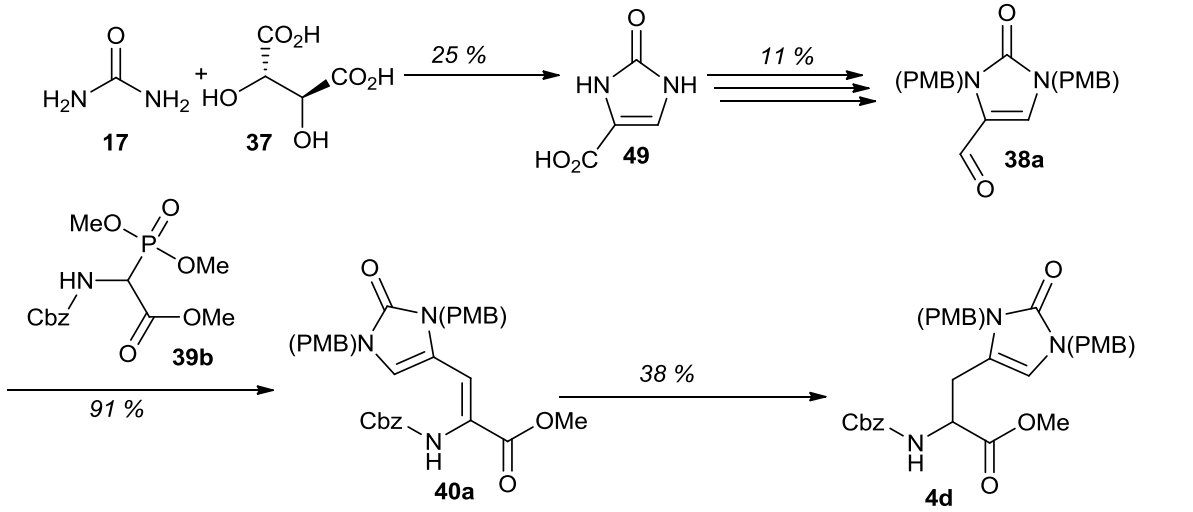

Scheme 5.2: Summary of synthesis of 2-oxo-histidine 4 from urea 17 and tartaric acid 37. Urea **17** and tartaric acid **37** were coupled together to form 4-carboxyimidazolin-2-one **49**. This was further derivatized to form 4-formylimidazolin-2-one **38a**, which was coupled to phosphonate **39b** using a Horner-Wadsworth-Emmons reaction to generate a dehydro-derivative of protected 2-oxo-L-histidine **40a**. Platinum-catalysed hydrogenation was then used to generate *N*(α)-Cbz, *N*(π),*N*(τ)-Bis(PMB)-2-oxo-His-OMe **4d**.

Since thesis writing has begun, the Wyatt lab has generated 2-oxo-L-histidine using an adaptation of a synthesis of the racemate reported by Lam *et al.* (Lam, A. K. Y., *et al.*, 2010). This adaptation is shown in Scheme 5.3 and includes the use of the Bamberger cleavage to generate the initial diamine pentanoic acid **83b**, thus avoiding several synthesis steps and ensuring only L-enantiomers are formed. Protection strategies are currently being investigated for this novel amino acid. Before its use in synthesising the Aβ peptide, this 2-oxo-histidine should be tested for its suitability to solid phase peptide synthesis by incorporating it into a short peptide sequence such as that for the tripeptide Thyrotropin Releasing Hormone (TRH) (Figure 5.3). This represents one of several future projects that can be extended from these syntheses of 2-oxo-histidine.

In conclusion, this thesis has shown that oxidation of Aβ has a profound influence on its fibrillisation and that incorporation of a stable oxidised histidine into Aβ is a realisable goal.

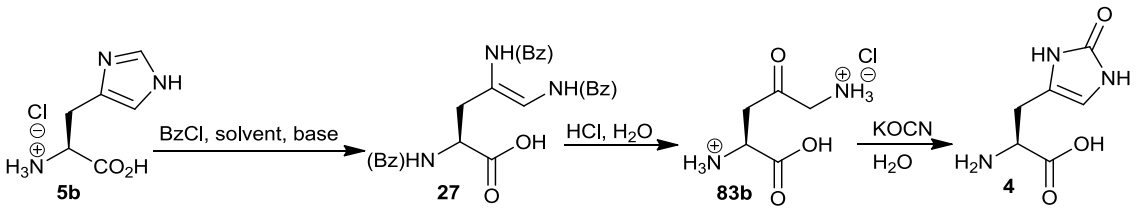

Scheme 5.3: Synthesis of 2-oxo-histidine 4 from L-histidine 5b.

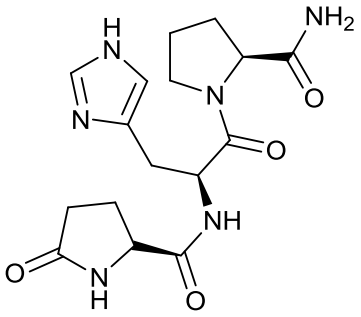

Figure 5.3: Thyrotropin Releasing Hormone (TRH).

Chapter 6

EXPERIMENTAL (FOR CHAPTERS 2 AND 3)

6.1. General procedures

^{31}P-NMR readings and some ^{1}H-NMR readings were performed on a Jeol JNMEX270 Spectrometer (^{1}H frequency 270 MHz, ^{31}P frequency 109.33 MHz). ^{13}C-NMR, DEPT-135, COSY, HSQC readings and the remaining ^{1}H-NMR readings were performed on either a Bruker AV400 Spectrometer or a Bruker AMX400 Spectrometer (both ^{1}H frequency 400 MHz, ^{13}C frequency 100.65 MHz). All measurements are done at room temperature. ^{31}P-NMR and ^{13}C-NMR were run as proton decoupled. In each case spectra are reported as; δ (in ppm), the number of nuclei in a particular chemical environment (determined by integration), the multiplicity (s = singlet, d = doublet, dd = doublet of doublet, t= triplet, q = quartet, m = multiplet), coupling constants if appropriate and assignment.

High-resolution mass spectrometry was performed at the EPSRC National Mass Spectrometry Service Centre using several ionisation techniques; positive electrospray (ESI), positive nano-electropray (NSI) and electron impact ionisation (EI). Reverse-phase-HPLC mass spectrometry was performed on an Agilent 1100 Series LC-MS with SL Ion Trap MSD.

ATR-IR was performed on a Bruker Tensor 37 spectrometer with a PIKE MIRacle ATR accessory. KBr-IR was performed on an FTIR-8300 spectrometer with samples dispersed in potassium bromide pellets.

Melting points were recorded using either a Reichert hot stage microscope apparatus or using capillary tubes in a Gallenkamp melting point instrument. Measurements are uncorrected and reported in degrees celsius (°C).

Thin layer chromatography (TLC) was performed on Merck silica gel 60F_{254} plates. Flash chromatography was conducted on either BDH silica gel (particle size 33-77 μm) or Zeoprep silica (particle size 40-63 μm).

1M, pH 7.2 sodium phosphate buffer was made up of 28 ml of sodium dihydrogenphosphate (2M, 13.8 g in 50 ml) and 72 ml of disodium hydrogen phosphate (2 M, 28.4 g in 100 ml) in 100 ml ultra-high-quality (UHQ) water. UHQ water was purified using a Millipore Simpak 2 system and has >18 MΩ.cm resistivity.

Activated manganese(IV) oxide (~85%, 5μm) was obtained from Sigma Aldrich. Tosyl chloride was purified by dissolution in with DCM, addition of petrol, filtration to remove insoluble impurities and evaporation of the filtrate**.** MeOH was distilled over magnesium and iodine. DMF, Et_2O and DCM were purified using a Solvent Purification System; M Braun MB SPS-800. THF was either dried using aforementioned solvent purification system or distilled under nitrogen with sodium metal and benzophenone. All other reagents were of reagent grade or better and used without further purification.

6.2. Experimental data

This thesis refers to the atoms of histidine as notated in Figure 6.1(A). However, the literature may label the atoms of histidine as denoted in Figure 6.1(B) as, historically, histidine atoms have been labelled differently depending on whether the context was organic chemistry (Figure 6.1 (A)) or biochemistry (Figure 6.1 (B)).

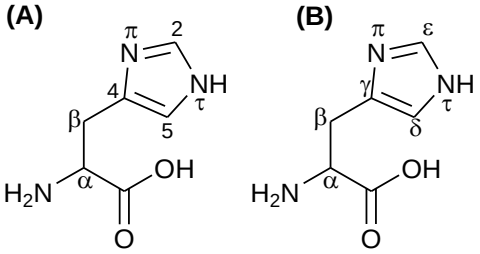

Figure 6.1: Labelling histidine 5. In both cases, the nitrogen atoms are labelled based on their proximity to the side chain; *pros* (near) with π and *tele* (far) with τ. Older papers may denote these as 1 or 3 with the order of this depending on whether the papers were by organic chemists or biochemists. In both cases the amino acid backbone is labelled using greek letters. **(A)** Labelling of histidine as defined by IUPAC. The carbon atom next to the τ-nitrogen is labelled 5 and the carbon between the two nitrogens is labelled 2. **(B)** Labelling of histidine more typical of that in biochemistry papers. In this case the ring carbons are labelled as a continuation of the backbone carbons with Greek letters. The carbon closest to the π-nitrogen is labelled γ whereas the carbon between the two nitrogens is called the ε-carbon.

His-OMe·2HCl 5c

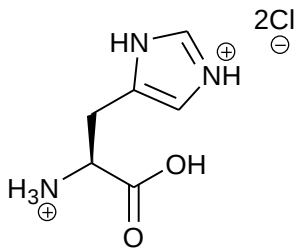

Based on the method described by Dancer *et al.* (Dancer, J., *et al.*, 1996), L-histidine hydrochloride **5e** (25.0 g, 0.13 mol) was suspended in methanol (250 ml). Thionyl chloride (20 ml, 0.28 mol) was added dropwise over 15 min. The mixture was refluxed for 6 h or until no solid remained. The mixture was concentrated *in vacuo* and ether was added to precipitate out the product. This was filtered off, washed with Et_2O and dried *in vacuo* over sodium hydroxide pellets to yield His-OMe·2HCl **5c** (14.5 g, 46 %) as a white powder; mp 204 - 205 °C dec (Lit. 205 – 206 °C dec (Hanford, B. O., *et al.*, 1968), Lit. 200 – 201 °C (Davis, N. C., 1956)); $[\alpha]_D$ + 17.9 (*c* 1.0 in methanol) (Lit. $[\alpha]_D$ + 10.8 *c* 1.0 in water (Gerhard, G. and Schunack, W., 1980)); ν_{max}(KBr)/cm^{-1} 3000 (NH), 1763 (CO).

N(α), *N*(τ)-DiBoc-His-OMe 5d

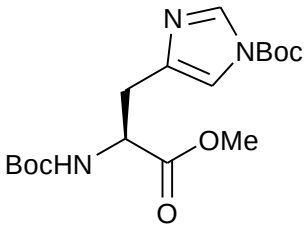

N(α), *N*(τ)-DiBoc-His-OMe **5d** was synthesised from His-OMe·2HCl (**1**) (9.68 g, 40 mmol) and Boc_2O (18.3 g, 84 mmol) using the method described by Brown *et al.* (Brown, T., *et al.*, 1982) and was obtained as a white solid (10.7 g, 72 %); mp 107 - 108 °C (Lit. 105 - 107 °C (Xu, J. and Yadan, J. C., 1995)); $[\alpha]_D$ + 28.8 (*c* 1.0 in DCM) (Lit. $[\alpha]_D$ + 23.3 *c* 1.0 in DCM (Xu, J. and Yadan, J. C., 1995)); ν_{max}(ATR)/cm^{-1} 3244 (NH),1739 (CO), 1702 (2 CO); δ_H(270 MHz; $CDCl_3$) 1.41 (9 H, s, C*H*$_3$ (Boc)), 1.57 (9H, s, C*H*$_3$ (Boc)), 2.99 (1 H, dd *J* 14.3 Hz and 4.9 Hz, β-CH*H*), 3.03 (1 H, dd, *J* 14.3 Hz and 4.9 Hz, β-C*H*H), 3.70 (3 H, s, OC*H*$_3$), 4.50 - 4.59 (1 H, m, α-C*H*), 5.69 (1 H, d, *J* 6.3 Hz, br, α-N*H*), 7.11 (1 H, s, Im 5-*H*), 7.96

(1 H, d, *J* 1.2 Hz, Im 2-*H*); δ_C(400 MHz; $CDCl_3$) 27.9 (3 *C*H_3), 28.3 (3 *C*H_3), 30.3 (*C*H_2), 52.3 (O*C*H_3), 53.2 (*C*H), 79.8 (*C*), 85.6 (*C*H), 136.9 (*C*), 138.7 (*C*H), 146.9 (*C*O), 155.5 (*C*O), 172.3 (*C*O).

_N_(α)-Boc-His-OMe 5a

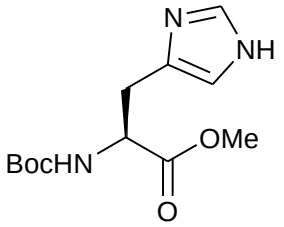

Two methods were used:

(A) Based on the method described by Dancer *et al.* (Dancer, J., *et al.*, 1996), *N*(α), *N*(τ)-DiBoc-His-OMe **5d** (1.00 g, 2.7 mmol) was suspended in anhydrous methanol (10 ml). Potassium carbonate (37 mg, 0.27 mmol) was added and the mixture was refluxed for 2 h. The mixture was then concentrated *in vacuo*. The resulting oil was partitioned between water and dichloromethane. The organic phase was dried over $MgSO_4$ to yield *N*(α)-Boc-His-OMe **5a** (400 mg, 55 %) as a viscous brown-yellow oil; $[\alpha]_D$ + 11.7 (*c* 1.0 in chloroform) (Lit. $[\alpha]_D$ − 11.7 *c* 1.0 in methanol (Hanford, B. O., *et al.*, 1968)); ν_{max}(KBr)/cm^{-1} 3369 (NH), 1740 (CO), 1701 (CO); δ_H(270 MHz; $CDCl_3$) 1.41 (9 H, s, CH_3 (Boc)), 2.98 – 3.17 (2 H, m, β-CH_2), 3.70 (3 H, s, OCH_3), 4.47 - 4.58 (1 H, m, α-C*H*), 5.71 - 5.84 (1 H, m, α-N*H*), 6.78 (1 H, s, Im 5-*H*), 7.52 (1 H, s, Im 2-*H*). δ_C (400 MHz; $CDCl_3$) 28.3 (3 *C*H_3), 29.8 (*C*H_2), 52.3 (O*C*H_3), 53.6 (*C*H), 80.0 (*C*), 116.2 (*C*H), 134.0 (*C*H), 135.2 (*C*), 155.61 (*C*O), 172.6 (*C*O).

(B) Based on the method described by Brown *et al.* (Brown, T., *et al.*, 1982), His-OMe·2HCl (**5c**) (12.3 g, 0.051 mol) was suspended in methanol (50 ml) and Boc_2O (11.3 g, 0.052 mol) was added. The mixture was cooled to 0 °C (ice/salt bath). Triethylamine (14 ml, 0.10 moles) was added dropwise and the reaction was left stirring overnight at room temperature. The mixture was then concentrated *in vacuo* and extracted into ethyl acetate (50 ml). The organic extract was washed with citric acid (5 x 25 ml), neutralized with $NaHCO_3$ and extracted into ethyl

acetate before dying over $MgSO_4$ to yield *N*(α)-Boc-His-OMe **5a** (1.58 g, 12 %) as a white glassy solid; mp 140.8 – 142.6 °C (Lit. 126.0 – 128.0 °C (Perfetti, R. B., *et al.*, 1976)); ν_{max}(KBr)/cm^{-1} 3308 (NH), 3120 (NH), 1748 (CO), 1699 (CO); δ_H(270 MHz; $CDCl_3$) 1.41 (9 H, s, C*H*$_3$ (Boc)), 3.01 – 3.13 (2 H, m, β-C*H*$_2$), 3.69 (3 H, s, OC*H*$_3$), 4.48 – 4.57 (1 H, m, α-C*H*), 5.58 – 5.69 (1 H, m, α-N*H*), 6.80 (1 H, s, Im 5-*H*), 7.56 (1 H, s, Im 2-*H*).

Dimethyldioxirane (DMDO) 21 solution in acetone

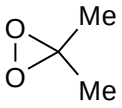

Dimethyldioxirane **21** solution in acetone was prepared using the vacuum distillation method described by Adam *et al.* (Adam, W., *et al.*, 1991). Sodium hydrogencarbonate (29.0 g, 0.35 mol) was dissolved in a mixture of water (127 ml) and acetone (96 ml) within the distillation flask and cooled to 0 °C (ice-salt bath). Oxone (60.0 g, 98 mmoles) was added in 5 portions over 15 min. The apparatus was evacuated to ca 15 mmHg using a water aspirator. The distillation flask was then gradually warmed to room temperature and the distillation started. Distillation was continued until the reactants stopped effervescing. The distillate (30 ml) was a solution of DMDO in acetone. The DMDO concentration of this was determined, by an iodine/thiosulfate back titration, to be 40 mM (1.7 % yield). The solution was stored over 4 Å molecular sieves at −20 °C for short periods.

Oxidation of *N*(α)-Boc-His-OMe 5a by DMDO in acetone

Based on the method used by Saladino *et al.* (Saladino, R., *et al.*, 1999) to synthesise *N*(α)-Boc-2-oxo-His-OMe **4a**, *N*(α)-Boc-His-OMe **5a** (329 mg, 1.2 mmol) was added to DMDO in acetone (40 mM, 30 ml, 1.2 mmol) and left to react under one of two possible reaction conditions; 12 h at r.t. **(A)** or 27 h at 2 °C **(B)**. The mixtures were then concentrated and dried *in vacuo* over phosphorus pentoxide to yield a yellow, glassy solid. This was purified by flash

chromatography using EtOAc-petrol (50:50 to 75:25) followed by further chromatography using EtOAc-DCM (10:90) to yield two colourless oils:

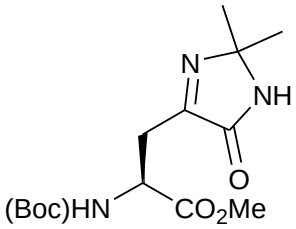

i) 2-Boc-amino-3-(2,2-dimethyl-5-oxo-2,5-dihydro-1*H*-imidazol-4-yl)propionic acid methyl ester **22** (7.4 mg, 2.0 %) (R_f 0.30 in 65 % EtOAc-DCM). Produced under conditions **(A)** and **(B)**. δ_H(400 MHz; $CDCl_3$) 1.44 (9 H, s, CH_3 (Boc)), 1.45 (3 H, s, 2-CCH_3), 1.46 (3 H, s, 2-CCH_3), 3.00 (2 H, dd, 10.8 Hz and 2.7 Hz, β-C*H*), 3.07 (2 H, dd, 10.8 Hz and 5.4 Hz, β-C*H*), 3.72 (3 H, s, OCH_3), 4.71 – 4.79 (1 H, m, α-C*H*), 5.77 (1 H, br, d, *J* 5.5 Hz, α-N*H*), 7.65 (1 H, s, br, τ-N*H*); δ_C(100.65 MHz; $CDCl_3$) 26.7 (H_3CCCH_3), 26.8 (H_3CCCH_3), 28.3 (3 CH_3 (Boc)), 30.8 (β-CH_2), 51.1 (α-*C*H), 52.4 (OCH_3), 80.0 (*C*), 81.9 (*C*), 155.4 (*C*O), 165.0 (*C*O), 171.7 (*C*O). Assignments based on 1D spectra, DEPT-135, COSY and HSQC analysis; *m/z* (ESI) found: 314.1713 ($M + H^+$) ($C_{14}H_{24}N_3O_5$ requires 314.1710).

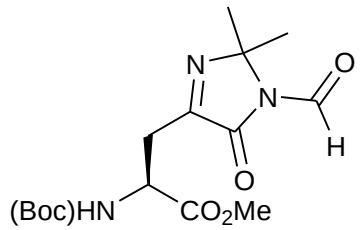

ii) 2-Boc-amino-3-(2,2-dimethyl-5-oxo-2,5-dihydro-1*H*-imidazol-4-yl)-*N*(τ)-formyl -propionic acid methyl ester (1 mg, 0.25 %) (R_f 0.40 in 65 % EtOAc-DCM). Produced under condition **(B)**. ν_{max}(KBr)/cm^{-1} 3369 (NH), 1750 (CO), 1706 (CO); δ_H(400 MHz; $CDCl_3$) 1.43 (9 H, s, CH_3 (Boc)), 1.61 (3 H, s, H_3CCCH_3), 1.62 (3 H, s, H_3CCCH_3), 2.98 (1 H, dd, *J* 10.4 Hz and 4.7 Hz, β-CH*H*), 3.04 (1 H, dd, *J* 10.5 Hz and 3.4 Hz, β-C*H*H), 3.71 (3 H, s, OCH_3), 4.70 – 4.79 (1 H, m, α-C*H*), 5.47 (1 H, d, *J* 7.9 Hz, N*H*), 9.02 (1 H, s, C*H*O); δ_C(100.65 MHz; $CDCl_3$) 24.6 (H_3CCCH_3), 24.8 (H_3CCCH_3), 28.3 (3 CH_3 (Boc)), 31.4 (β-CH_2), 51.0 (α-*C*H),

52.7 (O*C*H_3), 80.3 (*C*), 85.5 (*C*), 155.2 (*C*), 158.2 (H*C*), 162.6 (*C*), 163.5 (*C*), 171.3 (*C*). Assignments based on 1D spectra, DEPT-135, COSY and HSQC analysis; *m/z* (ESI) found: 342.1663 (M + H^+) ($C_{15}H_{24}N_3O_6$ requires 342.1660).

_N_(α)-Bz-His-OH 5b

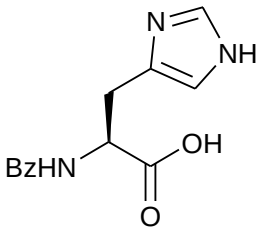

L-Histidine hydrochloride monohydrate **5e** (21.0 g, 0.10 mol) was dissolved in water (200 ml) and cooled to 0 °C. Benzoyl chloride (11.6 ml, 0.10 mol) and sodium bicarbonate (16.8 g, 0.20 mol) were added dropwise, concurrently. The mixture was then stirred at room temperature for 9 h. The solution was then acidified to pH 3.0 using HCl and the product precipitated. This was then air dried followed by re-crystallisation from methanol. A low melting point (< 190 °C) indicated the presence of impurities and so the product was then recrystallised from boiling ethanol, then methanol and diethyl ether to yield *N*(α)-Bz-His-OH (**5b**) (1.26 g, 5.0 %) as a yellow crystalline solid; mp 243 °C dec (Lit. 243 °C (Otani, T. T. and Briley, M. R., 1979)); ν_{max}(ATR)/cm^{-1} 3437 (NH), 3296 (NH), 1655 (CO), 1630 (CO); δ_H(270 MHz; $CDCl_3$) 3.00 – 3.09 (2 H, m, β-CH_2), 5.56- 5.64 (1 H, m, α-C*H*), 6.86 (1 H, s, Im 5-*H*), 7.44 – 7.57 (3 H, m, C*H* (Bz), 7.59 (1 H, s, Im 2-*H*), 7.79 – 7.68 (2 H, m, C*H* (Bz)), 8.73 (1 H, d, *J* 8.2 Hz, α-N*H*); δ_C(100.65 MHz; $CDCl_3$) 28.4 (*C*H_2), 52.8 (*C*H), 116.4 (*C*H), 127.2 (2 *C*H), 128.3 (2 *C*H), 131.3 (*C*), 133.9 (*C*), 134.0 (*C*), 134.8 (*C*), 166.1 (*C*O), 173.0 (*C*O).

N(α)-Bz-2-oxo-His-OH 4b (within crude products)

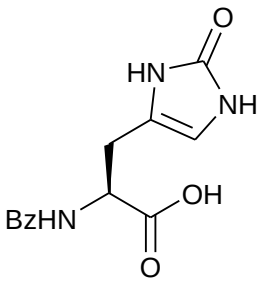

N(α)-Bz-His-OH **5b** (200 mg, 0.73 mmol) was dissolved in sodium phosphate pH 7.2 buffer (0.75 ml, pH 7.2) and ultra-high quality (UHQ) water (14.25 ml) to make a 50 mM solution of protected histidine. This solution was incubated for 26 h at r.t. with rapid mixing and the addition of aqueous ascorbic acid (17 ml, 50 mM) and aqueous copper(II) sulfate (15 ml, 0.5 mM). The pH of the solution was maintained by checking every 30 minutes for the first 6 h, adding small amounts of 1M NaOH and 2M HCl as necessary. A further 10 ml UHQ water was added at 21 h. Over the 26 h incubation the solution changed from colourless to brown. At 26 h the solution was concentrated *in vacuo* to leave a yellow oil which was dried over phosphorus pentoxide. ^{1}H-NMR showed evidence of peaks derived from ascorbate and thus further purification was attempted using a 8.0 ml Dowex AG 50W-X8, 60-140 mesh H^{+} form ion exchange resin. The material exited the column within the first ten fractions with a water based eluant. In addition, reverse phase analytical HPLC was performed on an Agilent Series 1100 machine on a Lichrosphere RP select B column run with acetonitrile and water. However, the product was still deemed impure by ^{1}H-NMR. All analyses are of the crude material; δ_{H}(270 MHz; DMSO) 2.89 – 3.17 (2 H, m, β-C*H*$_2$), 2.89 – 3.17 (1 H, m, α-C*H*), 3.48- 5.05 (>100 H, m, ascorbate and oxidized ascorbate), 6.29 (1 H, s, Im 5-*H*), 7.28-7.83 (5 H, m, C*H* (Bz)); *m/z* (RP-HPLC-MS, negative ion) found: 273.1 (16.5 %, *N*(α)-Bz-2-oxo-histidine **4b** – $2H^{+}$).

2,4,5-Tris(benzamido)pent-4-enoic acid methyl ester 27

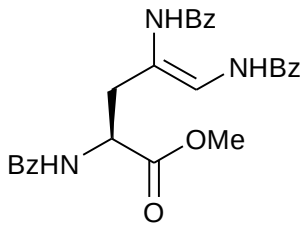

His-OMe·2HCl **5c** (1.00 g, 4.13 mmol) was suspended in a mixture of ethyl acetate (26 ml) and water (17 ml) and cooled to 0 °C. Benzoyl chloride (4.8 ml, 41.3 mmol) was added followed by aqueous sodium bicarbonate (6.5 g in 19.6 ml), each in three portions over a 45 min interval. The solution was then warmed to r.t. and left for 6.5 h. The product was then partitioned between water and ethyl acetate (2 x 15 ml). The combined organic extracts were dried over $MgSO_4$. The EtOAc extract was concentrated *in vacuo*. The compound was then triturated with diethyl ether and the resulting residue recrystallised from methanol to yield 2,4,5-Tris(benzamido)pent-4-enoic acid-methyl ester **27** (603 mg, 31 %) as a white powder; mp 212.0 – 213.1 °C (Lit. 213 - 215 °C (Trampota, M., 2009)); ν_{max}(ATR)/cm^{-1} 3315 (NH), 1743 (CO), 1674 (CO), 1640 (CO)1623 (CO); δ_H(270 MHz; $CDCl_3$) 2.85 (1 H, dd, *J* 14.2 Hz and 10.1 Hz, β-CH*H*), 3.20 (1 H, dd, *J* 14.2 Hz and 4.7 Hz, C*H*H), 3.63 (3 H, s, OCH_3), 4.71 (1 H, m, HNC*H*CO), 6.70 (1 H, d, *J* 9.4 Hz, HN*H*C=C), 7.42- 7.62 (9 H, m, C*H* (Bz)), 7.79 – 7.95 (6 H, m, C*H* (Bz)), 8.75 (1 H, d, *J* 8.2 Hz, *H*NCHCO), 9.54 (1 H, s,), 9.80 (1 H, d, *J* 9.4 Hz, C=CHN*H*); δ_C (100.65 MHz, $CDCl_3$) 38.6 (β-*C*H_2), 51.5 (α-*C*H), 53.2 (O*C*H_3), 114.6 (*C*-4), 116.1 (H*C*-5), 127.2 (2 *C*H), 127.4 (2 *C*H), 127.7 (2 *C*H), 128.7 (4 *C*H), 128.8 (2 *C*H), 132.0 (2 *C*H), 132.25 (*C*H), 132.31 (*C*), 132.9 (*C*), 133.4 (*C*), 166.1 (2 *C*O), 167.8 (*C*O), 172.2 (*C*O); *m/z* (RP-HPLC-MS, -ve ion) found: 470.1 (100 %, M - H^+) ($C_{27}H_{26}N_3O_5$ requires 470.17).

Bamberger reaction on *N*(α)-Boc-His-OMe 5a using BzCl

N(α)-Boc-His-OMe **5a** (500 mg, 1.9 mmol) was suspended in a mixture of ethyl acetate (26 ml) and water (17 ml) and cooled to 0 °C. Benzoyl chloride (2.2 ml, 15.7 mmol) was added followed by aqueous sodium hydrogencarbonate (6.5 g) in

water (19.6 ml), each in three portions over a 45 min interval. The solution was then warmed to r.t. and left for 19.5 h. The product was then partitioned between water and ethyl acetate (2 x 15 ml) and extracted twice into the organic layer. This organic layer was dried over $MgSO_4$. This was concentrated *in vacuo* and then purified twice by flash chromatography, both using EtOAc-petrol (10:90 to 30:70 and 20:80 to 30:70) to yield two colourless oils:

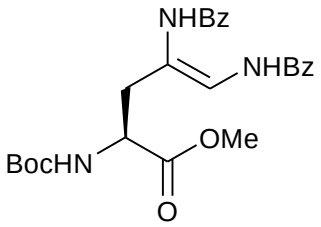

i) 4,5-Bis-benzamido-2-*tert*-butoxycarbonylamino-pent-4-enoic acid methyl ester **28** (180 mg, 20 %) (R_f 0.17 in 40 % EtOAc-DCM); ν_{max}(ATR)/cm^{-1} 3264 (NH), 1748 (CO), 1684 (CO), 1654 (CO), 1634 (CO); δ_H(400 MHz; $CDCl_3$); 1.43 (9 H, s, C*H*$_3$ (Boc)), 2.63 (1 H, dd, *J* 14.8 Hz and 5.7 Hz, C*H*H), 2.85 (1 H, dd, *J* 14.8 Hz and 5.7 Hz, CH*H*), 3.73 (3 H, s, OC*H*$_3$), 4.46 – 4.58 (1 H, m, HNC*H*CO), 5.46 (1 H, d, *J* 7.4 Hz, *H*NCHCO), 7.36 – 7.67 (7 H, m, C*H* (Bz) and C=C*H*NH), 7.87 - 8.10 (4 H, m, C*H* (Bz)); δ_C(400 MHz; $CDCl_3$) 28.2 (*C*H$_3$), 38.6 (*C*H$_2$), 52.6 (O*C*H$_3$), 52.9 (*C*H), 80.9 (*C*), 114.8 (*C*H), 115.9 (*C*), 127.4 (2 *C*H), 127.6 (2 *C*H), 128.6 (2 *C*H), 128.7 (2 *C*H), 131.9 (*C*H), 132.2 (*C*H), 133.49 (*C*), 133.54 (*C*), 155.8 (*C*O), 164.0 (*C*O), 166.0 (*C*O), 172.2 (*C*O); *m/z* (ESI) found: 468.2126 (M + H^+) ($C_{25}H_{29}N_3O_6$ requires 468.2129).

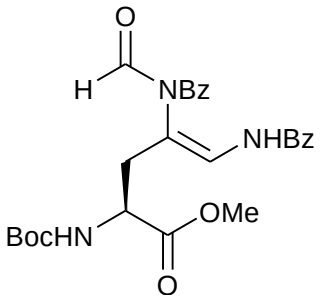

ii)5-Benzamido-4-(*N*-benzoyl, *N*-formylamino)-2-*tert*-(butoxycarbonylamino)pent-4-enoic acid methyl ester **28a** (30 mg, 3.2 %, R_f 0.30 in 40 % EtOAc-petrol); δ_H(400 MHz; $CDCl_3$); 1.40 (3 H, s, C*H*$_3$ (Boc)), 1.51 (6H, s, C*H*$_3$ (Boc)), 2.85 (1 H,

dd, *J* 12.3 Hz and 7.4 Hz, CH*H*), 3.01 (1 H, dd, *J* 12.3 Hz and 6.4 Hz, C*H*H), 3.74 (3 H, s, CO_2CH_3 (OMe)), 4.35 – 4.45 (1 H, m, HNC*H*CO), 6.65 (1 H, d, *J* 8.0 Hz, C=C*H*NH), 7.35 – 7.69 (10 H, m, C*H* (Bz)), 8.42 (1 H, s, br, *H*NCHCO), 9.17 (1 H, s, HNC*H*O), 10.0 (1H, d, *J* 8.0 Hz, C=CHN*H*).

2,4,5-Tris(methoxycarbonylamino)pent-4-enoic acid methyl ester 29

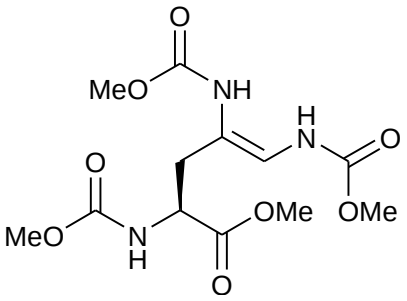

His-OMe·2HCl **5c** (500 mg, 2.1 mmol) was suspended in ethyl acetate (26 ml) and water (17 ml) and cooled to 0 °C (ice-salt bath). Methyl chloroformate (3.2 ml, 41.4 mmol) was added followed by aqueous sodium bicarbonate (6.5 g in 19.6 ml), each in three portions over 45 min. The solution was then warmed to r.t. and left for 6.5 h. The product was then partitioned between water and ethyl acetate (2 x 15 ml). The combined ethyl acetate extracts were dried over $MgSO_4$, concentrated *in vacuo*, dried over phosphorus pentoxide and purified by flash chromatography using Et_2O-DCM (10:90 to 50:50) to yield 2,4,5-tris(methoxycarbonylamino)pent-4-enoic acid methyl ester **29** (220 mg, 31 %) (R_f 0.21 in 50:50 Et_2O-DCM) as a colourless oil; δ_H(400 MHz; $CDCl_3$) 2.44 (1 H, dd, *J* 14.1 Hz and 7.9 Hz, C*H*H), 2.68 (1 H, dd, *J* 14.6 Hz and 4.4 Hz, CH*H*), 3.58 (3 H, s, OCH_3 (OMe)), 3.67 (3 H, s, OCH_3 (MeOCO)), 3.71 (3 H, s, CO_2CH_3 (MeOCO)), 3.72 (3 H, s, CO_2CH_3 (MeOCO)), 4.37 – 4.48 (1 H, m, HNC*H*CO), 5.67 (1 H, d, *J* 8.2 Hz, *H*NCHCO), 6.21 (1 H, d, *J* 8.7 Hz, HC=CN*H*), 6.62 (1 H, s, C=CHN*H*), 7.39 - 7.50 (1 H, m, C=C*H*NH).

4-carboxyimidazolin-2-one 49

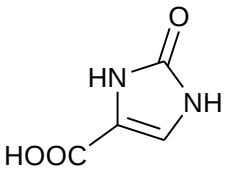

Using the procedure described by Baxter *et al.* (Baxter, R. L., *et al.*, 1992), urea **17** (65 g, 1.08 moles) and tartaric acid **37** (210 g, 1.40 moles) were ground together and added in small portions to stirring concentrated sulfuric acid (500 ml). The mixture was heated to 80 °C for 1h. The mixture was then cooled to 10 °C, poured over crushed ice (5 kg) and left to stand until a precipitate formed. This precipitate was filtered off, washed with water and dried over KOH pellets to yield 4-carboxyimidazolin-2-one **49** (34.1 g, 25 %) as a grey solid; mp 221 - 223 °C (Lit. 226 - 230 °C (Baxter, R. L., *et al.*, 1992), 1992. Lit. 232 – 235 °C (Zav'yalov, S. I., *et al.*, 2004); ν_{max}(ATR)/cm^{-1} 2972 (NH), 2820 (NH), 1741 (CO), 1647 (CO); δ_H (270 MHz, DMSO) 7.13 (1H, s, C*H*), 10.43 (1H, s, br, N*H*), 10.55 (1H, s, br, N*H*); δ_C (100.65 MHz, DMSO) 115.0 (*C*H), 118.2 (*C*), 154.4 (*C*O), 160.9 (*C*O).

Imidazolin-2-one 36

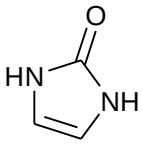

Using the procedure described by Baxter et al. (Baxter, R. L., *et al.*, 1992), 4-carboxyimidazolin-2-one **49** (16.7 g, 0.13 mol) was dissolved in aqueous potassium carbonate (17.9 g, 0.13 mol) and refluxed for 4 h. Charcoal (6.2 g) was added to the reaction mixture and this was refluxed for 30 min. The hot solution was filtered and concentrated *in vacuo*. The product was washed with ether (25 ml) and acetone (19 ml) to yield imidazolin-2-one **36** (8.6 g, 79 %) as a white solid; mp 216 – 220 °C (Lit. 238 – 240 °C (Baxter, R. L., *et al.*, 1992)); ν_{max}(ATR)/cm^{-1} 3024 (NH), 1631 (CO); δ_H (270 MHz; $CDCl_3$) 6.24 (2 H, s, C*H*), 9.79 (2 H, s, br, N*H*); δ_C (100.65 MHz; $CDCl_3$) 108.9 (2 *C*H), 155.4 (*C*O).

4-Methoxycarbonylimidazolin-2-one 52

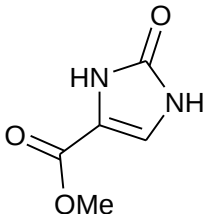

Using the procedure briefly described by Dransfield *et al.* (Dransfield, P. J., *et al.*, 2006), 4-carboxyimidazolin-2-one **49** (3 g, 23.4 mmol) was suspended in MeOH (60 ml). Thionyl chloride (6 ml, 82.6 mmol) was added slowly and the mixture was refluxed for 4 h. The mixture was concentrated *in vacuo* and dried over phosphorus pentoxide. The residue was recrystallised from MeOH to yield 4-methoxycarbonylimidazolin-2-one **52** (2.66 g, 80 %) as a grey powder; mp 284 - 286 °C dec (Lit. 280 °C (Stanovnik, B., *et al.*, 1979)); ν_{max}(ATR)/cm^{-1} 3144 (NH), 3013 (NH), 1728 (CO), 1670 (CO); δ_H (270 MHz; DMSO) 3.70 (s, 3H, OC*H*$_3$), 7.26 (s, 1H, C*H*), 10.60 (s, br, 1H, N*H*), 10.68 (s, br, 1H, N*H*); δ_C(400 MHz; DMSO) 51.7 (*C*H$_3$), 113.5 (*C*H), 118.6 (*C*), 153.9 (*C*O), 159.5 (*C*O).

1,3-Bis(PMB)-4-methoxycarbonylimidazolin-2-one 52a

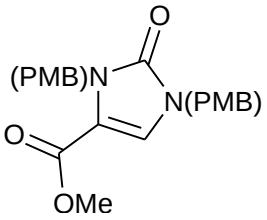

Sodium hydride (60% dispersion in mineral oil, 942 mg, 19.0 mmol) was washed with petroleum ether. The washed NaH was suspended in anhydrous DMF (28.5 ml). 4-Methoxycarbonylimidazolin-2-one **52** (1.12 g, 7.85 mmol) was added. The mixture was stirred under nitrogen for 30 min, by which time a viscous gel had formed. 4-Methoxybenzyl chloride (3.69 g, 19.0 mmol) was added slowly to the mixture and this was left stirring at r.t. under nitrogen for 20 h until the mixture had become a non-viscous liquid again. The mixture was diluted with Et_2O (200 ml), then washed twice with brine, dried with magnesium sulfate and concentrated *in vacuo* to yield a brown oil. This was purified by flash chromatography using

EtOAc-petrol (30:70 to 40:60) to yield a yellow oil (R_f 0.14 in 20% EtOAc in petrol). This was recrystallised from a mixture Et_2O and *n*-hexane to yield 1,3-bis(PMB)-4-methoxycarbonylimidazolin-2-one **52a** as fine white crystals (718 mg, 21%); mp 98.7 – 99.0 °C; IR (ATR) ν_{max}(ATR)/cm^{-1} 1724 (CO), 1676 (CO); δ_H (270 MHz, $CDCl_3$) 3.70 (3 H, s, OCH_3), 3.76 (3 H, s, O*C*H_3), 3.79 (3 H, s, O*C*H_3), 4.76 (2H, s, *C*H_2 (PMB)), 5.16 (2H, s, *C*H_2 (PMB)), 6.91-6.78 (4 H, m, Ar*H*), 6.89 (1 H, s, CH), 7.19 (2 H, d, *J* 8.7 Hz, Ar*H*), 7.32 (2 H, d, *J* 8.6 Hz, Ar*H*); δ_C (100.65 MHz, $CDCl_3$) 45.1 (*C*H_2 (PMB)), 47.2 (*C*H_2 (PMB)), 51.4 (O*C*H_3), 55.2 (O*C*H_3), 55.3 (O*C*H_3), 113.4 (*C*H (Ar)), 114.0 (2 *C*H (Ar)), 114.4 (*C*H (Ar)), 120.1 (*C*H (Ar)), 127.2 (*C*H (Ar)), 129.5 (*C*H (Ar)), 129.6 (2 *C*H (Ar)), 130.2 (*C*)), 153.4 (*C* (Ar)), 158.9 (*C* (Ar)), 159.6 (*C*O), 159.7 (*C*O); m.p 98.7 - 99.0 °C; *m/z* (ESI) found: 383.1602 (M + H^+) ($C_{21}H_{23}N_2O_5$ requires 383.1601).

1,3-Bis(PMB)-4(hydroxymethyl)imidazolin-2-one 53a

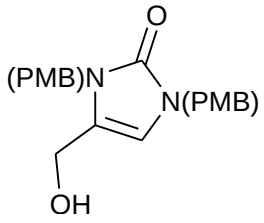

1,3-bis(PMB)-4-methoxycarbonylimidazolin-2-one **52a** (1.00 g, 2.61 mmol) was suspended in anhydrous DCM (19 ml) and cooled to − 78 °C (EtOAc/ice bath) under a nitrogen atmosphere. DIBAL-H (7.8 ml, 7.84 mmol in heptane) was added to the mixture and it was stirred at − 78 °C for 3 h 15 min. MeOH (4.8 ml) was added to quench the reaction. The mixture was allowed to warm to room temperature and then diluted with 2M HCl. The product was partitioned between DCM and water. The aqueous phase was extracted and three further times with DCM. The combined organic extracts were washed twice with brine. The organic phase was dried with sodium sulfate and concentrated *in vacuo* to yield 1,3-bis(PMB)-4-hydroxyimidazolin-2-one as a yellow oil. This was recrystallised from EtOAc and *n*-hexane to yield 1,3-bis(PMB)-4-(hydroxymethyl)imidazolin-2-one **53a** (850 mg, 92 %) as white crystals; m.p. 142.0 - 143.5 °C, ν_{max}(ATR)/cm^{-1} 3270 (OH), 2930 (CH_2), 1656

(CO); δ_H (270 MHz, $CDCl_3$) 3.76 (3 H, s, OCH_3), 3.78 (3 H, s, OCH_3), 4.20 (2 H, d, *J* 5.9 Hz, HOCH_2), 4.71 (2 H, s, CH_2), 4.90 (2 H, s, CH_2), 6.04 (1 H, s, C*H*), 6.78-6.90 (4 H, m, Ar*H* (PMB)), 7.15-7.28 (4 H, m, Ar*H* (PMB)); δ_C (100.65 MHz, $CDCl_3$) 44.5 (*C*H_2), 46.7 (*C*H_2), 55.4 (2 O*C*H_3), 108.9 (*C*H_2), 114.2 (*C*H), 114.3 (*C*H), 122.4 (*C*H), 128.8 (*C*H), 128.9 (*C*H), 129.6 (2 *C*), 129.9 (*C*), 153.8 (*C*) , 159.1 (*C*), 159.3 (*C*O); *m/z* (ESI) found: 355.1654 ($C_{20}H_{23}N_2O_4$ (M + H^+) requires 355.1652).

1,3-Bis(PMB)- 4-formylimidazolin-2-one 38a

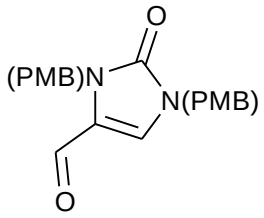

1,3-bis(PMB)-4(hydroxymethyl)imidazolin-2-one **53a** (920 mg, 2.60 mmol) was dissolved in anhydrous DCM (101 ml) under a nitrogen atmosphere. Activated manganese(IV) oxide (2.34 g, 26.9 mmol) was added. The mixture was stirred for 36 h and then filtered through celite with DCM washes. The filtrate was then concentrated *in vacuo* to yield a brown oil. The crude mixture was purified by flash chromatography using EtOAc-petrol (40:60) to yield 1,3-bis(PMB)-4-formylimidazolin-2-one **38a** (670 mg, 73 %) as a yellow oil (R_f 0.47 in 60% EtOAc:petrol); IR (ATR) ν_{max}(ATR)/cm^{-1} 1703 (CO), 1653 (CO); δ_H (270 MHz, $CDCl_3$) 3.75 (3 H, s, OCH_3), 3.78 (3 H, s, OCH_3), 4.78 (2 H, s, CH_2), 5.15 (2H, s, CH_2), 6.94-6.77 (4 H, m, Ar*H*), 6.89 (1 H, s, CH), 7.32 (2 H, d, *J* 8.6 Hz, Ar*H*), 7.38 (2 H, d *J* 8.9 Hz, Ar*H*), 9.12 (1H, s, C*H*O); δ_C (100.65 MHz, $CDCl_3$) 45.5 (*C*H_2), 47.5 (*C*H_2), 55.3 (*C*H_3), 55.4 (*C*H_3), 113.9 (*C*H), 114.6 (2 *C*H), 123.1 (2 *C*H), 127.4 (2 *C*H), 129.9 (2 *C*H), 130.0 (*C*), 153.3 (*C*), 159.2 (2 *C*), 159.9 (2 *C*), 176.8 (*C*O); *m/z* (ESI) found: 353.1499 (M + H^+) ($C_{20}H_{21}N_2O_4$ requires 353.1496).

***N*(α)-Cbz, *N*(π),*N*(τ)-Bis(PMB), α,β-dehydro-4,5-dihydro-2-oxo-His-OMe 40a**

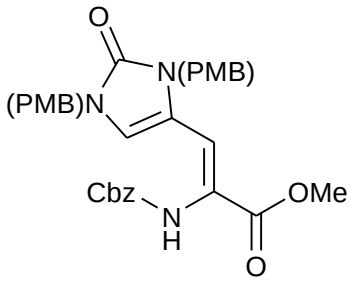

1,3-Bis(PMB)-4-formylimidazolin-2-one **38a** (580 mg, 1.65 mmol) and (±)-benzyloxycarbonyl-α-phosphonoglycine trimethyl ester **39b** (707 mg, 2.13 mmol) were suspended in anhydrous DCM (25 ml) under a nitrogen atmosphere. 1,8-Diazabicyclo[5.4.0]undec-7-ene (DBU) (0.32 ml, 2.13 mmol) was added slowly to the reaction mixture. This was left stirring for 4.5 h. The mixture was concentrated *in vacuo* to a give a yellow oil. Flash chromatography with EtOAc-DCM (20:80 to 100:0) yielded N(*α*)-Cbz, N(*π*),N(*τ*)-bis(PMB)-α,β-dehydro-oxo-His-OMe **40a** (840 mg, 91 %) as a yellow powdery solid (R_f 0.17 in 20% EtOAc-DCM); mp. 53.0 - 54.5°C; ν_{max}(ATR)/cm^{-1} 3252 (NH), 1725 (CO), 1682 (CO), 1632 (CO); δ_H (270 MHz, $CDCl_3$) 3.71 (3 H, s, OC*H*$_3$), 3.76 (3 H, s, OC*H*$_3$), 3.78 (3 H, s, OC*H*$_3$), 4.70 (2 H, s, C*H*$_2$ (PMB)), 4.88 (2 H, s, C*H*$_2$ (PMB)), 5.04 (s, 2H, C*H*$_2$ (Cbz)), 5.93 (1 H, s, br, N*H*), 6.49 (1 H, s, br, Im 5-*H*), 6.83 (4 H, d, *J* 7.9 Hz, Ar*H*), 7.40-7.06 (9 H, m, Ar*H*); δ_C (100.65 MHz, DMSO) 44.3 (*C*H$_2$ (PMB)), 47.1 (*C*H$_2$ (PMB)), 52.9 (O*C*H$_3$), 55.3 (2 O*C*H$_3$), 67.6 (*C*H$_2$ (Cbz)), 114.3 (2 *C*H (Ar)), 114.3 (2 *C*H (Ar)), 116.3 (*HC*-5), 117.6 (*C* (Ar)), 119.5 (β-*C*H), 121.0 (α-*C*), 128.2 (*C* (Ar)), 128.3 (2 *C*H (Ar)), 128.4 (2 *C*H (Ar)), 128.6 (2 *C*H (Ar)), 128.6 (2 *C*H (Ar)), 128.9 (*C* (Ar)), 129.4 (*C*H (Ar)), 152.6 (*C* (Ar)), 153.9 (*C* (Ar)), 159.2 (*C* (Ar)), 159.4 (*C*O), 165.0 (*C*O). Assignments based on 1D spectra, DEPT-135, COSY and HSQC analysis; *m/z* (EI) found: 558.2228 (M + H$^+$) ($C_{31}H_{32}N_3O_7$ requires 558.2235).

Hydrogenation of
***N*(α)-Cbz, *N*(π),*N*(τ)-Bis(PMB), α,β-dehydro-4,5-dihydro-2-oxo-His-OMe 40a**

The dehydro-derivative **40a** (340 mg, 0.609 mmol) and Adam's catalyst (PtO_2) (42.5 mg, 0.241 mmol) were suspended in methanol (42.5 ml) in a two-necked flask and stirred. The flask was evacuated via a three way tap and then connected to a hydrogen balloon (1 atm) for 4.5 h at r.t.. The mixture was then filtered through celite and concentrated *in vacuo* to yield a brown oil. This was purified by flash chromatography using EtOAc-DCM (10:90 to 30:70) to yield three colourless oils:

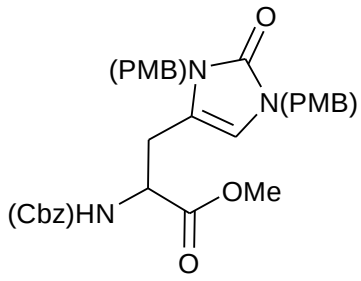

i) *N*(α)-Cbz, *N*(π), *N(τ)*-Bis(PMB)-2-oxo-His-OMe **4d** (140 mg, 38 %) (R_f 0.18 in 1:4 EtOAc-DCM); mp 110.5 – 111.5 °C; ν_{max}(ATR)/cm^{-1} 3179 (NH), 1739 (CO), 1713 (CO), 1655 (CO); δ_H(400 MHz; $CDCl_3$) 2.58 (1 H, dd, *J* 15.5 Hz and 6.3 Hz, β-C*H*H), 2.69 (1 H, dd, *J* 15.5 Hz and 5.2 Hz, β-CH*H*), 3.51 (3 H, s, OCH_3), 3.67 (3 H, s, OCH_3), 3.68 (3 H, s, OCH_3), 4.27-4.38 (1 H, m, α-C*H*), 4.59-4.62 (3 H, m, 1.5 CH_2 (PMB)), 4.77 (1H, d, *J* 16.0 Hz, C*H*H (PMB)), 4.98 (2 H, s, CH_2 (Cbz)), 5.26-5.34 (1 H, m, α-N*H*), 5.79 (1 H, s, Im 5-*H*), 6.73 (2 H, d, *J* 8.7 Hz, 2 Ar*H* (PMB)), 6.76 (2 H, d, *J* 8.7 Hz, 2 Ar*H* (PMB)), 7.04 (2 H, d, *J* 8.3 Hz, 2 Ar*H* (PMB)), 7.08 (2 H, d, *J* 8.3 Hz, 2 Ar*H* (PMB)), 7.22-7.28 (5 H, m, 5 Ar*H* (Cbz)); δ_C(100.65 MHz; $CDCl_3$) 28.1 (β-*C*H_2), 44.2 (*C*H_2 (PMB)), 46.6 (*C*H_2 (PMB)), 52.4 (α-*C*H), 52.9 (O*C*H_3), 55.25 (O*C*H_3), 55.27 (O*C*H_3), 67.2 (*C*H_2 (Cbz)), 108.2 (*HC*-5), 114.1 (2 *C*H (Ar)), 117.8 (*C*-4), 128.1 (2 *C*H (Ar)), 128.3 (2 *C*H (Ar)), 128.4 (2 *C*H (Ar)), 128.6 (2 *C*H (Ar)), 129.1 (*C* (Ar)), 129.3 (2 *C*H (Ar)), 129.5 (*C* (Ar)), 136.1 (*C* (Ar)), 153.6 (*C* (Ar)), 155.6 (*C* (Ar)), 159.0 (*C*O), 159.2 (*C*O), 171.5 (*C*O). Assignments based on 1D spectra, DEPT-135, COSY and HSQC analysis; *m/z* (ESI) found: 560.2383 ($M + H^+$) ($C_{31}H_{34}N_3O_7$ requires 560.2391).

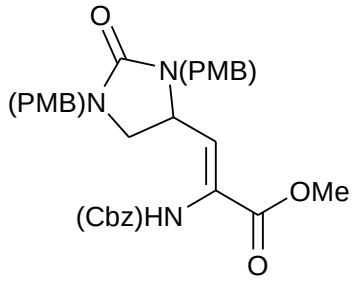

ii) *N*(α)-Cbz, *N*(π), *N*(τ)-Bis(PMB)-α,β-dehydro-4,5-dihydro-2-oxo-His-OMe **60** (100 mg, 21 %) (R_f 0.74 in 20 % EtOAc-DCM); mp 100 -104 °C; ν_{max}(ATR)/cm^{-1} 3208 (NH), 1740 (CO), 1716 (CO), 1664 (CO); δ_H(400 MHz; $CDCl_3$) 2.86 – 2.93 (1 H, m, Im 5-*H*H), 3.33 – 3.44 (1 H, m, Im 5-*H*H), 3.67 (3 H, s, OCH_3), 3.67 (3 H, s, OCH_3), 3.72 (3 H, s, OCH_3), 3.93 (1 H, d, *J* 14.8 Hz, C*H*H (PMB)), 4.06 (1 H, ddd, *J* 9.6 Hz, 6.8 Hz and 6.8 Hz, Im 4-*H*), 4.19 (1 H, d, *J* 14.8 Hz, C*H*H (PMB)), 4.33 (1 H, d, *J* 14.4 Hz, C*H*H (PMB)), 4.44 (1 H, d, *J* 14.8 Hz, C*H*H (PMB)), 4.99 (2 H, s, CH_2 (Cbz)), 6.13 (1 H, d, *J* 9.6 Hz, β-C*H*), 6.27 (1 H, s br, α-N*H*), 6.72 (2 H, d, *J* 6.8 Hz, 2 Ar*H* (PMB)), 6.78 (2 H, d, *J* 8.8 Hz, 2 Ar*H* (PMB)), 7.05 (2 H, d, *J* 8.4 Hz, 2 Ar*H* (PMB)), 7.12 (2 H, d, *J* 8.4 Hz, 2 Ar*H* (PMB)), 7.20-7.31 (5 H, m, 5 Ar*H* (Cbz)); δ_C(100.65 MHz; $CDCl_3$, TMS) 46.3 (H_2C-5), 46.8 (*C*H_2 (PMB)), 47.6 (*C*H_2(PMB)), 51.1 (H*C*-4), 52.8 (O*C*H_3), 55.2 (O*C*H_3), 55.3(O*C*H_3), 67.7 (*C*H_2(Cbz)), 113.8 (2 *C*H (Ar)), 114.0 (2*C*H (Ar)), 128.1 (2 *C*H (Ar)), 128.5 (2 *C*H (Ar)), 128.6 (2 *C*H (Ar)), 129.0 (2 *C* (Ar)), 129.3 (2 *C* (Ar)), 129.7 (2 *C*H (Ar)), 130.0 (2 *C*H (Ar)), 130.2 (β-*C*H), 135.5 (*C* (Ar)), 154.3 (*C*O), 159.0 (2 *C* (Ar)), 160.2(*C*O), 164.3 (*C*O). Assignments based on 1D spectra, DEPT-135, COSY and HSQC analysis; *m/z* (ESI) found: 560.2392 ($M + H^+$) ($C_{31}H_{34}N_3O_7$ requires 560.2391).

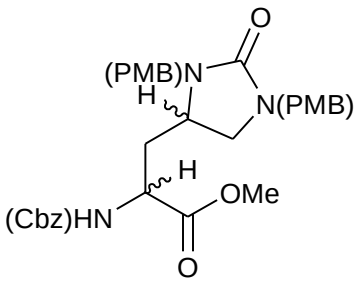

iii) *N*(α)-Cbz, *N*(π), *N(τ)*-Bis(PMB)-4,5-dihydro-2-oxo-His-OMe **61** (150 mg, 41 %, R_f 0.54 in 20 % EtOAc-DCM); 45:55 mixture of two diastereomers; mp 100.0 - 104.0 °C; ν_{max}(ATR)/cm^{-1} 3150 (NH), 1738 (CO), 1714 (CO), 1690

(CO); δ_H(400 MHz; $CDCl_3$); 1.59 (1 H, ddd, *J* 13.6 Hz, 7.6 Hz, 2.8 Hz, β-CH*H*), 2.20 (1 H, ddd, *J* 13.6 Hz, 6.8 Hz, 2.4 Hz, β-C*H*H), 2.74 (1 H, dd, *J* 8.4 Hz, 8.4 Hz, Im 5-*H*H), 3.14 (1H, dd, *J* 8.4 Hz and 8.4 Hz, Im 5-H*H*), 3.23-3.34 (1H, m, Im 4-*H*), 3.69 (3 H, s, OCH_3), 3.72 (3 H, s, OCH_3), 3.73 (3 H, s, OCH_3), 3.85 (1 H, d, *J* 9.2 Hz, C*H*H (PMB)), 3.89 (1 H, d, *J* 9.2 Hz, CH*H* (PMB)), 4.12-4.20 (1 H, m, α-C*H*), 4.65 (2H, s, CH_2 (PMB)), 5.00 (2 H, s, CH_2 (Cbz)), 6.73 – 6.83 (4H, m, 4 Ar*H* (PMB)), 7.07 – 7.15 (4H, m, 4 Ar*H* (PMB)), 7.24 - 7.31 (5 H, m, 5 Ar*H* (Cbz)); δ_C(100.65 MHz; $CDCl_3$); 45.2 (CH_2 (PMB)), 45.4 (CH_2 (PMB)), 47.5 (H_2C-5), 49.8 (H*C*-4), 51.3 (α-*C*H), 52.6 (OCH_3), 52.8 (OCH_3), 53.5 (β-CH_2), 55.3 (OCH_3), 67.2 (CH_2 (Cbz)) 114.0 (*C*H (Ar)), 128.1 (2 *C*H (Ar)), 128.2 (2 *C*H (Ar)), 128.4 (2 *C*H (Ar)), 128.6 (2 *C*H (Ar)), 129.0 (4 *C* (Ar)), 129.5 (2 *C*H (Ar)), 129.6 (2 *C*H (Ar)), 159.0 (*C* (Ar)), 160.5 (*C*O), 171.2 (*C*O), 172.1 (*C*O). Assignments based on 1D spectra, DEPT-135, COSY and HSQC analysis; *m/z* (ESI) found: 562.2547 ($M + H^+$) ($C_{31}H_{36}N_3O_7$ requires 562.2548).

Attempted mesylation/tosylation of 1,3-Bis(PMB)-4-(hydroxymethyl)imidazolin-2-one 53a: formation of 1, 3-bis(PMB)-5-methylimidazolidin-2,4-dione 74a

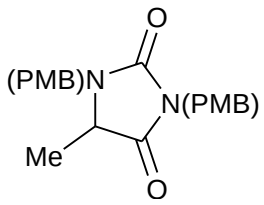

This dione was produced by two similar methods which both aimed to activate the alcohol of 1,3-bis(PMB)-4-(hydroxymethyl)imidazolin-2-one **53a**:

(A) 1,3-Bis(PMB)-4-(hydroxymethyl)imidazolin-2-one **53a** (110 mg, 0.268 mmol) was dissolved in anhydrous DCM (2 ml) and placed under a nitrogen atmosphere. The mixture was cooled to 0 °C and triethylamine (87.7 μl, 0.630 mmol) was added. Mesyl chloride (40.3 μl, 0.521 mmol) was added and the mixture was left for 120 h. The product was then partitioned between DCM and 2M HCl and extracted into the organic layer. The aqueous layer was washed twice with DCM

and these washings were added to the final organic layer. The combined organic extracts were dried with $MgSO_4$ and concentrated *in vacuo* to yield a brown oil. This was purified using flash chromatography with EtOAc-petrol (30:70 to 50:50) to yield 1,3-bis(PMB)-5-methylimidazolidin-2,4-dione **74a** (24 mg, 25 %) as a yellow oil (R_f 0.31 in 3:1 EtOAc-petrol); δ_H (400 MHz, $CDCl_3$) 1.30 (3 H, d, *J* 7 Hz, C*H*$_3$CH), 3.70 (1 H, q, *J* 8.7 Hz, CH$_3$*H*), 3.77 (6 H, s, 2 OC*H*$_3$), 4.47 (2 H, d, *J* 14.3 Hz, CH*H* (PMB)), 4.59 (2 H, d, *J* 14.3 Hz, CH*H* (PMB)), 6.83 (4 H, d, *J* 8.6 Hz, Ar*H*), 7.15 (2 H, d, *J* 8.6 Hz, Ar*H*), 7.34 (2 H, d, *J* 8.6 Hz, Ar*H*); *m/z* (ESI) found: 355.1656 ($M + H^+$) ($C_{20}H_{23}N_2O_4$ requires 355.1652).

(B) Sodium hydride (60% dispersion in mineral oil; 17.6 mg, 0.732 mmol) was washed with petroleum spirit. The washed NaH was suspended in anhydrous Et_2O (14 ml) under a nitrogen atmosphere and 1,3-bis(PMB)-4-(hydroxymethyl)imidazolin-2-one **53a** (150 mg, 0.365 mmol) was added. Tosyl chloride (83.7 mg, 0.439 mmol), which was purified first by washing with DCM and petrol and removing any precipitates of toluenesulfonic acid, was added and the mixture was left for 36 h. ^{1}H-NMR showed only starting material so more tosyl chloride (83.7 mg, 0.439 mmol) and a different base, pyridine (34.7 mg, 0.439 mmol) was added and the mixture was left stirring at r.t. for 24 h. The product was then partitioned between DCM and 2M HCl and extracted into the organic layer. The aqueous layer was washed twice with DCM and these washings were added to the final organic layer. This organic layer was dried with $MgSO_4$ and concentrated *in vacuo* to yield a brown oil. This was purified using flash chromatography with EtOAc-petrol (20:80 to 40:60) to yield 1,3-bis(PMB)-5-methylimidazolidin-2,4-dione (**74a**) (70 mg, 54 %) as a yellow oil (R_f 0.12 in 40:60 EtOAc-petrol); IR (ATR) ν_{max}(ATR)/cm^{-1} 2936 (NH), 2838 (NH), 1768 (CO), 1704 (CO); δ_H (400 MHz, $CDCl_3$) 1.24 (3 H, d, *J* 9.4 Hz, C*H*$_3$CH), 3.66 (1 H, q, *J* 9.4 Hz, CH$_3$C*H*), 3.70 (6 H, s, 2 OCH$_3$), 3.99 (2 H, d, *J* 10.1 Hz, CH*H* (PMB)), 4.49 (2 H, d, *J* 9.4 Hz, C*H*H (PMB)), 4.56 (2 H, d, *J* 9.5 Hz, CH*H* (PMB)), 4.81 (2 H, d, *J* 10.3 Hz, CH*H* (PMB)), 6.75 – 6.78 (4 H, m, Ar*H*), 7.08 (2 H, d, *J* 8.6 Hz, Ar*H*), 7.27 (2 H, d, *J* 8.6 Hz, Ar*H*); δ_C (100.65 MHz, $CDCl_3$) 15.1 (*C*H$_3$CH), 42.0 (*C*H$_2$ (PMB)), 44.0 (*C*H$_2$ (PMB)), 54.7 (*C*HCH$_3$),

55.26 (O*C*H_3), 55.30 (O*C*H_3), 114.0 (2 *C*H (Ar)), 114.3 (2 *C*H (Ar)), 128.5 (*C* (Ar)), 129.5 (2 *C*H (Ar)), 129.7 (*C* (Ar)), 130.1 (2 *C*H (Ar)), 156.1 (*C*O), 159.3 (*C* (Ar)), 159.4 (*C* (Ar)), 173.4 (*C*O). Assignments based on 1D spectra, DEPT-135, COSY and HSQC analysis.

N-(Benzyloxycarbonyl)-*α*-hydroxyglycine 57

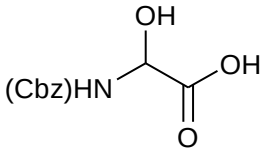

The title compound was synthesised from benzyl carbamate **55** (6.4 g, 42.3 mmol) and glyoxylic acid monohydrate 5**6** (4.3 g, 46.7 mmol) using the procedure described by Williams *et al.* (Williams, R. M., *et al.*, 1990) and obtained as a white powder (7.97 g, 84 %); mp 194.3 °C dec. (Lit. 196 – 198 °C dec. (Zoller, U. and Ben-Ishai, D., 1975)); ν_{max}(ATR)/cm^{-1} 3328 (NH), 1724 (CO), 1699 (CO); δ_H(270 MHz, $CDCl_3$) 3.40 (1 H, s br, O*H*), 5.05 (2 H, s, CH_2), 5.22 (1 H, d, *J* 8.9 Hz, C*H*), 7.43-7.28 (5 H, m, Ar*H*), 8.12 (1 H, d br, *J* 8.6 Hz, N*H*).

Ethyl *N*-(benzyloxycarbonyl)-*α*-ethoxyglycinate 58

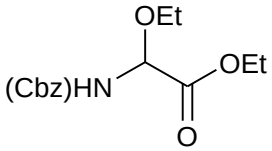

Using the method described by Williams *et al.*.(Williams, R. M., *et al.*, 1990) to synthesise ethyl *N*-(benzyloxycarbonyl)-*α*-methoxyglycinate but using ethanol (100 ml) in place of methanol, with *N*-(benzyloxycarbonyl)-*α*-hydroxyglycine 57 (6.00 g, 26.6 mmol) and concentrated sulfuric acid (1 ml), ethyl *N*-benzyloxycarbonyl-*α*-ethoxyglycinate **58** (7.43 g, 86 %) was obtained as a white powder; mp 69 - 70 °C (Lit. 71 – 72 °C (Kawai, M., *et al.*, 1996)); δ_H (270 MHz, $CDCl_3$) 1.21 (3 H, t, *J* 6.9 Hz, $HCOCH_2CH_3$), 1.29 (3 H, t, *J* 7.2 Hz, $OCOCH_2CH_3$), 3.60-3.80 (2 H, m, $HCOCH_2CH_3$), 4.22 (2 H, q, *J* 7.2 Hz, $OCOCH_2CH_3$), 5.12 (2 H, s, $ArCH_2$), 5.38 (1 H, d, *J* 9.4 Hz, C*H*), 5.94 (1 H, d, *J* 9.4 Hz, N*H*), 7.40-7.26 (5 H, m, Ar*H*).

Ethyl *N*-(benzyloxycarbonyl)-*α*-diethoxyphosphinylglycinate 39a

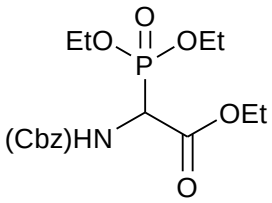

The title compound was prepared by analogy with the method described by Coleman and Carpenter (Coleman, R. S. and Carpenter, A. J., 1993) for making methyl *N*-(benzyloxycarbonyl)-*α*-dimethoxyphosphinylglycinate, but using ethyl esters. Thus reaction of phosphorus trichloride (1.97 ml, 5.79 mmol) and *N*-(benzyloxycarbonyl)-*α*-ethoxyglycinate **58** (2.00 g, 5.79 mmol) followed by addition of triethyl phosphite (1.46 ml, 5.79 mmol) gave ethyl *N*-(benzyloxycarbonyl)-*α*-diethoxyphosphinylglycinate **39a** (2.27 g, 92 %) as a colourless oil; δ_H (270 MHz, $CDCl_3$) 1.01-1.04 (9 H, m, 3 OCH_2CH_3), 4.01-4.18 (4 H, m, 2 $POCH_2CH_3$), 4.24 (2 H, q, *J* 7.2 Hz, $COCH_2CH_3$), 4.85 (1 H, d, *J* 9.4 Hz, PCH), 5.06 (1 H, d, *J* 12.1 Hz, ArC*H*H), 5.13 (1 H, d, *J* 12.1 Hz, ArCH*H*) 5.64 (1 H, d, *J* 9.4 Hz, N*H*), 7.33-7.25 (5 H, m, Ar*H*); δ_P (109.3 MHz, $CDCl_3$) 16.5 ($PO(OEt)_2$), 7.9 ($O{=}PH.(OEt)_2$ impurity, 17.6% peak intensity of δ 16.5 peak).

Methyl *N*-(acetyl)-*α*-dimethyoxyphosphinylglycinate 39c

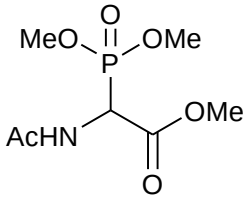

(±)-Benzyloxycarbonyl-α-phosphonoglycine trimethyl ester **39b** (2.00 g, 6.04 mmol), acetic anhydride (2.85 ml, 30.2 mmol) and 10 % palladium on carbon catalyst (100 mg) were suspended in acetic acid (17.3 ml). The flask was evacuated and then placed under hydrogen (1 atm) for 17 h. The mixture was then filtered through celite and concentrated *in vacuo* to yield a brown oil. This was recrystallised from EtOAc and hexane to yield methyl *N*-(acetyl)-*α*-dimethoxyphosphinylglycinate **39c** (1.13 g, 78 %) as a white powder; mp 85 – 86 °C (Lit. 88 – 89 °C (Schmidt, U., *et al.*, 1984), Lit. 88.0 -

88.5 °C (Mazurkiewicz, R. and Kuznik, A., 2006);; δ_H(270 MHz; $CDCl_3$) 2.06 (3 H, s, C*H*$_3$ (Ac)), 3.78 (3 H, d, *J* 5.4 Hz, POC*H*$_3$), 3.81 (3 H, s, OCOC*H*$_3$), 3.82 (3 H, d, *J* 5.4 Hz, POC*H*$_3$) 5.22 (1 H, dd, *J* 22.2 Hz, 8.9 Hz, HNC*H*CO), 6.45 (1 H, d, *J* 8.9 Hz, N*H*); δ_P (109.3 MHz, $CDCl_3$) 20.0 ($PO(OEt)_2$).

N(α)-Ac, *N(π),N(τ)*-Bis(PMB), α,β-dehydro-oxo-His-OMe 40b

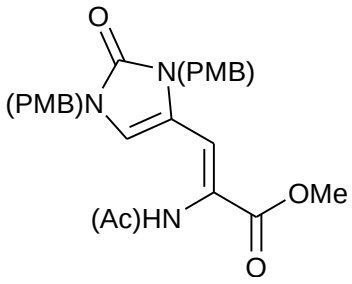

1,3-Bis(PMB)-4-formylimidazolin-2-one **38a** (240 mg, 0.681 mmol) and ethyl *N*-(acetyl)-*α*-dimethy(oxyphosphinyl)glycinate **39c** (243 mg, 1.02 mmol) were suspended in anhydrous DCM (12.0 ml) under a nitrogen atmosphere. 1,8-Diazabicyclo[5.4.0]undec-7-ene (DBU) (115 mg, 1.02 mmol) was added slowly to the reaction mixture. This was left stirring for 20 h. The mixture was concentrated *in vacuo* to yield a yellow oil. This was purified using flash chromatography with EtOAc-DCM (40:60 to 70:30) to yield *N(α)*-Ac, *N(π),N(τ)*-Bis(PMB), α,β-dehydro-oxo-His-OMe **40b** (190 mg, 60 %) as a white powder (R_f 0.19 in 40:60 EtOAc-DCM); mp 198 – 201 °C; ν_{max}(ATR)/cm^{-1} 3253 (NH), 1701 (CO), 1655 (CO), 1644 (CO); δ_H(400 MHz, $CDCl_3$) 1.92 (3 H, s br, C*H*$_3$CO), 3.67 (3 H, s, OC*H*$_3$), 3.70 (3 H, s, OC*H*$_3$), 3.72 (3 H, s, OC*H*$_3$), 4.70 (2 H, s, C*H*$_2$ (PMB)), 4.81 (2 H, s, C*H*$_2$ (PMB)), 6.28 (1 H, s br, β-C*H*), 6.77 (2 H, d, *J* 8.8 Hz, 2 Ar*H* (PMB)), 6.80 (2 H, d, *J* 8.8 Hz, 2 Ar*H* (PMB)), 6.90 (1 H, s br, α-N*H*), 7.05 (1 H, s br, Im 5-*H*), 7.12 (2 H, d, *J* 8.8 Hz, 2 Ar*H* (PMB)), 7.13 (2 H, d, *J* 8.8 Hz, 2 Ar*H* (PMB)); δ_C(100.65 MHz; $CDCl_3$); 44.3 (*C*H_2 (PMB)), 47.2 (*C*H_2 (PMB)), 52.6 (O*C*H_3), 55.28 (O*C*H_3), 55.34 (O*C*H_3), 114.2 (*C*H (Ar)), 114.3 (*C*H (Ar)), 116.4 (β-*C*H), 117.5 (*C* (Ar)), 119.3 (H*C*-5), 120.8 (α-*C*), 127.9 (*C* (Ar)), 128.6 (*C*H (Ar)), 128.9 (*C* (Ar)), 129.7 (*C*H (Ar)), 152.6 (*C*O), 159.2 (*C* (Ar)), 159.5 (*C* (Ar)), 165.1 (*C*O), 168.0 (*C*O). Assignments based on 1D

spectra, DEPT-135, COSY and HSQC analysis; *m/z* (EI) found: 465.1890 ($M + H^+$) ($C_{25}H_{27}N_3O_6$ requires 465.1894).

Attempted deprotection of 1,3-bis(PMB)-4-methoxycarbonylimidazole 52a using TFA

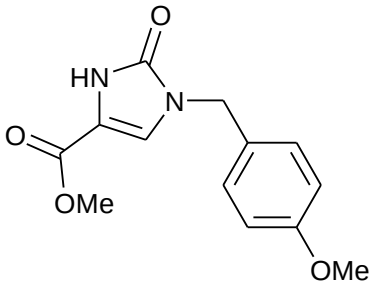

1,3-Bis(PMB)-4-methoxycarbonylimidazolin-2-one **52a** (60 mg, 0.157 mmol) was dissolved in a mixture of trifluoroacetic acid (1.9 ml) and thiophenol (32.1 µl, 0.314 mmol). This was refluxed under nitrogen for 51 h. Et_2O (~ 5 ml) was added gradually. The resultant white precipitate was filtered off and dried to give 1-PMB-4-methoxycarbonylimidazolin-2-one **70** (24.6 mg, 60%) a white solid; mp 172 - 173 °C; ν_{max}(ATR)/cm^{-1} 1717 (NH), 1676 (CO); δ_H(400 MHz, DMSO) 3.71 (3 H, s, OC*H*$_3$ (PMB)), 3.74 (3 H, s, CO_2CH_3 (OMe)), 4.68 (2 H, s, C*H*$_2$ (PMB)), 6.91 (1 H, d, *J* 8.8 Hz, Ar*H* (PMB)), 7.25 (1 H, d, *J* 8.8 Hz, Ar*H* (PMB)), 7.48 (1 H, s, HNCC*H*), 10.90 (1 H, s br, N*H*); δ_C(100.65 MHz; DMSO) 45.5 (*C*H$_2$ (PMB)), 51.3 (*C*H$_3$ (PMB)), 55.1 (*C*H$_3$ (OMe)), 112.1 (*C* (Ar)), 114.0 (*C*H (Ar)), 120.9 (H*C*-5), 129.2 (*C*H (Ar)), 152.7 (*C* (Ar)), 158.7 (*C* (Ar)), 159.3 (*C* (Ar)); 1D-NOE (400 MHz, DMSO), irradiated at δ 7.47 (HNCC*H*), NOE observed at δ 4.68 (1.33%, C*H*$_2$ (PMB)); *m/z* (ESI) found: 263.1031 ($M + H^+$) ($C_{13}H_{15}N_2O_4$ requires 263.1032).

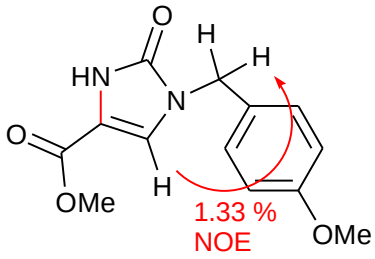

Attempted deprotection of 1,3-Bis(PMB)-4-methoxycarbonylimidazolin-2-one 52a using CAN

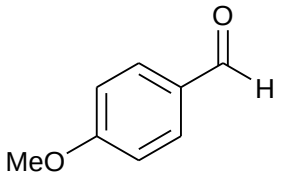

1,3-Bis(PMB)-4-methoxycarbonylimidazolin-2-one **52a** (200 mg, 0.523 mmol) was dissolved in a mixture of acetonitrile (12.7 ml) and water (3.91 ml). Cerium(IV) diammonium nitrate (2.29 g, 4.18 mmol) was added and the solution was stirred for 3 h at room temperature. The product was concentrated *in vacuo*. The resulting oil was then partitioned between EtOAc and water and extracted into the organic layer. This was then concentrated *in vacuo* and dried *in vacuo* over phosphorus pentoxide to yield 4-methoxybenzaldehyde **64** (200 mg, 99 %) as a colourless oil; δ_H(270 MHz, $CDCl_3$) 3.90 (3 H, s, OC*H*$_3$), 6.99 (2 H, d, *J* 8.9 Hz, Ar*H*), 7.83 (2 H, d, *J* 8.9 Hz, Ar*H*), 9.84 (1 H, s, C*H*O), which matches literature data (Moorthy, J. N., *et al.*, 2010).

Attempted deprotection of *N*(α)-Cbz, *N*(τ),*N*(π)-Bis(PMB)-2-oxo-His-OMe 4d using 8 mol. eq. CAN

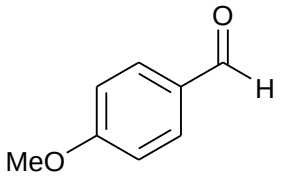

N(α)-Cbz, *N*(τ),*N*(π)-Bis(PMB)-2-oxo-His-OMe **4d** (60 mg, 0.107 mmol) was dissolved in a mixture of acetonitrile (2.6 ml) and water (0.8 ml). Cerium(IV) diammonium nitrate (469.3 mg, 0.856 mmol) was added and the solution was stirred for 3 h at room temperature. The mixture was then poured into water (4 ml) and EtOAc (4 ml) and then extracted into the organic layer. This organic layer was washed with saturated aqueous sodium hydrogen carbonate and water. It was then dried over $MgSO_4$. This was concentrated *in vacuo* to yield 4-methoxybenzaldehyde **64** (14 mg, 96 %) as a brown oil;; δ_H(270 MHz, $CDCl_3$)

3.87 (3 H, s, OC*H*$_3$), 6.98 (2 H, d, *J* 8.7 Hz, Ar*H*), 7.81 (2 H, d, *J* 8.7 Hz, Ar*H*), 9.85 (1 H, s, C*H*O), which matches literature data (Moorthy, J. N., *et al.*, 2010).

Attempted deprotection of *N*(α)-Cbz, *N*(τ),*N*(π)-Bis(PMB)-2-oxo-His-OMe 4d using 4 mol. eq. CAN

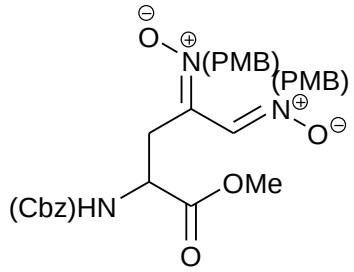

N(α)-Cbz, *N*(τ),*N*(π)-Bis(PMB)-2-oxo-His-OMe **4d** (60 mg, 0.107 mmol) was dissolved in a mixture of acetonitrile (2.6 ml) and water (790 μl). Cerium(IV) diammonium nitrate (235 mg, 0.428 mmol) was added and the solution was stirred for 30 min at room temperature. The mixture was then concentrated *in vacuo* and washed through a silica plug with acetonitrile. The eluate was diluted with DCM, washed with water to remove cerium ions and then was purified by flash chromatography, first using EtOAc-DCM (5:95 to 10:90) and then using methanol-$CHCl_3$ (2:98 to 5:95). This yielded 2-carboxybenzylamino-4,5-bis-(PMB-imino)pentanoic-acid methyl ester *N*(4), *N*(5)-dioxide **66** (2 mg, 3.3 %) as a colourless oil (R_f 0.11 in 2 % methanol-$CHCl_3$); ν_{max}(ATR)/cm^{-1} 1766 (C=O), 1704 (C=O), 1613 (C=N); δ_H(400 MHz; $CDCl_3$) 2.76 (1 H, d, *J* 16.4 Hz, N=CC*H*H), 3.00 (1 H, dm, *J* 16.4 Hz, N=CCH*H*), 3.66 (3 H, s, OC*H*$_3$), 3.69 (3 H, s, OC*H*$_3$), 3.71 (3 H, s, OC*H*$_3$), 4.51-4.57 (1 H, m, *H*CCH$_2$), 4.59 (2 H, s, C*H*$_2$ (PMB)), 4.67 (2 H, s, C*H*$_2$ (PMB)), 5.04 (2 H, s, C*H*$_2$ (Cbz)), 5.74 (1 H, d, *J* 7.2 Hz, N*H*), 6.67 (2 H, d, *J* 8.4 Hz, 2 Ar*H* (PMB)), 6.72 (2 H, d, *J* 8.4 Hz, 2 Ar*H* (PMB)), 6.92 (2H, d, *J* 7.6 Hz, 2 Ar*H* (PMB)), 7.12 (2H, d, *J* 7.6 Hz, 2 Ar*H* (PMB)), 7.25 – 7.32 (5 H, m, 5 Ar*H* (Cbz)), 8.64 (1H, s, *H*C=N); *m/z* (ESI) found: 564.2335 (M + H$^+$) ($C_{30}H_{34}N_3O_8$ requires 564.2340), 581.2599 (M + NH_4^+) ($C_{30}H_{37}N_4O_8$ requires 581.2611), 586.2149 (M + Na$^+$) ($C_{30}H_{33}N_3O_8Na$ requires 586.2165).

2,4-dimethoxybenzyl chloride 69

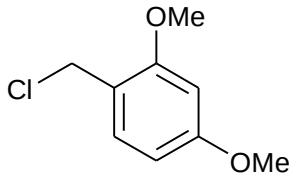

The title compound was synthesised using the procedure described by Nicoletti *et al.* (Nicoletti, T. M., *et al.*, 1990). 2,4-dimethoxybenzyl alcohol (1.00 g, 5.95 mmol), anhydrous thionyl chloride (910 µl, 12.6 mmol) and anhydrous pyridine (1 ml) were reacted in anhydrous DCM (6.5 ml) and yielded 2,4-dimethoxybenzyl chloride **69** (820 mg, 74 %) as a yellow oil; δ_H(270 MHz, $CDCl_3$) 3.80 (3 H, s, OC*H*$_3$), 3.85 (3 H, s, OC*H*$_3$), 4.62 (2 H, s, C*H*$_2$), 6.45 (1 H, d, *J* 5.4 Hz, Ar*H*), 6.46 (1 H, d, *J* 8.1 Hz, Ar*H*), 7.24 (1 H, d, *J* 8.9 Hz, Ar*H*) which matched the literature data (Nicoletti, T. M., *et al.*, 1990).

3,4-dimethoxybenzyl chloride 70

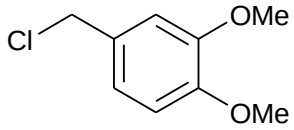

The title compound was synthesised using the procedure described by Howell *et al.* (Howell, S. J., *et al.*, 2001). 3,4-dimethoxybenzyl alcohol (1.00 g, 5.95 mmol), triethylamine (0.93 ml, 6.66 mmol) and thionyl chloride (0.66 ml, 9.09 mmol) were reacted in DCM (12.1 ml) and yielded 3,4-dimethoxybenzyl chloride **70** (510 mg, 46 %) as an off-white powder; δ_H(270 MHz, $CDCl_3$) 3.87 (3 H, s, OCH_3), 3.89 (3 H, s, OCH_3), 4.56 (2 H, s, CH_2), 6.81 (1 H, d, *J* 7.9 Hz, Ar*H*), 6.91 (1 H, s, Ar*H*), 6.92 (1 H, d, *J* 7.9 Hz, Ar*H*), which matched the literature data (Howell, S. J., *et al.*, 2001).

Protection of 4-methoxycarbonylimidazolin-2-one 52 with benzyl chloromethyl ether

Based on the literature preparation by Dransfield *et al.* (Dransfield, P. J., *et al.*, 2006), sodium hydride (60 % dispersion in mineral oil, 507 mg, 21.1 mmol) was

washed with petroleum spirit. The washed NaH was suspended in anhydrous DMF (26 ml). 4-Methoxycarbonylimidazolin-2-one **52** (1.00 g, 7.04 mmol) was added. The mixture was stirred under nitrogen for 30 min by which time a viscous gel had formed. Benzyl chloromethyl ether (2.9 ml, 21.1 mmol) was added slowly to the mixture and this was left stirring at r.t. under nitrogen for 18 h until the mixture has become a non-viscous liquid again. The mixture was diluted with Et_2O (30 ml), then washed twice with brine, dried with magnesium sulfate and concentrated *in vacuo* to yield a brown oil. This was purified by flash chromatography using EtOAc-petrol (30:70) to yield two products:

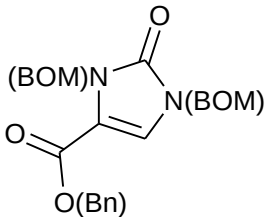

i) 1,3-Bis(BOM)-4-benzyloxycarbonylimidazolin-2-one **68** (586 mg, 17 %) as a colourless oil (R_f 0.45 in 40 % EtOAc-petrol); δ_H(400MHz; $CDCl_3$) 4.57 (2 H, s, C*H*$_2$ (BOM)), 4.63 (2 H, s, C*H*$_2$ (BOM)), 4.74 (2 H, s, C*H*$_2$ (BOM)), 5.13 (2 H, s, C*H*$_2$ (BOM)), 5.52 (4 H, s, 2 C*H*$_2$OBn), 7.09 (1 H, s, HNCC*H*), 7.23 – 7.41 (15 H, m, Ar*H* (BOM)); δ_C(100.65 MHz; $CDCl_3$); 71.2 (*C*H_2), 71.3 (*C*H_2), 71.4 (*C*H_2), 72.3 (*C*H_2), 72.8 (*C*H_2), 88.7 (*C*H_2), 114.0 (*C*H), 121.1 (*C*H), 127.68 (2 *C*H), 127.72 (2 *C*H), 127.88 (4 *C*H), 127.91 (*C*H), 128.06 (4 *C*H), 128.13 (*C*H), 128.3 (*C*), 136.8 (*C*), 137.0 (*C*), 137.8 (*C*), 153.7 (*C*), 158.3 (*C*).

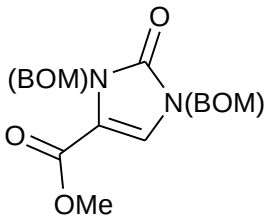

ii) 1,3-Bis(BOM)-4-methoxycarbonylimidazolin-2-one **52b** (484 mg, 12.4 %) as a colourless oil. (R_f 0.10 in 40 % EtOAc-petrol); δ_H(400MHz; $CDCl_3$) δ_H(400MHz; $CDCl_3$) 3.75 (3 H, s, OC*H*$_3$), 4.51 (2 H, s, C*H*$_2$ (BOM)), 4.59 (2 H, s, C*H*$_2$ (BOM)), 5.06 (2 H, s, C*H*$_2$ (BOM)), 5.48 (2 H, s, 2 C*H*$_2$ (BOM)), 7.13 (1 H, s, HNCC*H*), 7.15 – 7.32 (10 H, m, Ar*H* (BOM)).

1,3-Bis(BOM)-4-hydroxymethylimidazolin-2-one 53b

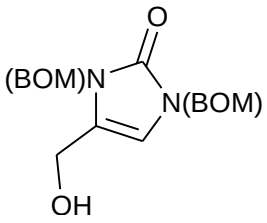

1,3-Bis(BOM)-4-methoxycarbonylimidazolin-2-one **52b** (1.6 g, 3.61 mmol) was suspended in anhydrous DCM (12.6 ml) and cooled to − 78 °C (EtOAc/ice bath) under a nitrogen atmosphere. DIBAL-H (31.0 ml, 31.2 mmol) was added to the mixture and it was stirred at − 78 °C for 7 h. MeOH (11.7 ml) was added to quench the reaction and the mixture was allowed to warm to room temperature. The mixture was diluted with 2M HCl and the product was extracted into DCM. The organic layer was washed twice more with brine. The organic layer was dried with magnesium sulfate and concentrated *in vacuo* to yield a yellow oil. This was purified using flash chromatography with EtOAc-petrol (40:60 to 70:30) to yield 1,3-bis(PMB)-4-hydroxyimidazolin-2-one **53b** (980 mg, 77 %) as a colourless oil (R_f 0.12 in 1:1 EtOAc-petrol); δ_H (400MHz; $CDCl_3$) 4.43 (2 H, s, C*H*$_2$), 4.52 (2 H, s, C*H*$_2$), 4.55 (2 H, s, C*H*$_2$), 5.02 (2 H, s, C*H*$_2$), 5.26 (2 H, s, C*H*$_2$), 6.29 (1 H, s, HNCC*H*), 7.20 – 7.38 (10 H, m, Ar*H* (BOM)).

1,3-Bis(BOM)-4-formylimidazolin-2-one 38b

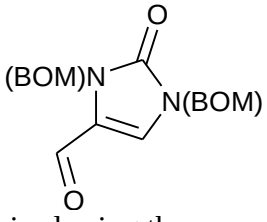

The title compound was synthesised using the procedure described by Dransfield *et al.* using 1,3-bis(BOM)-4-hydroxymethylimidazolin-2-one **53b** (545 mg, 1.54 mmol) and manganese dioxide (1.07 g, 12.3 mmol) in DCM (22 ml) to produce a yellow oil. This was purified using flash chromatography with EtOAc-petrol (40:60 to 50:50) to yield 1,3-bis(BOM)-4-formylimidazolin-2-one **38b** (302 mg, 56 %) as a colourless oil (R_f 0.18 in 50 % EtOAc-petrol); δ_H (400 MHz, $CDCl_3$) 4.61 (2 H, s, C*H*$_2$), 4.68 (2 H, s, C*H*$_2$), 5.19 (2 H, s, C*H*$_2$), 5.54

(2 H, s, CH_2), 7.15 (1 H, s, HNCC*H*), 7.25 – 7.41 (10 H, m, Ar*H* (BOM)), 9.34 (1 H, s, C*H*O).

_N_(α)-Cbz, _N_(π),_N_(τ)-Bis(BOM), α,β-dehydro-4,5-dihydro-2-oxo-His-OMe 40c

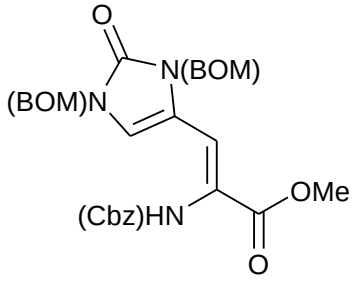

1,3-Bis(BOM)-4-formylimidazolin-2-one **38b** (232 mg, 0.66 mmol) and (±)-benzyloxycarbonyl-α-phosphonoglycine **39b** trimethyl ester (327 mg, 0.99 mmol) were suspended in anhydrous DCM (11.7 ml) under a nitrogen atmosphere. 1,8-Diazabicyclo[5.4.0]undec-7-ene (DBU) (0.148 ml, 0.99 mmol) was added slowly to the reaction mixture. This was left stirring for 16.5 h. The mixture was concentrated *in vacuo* to a brown-yellow oil. This was purified using flash chromatography with EtOAc-DCM (10:90 to 30:70) to yield *N*(α)-Cbz, *N*(π),*N*(τ)-Bis(BOM), α,β-dehydro-4,5-dihydro-2-oxo-His–OMe **40c** (110.2 mg, 29 %) as a colourless oil (R_f 0.55 in 60 % EtOAc-DCM); ν_{max}(ATR)/cm^{-1} 2953 (CH), 1716 (CO), 1704 (CO), 1655 (CO); δ_H(400 MHz; $CDCl_3$) 3.68 (3 H, s, OCH_3), 4.44 (2 H, s, CH_2 (Cbz)), 4.47 (2 H, s, *CH*$_2$ (BOM)), 4.96 (2 H, s, CH_2 (BOM)), 5.06 (2 H, s, CH_2 (BOM)), 5.14 (2 H, s, CH_2 (BOM)), 6.36 (1 H, s br, α-N*H*), 6.67 (1 H, s br, β-C*H*), 7.14 (1 H, s, Im 5-*H*), 7.20-7.40 (15 H, m, 3 Ph); δ_C(100.65 MHz; $CDCl_3$); 52.7 (*C*H$_3$), 67.7 (*C*H$_2$), 70.5 (*C*H$_2$), 70.7 (*C*H$_2$), 71.1 (*C*H$_2$), 72.7 (*C*H$_2$), 116.1 (*C*H), 118.3 (*C*), 118.5 (*C*H), 119.3 (*C*H), 123.9 (*C*), 127.7 (*C*), 127.9 (*C*H), 127.9 (*C*), 128.0 (*C*H), 128.3 (*C*O), 128.4 (*C*), 128.5 (*C*), 128.6 (*C*O), 135.9 (*C*), 137.0 (*C*), 137.2 (*C*), 152.9 (*C*), 153.7 (*C*), 165.0 (*C*). Assignments based on 1D spectra, DEPT-135, COSY and HSQC analysis; *m/z* (ESI) found: 558.2229 (M + NH_4^+) ($C_{31}H_{33}N_3O_7$ requires 558.2235).

Attempted mesylation/tosylation of 1,3-Bis(BOM)-4-(hydroxymethyl)imidazolin-2-one 52b: formation of 1, 3-bis(PMB)-5-methylimidazolidin-2,4-dione 74b

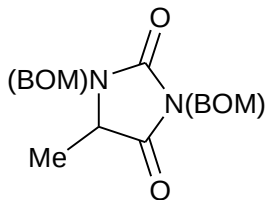

1,3-Bis(BOM)-4-hydroxymethylimidazolin-2-one **53b** (100 mg, 0.282 mmol) was dissolved in anhydrous DCM (1.8 ml) and placed under a nitrogen atmosphere. The mixture was cooled to 0 °C using an ice bath and triethylamine (94.4 µl, 0.677 mmol) was added. Mesyl chloride (43.7 µl, 0.564 mmol) was added and the mixture was left for 7 h. The product was then partitioned between DCM and 2M HCl. The aqueous layer was then washed twice with DCM and the combined organic layers were dried with $MgSO_4$ and concentrated *in vacuo* to yield a brown oil. This was purified by flash chromatography using EtOAc-petrol (30:70 to 50:50) to yield 1,3-bis(BOM)-5-methylimidazolidin-2,4-dione **74b** (50 mg, 38%) as a yellow oil (R_f 0.43 in 40% EtOAc-petrol): IR (ATR) ν_{max}(ATR)/cm^{-1} 2937 (NH), 2877 (NH), 1780 (CO), 1716 (CO); δ_H (400 MHz, $CDCl_3$) 1.31 (3 H, d, *J* 7.2 Hz, C*H*$_3$CH), 4.46 (1 H, q, J 7.2 Hz, CH$_3$C*H*), 4.58 (2 H, s, C*H*$_2$(BOM)), 4.68 (1 H, d, *J* 11.2 Hz, CH*H*(BOM)), 4.95 (2 H, s, C*H*$_2$ (BOM)), 4.97 (1 H, d, *J* 11.2 Hz, CH*H*(BOM)), 5.22 (2 H, s, C*H*$_2$(BOM)), 7.22 - 7.30 (10 H, m, 2 Ph); δ_C(100.65 MHz, $CDCl_3$); 15.2 (*C*H$_3$CH), 54.6 (*C*HCH$_3$), 68.2 (*C*H$_2$ (BOM)), 70.8 (*C*H$_2$ (BOM)), 71.0 (*C*H$_2$ (BOM)), 72.0 (*C*H$_2$ (BOM)), 127.5 (2 *C*H (Ar)), 127.82 (2 *C*H (Ar)), 127.84 (*C*HCH$_3$), 128.1 (2 *C*H (Ar)), 128.4 (*C*H (Ar)), 128.6 (*C*H (Ar)), 137.21 (*C* (Ar)), 137.6 (*C* (Ar)), 155.8 (*C*O), 173.3 (*C*O). Assignments based on 1D spectra, DEPT-135, COSY and HSQC analysis; *m/z* (ESI) found: 372.1916 (M + NH_4^+) ($C_{20}H_{26}N_3O_4$ requires 372.1918).

1,3-Bis(BOM)-2-oxo-imidazolin-4-methyl methyl carbonate 75

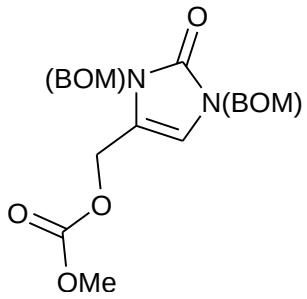

Two methods were used:

(A) 1,3-Bis(BOM)-4-hydroxymethylimidazolin-2-one **53b** (100 mg, 0.28 mmol) was dissolved in anhydrous DCM (0.7 ml). This was cooled to 0 °C. Pyridine (26.4 µl, 0.33 mmol) was added followed by methyl chloroformate (24.0 µl, 0.31 mmol). The mixture was allowed to warm to r.t. and then kept at r.t. for 5.5 h. Water (0.4 ml) was added and the product was extracted into ethyl acetate (0.7 ml). The organic layer was then washed with pH 7.4 phosphate buffer (2 x 0.7ml) and brine (2 x 0.7 ml), dried with $MgSO_4$ and concentrated *in vacuo* to yield a yellow oil. This was purified using flash chromatography with the column prepared with Et_3N and then run with EtOAc-petrol (30:70 to 80:20) to yield 1,3-bis(BOM)-2-oxo-imidazolin-4-methyl methyl carbonate **75** (41.6 mg, 36.0 %, R_f 0.19 in 50 % EtOAc-petrol); δ_H (400 MHz, $CDCl_3$) 3.69 (3 H, s, OCH_3), 4.48 (2 H, s, CH_2 (BOM)), 4.49 (2 H, s, CH_2 (BOM)), 4.94 (2 H, s, CH_2 (BOM)), 5.02 (2 H, s, CH_2 (BOM)), 5.17 (NCCH_2), 6.42 (1 H, s, NC*H*), 7.17-7.28 (10 H, m, 2 Ph); δ_C(100.65 MHz; $CDCl_3$); 55.0 (O*C*H_3), 59.2 (*C*H_2 (BOM)), 70.8 (NC*C*H_2), 70.9 (*C*H_2 (BOM)), 70.9 (*C*H_2 (BOM)), 78.0 (*C*H_2 (BOM)), 112.7 (*C*H (Ar)), 117.8 (*C* (Ar)), 127.8 (*C*H (Ar)), 127.8 (*C*H (Ar)), 127.9 (*C*H (Ar)), 128.0 (*C*H (Ar)), 128.3 (2 *C*H (Ar)), 128.4 (2 *C*H (Ar)), 128.5 (2 *C*H (Ar)), 137.1 (*C* (Ar)), 137.3 (*C* (Ar)), 137.7 (*C* (Ar)), 138.0 (*C* (Ar)), 153.8 (*C* (Ar)), 155.3 (*C* (Ar)). Assignments based on 1D spectra, DEPT-135, COSY and HSQC analysis.

(B) Sodium hydride (60 % dispersion in mineral oil, 13.1 mg, 0.55 mmol) was washed with petroleum spirit. The washed NaH was suspended in anhydrous THF (1 ml), then cooled to 0 °C. 1,3-Bis(BOM)-4-hydroxymethylimidazolin-2-one **53b**

(100 mg, 0.28 mmol) was added. Methyl chloroformate (48 μl, 0.62 mmol) was added and the mixture was allowed to warm to r.t. It was then stirred under nitrogen for 29 h. pH 7.4 phosphate buffer (0.5 ml, 10 mM) was added and the product was extracted into ethyl acetate (1 ml). The organic layer was then washed with pH 7.4 phosphate buffer (2 x 0.7ml) and brine (2 x 0.7 ml), dried with $MgSO_4$ and concentrated *in vacuo* to yield a yellow oil. This was purified using flash chromatography with the column prepped with Et_3N and then run with EtOAc-petrol (30:70) to yield 1,3-bis(BOM)-2-oxo-imidazolin-4-methyl methyl carbonate **75** (3.5 mg, 3.0 %, 0.18 in 50 % EtOAc-petrol); δ_H (400 MHz, $CDCl_3$) 3.69 (3 H, s, OC*H*$_3$), 4.49 (4 H, s, 2 C*H*$_2$ (BOM)), 4.95 (2 H, s, C*H*$_2$ (BOM)), 5.03 (2 H, s, C*H*$_2$ (BOM)), 5.18 (NCC*H*$_2$), 6.43 (1 H, s, NC*H*), 7.18-7.34 (10 H, m, Ar*H* (BOM)); *m/z* (ESI) found: 413.1704 ($M + H^+$) ($C_{22}H_{25}N_2O_6$ requires 413.1707).

2-Acetamido-2-[1,3-bis(benzyloxymethyl)5-methyl-2-oxo-2,3-dihydro-1H-imidazol-4-yl]-malonic acid diethyl ester 77

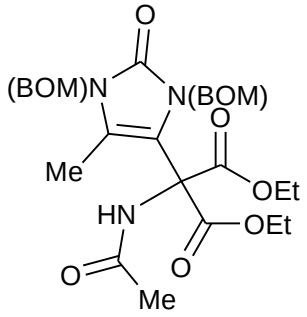

Sodium hydride (60 % dispersion in mineral oil, 2.64 mg, 0.11 mmol) was washed with petroleum ether. The washed NaH was suspended in anhydrous DMF (1.6 ml) under a nitrogen atmosphere. Diethyl acetamidomalonate **71** (23.9 mg, 0.11 mmol) was added and the mixture was left stirring at r.t. for 10 min. (*S*)-(-)-BINAP (6.29 mg, 0.01 mmol was then added followed by 1,3-bis(BOM)-2-oxo-imidazolin-4-methyl methyl carbonate **75** (40 mg, 0.11 mmol). Finally $[Pd(allyl)Cl]_2$ (0.92 mg, 2.53 μmol) was added. The flask was then evacuated and back-filled three times with nitrogen before heating to 80 ° C for 5 h. The flask was then cooled to r.t.. Water (2.5 ml) was added and the product was extracted into ethyl acetate (5 ml). The organic layer was washed with potassium -hydroxide solution (2 x 5 ml, 1 M), HCl (2 x 5 ml, 1 M) and brine

(3 x 5ml). This layer was then dried with $MgSO_4$ and concentrated *in vacuo* to yield a crude product which was then purified thrice using flash chromatography, twice with EtOAc-petrol (40:60 to 80:20 and then 40:60 to 100:0) and then with EtOAc-DCM (20:80) to yield 2-acetamido-2-[1,3-bis(benzyloxymethyl)5-methyl-2-oxo-2,3-dihydro-1*H*-imidazol-4-yl]-malonic acid diethyl ester **77** (5.1 mg, 8.4 %, R_f 0.26 in 30 % EtOAc-DCM); ν_{max}(ATR)/cm^{-1} 3319 (NH), 1747 (CO), 1670 (2 CO); δ_H (400 MHz, $CDCl_3$) 1.21 (3 H, t, *J* 7.2 Hz, CH_2CH_3), 1.78 (3 H, s, CH_3), 2.05 (3 H, s, CH_3), 4.12 – 4.28 (4 H, m, 2 CH_2CH_3), 4.51 (2 H, s, CH_2), 4.59 (2 H, s, CH_2), 5.06 (2 H, s, CH_2), 5.13 (2 H, s, CH_2), 7.22 – 7.32 (10 H, m, 2 Ph), 7.89 (1 H, s, br, NH); *m/z* (ESI) found: 554.2494 ($M + H^+$) ($C_{29}H_{36}N_3O_8$ requires 554.2497).

Chapter 7

REFERENCES

Adam, W. and Reinhardt, D. (1995) Epoxidation of vinylamides by dimethyldioxirane: first spectral evidence for enamine oxides. *Tetrahedron* **51** 12257-12262

Adam, W., Ahrweiler, M., Paulini, K., Reißig, H. U. and Voerckel, V. (1992) Dimethyldioxirane oxidation of enamines: First spectral evidence for enamine oxides by stabilization through N-silylation. *Chemische Berichte* **125** 2719-2721

Adam, W., Ahrweiler, M., Peters, K. and Schmiedeskamp, B. (1994) Oxidation of N-Acylindoles by Dimethyldioxirane and Singlet Oxygen: Substituent Effects on Thermally Persistent Indole Epoxides and Dioxetanes. *Journal of Organic Chemistry* **59** 2783-2789

Adam, W., Bialas, J. and Hadjiarapoglou, L. (1991) A convenient preparation of acetone solutions of dimethyldioxirane. *Chemische Berichte* **124** 2377-2377

Adams, J. D. J. (1991) Oxygen free radicals and Parkinson's disease. *Free Radical Biology and Medicine* **10** 161-169

Agarwal, S. and Sohal, R. S. (1993) Relationship between aging and susceptibility to protein oxidative damage. *Biochemical and Biophysical Research Communications* **194** 1203-1208

Aiman, C. E. and Daugs, E. D. Process for the production of 2-imidazolones. March 29, 1993 Merrell Dow Pharmaceuticals Inc. (Cincinnati, OH) *5338862*

Aizenstein, H. J., Nebes, R. D., Saxton, J. A., Price, J. C., Mathis, C. A., Tsopelas, N. D., Ziolko, S. K., James, J. A., Snitz, B. E., Houck, P. R., Bi, W., Cohen, A. D., Lopresti, B. J., DeKosky, S. T., Halligan, E. M. and Klunk, W. E. (2008) Frequent amyloid deposition without significant cognitive impairment among the elderly. *Archives of Neurology* **65** 1509-1517

Akama, K. T., Albanese, C., Pestell, R. G. and Van Eldik, L. J. (1998) Amyloid beta-peptide stimulates nitric oxide production in astrocytes through an NFkappaB-dependent mechanism. *Proceedings of the National Academy of Sciences* **95** 5795-5800

Aksenov, M. Y., Aksenova, M. V., Butterfield, D. A., Geddes, J. W. and Markesbery, W. R. (2001) Protein oxidation in the brain in Alzheimer's disease. *Neuroscience* **103** 373-383

Ali, F. E., Barnham, K. J., Barrow, C. J. and Separovic, F. (2003) Copper catalyzed oxidation of amino acids and Alzheimer's disease. *Letters in Peptide Science* **10** 405-412

Altman, J. and Wilchek, M. (1989) 5,6-Diaminocaproic Acid by Bamberger Ring Cleavage of Substituted Imidazoles. *Liebigs Annalen Der Chemie* **1989** 493-495

Altman, J., Grinberg, M. and Wilchek, M. (1990) Approach to chiral vicinal diacylamines by Bamberger ring cleavage of substituted imidazoles. *Liebigs Annalen Der Chemie* **1990** 339-343

Altman, J., Shoef, N., Wilchek, M. and Warshawsky, A. (1984) Bifunctional chelating agents. part 2. Synthesis of 1-(2-carboxyethyl)ethylenediaminetetra-acetic acid by ring cleavage of a substituted imidazole. *Journal of the Chemical Society Perkin Transactions 1* 59-62

Altman, J., Shoef, N., Wilchek, M. and Warshawsky, A. (1985) Ring opening of N-tosylhistamine with di-t-butyl pyrocarbonate: synthesis of 1,2-diamino-4-tosylaminobutane dihydrochloride. *Journal of the Chemical Society Chemical Communications* 1133-1134

Alzheimer, A. (1906) Regarding a Curious Disease of the Cortex *Meeting of South-West German Society of Alienists*

Andrés, J. I., Alonso, J. M., Díaz, A., Fernández, J., Iturrino, L., Martínez, P., Matesanz, E., Freyne, E. J., Deroose, F., Boeckx, G., Petit, D., Diels, G., Megens, A., Somers, M., Wauwe, J. V., Stoppie, P., Cools, M., Clerck, F. D., Peeters, D. and de Chaffoy, D. (2002) Synthesis and biological evaluation of imidazol-2-one and 2-cyanoiminoimidazole derivatives: novel series of PDE4 inhibitors. *Bioorganic & Medicinal Chemistry Letters* **12** 653-658

Anilkumar, G., Nambu, H. and Kita, Y. (2002) A Simple and Efficient Iodination of Alcohols on Polymer-Supported Triphenylphosphine. *Organic Process Research & Development* **6** 190-191

Antunes, F. and Cadenas, E. (2001) Cellular titration of apoptosis with steady state concentrations of H2O2: submicromolar levels of H2O2 induce apoptosis through fenton chemistry independent of the cellular thiol state. *Free Radical Biology and Medicine* **30** 1008-1018

Antzutkin, O. N., Balbach, J. J., Leapman, R. D., Rizzo, N. W., Reed, J. and Tycko, R. (2000) Multiple quantum solid-state NMR indicates a parallel, not antiparallel, organization of beta-sheets in Alzheimer's beta-amyloid fibrils. *Proceedings of the National Academy of Sciences* **97** 13045-13050

Armstrong, R. W., Tellew, J. E. and Moran, E. J. (1992) Stereoselective synthesis of (E)- and (Z)-1-azabicyclo[3.1.0]hex-2-ylidene dehydroamino acid derivatives. *Journal of Organic Chemistry* **57** 2208-2211

Ashley, J. N. and Harington, C. R. (1930) CCCXLII.—Synthesis of 1-2-thiolhistidine. *Journal of the Chemical Society (Resumed)* 2586

Atwood, C. S., Huang, X., Khatri, A., Scrapa, R. C., Kim, Y.-S., Moir, R. D., Tanzi, R. E., Rohrer, A. E. and Bush, A. I. (2000) Copper catalysed oxidation of Alzheimer Abeta. *Cellular and Molecular Biology* **46** 777-783

Atwood, C. S., Huang, X., Moir, R. D., Tanzi, R. E. and Bush, A. I. (1999) Role of free radicals and metal ions in the pathogenesis of Alzheimer's disease. *Metal ions in biological systems* **36** 309-364

Atwood, C. S., Martins, R. N., Smith, M. A. and Perry, G. (2002) Senile plaque composition and posttranslational modification of amyloid-beta peptide and associated proteins. *Peptides* **23** 1343–1350

Atwood, C. S., Obrenovich, M. E., Liu, T., Chan, H., perry, G., Smith, M. A. and Martins, R. N. (2003) Amyloid-beta: a chameleon walking in two worlds: a review of the trophic and toxic properties of amyloid-beta. *Brain Research Reviews* **43** 1-16

Bailey, P. D. (1992) An Introduction to Peptide Chemistry. John Wiley & Sons

Baldwin, J. E., Merritt, K. D. and Schofield, C. J. (1993) Synthesis of L-ornithines stereospecifically deuterated at C-3. *Tetrahedron Letters* **34** 3919-3920

Balleza-Tapia, H. and Pena, F. (2009) Pharmacology of the Intracellular Pathways Activated by Amyloid Beta Protein. *Mini Reviews in Medicinal Chemistry* **9** 724-740

Bamberger, E. (1893) Studien über Imidazole *Justus Liebegs Annalen der Chemie* **273** 267

Banerjee, D., Kumar, P. A., Kumar, B., Madhusoondanan, U. K., Nayak, S. and Jacob, J. (2002) Determination of absolute hydrogen peroxide concentration by spectrophotometric method. *current Science* **83** 1193-1194

Barnham, K. J., Ciccotosto, G. D., Tickler, A. K., Ali, F. E., Smith, D. G., Williamson, N. A., Lam, Y. H., Carrington, D., Tew, D., Kocak, G., Volitakis, I., Separovic, F., Barrow, C. J., Wade, J. D., Masters, C. L., Cherny, R. A., Curtain, C. C., Bush, A. I. and Cappai, R. (2003) Neurotoxic, redox-competent Alzheimer's beta-amyloid is released from lipid membrane by methionine oxidation. *Journal of Biological Chemistry* **278** 42959-42965

Barrow, C. and Zagorski, M. (1991) Solution structures of beta peptide and its constituent fragments: relation to amyloid deposition. *Science* **253** 179-182

Barrow, C. J. (1999) Synthesis, structure and neurotoxicity of the Abeta peptide of Alzheimer's Disease. *Protein and Peptide Letters* **6** 271

Barrow, C. J., Yasuda, A., Kenny, P. T. M. and Zagorski, M. G. (1992) Solution conformations and aggregational properties of synthetic amyloid [beta]-peptides of Alzheimer's disease : Analysis of circular dichroism spectra *Journal of Molecular Biology* **225** 1075-1093

Bartoli, G., Marcantoni, E. and Sambri, L. (2003) The CeCl3·nH2O/NaI System in Organic Synthesis: An Efficient Water Tolerant Lewis Acid Promoter. *Synlett* **2003** 2101-2116

Baruch-Suchodolsky, R. and Fischer, B. (2008) Soluble Amyloid beta 1-28-Copper(I)/Copper(II)/Iron(II) Complexes Are Potent Antioxidants in Cell-Free Systems. *Biochemistry* **47** 7796-7806

Baruch-Suchodolsky, R. and Fischer, B. (2009) Abeta40, either Soluble or Aggregated, Is a Remarkably Potent Antioxidant in Cell-Free Oxidative Systems. *Biochemistry* **48** 4354-4370

Baxter, R. L., Camp, D. J., Coutts, A. and Shaw, N. (1992) Synthesis and Biological-Activity of 9-Mercaptodethiobiotin - a Putative Biotin Precursor in Escherichia-Coli. *Journal of the Chemical Society Perkin Transactions 1* 255-258

Bayle-Lacoste, M., Moulines, J., Collignon, N., Boumekouez, A., de Tinguy-Moreaud, E. and Neuzil, E. (1990) Synthesis of 4-phosphono- and of 4-(phosphonomethyl)-dl-phenylalanine, two analogues of O-phosphotyrosine. *Tetrahedron* **46** 7793-7802

Behl, C. (1997) Amyloid beta-protein toxicity and oxidative stress in Alzheimer's disease. *Cell and Tissue Research* **290** 471-480

Behl, C., Davis, J. B., Lesley, R. and Schubert, D. (1994) Hydrogen peroxide mediates amyloid beta protein toxicity. *Cell* **77** 817-827

Benzing, W. C., Mufson, E. J. and Armstrong, D. M. (1993) Alzheimer's disease-like dystrophic neurites characteristically associated with senile plaques are not found within other neurodegenerative diseases unless amyloid -protein deposition is present. *Brain Research* **606** 10-18

Berlett, B. S. and Stadtman, E. R. (1997) Protein oxidation in aging, disease, and oxidative stress. *Journal of Biological Chemistry* **272** 20313-20316

Bernaducci, E., Schwindinger, W. F., Hugheg, J. L., Krogh-Jesperson, K. and Schugar, H. J. (1981) Electronic spectra of copper(II)-imidazole and copper(II)-pyrazole chromophores. *Journal of the American Chemical Society* **103** 1686-1691

Bernstein, S. L., Dupuis, N. F., Lazo, N. D., Wyttenbach, T., Condron, M. M., Bitan, G., Teplow, D. B., Shea, J.-E., Ruotolo, B. T., Robinson, C. V. and Bowers, M. T. (2009) Amyloid-beta

protein oligomerization and the importance of tetramers and dodecamers in the aetiology of Alzheimer's disease. *Nature Chemistry* **1** 326-331

Bhatia, R., Lin, H. and Lal, R. (2000) Fresh and globular amyloid protein (1–42) induces rapid cellular degeneration: evidence for AbetaP channel-mediated cellular toxicity. *FASEB JOURNAL* **14** 1233–1243

Bieschke, J., Siegel, S. J., Fu, Y. and Kelly, J. W. (2008) Alzheimer's Abeta peptides containing an isostructural backbone mutation afford distinct aggregate morphologies but analogous cytotoxicity. Evidence for a common low-abundance toxic structure(s)? *Biochemistry* **47** 50-59

Bieschke, J., Zhang, Q. H., Bosco, D. A., Lerner, R. A., Powers, E. T., Wentworth, P. and Kelly, J. W. (2006) Small molecule oxidation products trigger disease-associated protein misfolding. *Accounts of Chemical Research* **39** 611-619

Bieschke, J., Zhang, Q., Powers, E. T., Lerner, R. A. and Kelly, J. W. (2005) Oxidative metabolites accelerate Alzheimer's amyloidogenesis by a two-step mechanism, eliminating the requirement for nucleation. *Biochemistry* **44** 4977-4983

Bitan, G. and Teplow, D. B. (2004) Rapid photochemical cross-linking – a new tool for studies of metastable, amyloidogenic protein assemblies. *Accounts of Chemical Research* **37** 357-364

Bitan, G., Bogdan, T., Vollers, S. S., Lashuel, H. A., Condron, M. M., Straub, J. E. and Teplow, D. B. (2003) A Molecular Switch in Amyloid Assembly: Met35 and Amyloid beta-Protein Oligomerization. *Journal of the American Chemical Society* **125** 15359-15365

Bitan, G., Kirkitadze, M. D., Lomakin, A., Vollers, S. S., Benedek, G. B. and Teplow, D. B. (2003) Amyloid beta protein (Abeta) assembly: Abeta40 and Abeta42 oligomerize through distinct pathways. *Proceedings of the National Academy of Sciences* **100** 330-335

Blackley, H. K. L., Patel, N., Davies, M. C., Roberts, C. J., Tendler, S. J. B., Wilkinson, M. J. and Williams, P. M. (1999) Morphological development of beta(1-40) amyloid fibrils. *Experimental Neurology* **158** 437-443

Bladon, C. M. (1990) Synthesis of Heteroaromatic Thyrotropin-releasing Hormone Analogues. *Journal of the Chemical Society Perkin Transactions 1* 1151-1158

Blennow, K., de Leon, M. J. and Zetterberg, H. (2006) Alzheimer's disease *Lancet* **368** 387-403

Boger, D. L., Fink, B. E. and Hedrick, M. P. (2000) Total synthesis of distamycin A and 2640 analogues: A solution-phase combinatorial approach to the discovery of new, bioactive DNA binding agents and development of a rapid, high-throughput screen for determining relative DNA binding affinity or DNA sequence selectivity. *Journal of the American Chemical Society* **122** 6382-6394

Bondy, S. C., Guo-Ross, S. X. and Truong, A. T. (1998) Promotion of transition metal-induced reactive oxygen species formation by beta-amyloid. *Brain Research* **799** 91-96

Boros, S., Kamps, B., Wunderink, L., de Bruijin, W., de Jong, W. W. and Boelens, W. C. (2004) Transglutaminase catalyzes differential cross-linking of small heat shock proteins and amyloid-beta. *FEBS Letters* **576** 57-62

Bravo, A., Fontana, F., Fronza, G., Minisci, F. and Zhao, L. (1998) Molecule-Induced Homolysis versus Concerted Oxenoid Oxygen Insertion in the Oxidation of Organic Compounds by Dimethyldioxirane. *Journal of Organic Chemistry* **63** 254-263

Bretschneider, T., Miltz, W., Münster, P. and Steglich, W. (1988) New syntheses of [alpha]-amino acids based on n-acylimino acetates. *Tetrahedron* **44** 5403-5414

Bronfman, F. C., Garrido, J., Alvarez, A., Morgan, C. and Inestrosa, N. C. (1996) Laminin inhibits amyloid-beta-peptide fibrillation. *Neuroscience Letters* **218** 201-203

Brooke, G. M., Mohammed, S. and Whiting, M. C. (1997) A simple amide protecting group: synthesis of oligoamides of Nylon 6. *Chemical Communications* 1511-1512

Brown, T., Jones, J. H. and Richards, J. D. (1982) Further Studies on the Protection of Histidine Side Chains in Peptide Synthesis: The Use of the pi-Benzyloxymethyl Group. *Journal of the Chemical Society Perkin Transactions 1* 1553-1561

Buckle, D. R. and Rockell, C. J. M. (1982) Studies on V-Triazoles. 4. The 4-Methoxybenzyl Group, a Versatile N-Protecting Group for the Synthesis of N-Unsubstituted V-Triazoles. *Journal of the Chemical Society-Perkin Transactions 1* 627-630

Bull, S. D., Davies, S. G., Delgado-Ballester, S., Kelly, P. M., Kotchie, L. J., Gianotti, M., Laderas, M. and Smith, A. D. (2001) Asymmetric synthesis of beta-haloaryl beta-amino acid derivatives. *Journal of the Chemical Society-Perkin Transactions 1* 3112-3121

Burgemeister, K., Francio, G., Gego, V. H., Greiner, L. H., Hugl, H. and Leitner, W. (2007) Inverted Supercritical Carbon Dioxide/Aqueous Biphasic Media for Rhodium-Catalyzed Hydrogenation Reactions. *Chemistry - A European Journal* **13** 2798-2804

Burgess, L. E., Gross, E. K. M. and Jurka, J. (1996) The Preparation of alpha-Substituted, beta-Hydroxy Piperidines and Pyrrolidines: The Total Synthesis of Febrifugine. *Tetrahedron Letters* **1996** 3255-3258

Burgey, C. S., Stump, C. A., Nguyen, D. N., Deng, J. Z., Quigley, A. G., Norton, B. R., Bell, I. M., Mosser, S. D., Salvatore, C. A., Rutledge, R. Z., Kane, S. A., Koblan, K. S., Vacca, J. P., Graham, S. L. and Williams, T. M. (2006) Benzodiazepine calcitonin gene-related peptide (CGRP) receptor antagonists: Optimization of the 4-substituted piperidine. *Bioorganic & Medicinal Chemistry Letters* **16** 5052-5056

Burgoyne, D. L., Miao, S., Pathirana, C., Andersen, R. J., Ayer, W. A., Singer, P. P. and Kokke, W. C. M. C. (1991) The structure and partial synthesis of imbricatine, a benzyltetrahydroisoquinoline alkaloid from the starfish *Dermasterias imbricata*. *Canadian Journal of Chemistry* **69** 20-27

Burk, M. J., Allen, J. G. and Kiesman, W. F. (1998a) Highly Regio- and Enantioselective Catalytic Hydrogenation of Enamides in Conjugated Diene Systems: Synthesis and Application of alpha,gamma-Unsaturated Amino Acids. *Journal of the American Chemical Society* **120** 657-663

Burk, M. J., Bienewald, F., Challenger, S., Derrick, A. and Ramsden, J. A. (1999) Me-DuPHOS-Rh-Catalyzed Asymmetric Synthesis of the Pivotal Glutarate Intermediate for Candoxatril *Journal of Organic Chemistry* **64** 3290-3298

Burk, M. J., Feaster, J. E., Nugent, W. A. and Harlow, R. L. (1993) Preparation and use of C2-symmetric Bis(phospholanes): Production of alpha-amino acid derivatives via highly enantioselective hydrogenation reactions. *Journal of the American Chemical Society* **115** 10125-10138

Burk, M. J., Kalberg, C. S. and Pizzano, A. (1998b) Rh-DuPHOS-catalyzed enantioselective hydrogenation of enol esters. Application to the synthesis of highly enantioenriched alpha-hydroxy esters and 1,2-diols. *Journal of the American Chemical Society* **120** 4345-4353

Burkoth, T. S., Benzinger, T. L. S., Urban, V., Morgan, D. M., Gregory, D. M., Thiyagarajan, P., Botto, R. E., Meredith, S. C. and Lynn, D. G. (2000) Structure of the beta-Amyloid(10-35) Fibril. *Journal of the American Chemical Society* **122** 7883-7889

Busciglio, J., Gabuzda, D. H., Matsudaira, P. and Yankner, B. A. (1993) Generation of beta-amyloid in the secretory pathway in neuronal and nonneruonal cells. *Proceedings of the National Academy of Sciences* **90** 2092-2096

Bush, A. I. (2003) The metallobiology of Alzheimer's disease. *Trends in Neurosciences* **26** 207-214

Butterfield, D. A. and Stadtman, E. R. (1997) Protein oxidation processes in aging brain. *Advances in cell aging and gerontology.* **2** 161-191

Butterfield, D. A., Hensley, K., Harris, M., Mattson, M. and Carney, J. (1994) [beta]-Amyloid Peptide Free Radical Fragments Initiate Synaptosomal Lipoperoxidation in a Sequence-Specific Fashion: Implications to Alzheimer's Disease. *Biochemical and Biophysical Research Communications* **200** 710-715

Carling, R. W., Moore, K. W., Moyes, C. R., Jones, E. A., Bonner, K., Emms, F., Marwood, R., Patel, S., Patel, S., Fletcher, A. E., Beer, M., Sohal, B., Pike, A. and Leeson, P. D. (1999) 1-(3-Cyanobenzylpiperidin-4-yl)-5-methyl-4-phenyl-1,3-dihydroimidazol-2-one: A Selective High-Affinity Antagonist for the Human Dopamine D4 Receptor with Excellent Selectivity over Ion Channels. *Journal of Medicinal Chemistry* **42** 2706-2715

Carroll, A. R., Duffy, S. and Avery, V. M. (2009) Citronamides A and B, Tetrapeptides from the Australian Sponge *Citronia astra*. *Journal of Natural Products* **72** 764-768

Caruso, T., Bedini, E., De Castro, C. and Parrilli, M. (2006) Bronsted acidity of ceric ammonium nitrate in anhydrous DMF. The role of salt and solvent in sucrose cleavage *Tetrahedron* **62** 2350-2356

Casella, L. and Gulloti, M. (1983) Coordination modes of histidine. 4.Coordination structures in the copper(II)-L-histidine (1:2) system. *Journal of Inorganic Biochemistry* **18** 19-31

Castegna, A., Aksenov, M., Aksenova, M., Thongboonkerd, V., Klein, J. B., Pierce, W. M., Booze, R., Markesbery, W. R. and Butterfield, D. A. (2002) Proteomic identification of oxidatively modified proteins in Alzheimer's disease brain. Part I: creatine kinase BB, glutamine synthase, and ubiquitin carboxy-terminal hydrolase L-1. *Free Radical Biology and Medicine* **33** 562-571

Castellani (2009) Reexamining Alzheimer's Disease: Evidence for a Protective Role for Amyloid- beta Protein Precursor and Amyloid- beta. *Journal of Alzheimer's disease* **18** 447 -452

Chan, W. C. and White, P. D. (2004) Fmoc solid phase peptide synthesis Oxford University Press

Chen, Y. R. and Glabe, C. G. (2006) Distinct early folding and aggregation properties of Alzheimer amyloid-beta peptides Abeta40 and Abeta42: stable trimer or tetramer formation by Abeta42. *Journal of Biological Chemistry* **281** 24414-24422

Chern, C. Y., Huang, Y. P. and Kan, W. M. (2003) Selective N-debenzylation of amides with p-TsOH. *Tetrahedron Letters* **44** 1039-1041

Chevion, M. (1988) A site-specific mechanism for free radical induced biological damage: The essential role of redox active transition metals. *Free Radical Biology and Medicine* **5** 27-37

Chida, N., Ohtsuka, M. and Ogawa, S. (1993) Total Synthesis of (+)-Lycoricidine and Its 2-Epimer from D-Glucose. *Journal of Organic Chemistry* **58** 4441-4447

Choi, Y., George, C., Comin, M. J., Barchi Jr, J. J., Kim, H. S., Jacobson, K. A., Balzarini, J., Mitsuya, H., Boyer, P. L., Hughes, S. H. and Marquez, V. E. (2003) A Conformationally Locked Analogue of the Anti-HIV Agent Satvudine. An Important Correlation between Pseudorotation and Maximum Amplitude. *Journal of Medicinal Chemistry* **46** 3292-3299

Chromy, B. A., Nowak, R. J., Lambert, M. P., Viola, K. L., Chang, L., Velasco, P. T., Jones, B. W., Fernandez, S. J., Lacor, P. N., Horowitz, P., Finch, C. E., Krafft, G. A. and Klein, W. L. (2003) Self-Assembly of Abeta1-42 into Globular Neurotoxins. *Biochemistry* **42** 12749–12760

Ciattini, P. G., Morera, E. and Ortar, G. (1988) Horner Synthesis of Didehydroamino Acid Derivatives in a Liquid-Liquid Two-Phase System. *Synthesis* **2** 140-142

Clippingdale, A. B., Macris, M., Wade, J. D. and Barrow, C. J. (1999) Synthesis and secondary structural studies of penta(acetyl-Hmb)Abeta(1-40) *The Journal of Peptide Research* **53** 665-672

Cobley, C. J., Lennon, I. C., Praquin, C. and Zanotti-Gerosa, A. (2003) Highly Efficient Asymmetric Hydrogenation of 2-Methylenesuccinamic Acid Using a Rh-DuPHOS Catalyst. *Organic Process Research & Development* **7** 407-411

Cohen-Anisfeld, S. T. and Lansbury, P. T. (1993) A practical, convergent method for glycopeptide synthesis *Journal of the American Chemical Society* **115** 10531-10537

Coleman, R. S. and Carpenter, A. J. (1993) Stereoselective Bromination of Dehydroamino Acids with Controllable Retention or Inversion of Olefin Configuration. *Journal of Organic Chemistry* **58** 4452-4461

Coles, M., Bicknell, W., Watson, A. A., Fairlie, D. P. and Craik, D. J. (1998) Solution Structure of Amyloid beta-Peptide(1-40) in a Water-Micelle Environment. Is the Membrane-Spanning Domain Where We Think It Is? *Biochemistry* **37** 11064-11077

Colombo, R., Colombo, F. and Jones, J. H. (1984) Acid-labile histidine side-chain protection: the N()-t-butoxymethyl group. *J. Chem. Soc. Chem. Commun.* 292-293

Come, J. H., Fraser, P. E. and Lansbury Jr., P. T. (1993) A kinetic model for amyloid formation in the prion diseases: importance of seeding. *Proceedings of the National Academy of Sciences* **90** 5959-5963

Cooper (1985) Studies of the limited degradation of mucus glycoproteins. The mechanism of the peroxide reaction. *Biochemical Journal* **228** 615-626

Cornett, C. R., Markesbery, W. R. and Ehmann, W. D. (1998) Imbalances of trace elements related to oxidative damage in Alzheimer's disease brain. *Neurotoxicology* **19** 339-345

Cortez, R., Rivero, I. A., Somanathan, R., Aguirre, F., Ramirez, E. and Hong, E. (1991) Synthesis of Quinazolinedione Using Triphosgene. *ChemInform* **21** 285–292

Coyle, J. T. and Puttfarcken, P. (1993) Oxidative stress, glutamate, and neurodegenerative disorders. *Science* **262** 689-695

Crapper-McLachlan, D. R. C., Dalton, A. J., Kruck, T. P. A., Bell, M. Y., Smith, W. L., Kalow, W. and Andrews, D. F. (1991) Intramuscular desferrioxamine in patients with Alzheimer's disease. *Lancet* **337** 1304-1308

Crouch, P. J., Blake, R., Duce, J. A., Ciccotosto, G. D., Li, Q. X., Barnham, K. J., Curtain, C. C., Cherny, R. A., Cappai, R., Dyrks, T., Masters, C. L. and Trounce, I. A. (2005) Copper-dependent inhibition of human cytochrome c oxidase by a dimeric conformer of amyloid-beta1-42. *Journal of Neuroscience* **25** 672-679

Cuajungco, M. P., Goldstein, L. E., Nunomura, A., Smith, M. A., Lim, J. T., Atwood, C. S., Huang, X., Farrag, Y. W., Perry, G. and Bush, A. I. (2000) Evidence that the beta-amyloid plaques of Alzheimer's disease represent the redox-silencing and entombment of abeta by zinc. *Journal of Biological Chemistry* **275** 19439-19442

Curi, D., Pardini, V. L. and Viertier, H. (1999) Dimetildioxirane. 1. Oxidação de compostos de enxofre. *Química Nova* **22** 85-93

Dancer, J., Ford, M., Hamilton, K., Kilkelly, M., Lindell, S., O'Mahony, M. and Saville-Stones, E. (1996) Synthesis of Potent Inhibitors of Histidinol Dehydrogenase. *Bioorganic & Medicinal Chemistry Letters* **6** 2131-2136

Danielsson, J., Jarvet, J., Damberg, P. and Graslund, A. (2002) Translational diffusion measured by PFG-NMR on full length and fragments of the Alzheimer Abeta(1-40) peptide.

Determination of hydrodynamic radii of random coil peptides of varying length. *Magnetic Resonance in Chemistry* **40** S89-S97

Daumas, M., Vo-Quang, L., Vo-Quang, Y. and Le Goffic, F. (1989) A new synthesis of alpha-amino acids(E)-beta, gamma-enol ethers. *Tetrahedron Letters* **30** 5121-5124

Davis, N. C. (1956) *Journal of Biological Chemistry* **3** 935

Debenham, S. D., Debenham, J. S., Burk, M. J. and Toone, E. J. (1997) Synthesis of Carbon-linked Glycopeptides through Catalytic Asymmetric Hydrogenation. *Journal of the American Chemical Society* **119** 9897-9898

Deibel, M. A., Ehmann, W. D. and Markesbery, W. R. (1996) Copper, iron, and zinc imbalances in severely degenerated brain regions in Alzheimer's disease: possible relation to oxidative stress. *Journal of Neurological Science* **143** 137-142

Della Bianca, V., Dusi, S., Bianchini, E., Dal Pra , I. and Rossi, F. (1999) beta-Amyloid Activates the O¨-2 Forming NADPH Oxidase in Microglia, Monocytes, and Neutrophils. *Journal of Biological Chemistry* **274** 15493-15499

DeShong, P., Ramesh, S., Elango, V. and Perez, J. J. (1985) Total Synthesis of (+/-)-Tirandamycin A. *Journal of the American Chemical Society* **107** 5219-5224

DeSimone, R. W. and Blum, C. A. (2000) Substituted 3-(2-benzoxazyl)-benzimidazol-2-(1H)-ones: A new class of GABAA brain receptor ligands. *Bioorganic & Medicinal Chemistry Letters* **10** 2723-2726

Díaz, J. C., Linnehan, J., Pollard, H. and Arispe, N. (2006) Histidines 13 and 14 in the Abeta sequence are targets for inhibition of Alzheimer's disease Abeta ion channel and cytotoxicity. *Biological Research* **39** 447-460

Dikalov, S. I., Vitek, M. P. and Mason, R. P. (2004) Cupric–amyloid beta peptide complex stimulates oxidation of ascorbate and generation of hydroxyl radical. *Free Radical Biology and Medicine* **36** 340-347

Dikalov, S. I., Vitek, M. P., Maples, K. R. and Mason, R. P. (1999) Amyloid beta peptides do not form peptide-derived free radicals spontaneously, but can enhance metal-catalyzed oxidation of hydroxylamines to nitroxides. *Journal of Biological Chemistry* **274** 9392-9399

Dilley, A. S. and Romo, D. (2001) Enantioselective Strategy to the Spirocyclic Core of Palau'amine and Related Bisguanidine Marine Alkaloids. *Organic Letters* **3** 1535-1538

Diness, F. and Meldal, M. (2009) Imidazolones in Diastereoselective Cyclization Reactions and Cu(II)-Catalysed Cross-Coupling Reactions. *Chemistry: A European Journal* **15** 7044-7047

Ding, Q., Markesbury, W. R. and Chen, Q. (2005) Ribosome dysfunction in an early event in Alzheimer's disease. *Journal of Neuroscience* **25** 9171-9175

Dobeli, H., Draeger, N., Huber, G., Jakob, P., Schmidt, D., Seilheimer, B., Stuber, D., Wipf, B. and Zulauf, M. (1995) A Biotechnological Method Provides Access to Aggregation Competent Monomeric Alzheimer's beta42 Residue Amyloid Peptide. *Nature Biotechnology* **13** 988–993

Dobson, C. M. (1999) Protein misfolding, evolution, and disease. *Trends in Biochemical Sciences* **24** 329-332

Dong, J., Atwood, C. S., Anderson, V. E., Siedlak, S. L., Smith, M. A., Perry, G. and Carey, P. R. (2003) Metal binding and oxidation of amyloid-beta within isolated senile plaque cores: Raman microscopic evidence. *Biochemistry* **42** 2768-2773

Dong, J., Shokes, J. E., Scott, R. A. and Lynn, D. G. (2006) Modulating Amyloid Self-Assembly and Fibril Morphology with Zn(II). *Journal of the American Chemical Society* **128** 3540-3542

Drake, A. F. (1994) Chaper 16: Circular Dichroism Humana Press Inc, Totowa, NJ

Drake, J., Link, C. D. and Butterfield, D. A. (2003) Oxidative stress precedes fibrillar deposition of Alzheimer's disease amyloid beta-peptide (1-42) in a transgenic Caenorhabditis elegans model. *Neurobiology of Aging* **24** 415-420

Dransfield, P. J., Dilley, A. S., Wang, S. H. and Romo, D. (2006) A unified synthetic strategy toward oroidin-derived alkaloids premised on a biosynthetic proposal. *Tetrahedron* **62** 5223-5247

Dransfield, P. J., Shaohui Wang, S., Dilley, A. and Romo, D. (2005) Highly Regioselective Diels-Alder Reactions toward Oroidin Alkaloids: Use of a Tosylvinyl Moiety as a Nitrogen Masking Group with Adjustable Electronics. *Organic Letters* **7** 1679-1682

Duschinsky, R. and Dolan, L. A. (1946) Studies in the Imidazolone Series. The Synthesis of a Lower and a Higher Homolog of Desthiobiotin and of Related Substances. *Journal of the American Chemical Society* **68** 2350-2355

Dyrks, T., Dyrks, E., Hartmann, T., Masters, C. and Beyreuther, K. (1992) Amyloidogenicity of beta A4 and beta A4-bearing amyloid protein precursor fragments by metal-catalysed oxidation. *Journal of Biological Chemistry* **267** 18210-18217

Edamatsu, R., Mori, A. and Packer, L. (1995) The Spin-Trap N-tert-[alpha]-Phenylbutylnitrone Prolongs the Life Span of the Senescence-Accelerated Mouse. *Biochemical and Biophysical Research Communications* **211** 847-849

Eisenverg, H. (1971) Glutamate dehydrogenase: anatomy of a regulatory enzyme. *Accounts of Chemical Research* **4** 379-385

Esler, W. P., Stimson, E. R., Ghilardi, J. R., Vinters, H. V., Lee, J. P., Mantyh, P. W. and Maggio, J. E. (1996) In vitro growth of Alzheimer's disease beta-amyloid plaques displays first-order kinetics. *Biochemistry* **35** 749-757

Fabian, H., Szendrei, G. I., Mantsch, H. H., Greenberg, B. D. and Otvos Jr, L. (1994) Synthetic post-translationally modified human Abeta peptide exhibits a markedly increased tendency to form beta-pleated sheets in vitro. *European Journal of Biochemistry* **221** 959-964

Fabrello, A., Bachelier, A., Urrutigoity, M. and Kaick, P. (2010) Mechanistic analysis of the transition metal-catlysed hydrogenation of imines and functionalized enamines. *Coordination chemistry reviews* **254** 273-287

Fang, C.-L., Wu, W.-H., Liu, Q., Sun, X., Ma, Y., Zhao, Y.-F. and Li, Y.-M. (2010) Dual functions of beta-amyloid oligomer and fibril in Cu(II)-induced H2O2 production. *Regulatory Peptides* **163** 1-6

Farber, J. M. and Levine, R. L. (1986) Sequence of a peptide susceptible to mixed-function oxidation. Probable cation binding site in glutamine synthetase. *Journal of Biological Chemistry* **261** 4574-4578

Fenton, H. J. H. and Reginald, W. A. W. (1909) CXLVII.-isoIminazolone. *Journal of the Chemical Society, Transactions* **95** 1329-1334

Ferreira, S. T., Vieira, M. N. N. and De Felice, F. G. (2007) Soluble Protein Oligomers as Emerging Toxins in Alzheimer's and Other Amyloid Diseases. *IUBMB Life* **59** 332-345

Ferris, L., Haigh, D. and Moody, C. J. (1996) N-H insertion reactions of rhodium carbenoids. Part 2. Preparation of N-substituted amino(phosphoryl)acetates (N-substituted phosphorylglycine esters). *Journal of the Chemical Society Perkin Transactions 1* 2885-2888

Ferrone, F. A., Hofrichter, J. and Eaton, W. A. (1980) Kinetic studies on sickle hemoglobin polymerisation II, A double nucleation mechanism. *Journal of Molecular Biology* **183** 611-631

Fezoui, Y., Hartley, D. M., Harper, J. D., Khurana, R., Walsh, D. M., Condron, M. M., Selkoe, D. J., Lansbury, J., P. T. , Fink, A. L. and Teplow, D. B. (2000) An improved method of preparing the amyloid beta-protein for fibrillogenesis and neurotoxicity experiments. *Amyloid* **7** 166-178

Fiedler, H.-P., Kurth, R., Langharig, J., Delzer, J. and Zahner, H. (1982) Nikkomycins: Microbial inhibitors of chitin synthase. *Journal of Chemical Technology and Biotechnology* **32** 271-280

Forbes, I. T., Johnson, C. N. and Thompson, M. (1992) Syntheses of Functionalized Pyrido[2,3-B]Indoles *Journal of the Chemical Society-Perkin Transactions 1* 275-281

Forloni, G., Lucca, E., Angeretti, N., Della Torre, P. and Salmona, M. (1997) Amidation of beta-amyloid peptide strongly reduced the amyloidogenic activity without alteration of the neurotoxicity. *Journal of Neurochemistry* **69** 2048

Forster, M. J., Dubey, A., Dawson, K. M., Stutts, W. A., Lal, H. and Sohal, R. S. (1996) Age-related losses of cognitive function and motor skills in mice are associated with oxidative protein damage in the brain. *Proceedings of the National Academy of Sciences* **93** 4765-4769

Fraser, P. E., McLachlan, D. R., Surewicz, W. K., Mizzen, C. A., Snow, A. D., Nguyen, J. T. and Kirschner, D. A. (1994) Conformation and Fibrillogenesis of Alzheimer A[beta] Peptides with Selected Substitution of Charged Residues. *Journal of Molecular Biology* **244** 64-73

Frautschy, S. A., Baird, A. and Cole, G. M. (1991) Effects of injected Alzheimer beta-amyloid cores in rat brain. *Proceedings of the National Academy of Sciences* **88** 8362-8366

Frederikse, P. H., Garland, D., Zigler, J. S. and Piatigorsky, J. (1996) Oxidative Stress Increases Production of -Amyloid Precursor Protein and -Amyloid (A) in Mammalian Lenses, and A Has Toxic Effects on Lens Epithelial Cells. *Journal of Biological Chemistry* **271** 10169-10174

Frieden, C. and Goddette, D. W. (1983) Polymerization of actin and actin-like systems: evaluation of the time course of polymerization in relation to the mechanism. *Biochemistry* **22** 5836-5843

Fukuda, H., Shimizu, T., Nakajima, M., Mori, H. and Shirasawa, T. (1999) Synthesis, aggregation, and neurotoxicity of the alzheimer's Aß1-42 amyloid peptide and its isoaspartyl isomers *Bioorganic & Medicinal Chemistry Letters* **9** 953-956

Furuta, T., Katayama, M., Shibasaki, H. and Kasuya, Y. (1992) Synthesis of Selectively Multi-Labelled Histidines with Stable Isotopes and Chiral Synthesis of L-Histidine from L-Aspartic Acid. *Journal of the Chemical Society Perkin Transactions 1* 1643-1648

Gangopadhyay, S., Ali, M. and Banerjee, P. (1992) Kinetics and mechanism of the oxidation of histidine by dodecatungstocobaltate(III) and trans-cyclohexane-1, 2-diamine-N, N, N',

N'tetraacetatomanganate(III) in aqueous medium. *Journal of the Chemical Society Perkin Transactions 1* **2** 781-785

Garland, D., Russell, P. and Zigler, J. S. (1988) The oxidative modification of lens proteins. 347-353 Oxygen Radicals in Biology and Medicine Plenum New York

Garrison (1987) Reaction mechanisms in the radiolysis of peptides, polypeptides, and proteins. *Chemical Reviews* **87** 381-398

Geddes, J. W., Anderson, K. J. and Cotman, C. W. (1986) Senile plaques as aberrant sprout-stimulating structures. *Experimental Neurology* **94** 767-776

Gellermann, G. P., Byrnes, H., Striebinger, A., Ullrich, K., Mueller, R., Hillen, H. and Barghorn, S. (2008) A[beta]-globulomers are formed independently of the fibril pathway. *Neurobiology of Disease* **30** 212-220

Gerhard, G. and Schunack, W. (1980) Struktur-Wirkungs-Beziehungen bei Histaminanaloga, 20. Mitt. Absolute Konfiguration und histaminartige Wirkung der enantiomeren alpha-Methylhistamine. *Archiv Der Pharmazie* **313** 709-714

Ghezzo-Schoneich, E., Esch, S. W., Sharov, V. S. and Schoneich, C. (2001) Biological aging does not lead to the accumulation of oxidised Cu, Zn-superoxide dismutase in the liver of F344 rats. *Free Radical Biology and Medicine* **30** 858-864

Giaccone, G., Salmona, M., Tagliavini, F. and Forloni, G. (2005) Brain Dysfunction Associated with Amyloid Fibrils and Other Aggregated Proteins. Amyloid Proteins: The Beta Sheet Conformation and Disease. Wilay-VCH

Giannakopoulos, P., Herrmann, F. R., Bussiere, T., Bouras, C., Kovari, E., Perl, D. P., Morrison, J. H., Gold, G. and al., e. (2003) Tangle and neuron numbers, but not amyloid load, predict cognitive status in Alzheimer's disease. *Neurology* **60** 1495-1500

Gibson, F. S., Bergmeier, S. C. and Rapoport, H. (1994) Selective Removal of an N-Boc Protecting Group in the Presence of a Tert-Butyl Ester and Other Acid-Sensitive Groups. *Journal of Organic Chemistry* **59** 3216-3218

Giulian, D., Haverkamp, L. J., Yu, J. H., Karshin, M., Tom, D., Li, J., Kazanskaia, A., Kirkpatrick, J. and Roher, A. E. (1998) The HHQK domain of beta-amyloid provides a structural basis for the immunopathology of Alzheimer's disease. *Journal of Biological Chemistry* **273** 29719–29726

Giunta, S., Ronchi, P., Valli, B., Franceschi, C. and Galeazzi, L. (2000) Transformation of beta-amyloid (Abeta) (1-42) tyrosine to L-Dopa as the result of in vitro hydroxyl radical attack. *Amyloid* **7** 189-193

Glenner, G. G. and Wong, C. W. (1984) Alzheimer's disease: Initial report of the purification and characterization of a novel cerebrovascular amyloid protein. *Biochemical and Biophysical Research Communications* **120** 885-890

Glenner, G. G., Eanes, E. D. and Page, D. L. (1972) The relation of the properties of Congo red-stained amyloid fibrils to the beta-conformation. *Journal of Histochemistry & Cytochemistry* **20** 821-826

Glinka, T., Lomovskaya, O., Bostian, K. and Wallace, D. M. Polybasic bacterial efflux pump inhibitors and therapeutic uses thereof. Dec. 25, 2008 Mpex Pharmaceuticals, Inc. *US 2008/0318957 A1*

Gong, Y., Chang, L., Viola, K. L., Lacor, P. N., Lambert, M. P., Finch, C. E., Krafft, G. A. and Klein, W. L. (2003) Alzheimer's disease-affected brain: presence of oligomeric Abeta ligands (ADDLs) suggests a molecular basis for reversible memory loss. *Proceedings of the National Academy of Sciences* **100** 10417–10422

Grace, M. E., Loosemore, M. J., Semmel, M. L. and Pratt, R. F. (1980) Kinetics and Mechanism of the Bamberger Cleavage of Imidazole and of Histidine Derivatives by Diethyl Pyrocarbonate in Aqueous-Solution. *Journal of the American Chemical Society* **102** 6784-6789

Gravina, S. A., Ho, L., Eckman, C. B., Long, K. E., Otvos, L., Younkin, L. H., Suzuki, N. and Younkin, S. L. (1995) Amyloid beta protein (Abeta) in Alzheimer's disease brain. *Journal of Biological Chemistry* **270** 7013-7016

Greenlund, L. J. S., Deckwerth, T. L. and Johnson, E. M. J. (1995) Superoxide dismutase delays neuronal apoptosis: a role for reactive oxygen species in programmed neuronal death. *Neuron* **14** 303-315

Groenning, M., Olsen, L., van de Weert, M., Flink, J. M., Frokjaer, S. and Jørgensen, F. S. (2007) Study on the binding of Thioflavin T to [beta]-sheet-rich and non-[beta]-sheet cavities *Journal of Structural Biology* **158** 358-369

Gruener, N., Gozlan, O., Goldstein, T., Davis, J. B., Besner, I. and Iancu, T. C. (1991) Iron, transferrin and ferritin in cerebrospinal fluid of children. *Clinical Chemistry* **37** 263-265

Grunder-Klotz, E. and Ehrhardt, J.-D. (1991) The 3,4-dimethoxybenzyl moiety as a new N-protecting group of 1,2-thiazetidine 1,1-dioxides. *Tetrahedron Letters* **32** 751-752

Grundke-Iqbal, I., Fleming, J., Tung, Y.-C., Lassmann, H., K., I. and Joshi, J. G. (1990) Ferritin is a component of the neuritic (senile) plaque in Alzheimer dementia. *Acta Neuropathologica* **81** 105-110

Grundke-Iqbal, I., Iqbal, K., Quinlan, M., Tung, Y. C., Zaidi, M. S. and Wisniewska, H. M. (1986) Microtubule-associated protein tau. A component of Alzheimer paired helical filaments. *Journal of Biological Chemistry* **261** 6084-6089

Grundman, M. (2000) Vitamin E and Alzheimer disease: the basis for additional clinical trials. *American Journal of Clinical Nutrition* **71** 630S-636S

Guernik, S., Wolfson, A., Herskowitz, M., Greenspoon, N. and Geresh, S. (2001) A novel system consisting of Rh-DuPHOS and ionic liquid for asymmetric hydrogenations . *Chemical Communications* 2314-2315

Guilloreau, L., Combalbert, S., Sournia-Saquet, A., Mazarguil, H. and Faller, P. (2007) Redox Chemistry of Copper-Amyloid-beta: The Generation of Hydroxyl Radical in the Presence of Ascorbate is Linked to Redox-Potentials and Aggregation State. *Chembiochem* **8** 1317-1325

Haass, C. and Steiner, H. (2001) Protofibrils, the unifying toxic molecule of neurodegenerative disorders? *Nature Neuroscience* 859 - 860

Hagenmaier, H., Keckeisen, A., Zahner, H. and Kanig, W. A. (1979) Stoffwechselprodukte von Mikroorganismen, 182. Aufklarung der Struktur des Nucleosidantibiotikums Nikkomycin X. *Liebigs Annalen Der Chemie* **1979** 1494-1502

Hager, K., Kenklies, M., McAfoose, J., Engel, J. and Münch, G. (2007) Alpha-lipoic acid as a new treatment option for Alzheimer's disease--a 48 months follow-up analysis. *Journal of Neural Transmissions Supplement* **72** 189-193

Halliwell, B. (1992) Reactive oxygen speices and the central nervous system. *Journal of Neurochemistry* **59** 1609-1623

Halliwell, B. and Gutteridge, J. M. C. (1984) Oxygen toxicity, oxygen radicals, transition metals and disease. *Biochemistry Journal* **219** 1-14

Halliwell, B. and Gutteridge, J. M. C. (1985) The Importance of Free Radicals and Catalytic Metal Ions in Human Diseases. *Molecular Aspects of Medicine* **8** 89-193

Halpern, J. (1982) Mechanism and Stereoselectivity of Asymmetric Hydrogenation. *Science* **217** 401-407

Halverson, K., Fraser, P. E., Kirschner, D. A. and Lansbury, P. T. (1990) Molecular determinants of amyloid deposition in Alzheimer's disease: conformational studies of synthetic .beta.-protein fragments *Biochemistry* **29** 2639-2644

Hammadi, A., Nutzillard, J. M., Poulin, J. C. and Kagan, H. B. (1992) Diastereoselective Hydrogenation of Monodehydroenkephalins Controlled by Chiral Rhodium Catalysts. *Tetrahedron Assymetry* **3** 1247-1262

Hanford, B. O., Hylton, T. A., Wang, K.-T. and Weinstein, B. (1968) Amino acids and peptides. XVIII. Synthesis of a tetrapeptide sequence (A1-A4) of glucagon. *Journal of Organic Chemistry* **33** 4251-4255

Hardy, J. A. and Higgins, G. A. (1992) Alzheimer's disease: the amyloid cascade hypothesis. *Science* **256** 184-185

Hardy, J. and Selkoe, D. J. (2002) The Amyloid Hypothesis of Alzheimer's Disease: Progress and Problems on the Road to Therapeutics. *Science* **297** 353-356

Harper, J. D., Wong, S. S., Lieber, C. M. and Lansbury, P. T. J. (1999) Assembly of Ab amyloid protofibrils: an in vitro model for a possible early event in Alzheimer's disease. *Biochemistry* **38** 8972-8980

Harris, M. E., Hensley, K., Butterfield, D. A., Leedle, R. A. and Carney, J. M. (1995) Direct evidence of oxidative injury produced by the Alzheimer's [beta]-Amyloid peptide (1-40) in cultured hippocampal neurons. *Experimental Neurology* **131** 193-202

Hartley, D. M., Walsh, D. M., Ye, C. P., Diehl, T., Vasquez, S., Vassilev, P. M., Teplow, D. B. and Selkoe, D. J. (1999) Protofibrillar Intermediates of Amyloid beta -Protein Induce Acute Electrophysiological Changes and Progressive Neurotoxicity in Cortical Neurons. *Journal of Neuroscience* **19** 8876-8884

Hayashi, H., Kimura, N., Yamaguchi, H., Hasegawa, K., Yokoseki, T., Shibata, M., Yamamoto, N., Michikawa, M., Yoshikawa, Y., Terao, K., Matsuzaki, K., Lemere, C. A., Selkoe, D. J., Naiki, H. and Yanagisawa, K. (2004) A seed for Alzheimer amyloid in the brain. *Journal of Neuroscience* **24** 4894-4902

Hayashi, T., Shishido, N., Nakayama, K., Nunomura, A., Smith, M. A., Perry, G. and Nakamura, M. (2007) Lipid peroxidation and 4-hydroxy-2-nonenal formation by copper ion bound to amyloid-beta peptide. *Free Radical Biology and Medicine* **43** 1552-1559

He, W. and Barrow, C. J. (1999) The Abeta 3-Pyroglutamyl and 11-Pyroglutamyl Peptides Found in Senile Plaque Have Greater beta-Sheet Forming and Aggregation Propensities in Vitro than Full-Length Abeta. *Biochemistry* **38** 10871-10877

Head, E., Garzon-Rodriguez, W., Johnson, J. K., Lott, I. T., Cotman, C. W. and Glabe, C. (2001) Oxidation of Abeta and Plaques Biogenesis in Alzheimer's Disease and Down Syndrome. *Neurobiology of Disease* **8** 792-806

Heath, H., Lawson, A. and Rimington, C. (1951) 488. 2-Mercaptoglyoxalines. Part I. The Synthesis of Ergothioneine. *Journal of the Chemical Society (Resumed)* 2215-2217

Heegaard, P. M. H., Pedersen, H. G., Flink, J. and Boas, U. (2004) Amyloid aggregates of the prion peptide PrP106-126 are destabilised by oxidation and by the action of dendrimers *FEBS Letters* **577** 127-133

Hendrix, J. C., Halverson, K. J. and Lansbury Jr., P. T. (1992) A Convergent Synthesis of the Amyloid Protein of Alzheimer's Disease. *Journal of the American Chemical Society* **114** 7930-7931

Hensley, K., Carney, J. M., Mattson, M. P., Aksenova, M., Harris, M., Wu, J. F., Floyd, R. A. and Butterfield, D. A. (1994) A model for beta-amyloid aggregation and neurotoxicity based on free radical generation by the peptide: relevance to Alzheimer disease. *Proceedings of the National Academy of Sciences* **91** 3270-3274

Hensley, K., Hall, N., Subramaniam, R., Cole, P., Harris, M., Aksenov, M. Y., Aksenova, M., Gabbita, S. P., Wu, J. F., Carney, J. M., Lovell, M., Markesbery, W. R. and Butterfield, D. A. (1995) Brain regional correspondence between Alzheimer's disease histopathology and biomarkers of protein oxidation. *Journal of Neurochemistry* **65** 2146–2156

Hensley, K., Maidt, M. L., Yu, Z., Sang, H., Markesbery, W. R. and Floyd, R. A. (1998) Electrochemical analysis of protein nitrotyrosine and dityrosine in the Alzheimer brain indciates region-specific accumulation. *Journal of Neuroscience* **18** 8126-8132

Hernandez, J. N., Ramirez, M. A. and Martin, V. S. (2003) A new selective cleavage of N,N-dicarbamoyl-protected amines using lithium bromide. *Journal of Organic Chemistry* **68** 743-746

Hewitt, N. and Rauk, A. (2009) Mechanism of Hydrogen Peroxide Production by Copper-Bound Amyloid Beta Peptide: A Theoretical Study. *The Journal of Physical Chemistry B* **113** 1202-1209

Hilbert, G. E. (1932) The synthesis of 2-imidazolone-4-carboxylic acid and 2-imidazolone. *Journal of the American Chemical Society* **54** 3413-3419

Hilbich, C., Kisters-Woike, B., Reed, J., Masters, C. L. and Beyreuther, K. (1991) Aggregation and Secondary Structure of Synthetic Amyloid betaA4 Peptides of Alzheimer's Disease. *Journal of Molecular Biology* **218** 149-163

Hofmann, K. (1953) The 1-Acylbenzimidazoles and the Bamberger Reaction. 273-276 The Chemistry of Heterocyclic Compounds: Imidazole and its Derivatives. Interscience New York

Horner, L., Hoffmann, H. M. R. and Wippel, H. G. (1958) Phosphororganische Verbindungen, XII. Phosphinoxyde als Olefinierungsreagenzien. *Chemische Berichte* **91** 61-63

Horner, L., Hoffmann, H. M. R., Wippel, H. G. and Klahre, G. (1959) Phosphororganische Verbindungen, XX. Phosphinoxyde als Olefinierungsreagenzien. *Chemische Berichte* **92** 2499-2505

Hortschansky, P., Schroeckh, V., Christopeit, T., Zandomeneghi, G. and Fandrich, M. (2005) The aggregation kinetics of Alzheimer's beta-amyloid peptide is controlled by stochastic nucleation. *Protein Science* **14** 1753-1759

Hoshi, M., Sato, M., Matsumoto, S., Noguchi, A., Yasutake, K., Yoshida, N. and Sato, K. (2003) Spherical aggregates of beta-amyloid (amylospheroid) show high neurotoxicity and activate tau protein kinase I/glycogen synthase kinase-3beta. *Proceedings of the National Academy of Sciences of the United States of America* **100** 6370-6375

Hoshina, Y., Doi, T. and Takahashi, T. (2007) Synthesis of the octahydroindole unit of aeruginosins via asymmetric hydrogenation of the Diels-Alder adducts of 2-amido-2,4-pentadienoate. *Tetrahedron* **63** 12740-12746

Hou, L., Kang, I., Marchant, R. E. and Zagorski, M. G. (2002) Methionine 35 oxidation reduces fibril assembly of the amyloid abeta-(1-42) peptide of Alzheimer's disease *Journal of Biological Chemistry* **277** 40173-40176

Hou, L., Shao, H., Zhang, Y., Li, H., Menon, N. K., Neuhaus, E. B., Brewer, J. M., Byeon, I. J., Ray, D. G., Vitek, M. P., Iwashita, T., Makula, R. A., Przybyla, A. B. and Zagorski, M. G. (2004) Solution NMR studies of the A beta(1-40) and A beta(1-42) peptides establish that the Met35 oxidation state affects the mechanism of amyloid formation. *Journal of the American Chemical Society* **126** 1992-2005

Hovorka, S. W., Biesiada, H., Williams, T. D., Huhmer, A. and Schoneich, C. (2002) High Sensitivity of Zn2+ Insulin to Metal-Catalzed Oxidation: Detection of 2-Oxo-Histidine by Tandem Mass Spectroscopy. *Pharmaceutical Research* **19** 530-537

Howell, S. J., Spencer, N. and Philp, D. (2001) Recognition-mediated regiocontrol of a dipolar cycloaddition reaction. *Tetrahedron* **57** 4945-4954

Howlett, D. R., Jennings, K. H., Lee, D. C., Clark, M. S., Brown, F., Wetzel, R., Wood, S. J., Camilleri, P. and Roberts, G. W. (1995) Aggregation state and neurotoxic properties of Alzheimer Beta-Amyloid peptide. *Neurodegeneration* **4**

Huang, T. H. J., Yang, D.-S., Plaskos, N. P., Go, S., Yip, C. M., Fraser, P. E. and Chakrabartty, A. (2000) Structural studies of soluble oligomers of the alzheimer [beta]-amyloid peptide. *Journal of Molecular Biology* **297** 73-87

Huang, X., Atwood, C. S., Hartshorn, M. A., Multhaup, G., Goldstein, L. E., Scarpa, R. C., Cuajungco, M. P., Gray, D. N., Lim, J., Moir, R. D., Tanzi, R. E. and Bush, A. I. (1999a) The A beta peptide of Alzheimer's disease directly produces hydrogen peroxide through metal ion reduction. *Biochemistry* **38** 7609-7616

Huang, X., Atwood, C. S., Moir, R. D., Hartshorn, M. A., Tanzi, R. E. and Bush, A. I. (2004) Trace metal contamination initiates the apparent auto-aggregation, amyloidosis, and oligomerization of Alzheimer's Abeta peptides. *Journal of Biological Inorganic Chemistry* **9** 954-960

Huang, X., Cuajungco, M. P., Atwood, C. S., Hartshorn, M. A., Tyndall, J. D., Hanson, G. R., Stokes, K. C., Leopold, M., Multhaup, G., Goldstein, L. E., Scarpa, R. C., Saunders, A. J., Lim, J., Moir, R. D., Glabe, C., Bowden, E. F., Masters, C. L., Fairlie, D. P., Tanzi, R. E. and Bush, A. I. (1999) Cu(II) potentiation of alzheimer abeta neurotoxicity. Correlation with cell-free hydrogen peroxide production and metal reduction. *Journal of Biological Chemistry* **274** 37111-37116

Huffman, W. F., Holden, K. G., Buckley, T. F., Gleason, J. G. and Wu, L. (1977) Nuclear analogs of beta-lactam antibiotics. 1. The total synthesis of a 7-oxo-1,3-diazabicyclo[3.2.0]heptane-2-carboxylic acid via a versatile monocyclic beta-lactam intermediate. *Journal of the American Chemical Society* **99** 2352-2353

Hung, A., Griffin, M. D. W., Howlett, G. J. and Yarovsky, I. (2008) Effects of oxidation, pH and lipids on amyloidogenic peptide structure: implications for fibril formation? *European Biophysics Journal* **38** 99-110

Hureau, C. and Faller, P. (2009) Abeta-mediated ROS production by Cu ions: structural insights, mechanisms and relevance to Alzheimer's disease. *Biochimie* **91** 1212-1217

Hureiki, L., Croue, J. P. and Legube, B. (1994) Chlorination studies of free and combined amino acids. *Water Research* **28** 2521-2531

Imanaga, Y. (1955) Autooxidation of L-ascorbig acid and imidazole nucleus: 1. The effects of imidazole derivatives on the autooxidation of L-ascorbig acid. *Journal of Biochemistry* **42** 657-667

Inoue, K., Garner, C., Ackermann, B. L., Oe, T. and Blaire, L. A. (2006) Liquid chromatography/tandem mass spectrometry characterization of oxidised amyloid beta peptides as potential biomarkers of Alzheimer's disease. *Rapid Communications in Mass Spectrometry* **20** 911-918

Inouye, H., Fraser, P. E. and Kirschner, D. A. (1993) Structure of beta-crystallite assemblies formed by Alzheimer beta-amyloid protein analogues: analysis by x-ray diffraction. *Biophysical Journal* **64** 502-519

Jackson, R. F. W., Wishart, N., Wood, A., James, K. and Wythes, M. J. (1992) Preparation of Enantiomerically Pure Protected 4-Oxo-Alpha-Amino Acids and 3-Aryl-Alpha-Amino Acids from Serine. *Journal of Organic Chemistry* **57** 3397-3404

Jarrett, J. T. and Lansbury, P. T. (1993) Seeding "one-dimensional crystallization" of amyloid: A pathogenic mechanism in Alzheimer's disease and scrapie? *Cell* **73** 1055-1058

Jarrett, J. T., Berger, E. P. and Lansbury, P. T., Jr. (1993) The carboxy terminus of the beta amyloid protein is critical for the seeding of amyloid formation: implications for the pathogenesis of Alzheimer's disease. *Biochemistry* **32** 4693-4697

Jayaraman, S., Gantz, D. L. and Gursky, O. (2007) Effects of Oxidation on the Structure and Stability of Human Low-Density Lipoprotein. *Biochemistry* **46** 5790-5797

Jiang, D. L., Li, X. J., Liu, L., Yagnik, G. B. and Zhou, F. M. (2010) Reaction Rates and Mechanism of the Ascorbic Acid Oxidation by Molecular Oxygen Facilitated by Cu(II)-Containing Amyloid-beta Complexes and Aggregates. *Journal of Physical Chemistry B* **114** 4896-4903

Jiang, D., Men, L., Wang, J., Zhang, Y., Chickenyen, S., Wang, Y. and Zhou, F. (2007) Redox Reactions of Copper Complexes Formed with Different beta-Amyloid Peptides and Their Neuropathalogical Relevance. *Biochemistry* **46** 9270-9282

Jobling, M., Barrow, C., White, A., Masters, C., Collins, S. and Cappai, R. (1999) The synthesis and spectroscopic analysis of the neurotoxic prion peptide 106–126: Comparative use of manual Boc and Fmoc chemistry *Letters in Peptide Science* **6** 129-134

Johansson, A.-S., Bergquist, J., Volbracht, C., Paivio, A., Leist, M., Lannfelt, L. and Westlind-Danielsson, A. (2007) Attenuated amyloid-beta aggregation and neurotoxicity owing to methionine oxidation. *Neuroreport* **18** 559-563

Johansson, R. and Samuelsson, B. (1984) Regioselective Reductive Ring-opening of 4-Methoxybenzylidene Acetals of Hexopyranosides. Access to a Novel Protecting-group Stratgey. Part 1. *Journal of the Chemical Society Perkin Transactions 1* 2371-2374

Jones, R. G. and McLaughlin, K. C. (1949) Studies on Imidazoles. III. 1-Substituted Analogs of Histidine and Histamine. *Journal of the American Chemical Society* **71** 2444–2448

Jumnah, R. (1991) Cycloaddition reactions of 1,2-diacylaminoalkenes from Bamberger cleavage of imidazoles. BSc Dissertation, *Department of Chemistry, Queen Mary and Westfield College*

Kagan, B. (2005) Oligomers and Cellular Toxicity Amyloid Proteins: The Beta Sheet Conformation and Disease. Wilay-VCH

Kamihira, M., Naito, A., Tuzi, S., Nosaka, A. Y. and Saito, H. (2000) Conformational transitions and fibrillation mechanism of human calcitonin as studied by high-resolution solid state 13CNMR. *Protein Science* **9** 867-877

Kamijo, T., Yamamoto, R., Harada, H. and Iizuka, K. (1983) An Improved and Convenient Procedure for the Synthesis of 1-Substituted Imidazoles. *Chemical & Pharmaceutical Bulletin* **31** 1213-1221

Kamsler, A. and Segal, M. (2004) Hydrogen peroxide as a diffusible signal molecule in synaptic plasticity. *Molecular Neurobiology* **29** 167-178

Kang, J., Lee, J. H., Ahn, S. H. and Choi, J. S. (1998) Asymmetric Synthesis of a New Cylindrically Chiral and Air-Stable Ferrocenyldiphosphine and Its Application to Rhodium-Catalyzed Asymmetric Hydrogenation. *Tetrahedron Letters* **39** 5523-5526

Kang, J., Lemaire, H. G., Unterbeck, A., Salbaum, J. M., Masters, C. L., Grzeschik, K. H., Multhaup, G., Beyreuther, K. and Muller-Hill, B. (1987) The precursor of Alzheimer's disease amyloid A4 protein resembles a cell-surface receptor. *Nature* **325** 733-736

Karim, E. and Mahanti, M. K. (1992) Kinetics of oxidation of amino acids by quinolinium dichromate. *Polish Journal of Chemistry* **66** 1471-1476

Karr, J. W. and Szalai, V. A. (2008) Cu(II) binding to monomeric, oligomeric, and fibrillar forms of the Alzheimer's disease amyloid-beta peptide. *Biochemistry* **47** 5006-5016

Kato, M., Saito, H. and Abe, K. (1997) Nanomolar Amyloid beta Protein-Induced Inhibition of Cellular Redox Activity in Cultured Astrocytes. *Journal of Neurochemistry* **68** 1889-1895

Katzman, R., Terry, R., DeTeresa, R., Brown, T., Davies, P., Fuld, P., Renbing, X. and Peck, A. (1988) Clinical, pathological, and neurochemical changes in dementia: a subgroup with preserved mental status and numerous neocortical plaques. *Annals of Neurology* **23** 138-144

Kawai, M., Hosoda, K., Omori, Y., Yamada, K., Hayakawa, S., Yamamura, H. and Butsugan, Y. (1996) Preparation of Protected beta-Alkoxyglycines *Synthetic Communications: An International Journal for Rapid Communication of Synthetic Organic Chemistry* **26** 1545 - 1554

Kayed, R., Head, E., Thompson, J. L., McIntire, T. M., Milton, S. C., Cotman, C. W. and Glabe, C. G. (2003) Common Structure of Soluble Amyloid Oligomers Implies Common Mechanism of Pathogenesis. *Science* **300** 486-489

Khan, A., Dobson, J. P. and Exley, C. (2006) Redox cycling of iron by A beta(42). *Free Radical Biology and Medicine* **40** 557-569

Khandogin, J. and Brooks, C. L., 3rd (2007) Linking folding with aggregation in Alzheimer's beta-amyloid peptides. *Proceedings of the National Academy of Sciences* **104** 16880-16885

Khossravi, M. and Borchardt, D. R. (1998) Chemical Pathways of Peptide Degradation: IX. Metal-Catalyzed Oxidation of Histidine in Model Peptides. *Pharmaceutical Research* **15** 1096-1102

Khossravi, M. and Borchardt, R. T. (2000) Chemical pathways of peptide degradation. X: Effect of metal-catalyzed oxidation on the solution structure of a histidine-containing peptide fragment of human relaxin. *Pharmaceutical Research* **17** 851-858

Khossravi, M., Shire, S. J. and Borchardt, R. T. (2000) Evidence for the involvement of histidine A(12) in the aggregation and precipitation of human relaxin induced by metal-catalyzed oxidation. *Biochemistry* **39** 5876-5885

Khurana, R., Coleman, C., Ionescu-Zanetti, C., Carter, S. A., Krishna, V., Grover, R. K., Roy, R. and Singh, S. (2005) Mechanism of thioflavin T binding to amyloid fibrils *Journal of Structural Biology* **151** 229-238

Kidd, M. (1964) Alzheimer's disease – an electron microscopical study. *Brain* **87** 307-320

Kim, N. H. and Kang, J. H. (2003) Oxidative Modification of Neurofilament-L by Copper-catalyzed Reaction . *Journal of Biochemistry and Molecular Biology* **36** 488-492

Kim, Y. H., Berry, A. H., Spencer, D. S. and Stites, W. E. (2001) Comparing the effect on protein stability of methionine oxidation versus mutagenesis: steps toward engineering oxidative resistance in proteins. *Protein Engineering* **14** 343-347

Kim, Y. S., Moss, J. A. and Janda, K. D. (2004) Biological Tuning of Synthetic Tactics in Solid-Phase Synthesis: Application to Abeta(1-42). *Journal of Organic Chemistry* **69** 7776-7778

Kimoto, H., Kirk, K. L. and Cohen, L. A. (1978) A facile synthesis of 2-(trifluoromethyl)histamine and 2-(trifluoromethyl)-L-histidine. *Journal of Organic Chemistry* **43** 3403-3405

Kirschner, D. A., Abraham, C. and Selkoe, D. J. (1986) X-ray diffraction from intraneuronal paired helical filaments and extraneuronal amyloid fibers in Alzheimer disease indicates cross-beta conformation. *Proceedings of the National Academy of Sciences* **83** 503-507

Kish, S., Morito, C. and Hornykiewicz, O. (1986) Brain glutathione peroxidase in neurodegenerative disorders. *Molecular and Chemical Neuropathology* 23-28 PlacePublished Humana Press Inc.

Klegeris, A. and McGeer, P. L. (1997) beta-Amyloid protein enhances macrophage production of oxygen free radicals and glutamate. *Journal of Neuroscience Research* **49** 229-235

Klein, W. L., Stine, W. B. and Teplow, D. B. (2004) Small assemblies of unmodified amyloid beta-protein are the proximate neurotoxin in Alzheimer's disease. *Neurobiology of Aging* **25** 569-580

Knowles, W. S. (2002) Asymmetric Hydrogenation (Nobel Lecture). *Angewandte Chemie International Edition* **41** 1998-2007

Kontush, A. (2001) Amyloid-beta: an antioxidant that becomes a pro-oxidant and critically contributes to Alzheimer's disease. *Free Radical Biology and Medicine* **31** 1120-1131

Kontush, A., Berndt, C., Weber, W., Akopyan, V., Arlt, S., Schippling, S. and Beisiegel, U. (2001a) Amyloid-beta is an anti-oxidant for lipoproteins in cerebrospinal fluid and plasma. *Free Radical Biology and Medicine* **30** 119-128

Kontush, A., Donarski, N. and Beisiegel, U. (2001b) Resistance of human cerebrospinal fluid to in vitro oxidation is directly related to its amyloid-beta content. *Free Radical Research Communications* **35** 507-517

Korolainen, M., A., Goldsteins, G., Nyman, T. A., Alafuzoff, I., Koistinaho, J. and Pirttilä, T. (2006) Oxidative modification of proteins in the frontal cortex of Alzheimer's disease brain. *Neurobiology of Aging* **27** 42-53

Kosik, K. S. (1999) A notable cleavage: Winding up with beta-amyloid. *Proceedings of the National Academy of Sciences of the United States of America* **96** 2574-2576

Koudinov, A. R., Berezov, T. T. and Koudinova, N. V. (2001) The levels of soluble amyloid-beta in different high density lipoprotein subfractions distinguish Alzheimer's and normal aging cerebrospinal fluid: implication for brain cholesterol pathology? *Neuroscience Letters* **314** 115-118

Kowalik-Jankowska, T., Ruta, M., Wisniewska, K., Lankiewicz, L. and Dyba, M. (2004) Products of Cu(II)-catalyzed oxidation in the presence of hydrogen peroxide of the 1-10, 1-16 fragments of human and mouse amyloid beta peptide. *Journal of Inorganic Biochemistry* **98** 940-950

Kowall, N. W., Beal, M. F., Busciglio, J., Duffy, L. K. and Yankner, B. A. (1991) An in vivo model for the neurodegenerative effects of beta amyloid and protection by substance P. *Proceedings of the National Academy of Sciences* **88** 7247-7251

Krebs, M. R. H., Bromley, E. H. C. and Donald, A. M. (2005) The binding of thioflavin-T to amyloid fibrils: localisation and implications *Journal of Structural Biology* **149** 30-37

Kreuzfeld, H.-J., Dobler, C., Krause, H. W. and Facklam, C. (1993) Unusual amino acids. V. Asymmetric hydrogenation of (Z)-N-Acylamino-cinnamic acid derivatives bearing different protective groups. *Tetrahedron Asymmetry* **4** 2047-2051

Krogsgaard-Larsen, P., Nielsen, E. O. and Curtis, D. R. (1984) Ibotenic acid analogs. Synthesis and biological and in vitro activity of conformationally restricted agonists at central excitatory amino acid receptors. *Journal of Medicinal Chemistry* **27** 585-591

Kuo, Y. M., Emmerling, M. R., Vigo-Pelfrey, C., Kasunic, T. C., Kirkpatrick, J. B., Murdoch, G. H., Ball, M. J. and Roher, A. E. (1996) Water soluble Abeta(N-40N-42) oligomers in normal and Alzheimer disease brains. *Journal of Biological Chemistry* **271** 4077-4081

Kuo, Y.-M., Webster, S., Emmerling, M. R., De Lima, N. and Roher, A. E. (1998) Irreversible dimerization/tetramerization and post-translational modifications inhibit proteolytic degradation of A[beta] peptides of Alzheimer's disease. *Biochimica et Biophysica Acta (BBA) - Molecular Basis of Disease* **1406** 291-298

Kurahashi, T., Miyazaki, A., Suwan, S. and Isobe, M. (2001) Extensive Investigations on Oxidized Amino Acid Residues in H2O2-Treated Cu,Zn-SOD Protein with LC-ESI-Q-TOF-MS, MS/MS

for the Determination of the Copper-Binding Site. *Journal of the American Chemical Society* **123** 9268-9278

Kusumoto, Y., Lomakin, A., Teplow, D. B. and Benedek, G. B. (1998) Temperature dependence of amyloid beta-protein fibrillization. *Proceedings of the National Academy of Sciences* **95** 12277–12282

Kuwano, R. and Kondo, Y. (2004) Palladium-Catalyzed Benzylation of Active Methine Compounds without Additional Base: Remarkable Effect of 1,5-Cyclooctadiene. *Organic Letters* **6** 3545-3547

Lacor, P. N., Buniel, M. C., Furlow, P. W., Sanz Clemente, A., Velasco, P. T., Wood, M., Viola, K. L. and Klein, W. L. (2007) Abeta oligomer-induced aberrations in synapse composition, shape, and density provide a molecular basis for loss of connectivity in Alzheimer's disease. *Journal of Neuroscience* **27** 796-807

Lacor, P. N., Viola, K. L., Fernandez, S., Velasco, P. T., Bigio, E. H. and Klein, W. L. (2003) Targeting of synapses and memory-linked IEG protein Arc by ADDLs. *Society for Neuroscience Abstracts* 29

Laloo, D. and Mahanti, M. K. (1990) Kinetics of Oxidation of Amino-Acids by Alkaline Hexacyanoferrate(III). *Journal of Physical Organic Chemistry* **3** 799-802

Lam, A. K. Y., Hutton, C. A. and O'Hair, R. A. J. (2010) Role of 2-oxo and 2-thioxo modifications on the proton affinity of histidine and fragmentation reactions of protonated histidine. *Rapid Communications in Mass Spectrometry* **24** 2591-2604

Lambert, M. P., Barlow, A. K., Chromy, B. A., Edwards, C., Freed, R., Liosatos, M., Morgan, T. E., Rozovsky, I., Trommer, B., Viola, K. L., Wals, P., Zhang, C., Finch, C. E., Krafft, G. A. and Klein, W. L. (1998) Diffusible, nonfibrillar ligands derived from Abeta1-42 are potent central nervous system neurotoxins. *Proceedings of the National Academy of Sciences* **95** 6448-6453

Lanman, B. A., Overman, L. E., Paulini, R. and White, N. S. (2007) On the structure of Palau'amine: Evidence for the revised relative configuration from chemical synthesis. *Journal of the American Chemical Society* **129** 12896-12900

Lashuel, H. A., Hartley, D. M., Petre, B. M., Wall, J. S., Simon, M. N., Walz, T. and Lansbury, P. T., Jr. (2003) Mixtures of wild-type and a pathogenic (E22G) form of Abeta40 in vitro accumulate protofibrils, including amyloid pores. *Journal of Molecular Biology* **332** 795-808

Lassmann, G., Eriksson, L. A., Lendzian, F. and Lubitz, W. (2000) Structure of a transient neutral histidine radical in solution: EPR continuous-flow studies in a Ti3+/EDTA-Fenton system and density functional calculations. *Journal of Physical Chemistry A* **104** 9144-9152

Lászó, G. (2006) The hydrogen peroxide paradox. *Orvosi hetilap* **19** 887-893

Lazarus-Barlow, W. S. (1896) On the Initial Rate of Osmosis of Blood serum with reference to the Composition of "Physiological Saline Solution" in Mammals. *The Journal of Physiology* **20** 145-157

Lazo, N. D., Maji, S. K., Fradinger, E. A., Bitan, G. and Teplow, D. B. (2005) The Amyloid beta-Protein. Amyloid Proteins: The Beta Sheet Conformation and Disease. Wiley-VCH

Lee, H.-g., Zhu, X., Castellani, R. J., Nunomura, A., Perry, G. and Smith, M. A. (2007) Amyloid- beta in Alzheimer Disease: The Null versus the Alternate Hypotheses. *Journal of Pharmacology and Experimental Therapeutics* **321** 823-829

Lee, J. and Helmann, J. D. (2006) The PerR transcription factor sense H_2O_2 by metal-catalyzed oxidation. *Nature* **440** 363-367

Leigh, C. D. and Bertozzi, C. R. (2008) Synthetic studies toward Mycobacterium tuberculosis sulfolipid-I. *Journal of Organic Chemistry* **73** 1008-1017

Levine (1983) Oxidative modification of glutamine synthetase. I. Inactivation is due to loss of one histidine residue. *Journal of Biological Chemistry* **258** 11823-11827

Levine, H. (1993) Thioflavin-T Interaction with Synthetic Alzheimers-Disease Beta-Amyloid Peptides - Detection of Amyloid Aggregation in Solution. *Protein Science* **2** 404-410

Levine, H. (1995) Soluble multimeric Alzheimer [beta](1-40) pre-amyloid complexes in dilute solution. *Neurobiology of Aging* **16** 755-764

Levine, R. L., Mosoni, L., Berlott, B. S. and Stadtman, E. R. (1996) Methionine residues as endogenous antioxidants in proteins. *Proceedings of the National Academy of Sciences* **93** 15036-15040

Lewisch, S. A. and Levine, R. L. (1999) Determination of 2-Oxohistidine by Amino Acid Analysis. Methods in enzymology Gulf Professional Publishing

Li, M., Sunamoto, M., Ohnishi, K. and Ichmori, Y. (1996) beta-amyloid protein dependent nitric oxide production from microglial cells and neurotoxicity. *Brain Research* **720** 93-100

Liaw, S.-H., Villafrace, J. J. and Eisenberg, D. (1993) A Model for Oxidative Modifications of Glutamine Synthetase, Based on Crystal Structures of Mutant H269N and the Oxidised Enzyme. *Biochemistry* **32** 7999-8003

Lisowski, V., Enguehard, C., Lancelot, J. C., Caignard, D. H., Lambel, S., Leonce, S., Pierre, A., Atassi, G., Renard, P. and Rault, S. (2001) Design, synthesis and antiproliferative activity of tripentones: A new series of antitubulin agents. *Bioorganic & Medicinal Chemistry Letters* **11** 2205-2208

Liu, G., Men, P., Perry, G. and Smith, M. A. (2010) Nanoparticle and Iron Chelators as a Potential Novel Alzheimer Therapy. *Methods in Molecular Biology (Free Radicals and Antioxidant Protocols)* **610** 123-144

Liu, S. T., Howlett, G. and Barrow, C. J. (1999) Histidine-13 is a crucial residue in the zinc ion-induced aggregation of the A beta peptide of Alzheimer's disease. *Biochemistry* **38** 9373-9378

Lockhart, B. P., Benicourt, C., Junien, J.-L. and Privat, A. (1994) Inhibitors of free radical formation fail to attenuate direct beta-amyloid25-35 peptide-mediated neurotoxicity in rat hippocampal cultures. *Journal of Neuroscience* **39** 494-505

Lomakin, A., Chung, D. S., Benedek, G. B., Kirschner, D. A. and Teplow, D. B. (1996) On the nucleation and growth of amyloid beta-protein fibrils: Detection of nuclei and quantitation of rate constants. *Proceedings of the National Academy of Sciences of the United States of America* **93** 1125-1129

Lomakin, A., Teplow, D. B., Kirschner, D. A. and Benedek, G. B. (1997) Kinetic theory of fibrillogenesis of amyloid beta-protein. *Proceedings of the National Academy of Sciences* **94** 7942-7947

Loosemore, M. J. and Pratt, R. F. (1976) The irreversible cleavage of histidine residues by diethylpyrocarbonate (ethoxyformic anhydride). *FEBS Letters* **72** 155-158

Lorenzo, A. and Yankner, B. A. (1994) beta-Amyloid neurotoxicity requires fibril formation and is inhibited by congo red. *Proceedings of the National Academy of Sciences* **91** 12243-12247

Lorenzo, A., Matsudaira, P. and Yankner, B. A. (1993) The role of oxidation in the neurotoxicity of beta amyloid. *Society for Neuroscience Abstracts* **19** 184

Lovell, M. A., Ehmann, W. D., M., B. S. and Markesbery, W. R. (1995) Elevated thiobarbituric acid-reactive substances and antioxidant enzyme activity in the brain in Alzheimer's disease. *Neurology* **45** 1594-1601

Lovell, M. A., Robertson, J. D., Teesdale, W. J., Campbell, J. L. and Markesbery, W. R. (1998) Copper, iron and zinc in Alzheimer's disease senile plaques. *Journal of Neuroscience* **158** 47-52

Lovely, C. J., Du, H., He, Y. and Dias, H. V. R. (2004) Oxidative Rearrangement of Imidazoles with Dimethyldioxirane. *Organic Letters* **6** 735-738

Lue, L.-F., Kuo, Y.-M., Roher, A. E., Brachova, L., Shen, Y., Sue, L., Beach, T., Kurth, J. H., Rydel, R. E. and Rogers, J. (1999) Soluble Amyloid {beta} Peptide Concentration as a Predictor of Synaptic Change in Alzheimer's Disease. *American Journal of Pathology* **155** 853-862

Luhrs, T., Ritter, C., Adrian, M., Riek-Loher, D., Bohrmann, B., Dobeli, H., Schubert, D. and Riek, R. (2005) 3D structure of Alzheimer's amyloid-beta(1-42) fibrils. *Proceedings of the National Academy of Sciences* **102** 17342-17347

Lundt, B. F., Johansen, N. L., Vølund, A. and Markussen, J. (1978) Removal of t-Butyl and t-Butoxycarbonyl protecting groups with trifluoroacetic acid. *International Journal of Peptide and Protein Research* **12** 258-268

Ma, Z., Lu, J., Wang, W. and Chen, C. (2011) Revisiting the Kinnel-Scheuer hypothesis for the biosynthesis of palau'amine. *Chemical Communications* **47** 427-429

Maiti, P., Piacentini, R., Ripoli, C., Grassi, C. and Bitan, G. (2010) Surprising toxicity and assembly behaviour of amyloid beta-protein oxidized to sulfone. *Biochemical Journal* **433** 323-332

Marckwald, W. (1892) Ein Beitrag zur Kenntniss der Imidazole und der Constitution des Glyoxalins. *Berichte der deutschen chemischen Gesellschaft* **25** 2354-2373

Marino, S. T., Stachurska-Buczek, D., Huggins, D. A., Krywult, B. M., Sheehan, C. S., Nguyen, T., Choi, N., Parsons, J. G., Griffiths, P. G., James, I. W., Bray, A. M., White, J. M. and Boyce, R. S. (2004) Synthesis of Chiral Building Blocks for Use in Drug Discovery. *Molecules* **9** 405-426

Markesbery, W. R. (1997) Oxidative Stress Hypothesis in Alzheimer's Disease. *Free Radical Biology and Medicine* **23** 134-147

Martins, R. N., Harper, C. G., Stokes, G. B. and Masters, C. L. (1986) Increased Cerebral Glucose-6-Phosphate Dehydrogenase Activity in Alzheimer's Disease May Reflect Oxidative Stress. *Journal of Neurochemistry* **46**

Masters, C. L., Multhaup, G., Simms, G., Pottgiesser, J., Martins, R. N. and Beyreuther, K. (1985) Neuronal origin of a cerebral amyloid—neurofibrillary tangles of Alzheimer's-disease contain the same protein as the amyloid of plaque cores and blood-vessels. *EMBO Journal* **11** 2757-2763

Matsuoka, Y., Picciano, M., La Francois, J. and Duff, K. (2001) Fibrillar beta-amyloid evokes oxidative damage in a transgenic mouse model of Alzheimer's disease. *Neuroscience* **104** 609-613

Mattson, M. P., Fu, W., Waeg, G. and Uchida, K. (1997) 4-Hydroxynonenal, a product of lipid peroxidation, inhibits dephosphorylation of the microtubule-associated protein tau. *Neuroreport* **8** 2275-2281

Mazurkiewicz, R. and Kuznik, A. (2006) A new convenient synthesis of N-acyl-2-(dimethoxyphosphoryl)glycinates. *Tetrahedron Letters* **47** 3439-3442

McDonald, D. R., Brunden, K. R. and Landreth, G. E. (1997) Amyloid fibrils activate tyrosine kinase-dependent signalling and superoxide production in microglia. *Journal of Neuroscience* **17**

McLaurin, J. and Fraser, P. E. (2000) Effect of amino-acid substitutions on Alzheimer's amyloid-beta peptide–glycosaminoglycan interactions. *European Journal of Biochemistry* **267** 6353–6361

McLaurin, J., Yang, D., Yip, C. M. and Fraser, P. E. (2000) Review: modulating factors in amyloid-beta fibril formation. *Journal of Structural Biology* **130** 259-270

McLean, C. A., Cherny, R. A., Fraser, F. W., Fuller, S. J., Smith, M. J., Vbeyreuther, K., Bush, A. I. and Masters, C. L. (1999) Soluble pool of Abeta amyloid as a determinant of severity of neurodegeneration in Alzheimer's disease. *Annals of Neurology* **46** 860-866

Mears, R. J., Sailes, H. E., Watts, J. P. and Whiting, A. (2006) A stereoselective remote homochiral boronate ester-mediated aldol reaction. *Arkivoc* **i** 95-103

Mecocci, P., MacGarvey, U. and Beal, M. F. (1994) Oxidative damage to mitochondrial DNA is increased in Alzheimer's disease. *Annals of Neurology* **36** 747-750

Mecocci, P., MacGarvey, U., Kaufman, A. E., Koontz, D., Shoffner, J. M., Wallace, D. C. and Beal, M. F. (1993) Oxidative damage to mitochondrial DNA shows marked age-dependent increases in human brain. *Annals of Neurology* **34** 609-616

Meda, L., Cassatella, M. A., Szendrei, G. I., Otvos Jr, L., Baron, P., Villalba, M., Ferrari, D. and Rossi, F. (1995) Activation of microglial cells by beta-amyloid protein and interferon-gamma. *Nature* **374** 647-650

Mehta, P. D., Pirtilla, T., Mehta, S. P., Sersen, E. A., Aisen, P. S. and Wisniewska, H. M. (2000) Plasma and Cerebrospinal Fluid Levels of Amyloid {beta} Proteins 1-40 and 1-42 in Alzheimer Disease. *Archives of Neurology* **57** 100-105

Meister Winter, G. E. and Butler, A. (1996) Inactivation of vanadium bromoperoxidase: Formation of 2-oxohistidine. *Biochemistry* **35** 11805-11811

Melo, J. B., Sousa, C., Garcao, P., Oliveira, C. R. and Agostinho, P. (2009) Galantamine protects against oxidative stress induced by amyloid-beta peptide in cortical neurons. *European Journal of Neuroscience* **29** 455-464

Meyer-Luehmann, M., Spires-Jones, T. L., Prada, C., Garcia-Alloza, M., de Calignon, A., Rozkalne, A., Koenigsknecht-Talboo, J., Holtzman, D. M., Bacskai, B. J. and Hyman, B. T. (2008) Rapid appearance and local toxicity of amyloid-beta plaques in a mouse model of Alzheimer's disease. *Nature* **451** 720-724

Milton, S., Milton, R., Kates, S. and Glabe, C. (1999) Improved synthesis and purification of Alzheimer's Abeta 1-42 and analogs *Letters in Peptide Science* 151-156 PlacePublished Springer Netherlands

Misonou, H., Morishima-Kawashima, M. and Ihara, Y. (2000) Oxidative stress induces intracellular accumulation of amyloid beta-protein (Abeta) in human neuroblastoma cells. *Biochemistry* **39** 6951-1959

Miyakawa, T., Katsuragi, S., Watanabe, K., Shimoji, A. and Ikeuchi, Y. (1986) Ultrastructural studies of amyloid fibrils and senile plaques in human brain. *Acta Neuropathologica* **70** 202-208

Mizusaki, K. and Makisumi, S. (1981) Synthesis of four stereoisomers of gamma-Hydroxyarginine via the corresponding isomers of gamma-Hydroxyornithine. *Bulletin of the Chemical Society of Japan* **54** 470-472

Monji, A., Utsumi, H., Yoshida, I., Hashiko, S., Tashiro, K.-I. and Tashiro, N. (2001) The relationship between Abeta-associated free radical generation and Abeta fibril formation revealed by negative stain electron microscopy and thioflavine-T fluorometric assay. *Neuroscience Letters* **304** 65-68

Moorthy, J. N., Senapati, K. and Parida, K. N. (2010) 6-Membered Pseudocyclic IBX Acids: Syntheses, X-ray Structural Characterizations, and Oxidation Reactivities in Common Organic Solvents *The Journal of Organic Chemistry* **75** 8416-8421

Mori, S. and Barth, H. G. (1999) Size exclusion chromatography Springer

Mori, S., Iwakura, H. and Takechi, S. (1988) A New Amidoalkynylation Using Alkynylzinc Reagent. *Tetrahedron Letters* **29** 5391-5394

Morris, A. M., Watzky, M. A., Agar, J. N. and Finke, R. G. (2008) Fitting Neurological Protein Aggregation Kinetic Data via a 2-Step, Minimal/"Ockham's Razor" Model: The Finke-Watzky Mechanism of Nucleation Followed by Autocatalytic Surface Growth. *Biochemistry* **47** 2413-2427

Mucke, L., Masliah, E., Yu, G. Q., Mallory, M., Rockenstein, E. M., Tatsuno, G., Hu, K., Kholodenko, D., Johnson-Wood, K. and McConlogue, L. (2000) High-level neuronal expression of A(1–42) in wildtype human amyloid protein precursor transgenic mice: synaptotoxicity without plaque formation. *Journal of Neuroscience* **20** 4050-4058

Murakami, K., Irie, K., Morimoto, A., Ohigashi, H., Shindo, M., Nagao, M., Shimizu, T. and Shirasawa, T. (2003) Neurotoxicity and Physicochemical Properties of Abeta Mutant Peptides from Cerebral Amyloid Angiopathy. *Journal of Biological Chemistry* **278** 46179-46187

Murray, I. V. J., Sindoni, M. E. and Axelsen, P. H. (2005) Promotion of Oxidative Lipid Membrane Damage by Amyloid beta Proteins. *Biochemistry* **44** 12606-12613

Murray, M. M., Bernstein, S. L., Nyugen, V., Condron, M. M., Teplow, D. B. and Bowers, M. T. (2009) Amyloid beta Protein: A beta 40 Inhibits A beta 42 Oligomerization. *Journal of the American Chemical Society* **131** 6316-6317

Murray, R. W. and Singh, M. (1998) Synthesis of epoxides using dimethyldioxirane: trans-stilbene oxide. *Organic Syntheses* **9** 288-293

Nadal, R. C., Rigby, S. E. J. and Viles, J. H. (2008) Amyloid beta-Cu2+ Complexes in both Monomeric and Fibrillar Forms Do Not Generate H2O2 Catalytically but Quench Hydroxyl Radicals. *Biochemistry* **47** 11653-11664

Nagel, U. and Albrecht, J. (1998) The enantioselective hydrogenation of *N*-acyl dehydroamino acids. *Topics in Catalysis* **5** 3-23

Naiki, H., Higuchi, K., Hosokawa, M. and Takeda, T. (1989) Fluorometric determination of amyloid fibrils in vitro using the fluorescent dye, thioflavin T. *Analytical Biochemistry* **177** 244-249

Nakajima, M. (1958) *Nagasaki Medical Journal* **33** 825

Nakamura, M., Shishido, N., Nunomura, A., Smith, M. A., Perry, G., Hayashi, Y., Nakayama, K. and Hayashi, T. (2007) Three histidine residues of amyloid-beta peptide control the redox activity of copper and iron. *Biochemistry* **46** 12737-12743

Nakamura, S., Murayama, N., Noshita, T., Annoura, H. and Ohno, T. (2001) Progressive brain dysfunction following intracerebrocenticular infusion of beta(1-42)-amyloid peptide. *Brain Research* **912** 128-136

Naylor, E. M., Parmee, E. R., Colandrea, V. J., Perkins, L., Brockunier, L., Candelore, M. R., Cascieri, M. A., Colwell, L. F., Deng, L., Feeney, W. P., Forrest, M. J., Hom, G. J., MacIntyre, D. E., Strader, C. D., Tota, L., Wang, P.-R., Wyvratt, M. J., Fisher, M. H. and Weber, A. E. (1999) Human [beta]3 andrenergic receptor agonists containing imidazolidinone and imidazolone benzenesulfonamides. *Bioorganic & Medicinal Chemistry Letters* **9** 755-758

Naylor, R., Hill, A. and Barnham, K. J. (2008) Is covalently crosslinked Abeta responsible for synaptotoxicity in Alzheimer's disease? *Current Alzheimer research* **5** 533-539

Nelson, R. and Eisenberg, D. (2006) Structural models of amyloid-like fibrils. *Advances in Protein Science* **73** 235 - 282

Nelson, T. J. and Alkon, D. L. (2005) Oxidation of Cholesterol by Amyloid Precursor Protein and beta-Amyloid Peptide. *Journal of Biological Chemistry* **280** 7377-7387

Nichols, M. R., Moss, M. A., Reed, D. K., Lin, W.-L., Mukhopadhyay, R., Hoh, J. H. and Rosenberry, T. L. (2002) Growth of beta-Amyloid(1-40) Protofibrils by Monomer Elongation and Lateral Association. Characterization of Distinct Products by Light Scattering and Atomic Force Microscopy. *Biochemistry* **41** 6115-6127

Nicoletti, T. M., Raston, C. L. and Sargent, M. V. (1990) A New Synthesis of Anthraquinones Using Dihydro-Oxazoles and Grignard-Reagents Derived from Mg(Anthracene)(Thf)3. *Journal of the Chemical Society-Perkin Transactions 1* 133-138

Nicotera, T. M. Thioflavin T method for detection of amyloid polypeptide fibril aggregation.

Nilsberth, C., Westlind-Danielsson, A., Eckman, C. B., Condron, M. M., Axelman, K., Forsell, C., Stenh, C., Luthman, J., Teplow, D. B., Younkin, S. G., Naslund, J. and Lannfelt, L. (2001) The 'Arctic' APP mutation (E693G) causes Alzheimer's disease by enhanced A[beta] protofibril formation *Nature Neuroscience* **4** 887-893

Nishino, S. and Nishida, Y. (2001) Oxygenation of amyloid beta-peptide (1-40) by copper(II) complexand hydrogen peroxide system. *Inorganic Chemistry Communications* **4** 86-89

Nordberg, A. (2003) Toward an early diagnosis and treatment of Alzheimer's disease *Int Psychogeriatr* **15** 223-237

Nunomura, A., Perry, G., Aliev, G., Hirai, K., Takeda, A., Balraj, E. K., Jones, P. K., Ghanbari, H., Wataya, T., Shimohama, S., Chiba, S., Atwood, C. S., Petersen, R. B. and Smith, M. A. (2001) Oxidative damage is the earliest event in Alzheimer's disease. *Journal of Neuropathology and Experimental Neurology* **60** 759-767

Nunomura, A., Perry, G., Pappola, M. A., Wade, R., Hirai, K., Chiba, S. and Smith, M. A. (1999) RNA oxidation is a promient feature of vulnerable neurons in Alzheimer's disease. *Journal of Neuroscience* **19** 1959-1964

Nybo, M., Svehag, S.-E. and Nielsen, E. H. (1999) An ultrastructural study of amyloid intermediates in Ab1–42 fibrillogenesis. *Scandinavian Journal of Immunology* **49** 219-223

Oda, T., Walls, P., Osterburg, H. H., Johnson, S. A., Pasinetti, G. M., Morgan, T. E., Rozovsky, I., Stine, W. B., Snyder, S. W., Holzman, T. F., Krafft, G. A. and Finch, C. E. (1995) Clusterin (apo-J) alters the aggregation of Amyloid beta-peptide (Abeta1-42) and forms slowly sedimenting Abeta complexes that cause oxidative stress. *Experimental Neurology* **136** 22-31

Oddo, S., Vasilevko, V., Caccamo, A., Kitazawa, M., Cribbs, D. H. and LaFerla, F. M. (2006) Reduction of Soluble Abeta and Tau, but Not Soluble Abeta Alone, Ameliorates Cognitive Decline in Transgenic Mice with Plaques and Tangles. *Journal of Biological Chemistry* **281** 39413-39423

Olanow, C. W. (1993) A radical hypothesis for neurodegeneration. *Trends in Neurosciences* **16** 439-444

Oliver, C. N. (1987) Age-related changes in oxidized proteins. *Journal of Biological Chemistry* **262** 5488-5491

Opazo, C., Huang, X., Cherny, R. A., Moir, R. D., Roher, A. E., White, A. R., Cappai, R., Masters, C. L., Tanzi, R. E., Inestrosa, N. C. and Bush, A. I. (2002) Metalloenzyme-like Activity of Alzheimer's Disease beta-Amyloid:Cu-dependent catalytic conversion of dopamine, cholesterol, and biological reducing agents to neurotoxic H2O2. *Journal of Biological Chemistry* **277** 40302-40308

Orgogozo, J. M., Gilman, S., Dartigues, J. F., Laurent, B., Puel, M., Kirby, L. C., Jouanny, P., Dubois, B., Eisner, L., Flitman, S., Michel, B. F., Boada, M., Frank, A. and Hock, C. (2003) Subacute meningoencephalitis in a subset of patients with AD after Abeta42 immunization. *Neurology* **61** 46-54

Oswald, C. L., Carrillo-Marquez, T., Caggiano, L. and Jackson, R. F. W. (2008) Negishi cross-coupling reactions of alpha-amino acid-derived organozinc reagents and aromatic bromides. *Tetrahedron* **64** 681-687

Otani, T. T. and Briley, M. R. (1979) *N*-Benzoyl derivatives of amino acids and amino acid analogs as growth inhibitors in microbial antitumor screen. *Journal of Pharmaceutical Sciences* **68** 1366-1369

Otter, B. A., Falco, E. A. and Fox, J. J. (1968) Nucleosides. LII. Transformations of pyrimidine nucleosides in alkaline media. 1. Conversion of 5-haloarabinosyluracils to imidazoline nucleosides. *Journal of Organic Chemistry* **33** 3593-3600

Oyedele, T. A. O. (2011) Chemical modification of histidine as a route to unusual amino acids. MSci Advanced Chemistry Project, *SBCS, Queen Mary University of London*

Palmblad, M., Westlind-Danielsson, A. and Bergquist, J. (2002) Oxidation of methionine 35 attenuates formation of amyloid beta-peptide 1-40 oligomers. *Journal of Biological Chemistry* **277** 19506-19510

Paola, D., Domenicotti, C., Nitti, M., Vitali, A., Borghi, R., Cottalasso, D., Zaccheo, D., Odetti, P., Strocchi, P., Marinari, U. M., Tabaton, M. and Pronzato, M. A. (2000) Oxidative Stress Induces Increase in Intracellular Amyloid [beta]-Protein Production and Selective Activation of [beta]I and [beta]II PKCs in NT2 Cells. *Biochemical and Biophysical Research Communications* **268** 642-646

Patchornik, A., Berger, A. and Katchalski, E. (1957) Carbobenzoxy Derivatives of Histidine, Imidazole and Benzimidazole. *Journal of the American Chemical Society* **79** 6416-6420

Paterson, I., Burton, P. M., Cordier, C. J., Housden, M. P., Muhlthau, F. A. and Loiseleur, O. (2009) Toward the Total Synthesis of the Brasilinolides: Construction of a Differentially Protected C20-C38 Segment. *Organic Letters* **11** 693-696

Pereira, W. E., Hoyano, Y., Summons, R. E. and Bacon, V. A. (1973) Chlorination Studies II. The reaction of aqueous hypochlorous acid with alpha-amino acids and dipeptides. *Biochimica et Biophysica Acta* **313** 170-180

Perfetti, R. B., Anderson, C. D. and Hall, P. L. (1976) The chemical modification of papain with 1-ethyl-3-(3-dimethylaminopropyl)carbodiimide. *Biochemistry* **15** 1735-1736

Perkins, A. J., Hendrie, H. C., Callahan, C. M., Geo, S., Unverzagt, F. W., Yong, X., Hall, K. S. and Hui, S. L. (1999) Association of antioxidants with memory in a mutliethnic elderly sample using the Third National Health and Nutrition Examination Survey. *American Journal of Epidemiology* **150** 37-44

Pesaresi, M., Lovati, C., Bertora, P., Mailland, E., Galimberti, D., Scarpini, E., Quadri, P., Forloni, G. and Mariani, C. (2006) Plasma levels of beta-amyloid (1-42) in Alzheimer's disease and mild cognitive impairment. *Neurobiology of Aging* **27** 904-905

Petkova, A. T., Ishii, Y., Balbach, J. J., Antzutkin, O. N., Leapman, R. D., Delaglio, F. and Tycko, R. (2002) A structural model for Alzheimer's beta-amyloid fibrils based on experimental constraints from solid state NMR. *Proceedings of the National Academy of Sciences* **99** 16742-16747

Pike, C. J., Walencewicz, A. J., Glabe, C. G. and Cotman, C. W. (1991) In vitro aging of beta-amyloid protein causes peptide aggregation and neurotoxicity. *Brain Research* **563** 311-314

Pike, C. J., Walencewicz, A. J., Kosmoski, J., Cribbs, D. H., Glabe, C. G. and Cotman, C. W. (1995) Structure-Activity Analyses of beta-Amyloid Peptides: Contributions of the beta25-35 Region to Aggregation and Neurotoxicity. *Journal of Neurochemistry* **64** 253-265

Pinto, I., Sherigara, B. S. and Udupa, H. V. K. (1990) Electrolytically generated manganese(III) sulfate for the oxidation of L-histidine in aqueous sulfuric acid: a kinetic study. *Bulletin of the Chemical Society of Japan* **63** 3625-3231

Poon, H. F., Joshi, G., Sultana, R., Farr, S. A., Banks, W. A., Morley, J. E., Calabrese, V. and Butterfield, D. A. (2004) Antisense directed at the Abeta region of APP decrease brain oxidative markers in aged senescence accelerated mice. *Brain Research* **1018** 86-96

Popescu, B. F. G. and Nichol, H. (2011) Mapping Brain Metals to Evaluate Therapies for Neurodegenerative Disease. *CNS Neuroscience and Therapeutics* **17** 256-268

Pratico, D. (2008) Evidence of oxidative stress in Alzheimer's disease brain and antioxidant therapy. 70-78 Mitochondria and Oxidative Stress in Neurodegenerative Disorders Annals of the New York Academy of Sciences

Pratico, D., Uryu, K., Leight, S., Q., T. J. and Lee, V. M. (2001) Increased lipid peroxidation precedes amyloid plaque formation in an animal model of Alzheimer amyloidosis. *Journal of Neurochemistry* **21** 4183-4187

Premkumar, D. R. D., Smith, M. A., Richey, P. L., Petersen, R. B., Castellani, R., Kutty, R. K., Wiggert, B., G., P. and Kalaria, R. N. (1995) Induction of heme oxygenase-1 mRNA and protein in neocortex and cerebral vessels in Alzheimer's disease. *Journal of Neurochemistry* 1399-1402

Pridgen, L. N., Prol, J., Alexander, B. and Gillyard, L. (1989) Single-Pot Reductive Conversion of Amino-Acids to Their Respective 2-Oxazolidinones Employing Trichloromethyl Chloroformate as the Acylating Agent - a Multigram Synthesis. *Journal of Organic Chemistry* **54** 3231-3233

Puzzo, D., Privitera, L., Leznik, E., Fa, M., Staniszewski, A., Palmeri, A. and Arancio, O. (2008) Picomolar Amyloid- beta Positively Modulates Synaptic Plasticity and Memory in Hippocampus. *Journal of Neuroscience* **28** 14537

Qian, X., Zheng, B., Burke, B., Saindane, M. T. and Kronenthal, D. R. (2002) A Stereoselective Synthesis of BMS-262084, an Azetidinone-Based Tryptase Inhibitor. *Journal of Organic Chemistry* **67** 3595-3600

Qin, H.-L. and Panek, J. S. (2008) Total Synthesis of the Hsp90 Inhibitor Geldanamycin. *Organic Letters* **10** 2477-2479

Qin, Z. (2010) Effect of solvents, buffer systems, and ionic strength on the fibrillation of beta-amyloid peptides. *Alzheimers and Dementia* **6** S240

Quibell, M., Turnell, W. G. and Johnson, T. (1994) Preparation and Purification of beta-amyloid (1-43) via Soluble, Amide Backbone Protected Intermediates *J. Org. Chem.* **59** 1745-1750

Quibell, M., Turnell, W. G. and Johnson, T. (1995) Improved Preparation of Beta-Amyloid(1-43) - Structural Insight Leading to Optimized Positioning of N-(2-Hydroxy-4-Methoxybenzyl) (Hmb) Backbone Amide Protection *Journal of the Chemical Society-Perkin Transactions 1* 2019-2024

Rangappa, K. S., Chandraju, S. and Gowda, N. M. M. (1998) Manganese(III) oxidation of L-lysine and L-histidine in pyrophosphate solution: a kinetic and mechanistic study. *Synthetic Reactions in Inorganic Metal-Organic Chemistry* **28** 275-294

Rapoport, M., Dawson, H. N., Binder, L. I., Vitek, M. P. and Ferreira, A. (2002) Tau is essential to beta-amyloid-induced neurotoxicity. *Proceedings of the National Academy of Sciences* **99** 6363-6369

Ratcliffe, R. W. and Christensen, B. G. (1973) Total synthesis of [beta]-lactam antibiotics II. (±)-cephalothin. *Tetrahedron Letters* **14** 4649-4652

Reitz, D. B., Garland, D. J., Norton, M. B., Collins, J. T., Reinhard, E. J., Manning, R. E., Olins, G. M., Chen, S. T., Palomo, M. A., McMahon, E. G. and Koehler, K. F. (1993) N1-sterically hindered 2H-imidazol-2-one angiotensin II receptor antagonists: The conversion of surmountable antagonists to insurmountable antagonists. *Bioorganic & Medicinal Chemistry Letters* **3** 1055-1060

Ren, Y., Li, M. and Wong, N.-B. (2005) Prototropic tautomerism of imidazolone in aqueous solution: a density functional approach using the combined discrete/self-consistent reaction field (SCRF) models. *Journal of Molecular Modelling* **11** 167-173

Requena, J. s. R., Groth, D., Legname, G., Stadtman, E. R., Prusiner, S. B. and Levine, R. L. (2001) Copper-catalyzed oxidation of the recombinant SHa(29-231) prion protein. *Proceedings of the National Academy of Sciences of the United States of America* **98** 7170-7175

Retsky, K. L., Chen, K., Zeind, J. and Frei, B. (1998) Inhibition of copper-induced LDL oxidation by vitamin C is associated with decreased copper-binding to LDL and 2-oxo-histidine formation. *Free Radical Biology and Medicine* **26** 90-98

Riek, R., Guntert, P., Dobeli, H., Wipf, B. and Wuthrich, K. (2001) NMR studies in aqueous solution fail to identify significant conformational differences between the monomeric forms of two Alzheimer peptides with widely different plaque-competence, A beta(1-40)(ox) and A beta(1-42)(ox). *European Journal of Biochemistry* **268** 5930-5936

Ritchie, C. W., Bush, A. I., Mackinnon, A., Macfarlane, S., Mastwyk, M., MacGregor, L., Kiers, L., Cherny, R., Li, Q. X., Tammer, A., Carrington, D., Mavros, C., Volitakis, I., Xilinas, M., Ames, D., Davis, S., Beyreuther, K., Tanzi, R. E. and Masters, C. L. (2003) Metal-protein attenuation with iodochlorhydroxyquin (clioquinol) targeting Abeta amyloid deposition and toxicity in Alzheimer disease: a pilot phase 2 clinical trial. *Archives of Neurology* **60** 1685-1691

Rival, T., Page, R. M., Chandraratna, D. S., Sendall, T. J., Ryder, E., Liu, B., Lewis, H., Rosahl, T., Hider, R., Camargo, L. M., Shearman, M. S., Crowther, D. C. and Lomas, D. A. (2009) Fenton chemistry and oxidative stress mediate the toxicity of the beta-amyloid peptide in a *Drosophila* model of Alzheimer's disease. *European Journal of Neuroscience* **29** 1335-1347

Robakis, N. K., Ramakrishna, N., Wolfe, G. and Wisniewski, H. M. (1987) Molecular cloning and characterization of a cDNA encoding the cerebrovascular and the neuritic plaque amyloid peptides. *Proceedings of the National Academy of Sciences* **84** 4190–4194

Roberson, E. D., Scearce-Levie, K., Palop, J. J., Yan, F., Cheng, I. H., Wu, T., Gerstein, H., Yu, G. Q. and Mucke, L. (2007) Reducing endogenous tau ameliorates amyloid beta-induced deficits in an Alzheimer's disease mouse model. *Science* **316** 750-754

Roher, A. E., Chaney, M. O., Kuo, Y.-M., Webster, S. D., Stine, W. B., Haverkamp, L. J., Woods, A. S., Cotter, R. J., Tuohy, J. M., Krafft, G. A., Bonnell, B. S. and Emmerling, M. R. (1996) Morphology and Toxicity of Abeta-(1-42) Dimer Derived from Neuritic and Vascular Amyloid Deposits of Alzheimer's Disease. *Journal of Biological Chemistry* **271** 20631-20635

Roychaudhuri, R., Yang, M., Hoshi, M. M. and Teplow, D. B. (2009) Amyloid beta-Protein Assembly and Alzheimer Disease. *Journal of Biological Chemistry* **284** 4749-4753

Saido, T. C., Yamao-Harigaya, W., Iwatsubo, T. and Kawashima, S. (1996) Amino- and carboxyl-terminal heterogeneity of [beta]-amyloid peptides deposited in human brain. *Neuroscience Letters* **215** 173-176

Sakaitani, M., Hori, K. and Ohfune, Y. (1988) One-pot conversion of N-benzyloxycarbonyl group into N-tert-butoxycarbonyl group. *Tetrahedron Letters* **29** 2983-2984

Saladino, R., Mezzetti, M., Mincione, E., Torrini, I., Paradisi, M. P. and Mastropietro, G. (1999) A new and efficient synthesis of unnatural amino acids and peptides by selective 3,3-dimethyldioxirane side-chain oxidation. *Journal of Organic Chemistry* **64** 8468-8474

Sampson, W. R., Patsiouras, H. and Ede, N. J. (1999) The synthesis of 'difficult' peptides using 2-hydroxy-4-methoxybenzyl or pseudoproline amino acid building blocks: a comparative study. *Journal of Peptide Science* **5** 403-409

Samsonov, V. and Volodarskii, L. (1980) Preparation and some properties of 2H-imidazole 1,3-dioxides, derivatives of alicyclic 1,2-dioximes. *Chemistry of Heterocyclic Compounds* 628-633 PlacePublished Springer New York

Sano, M., Ernesto, C., Thomas, R. G., Klauber, M. R., Schafer, K., Grundman, M., Woodbury, M., Growdon, P. and al., e. (1997) A controlled trial of selegiline, alpha-tocopherol, or both as treatments for Alzheimer's disease. The Alzheimer's Disease Cooperative Study. *New England Journal of Medicine* **36** 1216–1222

Santa Maria, C., Reville, E., Ayala, A., De la Cruz, C. P. and Machadio, A. (1995) Changes in the histidine residues of Cu/Zn superoxide dismutase during aging. *FEBS Letters* **374** 85-88

Sarell, C. J., Syme, C. D., Rigby, S. E. J. and Viles, J. H. (2009) Copper(II) Binding to Amyloid-beta Fibrils of Alzheimer's Disease Reveals a Picomolar Affinity: Stoichiometry and Coordination Geometry Are Independent of Abeta Oligomeric Form. *Biochemistry* **48** 4388-4402

Sarell, C. J., Wilkinson, S. R. and Viles, J. H. (2010) Sub-stoichiometric levels of Copper2+ ions accelerate the kinetics of fibre formation and promote cell toxicity of amyloid-beta from Alzheimer's disease. *Journal of Biological Chemistry* **285** 41533-41540

Satyanarayana, M. V., Sundar, B. S. and Murti, P. S. R. (1993) Kinetics and mechanism of oxidation of a few alpha-amino acids by trichloroisocyanuric acid. *Oxidation Communications* **16** 362-372

Sawaya, M. R., Sambashivan, S., Nelson, R., Ivanova, M. I., Sievers, S. A., Apostol, M. I., Thompson, M. J., Balbirnie, M., Wiltzius, J. J. W., McFarlane, H. T., Madsen, A. O., Riekel, C. and Eisenberg, D. (2007) Atomic structures of amyloid cross-[bgr] spines reveal varied steric zippers **447** 453-457

Sayre, L. M., Zelasko, D. A., Harris, P. L., Perry, G., Salomon, R. G. and Smith, M. A. (1997) 4-Hydroxynonenal-derived advanced lipid peroxidation end products are increased in Alzheimer's disease. *Journal of Neuroscience* **68** 2092-2097

Schenck, H. L., Dado, G. P. and Gellman, S. H. (1996) Redox-Triggered Secondary Structure Changes in the Aggregated States of a Designed Methionine-Rich Peptide *Journal of the American Chemical Society* **118** 12487-12494

Schiewe, A. J., Margol, L., Soreghan, B. A., Thomas, S. N. and Yang, A. J. (2004) Rapid Characterization of Amyloid-beta Side-Chain Oxidation by Tandem Mass Spectrometry and the Scoring Algorithm for Spectral Analysis. *Pharmaceutical Research* **21** 1094-1102

Schlessinger, R. H., Bebernitz, G. R., Lin, P. and Poss, A. J. (1985) Total Synthesis of (-)-Tirandamycin-A. *Journal of the American Chemical Society* **107** 1777-1778

Schmidt, U., Griesser, H., Leitenberger, V., Lieberknecht, A., Mangold, R., Meyer, R. and Riedl, B. (1992) Diastereoselective Formation of (Z)-Didehydroamino Acid Esters. *Synthesis* **5** 487-490

Schmidt, U., Lieberknecht, A. and Wild, J. (1984) Amino Acids and Peptides; XLIII1. Dehydroamino Acids; XVIII2. Synthesis of Dehydroamino Acids and Amino Acids from N-Acyl-2-(dialkyloxyphosphinyl)-glycin Esters; II. *Synthesis* **1984** 53-60

Schmidt, U., Lieberknecht, A., Schanbacher, U., Beuttler, T. and Wild, J. (1982) Facile Preparation of *N*-Acyl-2-(diethoxyphosphoryl)glycine Esters and Their Use in the Synthesis of Dehydroamino Acid Esters. *Angewandte Chemie* **94** 797

Schoneich, C. (2000) Mechanisms of metal-catalyzed oxidation of histidine to 2-oxo-histidine in peptides and proteins. *Journal of Pharmaceutical and Biomedical Analysis* **21** 1093-1097

Schoneich, C. (2002) Redox processes of methionine relevant to beta-amyloid oxidation and Alzheimer's disease. *Archives of Biochemistry and Biophysics* **397** 370-376

Schoneich, C. (2004) Selective Cu2+/Ascorbate-Dependent Oxidation of Alzheimer's Disease beta-Amyloid Peptides. *Annals of the New York academy of science* **1012** 164-170

Schoneich, C. (2005) Methionine oxidation by reactive oxygen species: reaction mechanism and relevance to Alzheimer's disease. *Biochimica et Biophysica Acta* **1703** 111-119

Schoneich, C. and Williams, T. D. (2002) Cu(II)-catalyzed oxidation of beta-amyloid peptide targets His(13) and His(14) over His(6): Detection of 2-oxo-histidine by HPLC-MS/MS. *Chemical Research in Toxicology* **15** 717-722

Schoneich, C. and Williams, T. D. (2003) Cu(II)-catalyzed oxidation of Alzheimer's disease beta-amyloid peptide and related sequences: remarkably different sensitivities of neurotoxic betaAP1-40 and non-toxic betaAP40-1. *Cellular and Molecular Biology* **49** 753-761

Schweers, O., Mandelkow, E.-M., Biernat, J. and Mandelkow, E. (1995) Oxidation of cysteine-322 in the repeat domain of microtubule-associated protein tau controls the in vitro assembly of paired helical filaments. *Proceedings of the National Academy of Sciences* **92** 8463-8467

Seilheimer, B., Bohrmann, B., Bondolfi, L., Müller, F., Stüber, D. and Döbeli, H. (1997) The Toxicity of the Alzheimer's [beta]-Amyloid Peptide Correlates with a Distinct Fiber Morphology. *Journal of Structural Biology* **119** 59-71

Selkoe, D. J. (1994) Normal and abnormal biology of the beta-amyloid precursor protein. *Annual Review of Neuroscience* **17** 489-517

Selkoe, D. J. (2001) Alzheimer's Disease: Genes, Proteins, and Therapy *Physiology Review* **81** 741-766

Senior, K. (2002) Dosing in phase II trial of Alzheimer's vaccine suspended. *Lancet Neurology* **1** 3

Serrano, F. and Klann, E. (2004) Reactive oxygen species and synaptic plasticity in the aging hippocampus. *Ageing Research Reviews* **3** 431 – 443

Seubert, P., Vigo-Pelfrey, C., Esch, F., Lee, M., Dovey, H., Davis, D., Sinha, S., Schiossmacher, M., Whaley, J., Swindlehurst, C., McCormack, R., Wolfert, R., Selkoe, D., Lieberburg, I. and Schenk, D. (1992) Isolation and quantification of soluble Alzheimer's [beta]-peptide from biological fluids. *Nature* **359** 325-327

Shankar, G. M., Bloodgood, B. L., Townsend, M., Walsh, D. M., Selkoe, D. J. and Sabatini, B. L. (2007) Natural oligomers of the Alzheimer amyloid-beta protein induce reversible

synapse loss by modulating an NMDA-type glutamate receptor-dependent signalling pathway. *Journal of Neuroscience* **27** 2866-2875

Shankar, R. and Scott, A. I. (1993) A Convenient Synthesis of 2-(Diethoxyphosphoryl)Glycine and its derivatives. *Tetrahedron Letters* **34** 231-234

Shao, H., Jao, S.-c., Ma, K. and Zagorski, M. G. (1999) Solution structures of micelle-bound amyloid [beta]-(1-40) and [beta]-(1-42) peptides of Alzheimer's disease. *Journal of Molecular Biology* **285** 755-773

Shearer, J. and Szalai, V. A. (2008) The Amyloid-beta; Peptide of Alzheimer's Disease Binds CuI in a Linear Bis-His Coordination Environment: Insight into a Possible Neuroprotective Mechanism for the Amyloid-beta; Peptide. *Journal of the American Chemical Society* **130** 17826-17835

Shimshock, S. J., Waltermire, R. E. and DeShong, P. (1991) A Total Synthesis of (+/-)-Tirandamycin B. *Journal of the American Chemical Society* **113** 8791-8796

Shin, C.-g., Obara, T., Segami, S. and Yonezawa, Y. (1987) Convenient syntheses and reactions of two kinds of basic [alpha]-dehydroamino acid derivatives. *Tetrahedron Letters* **28** 3827-3830

Shinall, H., Song, E. S. and Hersh, L. B. (2005) Susceptibility of Amyloid beta Peptide Degrading Enzymes to Oxidative Damage: A Potential Alzheimer's Disease Spiral. *Biochemistry* **44** 15345-15350

Shipton, O. A., Leitz, J. R., Dworzak, J., Acton, C. E. J., Tunbridge, E. M., Denk, F., Dawson, H. N., Vitek, M. P., Wade-Martins, R., Paulsen, O. and Vargas-Caballero, M. (2011) Tau Protein Is Required for Amyloid beta-Induced Impairment of Hippocampal Long-Term Potentiation. *Journal of Neuroscience* **31**

Shustov, G. V. and Rauk, A. (1998) Mechanism of Dioxirane Oxidation of CH Bonds: Application to Homo- and Heterosubstituted Alkanes as a Model of the Oxidation of Peptides. *Journal of Organic Chemistry* **63** 5413-5422

Simakov, P. A., Choi, S.-Y. and Newcomb, M. (1998) Dimethyldioxirane hydroxylation of a hypersensitive radical probe: Supporting evidence for an oxene insertion pathway. *Tetrahedron Letters* **39** 8187-8190

Simic, M. G. (1978) Radiation chemistry of amino acids and peptides in aqueous solutions. *Journal of Agricultural and Food Chemistry* **26** 6-14

Simmons, L. K., May, P. C., Tomaselli, K. J., Rydel, R. E., Fuson, K. S., Brigham, E. F., Wright, S., Lieberburg, I., Becker, G. W., Brems, D. N. and Li, W. Y. (1994) Secondary structure of amyloid beta papetide correlates with neurotoxic activity in vitro. *Molecular Pharmacology* **45** 373-379

Sipe, J. D. (2000) Review: History of the Amyloid Fibril. *Journal of Structural Biology* **130** 88-98

Sivappa, R., Koswatta, P. and Lovely, C. J. (2007) Oxidative reactions of tetrahydrobenzimidazole derivatives with N-sulfonyloxaziridines. *Tetrahedron Letters* **48** 5771-5775

Sjogren, M., Davidsson, P., Wallin, A., Granerus, A. K., Grundstrom, E., Askmark, H., Vanmechelen, E. and Blennow, K. (2002) Decreased CSF-beta-amyloid 42 in Alzheimer's disease and amyotrophic lateral schlerosis may reflect mismetabolism of beta-amyloid induced by disparate mechanisms. *Dementia and Geriatric Cognitive Disorders* **13** 112-118

Smith, A. B., Leahy, J. W., Noda, I., Remiszewski, S. W., Liverton, N. J. and Zibuck, R. (1992) Total Synthesis of the Latrunculins. *Journal of American Chemical Society* **114** 2995-3007

Smith, C. D., Carney, J. M., Starke-Reed, P. E., Oliver, C. N., Stadtman, E. R., Floyd, R. A. and Markesbery, W. R. (1991) Excess brain protein oxidation and enzyme dysfunction in normal aging and in Alzheimer disease. *Proceedings of the National Academy of Sciences* **88** 10540-10543

Smith, D. G., Cappai, R. and Barnham, K. J. (2007) The redox chemistry of the Alzheimer's disease amyloid beta peptide. *Biochimica Et Biophysica Acta-Biomembranes* **1768** 1976-1990

Smith, D. G., Ciccotosto, G. D., Tew, D. J., Perez, K., Curtain, C. C., Boas, J. F., Masters, C. L., Cappai, R. and Barnham, K. J. (2010) Histidine 14 Modulates Membrane Binding and Neurotoxicity of the Alzheimer's Disease Amyloid- beta Peptide. *Journal of Alzheimer's disease* **19** 1371-1376

Smith, D. P., Smith, D. G., Curtain, C. C., Boas, J. F., Pilbrow, J. R., Ciccotosto, G. D., Lau, T. L., Tew, D. J., Perez, K., Wade, J. D., Bush, A. I., Drew, S. C., Separovic, F., Masters, C. L., Cappai, R. and Barnham, K. J. (2006) Copper-mediated amyloid-beta toxicity is associated with an intermolecular histidine bridge. *Journal of Biological Chemistry* **281** 15145-15154

Smith, M. A., Harris, P. L., Sayre, L. M. and Perry, G. (1997a) Iron accumulation in Alzheimer disease is a source of redox-generated free radicals. *Proceedings of the National Academy of Sciences* **94** 9866-9868

Smith, M. A., Hirai, K., Hsiao, K., Pappola, M. A., Richey Harris, P. L., Siedlak, S. L., Tabaton, M. and Perry, G. (1998) Amyloid-beta deposition in Alzheimer transgenic mice is associated with oxidative stress. *Journal of Neurochemistry* **70** 2212-2215

Smith, M. A., Kutty, R. K., Richey, P. L., Yan, S. D., Stern, D., Chader, G. J., Wiggert, B., B., P. R. and Perry, G. (1994a) Heme-oxygenase-1 is associated with the neurofibrillary pathology of Alzheimer's disease. *American Journal of Pathology* **145** 42-47

Smith, M. A., Richey Harris, P. L., Sayre, L. M., Beckman, J. S. and Perry, G. (1997b) Widespread peroxynitrite-mediated damage in Alzheimer's disease. *Journal of Neuroscience* **17** 2653-2657

Smith, M. A., Richey, P. L., Taneda, S., Kutty, R. K., Sayre, L. M., Monnier, V. M. and Perry, G. (1994b) Advanced Maillard Reaction End Products, Free Radicals, and Protein Oxidation in Alzheimer's Disease. *Annals of the New York academy of science* **738** 447-454

Smith, M. A., Taneda, S., Richey, P. L., Miyata, S., Yan, S.-D., Stern, D., Sayre, L. M., Monnier, V. M. and Perry, G. (1994c) Advanced Mailard reaction end products are associated with Alzheimer disease pathology. *Proceedings of the National Academy of Sciences* **91** 5710-5714

Smyth, M. S., Stefanova, I., Hartmann, F., Horak, I. D., Osherov, N., Levitzki, A. and Burke, T. R. (1993) Non-Amine Based Analogs of Lavendustin-a as Protein-Tyrosine Kinase Inhibitors. *Journal of Medicinal Chemistry* **36** 3010-3014

Snyder, E. M., Nong, Y., Almeida, C. G., Paul, S., Moran, T., Choi, E. Y., Nairn, A. C., Salter, M. W., Lombroso, P. J., Gouras, G. K. and Greengard, P. (2005) Regulation of NMDA receptor trafficking by amyloid-beta. *Nature Neuroscience* **8** 1051-1058

Snyder, S. W., Ladror, U. S., Wade, W. S., Wang, G. T., Barrett, L. W., Matayoshi, E. D., Krafft, G. A. and Holzman, T. F. (1994) Amyloid beta aggregation: selective inhibition of aggregation in mixtures of amyloid with different chain links. *Biophysical Journal* **10** 373-403

Sohal, R. S., Agarwal, S. and Sohal, B. H. (1995) Oxidative stress and aging in the Mongolian gerbil (Meriones unguiculatus). *Mechanisms of Ageing and Development* **81** 15-25

Sohma, Y., Hayashi, Y., Kimura, M., Chiyomori, Y., Taniguchi, A., Sasaki, M., Kimura, T. and Kiso, Y. (2005) The 'O-acyl isopeptide method' for the synthesis of difficult sequence-containing peptides: application to the synthesis of Alzheimer's disease-related amyloid beta peptide (A beta) 1-42 *Journal of Peptide Science* **11** 441-451

Sokolowska, M. and Bal, W. (2005) Cu(II) complexation by "non-coordinating" N-2-hydroxyethylpiperazine-N'-2-ethanesulfonic acid (HEPES buffer). *Journal of Inorganic Biochemistry* **99** 1653-1660

Solar, I., Dulitzky, J. and Shaklai, N. (1990) Hemin-promoted peroxidation of red cell cytoskeletal proteins *Archives of Biochemistry and Biophysics* **283** 81-89

Soto, C. (2004) Unfolding the role of protein misfolding in neurodegenerative diseases. *Nature Reviews Neuroscience* **4** 49-60

Spector, R. and Eels, J. (1984) Deoxynucleoside and vitamin transport into the central nervous system. *Federation Proceedings* **43** 196-200

Spires, T. L. and Hyman, B. T. (2004) Neuronal structure is altered by amyloid plaques. *Review of Neuroscience* **15** 267-278

Sponne, I., Fifre, A., Drouet, B., Klein, C., Koziel, V., Pincon- Raymond, M., Olivier, J. L., J., C. and Pillot, T. (2003) Apoptotic neuronal cell death induced by the non-fibrillar amyloid beta peptide proceeds through an early reactive oxygen speciesdependent cytoskeleton perturbation. *Journal of Biological Chemistry* **278** 3437 – 3445

Squitti, R., Barbati, G., Rossi, L., Ventriglia, M., Dal Forno, G., Cesaretti, S., Moffa, F., Caridi, I., Cassetta, E., Pasqualetti, P., Calabrese, L., Lupoi, D. and Rossini, P. M. (2006) Excess of nonceruloplasmin serum copper in AD correlates with MMSE, CSF beta-amyloid, and h-tau. *Neurology* **67** 76-82

Stadtman, E. R. (1990) Metal ion-catalyzed oxidation of proteins: biochemical modifications and biological consequences. *Free Radical Biology and Medicine* **9** 315-325

Stadtman, E. R. and Berlett, B. S. (1991) Fenton chemistry. Amino acid oxidation. *Journal of Biological Chemistry* **266** 17201-17211

Stadtman, E. R. and Berlett, B. S. (1997) Reactive Oxygen-Mediated Protein Oxidation in Aging and Disease. *Chemical Research in Toxicology* **10** 485-494

Stanovnik, B., Tisler, M. and Voncina, E. (1979) A Photo-rearrangement of S-Diazouracil. A Convenient Synthesis of 2-Oxo-4-imidazoline-4-carboxylic Acid Derivatives. *Heterocycles* **12** 761-764

Starke-Reed, P. E. and Oliver, C. N. (1989) Protein oxidation and proteolysis during aging and oxidative stress. *Archives of Biochemistry and Biophysics* **275** 559-567

StatSoft Electronic Statistics Textbook

Steinhuebel, D., Palucki, M. and Davies, I. W. (2006) Controlling Olefin Geometry with Pd Catalysis: Selective Formation of Z-olefins from Both E and Z-Allylic Carbonates. *Journal of Organic Chemistry* **71** 3282-3284

Stine, W. B., Jr., Dahlgren, K. N., Krafft, G. A. and LaDu, M. J. (2003) In vitro characterization of conditions for amyloid-beta peptide oligomerization and fibrillogenesis *Journal of Biological Chemistry* **278** 11612-11622

Subbarao, K. V., Richardson, J. S. and Ang, L. C. (1990) Autopsy samples of Alzheimer's cortex shows increased peroxidation in vitro. *Journal of Neurochemistry* **55** 342-345

Sultana, R. and Butterfield, D. A. (2008) Redox proteomics studies of in vivo amyloid beta-peptide animal models of Alzheimers disease: Insight into the role of oxidative stress. *Proteomics Clinical Applications* **2** 685-696

Sun, A. Y., Draczynska-Lusiak, B. and Sun, G. Y. (2001) Oxidized lipoproteins, amyloid peptides and Alzheimer's disease. *Neurotoxicity Research* **3** 167–178

Sundberg, R. J. and Martin, R. B. (1974) Interactions of histidine and other imidazole derivatives with transition metal ions in chemical and biological systems. *Chemical Reviews* **74** 471

Syme, C. D., Nadal, R. C., Rigby, S. E. and Viles, J. H. (2004) Copper binding to the amyloid-beta (Abeta) peptide associated with Alzheimer's disease: folding, coordination geometry, pH dependence, stoichiometry, and affinity of Abeta-(1-28): insights from a range of complementary spectroscopic techniques. *Journal of Biological Chemistry* **279** 18169-18177

Tabanella, S., Valancogne, I. and F. W. Jackson, R. (2003) Preparation of enantiomerically pure pyridyl amino acids from serine. *Organic & Biomolecular Chemistry* **1** 4254-4261

Tabaton, M., Nunzi, M. G., Xue, R., Usiak, M., Autilio-Gambetti, L. and Gambetti, P. (1994) Soluble amyloid beta-protein is a marker of Alzheimer amyloid in brain but not in cerebrospinal fluid. *Biochemical and Biophysical Research Communications* **200** 1598-1603

Takahashi, R. and Goto, S. (1990) Alteration of aminoacyl-tRNA synthetase with age: Heat labilization of the enzyme by oxidative damage. *Archives of Biochemistry and Biophysics* **277** 228-233

Talmard, C., Guilloreau, L., Coppel, Y., Mazarguil, H. and Faller, P. (2007) Amyloid-Beta Peptide forms monomeric complexes with Cu(II) and Zn(II) prior to aggregation. *Chemical and Biological Communications* **8** 163-165

Tam, J. P., Heath Jr, W. F. and Merrifield, R. B. Peptide Synthesis Reagents and Method of Use. March 26, 1985 Research Corporation *US 4507230*

Tapiola, T., Alafuzoff, I., Herukka, S.-K., Parkkinen, L., Hartikainen, P., Soininen, H. and Pirttila, T. (2009) Cerebrospinal Fluid beta -Amyloid 42 and Tau Proteins as Biomarkers of Alzheimer-Type Pathologic Changes in the Brain. *Archives of Neurology* **66** 382-393

Teplow, D. B. (2006) Preparation of amyloid beta-protein for structural and functional studies. *Methods in Enzymology* **413** 20-33

Terry, R. D., Gonatas, N. K. and Weiss, M. (1964) Ultrastructural studies in Alzheimer's presenile dementia. *American Journal of Pathology* **44** 269-297

Thenappan, A. and Burton, D. J. (1990) Reduction-Olefination of Esters: A New and Efficient Synthesis of alpha-Fluoro alpha,beta-Unsaturated Esters. *Journal of Organic Chemistry* **55** 4639-4642

Thinakaran, G. and Koo, E. H. (2008) Amyloid precursor protein trafficking, processing, and function. *Journal of Biological Chemistry* **283** 29615-29619

Thomas, T., Thomas, G., McLendon, C., Sutton, T. and Mullan, M. (1996) [beta]-Amyloid-mediated vasoactivity and vascular endothelial damage. *Nature* **380** 168-171

Thompson, C. M., Markesbery, W. R., Ehmann, W. D., Mao, Y.-X. and Vance, D. E. (1988) Regional brain trace-element studies in Alzheimer's disease. *Neurotoxicology* **9** 1-8

Thusius, D., Dessen, P. and Jallon, J.-M. (1975) Mechanism of bovine liver glutamate dehydrogenase self-association. *Journal of Molecular Biology* **92** 413-432

Tickler, A. K. and Wade, J. D. (2001) Improved preparation of amyloid-beta peptides using DBU as Nalpha-Fmoc deprotection reagent. *Journal of Peptide Science* **7** 488-494

Tickler, A. K., Clippingdale, A. B. and Wade, J. D. (2004) Amyloid-beta as a "difficult sequence" in solid phase peptide synthesis. *Protein and Peptide Letters* **11** 377-384

Torok, M., Milton, S., Kayed, R., Wu, P., McIntire, T., Glabe, C. and Langen, R. (2002) Structural and dynamic features of Alzheimer's Abeta peptide in amyloid fibrils studied by site-directed spin labelling. *Journal of Biological Chemistry* **277** 40810–40815

Trampota, M. Process for the synthesis of L-(plus)-Ergothioneine. 9 April 2009 McNamara, S. P. *WO 2009/045413 A1*

Traore, D. A. K., El Ghazouani, A., Jacquamet, L., Borel, F., Ferrer, J. L., Lascoux, D., Ravanat, J. L., Jaquinod, M., Blondin, G., Caux-Thang, C., Duarte, V. and Latour, J. M. (2009)

Structural and functional characterization of 2-oxo-histidine in oxidized PerR protein. *Nature Chemical Biology* **5** 53-59

Triguero, L., Singh, R. and Prabhakar, R. (2008a) Comparative Molecular Dynamics Studies of Wild-Type and Oxidized Forms of Full-Length Alzheimer Amyloid beta-Peptides Abeta(1-40) and Abeta(1-42). *The Journal of Physical Chemistry B* **112** 7123-7131

Triguero, L., Singh, R. and Prabhakar, R. (2008b) Molecular dynamics study to investigate the effect of chemical substitutions of methionine 35 on the secondary structure of the amyloid beta (A beta(1-42)) monomer in aqueous solution *Journal of Physical Chemistry B* **112** 2159-2167

Troncoso, J. C., Costello, A., Watson, A. L. J. and Johnson, G. V. (1993) In vitro polymerisation of oxidised tau into filaments. *Brain Research* **613** 313-316

Tsuji, K., Nukaya, H. and Kanaya, Y. Histidine-hydrogen peroxide adduct and process for preparing same. Tokai Denka Kogyo Kabushiki Kaisha (Tokyo, JP)

Turnbull, S., Tabner, B. J., El-Agnaf, O. M., Twyman, L. J. and Allsop, D. (2001) New evidence that the Alzheimer beta-amyloid peptide does not spontaneously form free radicals: an ESR study using a series of spin-traps. *Free Radical Biology and Medicine* **30** 1154-1162

Tycko, R. (2006) Molecular structure of amyloid fibrils: insights from solid-state NMR. *Quarterly Reviews of Biophysics* **39** 1-55

Uchida, K. (2003) Histidine and lysine as targets of oxidative modification. *Amino Acids* **25** 249-257

Uchida, K. and Kawakishi, S. (1986) Selective Oxidation of Imidazole Ring in Histidine Residues by the Ascorbic Acid-Copper Ion System. *Biochemical and Biophysical Research Communications* **138** 659-665

Uchida, K. and Kawakishi, S. (1989) Ascorbate-mediated specific oxidation of the imidazole ring in a histidine derivative. *Bioorganic Chemistry* **17** 330-343

Uchida, K. and Kawakishi, S. (1989a) Ascorbate-Mediated Specific Modification of Histidine-Containing Peptides. *Journal of Agricultural and Food Chemistry* **37** 897-901

Uchida, K. and Kawakishi, S. (1990) Reaction of a Histidyl Residue Analogue with Hydrogen Peroxide in the Presence of Copper(II) Ion. *Journal of Agricultural and Food Chemistry* **38** 660-664

Uchida, K. and Kawakishi, S. (1990a) Formation of the 2-Imidazolone Structure within a Peptide Mediated by a Copper(II) Ascorbate System. *Journal of Agricultural and Food Chemistry* **38** 1896-1899

Uchida, K. and Kawakishi, S. (1990c) Site-specific oxidation of angiotensin I by copper(II) and -ascorbate: Conversion of histidine residues to 2-imidazolones. *Archives of Biochemistry and Biophysics* **283** 20-26

Uchida, K. and Kawakishi, S. (1993) 2-Oxo-histidine as a novel biological marker for oxidatively modified proteins. *FEBS Letters* **332** 208-210

Uchida, K. and Kawakishi, S. (1994) Identification of oxidized histidine generated at the active site of Cu,Zn-Superoxide Dismutase exposed to H2O2. *Journal of Biological Chemistry* **269** 2405-2410

Ueda, J. I., Shimazu, Y. and Ozawa, T. (1995) Reactions of copper(II)-oligopeptide complexes with hydrogen peroxide: Effects of biological reductants. *Free Radical Biology and Medicine* **18** 929-933

Uversky, V. N., Li, J. and Fink, A. L. (2001) Evidence for a partially folded intermediate in alpha-synuclein fibril formation *Journal of Biological Chemistry* **276** 10737 - 10744

Uversky, V., Cooper, E., Bower, K., Li, J. and Fink, A. (2002) Accelerated alpha-synuclein fibrillation in crowded milieu *FEBS Lett* **515** 99 - 103

van den Berg, B., Wain, R., Dobson, C. M. and Ellis, R. J. (2000) Macromolecular crowding perturbs protein refolding kinetics: implications for folding inside the cell. *EMBO Journal* **19** 3870-3875

van der Merwe, P. (1928) Über einige neue Derivate des Histamins. *Hoppe-Seyler's Zeitschrift für physiologische Chemie* **177** 301-314

Varadarajan, S., Kanski, J., Aksenova, M., Lauderback, C. and Butterfield, D. A. (2001) Different mechanisms of oxidative stress and neurotoxicity for Alzheimer's Abeta(1-42) and Abeta(25-35). *Journal of the American Chemical Society* **123** 5625-5631

Varadarajan, S., Yatin, S., Kanski, J., Jahanshahi, F. and Butterfield, D. A. (1999) Methionine residue 35 is important in amyloid beta-peptide-associated free radical oxidative stress. *Brain Research Bulletin* **50** 133-141

Vaswani, R. G. and Chamberlin, A. R. (2008) Stereocontrolled Total Synthesis of (-)-Kaitocephalin. *Journal of Organic Chemistry* **73** 1661-1681

Velazquez, P., Cribbs, D. H., Poulos, T. L. and Tenner, A. J. (1997) Aspartate residue 7 in amyloid beta-protein is critical for classical complement pathway activation: implications for Alzheimer's disease pathogenesis. *Nature Medicine* **3** 77-79

Venti, A., Giordano, T., Eder, P., Bush, A. I., Lahiri, D. K., Greig, N. H. and Rogers, J. T. (2004) The Integrated Role of Desferrioxamine and Phenserine Targeted to an Iron-Responsive Element in the APP-mRNA 5'-Untranslated Region. *Annals of the New York Academy of Sciences* **1035** 34-48

Vestergaard, M., Kerman, K., Saito, M., Nagatani, N., Takamura, Y. and Tamiya, E. (2005) A rapid label-free electrochemical detection and kinetic study of Alzheimer's amyloid beta aggregation. *Journal of American Chemical Society* **127** 11892-11893

Vigo-Pelfrey, C., Lee, D., Keim, P., Lieberburg, I. and Schenk, D. B. (1993) Characterization of beta-amyloid peptide from human cerebrospinal fluid. *Journal of Neurochemistry* **61** 1965-1968

Vliegenthart, J. F. and Dorland, L. (1970) Study by mass spectrometry of amino acid sequences in peptides containing histidine. *Biochemical Journal* **117** 31P-32P

Vogt, W. (1995) Oxidation of methionyl residues in proteins: Tools, targets and reversal. *Free Radical Biology and Medicine* **18** 93-105

von Edlbacher, S. and von Segesser, A. (1937) Der Abbau des Histidins und anderer Imidazole durch Ascorbinsäure. *Biochemische Zeitschrift* **290** 370

Wade, J. D., Otvos Jr, L., Matthieu, M. N., Tickler, A. K., Tregear, G. W., Catimel, B., Rothacker, J. and Nice, E. (2003) Innovation Perspectives in Solid Phase Synthesis Mayflower Worldwide

Wadsworth, W. S. and Emmons, W. D. (1961) The Utility of Phosphonate Carbanions in Olefin Synthesis. *Journal of the American Chemical Society* **83** 1733-1738

Wadsworth, W. S. J. and Emmons, W. D. (1973) Ethyl cyclohexylideneacetate [Delta1-alpha-Cyclohexaneacetic acid, ethyl ester]. *Organic Syntheses Collective* **5** 549

Walker, M. A., Kaplita, K. P., Chen, T. and King, H. D. (1997) Synthesis of all Three Regioisomers of Pyridylalanine. *Synlett* **1997** 169,170

Walsh, D. M., Hartley, D. M., Kusumoto, Y., Fezoui, Y., Condron, M. M., Lomakin, A., Benedek, G. B., Selkoe, D. J. and Teplow, D. B. (1999) Amyloid beta-protein fibrillogenesis: Structure and biological activity of protofibrillar intermediates. *Journal of Biological Chemistry* **274** 25945-25952

Wan, L., Nie, G., Zhang, J., Luo, Y., Zhang, P., Zhang, Z. and Zhao, B. (2011) [beta]-Amyloid peptide increases levels of iron content and oxidative stress in human cell and Caenorhabditis elegans models of Alzheimer disease. *Free Radical Biology and Medicine* **50** 122-129

Wang, S., Dilley, A. S., Poullennec, K. G. and Romo, D. (2006) Planned and unplanned halogenations in route to selected oroidin alkaloids. *Tetrahedron* **62** 7155-7161

Wang, W., Zhang, J. Y., Xiong, C. Y. and Hruby, V. J. (2002) Design and synthesis of hydrophobic, bulky chi(2)-constrained phenylalanine and naphthylalanine derivatives. *Tetrahedron Letters* **43** 2137-2140

Warshawsky, A., Altman, J., Kahana, N., Aradyellin, R., Deshe, A., Hasson, H., Shoef, N. and Gottlieb, H. (1989) Ring Cleavage of N-Acylsulfonylhistamine and N-(Arylsulfonyl)Histamine with Di-Tert-Butyl Dicarbonate - a One-Pot Synthesis of 4-Acylamino-1,2-Diaminobutane and 4-Arylsulfonylamino-1,2-Diaminobutane. *Synthesis-Stuttgart* **11** 825-829

Watson, A. A., Fairlie, D. P. and Craik, D. J. (1998) Solution structure of methionine-oxidized amyloid beta-peptide (1-40). Does oxidation affect conformational switching? *Biochemistry* **37** 12700-12706

Watson, D. J., Dowdy, E. D., Li, W.-S., Wang, J. and Polniaszek, R. (2001) Electronic effects in the acid-promoted deprotection of *N*-2,4-dimethoxybenzyl maleimides. *Tetrahedron Letters* **42** 1827-1830

Watzky, M. A. and Finke, R. G. (1997) Transition Metal Nanocluster Formation Kinetic and Mechanistic Studies. A New Mechanism When Hydrogen Is the Reductant: Slow, Continuous Nucleation and Fast Autocatalytic Surface Growth. *Journal of the American Chemical Society* **119** 10382-10400

Wegner, A. and Engel, J. (1975) Kinetics of the cooperative association of actin to actin filaments. *Biophysical Journal* **3** 215-225

Weldon, D. T., Rogers, S. D., Ghilardi, J. R., Finke, M. P., Cleary, J. P., Ohare, E., Esler, W. P., Maggio, J. E. and al., e. (1998) Fibrillar beta-amyloid induces microglial phagocytosis, expression of inducible nitric oxide synthase, and loss of a select population of neurons in the rat CNS in vivo. *Journal of Neuroscience* **18** 2161-2173

Westerman, M. A., Chang, L., Frautschy, S., Kotilinek, L., Cole, G. and Klein, W. L. (2002) Ibuprofen reverses memory loss in transgenic mice modeling Alzheimer's disease. *Society for Neuroscience Abstracts* **28** 690–694

Westlind-Danielsson, A. and Arnerup, G. (2001) Spontaneous in vitro formation of supramolecular beta-amyloid structures, "betaamy balls", by beta-amyloid 1–40 peptide. *Biochemistry* **40** 14736–14743

Wetzel, R. (2006) Kinetics and Thermodynamics of Amyloid Fibril Assembly. *Accounts of Chemical Research* **39** 671-679

White, A. R., Bush, A. I., Beyreuther, K., Masters, C. L. and Cappai, R. (1999) Exacerbation of copper toxicity in primary neuronal cultures depleted of cellular glutathione. *Journal of Neurochemistry* **72** 2092-2098

Whittemore, N. A., Mishra, R., Kheterpal, I., Williams, A. D., Wetzel, R. and Serpersu, E. H. (2005) Hydrogen-deuterium (H/D) exchange mapping of Abeta 1-40 amyloid fibril secondary structure using nuclear magnetic resonance spectroscopy. *Biochemistry* **44** 4434-4441

Williams, A. D., Portelius, E., Kheterpal, I., Guo, J. T., Cook, K. D., Xu, Y. and Wetzel, R. (2004) Mapping abeta amyloid fibril secondary structure using scanning proline mutagenesis. *Journal of Molecular Biology* **335** 833-842

Williams, R. M., Aldous, D. J. and Aldous, S. C. (1990) General-Synthesis of Beta,Gamma-Alkynylglycine Derivatives. *Journal of Organic Chemistry* **55** 4657-4663

Windaus, A. and Langenbeck, W. (1922) Über das Verhalten einiger aus Imidazolen bereiteter Bis-[benzoyl-amino]-äthylen-Derivate gegenüber Säure-anhydriden. *Chemische Berichte* **55** 3706

Wong, S. F., Halliwell, B., Richmond, R. and Skowroneck, W. R. (1981) The role of superoxide and hydroxyl radicals in the degradation of hyaluronic acid induced by metal ions and by ascorbic acid. *Journal of Inorganic Biochemistry* **14** 127-134

Wood, J. L., Stoltz, B. M. and Dietrich, H.-J. (1995) Total Synthesis of (+)- and (-)-K252a. *Journal of American Chemical Society* **117** 10413-10414

Wood, J. L., Stoltz, B. M. and Goodman, S. N. (1996) Total synthesis of (+)-RK-286c, (+)-MLR-52, (+)-staurosporine, and (+)-K252a. *Journal of the American Chemical Society* **118** 10656-10657

Wood, J. L., Stoltz, B. M., Dietrich, H.-J., Pflum, D. A. and Petsch, D. T. (1997) Design and Implementation of an Efficient Synthetic Approach to Furanosylated Indolocarbazoles: Total Synthesis of (+)- and (-)-K252a. *Journal of the American Chemical Society* **119** 9641-9651

Wood, S. J., Maleeff, B., Hart, T. and Wetzel, R. (1996) Physical, morphological and functional differences between pH 5.8 and 7.4 aggregates of the Alzheimer's amyloid peptide Abeta. *Journal of Molecular Biology* **256** 870-877

Wu, C., Wang, Z., Lei, H., Duan, Y., Bowers, M. T. and Shea, J.-E. (2008) The Binding of Thioflavin T and Its Neutral Analog BTA-1 to Protofibrils of the Alzheimer's Disease A[beta]16-22 Peptide Probed by Molecular Dynamics Simulations. *Journal of Molecular Biology* **384** 718-729

Wu, J., Anwyl, R. and Rowan, M. J. (1995a) Amyloid selectively augments NMDA receptor-mediated synaptic transmission in rat hippocampus. *Neuroreport* **6** 2409-2413

Wu, J., Anwyl, R. and Rowan, M. J. (1995b) Amyloid-(1–40) increases long-term potentiation in rat hippocampus in vitro. *European Journal of Pharmacology* **284** R1-R3

Wuts, P. G. M. and Greene, T. W. (2006) Greene's Protective Groups in Organic Synthesis. Wiley-Interscience

Xu, J. and Yadan, J. C. (1995) Synthesis of L-(+)-Ergothioneine. *Journal of Organic Chemistry* **60** 6296-6301

Yamaura, M., Suzuki, T., Hashimoto, H., Yoshimura, J., Okamoto, T. and Shin, C. (1985) Oxidative Removal of N-(4-Methoxybenzyl) Group on 2,5-Piperazinediones with Cerium(IV) Diammonium Nitrate. *Bulletin of the Chemical Society of Japan* **58** 1413-1420

Yan, S. D., Chen, X., Fu, J., Chen, M., Zhu, H., Roher, A., Slattery, T., Zhao, L., Nagashima, M., Morser, J., Migheli, A., Nawroth, P., Stern, D. and Schmidt, A. (1996) RAGE and amyloid-beta peptide neurotoxicity in Alzheimer's disease. *Nature* **382** 685-691

Yan, Y., McCallum, S. A. and Wang, C. (2008) M35 Oxidation Induces Abeta40-like Structural and Dynamical Changes in Abeta42. *Journal of the American Chemical Society* **130** 5394-5395

Yanagisawa, K. and Matsuzaki, K. (2002) Cholesterol-dependent aggregation of amyloid beta-protein. *Annals of the New York academy of science* **977** 384-386

Yankner, B. A. (1996) Mechanisms of neuronal degeneration in Alzheimer's disease. *Neuron* **16** 921-932

Yankner, B. A., Duffy, L. K. and Kirschner, D. A. (1990) Neurotrophic and neurotoxic effects of amyloid beta protein: reversal by tachykinin neuropeptides. *Science* **250** 279-282

Yates, C. M., Butterworth, J., Tennant, M. C. and Gordon, A. (1990) Enzyme activities in relation to pH and lactate in postmortem brain in Alzheimer-type and other dementias. *Journal of Neurochemistry* **55** 1624-1630

Yatin, S. M., Varadarajan, S. and Butterfield, D. A. (2000) Vitamin E prevents Alzheimer's amyloid beta-peptide (1-42)-induced neuronal protein oxidation and reactive oxygen species production. *Journal of Alzheimer's disease* **2** 123-131

Yatin, S. M., Varadarajan, S., Link, C. D. and Butterfield, D. A. (1999) In vitro and in vivo oxidative stress associated with Alzheimer's amyloid beta-peptide. *Neurobiology of Aging* **20** 325-330

Yeung, K.-S., Meanwell, N. A., Qiu, Z., Hernandez, D., Zhang, S., McPhee, F., Weinheimer, S., Clark, J. M. and Janc, J. W. (2001) Structure-Activity Relationship Studies of a Bisbenzimidazole-Based, Zn2+-Dependent Inhibitor of HCV NS3 Serine Protease. *Bioorganic & Medicinal Chemistry Letters* **11** 2355-2359

Yokogi, M. and Kuwano, R. (2007) Use of acetate as a leaving group in palladium-catalyzed nucleophilic substitution of benzylic esters. *Tetrahedron Letters* **48** 6109-6112

Yong, S. H. and Karel, M. (1978) Reaction of histidine with metyl linoleate: characterisation of the histidine degredation products. *Journal of the American Oil Chemists' Society* **55** 352-357

Yong, W., Lomakin, A., Kirkitadze, M. D., Teplow, D. B., Chen, S.-H. and Benedek, G. B. (2002) Structure determination of micelle-like intermediates in amyloid beta-protein fibril assembly by using small angle neutron scattering. *Proceedings of the National Academy of Sciences* **99** 150-154

Yoon, I., Lee, K. H. and Cho, J. (2004) Gossypin protects primary cultured rat cortical cells from oxidative stress- and beta-amyloid-induced toxicity. *Archives of Pharmacolgical Research* **27** 545-459

Youdim, M. B. H. (1988) Iron in the brain:implications for Parkinson's and Alzheimer's diseases. *Mount Sunai Journal of Medicine* **55** 97-101

Youngman, L. D., Park, J.-Y. K. and Ames, B. (1992) Protein oxidation associated with aging is reduced by dietary restriction of protein calories. *Proceedings of the National Academy of Sciences* **89** 9112-9116

Yu, L., Edalji, R., Harlan, J. E., Holzman, T. F., Lopez, A. P., Labkovsky, B., Hillen, H., Barghorn, S., Ebert, U. and Richardson, P. L. (2009) Structural Characterization of a Soluble Amyloid beta -Peptide Oligomer. *Biochemistry* **48** 1870-1877

Zancanella, M. A. and Romo, D. (2008) Facile Synthesis of the Trans-Fused Azabicyclo[3.3.0]octane Core of the Palau'amines and the Tricyclic Core of the Axinellamines from a Common Intermediate. *Organic Letters* **10** 3685-3688

Zav'yalov, S. I., Radul, O. M., Gunar, V. I. and Rodionova, N. A. (2004) Synthesis of ethyl ester of alpha-oxodehydrodesthiobiotin. *Russian Chemical Bulletin* **21** 2270-2272

Zav'yalov, S. I., Rodionov, N. A., Radul, O. M. and Gunar, V. I. (1972) Synthesis of alpha-oxodehydrodesthiobiotin ethyl-ester. *Izvestiya Akademii Nauk SSSR-Seriya Khimicheskaya.* **10** 2335

Zhang, S., Iwata, K., Lachenmann, M. J., Peng, J. W., Li, S., Stimson, E. R., Lu, Y., Felix, A. M., Maggio, J. E. and Lee, J. P. (2000) The Alzheimer's peptide a beta adopts a collapsed coil structure in water. *Journal of Structural Biology* **130** 130-141

Zhang, X. and Foote, C. S. (1993) Dimethyldioxirane oxidation of indole derivatives. Formation of novel indole-2,3-epoxides and a versatile synthetic route to indolinones and indolines. *Journal of the American Chemical Society* **115** 8867-8868

Zhang, Y., McLaughlin, R., Goodyer, C. and LeBlanc, A. (2002) Selective cytotoxicity of intracellular amyloid beta peptide1–42 through p53andBax in cultured primaryhumanneurons. *Journal of Cell Biology* **156** 519-529

Zhang, Z., Rydel, R. E., Drzewiecki, G. J., Fuson, K., Wright, S., Wogulis, M., Audia, J. E., May, P. C. and Hyslop, P. A. (1996) Amyloid beta-mediated oxidative and metabolic stress in rat cortical neurons: no direct evidence for a role for H2O2 generation. *Journal of Neurochemistry* **67** 1595-1606

Zhao, F., Ghezzo-Schoneich, E., Aced, G. I., Hong, J., Milby, T. and Schoneich, C. (1997) Metal-catalysed oxidation of histidine in human growth hormone. *Journal of Biological Chemistry* **272** 9019-9029

Zhu, X. W., Lee, H. G., Casadesus, G., Avila, J., Drew, K., Perry, G. and Smith, M. A. (2005) Oxidative imbalance in Alzheimer's disease. *Molecular Neurobiology* **31** 205-217

Zirah, S., Kozin, S. A., Mazur, A. K., Blond, A., Cheminant, M., Ségalas-Milazzo, I., Debey, P. and Rebuffat, S. (2006) Structural changes of region 1-16 of the Alzheimer disease amyloid beta-peptide upon zinc binding and in vitro aging. *Journal of Biological Chemistry* **281** 2151-2161

Zoller, U. and Ben-Ishai, D. (1975) Amidoalkylation of Mercaptans with Glyoxylic Acid Derivatives. *Tetrahedron* **31** 863-866

Zou, K., Gong, J. S., Yanagisawa, K. and Michikawa, M. (2002) A novel function of monomeric amyloid beta-protein serving as an antioxidant molecule against metal-induced oxidative damage. *Journal of Neuroscience* **22** 4833-4841